Springer Proceedings in Mathematics & Statistics

Ansgar Steland
Ewaryst Rafajłowicz
Krzysztof Szajowski *Editors*

Stochastic Models, Statistics and Their Applications

Wrocław, Poland, February 2015

Springer

Springer Proceedings in Mathematics & Statistics

Volume 122

Springer Proceedings in Mathematics & Statistics

This book series features volumes composed of select contributions from workshops and conferences in all areas of current research in mathematics and statistics, including OR and optimization. In addition to an overall evaluation of the interest, scientific quality, and timeliness of each proposal at the hands of the publisher, individual contributions are all refereed to the high quality standards of leading journals in the field. Thus, this series provides the research community with well-edited, authoritative reports on developments in the most exciting areas of mathematical and statistical research today.

More information about series at www.springer.com/series/10533

Ansgar Steland • Ewaryst Rafajłowicz •
Krzysztof Szajowski
Editors

Stochastic Models, Statistics and Their Applications

Wrocław, Poland, February 2015

Springer

Editors
Ansgar Steland
Institute of Statistics
RWTH Aachen University
Aachen, Germany

Krzysztof Szajowski
Inst. of Mathematics and Computer Science
Wrocław University of Technology
Wrocław, Poland

Ewaryst Rafajłowicz
Dept. of Computer Engineering,
Control and Robotics
Wrocław University of Technology
Wrocław, Poland

Additional material to this book can be downloaded from http://extras.springer.com

ISSN 2194-1009 ISSN 2194-1017 (electronic)
Springer Proceedings in Mathematics & Statistics
ISBN 978-3-319-13880-0 ISBN 978-3-319-13881-7 (eBook)
DOI 10.1007/978-3-319-13881-7

Library of Congress Control Number: 2015931942

Springer Cham Heidelberg New York Dordrecht London

Printed on acid-free paper

Springer International Publishing AG Switzerland is part of Springer Science+Business Media (www.springer.com)

Preface

This volume presents papers collected on the occasion of the 12th Workshop on Stochastic Models, Statistics and Their Applications, jointly organized by the Institute of Mathematics and Computer Science of Wrocław University of Technology, the Institute of Computer Engineering, Control and Robotics, Wrocław University of Technology, and by the Institute of Statistics of RWTH Aachen University. This German series of workshops has been frequently held together with research groups from Poland, i.e. as German–Polish events. It has become more and more international and takes place at Wrocław for the second time.

We would like to thank the following colleagues who accepted our invitation to organize an invited session: Marco Burkschat (Aachen), Maik Döring (Hohenheim), Dietmar Ferger (Dresden), Elżbieta Ferenstein (Warsaw), Josef Högel (Ulm), Hajo Holzmann (Marburg), Piotr Jaworski (Warsaw), Uwe Jensen (Hohenheim), Sven Knoth (Hamburg), Wolfgang Kössler (Berlin), Jacek Koronacki (Warsaw), Adam Krzyżak (Montreal), Eckhard Liebscher (Merseburg), Ryszard Magiera (Wrocław), Mirek Pawlak (Winnipeg), Rainer Schwabe (Magdeburg), Wolfgang Schmid (Frankfurt Oder) Krzysztof Szajowski (Wrocław), Darus Uciński (Zielona Góra), Christian Weiss (Hamburg), Aleksander Weron (Wrocław) and Rafał Weron (Wrocław).

In order to prepare a volume representing the state of the art as well as most recent trends in active research areas related to the workshop topics, we asked the session organizers to invite their speakers and submit full papers. All submitted papers undergone an intensive and critical peer-review process by members of the program committee, session organizers and other recognized international experts, but the authors are entirely responsible for the content and final form of the papers. The editors would like to thank the colleagues who joined us as members of the proceedings' program committee and helped us in handling and reviewing the papers: Marco Burkschat (Aachen), Uwe Jensen (Hohenheim), Waltraud Kahle (Magdeburg) and Sven Knoth (Hamburg). We are also indebted to the excellent and prompt work of other referees. They did an excellent job and without their help it would not have been possible to finish the volume timely.

Part I presents the papers related to the invited plenary presentations held by Laszlo Györfi (Budapest University of Technology and Economics and Hungarian Academy of Sciences), Teresa Ledwina (Polish Academy of Sciences) and Marie Hŭsková (Charles University of Prague). Part II collects articles about theory and related topics. Papers addressing stochastic modeling, primarily in engineering and related areas, methodological aspects and simulations are presented in Part III. Papers devoted to new algorithms, their improvement and study, or applications are provided in Part IV.

The authors who have contributed to this volume come from Austria, Brazil, Canada, Croatia, Czech Republic, Finland, France, Germany, Greece, Hungary, Italy, Japan, Netherlands, Norway, Poland, Russia, Slovak Republic, Spain and USA. It is our intention and hope that the preparation of the articles for this volume as well as the talks and discussions at the workshop deepen existing cooperations and partnerships and stimulate new collaborations.

We acknowledge the support of M.Sc. Annabel Prause who has helped us in organizing the sessions and communicating with the session organizers. Dr. Mohammed Abujarad and M.Sc. Evgenii Sovetkin handled the page proofs. Stefanie Truong carefully prepared the list of contributors and Hassan Satvat helped to set up and maintain the workshop's website. Last but not least, we would like to thank Springer for publishing this volume. Especially, we thank Ms. Alice Blanck for her valuable cooperation and support and Mr. Frank Holzwarth for his technical assistance.

Aachen, Germany — Ansgar Steland
Wrocław, Poland — Krzysztof Szajowski
Ewaryst Rafajłowicz

November 2014

Organization

Committees

Program Committee:

Ansgar Steland
Marco Burkschat
Uwe Jensen
Waltraud Kahle
Sven Knoth
Ewaryst Rafajłowicz
Krzysztof Szajowski

Organizing Committee:

Krzysztof Szajowski
Mohammed Abujarad
Prause Annabel
Ewaryst Rafajłowicz
Ewa Skubalska-Rafajłowicz
Ansgar Steland

Contents

Contributors

Jorge Alberto Achcar Social Medicine-FMRP, University of São Paulo, São Paulo, Brazil, e-mail: achcar@fmrp.usp.br

Daniel Ambach Department of Business, European University Viadrina, Frankfurt Oder, Germany, e-mail: ambach@europa-uni.de

Michał Balcerek Institute of Mathematics and Computer Science, Wrocław University of Technology, Wrocław, Poland, e-mail: michal.balcerek@pwr.edu.pl

Moulinath Banerjee Department of Statistics, University of Michigan, Ann Arbor, USA, e-mail: moulib@umich.edu

Emílio Augusto Coelho Barros Department of Mathematics, Federal Technological University of Paraná, Cornélio Procópio, Brazil, e-mail: eabarros@utfpr.edu.br

Kris De Brabanter Department of Statistics, Iowa State University, Ames, USA, e-mail: kbrabant@iastate.edu

Roy Cerqueti Department of Economics and Management, University of Macerata, Macerata, Italy, e-mail: roy.cerrqueti@unimc.it

Hong Chen Department of Applied Mathematics and Statistics, University Hohenheim, Stuttgart, Germany, e-mail: hong.chen@uni-hohenheim.de

Julien Chevallier IPAG Lab, IPAG Business School, Paris, France, e-mail: julien.chevallier04@univ-paris8.fr

Carsten Croonenbroeck Department of Business, European University Viadrina, Frankfurt O. Germany, e-mail: croonenbroeck@europa-uni.de

Kai Erik Dahlen Molde University College, Molde, Norway, e-mail: kai.e.dahlen@himolde.no

Maik Döring Department of Applied Mathematics and Statistics, University of Hohenheim, Stuttgart, Germany, e-mail: Maik.Doering@uni-hohenheim.de

Boris Darkhovsky Institute for Systems Analysis, Russian Academy of Sciences, Moscow, Russia, e-mail: darbor2004@mail.ru

Thorsten Dickhaus Weierstrass Institute for Applied Analysis and Stochastics, Berlin, Germany, e-mail: Thorsten.Dickhaus@wias-berlin.de

Wenyu Du Department of Mathematical Sciences, Binghamton University, New York, USA, e-mail: wdu1@binghamton.edu

Jason Ernst Mathematics and Statistics, University of Guelph, Guelph, Canada, e-mail: jernst@uoguelph.ca

Paolo Falbo Department of Economics and Management, University of Brescia, Brescia, Italy, e-mail: paolo.falbo@unibs.it

Tina Felber Department of Mathematics, TU Darmstadt, Darmstadt, Germany, e-mail: tfelber@mathematik.tu-darmstadt.de

Robert Garthoff Chair for Quantitative Methods, European University Viadrina, Frankfurt O., Germany, e-mail: garthoff@europa-uni.de

Stephane Goutte Mathematical Finance, Energy Modelling and Econometrics, University of Paris, Paris, France, e-mail: stephane.goutte@univ-paris8.fr

Ulrike Graßhoff Institute for Operations Research, Humboldt-University, Berlin, Germany, e-mail: grasshou@hu-berlin.de

Gianfranco Guastaroba Department of Economics and Management, University of Brescia, Brescia, Italy, e-mail: gianfranco.guastaroba@unibs.it

László Györfi Department of Computer Science and Information Theory, TU Budapest, Budapest, Hungary, e-mail: lacigyorfi@gmail.com

Radoslav Harman Department of Applied Mathematics and Statistics, Comenius University, Bratislava, Slovak Republic, e-mail: harman@fmph.uniba.sk

Zygmunt Hasiewicz Institute of Computer Engineering, Control and Robotics, Wrocław University of Technology, Wrocław, Poland, e-mail: zygmunt.hasiewicz@pwr.edu.pl

Heinz Holling Department of Psychology and Sport Science, Westphälische Wilhelms – University Münster, Münster, Germany, e-mail: holling@uni-muenster.de

Šárka Hudecová Faculty of Mathematics and Physics, Charles University in Prague, Prague, Czech Republic, e-mail: hudecova@karlin.mff.cuni.cz

Ronald Huisman Erasmus School of Economics, Erasmus University, Rotterdam, The Netherlands, e-mail: rhuisman@ese.eur.nl

Marie Hušková Faculty of Mathematics and Physics, Charles University in Prague, Prague, Hungary, e-mail: huskova@karlin.mff.cuni.cz

Matylda Jabłońska-Sabuka Lappeenranta University of Technology, Lappeenranta, Finland, e-mail: matylda.jablonska-sabuka@lut.fi

Uwe Jensen Institute of Applied Mathematics and Statistics, University of Hohenheim, Stuttgart, Germany, e-mail: Jensen@uni-hohenheim.de

Wolfgang Kössler Institute for Informatics, Humboldt-University, Berlin, Germany, e-mail: koessler@informatik.hu-berlin.de

Takashi Kanamura Graduate School of Advanced Integrated Studies in Human Survivability, Kyoto University, Kyoto, Japan, e-mail: tkanamura@gmail.com

Michael Kohler Department of Mathematics, TU Darmstadt, Darmstadt, Germany, e-mail: kohler@mathematik.tu-darmstadt.de

Adam Krzyżak Department of Computer Science and Software Engineering, Concordia University, Montreal, Canada, e-mail: krzyzak@cs.concordia.ca

Anna Ławniczak Mathematics and Statistics, University of Guelph, Guelph, Canada, e-mail: alawnicz@uoguelph.ca

Teresa Ledwina Department of Mathematical Statistics, Polish Academy of Science, Warszawa, Poland, e-mail: ledwina@impan.pan.wroc.pl

Urszula Libal Institute of Computer Engineering, Control and Robotics, Wrocław University of Technology, Wrocław, Poland, e-mail: urszula.libal@pwr.edu.pl

Eckhard Liebscher Department of Computer Science and Communication Systems, University of Applied Sciences Merseburg, Merseburg, Germany, e-mail: eckhard.liebscher@hs-merseburg.de

Yu Liu Computer Science Department, Iowa State University, Ames, USA, e-mail: yuliu@iastate.edu

Henryk Maciejewski Computer and Discrete Systems Group, Wrocław University of Technology, Wrocław, Poland, e-mail: henryk.maciejewski@pwr.wroc.pl

Katarzyna Maciejowska Institute of Organization and Management, Wrocław University of Technology, Wrocław, Poland, e-mail: kmaciejo@gmail.com

Michal Marczyk Institute of Informatics, Silesian University of Technology, Gliwice, Poland, e-mail: michal.marczyk@polsl.pl

Edson Zangiacomi Martinez Department of Social Medicine, University of São Paulo, São Paulo, Brazil, e-mail: edson@fmrp.usp.br

Josmar Mazucheli Department of Statistics, UEM, Mazingá, Brazil, e-mail: jmazucheli@uem.br

Simos Meintanis Department of Economics, National and Kapodistrian University of Athens, Athens, Greece, e-mail: simosmei@econ.uoa.gr

George Michailidis Department of Statistics, University of Michigan, Ann Arbor, USA, e-mail: gmichail@umich.edu

Jan Mielniczuk Faculty of Mathematics and Information Science, Warsaw University of Technology, Warsaw, Poland, e-mail: miel@ipipan.waw.pl

Tobias Andreas Möller Mathematics and Statistics, Helmut-Schmidt-University, Hamburg, Germany, e-mail: moellert@hsu-hh.de

Grzegorz Mzyk Department of Control and Optimization, Wrocław University of Technology, Wrocław, Poland, e-mail: Grzegorz.Mzyk@pwr.edu.pl

Philipp Otto Chair for Quantitative Methods, European University Viadrina, Frankfurt O., Germany, e-mail: potto@europa-uni.de

Maciej Patan Institute of Control and Computation Engineering, University of Zielona Góra, Zielona Góra, Poland, e-mail: m.patan@issi.uz.zgora.pl

Cristian Pelizzari Department of Economics and Management, University of Brescia, Brescia, Italy, e-mail: cristian.pelizzari@unibs.it

Elisa Perrone Department of Applied Statistics, Johannes Kepler University of Linz, Linz, Austria, e-mail: elisa.perrone@jku.at

Monika Pietrowska Center for Translational Research and Molecular Biology of Cancer, Gliwice, Poland, e-mail: m_pietrowska@io.gliwice.pl

Alexandra Piryatinska Department of Mathematics, San Francisco State University, San Francisco, USA, e-mail: alpiryat@sfsu.edu

Joanna Polańska Institute of Informatics, Silesian University of Technology, Gliwice, Poland, e-mail: joanna.polanska@polsl.pl

Andrzej Polański Institute of Informatics, Silesian University of Technology, Gliwice, Poland, e-mail: andrzej.polanski@polsl.pl

Aleksey Polunchenko Department of Mathematical Sciences, Binghamton University, New York, USA, e-mail: aleksey@binghamton.edu

Zuzana Prášková Faculty of Mathematics and Physics, Charles University in Prague, Prague, Czech Republic, e-mail: praskova@karlin.mff.cuni.cz

Annabel Prause Institute of Statistics, RWTH Aachen University, Aachen, Germany, e-mail: Prause@stochastik.rwth-aachen.de

Pedro Puig Department of Mathematics, University of Barcelona, Barcelona, Spain, e-mail: ppuig@mat.uab.cat

Ewaryst Rafajłowicz Institute of Computer Engineering, Control and Robotics, Wrocław University of Technology, Wrocław, Poland,
e-mail: ewaryst.rafajlowicz@pwr.edu.pl

Adam Romanek Institute of Control and Computation Engineering, University of Zielona Góra, Zielona Góra, Poland, e-mail: m.patan@issi.uz.zgora.pl

Guillaume Sagnol Mathematical Optimization and Scientific Information, ZIB Berlin, Berlin, Germany, e-mail: sagnol@zib.de

Alessandro Sapio Department of Business and Economic Studies, Parthenope University of Naples, Naples, Italy, e-mail: alessandro.sapio@uniparthenope.it

Rainer Schwabe Institute for Mathematical Stochastics, Otto-von-Guericke-University, Magdeburg, Germany, e-mail: rainer.schwabe@ovgu.de

Sebastian Schweer Institute of Applied Mathematics, Heidelberg University, Heidelberg, Germany, e-mail: schweer@uni-heidelberg.de

Ewa Skubalska-Rafajłowicz Institute of Computer Engineering, Control and Robotics, Wrocław University of Technology, Wrocław, Poland,
e-mail: ewa.rafajlowicz@pwr.wroc.pl

Przemysław Śliwiński Institute of Computer Engineering, Control and Robotics, Wrocław University of Technology, Wrocław, Poland,
e-mail: przemyslaw.sliwinski@pwr.edu.pl

Grigory Sokolov Department of Mathematical Sciences, Binghamton University, New York, USA, e-mail: gsokolov@binghamton.edu

Moudar Soumaya Institute for Mathematical Stochastics, Otto-von-Guericke-University, Magdeburg, Germany, e-mail: moudar.soumaya@ovgu.de

Roberto Souza Department of Mathematics/Department of Social Medicine, Federal Technological University of Paraná, Paraná, Brazil,
e-mail: rmolinasouza@utfpr.edu.br

Bruno Di Stefano Nuptek Systems Ltd., Canada,
e-mail: bruno.distefano@nupteksystems.com

Ansgar Steland Institute of Statistics, RWTH Aachen University, Aachen, Germany, e-mail: Steland@stochastik.rwth-aachen.de

Krzysztof Szajowski Institute of Mathematics and Computer Science, Wrocław University of Technology, Wrocław, Poland,
e-mail: Krzysztof.Szajowski@pwr.edu.pl

Hubert Szymanowski Polish Academy of Science, Warsaw, Poland,
e-mail: miel@ipipan.waw.pl

Ivana Tomas Žiković Faculty of Economics, University of Rijeka, Rijeka, Croatia,
e-mail: itomas@efri.hr

Dariusz Uciński Institute of Control and Computation Engineering, University of Zielona Góra, Zielona Góra, Poland, e-mail: d.ucinski@issi.uz.zgora.pl

Paweł Wachel Institute of Computer Engineering, Control and Robotics, Wrocław University of Technology, Wrocław, Poland, e-mail: pawel.wachel@pwr.edu.pl

Christian Weiß Mathematics and Statistics, Helmut-Schmidt-University, Hamburg, Germany, e-mail: weissc@hsu-hh.de

Aleksander Weron Hugo Steinhaus Center, Wrocław University of Technology, Wrocław, Poland, e-mail: aleksander.weron@pwr.edu.pl

Rafał Weron Institute of Organization and Management, Wrocław University of Technology, Wrocław, Poland, e-mail: rafal.weron@pwr.edu.pl

Sjur Westgaard Department of Industrial Economics, Norwegian University of Science and Technology, Trondheim, Norway, e-mail: sjur.westgaard@iot.ntnu.no

Piotr Widlak Center for Translational Research and Molecular Biology of Cancer, Gliwice, Poland, e-mail: widlak@io.gliwice.pl

Agnieszka Wyłomańska Institute of Mathematics and Computer Science, Wrocław University of Technology, Wrocław, Poland,
e-mail: agnieszka.wylomanska@pwr.wroc.pl

Elena Yudovina Department of Mathematics, University of Minnesota, Minneapolis, USA, e-mail: eyudovin@umn.edu

Florian Ziel Chair for Quantitative Methods, European University Viadrina, Frankfurt O. Germany, e-mail: ziel@europa-uni.de

Sasa Zikovic Faculty of Economics, University of Rijeka, Rijeka, Croatia,
e-mail: szikovic@efri.hr

Radoslaw Zimroz Institute of Mining Engineering, Wrocław University of Technology, Wrocław, Poland, e-mail: radoslaw.zimroz@pwr.edu.pl

Part I
Plenary Papers

Chapter 1
Large Deviations of χ^2 Divergence Errors on Partitions

László Györfi

Abstract We discuss Chernoff-type large deviation results for χ^2 divergence errors on partitions. In contrast to the total variation and the I-divergence, the χ^2-divergence has an unconventional large deviation rate. In this paper we extend the result of Quine and Robinson in Ann. Stat. 13:727–742, 1985 from uniform distribution to arbitrary distribution.

1.1 Introduction

We consider the problem of testing an unknown probability distribution. The test statistics are derived from dissimilarity measures of probability measures, like ϕ-divergences introduced by Csiszár [7]. The three most important ϕ-divergences in mathematical statistics and information theory are the total variation distance, the information divergence and the χ^2-divergence.

If μ and ν are probability measures on $\mathbf{R}^d$ $(d \geq 1)$, then the applications of large deviation results in statistical analysis mainly concern the comparison of test procedures using Bahadur efficiencies. We consider the problem of testing hypotheses

$$H_0: \quad \nu = \mu \text{ versus} \quad H_1: \quad \nu \neq \mu$$

by means of test statistics $T_n = T_n(X_1, \ldots, X_n)$ where $X_1, X_2, \ldots$ are independent and identically distributed random vectors along ν. Considering two tests rejecting H_0 for large values of the statistics $T_{n,1}$ and $T_{n,2}$, then (see e.g. Bahadur [1], Groeneboom and Shorack [11]) the efficiency $e_{1,2}$ of $T_{n,1}$ with respect to $T_{n,2}$ is calculated through the Bahadur exact slopes $2b_1(\nu)$ and $2b_2(\nu)$ for testing against an alternative ν: $e_{1,2} = \frac{b_1(\nu)}{b_2(\nu)}$. The functions b_1 and b_2 are then given by

$$b_j(\nu) = g_j\big(\psi_j(\nu)\big), \quad j = 1, 2, \tag{1.1}$$

This work was partially supported by the European Union and the European Social Fund through project FuturICT.hu (grant no.: TAMOP-4.2.2.C-11/1/KONV-2012-0013).

L. Györfi (✉)
Department of Computer Science and Information Theory, Budapest University of Technology and Economics, Stoczek u.2, 1521 Budapest, Hungary
e-mail: gyorfi@cs.bme.hu

A. Steland et al. (eds.), *Stochastic Models, Statistics and Their Applications*,
Springer Proceedings in Mathematics & Statistics 122,
DOI 10.1007/978-3-319-13881-7_1

provided

$$T_{n,j} \to \psi_j(\nu) \text{ a.s.} \quad \text{as } n \to \infty \text{ under } H_1, \tag{1.2}$$

$$\lim_{n\to\infty} \mathbf{E}T_{n,j} = 0 \quad \text{as } n \to \infty \text{ under } H_0, \tag{1.3}$$

and

$$\lim_{n\to\infty} \frac{1}{n} \ln \mathbf{P}(T_{n,j} > \varepsilon) = -g_j(\varepsilon) \quad \text{under } H_0,\ \varepsilon > 0, \tag{1.4}$$

for $j = 1, 2$. Such a limit assumption on the tail of the distribution of $T_{n,j}$ means that

$$\mathbf{P}(T_{n,j} > \varepsilon) = e^{-n[g_j(\varepsilon)+o(1)]}.$$

Each of the divergence measures defined below, when applied to the distance between the null-hypothesis distribution μ and the empirical distribution μ_n, both restricted to a partition, does lead to a test procedure. Hence the large deviation results given in the subsequent sections offer the possibility to calculate exact Bahadur slopes for these tests. Quine and Robinson [21] derived large deviation results for test statistics for uniformity based on I-divergence and χ^2-divergence, i.e. for the classical likelihood ratio and chi-square goodness-of-fit tests. We also refer to Nikitin [20] for a survey on Bahadur efficiencies of different well-known tests.

1.2 The L_1 Error

If μ and ν are probability measures on $\mathbf{R}^d$ $(d \geq 1)$, then the *total variation distance* between μ and ν is defined by

$$V(\mu, \nu) = \sup_A \big|\mu(A) - \nu(A)\big|,$$

where the supremum is taken over all Borel sets A.

We now consider some goodness of fit tests for H_0 given in the Introduction. Assume a sample of independent, $\mathbf{R}^d$ valued random vectors $X_1, \ldots, X_n$, distributed according to a probability measure μ, and let μ_n denote the empirical measure.

Györfi and van der Meulen [13] introduced the test statistic

$$J_n = \sum_{j=1}^{m_n} \big|\mu(A_{n,j}) - \mu_n(A_{n,j})\big|,$$

based on a finite partition $\mathscr{P}_n = \{A_{n,1}, \ldots, A_{n,m_n}\}$, $(n \geq 2)$, of $\mathbf{R}^d$. These authors also showed that under H_0

$$\mathbf{P}(J_n \geq \varepsilon) \leq e^{-n(\frac{\varepsilon^2}{8}+o(1))}.$$

Let $\bar{\mu}_n$ and μ_n^* be the restrictions of μ and μ_n to the partition $\mathscr{P}_n$, then $J_n = 2V(\bar{\mu}_n, \mu_n^*)$.

Beirlant et al. [2] proved the following large deviation property: Assume that

$$\lim_{n\to\infty} \max_j \mu(A_{n,j}) = 0 \tag{1.5}$$

and

$$\lim_{n\to\infty} \frac{m_n \ln n}{n} = 0. \tag{1.6}$$

Then for all $0 < \varepsilon < 2$

$$\lim_{n\to\infty} \frac{1}{n} \ln \mathbf{P}\{J_n > \varepsilon\} = -g(\varepsilon), \tag{1.7}$$

where

$$g(\varepsilon) = \inf_{0<p<1-\varepsilon/2} \left(p \ln \frac{p}{p+\varepsilon/2} + (1-p) \ln \frac{1-p}{1-p-\varepsilon/2} \right). \tag{1.8}$$

Biau and Györfi [4] gave an equivalent form of the rate function g:

$$g(\varepsilon) = \max_{s>0} \left[s\varepsilon + 1 - \frac{2s}{e^{2s}-1} - \ln\left(\frac{e^{4s} - 2e^{2s} + 1}{2s(e^{2s}-1)} \right) \right].$$

Moreover, they proved that without having the non-atomic condition (1.5), there is a general, tight upper bound

$$\mathbf{P}\{J_n > \varepsilon\} \le 2^{m_n} e^{-ng(\varepsilon)}.$$

This upper bound implies strongly consistent tests for homogeneity and for independence (cf. Biau and Györfi [4], and Gretton and Györfi [10]).

Remark 1.1 In Lemma 5.1 in Bahadur [1] it was observed that $g(\varepsilon) = \frac{\varepsilon^2}{2}(1+o(1))$ as $\varepsilon \to 0$. Local Bahadur efficiencies of the test J_n with respect to other goodness-of-fit tests can now be computed on the basis of the above large deviation property.

1.3 The Information Divergence

The *information divergence* (also called I-divergence, Kullback–Leibler number, relative entropy) of μ and ν is defined by

$$I(\mu, \nu) = \sup_{\{A_j\}} \sum_j \mu(A_j) \log \frac{\mu(A_j)}{\nu(A_j)},$$

where the supremum is taken over all finite Borel measurable partitions $\{A_j\}$ of $\mathbf{R}^d$.

In the literature on goodness-of-fit testing the following statistic is related to the information divergence, namely the *(reversed) I-divergence statistic*

$$I_n = I(\mu_n^*, \bar{\mu}_n) = \sum_{j=1}^{m_n} \mu_n(A_{n,j}) \ln \frac{\mu_n(A_{n,j})}{\mu(A_{n,j})}.$$

Kallenberg [16] and Quine and Robinson [21] proved that under (1.5) and (1.6), for all $\varepsilon > 0$

$$\lim_{n\to\infty} \frac{1}{n} \ln \mathbf{P}\{I_n > \varepsilon\} = -\varepsilon,$$

which means that

$$\mathbf{P}\{I_n > \varepsilon\} = e^{-n(\varepsilon + o(1))}.$$

This leads to a goodness-of-fit tests based on I_n.

1.4 The χ^2-Divergence

The χ^2-*divergence measure* between μ and ν is defined by

$$\chi^2(\mu, \nu) = \sup_{\{A_j\}} \sum_j \frac{(\mu(A_j) - \nu(A_j))^2}{\nu(A_j)},$$

where again the supremum is taken over all finite Borel measurable partitions $\{A_j\}$ of $\mathbf{R}^d$.

Of course the best known goodness-of-fit test is based on the χ^2 statistic. We refer to Neyman [19], Watson [23] for some important historic references. See also Kallenberg et al. [17] for a more recent discussion. The χ^2 *or Pearson statistic* is given by

$$\chi_n^2 = \chi^2\big(\mu_n^*, \bar{\mu}_n\big) = \sum_{j=1}^{m_n} \frac{(\mu(A_{n,j}) - \mu_n(A_{n,j}))^2}{\mu(A_{n,j})},$$

Birgé and Massart [5], Castellan [6], and Mason, van Zwet [18] showed exponential upper bounds on the tail distribution of the χ^2-statistic. Concerning large deviations, Quine and Robinson [21] proved that if

$$\mu(A_{n,j}) = \frac{1}{m_n}, \quad j = 1, \ldots, m_n \tag{1.9}$$

and

$$\frac{m_n^{3/2} \ln n}{n \ln m_n} \to 0, \tag{1.10}$$

then for all $\varepsilon > 0$

$$\lim_{n\to\infty} \frac{\sqrt{m_n}}{n \ln m_n} \ln \mathbf{P}\big\{\chi_n^2 > \varepsilon\big\} = -\sqrt{\varepsilon}/2,$$

which means that

$$\mathbf{P}\big\{\chi_n^2 > \varepsilon\big\} = e^{-\frac{n \ln m_n}{\sqrt{m_n}}(\sqrt{\varepsilon}/2 + o(1))}.$$

Remark 1.2 Since $\mathbf{E}(I_n) \le \mathbf{E}(\chi_n^2) = \frac{m_n - 1}{n}$, (1.3) holds for the statistics I_n and χ_n^2 when $m_n/n \to 0$.

Remark 1.3 The previous large deviation result means that when $m_n \to \infty$, the Bahadur exact slope of the χ^2-test is identically zero. Another interpretation is that the tail of the χ^2-test statistic is of sub-exponential nature, that is, is heavier than an exponential tail. This is due to cells $A_{n,j}$ with small probabilities, which put too much weight on the squared difference $(\mu(A_{n,j}) - \mu_n(A_{n,j}))^2$. Based on the fact that the limit distribution properties of the I_n and the χ^2 divergences are equivalent (cf. Beirlant, Györfi [3], Györfi, Vajda [12]), there is a widespread believe in literature that the I-divergence test I_n and the χ^2-test have a similar behaviour. In contrast, their Bahadur slopes are quite different. Namely, Quine and Robinson [21], Harremoës and Vajda [14, 15] proved that the information divergence statistic is infinitely more Bahadur efficient than the χ^2 divergence statistic.

Next we extend this sub-exponential rate of convergence such that don't assume anything on the underlying distribution μ and on the partition $\mathscr{P}_n$.

Theorem 1.1 *Suppose* (1.5) *and that*

$$M_n := \frac{1}{\min\{\mu(A_{n,j});\, j = 1, \ldots, m_n\}} < \infty$$

holds such that

$$\frac{m_n M_n^{1/2} \ln n}{n \ln M_n} \to 0, \tag{1.11}$$

then for all $\varepsilon > 0$

$$\lim_{n\to\infty} \frac{\sqrt{M_n}}{n \ln M_n} \ln \mathbf{P}\{\chi_n^2 > \varepsilon\} = -\sqrt{\varepsilon}/2.$$

In the proof of our theorem we shall use the following lemma.

Lemma 1.1 (Sanov [22], see p. 16 in Dembo, Zeitouni [9], or Problem 1.2.11 in Csiszár and Körner [8].) *Let* Σ *be a finite set of measurable sets (alphabet),* $\mathscr{L}_n$ *be a set of types (possible empirical distributions) on* Σ*, and let* Γ *be a set of distributions on* Σ*. Then*

$$\left| \frac{1}{n} \ln \mathbf{P}\{\mu_n^* \in \Gamma\} + \inf_{\tau \in \Gamma \cap \mathscr{L}_n} I(\tau, \bar{\mu}_n) \right| \le \frac{|\Sigma| \ln(n+1)}{n} \tag{1.12}$$

where $|\Sigma|$ *denotes the cardinality of* Σ*.*

Proof of Theorem 1 Apply (1.12) for $\Sigma = \{A_{n,1}, \ldots, A_{n,m_n}\}$ such that

$$\Gamma = \{\tau\colon\ \chi^2(\tau, \bar{\mu}_n) \ge \varepsilon\}.$$

Then, according to (1.12),

$$\left| \frac{\sqrt{M_n}}{n \ln M_n} \ln \mathbf{P}\{\chi_n^2 \geq \varepsilon\} + \frac{\sqrt{M_n}}{\ln M_n} \inf_{\tau \in \Gamma \cap \mathscr{L}_n} I(\tau, \bar{\mu}_n) \right| \leq \frac{m_n M_n^{1/2} \ln(n+1)}{n \ln M_n}.$$

Therefore, because of (1.11),

$$\begin{aligned} \lim_{n\to\infty} \frac{\sqrt{M_n}}{n \ln M_n} \ln \mathbf{P}\{\chi_n^2 > \varepsilon\} &= - \lim_{n\to\infty} \frac{\sqrt{M_n}}{\ln M_n} \inf_{\tau \in \Gamma \cap \mathscr{L}_n} I(\tau, \bar{\mu}_n) \\ &= - \lim_{n\to\infty} \frac{\sqrt{M_n}}{\ln M_n} \inf_{\chi^2(\tau, \bar{\mu}_n) \geq \varepsilon} I(\tau, \bar{\mu}_n). \end{aligned}$$

Introduce the notations

$$\tilde{\tau} = (\tau_1, \ldots, \tau_{m_n})$$

and

$$\bar{\mu}_n = (\mu_1, \ldots, \mu_{m_n}).$$

Without loss of generality assume that

$$\mu_1 = \min_{i=1,\ldots,m_n} \{\mu_i\} = 1/M_n.$$

For fixed $\bar{\mu}_n$, let $\tau_1 > \mu_1$ be arbitrary, while put

$$\tau_i = \frac{1-\tau_1}{1-\mu_1} \mu_i,$$

$(i = 2, \ldots, m_n)$. Then

$$\begin{aligned} I(\tilde{\tau}, \bar{\mu}_n) = \sum_{i=1}^{m_n} \tau_i \ln \frac{\tau_i}{\mu_i} &= \tau_1 \ln \frac{\tau_1}{\mu_1} + \sum_{i=2}^{m_n} \tau_i \ln \frac{1-\tau_1}{1-\mu_1} \\ &= \tau_1 \ln \frac{\tau_1}{\mu_1} + (1-\tau_1) \ln \frac{1-\tau_1}{1-\mu_1} \\ &= I\big((\tau_1, 1-\tau_1), (\mu_1, 1-\mu_1)\big). \end{aligned}$$

Similarly, we get that

$$\begin{aligned} \chi^2(\tilde{\tau}, \bar{\mu}_n) &= \sum_{i=1}^{m_n} \frac{\tau_i^2}{\mu_i} - 1 \\ &= \frac{\tau_1^2}{\mu_1} + \sum_{i=2}^{m_n} \left(\frac{1-\tau_1}{1-\mu_1} \right)^2 \mu_i - 1 \\ &= \frac{\tau_1^2}{\mu_1} + \frac{(1-\tau_1)^2}{1-\mu_1} - 1 \\ &= \chi^2\big((\tau_1, 1-\tau_1), (\mu_1, 1-\mu_1)\big). \end{aligned}$$

For the notation

$$\lambda := \frac{\tau_1}{\mu_1}$$

and for arbitrary $\varepsilon > 0$, choose λ such that

$$\chi^2(\tilde{\tau}, \bar{\mu}_n) = \chi^2\big((\tau_1, 1-\tau_1), (\mu_1, 1-\mu_1)\big) = \varepsilon,$$

i.e.,

$$\lambda = 1 + \sqrt{\varepsilon(1-\mu_1)/\mu_1} = 1 + \sqrt{\varepsilon(M_n - 1)}.$$

Notice that this is a fair choice of λ, since because of (1.5) μ_1 can be small enough such that for any fixed ε,

$$\tau_1 = \lambda\mu_1 = \mu_1 + \sqrt{\varepsilon(1-\mu_1)\mu_1} < 1.$$

Then

$$I(\tilde{\tau}, \bar{\mu}_n) = I\big((\tau_1, 1-\tau_1), (\mu_1, 1-\mu_1)\big) = \lambda\mu_1 \ln\lambda + (1-\tau_1)\ln\frac{1-\tau_1}{1-\mu_1}.$$

Therefore

$$\begin{aligned}
&\frac{\sqrt{M_n}}{\ln M_n} \inf_{\chi^2(\tau,\bar{\mu}_n)\geq\varepsilon} I(\tau, \bar{\mu}_n) \\
&\quad\leq \frac{\sqrt{M_n}}{\ln M_n} I(\tilde{\tau}, \bar{\mu}_n) \\
&\quad= \frac{\sqrt{M_n}}{\ln M_n} I\big((\tau_1, 1-\tau_1), (\mu_1, 1-\mu_1)\big) \\
&\quad\leq \frac{\sqrt{M_n}}{\ln M_n}\left(\frac{(1+\sqrt{\varepsilon(M_n-1)})\ln(1+\sqrt{\varepsilon(M_n-1)})}{M_n} + \ln\frac{M_n}{M_n-1}\right) \\
&\quad\to \sqrt{\varepsilon}/2,
\end{aligned}$$

and the lower bound

$$\liminf_{n\to\infty} \frac{\sqrt{M_n}}{n\ln M_n} \ln \mathbf{P}\big\{\chi_n^2 > \varepsilon\big\} \geq -\sqrt{\varepsilon}/2$$

in the theorem is proved. Concerning the upper bound one can show along similar lines as in the proof of Theorem 3 in Beirlant et al. [2] that for all but finitely many n, $\tilde{\tau}$ is the minimizing distribution. □

References

1. Bahadur R (1971) Some limit theorems in statistics. SIAM, Philadelphia
2. Beirlant J, Devroye L, Györfi L, Vajda I (2001) Large deviations of divergence measures on partitions. J Stat Plan Inference 93:1–16
3. Beirlant J, Györfi L (1994) Pitman efficiencies of L_p-goodness-of-fit tests. Kybernetika 30:223–232

4. Biau G, Györfi L (2005) On the asymptotic properties of a nonparametric L_1-test of homogeneity. IEEE Trans Inf Theory 51:3965–3973
5. Birgé L, Massart P (1997) From model selection to adaptive estimation. In: Pollard D, Torgersen E, Yang G (eds) Festschrift for Lucien Lecam: research papers in probability and statistics. Springer, New York, pp 55–87
6. Castellan G (2003) Density estimation via exponential model selection. IEEE Trans Inf Theory 49:2052–2060
7. Csiszár I (1967) Information-type measures of divergence of probability distributions and indirect observations. Studia Sci Math Hung 2:299–318
8. Csiszár I, Körner J (1981) Information theory: coding theorems for memoryless systems. Academic Press, New York
9. Dembo A, Zeitouni O (1992) Large deviations techniques and applications. Jones and Bartlett Publishers
10. Gretton A, Györfi L (2010) Consistent nonparametric tests of independence. J Mach Learn Res 11:1391–1423
11. Groeneboom P, Shorack GR (1981) Large deviations of goodness of fit statistics and linear combinations of order statistics. Ann Probab 9:971–987
12. Györfi L, Vajda I (2002) Asymptotic distributions for goodness of fit statistics in a sequence of multinomial models. Stat Probab Lett 56:57–67
13. Györfi L, van der Meulen EC (1991) A consistent goodness-of-fit test based on the total variation distance. In: Roussas G (ed) Nonparametric functional estimation and related topics. Kluwer, Boston, pp 631–646
14. Harremoës P, Vajda I (2008) On the Bahadur-efficient testing of uniformity by means of the entropy. IEEE Trans Inf Theory 54:321–331
15. Harremoës P, Vajda I (2011) On Bahadur efficiency of power divergence statistics. http://arxiv.org/abs/1002.1493
16. Kallenberg WCM (1985) On moderate and large deviations in multinomial distributions. Ann Stat 13:1554–1580
17. Kallenberg WCM, Oosterhof J, Shriever BF (1985) The number of classes in chi-squared goodness-of-fit tests. J Am Stat Assoc 80:959–968
18. Mason DM, Van Zwet WR (1987) A refinement of the KMT inequality for the uniform empirical process. Ann Probab 15:871–884
19. Neyman J (1949) Contribution to the theory of the χ^2 test. In: Proceedings of the first Berkeley symposium on mathematical statistics and probability. Berkeley University Press, Berkeley, pp 239–273
20. Nikitin Ya (1995) Asymptotic efficiency of nonparametric tests. Cambridge University Press, Cambridge
21. Quine MP, Robinson J (1985) Efficiencies of chi-square and likelihood ratio goodness-of-fit tests. Ann Stat 13:727–742
22. Sanov IN (1957) On the probability of large deviations of random variables. Mat Sb 42:11–44. (English translation in Sel Transl Math Stat Prob, 1:213–244 (1961).)
23. Watson GS (1958) On chi-squared goodness-of-fit tests for continuous distributions. J R Stat Soc B 20:44–61

Chapter 2
Detection of Changes in INAR Models

Šárka Hudecová, Marie Hušková, and Simos Meintanis

Abstract In the present paper we develop on-line procedures for detecting changes in the parameters of integer valued autoregressive models of order one. Tests statistics based on probability generating functions are constructed and studied. The asymptotic behavior of the tests under the null hypothesis as well as under certain alternatives is derived.

2.1 Introduction

Studying the stability in time series is one of the important tasks of data analysis. In many cases such tasks are formulated in terms of hypothesis testing (stability of the system versus system instability) or as an estimation problem whereby certain unknown quantities defining the system are estimated in order to detect a possible change in the values of these quantities. This area is known as change point analysis or structural break problem. Corresponding procedures come in two basic variants: off-line (with all data being available at the beginning of the analysis) or on-line procedures whereby observations arrive sequentially (one at a time) and statistical analysis is performed with each incoming observation.

Š. Hudecová · M. Hušková (✉)
Department of Statistics, Charles University of Prague, Sokolovská 83, 186 75 Praha 8, Czech Republic
e-mail: huskova@karlin.mff.cuni.cz

Š. Hudecová
e-mail: hudecova@karlin.mff.cuni.cz

S. Meintanis
Department of Economics, National and Kapodistrian University of Athens, 1 Sophocleous Str., and Aristidou Str., 105 59 Athens, Greece
e-mail: simosmei@econ.uoa.gr

S. Meintanis
Unit for Business Mathematics and Informatics, North–West University, Potchefstroom, South Africa

A. Steland et al. (eds.), *Stochastic Models, Statistics and Their Applications*,
Springer Proceedings in Mathematics & Statistics 122,
DOI 10.1007/978-3-319-13881-7_2

So far the change-point problem has been studied mostly in time series with continuous observations and consequently there is a huge literature on the problem, either in classical ARMA-type time series or more recently in the popular GARCH model; see for instance a recent survey paper [3].

There is a current interest however in studying the same problem with time series of counts. This interest has been developed along with the introduction of several corresponding models for such time series, which in turn is due to the fact that count time series can prove useful in the analysis of data occurring in many applications, such as finance (occurrence of events in a time period), climatology [16], medicine, etc.

There are only a few papers dealing with detection of changes in integer valued time series, a review of recent results can be found in [7] and [13]. In *the off-line* setting, [10] derived results on likelihood ratio type statistics for detection of a change in binary autoregressive time series, while [8] published results on CUSUM type test statistics. Papers [9, 14] and [6] proposed and studied procedures in Poisson autoregressive models.

The on-line procedures for detection of changes were studied in [19, 20] and by [17] and [18] in connection of control charts, while in [14] the authors developed and studied sequential CUSUM type procedures in various integer valued time series.

Here we focus on detection of changes in integer-valued autoregressive (INAR) time series. The INAR model of order one (INAR(1) for short) (see [1, 2, 15]) is specified by Eq. (2.1) below, and it incorporates a Bernoulli probability parameter as well as another parameter indexing the family of the so-called innovations. In what follows we develop detector statistics for detecting changes in these parameters in the context of INAR(1) models. As already mentioned we will work with monitoring schemes and hence propose sequential-type detector statistics. In the remainder of the paper we introduce the INAR process and the test statistics in Sect. 2.2, while in Sect. 2.3 we derive the limit properties of the procedures under the null as well as under a certain class of alternatives. The proofs are postponed in Sect. 2.4.

2.2 Model and Procedures

The INAR(1) process $\{Y_t\}$ is defined by the equation

$$Y_t = p \circ Y_{t-1} + e_t, \tag{2.1}$$

where $p \circ Y_{t-1}$ denotes a sum of Y_{t-1} independent Bernoulli variables all of which are independent of Y_{t-1}, the parameter $p \in (0, 1)$ denotes the probability of the aforementioned Bernoulli variables and $\{e_t\}$ is a sequence (often referred to as 'innovations') of independent and identically distributed (i.i.d.) nonnegative integer valued random variables with finite second moment and probability generating function (PGF) denoted by $g_e(u)$that is assumed to belong to a given family, i.e., $g_e(\cdot) \in \mathcal{G}_\Theta = \{g_e(u;\theta);\ u \in [0,1],\ \theta \in \Theta\}$ with Θ being an open subset of R.

Under the above conditions the sequence $\{Y_t\}$ is stationary and ergodic. Given the family $\mathcal{G}_\Theta$ of possible PGF for $\{e_t\}$ the model depends on two parameters $(p, \theta) \in$

$(0, 1) \times \Theta$. In this connection we note that while the Poisson family has been by far the most studied case, alternative families for $\{e_t\}$ such as the zero-inflated Poisson of [12], and the Poisson mixture of [16], have also been considered.

The proposed sequential test procedures for detecting changes in INAR(1) processes will be based on properties of probability generating function (PGF) of the observed variables. In this connection recall that the PGF of a random variable Y is defined as

$$g_Y(u) = Eu^Y, \quad u \in [0, 1],$$

and that under very mild conditions this PGF uniquely determines the underlying distribution function of Y. The empirical version of the PGF is defined by

$$\widehat{g}_{Y,n}(u) = \frac{1}{n}\sum_{i=1}^{n} u^{Y_i}, \quad u \in [0, 1],$$

and was employed by [11] in the context of goodness-of-fit testing with certain integer valued time series. This empirical PGF can be further used as the main tool for the construction of detector statistics in count time series of a more general nature. This is in fact a subject of a research project which is already in progress. Here, however, and in order to stay within a relatively simple context, we focus on procedures for detecting changes in the parameters of INAR(1) processes.

We are interested in investigating whether or not the parameters (p, θ) are the same during the observational period. Toward this we introduce a slightly more general model

$$Y_t = p_t \circ Y_{t-1} + e_t, \tag{2.2}$$

where $p_t \circ Y_{t-1}$ denotes a sum of Y_{t-1} independent Bernoulli variables all of which are independent of Y_{t-1} and all have a success probability $p_t \in (0, 1)$, and $\{e_t\}$ is a sequence of independent nonnegative integer valued random variables with finite second moments such that PGF of e_t is $g_e(u; \theta_t)$, $\theta_t \in \Theta$.

We consider a sequential setup where the observations arrive one after the other and, additionally, assume that a historical data set (or training data) $Y_1, \ldots, Y_m$ following the INAR(1) model specified in Eq. (2.1) are given. Then we wish to test the null hypothesis:

$$H_0\colon \quad (p_t, \theta_t) = (p_0, \theta_0), \quad 1 \le t < \infty,$$

against the alternative

$$\begin{aligned} H_1\colon \quad & \text{there exist } t_0 \text{ such that } (p_t, \theta_t) = (p_0, \theta_0), \quad 1 \le t \le m + t_0 \\ & \text{but } (p_t, \theta_t) = \left(p^0, \theta^0\right) \quad m + t_0 < t < \infty, \quad (p_0, \theta_0) \ne \left(p^0, \theta^0\right), \end{aligned}$$

where the parameters p_0, $p^0 \in (0, 1)$ and $\theta_0, \theta^0 \in \Theta$ are unknown, and where $m + t_0$ is an unknown change point. Clearly we are interested in testing the null hypothesis that the parameters (p_0, θ_0) do not change, which means that model (2.1) holds true with $(p, \theta) = (p_0, \theta_0)$ while under the alternative the first $m + t_0$ observations follow

model (2.1) with parameter (p_0, θ_0) and afterwards it changes to another INAR(1) model with parameter values (p^0, θ^0).

For detection of changes in the above model we apply the method developed in [5] which was first applied in the context of linear regression and later on extended to various other setups. In principle, we estimate the unknown parameters from the historical data, then, having $m + t$ observations, we calculate the test statistic $Q(m, t)$ that is sensitive w.r.t. a change in either of the parameters and according to value of this statistic, we decide whether a change in either of the parameters is indicated or not. In case of no indication of a change we continue with the next observation. We note in this context of change-detection for the parameters of a certain model, CUSUM type procedures are often used. Another possibility is to use some functionals of estimators of unknown parameters based on historical data $Y_1, \ldots, Y_m$ and on $Y_{m+1}, \ldots, Y_{m+t}$, $t = 1, 2, \ldots$.

Here we deal with procedures based on probability generating function utilizing the following property of the PGF of $\{Y_t\}$ under model (2.2)

$$E\left(u^{Y_t}|Y_{t-1}\right) = \left(1 + p_t(u-1)\right)^{Y_{t-1}} g_e(u;\theta_t), \quad t \geq 1,\ u \in [0,1],$$
$$E\left(u^{Y_t}\right) = E\left(1 + p_t(u-1)\right)^{Y_{t-1}} g_e(u;\theta_t), \quad t \geq 1,\ u \in [0,1].$$

Then under model (2.2), the quantities

$$\sum_{s=1}^{t}\left(u^{Y_s} - \left(1 + p_s(u-1)\right)^{Y_{s-1}} g_e(u;\theta_s)\right), \quad t \geq 2,$$

are partial sums of martingale differences for fixed $u \in [0,1]$ which prompts the idea of utilizing these quantities for constructing test procedures.

We suggest to test the null hypothesis H_0 by means of the test statistics based on the first $m + t$ observations

$$S_m(t) = \int_0^1 \left(Q_{m,m+t}(u, \widehat{p}_m, \widehat{\theta}_m) - \frac{t}{m} Q_{0,m}(u, \widehat{p}_m, \widehat{\theta}_m) \right)^2 w(u)du, \quad t \geq 1, \quad (2.3)$$

where $w(u)$ is a nonnegative weight function and

$$Q_{\ell,j}(u, \widehat{p}_m, \widehat{\theta}_m) = \frac{1}{\sqrt{m}} \sum_{s=\ell+1}^{j} \left(u^{Y_s} - \left(1 + \widehat{p}_m(u-1)\right)^{Y_{s-1}} g_e(u;\widehat{\theta}_m)\right),$$
$$\ell, j = 0, \ldots$$

with $(\widehat{p}_m, \widehat{\theta}_m)$ being estimators of (p, θ) based on the historical data $Y_1, \ldots, Y_m$.

The null hypothesis is rejected as soon as for some t

$$S_m(t)/q_\gamma^2(t/m) \geq c,$$

for an appropriately chosen c, where

$$q_\gamma(s) = (1+s)\left(\frac{s}{s+1}\right)^\gamma, \quad s \in (0,\infty),\ \gamma \in [0, 1/2),$$

is a boundary function. (Possible choices of boundary functions $q_\gamma(s)$ are discussed, e.g., in [4].) In this case, we usually stop and confirm a change, otherwise we continue monitoring. The related stopping rule is defined as

$$\tau_m(\gamma, T) = \inf\{1 \le t \le mT\colon\ S_m(t)/q_\gamma^2(t/m) \ge c\},$$
$$\tau_m(\gamma, T) = \infty \quad \text{if } S_m(t)/q_\gamma^2(t/m) < c \text{ for all } 1 \le t \le Tm,$$

for some fixed integer $T > 0$. It is required that under H_0

$$\lim_{m\to\infty} P\big(\tau_m(\gamma, T) < \infty\big) = \alpha$$

for prechosen $\alpha \in (0, 1)$ and under alternatives

$$\lim_{m\to\infty} P\big(\tau_m(\gamma, T) < \infty\big) = 1.$$

The former requirement guarantees asymptotic level α, while the later one ensures consistency. Hence in order to get an approximation for $c = c_\alpha$, the limit behavior $(m \to \infty)$ of

$$\max_{1\le t\le mT} S_m(t)/q_\gamma^2(t/m) \tag{2.4}$$

under H_0 has to be studied, while for consistency one has to investigate its limit behavior under alternatives. Both tasks are taken up in the next section.

The question of the optimal choices of the weight function w and the boundary function q_γ in order the detection lag is as small as possible remains open. Some practical recommendations are in the next section.

2.3 Asymptotic Results

Consider the INAR(1) process in Eq. (2.2) and denote the true value of $\vartheta = (p, \theta)$ under the null hypothesis H_0 by $\vartheta_0 = (p_0, \theta_0)$. To study the limit distribution under the null hypothesis H_0 we assume the following:

(A.1) $\{Y_t\}_{t\in\mathcal{N}}$ is a sequence of random variables satisfying (2.1) with $\{e_t\}_{t\in\mathcal{N}}$ being a sequence of i.i.d. discrete nonnegative random variables with finite second moment and PGF $g_e(\cdot;\theta)$, $\theta \in \Theta$, where Θ is an open subset of $\mathcal{R}$.

(A.2) $g_e(u;\theta)$ has the first partial derivative w.r.t. θ for all $u \in [0, 1]$ fulfilling Lipschitz condition:

$$\left|\frac{\partial g_e(u;\theta)}{\partial\theta} - \frac{\partial g_e(u;\theta)}{\partial\theta}\bigg|_{\theta=\theta_0}\right| \le D_1|\theta_0 - \theta|v(u),$$
$$u \in [0, 1],\ |\theta - \theta_0| \le D_2,$$

and

$$\left|\frac{\partial g_e(u;\theta)}{\partial\theta}\right| \le D_3 v(u), \quad u \in [0, 1],\ |\theta - \theta_0| \le D_2$$

for some $D_j > 0$, $j = 1, 2, 3$, and some measurable function $v(\cdot)$.

(A.3) $0 < \int_0^1 w(u)du < \infty$, $\int_0^1 w(u)v^2(u)du < \infty$.

(A.4) $\widehat{\vartheta}_m = (\widehat{p}_m, \widehat{\theta}_m)'$ is estimator of $\vartheta_0 = (p_0, \theta_0)'$ satisfying

$$\sqrt{m}(\widehat{\vartheta}_m - \vartheta_0) = O_P(1).$$

Assumption (A.3) is satisfied by rather wide class of weight function w. Simple practical choices are $w(u) = u^a$, $u \in [0, 1]$, $a \geq 0$.

In the following theorem we formulate the main assertion on limit behavior of our test statistic defined in Eq. (2.4) under the null hypothesis H_0.

Theorem 2.1 *Let assumptions* (A.1)–(A.4) *be satisfied in model* (2.1). *Then under the null hypothesis* H_0 *the limit distribution* $(m \to \infty)$ *of* $\max_{1 \leq t \leq mT} S_m(t)/q_\gamma^2(t/m)$ *with* $T > 0$ *fixed is the same as that of*

$$\sup_{s \in (0, T/(T+1))} \int_0^1 \frac{1}{s^{2\gamma}} Z^2(s, u; p_0, \theta_0) w(u) du,$$

where $\{Z(s, u; p, \theta); s \in (0, T/(T+1)), u \in [0, 1]\}$ *is a Gaussian process with zero mean and covariance structure described by*

$$\begin{aligned} &cov\big(Z(s_1, u_1; p, \theta), Z(s_2, u_2; p, \theta)\big) \\ &\quad = \min(s_1, s_2) E\big(u_1^{Y_2} - E\big(u_1^{Y_2}|Y_1\big)\big)\big(u_2^{Y_2} - E\big(u_2^{Y_2}|Y_1\big)\big) \end{aligned}$$

where

$$E\big(u^{Y_2}|Y_1\big) = \big(1 + p(u-1)\big)^{Y_1} g_e(u; \theta).$$

The explicit form of the limit distribution is not known. In order to approximate this distribution one can replace the unknown parameters and covariance structure by the respective estimators based on historical data and simulate the resulting process. Another possibility is to use parametric bootstrap by estimating (p, θ) from the historical data and then generate bootstrap observations along Eq. (2.1) with (p, θ) replaced by their estimators. This possibility also leads to an asymptotically correct approximation of the limit null distribution of the test statistic.

Next we shortly discuss the limit behavior of our test statistic under the following class of alternatives:

$\widetilde{H}_1$: there exists $0 < \nu_0 < T$ such that for $t_0 = \lfloor m\nu_0 \rfloor$ variables $\{Y_t\}_{t \leq m+t_0}$ follow (2.2) with (p_0, θ_0) and $\{Y_{m+t_0+t}\}_{t \geq 1} =^d \{Y_t^0\}_{t \geq 1}$, where $\{Y_t^0\}_{t \geq 1}$ follow (2.2) with $(p^0, \theta^0) \neq (p_0, \theta_0)$.

Notice that $\widetilde{H}_1$ slightly differs from the alternative H_1. In particular, $\widetilde{H}_1$ assumes that the process $\{Y_t\}$ changes from one INAR(1) process to another one, both possibly strictly stationary. This simplifies the formulation of the succeeding theorem and the corresponding proof.

Theorem 2.2 *Let* $\{Y_t\}_{t \leq m+t_0}$ *and* $\{Y_t^0\}_{t \geq 1}$ *from* $\widetilde{H}_1$ *satisfy assumptions* (A.1) *with parameters* (p_0, θ_0) *and* (p^0, θ^0), *respectively, and let also* (A.2)–(A.4) *be satisfied.*

Then under the alternative hypothesis $\widetilde{H}_1$ *for any* $\nu_0 < s < T$

$$\frac{1}{m} S_m\big(\lfloor ms \rfloor\big) \to (s-\nu_0) \int_0^1 \Big(E\big[\big(1+p^0(u-1)\big)^{Y_1^0} g_e\big(u,\theta^0\big) - \big(1+p_0(u-1)\big)^{Y_1} g_e(u,\theta_0)\big]\Big)^2 w(u)du$$

in probability as $m \to \infty$.

Studying carefully the proofs one realizes that the proposed test procedures are sensitive not only w.r.t. changes in the parameters p and/or θ but also w.r.t. changes that leave these parameters invariant but involve a change in the distribution (and hence the PGF) of the innovations e_t.

2.4 Proofs

Due to the space restriction and due to a certain similarity to the proof of Theorem 4.1 in [11] we present only main steps of the proof of our Theorem 1.

By the Taylor expansion of $Q_{m,m+t}(u, \widehat{p}_m, \widehat{\theta}_m) - \frac{t}{m} Q_{0,m}(u, \widehat{p}_m, \widehat{\theta}_m)$ at p_0, θ_0 and by convergence properties of stationary sequences we realize that under H_0 the limit behavior of $\max_{1\le t\le mT} S_m(t)/q_\gamma^2(t/m)$ does not change if the estimators $\widehat{p}_m, \widehat{\theta}_m$ are replaced by their true values p_0, θ_0.

Since $Q_{m,m+t}(u, p_0, \theta_0)$ and $Q_{0,m}(u, p_0, \theta_0)$ are partial sums of bounded martingale differences we can apply theorems on their limit behavior. The proof can be finished combining the arguments in the last part of the proof of Theorem 4.1 in [11] and the proof of Theorem 1 in [4].

Acknowledgements The research of Simos Meintanis was partially supported by grant number 11699 of the Special Account for Research Grants of the National and Kapodistrian University of Athens (ELKE). The research of Marie Hušková was partially supported by grant GAČR P201/12/1277 and by AP research network grant Nr. P7/06 of the Belgian government (Belgian Science Policy). The research of Šárka Hudecová was partially supported by the Czech Science Foundation project DYME Dynamic Models in Economics No. P402/12/G097.

References

1. Al-Osh MA, Alzaid AA (1987) First-order integer-valued autoregressive (INAR(1)) process. J Time Ser Anal 8:261–275
2. Alzaid AA, Al-Osh MA (1988) First-order integer-valued autoregressive (INAR(1)) process: distributional and regression properties. Stat Neerl 42:53–61
3. Aue A, Horváth L (2013) Structural breaks in time series. J Time Ser Anal 34:1–16
4. Aue A, Horváth L, Hušková M, Kokoszka P (2006) Change-point monitoring in linear models with conditionally heteroskedastic errors. Econom J 9:373–403
5. Chu C-SJ, Stinchcombe M, White H (1996) Monitoring structural change. Econometrica 64:1045–1065

6. Doukhan P, Kengne W (2013) Inference and testing for structural change in time series of counts model. Available via ArXiv http://arxiv.org/pdf/1305.1751v1.pdf. Cited 13 Sep 2014
7. Fokianos K (2012) Count time series models. In: Subba Rao T, Subba Rao S, Rao CR (eds) Handbook of statistics. Time series — methods and applications, vol 30. Elsevier, Amsterdam, pp 315–348
8. Fokianos K, Gombay E, Hussein A (2014) Retrospective change detection for binary time series models. J Stat Plan Inference 145:102–112
9. Franke J, Kirch C, Tadjuidje Kamgaing J (2012) Changepoints in time series of counts. J Time Ser Anal 33(5):757–770
10. Hudecová Š (2013) Structural changes in autoregressive models for binary time series. J Stat Plan Inference 143(10):1744–1752
11. Hudecová Š, Hušková M, Meintanis S (2014) Tests for time series of counts based on the probability generating function. Statistics, doi:10.1080/02331888.2014.979826 (in press)
12. Jadi MA, Jones G, Lai CD (2012) First-order integer valued AR processes with zero inflated Poisson innovations. J Time Ser Anal 33(6):954–963
13. Kirch C, Tadjuidje Kamgaing J (2015) Detection of change points in discrete valued time series. In: Davis RA, Holan SA, Lund RB, Ravishanker N (eds) Handbook of discrete valued time series. Chapman & Hall, London
14. Kirch C, Tadjuidje Kamgaing J (2014) Monitoring time series based on estimating functions. Preprint. Available at http://www.math.kit.edu/stoc/~ckirch/seite/publications. Cited 13 Sep 2014
15. McKenzie E (1985) Some simple models for discrete variate time series. Water Resour Bull 21:645–650
16. Pavlopoulos H, Karlis D (2008) INAR(1) modeling of overdispersed count series with an environmental application. Environmetrics 19(4):369–393
17. Weiss CH (2009) Modelling time series of counts with overdispersion. Stat Methods Appl 18:507–519
18. Weiss CH (2011) Detecting mean increases in Poisson INAR(1) processes with EWMA control charts. J Appl Stat 38(2):338–398
19. Weiss CH, Testik MC (2011) The Poisson INAR(1) CUSUM chart under overdispersion and estimation error. IIE Trans 43:805–818
20. Yontay P, Weiss CH, Testik MC (2013) A two-sided cumulative sum chart for first-order integer-valued autoregressive processes of Poisson counts. Qual Reliab Eng Int 29(1):33–42

Chapter 3
Visualizing Association Structure in Bivariate Copulas Using New Dependence Function

Teresa Ledwina

Abstract Measuring a strength of dependence of random variables is an important problem in statistical practice. We propose a new function valued measure of dependence of two random variables. It allows one to study and visualize explicit dependence structure, both in some theoretical models and empirically, without prior model assumptions. This provides a comprehensive view of association structure and makes possible much detailed inference than based on standard numeric measures of association. In this contribution, we focus on copula-based variant of the measure. We present theoretical properties of the new measure of dependence and discuss estimation of it. Some artificial and real data examples illustrate the behavior and practical utility of the measure and its estimator.

3.1 Introduction

Measuring a strength of dependence of two random variables has long history and wide applications. Detailed information can be found in Drouet Mari and Kotz [9] as well as Balakrishnan and Lai [2], for example. Most of measures of dependence, introduced in vast literature on the subject, are scalar ones. Such indices are called global measures of dependence. However, nowadays there is strong evidence that an attempt to represent complex dependence structure via a single number can be misleading. To overcome this drawback, some local dependence functions have been introduced as well. In particular, Kowalczyk and Pleszczyńska [14] invented function valued measure of monotonic dependence, based on some conditional expectations and adjusted to detect dependence weaker than the quadrant one. Next, Bjerve and Doksum [5], Bairamov et al. [1] and Li et al. [17], among others, introduced local dependence measures based on regression concepts. See the last mentioned paper for more information. Holland and Wang [11] defined the local dependence function, which mimics cross-product ratios for bivariate densities and treats the two variables in a symmetrical way. This function valued measure has several appealing

T. Ledwina (✉)
Institute of Mathematics, Polish Academy of Sciences, ul. Kopernika 18, 51-617 Wrocław, Poland
e-mail: ledwina@impan.pan.wroc.pl

A. Steland et al. (eds.), *Stochastic Models, Statistics and Their Applications*,
Springer Proceedings in Mathematics & Statistics 122,
DOI 10.1007/978-3-319-13881-7_3

properties and received considerable attention in the literature; cf. Jones and Koch [13] for discussion and references. However, on the other hand, this measure has some limitations: it is not normalized, requires existence of densities of the bivariate distribution, and is intimately linked to strong form of dependence, the likelihood ratio dependence. Recently, Tjøstheim and Hufthammer [21] extensively discussed the role and history of local dependence measures in finance and econometrics. They also proposed the new local dependence measure, the local correlation function, based on approximating of bivariate density locally by a family of Gaussian densities. Similarly as the measure of Holland and Wang [11], this measure treats both variables on the same basis. Though the idea behind the construction of this measure is intuitive one its computation and estimation is a difficult and complex problem. In Berentsen et al. [3] this theory is applied to describe dependence structure of different copula models. In particular, this work strongly emphasizes a need for intuitive and informative diagnostic plots.

In this paper, we propose the new function valued measure of dependence of two random variables X and Y and present its properties. The measure has simple form and its definition exploits cumulative distribution functions (cdf's), only. In particular, we do not assume existence of a density of the observed vector. We focus here on copula-based variant of the measure which corresponds to some cdf on $[0, 1]^2$ with uniform marginals. General case is presented in Ledwina [15]. The measure takes values in $[-1, 1]$ and treats both variables in a symmetrical way. The measure preserves the correlation order, or equivalently the concordance order, which is the quadrant order restricted to the class of distributions with fixed marginals. In particular, it is non-negative (non-positive) if and only if X and Y are positively (negatively) quadrant dependent. Quadrant dependence is relatively weak, intuitive and useful dependence notion, widely used in insurance and economics; see Dhaene et al. [8] for an evidence and further references. The new measure obeys several properties formulated in the literature as useful or desirable. It allows for readable visualization of departures from independence. Simple and natural estimator of the copula-based measure in the i.i.d. case is proposed and its appealing properties are discussed. The estimator is simply standardized empirical copula. Due to theoretical results proved in Ledwina and Wyłupek [16], the estimator can be effectively exploited to assess graphically underlying bivariate dependence structure and to build some formal local and global tests. For some details see Sect. 3.3. Two illustrative examples are given in Sect. 3.3 to support utility of the new solution.

3.2 Copula-based measure of dependence and its estimate

Consider a pair of random variables X and Y with joint cdf H and marginals F and G. In this paper, to avoid technicalities and to concentrate on the main idea, we restrict attention to cdf's H with continuous marginals. Under such a restriction there exists a unique copula C such that $H(x, y) = C(F(x), G(y))$. In other words, C is the restriction to the unit square of the joint cdf of $U = F(X)$ and $V = G(Y)$.

The copula captures the dependence structure among X and Y, irrespective of their marginal cdf's. This is important in many applications. For the related discussion see Póczos et al. [19]. Below we show that properly standardized copula function can be seen to be well defined function valued dependence measure.

Namely, set

$$q(u,v) = q_C(u,v) = \frac{C(u,v) - uv}{\sqrt{uv(1-u)(1-v)}}, \quad (u,v) \in (0,1)^2, \tag{3.1}$$

and define additionally $w(u,v) = 1/\sqrt{uv(1-u)(1-v)}$.

Following Ledwina and Wyłupek [16], notice that the value of q at (u,v) can be interpreted as correlation coefficient of two specific functions of U and V. Namely, for $u \in (0,1)$ and $s \in [0,1]$ consider

$$\phi_u(s) = -\sqrt{(1-u)/u}\mathbb{1}_{[0,u]}(s) + \sqrt{u/(1-u)}\mathbb{1}_{(u,1]}(s).$$

Then

$$q(u,v) = E_C\big[\phi_u(U)\cdot\phi_v(V)\big] = Cov_C\big(\phi_u(U),\phi_v(V)\big) = Corr_C\big(\phi_u(U),\phi_v(V)\big). \tag{3.2}$$

Remark 3.1 The last expression in (3.2) shows indeed that the function q is based on aggregated local correlations. Moreover, the second expression in (3.2) implies that $q(u,v)$ can be interpreted as Fourier coefficient of C pertaining to the quasi-monotone function $\phi_u(s)\cdot\phi_v(t)$, $(s,t) \in [0,1]^2$.

The measure q fulfills natural postulates, motivated by the axioms formulated in Schweizer and Wolff [20] and updated in Embrechts et al. [10].

Proposition 3.1 *The copula based measure of dependence q, given by (3.1), has the following properties.*

1. $-1 \le q(u,v) \le 1$ *for all* $(u,v) \in (0,1)^2$.
2. *By Fréchet–Hoeffding bounds for copulas, the property* 1 *can be further sharpened to* $B_*(u,v) \le q(u,v) \le B^*(u,v)$, $(u,v) \in (0,1)^2$, *where* $B_*(u,v) = w(u,v) \times [\max\{u+v-1,0\} - uv]$ *and* $B^*(u,v) = w(u,v)[\min\{u,v\} - uv]$.
3. q *is maximal (minimal) if and only if* $Y = f(X)$ *and* f *is strictly increasing (decreasing) a.s. on the range of* X.
4. $q(u,v) \equiv 0$ *if and only if* X *and* Y *are independent.*
5. *The equation* $q(u,v) \equiv c$, c *a constant, can hold true if and only if* $c = 0$.
6. q *is non-negative (non-positive) if and only if* (X,Y) *are positively (negatively) quadrant dependent.*
7. q *is invariant to strictly increasing a.s. on ranges of* X *and* Y, *respectively, transformations.*
8. *If* X *and* Y *are transformed by strictly decreasing a.s. functions then* $q(u,v)$ *transforms to* $q(1-u,1-v)$.
9. *If* f *and* g *are strictly decreasing a.s. on ranges of* X *and* Y, *respectively, then* q*'s for the pairs* $(f(X),Y)$ *and* $(X,g(Y))$ *take the forms* $-q(1-u,v)$ *and* $-q(u,1-v)$, *accordingly.*

10. *q respects concordance ordering, i.e. for cdf's H_1 and H_2 with the same marginals and pertaining copulas C_1 and C_2, $H_1(x, y) \le H_2(x, y)$ for all $(x, y) \in \mathbb{R}^2$ implies $q_{C_1}(u, v) \le q_{C_2}(u, v)$ for all $(u, v) \in (0, 1)^2$.*
11. *If (X, Y) and (X_n, Y_n), $n = 1, 2, \ldots$, are pairs of random variables with joint cdf's H and H_n, and the pertaining copulas C and C_n, respectively, then weak convergence of $\{H_n\}$ to H implies $q_{C_n}(u, v) \to q_C(u, v)$ for each $(u, v) \in (0, 1)^2$.*

Proof The property 1 follows from (3.2), 3 is a consequence of 2. To justify 5 observe that the equation is equivalent to $C(u, v) = C_c(u, v) = uv + c\sqrt{uv(1-u)(1-v)}$. Since C is quasi-monotone, then $C_c(u, v)$ should also possess such a property. Since $C_c(u, v)$ is absolutely continuous then quasi-monotonicity is equivalent to $\frac{\partial^2}{\partial u \partial v} C_c(u, v) \ge 0$ for almost all $(u, v) \in [0, 1]^2$ (in the Lebesgue measure); cf. Cambanis et al. [7]. However, $\frac{\partial^2}{\partial u \partial v} C_c(u, v) = 1 + c[u - 1/2][v - 1/2]w(u, v)$ and for $c \neq 0$ this expression can be negative on the set of positive Lebesgue measure. Properties 7–9 follow from Theorem 3 in Schweizer and Wolff [20]. The convergence in 11 is due to continuity of C. The remaining properties are immediate. □

Remark 3.2 The properties 4 and 7–9 provide some compromise to too demanding postulates P4 and P5 discussed in Embrechts et al. [10]. The property 5 is very different from respective property of the local dependence function of Holland and Wang [11] which is constant for the bivariate normal distribution and some other models; cf. Jones [12] for details.

Now, we discuss briefly estimation of q. Let $(X_1, Y_1), \ldots, (X_n, Y_n)$ be a random sample from cdf H. Furthermore, let R_i be the rank of X_i, $i = 1, \ldots, n$, in the sample $X_1, \ldots, X_n$ and S_i the rank of Y_i, $i = 1, \ldots, n$, within $Y_1, \ldots, Y_n$. Simple estimate of C has the form

$$C_n(u, v) = \frac{1}{n} \sum_{i=1}^{n} \mathbb{1}\left(\frac{R_i}{n+1} \le u, \frac{S_i}{n+1} \le v \right), \quad (u, v) \in [0, 1]^2. \tag{3.3}$$

We shall consider the following estimator of q.

$$Q_n(u, v) = w(u, v)\big[C_n(u, v) - uv\big] = \frac{C_n(u, v) - uv}{\sqrt{uv(1-u)(1-v)}}, \quad (u, v) \in (0, 1)^2. \tag{3.4}$$

Moreover, we set

$$L_n(u, v) = \sqrt{n} Q_n(u, v) \tag{3.5}$$

for the standardized version of this estimate. So, L_n is the standardized empirical copula. Simple algebra yields that for any $(u, v) \in (0, 1)^2$ it holds

$$L_n(u, v) = \frac{1}{\sqrt{n}} \sum_{i=1}^{n} \phi_u\left(\frac{R_i}{n+1} \right) \phi_v\left(\frac{S_i}{n+1} \right) + O\left(\frac{1}{\sqrt{n}} \right). \tag{3.6}$$

Table 3.1 Simulated critical values of the test rejecting independence for large values of $|L_n(u, v)|$ for two selected (u, v), versus n and α

(u, v)	$\alpha = 0.01$					$\alpha = 0.05$				
	n					n				
	200	300	400	500	600	200	300	400	500	600
$(\frac{1}{2}, \frac{1}{2})$	2.546	2.540	2.600	2.504	2.613	1.980	1.848	2.000	1.968	1.960
$(\frac{1}{16}, \frac{1}{16})$	2.753	2.879	2.933	2.349	2.591	1.546	1.894	2.080	1.586	1.894

Therefore, up to deterministic term of the order $O(1/\sqrt{n})$, the standardized estimator $L_n(u, v)$ is a linear rank statistic with the quasi-monotone score generating function $\phi_u \cdot \phi_v$. Moreover, the definition of L_n and Proposition 1 in Ledwina and Wyłupek [16] yield that

$$P_{C_1}\big(L_n(u, v) \geq c\big) \geq P_{C_2}\big(L_n(u, v) \geq c\big) \tag{3.7}$$

for any $(u, v) \in (0, 1)^2$, any c, any n, and any two copulas C_1 and C_2 such that C_1 has larger quadrant dependence than C_2. Summarizing the above mentioned results, let us note that under independence $L_n(u, v)$ is distribution free. So, given n, under independence, the significance of the obtained values of this statistic can be easily assessed on a basis of simple simulation experiment. For large n one can rely on asymptotic $N(0, 1)$ law of $L_n(u, v)$. Due to (3.7), similar conclusions follow if one likes to verify hypothesis asserting that $q_C(u, v) \geq 0$. In particular, given n, we are able to control the significance level over the whole set of positively quadrant dependent distributions. Moreover, (3.7) implies that different levels of strength of quadrant dependence of the underlying H's shall be adequately quantified by order preserving $L_n(u, v)$'s. These results make the values of $L_n(u, v)$, $(u, v) \in (0, 1)^2$, a useful diagnostic tool allowing for easy graphical presentation and precise evaluation of significance of different types of departures from independence. Heat map of $L_n(u, v)$'s helps also to recognize regions in $(0, 1)^2$ in which independence, positive quadrant dependence and, in consequence, some stronger forms of positive dependence, etc are invalidated. This is obviously not the case when ones relies on graphs of $C_n(u, v)$ or $C_n(u, v) - uv$, solely. Moreover, without using the 'magnifying glass' $w(u, v)$ departures from independence can be hardly seen in some cases.

To close, note that, given u and v, the score generating function $\phi_u \cdot \phi_v$, appearing in (3.6), is not smooth one and takes on at most four possible values, only. This causes that, under independence, the convergence of $L_n(u, v)$ to the limiting $N(0, 1)$ law is not very fast. Moreover, the rate of convergence is expected to depend on u and v, with the least favorable situation when (u, v) is close to the vertices of the unit square. We illustrate these aspects in Table 3.1, where simulated critical values of the test rejecting independence for large values of $|L_n(u, v)|$ are given under two choices of (u, v)'s, five different sample sizes, and two selected significance levels α.

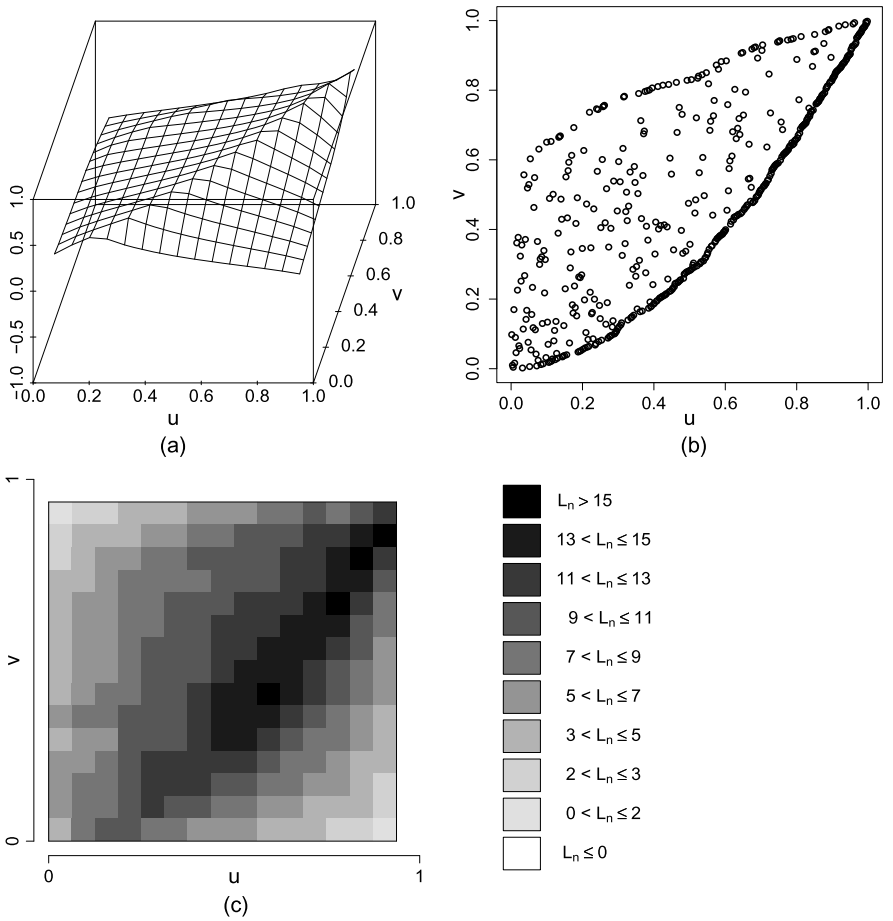

Fig. 3.1 **(a)**: dependence function $q(u, v)$ for the Mai–Scherer copula; **(b)**: scatter plot of $(R_i/(n+1), S_i/(n+1))$, $i = 1, \ldots, n$, $n = 500$, of simulated observations from the copula; **(c)**: standardized estimator $L_n(u, v)$ of $q(u, v)$ on the grid $\mathbb{G}_{16}$. $L_* = 1.5$, $L^* = 16.1$

3.3 Illustration

3.3.1 Example 1: Extreme Value Copula

We start with simulated data set of size $n = 500$ from Mai–Scherer copula given by $C(u, v) = C_{a,b}(u, v) = \min\{u^a, v^b\} \min\{u^{1-a}, v^{1-b}\}$, $a = 0.9$, $b = 0.5$; cf. Mai and Scherer [18], p. 313. The copula possesses a singular part. In Fig. 3.1 we show dependence functions $q(u, v)$ for this model. The function is accompanied by scatter plots of pseudo-observations $(R_i/(n+1), S_i/(n+1))$, $i = 1, \ldots, 500$, from the simulated sample. The scatter plot nicely exhibits the singularity. Panel (c) in this figure displays respective heat map of standardized correlations $L_n(u, v)$'s calcu-

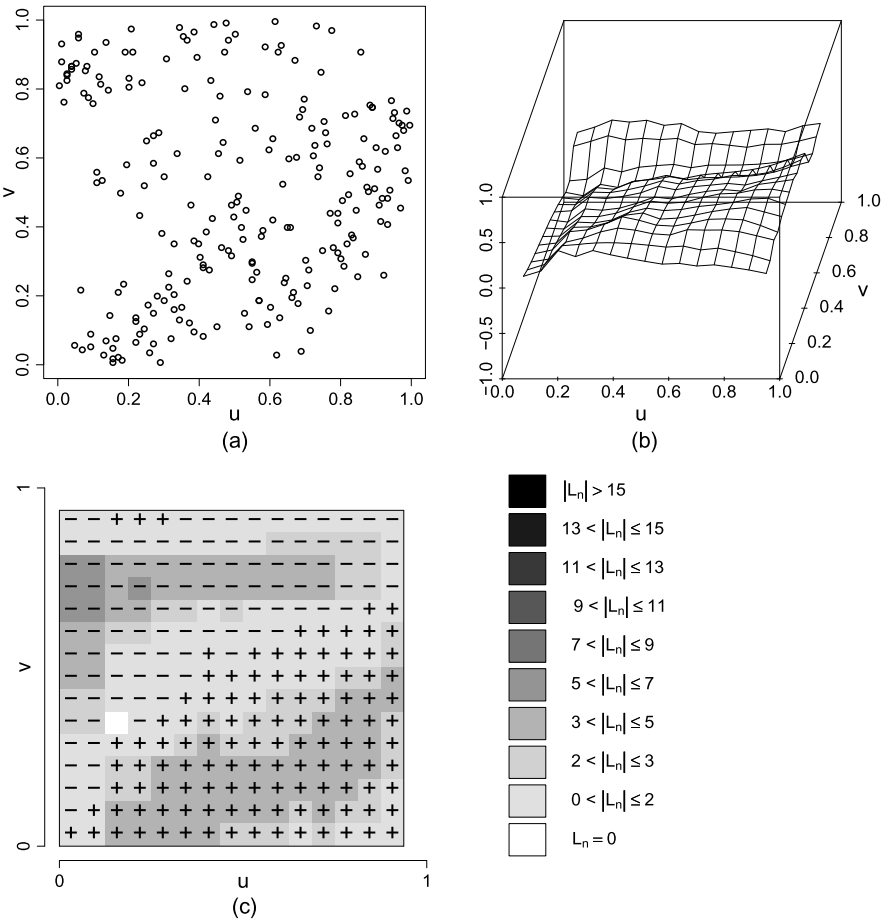

Fig. 3.2 **(a)**: scatter plot of $(R_i/(n+1), S_i/(n+1))$, $i = 1, \ldots, n$, $n = 230$, for aircraft data; **(b)**: estimator $Q_n(u, v)$ of $q(u, v)$ on the grid $\mathbb{G}_{16}$; **(c)**: standardized estimator $L_n(u, v) = \sqrt{n} Q_n(u, v)$ on the grid $\mathbb{G}_{16}$. $L_* = -6.5$, $L^* = 4.6$

lated on the grid $\mathbb{G}_{16} = \{(u, v) : u = i/16, v = j/16,\ i, j = 1, \ldots, 15\}$. Each of 225 squares of size 0.0625×0.0625 represents the respective value of L_n in its upper-right corner. To simplify reading, the heat map is accompanied with two numbers

$$L_* = \min_{1 \le i,j \le 15} L_n(i/16, j/16) \quad \text{and} \quad L^* = \max_{1 \le i,j \le 15} L_n(i/16, j/16).$$

The copula represents positively quadrant dependent distribution. Under such dependence large values of U tend to associate large values of V and similar pattern applies to small values. This tendency is nicely seen in the figure. The points of the grid $\mathbb{G}_{16}$ in which the estimated correlations Q_n are significant on the levels 0.05 and 0.01 can be easily identified; cf. Table 3.1 and related comments. Some possibility of testing for positive local and/or global dependence is sketched in Sect. 3.3.2.

Next example follows similar pattern. It concerns real data set considered earlier by Jones and Koch [13] and Berentsen and Tjøstheim [4]. However, in contrast to our approach based on scatter plots, they investigated the original bivariate observations. Below we use the same scale of intensity of colors in the heat map as above. This allows one to compare how different degrees of association are reflected by our estimators.

3.3.2 Example 2: Aircraft Data

Consider $n = 230$ aircraft span and speed data, on log scales, from years 1956–1984, reported and analyzed in Bowman and Azzalini [6]. We summarize the data in Fig. 3.2. Since in this example both negative and positive correlations appear, we added respective signs to the colors in the heat map. The figure exhibits that small and moderately large values of log speed are positively associated with log span, while for the remaining cases the relation is reversed. Two, approximately symmetrically located, regions of relatively strong dependence are seen. In general, in this example, the strength of dependence is weaker than in the previous case.

Bowman and Azzalini [6], p. 42, used these data to discuss some drawbacks of standard correlation measures when applied to invalidate independence. Indeed, for these data classical Pearson's, Spearman's and Blomqvist's rank statistics for assessing lack of association yield simulated p-values 0.81, 0.74, and 0.79, respectively. Kendall's rank correlation gives simulated p-value 0.31, which also seems to be too high, when one is looking at the magnitude of standardized local correlations in Fig. 3.2. Combining the local correlations into global statistic $L^o = \max_{1\le i,j\le 15} |L_n(i/16, j/16)|$, with large values being significant, basing on 10 000 Monte Carlo runs, we get p-value 0 for such global independence test. This shows that local correlations prove to be more informative than each of the above mentioned single classical global indices of association. Moreover, statistics L_* and L^* can be successfully applied to detect positive and negative quadrant dependence; cf. Ledwina and Wyłupek [16] for details on a very similar solution to L_*.

For further examples and more detailed discussion see Ledwina [15].

Acknowledgements Research was supported by the Grant N N201 608440 from the National Science Center, Poland. The author thanks Dr. Grzegorz Wyłupek for his help in preparing figures and the table of this article and for useful remarks. The author also thanks a referee for the careful reading of the manuscript and the useful comments.

References

1. Bairamov I, Kotz S, Kozubowski TJ (2003) A new measure of linear local dependence. Statistics 37:243–258
2. Balakrishnan N, Lai Ch-D (2009) Continuous bivariate distributions. Springer, Dordrecht

3. Berentsen G, Støve B, Tjøstheim D, Nordbø T (2014) Recognizing and visualizing copulas: an approach using local Gaussian approximation. Insur Math Econ 57:90–103
4. Berentsen G, Tjøstheim D (2014) Recognizing and visualizing departures from independence in bivariate data using local Gaussian correlation. Stat Comput 24:785–801
5. Bjerve S, Doksum K (1993) Correlation curves: measures of association as function of covariate values. Ann Stat 21:890–902
6. Bowman AW, Azzalini A (1997) Applied smoothing techniques for data analysis. Clarendon Press, Oxford
7. Cambanis S, Simons G, Stout W (1976) Inequalities for $Ek(X, Y)$ when marginals are fixed. Z Wahrscheinlichkeitstheor Verw Geb 36:285–294
8. Dhaene J, Denuit M, Vanduffel S (2009) Correlation order, merging and diversification. Insur Math Econ 45:325–332
9. Drouet Mari D, Kotz S (2001) Correlation and dependence. Imperial College Press, London
10. Embrechts P, McNeil A, Straumann D (2002) Correlation and dependency in risk management: properties and pitfalls. In: Dempster M, Moffatt H (eds) Risk management: value at risk and beyond. Cambridge University Press, Cambridge, pp 176–223
11. Holland PW, Wang YJ (1987) Dependence function for continuous bivariate densities. Commun Stat, Theory Methods 16:863–876
12. Jones MC (1998) Constant local dependence. J Multivar Anal 64:148–155
13. Jones MC, Koch I (2003) Dependence maps: local dependence in practice. Stat Comput 13:241–255
14. Kowalczyk T, Pleszczyńska E (1977) Monotonic dependence functions of bivariate distributions. Ann Stat 5:1221–1227
15. Ledwina T (2014) Dependence function for bivariate cdf's. arXiv:1405.2200v1 [stat.ME]
16. Ledwina T, Wyłupek G (2014) Validation of positive quadrant dependence. Insur Math Econ 56:38–47
17. Li R, Cheng Y, Fine JP (2014) Quantile association regression models. J Am Stat Assoc 109:230–242
18. Mai J-F, Scherer M (2011) Bivariate extreme-value copulas with discrete Pikands dependence measure. Extremes 14:311–324
19. Póczos B, Ghahramani Z, Schneider J (2012) Copula-based kernel dependency measures. In: Proceedings of the 29th international conference on machine learning. Omnipress, New York, pp 775–782
20. Schweizer B, Wolff EF (1981) On nonparametric measures of dependence for random variables. Ann Stat 9:879–885
21. Tjøstheim D, Hufthammer KO (2013) Local Gaussian correlation: a new measure of dependence. J Econom 172:33–48

Part II
Theory and Related Topics

Chapter 4
Smoothed Nonparametric Derivative Estimation Based on Weighted Difference Sequences

Kris De Brabanter and Yu Liu

Abstract We present a simple but effective fully automated framework for estimating derivatives nonparametrically based on weighted difference sequences. Although regression estimation is often studied more, derivative estimation is of equal importance. For example in the study of exploration of structures in curves, comparison of regression curves, analysis of human growth data, etc. Via the introduced weighted difference sequence, we approximate the true derivative and create a new data set which can be smoothed by any nonparametric regression estimator. However, the new data sets created by this technique are no longer independent and identically distributed (i.i.d.) random variables. Due to the non-i.i.d. nature of the data, model selection methods tend to produce bandwidths (or smoothing parameters) which are too small. In this paper, we propose a method based on bimodal kernels to cope with the non-i.i.d. data in the local polynomial regression framework.

4.1 Introduction

The popularity of nonparametric methods have increased since their introduction in the mid 1950s and early 1960s. One of the main reasons for their popularity is the flexibility these methods possess. Since their introduction, many of their properties have been rigorously investigated, see e.g. [6]. Most of the properties have been established for nonparametric regression estimation, but not as much for nonparametric derivative estimation even though the derivative of the regression estimate is of great importance as well (e.g. inference about slopes of the regression estimates). See e.g. comparison of regression curves [8], trend analysis in time series [11], the exploration of structures in curves [1], analysis of human growth data [10], etc.

K. De Brabanter (✉)
Department of Statistics and Department of Computer Science, Iowa State University, 2419 Snedecor Hall, Ames, IA, 50010-1210, USA
e-mail: kbrabant@iastate.edu

Y. Liu
Department of Computer Science, Iowa State University, Atanasoff Hall, Ames, IA, USA
e-mail: yuliu@iastate.edu

A. Steland et al. (eds.), *Stochastic Models, Statistics and Their Applications*,
Springer Proceedings in Mathematics & Statistics 122,
DOI 10.1007/978-3-319-13881-7_4

In general there exist two approaches to nonparametric derivative estimation: Regression/smoothing splines and local polynomial regression. Spline derivative estimators can achieve the optimal L_2 rate of convergence [13]. Further asymptotic theoretical properties (bias, variance and normality) were studied by [15]. However, to introduce more flexibility in the smoothing process and to overcome the choosing of the knots, smoothing splines are a very attractive method for derivative estimation. However, choosing the smoothing parameter is still difficult [9]. According to [9], data-driven methods are in general not the right way to deal with these problems and user intervention is recommended. Also, the smoothing parameter for a smoothing spline depends on the integer q while minimizing $\sum_{i=1}^{n}(\hat{m}^{(q)}(x_i) - m^{(q)}(x_i))^2$ [14].

In the context of kernel regression estimation, [7] proposed a generalized version of the cross-validation technique to estimate the first derivative via kernel smoothing using difference quotients. Unfortunately, the variance of difference quotients is proportional to the square of sample size. Consequently, the estimation will be rendered useless due to this large variance. On the other hand, the local polynomial framework [5] offers a nice way of estimating derivatives.

Consider the bivariate data $(X_1, Y_1), \ldots, (X_n, Y_n)$ which form an independent and identically distributed (i.i.d.) sample from a population (X, Y). Denote by $m(X) = \mathbf{E}[Y|X]$ the regression function. The data is regarded to be generated from the model

$$Y = m(X) + e, \tag{4.1}$$

where $\mathbf{E}[e|X] = 0$, $\mathbf{Var}[e|X] = \sigma_e^2 < \infty$ and X and e are independent. The aim of this paper is to estimate the derivative m' of the regression function m. In this paper we choose the local polynomial regression estimator to smooth the data.

This paper is organized as follows: Sect. 4.2 gives a short overview of derivative estimation in the fixed design setting and extends these results to the random design. Section 4.3 describes how to obtain a bandwidth for the local polynomial regression estimator in case of correlated errors in random design. Section 4.4 provides a simulation study of the proposed methodology. Finally, Sect. 4.5 states the conclusions and discusses options for further research.

4.2 Derivative Estimation via a Weighted Difference Sequence

4.2.1 Fixed Design

If $\mathscr{X}$ denotes the closed real interval $[a, b]$ then $x_i = a + (i-1)(b-a)/(n-1)$ and denote $d(\mathscr{X}) = b - a$. In what follows, we assume that the data is ordered i.e. $x_1 \leq x_2 \leq \cdots \leq x_n$. As mentioned in the introduction, for equispaced design the use of difference quotients $(Y_i - Y_{i-1})/(x_i - x_{i-1})$ may be natural, but their variances are $O(n^2)$. Therefore, it is appropriate to reduce the variance by using the following

weighted symmetric difference sequence to obtain the first order (noisy) derivative estimator

$$Y_i^{(1)} = Y^{(1)}(x_i) = \sum_{j=1}^{k} w_{i,j} \cdot \left(\frac{Y_{i+j} - Y_{i-j}}{x_{i+j} - x_{i-j}} \right), \tag{4.2}$$

where the weights $w_{i,1}, \ldots, w_{i,k}$ sum up to one. Next, we need to determine the weights such that the variance is minimized. Assume model (4.1) holds with equispaced design and let $\sum_{j=1}^{k} w_j = 1$. Then, for $k+1 \le i \le n-k$, the weights

$$w_{i,j} = w_j = \frac{6j^2}{k(k+1)(2k+1)}, \quad j = 1, \ldots, k \tag{4.3}$$

minimize the variance of $Y_i^{(1)}$ in (4.2), see [3]. Under this design setting, assume that m is twice continuously differentiable on $\mathscr{X} \subseteq \mathbb{R}$. If the second order derivative of m is finite on $\mathscr{X}$, then for the weights (4.3), it follows that [3]

$$\text{bias}\big(Y_i^{(1)}\big) = O\big(n^{-1}k\big) \quad \text{and} \quad \mathbf{Var}\big(Y_i^{(1)}\big) = O\big(n^2k^{-3}\big)$$

uniformly for $k+1 \le i \le n-k$. Explicit bias and variance expressions for the interior and boundary region are given in [3]. If $k \to \infty$ as $n \to \infty$ such that $nk^{-3/2} \to 0$ and $n^{-1}k \to 0$ and under the previous stated assumptions, we have that for $\varepsilon > 0$

$$\mathbf{P}\big(\big|Y_i^{(1)} - m'(x_i)\big| \ge \varepsilon\big) \to 0.$$

The tuning factor k can be chosen via the rule of thumb

$$\hat{k} = \left\lfloor \left(\frac{16\,\hat{\sigma}_e^2}{(\sup_{x_0 \in \mathscr{X}} |\hat{m}^{(2)}(x_0)|)^2\, d(\mathscr{X})^4} \right)^{1/5} n^{4/5} \right\rfloor,$$

where $\lfloor \alpha \rfloor$ is the largest integer not greater than α. The error variance can be estimated by means of any consistent error variance estimator and $\sup_{x_0 \in \mathscr{X}} |\hat{m}^{(2)}(x_0)|$ can be obtained by fitting a local polynomial regression estimate of order $p = 3$ leading to the following (rough) estimate of the second derivative $\hat{m}^{(2)}(x_0) = 2\hat{\beta}_2$. By Jensen's inequality we obtain the L_1 rate of convergence

$$\mathbf{E}\big|Y_i^{(1)} - m'(x_i)\big| = O\big(n^{-1/5}\big).$$

A similar analysis can be made for higher order derivatives. We refer the reader to [3].

4.2.2 Random Design

We assume that a density function f exists for the design points $X_i \in [a, b]$ for all $i = 1, \ldots, n$. As before, we assume that the data is ordered i.e. $X_1 \le X_2 \le \cdots \le X_n$. Similarly, we need to find a sequence of weights such that the variance of (4.2) is minimized. Under the constraint that the weights have to sum up to 1, we have for $k+1 \le i \le n-k$ and $j = 1, \ldots, k$

$$\mathbf{Var}\big(Y_i^{(1)}\big|X_{i+j},\ldots,X_{i-j}\big) = 2\sigma_e^2\left[\frac{1}{(X_{i+1}-X_{i-1})^2}\left(1-\sum_{j=2}^{k} w_{i,j}\right)^2 + \sum_{j=2}^{k}\frac{w_{i,j}^2}{(X_{i+j}-X_{i-j})^2}\right].$$

Setting the partial derivatives to zero and normalizing the weights such that they sum up to 1, yield the following finite sample weights

$$w_{i,j} = \frac{(X_{i+j}-X_{i-j})^2}{\sum_{l=1}^{k}(X_{i+l}-X_{i-l})^2}. \tag{4.4}$$

For further asymptotic analysis, the term $X_{i+j}-X_{i-j}$ needs to rewritten as a function of the design density f. Since our data is sorted, we can use the following approximation

$$X_{i+j}-X_{i-j} = \frac{2j}{nf(X_i)} + o_p(j/n).$$

Assuming m is twice continuously differentiable $\mathscr{X}\subseteq\mathbb{R}$, $m^{(2)}$ is finite on $\mathscr{X}$ and using the weights (4.4) gives for $k+1\le i\le n-k$ and $j=1,\ldots,k$

$$\begin{aligned}
\big|\mathrm{bias}\big(Y_i^{(1)}\big|X_{i-j},\ldots,X_{i+j}\big)\big| &\le \sup_{x\in\mathscr{X}}\big|m^{(2)}(x)\big|\left|\sum_{j=1}^{k} w_{i,j}\frac{(X_{i+j}-X_{i-j})}{4}\right| \\
&= \frac{3k(k+1)\sup_{x\in\mathscr{X}}|m^{(2)}(x)|}{4n(2k+1)f(X_i)} + o_p\big(kn^{-1}\big) \\
&= O_p\big(kn^{-1}\big) \\
\mathbf{Var}\big(Y_i^{(1)}\big|X_{i-j},\ldots,X_{i+j}\big) &= 2\sigma_e^2\sum_{j=1}^{k}\frac{w_{i,j}^2}{(X_{i+j}-X_{i-j})^2} \\
&= \frac{3\sigma_e^2 n^2 f^2(X_i)}{k(k+1)(2k+1)} + o_p\big(n^2k^{-3}\big) = O_p\big(n^2k^{-3}\big).
\end{aligned}$$

For a density f bounded away from zero, $m^{(2)}$ finite on $\mathscr{X}$, $k\to\infty$ as $n\to\infty$ such that $nk^{-3/2}\to 0$ and $n^{-1}k\to 0$, it follows that for $\varepsilon>0$,

$$\mathbf{P}\big(\big|Y_i^{(1)}-m'(X_i)\big|\ge\varepsilon\big)\to 0.$$

The asymptotic mean squared error of the first order derivative estimator can be upperbounded by

$$\mathrm{MSE}\big(Y_i^{(1)}\big|X_{i-j},\ldots,X_{i+j}\big) \le \frac{9k^2(k+1)^2\sup_{x\in\mathscr{X}}^2|m^{(2)}(x)|}{16n^2(2k+1)^2f^2(X_i)} + \frac{3\sigma_e^2n^2f^2(X_i)}{k(k+1)(2k+1)}.$$

Minimizing the above expression w.r.t. k results in a value for k depending on X_i and is given by

$$k(X_i) = \left(\frac{16\sigma_e^2 f^4(X_i)}{\sup_{x\in\mathscr{X}}^2|m^{(2)}(x)|}\right)^{1/5} n^{4/5}. \tag{4.5}$$

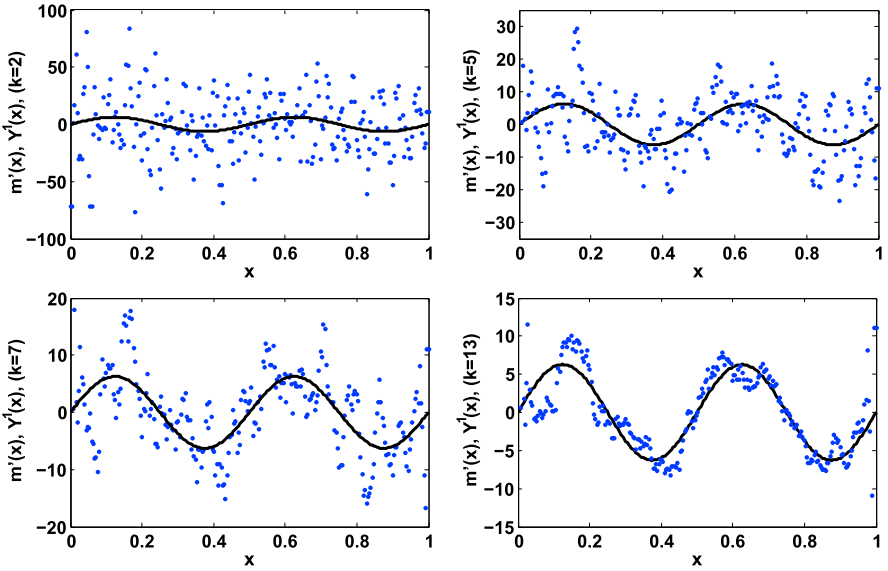

Fig. 4.1 Simulated data set of size $n = 250$ from model (4.1) with $m(X) = \sin^2\{2\pi(X - 0.5)\}$, $X \sim U[0, 1]$ and $e \sim N(0, 0.1^2)$. The *full line* shows the true first order derivative, the data points show the empirical first order derivatives for $k \in \{2, 5, 7, 13\}$

In order to obtain an estimator for $k(X_i)$, one needs to replace σ_e^2 and $f(X_i)$ by their consistent estimators. As in fixed design, the supremum of the absolute value of the second order derivative function can be obtained by fitting a local cubic fit to the original data. A global k can be obtained by minimizing the asymptotic mean integrated squared error (AMISE) resulting into

$$k = \left(\frac{16\sigma_e^2 \int f^2(x)\,dx}{\sup_{x \in \mathscr{X}} |m^{(2)}(x)| \int \frac{1}{f^2(x)}\,dx} \right)^{1/5} n^{4/5}. \tag{4.6}$$

The expressions for a varying and global k can take any positive value. To be used in practice, we round the value down to the smallest integer. The density f can be estimated by e.g. kernel density estimation. The bandwidth of the kernel for density estimation can be obtained by the solve-the-equation plug-in bandwidth selector [12].

It immediately follows that the L_2 rate of convergence in random design yields (for $k + 1 \le i \le n - k$ and $j = 1, \ldots, k$)

$$\mathbf{E}\big(|Y_i^{(1)} - m'(X_i)|^2 \big| X_{i-j}, \ldots, X_{i+j}\big) = O_p\big(n^{-1/5}\big).$$

It can be shown that using a local varying k always leads to an improvement over a global k. In order to reduce the bias at the boundaries, some corrections also need be to be taken into account. Figure 4.1 displays the empirical derivative for $k \in \{2, 5, 7, 13\}$ generated from model (4.1) with $m(X) = \sin^2\{2\pi(X - 0.5)\}$ where $X \sim U[0, 1]$, $n = 250$ and $e \sim N(0, 0.1^2)$.

4.3 Smoothing the Noisy Derivative Data

It is clear that for the newly generated data set the independence assumption is no longer valid since it is a weighted sum of differences of the original data set. In such cases, it is known that data-driven bandwidth selectors and plug-ins break down [2]. In [4], the authors extend this approach to the random design setting. In order to fit the newly obtained data set, we consider the following model for the first order derivative:

$$Y^{(1)}(X) = m'(X) + \varepsilon$$

where $\mathbf{E}[\varepsilon|X] = 0$ and $\mathbf{Cov}(\varepsilon_i, \varepsilon_j|X_i, X_j) = \sigma_e^2 \rho_n(X_i - X_j)$. If the following holds: f continuous and bounded away from zero, $\int K(u)\,du = 1$, $K \geq 0$ and symmetric, $\lim_{|u|\to\infty} |uK(u)| = 0$, $\sup_u |K(u)| < \infty$, ρ_n is a stationary, symmetric correlation function with $|\rho_n(x)| \leq 1, \forall x$ and $\rho_n(0) = 1$. Further assume short range correlation i.e., $\exists \xi > 0 : \int |\rho_n(t)| I(h^{-1}t \geq \xi)\,dt = o(\int |\rho_n(t)|\,dt)$ and $n \int |\rho_n(t-x)| f(t)\,dt = O(1)$; then for a kernel K satisfying $K(0) = 0$, $h \to 0$ and $nh \to \infty$ as $n \to \infty$, the correlation structure is removed in the model selection procedure without any prior knowledge about its structure. Since these bimodal kernels introduce extra variance into the estimate, we develop a relation between the bandwidth h of a unimodal kernel K and the bandwidth h_b of a bimodal kernel $\overline{K}$. Consequently, the estimate based on this bandwidth will be smoother than the one based on a bimodal kernel. A remarkable consequence of using a kernel K satisfying $K(0) = 0$ is that we do not need to use cross-validation (leave-one-out, v-fold, etc.), but simply minimizing the residual sum of squares suffices to obtain the value for the bandwidth h! It is easily verified that for local polynomial regression (p odd)

$$\hat{h} = C_p(K, \overline{K})\hat{h}_b,$$

where

$$C_p(K, \overline{K}) = \left[\frac{\int K_p^{\star 2}(u)\,du \{\int u^{p+1} \overline{K}_p^{\star}(u)\,du\}^2}{\int \overline{K}_p^{\star 2}(u)\,du \{\int u^{p+1} K_p^{\star}(u)\,du\}^2} \right]^{1/(2p+3)}.$$

The factor $C_p(K, \overline{K})$ is easy to calculate. We take $\overline{K}(u) = (2/\sqrt{\pi})u^2 \exp(-u^2)$ as bimodal kernel. $K_p^{\star}$ denotes the equivalent kernel, see [5]. For a Gaussian (unimodal) kernel and three different values of p, the factor $C_p(K, \overline{K})$ equals 1.16231, 1.01431 and 0.94386 for $p = 1, 3, 5$ respectively.

4.4 Simulation

In a first simulation, consider the following two functions $m(X) = 1 - 6X + 36X^2 - 53X^3 + 22X^5$ and $m(X) = \sin(2\pi X)$ with $n = 500$ generated from a uniform distribution on $[0, 1]$. The error variance was taken to be $\sigma_e^2 = 0.05$ and $e \sim N(0, \sigma_e^2)$ for both functions. The value of k was obtained via (4.6) which was 6 and 7 respectively for the first and second function (see Fig. 4.2). We used local cubic regression

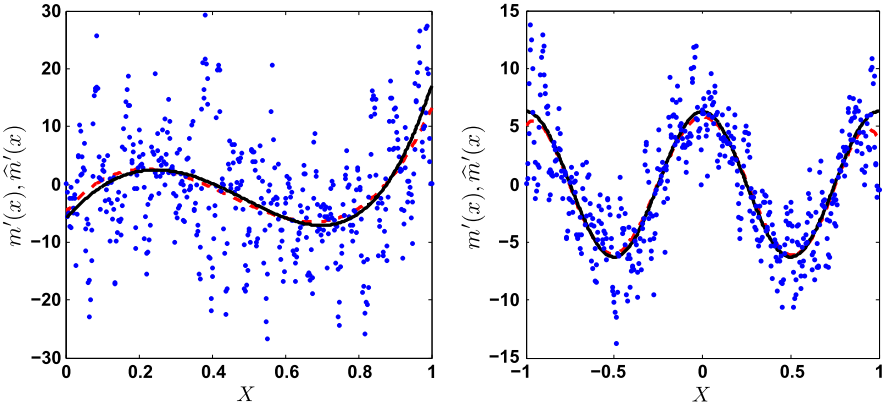

Fig. 4.2 First order derivative estimation. Estimated derivative by the proposed method (*full line*) and true derivative (*dashed line*) for both functions. The value of k (global) was obtained via (4.6)

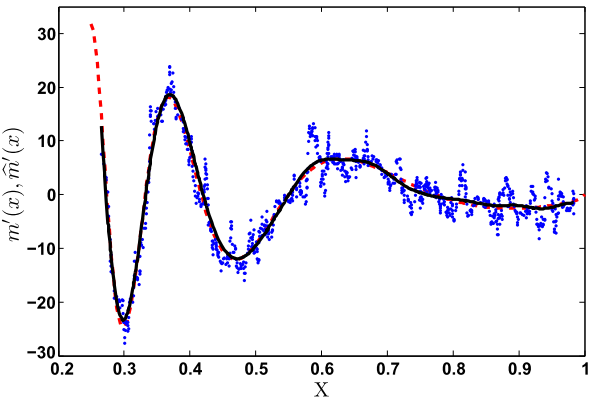

Fig. 4.3 First order derivative estimation. Estimated derivative by the proposed method (*full line*) for a varying k and true derivative (*dashed line*)

($p = 3$) with a Gaussian kernel to smooth the data. The bandwidths were selected via the procedure discussed in Sect. 4.3.

In the second simulation, we illustrate the proposed estimator of the first order derivative when k is a function of X, see (4.5). We consider the function $m(X) = \sqrt{X(1-X)}\sin((2.1\pi)/(X+0.05))$, $X \sim U[0.25, 1]$, $n = 1000$ and $e \sim N(0, 0.1^2)$. The density was estimated using kernel density estimation in combination with the solve-the-equation bandwidth selector. The value of k varied between 8 and 17. Figure 4.3 shows the result.

4.5 Conclusion

We proposed a methodology to estimate first order derivatives in the random design setting without estimating the regression function via smoothing a weighted differ-

ence sequence. We derived L_2 rates and established consistency of the estimator. The newly created data sets are no longer independent and identically distributed random variables. Therefore, we used bimodal kernels in the local polynomial regression framework. Future research will include the study of higher order derivatives and behavior at the boundaries in the random design setting.

References

1. Chaudhuri P, Marron JS (1999) SiZer for exploration of structures in curves. J Am Stat Assoc 94(447):807–823
2. De Brabanter K, De Brabanter J, Suykens JAK, De Moor B (2011) Kernel regression in the presence of correlated errors. J Mach Learn Res 12:1955–1976
3. De Brabanter K, De Brabanter J, Gijbels I, De Moor B (2012) Derivative estimation with local polynomial fitting. J Mach Learn Res 14:281–301
4. De Brabanter K, Gijbels I, Opsomer J (2014) Local polynomial regression with correlated errors in random design. Manuscript in preparation
5. Fan J, Gijbels I (1996) Local polynomial modeling and its applications. Chapman & Hall, London
6. Györfi L, Kohler M, Krzyżak A, Walk H (2002) A distribution-free theory of nonparametric regression. Springer, Berlin
7. Müller H-G, Stadtmüller U, Schmitt T (1987) Bandwidth choice and confidence intervals for derivatives of noisy data. Biometrika 74(4):743–749
8. Park C, Kang K-H (2008) SiZer analysis for the comparison of regression curves. Comput Stat Data Anal 52(8):3954–3970
9. Ramsay JO (1998) Derivative estimation. In: StatLib – S-News, Thursday, 12 March, 1998. Available via http://www.math.yorku.ca/Who/Faculty/Monette/S-news/0556.html
10. Ramsay JO, Silverman BW (2002) Applied functional data analysis. Springer, Berlin
11. Rondonotti V, Marron JS, Park C (2007) SiZer for time series: a new approach to the analysis of trends. Electron J Stat 1:268–289
12. Sheather SJ, Jones MC (1991) A reliable data-based bandwidth selection method for kernel density estimation. J R Stat Soc, Ser B, Stat Methodol 53:683–690
13. Stone C (1985) Additive regression and other nonparametric models. Ann Stat 13(2):689–705
14. Wahba G, Wang Y (1990) When is the optimal regularization parameter insensitive to the choice of loss function? Commun Stat, Theory Methods 19(5):1685–1700
15. Zhou S, Wolfe DA (2000) On derivative estimation in spline regression. Stat Sin 10(1):93–108

Chapter 5
Model Selection Using Cramér–von Mises Distance

Hong Chen, Maik Döring, and Uwe Jensen

Abstract In this paper we consider a model selection problem for the distribution function of lifetimes in the presence of covariates. We propose a new model selection method by defining the closeness between two distribution functions by the Cramér–von Mises distance. This distance is used mostly in the literature to conduct goodness of fit tests. Given a set of data and two competing classes of parametric distribution functions, we define a test statistic, to decide which class approximates the underlying distribution better. With increasing sample size the asymptotic normality property of our test statistic is shown under suitable conditions. As an example, we apply our method to a real data set of lifetimes of DC-motors, which depend on the covariate *load*.

5.1 Introduction

We are interested in the distribution of lifetimes of mechatronical systems in the presence of covarivates. For that matter we consider a model selection problem for the distribution function of the lifetimes. In a case study endurance tests on DC-motors under particular load levels have been conducted at the Institute of Design and Production in Precision Engineering of the University Stuttgart (see [2, 3]). For each of the predetermined load levels, the lifetimes of several objects have been observed. We denote the values of the load levels as z_i with $i = 1, 2, \ldots, m$, $m \in \mathbb{N}$ and the underlying distribution function of the lifetime of the motor for the load level z as $H(\cdot|z)$. We want to answer the question, which parametric class of distributions provides a good approximation for H.

H. Chen (✉) · M. Döring · U. Jensen
Institute of Applied Mathematics and Statistics, University of Hohenheim, 70593 Stuttgart, Germany
e-mail: hong.chen@uni-hohenheim.de

M. Döring
e-mail: maik.doering@uni-hohenheim.de

U. Jensen
e-mail: jensen@uni-hohenheim.de

A. Steland et al. (eds.), *Stochastic Models, Statistics and Their Applications*,
Springer Proceedings in Mathematics & Statistics 122,
DOI 10.1007/978-3-319-13881-7_5

Let two potential model classes of distribution functions be

$$F = \left\{F(\cdot|\theta, z); \theta \in \Theta, z \in \mathbb{R}^d\right\} \quad \text{and} \quad G = \left\{G(\cdot|\gamma, z); \gamma \in \Gamma, z \in \mathbb{R}^d\right\},$$

where $\Theta \subset \mathbb{R}^p$ and $\Gamma \subset \mathbb{R}^q$ are compact subsets. As an example, $F(\cdot|\theta, z)$ can be an exponential and $G(\cdot|\gamma, z)$ a Weibull distribution for each values of (θ, γ, z). The aim of this paper is to decide which model class lies closer to the underlying distribution. Then the distribution function $H(\cdot|z)$ for a given value of z can be estimated with that model. Notice that the two competing model classes may be nested, overlapping or disjoint. Moreover, both, only one or neither of the models may contain the underlying distribution function.

In the literature, various model selection methods have been discussed like Akaike information criterion [1], Bayesian information criterion [10] or Mallows's C_p [7]. See also [4] for a summary of these methods. Unlike these methods, Vuong [12] adopted the classical hypothesis testing framework and used the Kullback–Leibler Information Criterion (KLIC) as a measure of distance between two distributions. As we are interested in H, it would be reasonable to define a goodness of fit criterion based on distribution functions.

On the other hand, goodness of fit tests based on empirical processes have been used for a long time, see for example [5, 6] and [8, 9] for the case with censored data. In these papers, the Cramér–von Mises distance between the fitted distribution function and the empirical distribution function is used to construct tests.

In this paper we propose to use such distance measures for the construction of a test to decide if F or G approximates H better. Unlike the KLIC, our distance measure has a simpler interpretation. We introduce a test statistic, which is defined by the distance measure of different estimates of H according to F and G. Here the unknown parameters θ and γ are estimated by the maximum likelihood method.

To provide critical values the asymptotic normality property of our test statistic is shown. For that purpose, we assume that the following regularity conditions hold true, which are mainly based on the likelihood theory. They are formulated in terms of F and it is understood that corresponding assumptions are also made on G.

A.1 For $\theta \in \Theta$ and $i = 1, \ldots, m$, the distribution $F(\cdot|\theta, z_i)$ has a density function $f(\cdot|\theta, z_i) : \mathbb{R} \to \mathbb{R}^+$, which is strictly positive $H(\cdot|z_i)$-a.s.

A.2 The function $\log f$ is twice continuously differentiable in θ on Θ. Let $\dot{f}$ denote the derivative of f with respect to θ.

A.3 For $\theta \in \Theta$ and $i = 1, \ldots, m$ the functions $\log f(\cdot|\theta, z_i)$, $\dot{f}(\cdot|\theta, z_i)/f(\cdot|\theta, z_i)$ and $\partial^2 \log f(\cdot|\theta, z_i)/\partial\theta^2$ are dominated by $H(\cdot|z_i)$-integrable functions independent of θ. Hence, we can define

$$A_f(\theta) := \sum_{i=1}^{m} \int_0^\infty \frac{\partial^2 \log f(x|\theta, z_i)}{\partial\theta^2} dH(x|z_i).$$

A.4 The function $\sum_{i=1}^m \int_0^\infty \log f(x|\cdot, z_i) dH(x|z_i)$ has a unique maximum on Θ at θ_*, where θ_* is an interior point of Θ with $A_f(\theta_*) \neq 0$. The value θ_* is called the pseudo-true value of θ for the model F.

A.5 The derivative of F with respect to θ exists and is denoted as $\dot{F}$, which is bounded and continuous for all $(x, \theta) \in [0, \infty) \times \delta(\theta_*)$, where $\delta(\theta_*)$ is an open neighborhood of θ_* in Θ.

A.6 For $i = 1, \ldots, m$ the function $\dot{f}^2(\cdot|\theta_*, z_i)/f^2(\cdot|\theta_*, z_i)$ is $H(\cdot|z_i)$-integrable.

The rest of this paper is organized as follows. In Sect. 5.2, the results for the univariate case are presented. The case with a covariate will be treated in Sect. 5.3. In the end, we give a short conclusion.

5.2 Model Selection Between Two Parametric Model Classes

In this section we consider the univariate case, i.e. $m = 1$, omitting the covariate z in the argument of the functions. Let $X_1, X_2, \ldots, X_n$ be i.i.d. random variables with values in $\mathbb{R}^+$ and distribution function H. The two competing classes of parametric distributions reduce to

$$F = \left\{F(\cdot|\theta); \theta \in \Theta \subset \mathbb{R}^p\right\} \quad \text{and} \quad G = \left\{G(\cdot|\gamma); \gamma \in \Gamma \subset \mathbb{R}^q\right\}.$$

For the sake of simplicity, we assume $p = q = 1$. The results can be generalized to the case with $p > 1$ or $q > 1$ directly. The log likelihood function for the model F is defined as

$$\log L(X_1, \ldots, X_n, \theta) := \sum_{i=1}^{n} \log f(X_i|\theta).$$

Let the maximum likelihood estimator be $\hat{\theta}_n$, such that

$$\log L(X_1, \ldots, X_n, \hat{\theta}_n) = \sup_{\theta \in \Theta} \log L(X_1, \ldots, X_n, \theta).$$

According to Theorem 2.2 in [13], under A.1–A.4, $\hat{\theta}_n$ exists and convergences to θ_* almost surely. In our paper the convergences hold for $n \to \infty$. We define the distance between a model class F and a distribution function H by

$$d_H(F) = \int_0^\infty \big(H(x) - F(x|\theta_*)\big)^2 dH(x).$$

Hence, the model with less distance can be viewed as closer to H. Let γ_* and $\hat{\gamma}_n$ denote the pseudo-true value of γ for the model G and its maximum likelihood estimator. Therefore, we propose a test of the null hypothesis

$$H^0: \quad d_H(F) = d_H(G)$$

meaning that the two models are equally close to H, against

$$H^F: \quad d_H(F) < d_H(G)$$

meaning F is closer to H than G or against

$$H^G: \quad d_H(F) > d_H(G)$$

meaning G is closer to H than F. In practice, H, θ_* and γ_* are unknown, however, the difference of the distances can be estimated by the statistic

$$T_n := \int_0^\infty \big(H_n(x) - F(x|\hat{\theta}_n)\big)^2 dH_n(x) - \int_0^\infty \big(H_n(x) - G(x|\hat{\gamma}_n)\big)^2 dH_n(x),$$

where H_n is the empirical distribution function of $X_1, \ldots, X_n$. Let $g(\cdot|\gamma)$ and $\dot{g}$ denote the density function of $G(\cdot|\gamma)$ and the derivative of g with respect to γ, respectively. For the description of the asymptotic variance σ^2 of our test statistic we denote

$$\begin{aligned}
C^f &:= A_f^{-1}(\theta_*) \int_0^\infty \big(H(x) - F(x|\theta_*)\big)\dot{F}(x|\theta_*) dH(x),\\
C^g &:= A_g^{-1}(\gamma_*) \int_0^\infty \big(H(x) - G(x|\gamma_*)\big)\dot{G}(x|\gamma_*) dH(x),\\
N(x) &:= 2C^f \frac{\dot{f}(x|\theta_*)}{f(x|\theta_*)} + \big(H(x) - F(x|\theta_*)\big)^2\\
&\quad - 2C^g \frac{\dot{g}(x|\gamma_*)}{g(x|\gamma_*)} - \big(H(x) - G(x|\gamma_*)\big)^2\\
&\quad - 2\int_0^x \big(G(u|\gamma_*) - F(u|\theta_*)\big) dH(u),\\
\sigma^2 &:= \int_0^\infty N^2(x) dH(x) - \left(\int_0^\infty N(x) dH(x)\right)^2.
\end{aligned}$$

For $H \in F \cap G$ it follows under $A.4$ that $H = F(\cdot|\theta_*) = G(\cdot|\gamma_*)$, hence $\sigma^2 = 0$. In this case $N(0, \sigma^2)$ denotes the degenerate normal distribution.

Theorem 5.1 *Let A.1–A.6 be satisfied. If H^0 holds, then $\sqrt{n}T_n \xrightarrow{d} N(0, \sigma^2)$. If H^F holds, then $\sqrt{n}T_n$ tends to $-\infty$ almost surely. If H^G holds, then $\sqrt{n}T_n$ tends to $+\infty$ almost surely.*

Proof First, we write

$$\begin{aligned}
H_n(x) - F(x|\hat{\theta}_n) = \big(H(x) - F(x|\theta_*)\big) - \big(F(x|\hat{\theta}_n) - F(x|\theta_*)\big)\\
+ \big(H_n(x) - H(x)\big).
\end{aligned}$$

Hence, we have

$$\begin{aligned}
&\int_0^\infty \big(H_n(x) - F(x|\hat{\theta}_n)\big)^2 dH_n(x)\\
&= -2\int_0^\infty \big(F(x|\hat{\theta}_n) - F(x|\theta_*)\big)\big(H(x) - F(x|\theta_*)\big) dH_n(x)\\
&\quad + \int_0^\infty \big(H(x) - F(x|\theta_*)\big)^2 dH_n(x)\\
&\quad + 2\int_0^\infty \big(H_n(x) - H(x)\big)\big(H(x) - F(x|\theta_*)\big) dH_n(x)
\end{aligned}$$

$$
\begin{aligned}
&+\int_0^\infty \big(F(x|\hat{\theta}_n)-F(x|\theta_*)\big)^2 dH_n(x)\\
&-2\int_0^\infty \big(H_n(x)-H(x)\big)\big(F(x|\hat{\theta}_n)-F(x|\theta_*)\big)dH_n(x)\\
&+\int_0^\infty \big(H_n(x)-H(x)\big)^2 dH_n(x). \qquad (5.1)
\end{aligned}
$$

The first term in (5.1) can be written as

$$
-2\int_0^\infty \big(F(x|\hat{\theta}_n)-F(x|\theta_*)\big)\big(H(x)-F(x|\theta_*)\big)dH(x)+o_p(1/\sqrt{n})
$$

and the third term

$$
2\int_0^\infty \big(H_n(x)-H(x)\big)\big(H(x)-F(x|\theta_*)\big)dH(x)+o_p(1/\sqrt{n}),
$$

respectively. Next, we show that the fourth term in (5.1) converges to 0 in probability. By Theorem 3.2 in [13], under A.1–A.4, $\sqrt{n}(\hat{\theta}_n-\theta_*)$ is asymptotically normal. Given A.5,

$$
\begin{aligned}
&\sqrt{n}\int_0^\infty \big(F(x|\hat{\theta}_n)-F(x|\theta_*)\big)^2 dH_n(x)\\
&\quad\le \sup_x \sqrt{n}\big(F(x|\hat{\theta}_n)-F(x|\theta_*)\big)^2\\
&\quad= \sup_x \sqrt{n}\dot{F}^2(x|\tilde{\theta}_n)(\hat{\theta}_n-\theta_*)^2 \xrightarrow{P} 0,
\end{aligned}
$$

where $\tilde{\theta}_n$ lies between $\hat{\theta}_n$ and θ_*. Analogously, for the fifth term, since $\sup_x |H_n(x)-H(x)| \xrightarrow{\text{a.s.}} 0$,

$$
\sqrt{n}\int_0^\infty \big(H_n(x)-H(x)\big)\big(F(x|\hat{\theta}_n)-F(x|\theta_*)\big)dH_n(x) \xrightarrow{P} 0.
$$

The same holds true for $\int_0^\infty (H_n(x)-G(x|\hat{\gamma}_n))^2 dH_n(x)$. It follows that

$$
\begin{aligned}
&\sqrt{n}T_n-\sqrt{n}\big(d_H(F)-d_H(G)\big)\\
&\quad=-2\sqrt{n}\int_0^\infty \big(F(x|\hat{\theta}_n)-F(x|\theta_*)\big)\big(H(x)-F(x|\theta_*)\big)dH(x)\\
&\qquad+\sqrt{n}\int_0^\infty \big(H(x)-F(x|\theta_*)\big)^2 d\big(H_n(x)-H(x)\big)\\
&\qquad+2\sqrt{n}\int_0^\infty \big(G(x|\hat{\gamma}_n)-G(x|\gamma_*)\big)\big(H(x)-G(x|\gamma_*)\big)dH(x)\\
&\qquad-\sqrt{n}\int_0^\infty \big(H(x)-G(x|\gamma_*)\big)^2 d\big(H_n(x)-H(x)\big)\\
&\qquad+2\sqrt{n}\int_0^\infty \big(H_n(x)-H(x)\big)\big(H(x)-F(x|\theta_*)\big)dH(x)\\
&\qquad-2\sqrt{n}\int_0^\infty \big(H_n(x)-H(x)\big)\big(H(x)-G(x|\gamma_*)\big)dH(x)+o_p(1). \qquad (5.2)
\end{aligned}
$$

By A.5, the first term in (5.2) can be written as

$$-2\sqrt{n}(\hat{\theta}_n - \theta_*) \int_0^\infty \dot{F}(x|\theta_*)\big(H(x) - F(x|\theta_*)\big)dH(x) + o_p(1).$$

By A.3, A.4 and the proof of Theorem 3.2 in [13], we have

$$\begin{aligned}\sqrt{n}(\hat{\theta}_n - \theta_*) &= -A_f^{-1}(\theta_*)n^{-1/2}\sum_{i=1}^{n}\frac{\dot{f}(X_i|\theta_*)}{f(X_i|\theta_*)} + o_p(1)\\ &= -A_f^{-1}(\theta_*)\sqrt{n}\int_0^\infty \frac{\dot{f}(x|\theta_*)}{f(x|\theta_*)}dH_n(x) + o_p(1)\\ &= -A_f^{-1}(\theta_*)\sqrt{n}\int_0^\infty \frac{\dot{f}(x|\theta_*)}{f(x|\theta_*)}d\big(H_n(x) - H(x)\big) + o_p(1).\end{aligned}$$

A similar result holds true for the third term in (5.2). Since $\phi(x) = \int_0^x (H(u) - F(u|\theta_*))dH(u)$ is of bounded variation on $[0, T]$ for each $T < +\infty$, it follows from A.6 that

$$\begin{aligned}&\sqrt{n}T_n - \sqrt{n}\big(d_H(F) - d_H(G)\big)\\ &\xrightarrow{P} 2C^f\int_0^\infty \frac{\dot{f}(x|\theta)}{f(x|\theta)}dB^0\big(H(x)\big) + \int_0^\infty \big(H(x) - F(x|\theta_*)\big)^2 dB^0\big(H(x)\big)\\ &\quad - 2C^g\int_0^\infty \frac{\dot{g}(x|\gamma)}{g(x|\gamma)}dB^0\big(H(x)\big) - \int_0^\infty \big(H(x) - G(x|\gamma_*)\big)^2 dB^0\big(H(x)\big)\\ &\quad - 2\int_0^\infty\int_0^x \big(G(u|\gamma_*) - F(u|\theta_*)\big)dH(u)dB^0\big(H(x)\big)\\ &= \int_0^\infty N(x)dB^0\big(H(x)\big),\end{aligned}$$

where B^0 denotes a Brownian bridge process on $[0, 1]$, see Theorem 4.4.1 on page 283 in [11]. Since $N^2(x)$ is H-integrable, we have that $\int_0^\infty N(x)dB^0(H(x))$ is $N(0, \sigma^2)$ distributed and the theorem follows. □

Moreover, the variance σ^2 can be estimated consistently by

$$\hat{\sigma}_n^2 := \int_0^\infty \hat{N}_n^2(x)dH_n(x) - \left(\int_0^\infty \hat{N}_n(x)dH_n(x)\right)^2,$$

where

$$\begin{aligned}\hat{N}_n(x) := {}& 2\hat{C}_n^f\frac{\dot{f}(x|\hat{\theta}_n)}{f(x|\hat{\theta}_n)} + \big(H_n(x) - F(x|\hat{\theta}_n)\big)^2\\ &- 2\hat{C}_n^g\frac{\dot{g}(x|\hat{\gamma}_n)}{g(x|\hat{\gamma}_n)} - \big(H_n(x) - G(x|\hat{\gamma}_n)\big)^2\\ &- 2\int_0^x \big(G(u|\hat{\gamma}_n) - F(u|\hat{\theta}_n)\big)dH_n(u),\end{aligned}$$

$$\hat{C}_n^f := \hat{A}_f^{-1}(\hat{\theta}_n) \int_0^\infty \big(H_n(x) - F(x|\hat{\theta}_n)\big)\dot{F}(x|\hat{\theta}_n) dH_n(x),$$

$$\hat{C}_n^g := \hat{A}_g^{-1}(\hat{\gamma}_n) \int_0^\infty \big(H_n(x) - G(x|\hat{\gamma}_n)\big)\dot{G}(x|\hat{\gamma}_n) dH_n(x),$$

$$\hat{A}_f(\theta) := \int_0^\infty \frac{\partial^2 \log f(x|\theta)}{\partial\theta^2} dH_n(x) \quad \text{and} \quad \hat{A}_g(\theta) := \int_0^\infty \frac{\partial^2 \log g(x|\theta)}{\partial\theta^2} dH_n(x).$$

If $\sigma^2 > 0$ and H^0 holds true, we have that

$$\frac{\sqrt{n}T_n}{\hat{\sigma}_n} \xrightarrow{d} N(0,1).$$

Therefore, for a given significance level α, we decide for the hypothesis H^0, if $|\sqrt{n}T_n/\hat{\sigma}_n| \le z_{1-\alpha/2}$, where z_α denotes the α-quantile of a standard normal distribution. The hypothesis H^F or H^G will be accepted, if $\sqrt{n}T_n/\hat{\sigma}_n > z_{1-\alpha/2}$ or $\sqrt{n}T_n/\hat{\sigma}_n < -z_{1-\alpha/2}$, respectively. However, we propose to use the model with less parameters, ever if H^0 is not rejected. The case $\sigma^2 = 0$, where we have that $\sqrt{n}T_n \to 0$ under H^0, will be considered in a forthcoming paper.

5.3 The Case with Covariate

Unlike the regular regression analysis, we assume that for each covariate value z_i, $i = 1, 2, \ldots, m$, there are n random variables $X_{i1}, X_{i2}, \ldots, X_{in}$ with values in $\mathbb{R}^+$. Further, we assume that all random variables are independent and for each i, X_{ij} follow the same distribution function $H(\cdot|z_i)$. Hence we can estimate $H(\cdot|z_i)$ by the empirical distribution function denoted as $H_n(\cdot|z_i)$.

Given the two competing classes F and G as in the introduction of this paper, the maximum likelihood estimators $\hat{\theta}_n$ and $\hat{\gamma}_n$ for θ_* and γ_* can be defined similarly as in the univariate case. Further, we define the distance from the two models to the underlying distribution H as

$$d_H^Z(F) = \sum_{i=1}^m d_{H(\cdot|z_i)}\big(F(\cdot|\theta_*, z_i)\big), \qquad d_H^Z(G) = \sum_{i=1}^m d_{H(\cdot|z_i)}\big(G(\cdot|\gamma_*, z_i)\big).$$

For each i let σ_i and $\hat{\sigma}_i$ be the conditional version of σ and $\hat{\sigma}$ and the statistic T_n^Z be

$$T_n^Z := \sum_{i=1}^m \bigg(\int_0^\infty \big(H_n(x|z_i) - F(x|\hat{\theta}_n, z_i)\big)^2 dH_n(x|z_i) - \int_0^\infty \big(H_n(x|z_i) - G(x|\hat{\gamma}_n, z_i)\big)^2 dH_n(x|z_i) \bigg).$$

Corollary 5.2 *Let A.1–A.6 be satisfied. If $d_H^Z(F) = d_H^Z(G)$, then $\sqrt{n}T_n^Z \xrightarrow{d} N(0, \sum_{i=1}^m \sigma_i^2)$ and $\hat{\sigma}_i \xrightarrow{a.s.} \sigma_i$, $i = 1, \ldots, m$. If $d_H^Z(F) < d_H^Z(G)$, then $\sqrt{n}T_n^Z$ tends to $-\infty$ almost surely. If $d_H^Z(F) > d_H^Z(G)$, then $\sqrt{n}T_n^Z$ tends to $+\infty$ almost surely.*

We apply our test to the lifetime data of the DC-motors. For each of the five load levels (2.5, 3.75, 5, 6.25, 7.5 mNm) we observed 16 lifetimes (see [2, 3]). As an example, we want to select between the classes of the two-parametric Weibull distributions and of the lognormal distributions.

$$F = \left\{ Wei(\theta_1 + \theta_2 \cdot z, \theta_3 + \theta_4 \cdot z);\ \theta_1 + \theta_2 \cdot z > 0, \theta_3 + \theta_4 \cdot z > 0 \right\},$$
$$G = \left\{ \mathrm{Log}\, N\left(\gamma_1 + \gamma_2 \cdot z, (\gamma_3 + \gamma_4 \cdot z)^2\right);\ \gamma_3 + \gamma_4 \cdot z > 0 \right\}.$$

According to our data we get the estimates $n^{1/2} T_n^Z \approx 0.0274$ and $\sum_{i=1}^{5} \hat{\sigma}_i^2 \approx 0.0067$. Hence, we get the p-value ≈ 0.7382 and decide for H^0. This means, the two model classes do not approximate the distribution of the lifetimes significantly differently. However, the test statistic is positive, so we recommend the Weibull model.

5.4 Conclusion

In this paper, we applied the Cramér–von Mises distance to describe the closeness between two distributions. Other measures like Anderson–Darling distance or a weighted version of Cramér–von Mises could also be used. The Cramér–von Mises goodness of fit test is based, under different assumptions, on the asymptotic distribution of $n \cdot d_{H_n}(F)$. We showed that $n^{1/2} \cdot (d_{H_n}(F(\cdot|\hat{\theta}_n)) - d_{H_n}(G(\cdot|\hat{\gamma}_n)))$ is asymptotically normal under H^0, where the variance σ^2 can be estimated consistently. For $\sigma^2 > 0$ we stated a model selection method and the case $\sigma^2 = 0$ will be investigated in a forthcoming paper.

According to our data example, the empirical distribution function is available for each $i = 1, \ldots, m$. This motivates us to consider the asymptotics as $n \to \infty$ for fixed m. A different point of view is to investigate the asymptotics for $m \to \infty$.

Moreover, the two competing distribution classes here are both parametric. The extension to semiparametric and nonparametric classes or the case with censored data will be part of future work.

Acknowledgements We thank the DFG (German Research Foundation) for the support and funding of this research project (Ge: Je 162/10-1, Schi 457/12-1).

References

1. Akaike H (1973) Information theory and extension of the maximum likelihood principle. In: Petrov V, Csáki F (eds) Proceedings of the second international symposium on information theory, Akademiai Kiádo, Budapest, pp 267–281
2. Bobrowski S, Döring M, Jensen U, Schinköthe W (2011) Reliability prediction using the cox proportional Hazards model. In: 56th international scientific colloquium, Ilmenau
3. Bobrowski S, Döring M, Jensen U, Schinköthe W (2013) Reliability prediction for mechatronic drive systems. In: 9th GMM/ETG Fachtagung Innovative Klein- und Mikroantriebstechnik, Nürnberg

4. Claeskens G, Hjort NL (2009) Model selection and model averaging. Cambridge University Press, Cambridge
5. Durbin J (1973) Weak convergence of the sample distribution function when parameters are estimated. Ann Stat 1(2):279–290
6. Khmaladze E (1981) Martingale approach in the theory of goodness-of-fit tests. Theory Probab Appl 26(2):240–257
7. Mallows CL (1973) Some comments on C_p. Technometrics 15(4):661–675
8. Ren J (1995) Generalized Cramér–von Mises tests of goodness of fit for doubly censored data. Ann Inst Stat Math 47(3):525–549
9. Ren J (2003) Goodness of fit tests with interval censored data. Scand J Stat 30(1):211–226
10. Schwartz G (1978) Estimating the dimension of a model. Ann Stat 6(2):461–464
11. Shorack GR, Wellner JA (1986) Empirical processes with applications to statistics. Wiley, New York
12. Vuong QH (1989) Likelihood ratio tests for model selection and non-Nested hypotheses. Econometrica 57(2):307–333
13. White H (1982) Maximum likelihood estimation of misspecified models. Econometrica 50(1):1–25

Chapter 6
Rate of Convergence of a Change Point Estimator in a Misspecified Regression Model

Maik Döring

Abstract A parametric estimation problem is considered in a misspecified regression model, where the regression function has a smooth change point. The focus lies on regression functions, which are continuous at the change point. Here, it is not assumed that the true regression function belongs to the model class. However, there exists a pseudo change point, such that the related regression function gives a reasonable approximation. With increasing sample size the asymptotic behavior is investigated of the least squares estimates of the change point. The consistency of the change point estimator for the pseudo estimator is shown. It turns out that the rate of convergence depends on the order of smoothness of the regression function at the change point.

6.1 Introduction

Change point models are being used in many fields, for instance, archaeology, econometrics, epidemiology, medicine and reliability. The problem to estimate the location of a change point in a regression model has been studied in the literature to some extent. In most cases locating a jump discontinuity is considered and properties of the estimators are studied, see for example [1, 2]. Müller [10] investigates the problem of estimating a jump change point in the derivative of some order of the regression function. A change of the slope of a linear function was considered for example in [4, 5]. Hušková [6, 7] considers a least squares type estimator of the parameters in a location model with gradual changes in a fixed design setup.

Here the focus lies on regression functions, which are continuous at the change point in a random design regression model. Suppose an experimenter use such regression functions with a change point, but the true underlying regression function does not belong to the model. What is the asymptotic behavior of the least squares estimator for the change point? It is shown under suitable conditions, that the pro-

M. Döring (✉)
Institute of Applied Mathematics and Statistics, University of Hohenheim, 70593 Stuttgart, Germany
e-mail: maik.doering@uni-hohenheim.de

A. Steland et al. (eds.), *Stochastic Models, Statistics and Their Applications*,
Springer Proceedings in Mathematics & Statistics 122,
DOI 10.1007/978-3-319-13881-7_6

posed change point estimator is consistent for a pseudo change point. Further, the rate of convergence is studied.

Let for $n \in \mathbb{N}$ the observations $(X, Y), (X_1, Y_1), \ldots, (X_n, Y_n)$ be i.i.d. $\mathbb{R}^2$-valued random variables. It is assumed that the distribution of X is absolutely continuous with a density function d_X, which is uniformly bounded on the unit interval $[0, 1]$. Further it is assumed that the response variables Y_i are given by the following regression model

$$Y_i = f(X_i) + \varepsilon_i, \quad 1 \le i \le n,\ n \in \mathbb{N},$$

where $f : \mathbb{R} \to \mathbb{R}$ is an unknown continuous function. Let $\varepsilon, \varepsilon_1, \ldots, \varepsilon_n$ for $n \in \mathbb{N}$ be i.i.d. real valued random variables. It is required that $E(\varepsilon|X) = 0$ a.s. and that the random variable ε is suitably integrable. The function f should be approximated by a parametric regression function $f_\theta : \mathbb{R} \to \mathbb{R}$ with an unknown change point $\theta \in (0, 1)$ and known exponent $q \in (0, \infty)$ given by

$$f_\theta(x) := (x - \theta)^q 1_{(\theta,1]}(x),$$

where 1_A is the indicator function of a set A. Observe that for small values of q, the function $\theta \to f_\theta(x)$ is not differentiable in θ. The least squares error is considered for any possible change point. For $\theta \in [0, 1]$ and $n \in \mathbb{N}$ define

$$M_n(\theta) := -\frac{1}{n} \sum_{i=1}^{n} \big(Y_i - f_\theta(X_i)\big)^2.$$

For $n \in \mathbb{N}$ our estimator is defined as the maximizing point of M_n:

$$\hat{\theta}_n := \operatorname*{argmax}_{\theta \in [0,1]} M_n(\theta).$$

Here, the limit behavior will be studied of the least squares estimator $\hat{\theta}_n$. The model is misspecified in that f does not belong to the model. But, it is assumed that a pseudo change point $\theta_* \in (0, 1)$ exists with

$$E\big(f(X) - f_{\theta_*}(X)\big)^2 < E\big(f(X) - f_\theta(X)\big)^2 \quad \forall \theta \neq \theta_*. \tag{6.1}$$

This means in particular, that θ_* is a unique maximizer of $E(M_n)$. The consistency of the proposed estimator is shown, i.e. $\hat{\theta}_n \to \theta_*$ as $n \to \infty$. In order to get a rate of convergence, it is assumed that constants $\alpha > 0$ and $C > 0$ exist, such that for all $\theta \in [0, 1]$

$$-E\big(f(X) - f_\theta(X)\big)^2 + E\big(f(X) - f_{\theta_*}(X)\big)^2 < -C|\theta - \theta_*|^\alpha. \tag{6.2}$$

It turns out that the rate of convergence of $\hat{\theta}_n$ depends on α and q.

The paper is organized as follows. Consistency is shown in Sect. 6.2 and the rate of convergence of the estimator is considered in Sect. 6.3. In Sect. 6.4 some conclusions are given.

6.2 Consistency

To analyze the asymptotic behavior of the change point estimator, the theory of M-estimators and empirical processes is used. For a fuller treatment see for example [9, 12].

Theorem 6.1 *Let $E(|\varepsilon||X) < C_1$ a.s. for some positive constant C_1 and assume that (6.1) holds true. Then*

$$\lim_{n\to\infty} \hat{\theta}_n \to \theta_* \ a.s.$$

Proof It is to check whether all assumptions of the well-known argmax theorem are satisfied. Let for $\theta \in [0, 1]$ the functions $m_\theta : \mathbb{R}^2 \to \mathbb{R}$ be defined by

$$m_\theta(\mathfrak{e}, x) := -2\mathfrak{e}\big(f(x) - f_\theta(x)\big) - \big(f(x) - f_\theta(x)\big)^2.$$

Observe that $M_n(\theta) = \tilde{M}_n(\theta) - \frac{1}{n}\sum_{i=1}^n \varepsilon_i^2$, where

$$\tilde{M}_n(\theta) := \frac{1}{n}\sum_{i=1}^n m_\theta(\varepsilon_i, X_i).$$

It follows that M_n and $\tilde{M}_n$ have the same maximizers. The random variables ε_i, $1 \le i \le n$ are i.i.d. as well as X_i, $1 \le i \le n$ and $E(\varepsilon|X) = 0$ a.s., hence

$$E\big(\tilde{M}_n(\theta)\big) = E\big(m_\theta(\varepsilon, X)\big) = -E\Big(\big(f(X) - f_\theta(X)\big)^2\Big) =: \tilde{M}(\theta).$$

The function $\tilde{M}$ is continuous and by (6.1) it follows that θ_* is a well separated maximizer of $\tilde{M}$. The definition of the estimator yields $\tilde{M}_n(\hat{\theta}_n) = \sup_{\theta\in[0,1]} \tilde{M}_n(\theta)$ directly. Next it is shown that $\lim_{n\to\infty} \sup_{\theta\in[0,1]} |\tilde{M}_n(\theta) - \tilde{M}(\theta)| = 0$ a.s.

Let $\mathcal{M} := \{m_\theta \colon \theta \in [0, 1]\}$ be a set of function. Thus the following representation is given.

$$\sup_{\theta\in[0,1]} \big|\tilde{M}_n(\theta) - \tilde{M}(\theta)\big| = \sup_{m\in\mathcal{M}} \left|(1/n)\sum_{i=1}^n m(\varepsilon_i, X_i) - Em(\varepsilon, X)\right|.$$

For $\eta > 0$ let $N_{[]}(\eta, \mathcal{M}, L_1)$ be the bracketing number of the class of functions $\mathcal{M}$ related to the L_1-norm, i.e. $\|m\|_{L_1} = E(|m(\varepsilon, X)|)$, for details see Van der Vaart [12, Chap. 19]. It will be shown that the bracketing number $N_{[]}(\eta, \mathcal{M}, L_1)$ of the class $\mathcal{M}$ is finite for any $\eta > 0$, hence $\mathcal{M}$ is a Glivenko-Cantelli class by Theorem 19.4 in [12] and the assertion follows.

Let $0 \le \theta_1 < \theta_2 \le 1$ and fix $\mathfrak{e}$ and x. Then the function $m_{(\cdot)}(\mathfrak{e}, x) : [\theta_1, \theta_2] \to \mathbb{R}$ has at least one minimizer $\underline{\theta}$ and one maximizer $\overline{\theta}$. Hence

$$\begin{aligned}&\sup_{\theta\in[\theta_1,\theta_2]} m_\theta(\mathfrak{e}, x) - \inf_{\theta\in[\theta_1,\theta_2]} m_\theta(\mathfrak{e}, x)\\ &= -2\mathfrak{e}\big(f(x) - f_{\overline{\theta}}(x)\big) - \big(f(x) - f_{\overline{\theta}}(x)\big)^2 + 2\mathfrak{e}\big(f(x) - f_{\underline{\theta}}(x)\big)\end{aligned}$$

$$
\begin{aligned}
&+\big(f(x)-f_{\underline{\theta}}(x)\big)^2\\
&=\big(2\mathfrak{e}+2f(x)-f_{\overline{\theta}}(x)-f_{\underline{\theta}}(x)\big)\cdot\big(f_{\overline{\theta}}(x)-f_{\underline{\theta}}(x)\big)\\
&\le C_1\cdot|\mathfrak{e}|\cdot\big(f_{\theta_1}(x)-f_{\theta_2}(x)\big), \qquad (6.3)
\end{aligned}
$$

where C_1 is a positive constant and independent of θ_1 and θ_2. The last inequality follows since the function f is decreasing in θ. Let $\tilde{C}$ be a positive generic constant. Since the density d_X of the distribution X is uniformly bounded on the unit interval and by $E(|\varepsilon||X)<C$ a.s. it follows that

$$
\begin{aligned}
&E\Big(\sup_{\theta\in[\theta_1,\theta_2]} m_\theta(\varepsilon,X)-\inf_{\theta\in[\theta_1,\theta_2]} m_\theta(\varepsilon,X)\Big)\\
&\le\tilde{C}\left(\int_{\theta_1}^1(x-\theta_1)^q dx-\int_{\theta_2}^1(x-\theta_2)^q dx\right)\le\tilde{C}(\theta_2-\theta_1).
\end{aligned}
$$

Using standard methods it follows for any $\eta>0$ that $N_{[\,]}(\eta,\mathcal{M},L_1)\le\tilde{C}/\eta<\infty$.

Hence $\lim_{n\to\infty}\sup_{\theta\in[0,1]}|\tilde{M}_n(\theta)-\tilde{M}(\theta)|=0$ a.s. Thus all assumptions of Theorem 2.12 in [9] are satisfied and the assertion follows. □

6.3 Rate of Convergence

The rate of convergence is determined by α of (6.2) and q. Standard methods for the analysis, like Taylor expansion, are not applicable for small values of q, since the regression function $\theta\to f_\theta(x)$ is not differentiable.

Theorem 6.2 *Let $E(\varepsilon^2|X)<C_2$ a.s. for some positive constant C_2 and assume that (6.2) holds true. Then for $0<q<1/2$ and $\alpha>q+1$*

$$
n^{1/(2\alpha-2q-1)}\cdot(\hat{\theta}_n-\theta_*)=O_P(1),
$$

and for $1/2<q$ and $\alpha>1$

$$
n^{1/(2\alpha-2)}\cdot(\hat{\theta}_n-\theta_*)=O_P(1).
$$

Proof The main step of the proof is to show that there exists a constant $C>0$ such that for every sufficiently small $\delta>0$

$$
\begin{aligned}
&E\left(\sup_{\theta_0-\delta<\theta<\theta_0+\delta}\left|\frac{1}{\sqrt{n}}\sum_{i=1}^n\big(m_\theta(\varepsilon_i,X_i)-m_{\theta_*}(\varepsilon_i,X_i)\right.\right.\\
&\left.\left.-E\big(m_\theta(\varepsilon_i,X_i)\big)+E\big(m_{\theta_*}(\varepsilon_i,X_i)\big)\big)\right|\right)\le C\delta^{\beta(q)},
\end{aligned}
$$

where

$$
\beta(q):=\begin{cases}q+1/2 & 0<q<1/2\\ 1 & 1/2<q.\end{cases}
$$

For $0 < \delta$ let $\mathcal{M}_\delta$ be the following class of measurable functions:

$$\mathcal{M}_\delta := \{m_\theta - m_{\theta_*} \colon \theta_* - \delta < \theta < \theta_* + \delta\}.$$

With $C_1 > 0$ of (6.3) let $M_\delta : \mathbb{R}^2 \to \mathbb{R}$ be a measurable function defined by

$$M_\delta(\mathfrak{e}, x) := C_1|\mathfrak{e}|\big(f_{\theta_*-\delta}(x) - f_{\theta_*+\delta}(x)\big).$$

Observe that the function M_δ is non-negative since the function f is decreasing in θ. The function M_δ is an envelope function of the class $\mathcal{M}_\delta$, i.e. $|m(\mathfrak{e}, x)| \le M_\delta(\mathfrak{e}, x)$ for all $x \in \mathbb{R}$, $\mathfrak{e} \in \mathbb{R}$ and for all $m \in \mathcal{M}_\delta$. Let $\tilde{C}$ be a positive generic constant. Since the density d_X of the distribution X is uniformly bounded on the unit interval, by Lemma 8 in [3] and $E(\varepsilon^2|X) < C$ a.s. it follows that

$$\|M_\delta\|_{L_2} \le \tilde{C}\delta^{\beta(q)} \tag{6.4}$$

where the L_2-norm is defined by $\|M_\delta\|_{L_2}^2 = E(|M_\delta(\varepsilon, X)|^2)$.

For $\eta > 0$ let $N_{[\,]}(\eta, \mathcal{M}_\delta, L_2)$ be the bracketing number of the class of functions $\mathcal{M}_\delta$ related to the L_2-norm. Analogously to (6.4), in view of (6.3), it follows that, for $0 \le \theta_1 < \theta_2 < 1$,

$$\begin{aligned} &E\Big(\Big|\sup_{\theta_1\le\theta\le\theta_2}\big(m_\theta(\varepsilon, X) - m_{\theta_*}(\varepsilon, X)\big) - \inf_{\theta_1\le\theta\le\theta_2}\big(m_\theta(\varepsilon, X) - m_{\theta_*}(\varepsilon, X)\big)\Big|^2\Big) \\ &\quad \le E\big(C_1^2\varepsilon^2\big(f_{\theta_1,q}(X) - f_{\theta_2,q}(X)\big)^2\big) \le \tilde{C}(\theta_2 - \theta_1)^{2\beta(q)}. \end{aligned}$$

Using standard methods it follows that for any $\eta > 0$

$$\ln\big(N_{[\,]}(\eta, \mathcal{M}_\delta, L_2)\big) \le \ln\big(\tilde{C}\delta\eta^{-1/\beta(q)}\big) = \big(1/\beta(q)\big)\ln\big((\tilde{C}\delta)^{\beta(q)}/\eta\big).$$

Hence by Corollary 19.35 in [12] it follows that

$$\begin{aligned} &E\Bigg(\sup_{\theta_0-\delta<\theta<\theta_0+\delta}\Bigg|\frac{1}{\sqrt{n}}\sum_{i=1}^n\big(m_\theta(\varepsilon_i, X_i) - m_{\theta_*}(\varepsilon_i, X_i) \\ &\qquad - E\big(m_\theta(\varepsilon_i, X_i)\big) + E\big(m_{\theta_*}(\varepsilon_i, X_i)\big)\big)\Bigg|\Bigg) \\ &= E\Bigg(\sup_{m\in\mathcal{M}}\Bigg|\frac{1}{\sqrt{n}}\sum_{i=1}^n\big(m(\varepsilon_i, X_i) - E\big(m(\varepsilon_i, X_i)\big)\big)\Bigg|\Bigg) \\ &\le \tilde{C}\int_0^{\|M_\delta\|_{L_2}}\big(\max\big\{1, \ln\big(N_{[\,]}(\eta, \mathcal{M}_\delta, L_2)\big)\big\}\big)^{1/2}d\eta \\ &\le \tilde{C}\int_0^{\delta^{\beta(q)}}\sqrt{\delta^{\beta(q)}/\eta}\,d\eta \le \tilde{C}\delta^{\beta(q)}. \end{aligned}$$

The definition of our estimator yields $\tilde{M}_n(\hat{\theta}_n) \ge \tilde{M}_n(\theta_*)$ and by Theorem 6.1 it follows that $\hat{\theta}_n \to \theta_*$. By (6.2) all assumptions of Theorem 5.52 in [12] are satisfied with α and $\beta(q)$. Hence $n^{1/(2\alpha-2\beta(q))}(\hat{\theta}_n - \theta_*) = O_P(1)$ and the assertion follows. □

6.4 Discussion and Conclusion

It was shown that the least squares estimator for the change point is consistent for a pseudo change point. Further the rate of convergence of the change point estimator was analyzed. A quite simple model was considered, since the focus lies on the investigation of the different rates of convergence of $\hat{\theta}_n$ depending on q and α. Future work is to show under additional conditions that the rates are optimal. For small values of q the estimator shows a non-regular asymptotic behavior, since the regression function is not differentiable in θ. If q is large and assumption (6.1) holds true, then it follows that $\alpha = 2$, hence $n^{1/2}(\hat{\theta}_n - \theta_*) = O_P(1)$. In this case the estimator is asymptotically normal. In the following two particular types of functions f are discussed.

1. The true model: $f = f_{\theta_0}$ with $\theta_0 \in (0, 1)$.
   It follows that $\theta_0 = \theta_*$ and $\alpha = 2\beta(q)$, hence

$$\begin{aligned} \hat{\theta}_n &\to \theta_0 \text{ a.s.} \\ n^{1/(2q+1)} \cdot (\hat{\theta}_n - \theta_0) &= O_P(1) \quad \text{for } 0 < q < 1/2, \\ n^{1/2} \cdot (\hat{\theta}_n - \theta_0) &= O_P(1) \quad \text{for } 1/2 < q. \end{aligned}$$

   In [3] the convergence in distribution of the estimator was shown. For $q > 1/2$ the estimator is asymptotically normal and for $0 < q < 1/2$ the change point estimator converges to a maximizer of a fractional Brownian motion with drift. For $q = 1/2$ the rate $(n \ln n)^{1/2}$ was proven. But in the last case the limiting distribution is also normal. Such non-regular behavior occurs also in similar models, see for instance [6–8, 11].
2. A quite similar model: $f(x) = (x - \theta_0)^{q_0} 1_{(\theta_0, 1]}(x)$ with $\theta_0 \in (0, 1)$ and $q_0 \neq q$.
   The function f is decreasing in θ_0 and q_0, i.e. for all $x \in [0, 1]$

$$\begin{aligned} (x - \theta_1)^{q_0} 1_{(\theta_1, 1]}(x) &\geq (x - \theta_2)^{q_0} 1_{(\theta_2, 1]}(x) \quad \theta_1 < \theta_2, \\ (x - \theta_0)^{q_1} 1_{(\theta_0, 1]}(x) &\geq (x - \theta_0)^{q_2} 1_{(\theta_0, 1]}(x) \quad q_1 < q_2. \end{aligned}$$

   This gives for $q_0 < q$ and $\theta_1 < \theta_0 < \theta_2$ that

$$f_{\theta_2} \leq f_{\theta_0} \leq \min\{f, f_{\theta_1}\} \quad \text{and} \quad \tilde{M}(\theta_2) < \tilde{M}(\theta_0) < \tilde{M}(\theta_1).$$

   It follows for $q_0 < q$ that $\theta_0 > \theta_*$. The same conclusion can be drawn for $q_0 > q$, which implies that $\theta_0 < \theta_*$. Hence the estimator is not consistent for θ_0,

$$\hat{\theta}_n \to \theta_* \neq \theta_0 \text{ a.s.}$$

   Such situation occurs in models with continuous and stepwise linear functions. That means, regression function with $q = 1$ are postulated. For example let X uniformly distributed on the unit interval, then

$$\begin{aligned} \frac{\partial}{\partial \theta} \tilde{M}(\theta) &= \frac{\partial}{\partial \theta} \Big(-E\big((X - \theta_0)^{q_0} 1_{(\theta_0, 1]}(X) - (X - \theta) 1_{(\theta, 1]}(X) \big)^2 \Big) \\ &= -\frac{2}{q_0 + 1} (1 - \theta_0)^{q_0 + 1} + \frac{2}{q_0 + 1} \big(\max\{\theta, \theta_0\} - \theta_0 \big)^{q_0 + 1} + (1 - \theta)^2. \end{aligned}$$

For $q_0 < 1$, since $\theta_0 > \theta_*$, it follows that

$$\frac{\partial}{\partial\theta}\tilde{M}(\theta) = 0 \quad \Longleftrightarrow \quad \frac{2}{q_0+1}(1-\theta_0)^{q_0+1} = (1-\theta)^2.$$

Therefore, the pseudo change point is given by

$$\theta_* = 1 - \big(2/(q_0+1)\big)^{1/2}(1-\theta_0)^{(q_0+1)/2}.$$

For $q_0 > 1$, since $\theta_0 < \theta_*$, the pseudo change point θ_* solves the following equation

$$0 = -\frac{2}{q_0+1}(1-\theta_0)^{q_0+1} + \frac{2}{q_0+1}(\theta-\theta_0)^{q_0+1} + (1-\theta)^2.$$

Observe that $\theta = 1$ is a solution of the above equation, but it minimizes the function $\tilde{M}$. For q_0 close to one, it follows as expected that θ_* is close to θ_0. Further it can be shown that $\alpha = 2$ and by standard methods the asymptotic normality property of the change point estimator.

Acknowledgements The author would like to thank the Associate Editor and Reviewer for their careful reading and comments. These comments and suggestions have been helpful for revising and improving the manuscript.

References

1. Csörgö M, Horváth L (1997) Limit theorems in change-point analysis. Wiley, New York
2. Dempfle A, Stute W (2002) Nonparametric estimation of a discontinuity in regression. Stat Neerl 56:233–242
3. Döring M, Jensen U (2014) Smooth change point estimation in regression models with random design. Ann Inst Stat Math. doi:10.1007/s10463-014-0467-8
4. Feder PL (1975) On asymptotic distribution theory in segmented regression problems. Ann Stat 3:49–83
5. Hinkley D (1971) Inference in two-phase regression. J Am Stat Assoc 66:736–743
6. Hušková M (1999) Gradual changes versus abrupt changes. J Stat Plan Inference 76:109–125
7. Hušková M (2001) A note on estimators of gradual changes. In: de Gunst M, Klaassen C, van der Vaart A (eds) State of the art in probability and statistics. Institute of mathematical statistics lecture notes – monograph series, vol 36, pp 345–358. Beachwood
8. Ibragimov IA, Has'minskii RZ (1981) Statistical estimation – asymptotic theory. Springer, New York
9. Kosorok MR (2008) Introduction to empirical processes and semiparametric inference. Springer, New York
10. Müller HG (1992) Change-points in nonparametric regression analysis. Ann Stat 20:737–761
11. Prakasa Rao BLS (1985) Asymptotic theory of least squares estimator in a nonregular nonlinear regression models. Stat Probab Lett 3:15–18
12. Van der Vaart AW (1998) Asymptotic statistics. Cambridge University Press, Cambridge

Chapter 7
An Exact Formula for the Average Run Length to False Alarm of the Generalized Shiryaev–Roberts Procedure for Change-Point Detection under Exponential Observations

Wenyu Du, Grigory Sokolov, and Aleksey S. Polunchenko

Abstract We derive analytically an exact closed-form formula for the standard minimax Average Run Length (ARL) to false alarm delivered by the Generalized Shiryaev–Roberts (GSR) change-point detection procedure devised to detect a shift in the baseline mean of a sequence of independent exponentially distributed observations. Specifically, the formula is found through direct solution of the respective integral (renewal) equation, and is a general result in that the GSR procedure's nonnegativ headstart is not restricted to a bounded range, nor is there a "ceiling" value for the detection threshold. Apart from the theoretical significance (in change-point detection, exact closed-form performance formulae are typically either difficult or impossible altogether to get, especially for the GSR procedure), the obtained formula is also useful to a practitioner: in cases of practical interest, the formula is a function linear in both the detection threshold and the headstart, and, therefore, the ARL to false alarm of the GSR procedure can be easily computed.

7.1 Introduction

Quickest change-point detection is concerned with the design and analysis of reliable statistical machinery for rapid detection of changes that may spontaneously affect a "live" process, continuously monitored via sequentially made observations. See, e.g., [24] or [33, Part II]. A quickest change-point detection procedure is a stopping time adapted to the observed data, and is a rule whereby one is to stop and "sound an alarm" that the characteristics of the observed process may have (been) changed. A "good" (i.e., optimal or nearly optimal) detection procedure is one that

W. Du (✉) · G. Sokolov · A.S. Polunchenko
Department of Mathematical Sciences, State University of New York at Binghamton, Binghamton, NY 13902-6000, USA
e-mail: wdu1@binghamton.edu

G. Sokolov
e-mail: gsokolov@binghamton.edu

A.S. Polunchenko
e-mail: aleksey@binghamton.edu

A. Steland et al. (eds.), *Stochastic Models, Statistics and Their Applications*, Springer Proceedings in Mathematics & Statistics 122,
DOI 10.1007/978-3-319-13881-7_7

minimizes (or nearly minimizes) the desired detection delay penalty, subject to a constraint on the false alarm risk. For an overview of the major optimality criteria see, e.g., [18, 23, 32, 38] or [33, Part II].

A problem particularly persistent in applied change-point detection (e.g., in quality control) is evaluation of detection procedures' performance. To that end, the ideal would be to have the needed performance metrics expressed exactly and in a closed and simple form. However, this is generally quite difficult mathematically, if at all possible. Part of the reason is that the renewal equations that many popular performance metrics satisfy are Fredholm integral equations of the second kind (possibly written as equivalent differential equations), and such equations seldom allow for an analytical solution. As a result, the standard practice has been to evaluate the performance numerically (one particularly popular approach has been to devise an asymptotic approximation of some sort). Nevertheless, some exact performance formulae have been derived explicitly, although primarily for the "mainstream" detection methods. For instance, a number of characteristics of the celebrated CUSUM "inspection scheme" (due to [13]) have been expressed explicitly, e.g., in [1, 2, 6, 7, 25, 37],[1] although for only a handful of scenarios. Likewise, exact closed-form formulae for various performance metrics of the famous EWMA chart (due to [26]) in an exponential scenario have been established, e.g., in [3, 12, 21] (see footnote 1).

However, the corresponding progress made to date for the classical Shiryaev–Roberts (SR) procedure (due to [27–29]) is far more modest (except for the continuous-time case), and especially little has been done for the Generalized SR (GSR) procedure, which was introduced recently in [11] as a "headstarted" version of the classical SR procedure. Since the latter is a special case of the GSR procedure (when the headstart is zero), from now on we will follow [34] and use the term "GSR procedure" to refer to both procedures. As a matter of fact, to the best of our knowledge, exact and explicit formulae for a small subset of characteristics of the GSR procedure have been obtained only in [4, 9, 10, 14, 22, 23, 35, 40]. The purpose of this work is to add on to this list. Specifically, we obtain an exact, closed-form formula for the standard (minimax) Average Run Length (ARL) to false alarm delivered by the GSR procedure devised to detect a jump in the common baseline mean of a sequence of independent exponentially distributed observations. The formula is found analytically, through direct solution of the respective renewal (integral) equation, and is valid for an arbitrary (nonnegative) headstart, with the detection threshold not restricted from above. Furthermore, the formula is remarkably simple (it is a function linear in the detection threshold and in the headstart) and, unlike its complicated and cumbersome CUSUM and EWMA counterparts, *can* be used to compute the GSR procedure's ARL to false alarm (in the exponential scenario) essentially "*by hand*". This would clearly be of aid to a practitioner.

[1] By no means is this an exhaustive list of available papers on the subject.

7.2 Preliminaries

The centerpiece of this work is the (minimax) Average Run Length (ARL) to false alarm of the Generalized Shiryaev–Roberts (GSR) detection procedure (due to [11]) considered in the context of the basic minimax quickest change-point detection problem (see, e.g., [8, 14]). As a performance metric, the ARL to false alarm was apparently introduced in [13]; see also, e.g., [8].

Let $f_\infty(x)$ and $f_0(x)$ denote, respectively, the observations' pdf in the pre- and post-change regime. Let $\Lambda_n \triangleq f_0(X_n)/f_\infty(X_n)$ be the "instantaneous" likelihood ratio (LR) for the n-th data point, X_n. The GSR procedure (due to [11]) is then formally defined as the stopping time

$$\mathscr{S}_A^r \triangleq \inf\bigl\{n \geq 1 \colon R_n^r \geq A\bigr\}, \quad \text{such that } \inf\{\varnothing\} = \infty, \tag{7.1}$$

where $A > 0$ is a detection threshold used to control the false alarm risk, and

$$R_{n+1}^r = \bigl(1 + R_n^r\bigr)\Lambda_{n+1} \quad \text{for } n = 0, 1, \ldots \text{ with } R_0^r = r \geq 0, \tag{7.2}$$

is the GSR detection statistic. We remark that $R_0^r = r \geq 0$ is a design parameter referred to as the headstart and, in particular, when $R_0^r = r = 0$, the GSR procedure is equivalent to the classical Shiryaev–Roberts (SR) procedure (due to [27–29]); a brief account of the SR procedure's history may be found, e.g., in [16]. Albeit "young" (the GSR procedure was proposed in 2011), it has already been shown (see, e.g., [17, 22, 30, 34, 35]) to possess very strong optimality properties, not exhibited by the CUSUM scheme or the EWMA chart; in fact, in certain scenarios, the latter two charts have been found experimentally to be inferior to the GSR procedure.

Let $\mathbb{P}_\infty$ ($\mathbb{E}_\infty$) be the probability measure (expectation) induced by the observations in the pre-change regime, i.e., when $X_n \propto f_\infty(x)$ for *all* $n \geq 1$. The ARL to false alarm of the GSR procedure is defined as $\mathrm{ARL}(\mathscr{S}_A^r) \triangleq \mathbb{E}_\infty[\mathscr{S}_A^r]$. A key property of the GSR statistic (7.2) is that the sequence $\{R_n^r - n - r\}_{n\geq 0}$ is a zero-mean $\mathbb{P}_\infty$-martingale, i.e., $\mathbb{E}_\infty[R_n^r - n - r] = 0$ for all $n \geq 0$ and all r. This and Doob's Optional stopping (sampling) theorem (see, e.g., [33, Theorem 2.3.1, p. 31]) imply that $\mathbb{E}_\infty[R_{\mathscr{S}_A^r} - \mathscr{S}_A^r - r] = 0$, so that $\mathrm{ARL}(\mathscr{S}_A^r) = \mathbb{E}_\infty[R_{\mathscr{S}_A^r}] - r \geq A - r$. As a result, to ensure that $\mathrm{ARL}(\mathscr{S}_A^r) \geq \gamma$ for a desired $\gamma > 1$, it suffices to pick A and r from the solution set of the inequality $A - r \geq \gamma$ and such that $A > 0$ and $r \geq 0$.

A more accurate result is the approximation $\mathrm{ARL}(\mathscr{S}_A^r) \approx (A/\xi) - r$ valid for sufficiently large $A > 0$; see, e.g., [15, Theorem 1] or [34]. To define ξ, let $S_n \triangleq \sum_{i=1}^n \log \Lambda_n$ for $n \geq 1$, and let $\tau_a \triangleq \inf\{n \geq 1 \colon S_n \geq a\}$ for $a > 0$ (again, with the understanding that $\inf\{\varnothing\} = \infty$). Then $\kappa_a \triangleq S_{\tau_a} - a$ is the so-called "overshoot" (excess over the level $a > 0$ at stopping), and $\xi \triangleq \lim_{a\to\infty} \mathbb{E}_0[e^{-\kappa_a}]$, and is referred to as the "limiting average exponential overshoot"; here $\mathbb{E}_0$ denotes the expectation under the probability measure induced by the observations in the post-change regime, i.e., when $X_n \propto f_0(x)$ for *all* $n \geq 1$. In general, ξ is clearly between 0 and 1, and is a model-dependent constant, which falls within the scope of nonlinear renewal theory; see, e.g., [39], [38, Section II.C] or [33, Section 2.6].

We now state the main equation that we shall deal with (and, in fact, solve analytically) in the next section in a certain exponential scenario. Let $P_\infty^\Lambda(t) \triangleq$

$\mathbb{P}_\infty(\Lambda_1 \le t)$, $t \ge 0$, be the cdf of the LR under probability measure $\mathbb{P}_\infty$. Let $R_0^{r=x} = r = x \ge 0$ be fixed and define

$$\mathscr{K}_\infty(x, y) \triangleq \frac{\partial}{\partial y}\mathbb{P}_\infty\big(R_{n+1}^r \le y \big| R_n^r = x\big) = \frac{\partial}{\partial y} P_\infty^\Lambda\left(\frac{y}{1+x}\right), \quad \text{for } x, y \ge 0, \quad (7.3)$$

i.e., the transition probability density kernel for the homogeneous Markov process $\{R_n^r\}_{n\ge 0}$ under probability measure $\mathbb{P}_\infty$.

From now on, let $\ell(x, A) \triangleq \mathrm{ARL}(\mathscr{S}_A^{r=x})$. It is shown, e.g., in [11], that $\ell(x, A)$ is governed by the renewal equation

$$\ell(x, A) = 1 + \int_0^A \mathscr{K}_\infty(x, y)\ell(y, A)\, dy, \quad (7.4)$$

where $x \ge 0$ and $A > 0$. The question of existence and uniqueness of solution for this equation has been answered in the affirmative, e.g., in [11]. It is this equation, viz. the exact solution thereof in a specific exponential scenario, that is the centerpiece of this work.

Equation (7.4) is a Fredholm (linear) integral equation of the second kind. Since for such equations an analytical solution is rarely a possibility, they are usually solved numerically. Numerical schemes specifically for Eq. (7.4) have been developed and applied, e.g., in [11, 20, 36]. However, it turns out that in a certain exponential scenario it is possible to solve (7.4) analytically, and, more importantly, the solution is a simple linear function of x and A, just as one would expect from the approximation $\mathrm{ARL}(\mathscr{S}_A^r) \approx (A/\xi) - r$ mentioned earlier. This is the main result of this paper, it generalizes [5, Proposition 1], and the details are given in the next section.

7.3 The Main Result

We are now in a position to establish the main result of this work, i.e., derive analytically an exact closed-form formula for the ARL to false alarm exhibited by the GSR procedure (7.1)–(7.2) "tasked" to detect a change in the baseline (common) mean of a series of independent exponentially distributed observations. More concretely, suppose the observations' pre- and post-change pdf's are

$$f_\infty(x) = e^{-x}\mathbb{1}_{\{x\ge 0\}} \quad \text{and} \quad f_0(x) = \frac{1}{1+\theta} e^{-x/(1+\theta)}\mathbb{1}_{\{x\ge 0\}}, \quad (7.5)$$

respectively, where $\theta > 0$, a known parameter with an obvious interpretation: it is the magnitude of the shift in the mean of the exponential distribution, so that the higher (lower) the value of θ, the more (less) contrast the mean shift is, and the easier (harder) it is to detect. We shall from now on refer to this scenario as the $\mathscr{E}(1)$-to-$\mathscr{E}(1+\theta)$ model, to reflect not only the throughout "exponentiality" of the data, but also that their mean is 1 pre-change and $1 + \theta > 1$ post-change. For a motivation to consider this model, see, e.g., [4, 31], or [33, Section 3.1.6].

To "tailor" the general equation (7.4) on the ARL to false alarm to the $\mathscr{E}(1)$-to-$\mathscr{E}(1+\theta)$ model, the first step is to find $\Lambda_n \triangleq f_0(X_n)/f_\infty(X_n)$. To that end, it is easy to see from (7.5) that

$$\Lambda_n = \frac{1}{1+\theta}\exp\left\{\frac{\theta}{1+\theta}X_n\right\}, \quad n \geq 1, \tag{7.6}$$

and we note that since $X_n \geq 0$ w.p. 1 for all $n \geq 1$ under any probability measure, it can be deduced that $\Lambda_n \geq 1/(1+\theta)$ w.p. 1 for all $n \geq 1$, also under any probability measure. The latter inequality is a circumstance with consequences, which are illustrated in the following two results.

Lemma 7.1 *For the $\mathscr{E}(1)$-to-$\mathscr{E}(1+\theta)$ model (7.5), the pre-change transition probability density kernel, $\mathscr{K}_\infty(x, y)$, defined by (7.3), is given by the formula*:

$$\mathscr{K}_\infty(x, y) = \theta^{-1}(1+\theta)^{-1/\theta} y^{-2-1/\theta}(1+x)^{1+1/\theta}\mathbb{1}_{\{y \geq (1+x)/(1+\theta)\}}, \tag{7.7}$$

where it is understood that $x \geq 0$.

Proof The desired result can be established directly from (7.3), i.e., the definition of the pre-change transition probability density kernel, $\mathscr{K}_\infty(x, y)$, combined with (7.6), i.e., the formula for the LR specific to the $\mathscr{E}(1)$-to-$\mathscr{E}(1+\theta)$ model (7.5). The presence of the indicator function in the right-hand side of (7.7) is an implication of the aforementioned inequality $\Lambda_n \geq 1/(1+\theta)$ valid w.p. 1 for all $n \geq 1$ and under any probability measure. □

Now, with (7.7) put in place of $\mathscr{K}_\infty(x, y)$ in the general equation (7.4) the latter takes on the form

$$\ell(x, A) = 1 + \theta^{-1}(1+\theta)^{-1/\theta}(1+x)^{1+1/\theta}\int_{(1+x)/(1+\theta)}^{A} y^{-2-1/\theta}\ell(y, A)\,dy, \tag{7.8}$$

where $x \geq 0$ and $A > 0$, and we recall that $\ell(x, A) \triangleq \mathbb{E}_\infty[\mathscr{S}_A^{r=x}]$. It is this equation that we shall now attempt solve explicitly. To that end, a natural point of departure here would be the aforementioned approximation $\mathrm{ARL}(\mathscr{S}_A^r) \approx (A/\xi) - r$, where ξ is the limiting average exponential overshoot formally defined in the preceding section. It is known (see, e.g., [31]) that $\xi = 1/(1+\theta) \in (0, 1)$ for the $\mathscr{E}(1)$-to-$\mathscr{E}(1+\theta)$ model (7.5). Hence, at least for large enough A's, the solution to (7.8) should behave roughly as $\ell(x, A) \approx A(1+\theta) - x$. As will be shown shortly, this is, in fact, precisely the behavior of the solution, without A having to be large. However, the aforementioned fact that $\Lambda_n \geq 1/(1+\theta)$ w.p. 1 under any measure makes things a bit complicated.

Lemma 7.2 *For the $\mathscr{E}(1)$-to-$\mathscr{E}(1+\theta)$ model (7.5), at each epoch $n \geq 0$ and under any probability measure, the GSR statistic R_n^r has a* deterministic *lower bound, i.e.,*

$R_n^r \geq B_n^r$ *w.p.* 1, *for each* $n \geq 0$ *and under any probability measure, where*

$$B_n^r \triangleq \frac{1}{\theta}\left[1 - \frac{1}{(1+\theta)^n}\right] + \frac{r}{(1+\theta)^n}, \quad n \geq 0, \tag{7.9}$$

and r *is the GSR statistic's headstart, i.e.,* $R_0^r = r \geq 0$.

Proof It is merely a matter of "unfolding" the recursion $R_n^r = (1 + R_{n-1}^r)\Lambda_n$, $n \geq 1$, one term at a time, and applying, at each step, the inequality $\Lambda_n \geq 1/(1+\theta)$ valid w.p. 1 under any probability measure. □

At this point note that since $1 + \theta > 1$, the lower bound sequence $\{B_n^r\}_{n\geq 0}$ given by (7.9) is such that *(a)* for $r \leq 1/\theta$, it increases monotonically with n, i.e., $r \equiv B_0^r \leq B_1^r \leq B_2^r \leq \ldots$, when $r \leq 1/\theta$, and *(b)* $\lim_{n\to\infty} B_n^r = 1/\theta$, irrespective of $R_0^r = r \geq 0$. Hence, when $A < 1/\theta$, the GSR statistic, $\{R_n^r\}_{n\geq 0}$, is guaranteed to either hit or exceed the level $A > 0$ within at most m steps, where $m \equiv m(r, A, \theta)$ is found from the inequality $B_m^r \geq A$, i.e.,

$$m \equiv m(r, A, \theta) \triangleq \begin{cases} \left\lceil \left(\log \frac{1-\theta r}{1-\theta A}\right) / \log(1+\theta) \right\rceil, & \text{for } r < A\ (< 1/\theta); \\ 1, & \text{for } r \geq A, \end{cases}$$

with $\lceil x \rceil$ denoting the usual "ceiling" function. Therefore, the general solution to (7.8) is dependent upon whether $A < 1/\theta$ or $A \geq 1/\theta$. In the latter case, the (exact) solution is given by the following theorem, which is the main result of this paper.

Theorem 7.1 *For the* $\mathscr{E}(1)$*-to-*$\mathscr{E}(1+\theta)$ *model* (7.5), *if the detection threshold,* $A > 0$, *is set so that* $A \geq 1/\theta$, *then the ARL to false alarm of the GSR procedure is given by the formula*:

$$\ell(x, A) = 1 + (1+\theta)\left(A - \frac{1+x}{1+\theta}\right)\mathbb{1}_{\{(1+x)/(1+\theta)\leq A\}}, \tag{7.10}$$

and it is understood that $x \geq 0$.

Proof It is sufficient to insert (7.10) into Eq. (7.8) and directly verify that the latter does, in fact, "check out". The condition that $A \geq 1/\theta$ "protects" against the situation described in Lemma 7.2 and in the discussion following it. □

The special case of Theorem 7.1 when $R_0^{r=x} = r = x \geq 0$ (i.e., when there is no headstart) was previously established in [4, Proposition 1] using the memorylessness of the exponential distribution. It is also noteworthy that formula (7.10) as well as Eq. (7.8) are actually valid for $x \geq -1$; the same can also be said about the general equation (7.4).

We conclude this section with a brief analysis of the case when $A < 1/\theta$. Recall that the integral in the right-hand side of (7.8) plays no role, unless $(1+x)/(1+\theta) < A$. For this condition to hold when $A < 1/\theta$, it must be the case that $(1+x)/(1+\theta) < 1/\theta$, i.e., that $x < 1/\theta$. Hence, if $A < 1/\theta$, then $\ell(x, A) \equiv 1$ for all

$x \geq 1/\theta$. To obtain $\ell(x, A)$ explicitly for $x < 1/\theta$, note that if $x < 1/\theta$, the function $h(x) \triangleq (1 + x)/(1 + \theta)$, i.e., the lower limit of integration in the integral in the right-hand side of (7.8), is such that $h(x) \geq x$. As a result, the nature of the integral equation becomes such that the unknown function, $\ell(x, A)$, is dependent *solely* upon the values it assumes for higher x's, and since $\ell(x, A) \equiv 1$ for $x \geq 1/\theta$, one can iteratively work out backwards the solution for any $x \geq 0$. However, this process involves formidable integrals, and only the first few steps seem to be feasible to actually carry out.

While an explicit formula for the ARL to false alarm of the GSR procedure when $A < 1/\theta$ turned out to be problematic to get, from a practical standpoint it might not be worthwhile altogether, for the formula for $A \geq 1/\theta$ alone, i.e., Theorem 7.1, is sufficient. Specifically, since $\mathrm{ARL}(\mathscr{S}_A^r) \geq A - r$, the formula for the ARL to false alarm when $A > 1/\theta$, i.e., formula (7.10), will never yield ARL's lower than $(1/\theta) - r$. However, the size of this "blind spot" is not necessarily large, unless θ is very small, which is to say that the change in the mean in the $\mathscr{E}(1)$-to-$\mathscr{E}(1 + \theta)$ model (7.5) is faint and not worthy of detection to begin with. As an illustration of this point, consider the original SR procedure ($r = 0$) and suppose that θ is 0.01, which, from a practical standpoint, can hardly be considered a "change" in the first place. Yet, since $1/\theta$ in this case is 100, the linear formula for the ARL to false alarm will never yield a value of 100 or less. However, this is unlikely to be of inconvenience to a practitioner, as in most applications the ARL to false alarm is set to be at least in the hundreds, and, when $\theta = 0.01$, these levels of the ARL to false alarms *would be* obtainable through formula (7.10).

7.4 Concluding Remarks

This contribution is part of the authors' ongoing effort (manifested, e.g., in [19, 20], and, with other collaborators, e.g., in [11, 22, 34, 35]) to "pave the way" for further research on the theory and application of the GSR procedure. To that end, case studies involving "stress-testing" the GSR procedure on real data are still an "uncharted territory" and would be of particular interest. Hopefully, the result obtained in this work, the data-analytic advantages pointed out in [5], and the strong optimality properties established, e.g., in [17, 22, 30, 34, 35], will help the GSR procedure rightly stand out as the top tool for change-point detection.

Acknowledgements The authors would like to thank Prof. Sven Knoth of the Helmut Schmidt University, Hamburg, Germany, and Prof. Ansgar Steland of the RWTH Aachen University, Aachen, Germany, for the invitation to contribute this work to the 12-th German–Polish Workshop on Stochastic Models, Statistics and Their Applications. Constructive feedback provided by Dr. Ron Kenett of Israel-based KPA Ltd. (www.kpa-group.com), by Prof. William H. Woodall of Virginia Polytechnic Institute, Blacksburg, Virginia, USA, and by the two anonymous referees is greatly appreciated as well.

The effort of A.S. Polunchenko was supported, in part, by the Simons Foundation (www.simonsfoundation.org) via a Collaboration Grant in Mathematics (Award # 304574) and by the Research Foundation for the State University of New York at Binghamton via an Interdisciplinary Collaboration Grant (Award # 66761).

Last but not least, A.S. Polunchenko is also indebted to the Office of the Dean of the Harpur College of Arts and Sciences at the State University of New York at Binghamton for the support provided through the Dean's Research Semester Award for Junior Faculty granted for the Fall semester of 2014.

References

1. DeLucia J, Poor HV (1997) Performance analysis of sequential tests between Poisson processes. IEEE Trans Inf Theory 43(1):221–238
2. Gan FF (1992) Exact run length distributions for one-sided exponential CUSUM schemes. Stat Sin 2:297–312
3. Gan FF (1998) Designs of one- and two-sided exponential EWMA charts. J Qual Technol 30(1):55–69
4. Kenett R, Pollak M (1986) A semi-parametric approach to testing for reliability growth, with application to software systems. IEEE Trans Reliab 35(3):304–311
5. Kenett R, Pollak M (1996) Data-analytic aspects of the Shiryaev–Roberts control chart: Surveillance of a non-homogeneous Poisson process. J Appl Stat 23(1):125–138
6. Knoth S (1995) Quasistationäre CUSUM-Verfahren bei Erlangverteilung. Ph.D. thesis, TU. Chemnitz–Zwickau, Germany (in German)
7. Knoth S (1998) Exact average run lengths of CUSUM schemes for Erlang distributions. Seq Anal 17(2):173–184
8. Lorden G (1971) Procedures for reacting to a change in distribution. Ann Math Stat 42(6):1897–1908
9. Mei Y (2006) Comments on "A note on optimal detection of a change in distribution," by Benjamin Yakir. Ann Stat 34(3):1570–1576
10. Mevorach Y, Pollak M (1991) A small sample size comparison of the CUSUM and Shiryaev–Roberts approaches to changepoint detection. Am J Math Manag Sci 11(3&4):277–298
11. Moustakides GV, Polunchenko AS, Tartakovsky AG (2011) A numerical approach to performance analysis of quickest change-point detection procedures. Stat Sin 21(2):571–596
12. Novikov A (1990) On the first exit time of an autoregressive process beyond a level and an application to the "disorder" problem. Theory Probab Appl 35(2):269–279
13. Page ES (1954) Continuous inspection schemes. Biometrika 41(1&2):100–115
14. Pollak M (1985) Optimal detection of a change in distribution. Ann Stat 13(1):206–222
15. Pollak M (1987) Average run lengths of an optimal method of detecting a change in distribution. Ann Stat 15(2):749–779
16. Pollak M (2009) The Shiryaev–Roberts changepoint detection procedure in retrospect—Theory and practice. In: Proceedings of the 2nd International Workshop on Sequential Methodologies, University of Technology of Troyes, Troyes, France
17. Pollak M, Tartakovsky AG (2009) Optimality properties of the Shiryaev–Roberts procedure. Stat Sin 19:1729–1739
18. Polunchenko AS, Sokolov G, Du W (2013) Quickest change-point detection: A bird's eye view. In: Proceedings of the 2013 Joint Statistical Meetings, Montréal, Québec, Canada
19. Polunchenko AS, Sokolov G, Du W (2014) Efficient performance evaluation of the Generalized Shiryaev–Roberts detection procedure in a multi-cyclic setup. Appl Stoch Models Bus Ind 30(6):723–739
20. Polunchenko AS, Sokolov G, Du W (2014) An accurate method for determining the pre-change run-length distribution of the Generalized Shiryaev–Roberts detection procedure. Seq Anal 33(1):112–134
21. Polunchenko AS, Sokolov G, Tartakovsky AG (2014) Optimal design and analysis of the Exponentially Weighted Moving Average chart for exponential data. Sri Lankan J Appl Statist. doi:10.4038/sljastats.v5i4.7784

22. Polunchenko AS, Tartakovsky AG (2010) On optimality of the Shiryaev–Roberts procedure for detecting a change in distribution. Ann Stat 38(6):3445–3457
23. Polunchenko AS, Tartakovsky AG (2012) State-of-the-art in sequential change-point detection. Methodol Comput Appl Probab 44(3):649–684
24. Poor HV, Hadjiliadis O (2009) Quickest detection. Cambridge University Press, New York
25. Regula G (1975) Optimal CUSUM procedure to detect a change in distribution for the Gamma family. Ph.D. thesis, Case Western University, Cleveland, OH
26. Roberts SW (1959) Control chart tests based on geometric moving averages. Technometrics 1(3):239–250
27. Roberts SW (1966) A comparison of some control chart procedures. Technometrics 8(3):411–430
28. Shiryaev AN (1961) The problem of the most rapid detection of a disturbance in a stationary process. Sov Math Dokl 2:795–799
29. Shiryaev AN (1963) On optimum methods in quickest detection problems. Theory Probab Appl 8(1):22–46
30. Shiryaev AN, Zryumov PY (2009) On the linear and nonlinear generalized Bayesian disorder problem (discrete time case). In: Delbaen F, Rásonyi M, Stricker Ch (eds) Optimality and risk—Modern trends in mathematical finance. The Kabanov Festschrift. Springer, Berlin, pp 227–235
31. Tartakovsky AG, Ivanova IV (1992) Comparison of some sequential rules for detecting changes in distributions. Probl Inf Transm 28(2):117–124
32. Tartakovsky AG, Moustakides GV (2010) State-of-the-art in Bayesian changepoint detection. Seq Anal 29(2):125–145
33. Tartakovsky A, Nikiforov I, Basseville M (2014) Sequential analysis: Hypothesis testing and changepoint detection. CRC Press, Boca Raton
34. Tartakovsky AG, Pollak M, Polunchenko AS (2012) Third-order asymptotic optimality of the Generalized Shiryaev–Roberts changepoint detection procedure. Theory Probab Appl 56(3):457–484
35. Tartakovsky AG, Polunchenko AS (2010) Minimax optimality the Shiryaev–Roberts procedure. In: Proceedings of the 5th International Workshop in Applied Probability, Universidad Carlos III de Madrid, Colmenarejo Campus, Spain
36. Tartakovsky AG, Polunchenko AS, Moustakides GV (2009) Design and comparison of Shiryaev–Roberts- and CUSUM-type change-point detection procedures. In: Proceedings of the 2nd International Workshop on Sequential Methodologies, University of Technology of Troyes, Troyes, France
37. Vardeman S, Ray D (1985) Average run lengths for CUSUM schemes when observations are exponentially distributed. Technometrics 27(2):145–150
38. Veeravalli VV, Banerjee T (2013) Quickest change detection. In: Chellappa R, Theodoridis S (eds) Academic press library in signal processing: Array and statistical signal processing, vol 3. Academic Press, Oxford, pp 209–256
39. Woodroofe M (1982) Nonlinear renewal theory in sequential analysis. SIAM, Philadelphia
40. Yakir B (1997) A note on optimal detection of a change in distribution. Ann Stat 25(5):2117–2126

Chapter 8
Adaptive Density Estimation from Data Containing Bounded Measurement Errors

Tina Felber, Michael Kohler, and Adam Krzyżak

Abstract We consider the problem of density estimation using noisy data containing small measurement errors. The only assumption on these errors is that the maximal measurement error is bounded by some real number converging to zero for sample size tending to infinity. We estimate the density by a standard kernel density estimate applied to the noisy data and propose data-dependent method for choosing its bandwidth. We derive an adaptation result for this estimate and analyze the expected L1 error of our density estimate depending on the smoothness of the density and the size of the maximal measurement error.

8.1 Introduction

Let X be a real-valued random variable with distribution μ and let $\mathscr{B}$ be the sigma field of all Borel sets on the real line. We are interested in estimating μ from a sample $X_1, \ldots, X_n$ of X, i.e., from data

$$\mathscr{D}_n = \{X_1, \ldots, X_n\},$$

where X, X_1, X_2, ... are independent and identically distributed random variables.

It was shown in Devroye and Györfi [9], that no estimate $\hat{\mu}_n = \hat{\mu}_n(\cdot, \mathscr{D}_n)$ exists which can estimate μ consistently for all distributions, i.e., no estimate satisfies

$$\sup_{B \in \mathscr{B}} \left| \hat{\mu}_n(B) - \mu(B) \right| \to 0 \quad \text{a.s.} \quad (n \to \infty) \tag{8.1}$$

T. Felber (✉) · M. Kohler
Fachbereich Mathematik, Technische Universität Darmstadt, Schlossgartenstr. 7, 64289 Darmstadt, Germany
e-mail: tfelber@mathematik.tu-darmstadt.de

M. Kohler
e-mail: kohler@mathematik.tu-darmstadt.de

A. Krzyżak (✉)
Department of Computer Science and Software Engineering, Concordia University, 1455 De Maisonneuve Blvd. West, Montreal, Quebec, Canada H3G 1M8
e-mail: krzyzak@cs.concordia.ca

A. Steland et al. (eds.), *Stochastic Models, Statistics and Their Applications*, Springer Proceedings in Mathematics & Statistics 122,
DOI 10.1007/978-3-319-13881-7_8

for all distributions. However, it is possible to construct a consistent density estimate if a density f of X exists, i.e., if μ is given by

$$\mu(B) = \int_B f(x)\,dx \quad (B \in \mathscr{B}),$$

then we can construct a density estimate which satisfies (8.1) for all distributions or we can estimate f by $f_n(\cdot) = f_n(\cdot, \mathscr{D}_n)$ which is a density satisfying

$$\int \left| f_n(x) - f(x) \right| dx \to 0 \quad \text{a.s.} \quad (n \to \infty) \tag{8.2}$$

for all densities f.

In particular one can estimate f from $\mathscr{D}_n$ by a kernel density estimate

$$f_n(x) = \frac{1}{n \cdot h_n} \sum_{i=1}^{n} K\left(\frac{x - X_i}{h_n} \right) \tag{8.3}$$

(cf., Rosenblatt [18] and Parzen [15]) with a kernel K $K : \mathbb{R} \to \mathbb{R}$ which is a density itself (e.g., the naive kernel $K = \frac{1}{2} \cdot I_{[-1,1]}$) and a bandwidth $h_n > 0$. If h_n satisfies

$$h_n \to 0 \quad (n \to \infty) \quad \text{and} \quad n \cdot h_n \to \infty \quad (n \to \infty) \tag{8.4}$$

then the estimate f_n is universally consistent, i.e.,

$$\int_{\mathbb{R}} \left| f_n(x) - f(x) \right| dx \to 0 \quad \text{a.s.} \quad (n \to \infty)$$

for all densities f see, e.g., Mnatsakanov and Khmaladze [14], Devroye [5] and the books on density estimation by Devroye and Györfi [8], Devroye [7] and Devroye and Lugosi [10].

Regarding the rate of convergence it is well-known, that without imposing smoothness conditions on f the rate of convergence of the L_1 error of any estimate may be arbitrarily slow (cf., e.g., Devroye [6] or Theorem 2, p. 256 in Devroye and Györfi [8]).

One can show the optimal minimax rate of convergence

$$\mathbf{E} \int_{\mathbb{R}} \left| f_n(x) - f(x) \right| dx \le c_2 \cdot n^{-\frac{r}{2 \cdot r + 1}}, \tag{8.5}$$

for kernel density estimate f_n with naive kernel and bandwidth $h_n = c_1 \cdot n^{-\frac{1}{2 \cdot r + 1}}$ under the conditions that the distribution of X has compact support and f is Hölder continuous with exponent $r \in (0, 1]$ and Hölder constant C, i.e.,

$$\left| f(x) - f(z) \right| \le C \cdot |x - z|^r \quad \text{for all } x, z \in \mathbb{R}$$

(cf., e.g., Devroye and Lugosi [10], Ex. 15.14).

The optimal bandwidth depends on the smoothness of the density measured above by exponent r, which in practice is typically unknown. One solution is to construct adaptive kernel estimates with a bandwidth $\hat{h} = \hat{h}(\mathscr{D}_n)$ satisfying

$$\mathbf{E}\int_{\mathbb{R}}\left|f_{n,\hat{h}}(x)-f(x)\right|dx \le c_3\cdot\min_h \mathbf{E}\int_{\mathbb{R}}\left|f_{n,h}(x)-f(x)\right|dx+\varepsilon_n \tag{8.6}$$

for some constant $c_3 > 0$ and some ε_n converging to zero faster than the expected L_1 error of the kernel density estimate with the optimal bandwidth. Devroye and Lugosi [10] suggested an adaptive choice of the bandwidths by so-called Yatracos combinatorial method, see Yatracos [20]. For this choice they proved that inequality (8.6) holds with c_3 arbitrarily close to 3 and $\varepsilon_n = \log(n)/\sqrt{n}$ (cf., Theorem 11.1 in Devroye and Lugosi [10]).

In this paper we assume that instead of accurate data $\mathscr{D}_n$ we have data

$$\bar{\mathscr{D}}_n = \{\bar{X}_{1,n},\dots,\bar{X}_{n,n}\},$$

containing measurement errors. We assume that the measurement errors $\bar{X}_{i,n} - X_i$ are small in some sense (see Eq. (8.9) below). Such problems were studied by several authors. In Rafajłowicz [17] the errors are due to grouping of observations and in Pawlak and Stadtmüller [16] are due to grouping and jitter. The cases of round-off errors in data were investigated by Delattre and Jacod [4] and micro-structure noise which was attenuated by partial means was investigated in Ait-Sahalia, Mykland and Zhang [1], Schmisser [19] and Comte, Genon-Catalot and Samson [3]. In general, very little is assumed about these errors. The errors do not need to be independent or identically distributed, they do not need to have expectation zero, the noise density does not need to be known, or it may not be possible to estimate such a density, so estimates for convolution problems (see, e.g., Meister [13] and the literature cited therein) are not applicable in the context of this paper. Note also that our set-up is triangular, i.e., for sample size n we do not observe the first n observations of one given sequence of observations with measurement errors, instead for each sample size the complete sequence is allowed to be changed.

Suppose that there exists an upper bound on the average measurement error

$$\frac{1}{n}\sum_{i=1}^{n}|\bar{X}_{i,n}-X_i|.$$

Then we can ignore the errors completely and we can estimate f by the standard kernel density estimate

$$g_n(x) = g_{n,h_n}(x) = \frac{1}{n\cdot h_n}\sum_{i=1}^{n} K\left(\frac{x-\bar{X}_{i,n}}{h_n}\right). \tag{8.7}$$

Since for the naive kernel K we have

$$\int_{\mathbb{R}}\left|K\left(\frac{x-u}{h}\right)-K\left(\frac{x-v}{h}\right)\right|dx \le \min\{2h,|u-v|\} \quad (u,v\in\mathbb{R},h>0)$$

it follows that for naive kernel K we have

$$\int_{\mathbb{R}}\left|g_n(x)-f_n(x)\right|dx \le \frac{1}{n\cdot h_n}\sum_{i=1}^{n}|\bar{X}_{i,n}-X_i|. \tag{8.8}$$

Consequently it is straightforward to derive consistency and rate of convergence results for g_n from the corresponding results for f_n (cf., e.g., Theorem 2 in Bott, Devroye and Kohler [2] and Theorem 1 in Felber, Kohler and Krzyżak [11]). However, it is not clear how to estimate the bandwidth in a data-driven way given only data with measurement errors.

In Felber, Kohler and Krzyżak [11] it was assumed that an additional sample from X was available and it was used to estimate the distribution of X by its empirical distribution. Then the combinatorial method of Devroye and Lugosi [10] was used to choose the bandwidth of a kernel density estimate adaptively using real and artificial data. For this estimate it was possible to show an adaptation result with error term of order $\sqrt{\log(n)/n}$, where n was the size of the sample of X, however due to this error term it was not possible to achieve the rates of convergence for the L_1 error of the density estimate faster than $1/\sqrt{n}$. In this paper we assume that we have a huge sample of data with additional small measurement errors available (and we will see that in this case (8.5) is no longer the optimal rate of convergence), and we show that if these additional measurement errors are small enough, we can achieve faster L_1 rates of convergence than $1/\sqrt{n}$.

We achieve that by the combinatorial method of Devroye and Lugosi [10] assuming that the data contains additional small measurement errors, i.e., we estimate the distribution of X by the empirical measure of the sample with additional measurement errors and analyze how this effects the error bound of the method. The main result states that for data satisfying the deterministic upper bound δ_n on the measurement errors, i.e.,

$$\max_{i=1,\dots,n} |\bar{X}_{i,n} - X_i| \le \delta_n, \tag{8.9}$$

the error of the density estimate with the corresponding adaptive bandwidth $\hat{h} = \hat{h}(\bar{\mathcal{D}}_n) \in \mathcal{P}_n$ satisfies

$$\begin{aligned} &\mathbf{E} \int_{\mathbb{R}} \left| g_{n_l,\hat{h}}(x) - f(x) \right| dx \\ &\quad \le 3 \cdot \min_{h \in \mathcal{P}_n} \mathbf{E} \int_{\mathbb{R}} \left| g_{n_l,h}(x) - f(x) \right| dx + c_4 \cdot \log(n)/\sqrt{n_t} + c_5 \cdot n_l \cdot \delta_n \end{aligned} \tag{8.10}$$

whenever the density f is bounded, where $n_l + n_t = n$.

Throughout the paper we use the following notation: The sets of natural numbers, non-negative real numbers and real numbers are denoted by $\mathbb{N}$, $\mathbb{R}_+$ and $\mathbb{R}$, respectively. Let $D \subseteq \mathbb{R}^d$ and let $h : \mathbb{R}^d \to \mathbb{R}$ be a real-valued function defined on $\mathbb{R}^d$. We write $x = \arg\max_{z \in D} h(z)$ if $\max_{z \in \mathcal{D}} h(z)$ exists and if x satisfies

$$x \in D \quad \text{and} \quad h(x) = \max_{z \in \mathcal{D}} h(z).$$

For $h : \mathbb{R}^d \to \mathbb{R}$

$$\|h\|_\infty = \sup_{x \in \mathbb{R}^d} \left| h(x) \right|$$

is its supremum norm, and the supremum norm of h on a set $A \subseteq \mathbb{R}^d$ is denoted by

$$\|h\|_{\infty,A} = \sup_{x \in A} \big|h(x)\big|$$

The support of a probability measure μ defined on the Borel sets in $\mathbb{R}^d$ is abbreviated by

$$supp(\mu) = \big\{x \in \mathbb{R}^d \colon\ \mu\big(S_r(x)\big) > 0 \text{ for all } r > 0\big\},$$

where $S_r(x)$ is the ball of radius r around x. The indicator function of a set A is denoted by I_A.

In the next section we will present the main result.

8.2 Main Result

The combinatorial approach to adaptive choice of bandwidth is based on Scheffé's Lemma (cf., e.g., Devroye and Györfi [8]) stating that L_1 error of an arbitrary density estimate $f_{n,h}$ is given by

$$\begin{aligned}\int_{\mathbb{R}} \big|f_{n,h}(x) - f(x)\big|\,dx &= 2 \cdot \left(\int_{[f_{n,h} > f]} f_{n,h}(x)\,dx - \int_{[f_{n,h} > f]} f(x)\,dx\right) \\ &= 2 \cdot \sup_{B \in \mathscr{B}} \left|\int_B f_{n,h}(x)\,dx - \int_B f(x)\,dx\right|,\end{aligned}$$

where

$$[f_{n,h} > f] = \big\{x \in \mathbb{R} \colon\ f_{n,h}(x) > f(x)\big\}.$$

Since

$$\int_B f(x)\,dx = \mathbf{P}_X(B)$$

is unknown the main idea of the combinatorial method of Devroye and Lugosi [10] is to estimate $\mathbf{P}_X(B)$ by an empirical measure μ_n based on a sample of X, to consider the sets of the form

$$\mathscr{A} = \big\{[f_{n,h_1} > f_{n,h_2}] \colon\ h_1, h_2 > 0\big\}$$

and to choose the bandwidth by minimizing the following expression

$$\sup_{A \in \mathscr{A}} \left|\int_A f_{n,h}(x)\,dx - \mu_n(A)\right|$$

with respect to h. Due to technical reasons a sample splitting is used, i.e., the density estimate is computed with the first part of a sample of X and the empirical measure is based only on the second part of this sample.

In our problem we cannot compute the empirical measure μ_n, since a sample of X is not available. The idea is to use instead our sample with small measurement errors to compute a corresponding empirical measure and to analyze the influence of

these additional small measurement errors on the above bandwidth selection problem.

We start by splitting our sample with additional small measurement errors in two parts of size n_l and n_t, resp., where $n_l + n_t = n$. We use the first part to define kernel density estimates via

$$g_{n_l,h}(x) = \frac{1}{n_l \cdot h} \sum_{i=1}^{n_l} K\left(\frac{x - \bar{X}_{i,n}}{h}\right),$$

and use the second part to define a corresponding empirical measure by

$$\hat{\mu}_{n_t}(A) = \frac{1}{n_t} \sum_{i=n_l+1}^{n} I_A(\bar{X}_{i,n}).$$

Next we choose a finite set of bandwidths $\mathscr{P}_n \subseteq (0, \infty)$ from which we want to select the best one, and set

$$\mathscr{A}_n = \left\{[g_{n_l,h_1} > g_{n_l,h_2}]\colon\ h_1, h_2 \in \mathscr{P}_n, h_1 \neq h_2\right\}.$$

Then we define our data-driven choice of the bandwidth by minimizing

$$\Delta_n(h) = \sup_{A \in \mathscr{A}_n} \left| \int_A g_{n_l,h}(x)\, dx - \hat{\mu}_{n_t}(A) \right|$$

with respect to $h \in \mathscr{P}_n$, i.e., we set

$$\hat{h}_n = \hat{h}_n(\bar{\mathscr{D}}_n) = \arg\min_{h \in \mathscr{P}_n} \Delta_n(h).$$

Here the minimum above indeed exists since the set $\mathscr{P}_n$ is finite. Our main result is the following bound on the L_1 error of $g_{n_l,\hat{h}_n}$.

Theorem 8.1 *Let $X, X_1, X_2, \ldots$ be independent and identically distributed random variables with density f. For $n \in \mathbb{N}$ let $\bar{X}_{1,n}, \ldots, \bar{X}_{n,n}$ be arbitrary random variables satisfying*

$$\max_{i=1,\ldots,n} |\bar{X}_{i,n} - X_i| \leq \delta_n$$

for some $\delta_n \in \mathbb{R}_+$. Let $n_l = n_l(n), n_t = n_t(n) \in \mathbb{N}$ be such that $n_l + n_t = n$. Let K be the naive kernel, let $\mathscr{P}_n \subseteq (\delta_n, \infty)$ be a finite set, and define $g_{n_l,h}$ and $\hat{h}_n$ as above. Then the following bounds on the expected L_1 error of $g_{n_l,\hat{h}_n}$ hold:

(a) *If the density f of X is bounded, then bound (8.10) holds.*
(b) *If the density f of X satisfies*

$$\int_{\mathbb{R}} f(x)^2 dx < \infty,$$

then

$$\mathbf{E}\int \left|g_{n_l,\hat{h}_n}(x) - f(x)\right| dx$$
$$\leq 3 \cdot \min_{h \in \mathscr{D}_n} \mathbf{E}\int \left|g_{n_l,h}(x) - f(x)\right| dx + c_8 \cdot \sqrt{\frac{\log n}{n_t}} + c_9 \cdot \sqrt{n_l \cdot \delta_n}.$$

By using (8.8) we can relate the L_1 error of our density estimate to the best L_1 error of a kernel density estimate based on a sample from X without additional measurement errors. The proof of Theorem 8.1 and further details concerning applications of the proposed approach to the simulation model can be found in Felber, Kohler and Krzyżak [12].

Acknowledgements The first two authors would like to thank the German Research Foundation (DFG) for funding this project within the Collaborative Research Centre 805 and the last author acknowledges research support from the Natural Sciences and Engineering Research Council of Canada.

References

1. Ait-Sahalia Y, Mykland PA, Zahng L (2011) Ultra high frequency volatility estimation with dependent microstructure noise. J Econom 160:160–175
2. Bott A-K, Devroye L, Kohler M (2013) Estimation of a distribution from data with small measurement errors. Electron J Stat 7:2457–2476
3. Comte F, Genon-Catalot V, Samson A (2013) Nonparametric estimation for stochastic differential equations with random effects. Stoch Process Appl 123:2522–2551
4. Delattre S, Jacod J (1997) A central limit theorem for normalized functions of the increments of a diffusion process, in the presence of round-off errors. Bernoulli 3:1–28
5. Devroye L (1983) The equivalence in L1 of weak, strong and complete convergence of kernel density estimates. Ann Stat 11:896–904
6. Devroye L (1983) On arbitrarily slow rates of global convergence in density estimation. Z Wahrscheinlichkeitstheor Verw Geb 62:475–483
7. Devroye L (1987) A course in density estimation. Birkhäuser, Basel
8. Devroye L, Györfi L (1985) Nonparametric density estimation. The L1 view. Wiley series in probability and mathematical statistics: tracts on probability and statistics. Wiley, New York
9. Devroye L, Györfi L (1990) No empirical probability measure can converge in the total variation sense for all distributions. Ann Stat 18:1496–1499
10. Devroye L, Lugosi G (2001) Combinatorial methods in density estimation. Springer, New York
11. Felber T, Kohler M, Krzyżak A (2014) Adaptive density estimation based on real and artificial data. J Nonparametric Stat. doi:10.1080/10485252.2014.969729
12. Felber T, Kohler M, Krzyżak A (2014) Adaptive density estimation from data with small measurement errors. Unpublished manuscript. http://www3.mathematik.tu-darmstadt.de/hp/stochastik-homepages/kohler-michael/publikationen.html
13. Meister A (2009) Deconvolution problems in nonparametric statistics. Lecture notes in statistics, vol 193. Springer, Berlin
14. Mnatsakanov RM, Khmaladze EV (1981) On L_1-convergence of statistical kernel estimators of distribution densities. Sov Math Dokl 23:633–636
15. Parzen E (1962) On the estimation of a probability density function and the mode. Ann Math Stat 33:1065–1076

16. Pawlak M, Stadtmüller U (2001) Statistical aspects of sampling for noisy and grouped data. In: Modern sampling theory. Birkhäuser, Boston, pp 317–342
17. Rafajłowicz E (1997) Consistency of orthogonal series density estimators based on grouped observations. IEEE Trans Inf Theory 43:283–285
18. Rosenblatt M (1956) Remarks on some nonparametric estimates of a density function. Ann Math Stat 27:832–837
19. Schmisser E (2011) Non-parametric drift estimation for diffusions from noisy data. Stat Decis 28:119–150
20. Yatracos YG (1985) Rates of convergence of minimum distance estimators and Kolmogorov's entropy. Ann Stat 13:768–774

Chapter 9
Poisson Model with Three Binary Predictors: When are Saturated Designs Optimal?

Ulrike Graßhoff, Heinz Holling, and Rainer Schwabe

Abstract In this paper, Poisson regression models with three binary predictors are considered. These models are applied to rule-based tasks in educational and psychological testing. To efficiently estimate the parameters of these models locally D-optimal designs will be derived. Eight out of all 70 possible saturated designs are proved to be locally D-optimal in the case of active effects. Two further saturated designs which are the classical fractional factorial designs turn out to be locally D-optimal for vanishing effects.

9.1 Introduction

Many educational and psychological tests, e.g. measuring human abilites, yield count data. Usually, such tests contain items with different difficulties. The difficulties are often determined by certain binary characteristics or rules of the items. In many cases the data of such tests are distributed according to a Poisson distribution. Thus, a Poisson regression model with binary explanatory variables is the adequate statistical model to describe the data of such tests.

Such a Poisson regression model can be considered as a particular case of a generalized linear model with canonical exponential link. This facilitates the calculation of the likelihood and of the information matrix. The latter may serve as a characteristic of the quality of a design, i.e. for the choice of the explanatory variables in

U. Graßhoff
School of Business and Economics, Humboldt University, Unter den Linden 6, 10 099 Berlin, Germany
e-mail: grasshou@hu-berlin.de

H. Holling (✉)
Institute of Psychology, University of Münster, Fliednerstr. 21, 48 149 Münster, Germany
e-mail: holling@uni-muenster.de

R. Schwabe
Institute for Mathematical Stochastics, Otto-von-Guericke University, PF 4120, 39 016 Magdeburg, Germany
e-mail: rainer.schwabe@ovgu.de

A. Steland et al. (eds.), *Stochastic Models, Statistics and Their Applications*,
Springer Proceedings in Mathematics & Statistics 122,
DOI 10.1007/978-3-319-13881-7_9

experimental settings, because the asymptotic covariance matrix of the maximum likelihood estimator is proportional to the inverse of the information matrix.

For continuous predictors optimal designs have been derived by Rodríguez-Torreblanca and Rodríguez-Díaz [5] for one explanatory variable and by Russell et al. [6] in the case of additive linear effects of the explanatory variables in the linear predictor. Wang et al. [8] derived numerical results, when there is an additional interaction term which describes a synergetic or antagonistic effect. As in all underlying models which are non-linear in their parameters the optimal designs may depend on the true parameter values, which results in the determination of locally optimal designs.

In the case of two binary explanatory variables Graßhoff et al. [2] characterize optimal designs, when there are additive effects. A similar result has been obtained by Yang et al. [9] for binary response. For count data this result is extended in Graßhoff et al. [3] to an arbitrary number K of explanatory variables. In particular they established that certain saturated designs are optimal, when the effect sizes are sufficiently large.

Since saturated designs result in experiments which can be performed quite easily, the natural question arises, which saturated designs may be optimal and under which parameter constellations. In the present note we will show that in the case of $K = 3$ binary predictors only that particular class of saturated designs described in Graßhoff et al. [3] may be optimal—with the only exceptional situation of vanishing effect sizes, where a 2^{3-1} fractional factorial design is optimal. All other saturated designs cannot be locally optimal under any parameter settings.

9.2 Model Description, Information and Design

For each observation of counts the response variable Y is assumed to follow a Poisson distribution $\mathrm{Po}(\lambda)$ with intensity $\lambda = \lambda(\mathbf{x}; \boldsymbol{\beta})$, which depends on the experimental settings $\mathbf{x}$ of the explanatory variables and a parameter vector $\boldsymbol{\beta}$ of interest describing the effects of these explanatory variables. Under the exponential link this dependence is specified by $\lambda(\mathbf{x}; \boldsymbol{\beta}) = \exp(\mathbf{f}(\mathbf{x})^\top \boldsymbol{\beta})$, where $\mathbf{f}$ is a vector of known regression functions.

In the present setting of binary explanatory variables we code these by a base level $x_k = 0$ and an active level $x_k = 1$ for each variable x_k. Here we focus on $K = 3$ predictors with additive effects, hence $\mathbf{x} = (x_1, x_2, x_3) \in \{0, 1\}^3$ and the regression function is $\mathbf{f}(\mathbf{x}) = (1, x_1, x_2, x_3)^\top$. Then the intensity decomposes according to $\lambda(\mathbf{x}; \boldsymbol{\beta}) = \exp(\beta_0 + \beta_1 x_1 + \beta_2 x_2 + \beta_3 x_3)$. The parameter vector $\boldsymbol{\beta} = (\beta_0, \ldots, \beta_3)^\top$ has $p = 4$ components, where β_0 is a baseline parameter and β_k is the effect of the kth explanatory variable which results in a relative change of intensity by the factor $\exp(\beta_k)$, when the kth variable is active.

In the present situation of a generalized linear model with canonical link the Fisher information of a single observation equals $\mathbf{M}(\mathbf{x}; \boldsymbol{\beta}) = \lambda(\mathbf{x}; \boldsymbol{\beta}) \mathbf{f}(\mathbf{x}) \mathbf{f}(\mathbf{x})^\top$, which depends on the setting $\mathbf{x}$ and additionally on $\boldsymbol{\beta}$ through the intensity. Under the assumption of independent observations the normalized information matrix

is defined by $\mathbf{M}(\xi;\boldsymbol{\beta}) = \frac{1}{N}\sum_{i=1}^{N}\mathbf{M}(\mathbf{x}_i;\boldsymbol{\beta})$ for an exact design ξ consisting of N design points $\mathbf{x}_1,\ldots,\mathbf{x}_N$.

For analytical purposes we will make use of the concept of approximate designs ξ with mutually different design points $\mathbf{x}_1,\ldots,\mathbf{x}_n$, say, and corresponding (real valued) weights $w_i = \xi(\mathbf{x}_i) \geq 0$ with $\sum_{i=1}^{n} w_i = 1$ in the spirit of Kiefer [4]. For such an approximate design the information matrix is more generally defined as $\mathbf{M}(\xi;\boldsymbol{\beta}) = \sum_{i=1}^{n} w_i \lambda(\mathbf{x}_i;\boldsymbol{\beta})\mathbf{f}(\mathbf{x}_i)\mathbf{f}(\mathbf{x}_i)^\top$.

As common in generalized linear models the information matrix and, hence, optimal designs will depend on the parameter vector $\boldsymbol{\beta}$. For measuring the quality of a design we will use the popular D-criterion. More precisely, a design ξ will be called locally D-optimal at $\boldsymbol{\beta}$ if it maximizes the determinant of the information matrix $\mathbf{M}(\xi;\boldsymbol{\beta})$.

For the present Poisson model the intensity and, hence, the information is proportional to the baseline intensity $\exp(\beta_0)$, i.e. $\mathbf{M}(\xi;\boldsymbol{\beta}) = \exp(\beta_0)\mathbf{M}_0(\xi;\boldsymbol{\beta})$, where $\mathbf{M}_0(\xi;\boldsymbol{\beta})$ is the information matrix in the standardized situation when $\beta_0 = 0$. Thus design optimization does not depend on β_0, and $\det(\mathbf{M}_0(\xi;\boldsymbol{\beta}))$ has to be maximized only in dependence on β_1, β_2 and β_3, which means that we can assume the standardized case ($\beta_0 = 0$) in the following.

9.3 Saturated Designs

A design is called saturated, if the number n of distinct design points is equal to the number of parameters ($n = p$). For saturated designs it is well-known that the D-optimal weights are uniform ($w_i = 1/p$). Hence, optimization in the class of saturated designs has only to be done with respect to the choice of the settings $\mathbf{x}_1,\ldots,\mathbf{x}_p$.

In the present situation the dimension is $p = 4$, and we want to characterize which of the saturated designs can be optimal, i.e. which choice $\mathbf{x}_{i_1},\ldots,\mathbf{x}_{i_4}$ of four out of the eight possible settings $\mathbf{x}_0,\ldots,\mathbf{x}_7 \in \{0,1\}^3$ results in a locally D-optimal design for any parameter constellation $\boldsymbol{\beta}$. For notational reasons we enumerate the possible settings $\mathbf{x}_i = (x_{i1}, x_{i2}, x_{i3})$ according to the reversed binary number representation $i = \sum_{k=1}^{3} x_{ik}2^{k-1}$ for the index i by their components x_{ik}. This means for example $\mathbf{x}_0 = (0,0,0)$, $\mathbf{x}_4 = (0,0,1)$ and $\mathbf{x}_7 = (1,1,1)$. We can visualize these eight design points as the vertices of a three dimensional cube with edge length 1 placed in the first octant (see Fig. 9.1). Further we denote by $\lambda_i = \lambda(\mathbf{x}_i;\boldsymbol{\beta})$ the intensities of the eight possible settings.

In total, there are $\binom{8}{4} = 70$ different saturated designs with uniform weights. Denote by $\mathscr{I} = \{i_1,\ldots,i_4\}$ the index set of settings in such a saturated design and by $\xi_{\mathscr{I}}$ the design itself.

First of all we can exclude 12 of the 70 saturated designs, for which the design points are located on a plane, i.e. a two-dimensional affine subspace, and which, hence, result in a singular information matrix with determinant equal to zero. These excluded designs consist of the six faces of the cube, for example

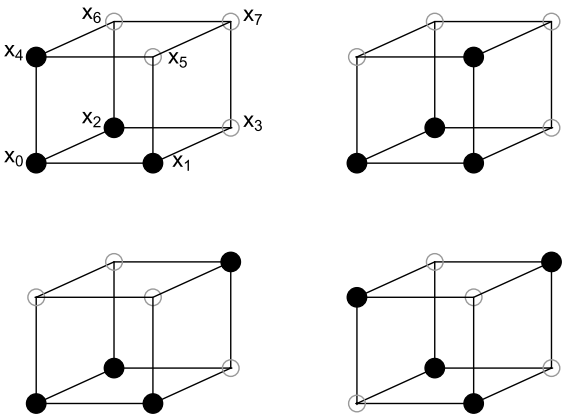

Fig. 9.1 The four relevant types of saturated designs on $\mathscr{X} = \{0, 1\}^3$

$\mathscr{I} = \{0, 1, 4, 5\}$, and the six diagonal planes connecting two opposite edges, for example $\mathscr{I} = \{0, 1, 6, 7\}$.

The remaining 58 designs can be assigned to four different equivalence classes with respect to permutations of the levels $\{0, 1\}$ for each explanatory variable x_k and among the explanatory variables $k = 1, 2, 3$ themselves. For each of these equivalence classes a representative is exhibited in Fig. 9.1.

The eight saturated designs in the first class (represented in the upper left panel of Fig. 9.1) can be characterized by a vertex $\mathbf{x} = (x_1, x_2, x_3)$ as follows: These "tripod-type" designs contain $\mathbf{x}$ as a central vertex ("head") and additionally all three adjacent vertices ("legs") $(1 - x_1, x_2, x_3)$, $(x_1, 1 - x_2, x_3)$ and $(x_1, x_2, 1 - x_3)$, respectively, as settings and will be denoted by $\xi_{\mathbf{x}}$. For example, the design $\xi_{\mathbf{0}}$ is exhibited in the upper left panel of Fig. 9.1 and is described by the index set $\mathscr{I} = \{0, 1, 2, 4\}$. In Graßhoff et al. [3] it is shown that the saturated design $\xi_{\mathbf{0}}$ is optimal when all effect sizes are negative and their modulus is sufficiently large. Using symmetry considerations the latter condition can be extended to all "tripod-type" designs $\xi_{\mathbf{x}}$, when the appropriate "head" $\mathbf{x} = (x_1, x_2, x_3)$ is chosen for which $x_k = 0$, when β_k is negative, and $x_k = 1$, when β_k is positive. In particular, this means that $\mathbf{x}$ is the setting with the highest intensity $(\lambda(\mathbf{x}; \boldsymbol{\beta}) = \max_{i=0,\ldots,7} \lambda_i)$.

The second class are "snake-type" designs represented in the upper right panel of Fig. 9.1, where the four settings are located on a linear graph not contained in a plane. By symmetry there are 24 saturated designs of that type, and a representative is shown in Fig. 9.1 for $\mathscr{I} = \{0, 1, 2, 5\}$. In the third class the saturated designs consist of three settings on one of the faces of the cube and the isolated opposite vertex as the fourth setting. Also in this class there are 24 different designs, which are equivalent with respect to symmetries. One representative is exhibited in the lower left panel of Fig. 9.1 with $\mathscr{I} = \{0, 1, 2, 7\}$. Saturated designs of these two types can never be locally D-optimal, as will be proved in the subsequent section.

The last two saturated designs are the classical fractional factorial designs. One of these is reported in the lower right panel of Fig. 9.1, where $\mathscr{I} = \{1, 2, 4, 7\}$. The other fractional factorial design is supported by the complementary four design points ($\mathscr{I} = \{0, 3, 5, 6\}$). These fractional factorial designs are well-known to be

D-optimal in the corresponding linear model ($\mathrm{E}(Y(\mathbf{x})) = \beta_0 + \beta_1 x_1 + \beta_2 x_2 + \beta_3 x_3$) with three binary predictors and no interaction. In the case of no active effects, $\beta_1 = \beta_2 = \beta_3 = 0$, the information matrix of the present Poisson count model turns out to be proportional to that in the linear model for any design ξ. Hence, the fractional factorial designs can be seen to be locally D-optimal in the Poisson model for vanishing effects ($\beta_k = 0$) of the predictors. For all other parameter constellations the fractional factorial cannot be locally D-optimal, as will be indicated in the next section.

9.4 Proofs of Non-optimality

Due to symmetry considerations it suffices to show that the representatives given in the previous section cannot be locally D-optimal for any parameter value $\boldsymbol{\beta}$. To do so we will make use of the celebrated Kiefer–Wolfowitz equivalence theorem (see Silvey [7]) in the version of Fedorov [1] which incorporates explicitly an intensity function λ.

Denote by $\psi_{\boldsymbol{\beta}}(\mathbf{x}; \xi) = \lambda(\mathbf{x}; \boldsymbol{\beta}) \mathbf{f}(\mathbf{x})^\top \mathbf{M}(\xi; \boldsymbol{\beta})^{-1} \mathbf{f}(\mathbf{x})$ the sensitivity function for a design ξ given $\boldsymbol{\beta}$. Then the equivalence theorem states that the design ξ is locally D-optimal at $\boldsymbol{\beta}$ if and only if $\psi_{\boldsymbol{\beta}}(\mathbf{x}; \xi) \le p$ for all possible settings $\mathbf{x}$. Note that, in general, for a saturated design equality is attained, $\psi_{\boldsymbol{\beta}}(\mathbf{x}; \xi) = p$, on its support points $\mathbf{x}_{i_1}, \ldots, \mathbf{x}_{i_p}$. Hence, the inequality has only to be checked for the remaining settings $\mathbf{x} \neq \mathbf{x}_{i_1}, \ldots, \mathbf{x}_{i_p}$. In the following we will suppress the dependence on the parameter vector $\boldsymbol{\beta}$ to facilitate the notation.

For a saturated design $\xi_{\mathscr{J}}$ the information matrix $\mathbf{M}(\xi_{\mathscr{J}}) = \frac{1}{p} \mathbf{F}_{\mathscr{J}}^\top \boldsymbol{\Lambda}_{\mathscr{J}} \mathbf{F}_{\mathscr{J}}$ can be decomposed into a product of the essential design matrix $\mathbf{F}_{\mathscr{J}} = (\mathbf{f}(\mathbf{x}_{i_1}), \ldots, \mathbf{f}(\mathbf{x}_{i_p}))^\top$ and the diagonal matrix $\boldsymbol{\Lambda}_{\mathscr{J}} = \mathrm{diag}(\lambda(\mathbf{x}_{i_1}), \ldots, \lambda(\mathbf{x}_{i_p}))$ of corresponding intensities. Note that these matrices are $p \times p$ square matrices and can be individually inverted. Because of $\mathbf{M}(\xi_{\mathscr{J}})^{-1} = p \mathbf{F}_{\mathscr{J}}^{-1} \boldsymbol{\Lambda}_{\mathscr{J}}^{-1} \mathbf{F}_{\mathscr{J}}^{-\top}$ the sensitivity function simplifies, and the condition of the equivalence theorem reduces to

$$\frac{1}{p} \psi(\mathbf{x}_i; \xi_{\mathscr{J}}) = \lambda(\mathbf{x}_i) \big(\mathbf{F}_{\mathscr{J}}^{-\top} \mathbf{f}(\mathbf{x}_i) \big)^\top \boldsymbol{\Lambda}_{\mathscr{J}}^{-1} \big(\mathbf{F}_{\mathscr{J}}^{-\top} \mathbf{f}(\mathbf{x}_i) \big) \le 1$$

for all $i \notin \mathscr{J}$, where $\mathbf{F}^{-\top}$ denotes the inverse of the transpose of $\mathbf{F}$.

For the present situation we recall that $p = 4$ and $\lambda(\mathbf{x}_i) = \lambda_i$, where $\lambda_0 = 1$, $\lambda_3 = \lambda_1 \lambda_2$, $\lambda_5 = \lambda_1 \lambda_4$, $\lambda_6 = \lambda_2 \lambda_4$ and $\lambda_7 = \lambda_1 \lambda_2 \lambda_4$.

Now for the "snake-type" design we consider the representative $\xi_{\mathscr{J}}$ of Fig. 9.1 specified by $\mathscr{J} = \{0, 1, 2, 5\}$. For this design the essential design matrix and its inverse are given by

$$\mathbf{F}_{\mathscr{J}} = \begin{pmatrix} 1 & 0 & 0 & 0 \\ 1 & 1 & 0 & 0 \\ 1 & 0 & 1 & 0 \\ 1 & 1 & 0 & 1 \end{pmatrix} \quad \text{and} \quad \mathbf{F}_{\mathscr{J}}^{-1} = \begin{pmatrix} 1 & 0 & 0 & 0 \\ -1 & 1 & 0 & 0 \\ -1 & 0 & 1 & 0 \\ 0 & -1 & 0 & 1 \end{pmatrix}.$$

Then $\mathbf{F}_{\mathscr{J}}^{-\top}\mathbf{f}(\mathbf{x}) = (1 - x_1 - x_2, x_1 - x_3, x_2, x_3)^\top$, and the conditions of the equivalence theorem become

$$\lambda(\mathbf{x})\big((1 - x_1 - x_2)^2 + (x_1 - x_3)^2/\lambda_1 + x_2^2/\lambda_2 + x_3^2/\lambda_5\big) \le 1.$$

In the case $\mathbf{x}_3 = (1, 1, 0)$ this condition reduces to $\lambda_1\lambda_2 + \lambda_1 + \lambda_2 \le 1$, and in the case $\mathbf{x}_4 = (0, 0, 1)$ the condition is equivalent to $\lambda_1\lambda_4 + \lambda_4 + 1 \le \lambda_1$. This leads to a contradiction, because these conditions require $\lambda_1 < 1$ for $\mathbf{x}_3$ and $\lambda_1 > 1$ for $\mathbf{x}_4$, respectively. Consequently there exists no $\boldsymbol{\beta}$ for which the "snake-type" saturated design $\xi_{\mathscr{J}}$ can be locally D-optimal.

Similarly, for the designs with an isolated setting we consider the representative $\xi_{\mathscr{J}}$ of Fig. 9.1 specified by $\mathscr{J} = \{0, 1, 2, 7\}$. The essential design matrix and its inverse are

$$\mathbf{F}_{\mathscr{J}} = \begin{pmatrix} 1 & 0 & 0 & 0 \\ 1 & 1 & 0 & 0 \\ 1 & 0 & 1 & 0 \\ 1 & 1 & 1 & 1 \end{pmatrix} \quad \text{and} \quad \mathbf{F}_{\mathscr{J}}^{-1} = \begin{pmatrix} 1 & 0 & 0 & 0 \\ -1 & 1 & 0 & 0 \\ -1 & 0 & 1 & 0 \\ 1 & -1 & -1 & 1 \end{pmatrix}.$$

Then $\mathbf{F}_{\mathscr{J}}^{-\top}\mathbf{f}(\mathbf{x}) = (1 - x_1 - x_2 + x_3, x_1 - x_3, x_2 - x_3, x_3)^\top$, and the conditions of the equivalence theorem become

$$\lambda(\mathbf{x})\big((1 - x_1 - x_2 + x_3)^2 + (x_1 - x_3)^2/\lambda_1 + (x_2 - x_3)^2/\lambda_2 + x_3^2/\lambda_7\big) \le 1.$$

In the case $\mathbf{x}_3 = (1, 1, 0)$ this condition reduces again to $\lambda_1\lambda_2 + \lambda_1 + \lambda_2 \le 1$, and in the case $\mathbf{x}_5 = (1, 0, 1)$ the condition is equivalent to $\lambda_1\lambda_2\lambda_4 + \lambda_1\lambda_4 + 1 \le \lambda_2$. This leads to a contradiction, because these conditions require $\lambda_2 < 1$ for $\mathbf{x}_3$ and $\lambda_2 > 1$ for $\mathbf{x}_5$, respectively. Consequently there exists no $\boldsymbol{\beta}$ for which the saturated design $\xi_{\mathscr{J}}$ with an isolated setting can be locally D-optimal.

Finally, the fractional factorial design $\xi_{\mathscr{J}}$ of Fig. 9.1 is specified by $\mathscr{J} = \{1, 2, 4, 7\}$, and the essential design matrix and its inverse are

$$\mathbf{F}_{\mathscr{J}} = \begin{pmatrix} 1 & 1 & 0 & 0 \\ 1 & 0 & 1 & 0 \\ 1 & 0 & 0 & 1 \\ 1 & 1 & 1 & 1 \end{pmatrix} \quad \text{and} \quad \mathbf{F}_{\mathscr{J}}^{-1} = \frac{1}{2}\begin{pmatrix} 1 & 1 & 1 & -1 \\ 1 & -1 & -1 & 1 \\ -1 & 1 & -1 & 1 \\ -1 & -1 & 1 & 1 \end{pmatrix}.$$

For $i = 0, 3, 5$, and 6 the conditions of the equivalence theorem are equivalent to

$$\lambda_i(\lambda_2\lambda_4 + \lambda_1\lambda_4 + \lambda_1\lambda_2 + 1) \le 4\lambda_1\lambda_2\lambda_4.$$

For $i = 3$ this condition reduces to $\lambda_2\lambda_4 + \lambda_1\lambda_4 + \lambda_1\lambda_2 + 1 \le 4\lambda_4$, which requires $\lambda_4 > 1/4$. If we rearrange this inequality to $\lambda_2(\lambda_4 + \lambda_1) \le 4\lambda_4 - \lambda_1\lambda_4 - 1$. The right hand side provides an upper bound $\lambda_1 < (4\lambda_4 - 1)/\lambda_4$ for λ_1. Similarly, if we rearrange the condition for $i = 0$, then $\lambda_1\lambda_4 + 1 \le \lambda_2(4\lambda_1\lambda_4 - \lambda_1 - \lambda_4)$ provides a lower bound $\lambda_1 > \lambda_4/(4\lambda_4 - 1)$. These two bounds can only be satisfied simultaneously if $\lambda_4 > 1/3$.

Moreover, the above conditions yield the following inequalities

$$\frac{\lambda_1\lambda_4+1}{4\lambda_1\lambda_4-\lambda_1-\lambda_4} \le \lambda_2 \le \frac{4\lambda_4-\lambda_1\lambda_4-1}{\lambda_1+\lambda_4},$$

which cannot be satisfied simultaneously if $1/3 < \lambda_4 < 1$.

Analogously, from the conditions for $i = 5$ and 6, respectively, we obtain the inequality $1/(4-\lambda_4) < 4-\lambda_4$, which requires $\lambda_4 < 3$, and

$$\frac{\lambda_1\lambda_4+1}{4-\lambda_1-\lambda_4} \le \frac{4\lambda_1-\lambda_1\lambda_4-1}{\lambda_1+\lambda_4}.$$

This inequality cannot be satisfied for $1 < \lambda_4 < 3$. Hence, local D-optimality can only be achieved, when $\lambda_4 = 1$, i.e. $\beta_3 = 0$.

Symmetry considerations lead to the same result for λ_1 and λ_2. As a consequence fractional factorial designs are locally D-optimal only if $\beta_1 = \beta_2 = \beta_3 = 0$.

Acknowledgements This work was partly supported by grant Ho1286-6 of the Deutsche Forschungsgemeinschaft.

References

1. Fedorov VV (1972) Theory of optimal experiments. Academic Press, New York
2. Graßhoff U, Holling H, Schwabe R (2013) Optimal design for count data with binary predictors in item response theory. In: Uciński D, Atkinson AC, Patan M (eds) mODa10 — advances in model-oriented design and analysis. Springer, Cham, pp 117–124
3. Graßhoff U, Holling H, Schwabe R (2014) Optimal design for the rasch Poisson counts model with multiple binary predictors. Technical report
4. Kiefer J (1974) General equivalence theory for optimum designs (approximate theory). Ann Stat 2:849–879
5. Rodríguez-Torreblanca C, Rodríguez-Díaz JM (2007) Locally D- and c-optimal designs for Poisson and negative binomial regression models. Metrika 66:161–172
6. Russell K, Woods D, Lewis S, Ecclestone J (2009) D-optimal designs for Poisson regression models. Stat Sin 19:721–730
7. Silvey D (1980) Optimal design. Chapman & Hall, London
8. Wang Y, Myers RH, Smith EP, Ye K (2006) D-optimal designs for Poisson regression models. J Stat Plan Inference 136:2831–2845
9. Yang J, Mandal A, Majumdar D (2012) Optimal designs for two-level factorial experiments with binary response. Stat Sin 22:885–907

Chapter 10
Computing D-Optimal Experimental Designs for Estimating Treatment Contrasts Under the Presence of a Nuisance Time Trend

Radoslav Harman and Guillaume Sagnol

Abstract We prove a mathematical programming characterization of approximate partial D-optimality under general linear constraints. We use this characterization with a branch-and-bound method to compute a list of all exact D-optimal designs for estimating a pair of treatment contrasts in the presence of a nuisance time trend up to the size of 24 consecutive trials.

10.1 Introduction

Consider the linear regression model $Y = \mathbf{F}\beta + \varepsilon$, where $Y = (Y_1, \ldots, Y_n)^T$ is a vector of observations, $\beta \in \mathbb{R}^m$ is an unknown parameter, $\mathbf{F} = (\mathbf{f}(x_1), \ldots, \mathbf{f}(x_n))^T$ is an $n \times m$ design matrix, and $\varepsilon = (\varepsilon_1, \ldots, \varepsilon_n)^T$ is a vector of random errors with $E(\varepsilon) = \mathbf{0}_n$, $Var(\varepsilon) = \sigma^2\mathbf{I}_n$, $\sigma^2 \in (0, \infty)$. Suppose that the function $\mathbf{f}: \mathfrak{X} \to \mathbb{R}^m$, where $\mathfrak{X}$ is a finite design space, is known and fixed, but the design points $x_1, \ldots, x_n$ can be chosen in $\mathfrak{X}$ according to the objective of the experiment, see, e.g., [2, 6, 8].

A typical objective is to estimate a linear parameter subsystem $\mathbf{A}^T\beta$, where $\mathbf{A}$ is a full-rank $m \times s$ matrix, $s \leq m$. It is a well-known fact that an unbiased linear estimator of $\mathbf{A}^T\beta$ exists if and only if the estimability condition $\mathscr{C}(\mathbf{A}) \subseteq \mathscr{C}(\mathbf{M})$ is satisfied, where $\mathbf{M} = \mathbf{F}^T\mathbf{F}$ is the moment matrix and $\mathscr{C}$ denotes the linear space generated by the columns of a matrix. In this case, the best linear unbiased estimator of $\mathbf{A}^T\beta$ is $\hat{\beta}_{\mathbf{A}} = \mathbf{A}^T\mathbf{M}^-\mathbf{F}^TY$, and the estimator does not depend on the choice of the generalized inverse $\mathbf{M}^-$. Moreover, $Var(\hat{\beta}_{\mathbf{A}}) = \sigma^2\mathbf{A}^T\mathbf{M}^-\mathbf{A}$ is non-singular.

Let $\mathbf{N}_{\mathbf{A}}(\mathbf{M}) = \min_{\mathbf{L}} \mathbf{L}\mathbf{M}\mathbf{L}^T$, where the minimum is taken on the set of all $s \times m$ matrices $\mathbf{L}$ such that $\mathbf{L}\mathbf{A} = \mathbf{I}_s$, with respect to the Loewner ordering $\preceq$ (for symmetric $s \times s$ matrices $\mathbf{N}_1, \mathbf{N}_2$ we define $\mathbf{N}_1 \preceq \mathbf{N}_2$ iff $\mathbf{N}_2 - \mathbf{N}_1$ is non-negative definite). The matrix $\mathbf{N}_{\mathbf{A}}(\mathbf{M})$ can be interpreted as the amount of information that the

R. Harman (✉)
Faculty of Mathematics, Physics and Informatics, Comenius University, Mlynská dolina, 84248 Bratislava, Slovakia
e-mail: harman@fmph.uniba.sk

G. Sagnol
Dept. Optimization, Zuse Institut Berlin, Takustr. 7, 14195 Berlin, Germany
e-mail: sagnol@zib.de

A. Steland et al. (eds.), *Stochastic Models, Statistics and Their Applications*, Springer Proceedings in Mathematics & Statistics 122,
DOI 10.1007/978-3-319-13881-7_10

experiment conveys about $\mathbf{A}^T\beta$, see [8, Chapter 3]. Hence, $\mathbf{N}_\mathbf{A}(\mathbf{M})$ is called the information matrix for $\mathbf{A}^T\beta$. The information matrix is non-singular if and only if the estimability condition is satisfied, in which case $\mathbf{N}_\mathbf{A}(\mathbf{M}) = (\mathbf{A}^T\mathbf{M}^-\mathbf{A})^{-1}$. For estimating the entire parameter β, we have $\mathbf{N}_{\mathbf{I}_m}(\mathbf{M}) = \mathbf{M}$.

To measure the quality of estimation of $\mathbf{A}^T\beta$, we will use the criterion of D-optimality defined by $\Phi(\mathbf{N}) = (\det(\mathbf{N}))^{1/s}$ for $\mathbf{N} \in \mathscr{S}_+^s$, where $\mathscr{S}_+^s$ is the set of all non-negative definite $s \times s$ matrices. Note that Φ is concave, continuous, positive homogeneous and Loewner-isotonic on $\mathscr{S}_+^s$, i.e., it is an information function [8, Chapter 5]. The composition $\Phi(\mathbf{N}_\mathbf{A}(\cdot)) : \mathscr{S}_+^m \to [0, \infty)$ is again an information function, and it is called the criterion of partial D-optimality, or $D_\mathbf{A}$-optimality (e.g., [6, Section IV.3] and [2, Section 10.2]). Explicitly, the criterion of $D_\mathbf{A}$-optimality is $\Phi_\mathbf{A}(\mathbf{M}) = (\det(\mathbf{A}^T\mathbf{M}^-\mathbf{A}))^{-1/s}$ if $\mathscr{C}(\mathbf{A}) \subseteq \mathscr{C}(\mathbf{M})$ and $\Phi_\mathbf{A}(\mathbf{M}) = 0$ otherwise.

Since the moment matrix $\mathbf{M} = \sum_i \mathbf{f}(x_i)\mathbf{f}^T(x_i)$ does not depend on the order of $x_1, \ldots, x_n$, we can represent an exact experimental design by a function $\xi : \mathfrak{X} \to \{0, 1, 2, \ldots\}$ such that $\xi(x)$ means the number of trials to be performed in $x \in \mathfrak{X}$. We will denote the set of all exact designs by Ξ^E. Note that the moment matrix corresponding to $\xi \in \Xi^E$ can be written as $\mathbf{M} = \mathbf{M}(\xi) = \sum_{x\in\mathfrak{X}} \xi(x)\mathbf{f}(x)\mathbf{f}^T(x)$.

An approximate experimental design is *any* function $\xi : \mathfrak{X} \to [0, \infty)$, which we understand as a relaxation of an exact design. The set of all approximate designs will be denoted by Ξ^A. The moment matrix $\mathbf{M}(\xi)$ of any $\xi \in \Xi^A$ is defined by the same formula as for the exact designs. For all $\xi \in \Xi^A$, let $\mathbf{N}_\mathbf{A}(\xi) := \mathbf{N}_\mathbf{A}(\mathbf{M}(\xi))$.

The usual constraint on an experimental design is that we are given a required size n of the experiment, i.e., we restrict the search to the designs ξ satisfying $\sum_{x\in\mathfrak{X}} \xi(x) = n$. Such designs will be called size-n-constrained. However, in practice the designs must often satisfy additional constraints, which can represent restrictions on the experimental budget and the availability of material, see, e.g., [3]. Moreover, the ability to compute approximate optimal designs under more general constraints may be used as a key component of algorithms for computing optimal exact designs, such as the branch-and-bound (BNB) method that we propose in Sect. 10.3.1.

In this paper, we will consider general linear constraints of the form

$$\sum_{x\in\mathfrak{X}} c(j, x)\xi(x) \le b(j) \quad \text{for all } j = 1, \ldots, k, \tag{10.1}$$

where $c : \{1, \ldots, k\} \times \mathfrak{X} \to \mathbb{R}$ and $b : \{1, \ldots, k\} \to \mathbb{R}$. Given any fixed ordering on $\mathfrak{X}$, the coefficient $c(j, x)$ can be arranged to a matrix $\mathbf{C}$ of type $k \times |\mathfrak{X}|$ and $b(j)$ can be arranged to a vector $\mathbf{b}$ of length k. Note that each design can be represented by an $|\mathfrak{X}|$-dimensional vector with non-negative components. Accordingly, Ξ^E corresponds to $\{0, 1, 2, \ldots\}^{|\mathfrak{X}|}$ and Ξ^A corresponds to $[0, \infty)^{|\mathfrak{X}|}$.

The designs satisfying (10.1) will be called $(\mathbf{C}, \mathbf{b})$-designs. We will assume that there exists at least one exact $(\mathbf{C}, \mathbf{b})$-design ξ, such that $\mathbf{A}^T\beta$ is estimable under ξ, and the set of all approximate $(\mathbf{C}, \mathbf{b})$-designs is bounded. The sets of all exact and approximate $(\mathbf{C}, \mathbf{b})$-designs will be denoted by $\Xi^E_{\mathbf{C},\mathbf{b}}$ and $\Xi^A_{\mathbf{C},\mathbf{b}}$ respectively. Evidently, $\Xi^E_{\mathbf{C},\mathbf{b}} = \Xi^A_{\mathbf{C},\mathbf{b}} \cap \mathbb{Z}^{|\mathfrak{X}|}$ is a finite subset of the compact and convex set $\Xi^A_{\mathbf{C},\mathbf{b}}$.

Let ξ_E^* be an exact $(\mathbf{C}, \mathbf{b})$-design, $\mathbf{A}^T\beta$ be estimable under ξ_E^* and $\Phi(\mathbf{N}_\mathbf{A}(\xi_E^*)) = \sup\{\Phi(\mathbf{N}_\mathbf{A}(\xi_E))\colon\ \xi_E \in \tilde{\Xi}^E_{\mathbf{C},\mathbf{b}}\}$, where $\tilde{\Xi}^E_{\mathbf{C},\mathbf{b}} := \{\xi_E \in \Xi^E_{\mathbf{C},\mathbf{b}}\colon\ \mathscr{C}(\mathbf{A}) \subseteq \mathscr{C}(\mathbf{M}(\xi_E))\}$. We will call ξ_E^* a $D_\mathbf{A}$-optimal exact $(\mathbf{C}, \mathbf{b})$-design. Analogously, we define a $D_\mathbf{A}$-optimal approximate $(\mathbf{C}, \mathbf{b})$-design and the symbol $\tilde{\Xi}^A_{\mathbf{C},\mathbf{b}}$. Compactness of $\Xi^A_{\mathbf{C},\mathbf{b}} \neq \emptyset$ and the continuity of $\Phi_\mathbf{A}$ imply the existence of a $D_\mathbf{A}$-optimal approximate $(\mathbf{C}, \mathbf{b})$-design ξ_A^*. The value $\Phi(\mathbf{N}_\mathbf{A}(\xi_A^*))$ will be called the $D_\mathbf{A}$-optimal value of $\Xi^A_{\mathbf{C},\mathbf{b}}$.

Computing $D_\mathbf{A}$-optimal approximate designs is a problem of convex optimization. The size-n-constrained $D_\mathbf{A}$-optimal approximate designs can be computed, to any given precision, by a Fedorov–Wynn vertex direction algorithm or by a multiplicative algorithm (e.g., [15]). However, it is difficult to use the classical algorithms to compute $D_\mathbf{A}$-optimal approximate designs under multiple linear constraints (cf. [3]). In this paper, we show that the problem of $D_\mathbf{A}$-optimal approximate designs under (10.1) can be cast as a max-det programming problem [13], which can be efficiently solved by readily available software.

Computing $D_\mathbf{A}$-optimal exact designs with constraints is in general a challenging problem of discrete optimization. To find the provably $D_\mathbf{A}$-optimal exact designs in small to medium-size problems, it is possible to use the complete enumeration of all permissible designs, or more efficient enumeration methods. For instance, in [14] a BNB method is used for computing $D_{\mathbf{I}_m}$-optimal exact size-n-constrained designs and in [11] a BNB method is used to compute $D_{\mathbf{I}_m}$-optimal exact directly constrained designs. In this paper, we propose a specific BNB algorithm for computing $D_\mathbf{A}$-optimal exact designs for the estimation of a set of treatment contrasts.

For large problems it is unrealistic to expect a rapid algorithm that always provides perfectly $D_\mathbf{A}$-optimal exact designs. To find an efficient size-n-constrained exact design, it is possible to use an exchange heuristic, cf. [2, Chapter 12].

10.2 A Mathematical Programming Characterization of $D_\mathbf{A}$-Optimal Constrained Approximate Designs

The following lemma is a simple consequence of the Schur complement characterization of positive semidefinite matrices (e.g. [8, Section 3.12]). Recently, this lemma has also been used to compute the support points of optimal designs [7, Section 6]. The symbol $\mathscr{S}^s_{++}$ denotes the set of all positive definite $s \times s$ matrices.

Lemma 10.1 *Let* $\mathbf{A}$ *be an* $m \times s$ *matrix of full rank,* $m \geq s$*, let* $\mathbf{M} \in \mathscr{S}^m_+$*, and let* $\mathbf{N} \in \mathscr{S}^s_{++}$*. Then the following two statements are equivalent*: (*i*) $\mathscr{C}(\mathbf{A}) \subseteq \mathscr{C}(\mathbf{M})$ *and* $\mathbf{N} \preceq (\mathbf{A}^T\mathbf{M}^-\mathbf{A})^{-1}$ *for any*[1] *generalized inverse* $\mathbf{M}^-$ *of* $\mathbf{M}$; (*ii*) $\mathbf{ANA}^T \preceq \mathbf{M}$.

Let $\mathscr{I} = \{\mathbf{N} \in \mathscr{S}^s_{++}\colon\ \mathbf{N} = (\mathbf{A}^T\mathbf{M}(\xi)^-\mathbf{A})^{-1}$ for some $\xi \in \tilde{\Xi}^A_{\mathbf{C},\mathbf{b}}\}$ and let $\tilde{\mathscr{I}} = \{\tilde{\mathbf{N}} \in \mathscr{S}^s_{++}\colon\ \mathbf{A}\tilde{\mathbf{N}}\mathbf{A}^T \preceq \mathbf{M}(\xi)$ for some $\xi \in \Xi^A_{\mathbf{C},\mathbf{b}}\}$.

[1] If $\mathscr{C}(\mathbf{A}) \subseteq \mathscr{C}(\mathbf{M})$, then $\mathbf{A}^T\mathbf{M}^-\mathbf{A}$ does not depend on the choice of the generalized inverse of $\mathbf{M}$.

Lemma 10.2 *$\mathscr{I} \subseteq \tilde{\mathscr{I}}$ and for each $\tilde{\mathbf{N}} \in \tilde{\mathscr{I}}$ there is some $\mathbf{N} \in \mathscr{I}$ such that $\tilde{\mathbf{N}} \preceq \mathbf{N}$.*

Proof If $\mathbf{N} \in \mathscr{I}$ then, trivially, condition (i) of Lemma 10.1 is satisfied for some $\mathbf{M} = \mathbf{M}(\xi)$ such that $\xi \in \Xi^A_{\mathbf{C},\mathbf{b}}$. Hence, the part (ii) of Lemma 10.1 holds, i.e., $\mathbf{A}\mathbf{N}\mathbf{A}^T \preceq \mathbf{M}$, which implies $\mathbf{N} \in \tilde{\mathscr{I}}$. Thus $\mathscr{I} \subseteq \tilde{\mathscr{I}}$. Let $\tilde{\mathbf{N}} \in \tilde{\mathscr{I}}$ and let $\mathbf{M} = \mathbf{M}(\xi)$, $\xi \in \Xi^A_{\mathbf{C},\mathbf{b}}$, be such that $\mathbf{A}\tilde{\mathbf{N}}\mathbf{A}^T \preceq \mathbf{M}$. Note that by Lemma 10.1 we have $\mathscr{C}(\mathbf{A}) \subseteq \mathscr{C}(\mathbf{M})$, i.e., we can set $\mathbf{N} = (\mathbf{A}^T\mathbf{M}^-\mathbf{A})^{-1} \in \mathscr{S}^s_{++}$. Hence, also by Lemma 10.1, we have $\tilde{\mathbf{N}} \preceq (\mathbf{A}^T\mathbf{M}^-\mathbf{A})^{-1} = \mathbf{N}$, which was to be proved. □

Theorem 10.1 (i) *The set of information matrices of all $D_{\mathbf{A}}$-optimal approximate $(\mathbf{C}, \mathbf{b})$-designs is identical to the set of all solutions $\mathbf{N}^*$ of the problem*

$$\max \Phi(\mathbf{N}) \quad \text{s.t. } \mathbf{N} \in \mathscr{S}^s_{++},\ \mathbf{A}\mathbf{N}\mathbf{A}^T \preceq \mathbf{M}(\xi),\ \xi \in \Xi^A_{\mathbf{C},\mathbf{b}}. \tag{10.2}$$

(ii) *If $\mathbf{N}^*$ is any solution of (10.2), and $\xi^* \in \Xi^A_{\mathbf{C},\mathbf{b}}$ is any design satisfying $\mathbf{A}\mathbf{N}^*\mathbf{A}^T \preceq \mathbf{M}(\xi^*)$, then ξ^* is a $D_{\mathbf{A}}$-optimal approximate $(\mathbf{C}, \mathbf{b})$-design.*

Proof (i) As $\Phi : \mathscr{S}^s_+ \to [0, \infty)$ vanishes on $\mathscr{S}^s_+ \setminus \mathscr{S}^s_{++}$ and is positive on $\mathscr{S}^s_{++}$, the set of information matrices of all $D_{\mathbf{A}}$-optimal approximate $(\mathbf{C}, \mathbf{b})$-designs is the set of all solutions of the problem $\max \Phi(\mathbf{N})$ s.t. $\mathbf{N} \in \mathscr{I}$. Moreover, note that Φ is strictly Loewner isotonic in the sense that if $\tilde{\mathbf{N}}, \mathbf{N} \in \mathscr{S}^s_{++}$ satisfy $\tilde{\mathbf{N}} \preceq \mathbf{N}$ and $\tilde{\mathbf{N}} \neq \mathbf{N}$, then $\Phi(\tilde{\mathbf{N}}) < \Phi(\mathbf{N})$. Therefore, we see from Lemma 10.2 that the set of information matrices of all $D_{\mathbf{A}}$-optimal approximate $(\mathbf{C}, \mathbf{b})$-designs is equal to the set of all solutions of the problem $\max \Phi(\tilde{\mathbf{N}})$ s.t. $\tilde{\mathbf{N}} \in \tilde{\mathscr{I}}$.

(ii) Let $\mathbf{N}^*$ be any solution of (10.2), and let $\xi^* \in \Xi^A_{\mathbf{C},\mathbf{b}}$ satisfy $\mathbf{A}\mathbf{N}^*\mathbf{A}^T \preceq \mathbf{M}(\xi^*)$. By Lemma 10.1 we have $\mathscr{C}(\mathbf{A}) \subseteq \mathscr{C}(\mathbf{M}(\xi^*))$ and $\mathbf{N}^* \preceq (\mathbf{A}^T\mathbf{M}^-(\xi^*)\mathbf{A})^{-1} = \mathbf{N}_{\mathbf{A}}(\xi^*)$. Since $\mathbf{N}_{\mathbf{A}}(\xi^*)$ satisfies the constraints in (10.2) (cf. Sect. 3.14 in [8]), and since Φ is Loewner isotonic, we conclude that $\Phi(\mathbf{N}_{\mathbf{A}}(\xi^*)) \leq \Phi(\mathbf{N}^*) \leq \Phi(\mathbf{N}_{\mathbf{A}}(\xi^*))$. □

By Theorem 10.1, computing $D_{\mathbf{A}}$-optimal approximate $(\mathbf{C}, \mathbf{b})$-designs can be cast as a problem of max-det programming, see [13]. A similar result appeared in [5, Section V.E] (with a different max-det formulation), for the case of a Bayesian framework with a prior density $\beta \sim \mathcal{N}(0, \Sigma)$. Max-det programs can be automatically reformulated as semidefinite programs (SDPs) by user-friendly interfaces such as PICOS [10]. SDPs is a class of optimization problems that are efficiently solvable by algorithms implemented in freely available software, for instance CVXOPT [12].

It is also worth mentioning that in the proof of Theorem 10.1 we did not use specific properties of D-optimality, except for the fact that Φ is a strictly Loewner isotonic information function vanishing on singular information matrices. Hence, we can use Theorem 10.1 also with many other criteria.

10.3 $D_{\mathbf{A}}$-Optimal Designs for Estimating a Set of Contrasts of Treatment Effects Under the Presence of a Time Trend

Suppose that we intend to perform n trials in a time sequence. For each trial $t \in \{1, \dots, n\}$ we select a treatment $u(t) \in \{1, \dots, v\}$, $v \geq 2$, with its effect $\tau_{u(t)} \in \mathbb{R}$. In addition to the treatment effects, the mean value of the response may depend on a nuisance time trend, which can be approximated by a polynomial of degree d. Hence, a natural model for the responses is

$$Y_t = \tau_{u(t)} + \theta_1 p_0(t) + \cdots + \theta_{d+1} p_d(t) + \varepsilon_t; \quad t = 1, \dots, n, \tag{10.3}$$

where $\theta_1, \dots, \theta_{d+1}$ are the parameters of the trend, $p_0, \dots, p_d$ are polynomials of degrees $0, \dots, d$, and $\varepsilon_1, \dots, \varepsilon_n$ are i.i.d. errors with zero mean and variance $\sigma^2 \in (0, \infty)$. In this model, we have $\mathfrak{X} = \{1, \dots, v\} \times \{1, \dots, n\}$ and $\mathbf{f}(u, t) = (\mathbf{e}_u^T, \mathbf{p}^T(t))^T$, where $\mathbf{e}_u \in \mathbb{R}^v$ is the standard u-th unit vector and $\mathbf{p}(t) = (p_0(t), \dots, p_d(t))^T$. The vector of model parameters is $\beta = (\tau_1, \dots, \tau_v, \theta_1, \dots, \theta_{d+1})^T$, but we suppose that only $s = v - 1$ contrasts $\tau_2 - \tau_1, \dots, \tau_v - \tau_1$ are of interest. Hence, we will focus on $\mathbf{A}^T\beta$, where $\mathbf{A}^T = (-\mathbf{1}_s, \mathbf{I}_s, \mathbf{0}_{s\times(d+1)})$, $s = v - 1$.

The moment matrix of any design ξ can be expressed in the form

$$\mathbf{M}(\xi) = \begin{pmatrix} \mathbf{M}_{11}(\xi) & \mathbf{M}_{12}(\xi) \\ \mathbf{M}_{12}^T(\xi) & \mathbf{M}_{22}(\xi) \end{pmatrix},$$

where $\mathbf{M}_{11}(\xi)$ is diagonal with $\sum_t \xi(1, t), \dots, \sum_t \xi(v, t)$ on the diagonal, $\mathbf{M}_{12}(\xi) = (\sum_t \xi(1, t)\mathbf{p}(t), \dots, \sum_t \xi(v, t)\mathbf{p}(t))^T$ and $\mathbf{M}_{22}(\xi) = \sum_t (\sum_u \xi(u, t))\mathbf{p}(t)\mathbf{p}^T(t)$. If ξ is exact, then the diagonal elements of the matrix $\mathbf{M}_{11}(\xi)$ can be interpreted as replication numbers of individual treatments.

A usual assumption of an experiment modeled by (10.3) is that exactly one treatment is assigned to each time, therefore any permissible design ξ must satisfy

$$\sum_{u=1}^{v} \xi(u, t) = 1; \quad t = 1, \dots, n. \tag{10.4}$$

If ξ satisfies (10.4), then $\mathbf{M}_{22}(\xi)$ does not depend on ξ. Moreover, it is simple to show that $\mathbf{N}_{\mathbf{A}}(\xi)$ does not depend on the choice of $p_0, \dots, p_d$ (provided that p_i has degree i), but a suitable choice of the polynomials can lead to simpler computations. We used discrete orthogonal polynomials which makes $\mathbf{M}_{22}(\xi)$ diagonal.

For any system of $v - 1$ independent contrasts of treatments, the $D_{\mathbf{A}}$-optimal designs are the same; the system $\tau_2 - \tau_1, \dots, \tau_v - \tau_1$ is chosen only for technical convenience. Also, note that for $\xi_1, \xi_2 \in \Xi^E$ we have $\Phi(\mathbf{N}_{\mathbf{A}}(\xi_1)) = \Phi(\mathbf{N}_{\mathbf{A}}(\xi_2))$ if the designs differ only in the labeling of treatments or if ξ_1 is only the time-reversed version of ξ_2. Hence, we can call such designs isomorphic.

The study of "trend-resistant" or "systematic" designs dates back to Cox [4], who studied sequences involving two or three treatments under the presence of quadratic and cubic time trends. The extensive combinatorial theoretical results that followed are usually restricted to the so-called trend-free orthogonal designs, with a focus on selecting a suitable permutation of treatments, or combinations of factor levels, see,

e.g., [9] for a survey. In [1] the authors propose a more universal approach based on optimality criteria. Compared to the combinatorial design results, the optimal design approach covers many more practical situations, e.g., it can be applied if the orthogonality is not attainable, the time points are not evenly spaced, or the time trend is non-polynomial.

In contrast to [1], we will use a BNB algorithm. This algorithm always results in a catalogue of perfectly $D_{\mathbf{A}}$-optimal exact designs, although the time requirements are higher compared to the heuristic used in [1], especially for large n.

10.3.1 The BNB Algorithm

Let $a_1, \ldots, a_n \in \{0, 1, \ldots, v\}$. We define the template $[a_1, \ldots, a_n]$ to be the set $\{\xi \in \Xi^A$: Eq. (10.4) holds and $(a_t \neq 0 \Rightarrow \xi(a_t, t) = 1)$ for all $t\}$. In particular, $[0, \ldots, 0]$ corresponds to the set of all approximate designs satisfying (10.4). We call a template $[a_1, \ldots, a_n]$ exact if $a_t > 0$ for all t, and composite if $a_t = 0$ for some t. Note that exact templates are singletons, whose only element is the design using treatments $a_1, \ldots, a_n$ for the times $1, \ldots, n$. Clearly, for any selection $a_1, \ldots, a_n \in \{0, 1, \ldots, v\}$ the template $[a_1, \ldots, a_n]$ is equal to $\Xi^A_{\mathbf{C},\mathbf{b}}$ for some $\mathbf{C}$ and $\mathbf{b}$. Thus, the $D_{\mathbf{A}}$-optimal approximate design on any template can be computed using Theorem 10.1.

By a complete enumeration tree we will call any directed v-ary tree, with vertices corresponding to templates, satisfying: (1) The root template is $[0, \ldots, 0]$; (2) Any non-terminal template $[a_1, \ldots, a_n]$ is composite, and its v child nodes are $[a_1, \ldots, a_{t^*-1}, u, a_{t^*+1}, \ldots, a_n]$, $u = 1, \ldots, v$, where t^* is selected such that $a_{t^*} = 0$. Therefore, the set of all permissible exact designs of a parent template is a disjunctive union of the sets of all permissible exact designs of its child templates; (3) The v^n terminal templates are the exact templates $[a_1, \ldots, a_n]$, $a_1, \ldots, a_n \in \{1, \ldots, v\}$.

Suppose that we have constructed a sub-tree of a complete enumeration tree. Let Ξ correspond to a terminal template of the sub-tree. If the $D_{\mathbf{A}}$-optimal value of Ξ is smaller than the value of the $D_{\mathbf{A}}$-optimality criterion of the best available exact design then Ξ does not contain any $D_{\mathbf{A}}$-optimal exact design. Hence, we can "prune" the branch of the tree, i.e., skip constructing the descendants of Ξ. This idea allows us to circumvent the construction of most of the complete enumeration tree, yet the terminal exact nodes of the final tree contain all $D_{\mathbf{A}}$-optimal exact designs.

To fully specify the BNB method, we need to define the branching rule, that is, how to select the next composite template to be "refined" by constructing its child nodes, and which child nodes should be created. At each step, we choose the composite template $\Xi^* = [a_1^*, \ldots, a_n^*]$ with the highest $D_{\mathbf{A}}$-optimal value. Then we form its v child templates $[a_1^*, \ldots, a_{t^*-1}^*, u, a_{t^*+1}^*, \ldots, a_n^*]$, $u = 1, \ldots, v$, such that t^* is selected to maximize the entropy of the distribution given by the pmf $\xi^*(\cdot, t)$, where ξ^* is an optimal approximate design on Ξ^*. The rationale behind this selection is that if the marginal design $\xi^*(\cdot, t^*)$ has a high "uncertainty", fixing the

treatments for the time t^* often makes the $D_{\mathbf{A}}$-optimal values of the child templates smaller than the threshold given by the $D_{\mathbf{A}}$-optimal value of the best available exact design.

In the actual implementation of our algorithm, all templates are stored in one of the lists `closed`, `open`, and `exact` (that is, the BNB tree itself is constructed only implicitly). The list `closed` is continually updated to include the templates that cannot contain any $D_{\mathbf{A}}$-optimal exact design, since their $D_{\mathbf{A}}$-optimal values are smaller than the $D_{\mathbf{A}}$-optimal value $\Phi^*_{\max}$ of the best available exact design. The list `open` comprises the composite templates that still can contain an optimal exact design. Finally, the list `exact` contains the exact templates with the criterial value exactly $\Phi^*_{\max}$. The algorithm terminates once the list `open` is empty, which corresponds to the moment when the list `exact` contains all $D_{\mathbf{A}}$-optimal designs.

10.4 Example

In this section, we will show the results of the BNB algorithm when applied to the problem of computing $D_{\mathbf{A}}$-optimal exact designs from Section 10.3 for $v = 3$ treatments, the cubic ($d = 3$) time trend, and $n = 6, \ldots, 24$ trials.

For some n, there may exist $D_{\mathbf{A}}$-optimal exact designs that differ with respect to a secondary criterion. From the set of all $D_{\mathbf{A}}$-optimal exact designs computed by the BNB algorithm, we generated the complete list of all $D_{\mathbf{A}}$-optimal exact designs, and from each class Ξ^* of mutually isomorphic $D_{\mathbf{A}}$-optimal exact designs we selected:

1. A design ξ^A that is A-optimal in Ξ^* (see [2, Section 10.1]).
2. A design $\xi^\dagger$ that is symmetric in the sense $Var(\hat{\beta}_{\mathbf{c}_2}(\xi^\dagger)) = Var(\hat{\beta}_{\mathbf{c}_3}(\xi^\dagger))$, provided that Ξ^* contains a design with this property. For $j \in \{2, 3\}$, the symbol $\hat{\beta}_{\mathbf{c}_j}(\xi^\dagger)$ denotes the BLUE of $\tau_j - \tau_1$ under the design $\xi^\dagger$.
3. A design $\xi^\leftrightarrow$ that is symmetric with respect to the reversal of time, i.e., satisfying $\xi^\leftrightarrow(u, t) = \xi^\leftrightarrow(u, n + 1 - t)$ for all $u \in \{1, 2, 3\}$ and $t \in \{1, \ldots, n\}$, provided that Ξ^* contains a design with this property.

The selected $D_{\mathbf{A}}$-optimal exact designs ξ^A, $\xi^\dagger$, $\xi^\leftrightarrow$ are not necessarily distinct. The results are summarized in the following list.

(**6**) $212313^{A,\dagger}$; (**7**) $1231231^{A,\dagger}$; (**8**) $12311231^{A,\dagger}$; (**9**) $123121321^{A,\leftrightarrow}$;
(**10**) $1232113231^{A,\dagger}$; (**11**) 23113221312^{A}; (**12**) $312213312213^{A,\leftrightarrow}$;
(**13**) $1233211123321^{A,\leftrightarrow}$; (**14**) $312123131221 3^{A}$; (**15**) $123322111332231^{A,\dagger}$;
(**16**) $1233212113132231^{A,\dagger}$; (**17a**) $31221133233112213^{A,\leftrightarrow}$;
(**17b**) $12332121312123321^{A,\leftrightarrow}$; (**18a**) $132232131131232231^{A,\leftrightarrow}$;
(**18b**) $231131232232131132^{\dagger,\leftrightarrow}$; (**18c**) $231132132231231132^{A,\leftrightarrow}$;
(**18d**) $123321321123123321^{\dagger,\leftrightarrow}$; (**19a**) $312122313131322121 3^{A,\leftrightarrow}$;
(**19b**) $1233211321231123321^{A,\leftrightarrow}$; (**20**) $123231321122131323 21^{A}$;
(**21a**) $12323311213212233131 2^{A}$; (**21b**) $231311223213233112123^{\dagger}$;

(**22**) $123312231123112331223 1^{A,\dagger}$; (**23a**) $123312223113113222133 21^{A,\leftrightarrow}$;
(**23b**) $231123331221221333211 32^{\dagger,\leftrightarrow}$; (**23c**) $312213132312132313122 13^{A,\leftrightarrow}$;
(**23d**) $231132321231321232311 32^{\dagger,\leftrightarrow}$; (**24a**) $231132132321123231231 132^{A,\leftrightarrow}$;
(**24b**) $123321321213312123123321^{\dagger,\leftrightarrow}$; (**24c**) $123321321123321123123321^{A,\leftrightarrow}$;
(**24d**) $312213213312213312312213^{\dagger,\leftrightarrow}$.

Note that the $D_{\mathbf{A}}$-optimal designs for the model with the cubic time trend are model-robust in the sense that they are either perfectly optimal, or very efficient for the models with polynomial trends of degrees 0 (i.e., if there is no trend), 1 as well as 2. For $n \geq 7$ ($n \geq 13$, $n \geq 17$), these efficiencies are higher than 0.9 (0.99, 0.999).

10.5 Conclusions

We described a mathematical programming characterization of $D_{\mathbf{A}}$-optimal approximate designs under linear constraints and a BNB method for computing $D_{\mathbf{A}}$-optimal exact designs for estimating a set of treatment contrasts in the presence of a nuisance trend. In the illustrative example the nuisance parameters specify an unknown cubic time trend, but the algorithm can be analogously used for a large variety of other models, where the nuisance parameters represent any time trend, any spatial trend or the effects of blocks.

The main advantage of the BNB algorithm, compared to heuristic local-search methods is that it provides a complete list of perfectly optimal exact designs. The list can be used to select the best design according to a secondary criterion. Moreover, the list can motivate (or disprove) theoretical conjectures, or support the intuition about the desirable properties of designs. Note also that the mathematical programming approach permits adding linear constraints on the design that can represent, for example, constraints on the total cost of the experiment.

Acknowledgements The research of the first author was supported by the VEGA 1/0163/13 grant of the Slovak Scientific Grant Agency.

References

1. Atkinson AC, Donev AN (1996) Experimental designs optimally balanced for trend. Technometrics 38(4):333–341
2. Atkinson AC, Donev AN, Tobias RD (2007) Optimum experimental designs, with SAS. Oxford University Press, New York
3. Cook D, Fedorov V (1995) Constrained optimization of experimental design. Statistics 26(2):129–148
4. Cox DR (1951) Some systematic experimental designs. Biometrika 38(3/4):312–323
5. Joshi S, Boyd S (2009) Sensor selection via convex optimization. IEEE Trans Signal Process 57(2):451–462
6. Pázman A (1986) Foundations of optimum experimental design. Reidel, Dordrecht

7. Papp D (2012) Optimal designs for rational function regression. J Am Stat Assoc 107(497):400–411
8. Pukelsheim F (2006) Optimal design of experiments. SIAM, Philadelphia
9. Tack L, Vandebroek M (2001) $(\mathscr{D}_t, c)$-optimal run orders. J Stat Plan Inference 98(1-2):293–310
10. Sagnol G (2012) Picos, a python interface to conic optimization solvers. Technical report 12-48. ZIB: http://picos.zib.de
11. Uciński D, Patan M (2007) D-optimal design of a monitoring network for parameter estimation of distributed systems. J Glob Optim 39(2):291–322
12. Vandenberghe L (2010) The CVXOPT linear and quadratic cone program solvers. http://cvxopt.org/documentation/coneprog.pdf
13. Vandenberghe L, Boyd S, Wu SP (1998) Determinant maximization with linear matrix inequality constraints. SIAM J Matrix Anal Appl 19(2):499–533
14. Welch WJ (1982) Branch-and-bound search for experimental designs based on D-optimality and other criteria. Technometrics 24(1):41–48
15. Yu Y (2010) Monotonic convergence of a general algorithm for computing optimal designs. Ann Stat 38(3):1593–1606

Chapter 11
Variable Inspection Plans for Continuous Populations with Unknown Short Tail Distributions

Wolfgang Kössler

Abstract The ordinary variable inspection plans are sensitive to deviations from the normality assumption. A new variable inspection plan is constructed that can be used for arbitrary continuous populations with short tail distributions. The peaks over threshold method is used, the tails are approximated by a generalized Pareto distribution, their parameters and the fraction defective are estimated by a moment method proposed in a similar form by Smith and Weissman in J. R. Stat. Soc. B 47:285–298, 1985. The estimates of the fraction defective are asymptotically normal. It turns out that their asymptotic variances do not differ very much for the various distributions. Therefore we may fix the variance and use the known asymptotic distribution for the construction of the inspection plans. The sample sizes needed to satisfy the two-point conditions are much less than that for attribute plans.

11.1 Introduction

We consider a lot of units having a quality characteristic $\mathbf{X}$ with a (unknown) continuous cumulative distribution function (cdf) F. Given a sample $X_1, \ldots, X_n$ a decision is to be made whether the lot is to be accepted or not. For simplicity we assume only lower specification limits L, but the procedure can be extended to the two-sided case of lower and upper specification limits. The fraction defective p_L of the lot is defined by

$$p_L = P(\mathbf{X} < L) = F(L).$$

We intend to construct reasonable estimates $\hat{p}$ of p based on the sample. Our variable inspection plan is then defined by: If $\hat{p} \leq c$ the lot will be accepted else it will be rejected. Denote by

$$L^{n,c}(p) := P_p(\hat{p} \leq c), \quad 0 < p < 0.5$$

W. Kössler (✉)
Institute of Computer Science, Humboldt-Universität, Berlin, Germany
e-mail: koessler@informatik.hu-berlin.de

A. Steland et al. (eds.), *Stochastic Models, Statistics and Their Applications*,
Springer Proceedings in Mathematics & Statistics 122,
DOI 10.1007/978-3-319-13881-7_11

the operating characteristic (OC). Variable inspection plans (n, c) are computed by minimizing the sample size n while meeting the so-called two-point conditions ($0 < p_1 < p_2 < 1, 0 < \beta < 1 - \alpha$)

$$L^{n,c}(p_1) \geq 1 - \alpha \quad \text{and} \quad L^{n,c}(p_2) \leq \beta, \tag{11.1}$$

where p_1 and p_2 are the accepted and rejected quality level, respectively. The ordinary variable inspection plan (ML plan, cf. e.g. Uhlmann [13], for the two-sided case see Bruhn-Suhr and Krumbholz [2]) is very sensitive with respect to deviations from the normal distribution assumption (cf. Kössler and Lenz [5, 6]).

In this paper we construct variable inspection plans which do not rely on the normality assumption and which require less sample sizes than the attribute plan. The main idea is that nonconforming items X_i occur in the lower tail of the underlying cdf, namely $X_i < L = F^{-1}(p_L)$ with the (unknown) fraction defective $p = p_L$. Additionally, items X_i with $X_i \approx L$, $X_i > L$ can be considered suspicious. They also should be considered in inspection plans. Whereas in Kössler [4] we assumed that the underlying density has not too short tails to obtain Maximum Likelihood estimates we consider the short tail case here and use a (moment) estimate proposed by Smith [10] and Smith and Weissman [11].

In Sect. 11.2 we apply the peak over threshold method, approximate the tails of the density by a generalized Pareto distribution (GPD) and estimate their parameters and the fraction defective in Sect. 11.3. Using the asymptotic normality of all these estimators we compute inspection plans meeting the conditions (11.1) at least approximately in Sect. 11.4. Comparisons of the various sampling plans in Sect. 11.5 show that the necessary sample sizes for the new plan are much less than that for the attribute sampling plan. Simulation studies performed in Sect. 11.6 show that this method works quite well even for relatively small sample sizes.

11.2 Approximation of the Tails by a GPD

We assume that we have a short tail density with a lower endpoint x_0 which may be set to zero without restriction to the generality, more precisely, we assume that the underlying density is in the domain of attraction of the Weibull (cdf $G_\gamma(x) = 1 - \exp(-x^\gamma)$, tail index $\gamma > 0$, $x > 0$). Let $t = t_L$ be a lower threshold value and $0 < y < t$. The conditional cdf $F_t(y)$ of $t - X$ conditioned under $X < t$,

$$F_t(y) = \frac{F(t) - F(t - y)}{F(t)}, \tag{11.2}$$

can be approximated by a generalized Pareto cdf,

$$GPD(y; \sigma, k) := 1 - \left(1 - \frac{ky}{\sigma}\right)^{\frac{1}{k}} \quad k, \sigma > 0,\ 0 < y < \frac{\sigma}{k}$$

as was shown by Pickands [8, Theorem 7]. The parameters $k = \frac{1}{\gamma} > 0$ and $\sigma(t) = k(t - x_0) = kt$ are given by the extreme value distribution theory, cf. e.g. Falk [3].

To approximate the fraction defective p_L let $t = t_L$ be fixed, $t > L = F^{-1}(p_L)$ and $y = y_L = t - L$. We obtain from (11.2):

$$p_L = F(L) = F(t) - F_t(y) \cdot F(t) \approx F(t)\left(1 - \frac{ky}{\sigma}\right)^{\frac{1}{k}}.$$

11.3 Estimation of the Fraction Defective

Define the threshold by $t_L = F^{-1}(q)$ for given q, $0 < q < 0.5$ and estimate it by $\hat{t}_L = X_{(m+1)}$, where $m := \lfloor nq \rfloor$ and $X_{(i)}$ is the ith order statistics of the sample. Let $\hat{y}_L = \hat{t}_L - L$ and $(\hat{k}_L, \hat{\sigma}_L)$ be a consistent estimate of (k_L, σ_L) in the GPD-model. Then

$$\hat{p}_L = q \cdot \begin{cases} (1 - \frac{\hat{k}_L \hat{y}_L}{\hat{\sigma}_L})^{\frac{1}{\hat{k}_L}} & \text{if } \hat{k}_L \neq 0 \\ e^{-\frac{\hat{y}_L}{\hat{\sigma}_L}} & \text{if } \hat{k}_L = 0 \end{cases} \tag{11.3}$$

is a consistent estimate of p_L.

Note that $\hat{y}_L$ is random, and the estimate (11.3) is well defined if $\hat{y}_L \geq 0$ and if

$$\hat{k}_L \hat{y}_L < \hat{\sigma}_L. \tag{11.4}$$

In the few cases that $\hat{y}_L < 0$ we may reject the lot without further computations because these cases indicate low quality.

For the estimation of the parameters we might use Maximum Likelihood estimates. This procedure was pursued in Kössler [4]. However, if $k > 0.5$ the ML estimates are not asymptotically normal ($k \leq 1$) or they do not exist ($k > 1$). For the short tail densities here we use an estimate (SW estimate) proposed by Smith and Weissman [11, Eq. (4.3)], and Smith [10, Sect. 7],

$$\hat{k}_L = \frac{1}{m} \sum_{i=2}^{m} \log \frac{X_{(m+1)} - X_{(1)}}{X_{(i)} - X_{(1)}} \tag{11.5}$$

$$\hat{\sigma}_L = \hat{k}_L (X_{(m+1)} - X_{(1)}). \tag{11.6}$$

The estimate for k_L may be motivated by the moment equation $E(-\log(1 - \frac{kY}{\sigma})) = k$ if Y is a random variable, $Y \sim GPD(\sigma, k)$, cf. Smith [10]. The estimate for σ_L is motivated by $\sigma_L = k_L(t_L - x_0)$ if $k_L > 0$, and the in praxis unknown lower endpoint x_0 is estimated by the smallest observation $X_{(1)}$.

If $X_{(1)} < L$ then condition (11.4) is satisfied and consistent estimates $\hat{p}_L$ of the fraction defective p_L are obtained by inserting $\hat{k}_L$ and $\hat{\sigma}_L$ in (11.3). In the case of $X_{(1)} \geq L$ we may set $\hat{p}_L := 0$ as it indicates good quality. However, a slight negative bias may be introduced.

Note that we also investigated various other estimates of (k, σ), moment estimates (MOM), probability weighted moment estimates (PWM) and elemental percentile moment estimates (EPM) (see e.g. Beirlant [1] and references therein). The

asymptotic variances of the MOM and PWM estimates are much larger than that of estimates (11.5) and (11.6), a result that is confirmed by finite sample simulation studies. Simulations with the EPM method show that their bias is slightly less than that for the SW estimate but the variances are much higher for the EPM estimates.

Under certain conditions on the convergence of $t \to x_o$, $L \to x_o$ if $n \to \infty$ the SW-estimate $\hat{p}_L$ is asymptotically normally distributed with expectation zero and variance $V(p_L)$,

$$\sqrt{m}\frac{\hat{p}_L - p_L}{p_L} \to \mathcal{N}\big(0, V(p_L)\big) \tag{11.7}$$

(cf. Smith [10, Ch. 8]). To obtain a closed relation for the variance $V(p_L)$ dependent on the cdf F we follow the arguments of Smith [10, Ch. 8].

Let z, $z > 0$, be fixed and define the sequences p_m, q_m, $p_m \to 0$, $q_m \to 0$, $0 < p_m < q_m$ in the same way as in Smith [10] by

$$z = 1 - \frac{k y_m}{\sigma_m} = 1 - \frac{k(t_{L,m} - L_m)}{\sigma_m} = 1 - \frac{k(F^{-1}(q_m) - F^{-1}(p_m))}{\sigma_m}, \tag{11.8}$$

where $y_m := t_{L,m} - L_m = F^{-1}(q_m) - F^{-1}(p_m)$, and k and σ_m are the parameters given by the GPD approximation of the conditional probability (11.2) which depend on the sequence of the threshold values $t_{L,m} = F^{-1}(q_m)$.

The asymptotic variance $V = V_F$ for $p_m, q_m \to 0$ is then given by

$$V_F = 1 - q_m + \mathbf{c}^T \mathbf{S} \mathbf{c}, \tag{11.9}$$

where

$$\mathbf{c}^T = \left(-\frac{1}{k}\left(\frac{1}{z} - 1\right), \frac{\log z}{k^2} + \frac{1}{k^2}\left(\frac{1}{z} - 1\right)\right) \quad \text{and} \quad \mathbf{S} = \begin{pmatrix} 1 & k \\ k & k^2 \end{pmatrix}. \tag{11.10}$$

The term $\mathbf{c}^T \mathbf{S} \mathbf{c}$ in (11.9) becomes $\mathbf{c}^T \mathbf{S} \mathbf{c} = \frac{1}{k^2} \log^2 z$, where z is defined by (11.8) with $\sigma_m = k t_{L,m}$. Interestingly, if the cdf F is GPD or Weibull the term $\mathbf{c}^T \mathbf{S} \mathbf{c}$ is independent of k.

For further investigation of the variance term we considered the following short tail densities, the GPD, the Weibull, the Beta, the Gamma and the Burr, all with various values of the parameter k. From the matrices $\mathbf{S}$ in the ML and SW cases (cf. Smith [10]) it may be seen that for $k = 0.5$ the asymptotic variances of the ML and SW estimates are the same. Moreover, it turns out that the asymptotic variances of the SW estimates of $\hat{p}_L$ in the case of short tails are often similar to that of the ML estimate in the (long tail) Pareto ($k = -1$) case where we had an upper specification limit (Kössler [4, Eq. (14), Table 3]). Exceptions are the Gamma with $k = 0.25$, and the Burr with $k = 0.25$ or $k = 0.5$. An explanation of the latter facts may be that the speed of convergence of $q_m \to 0$ must be faster in that cases, cf. convergence conditions SR1 or SR2 of Smith [10].

However, if the ratios of the fraction defective p_L and the used tail fraction q are not too small then the dissimilarities are not so large.

The similarities of the asymptotic variances will allow us to use the variance $V(p)$ obtained for the ML estimate in the (reverse) Pareto ($k = -1$) case for the

determination of the sampling plan later on. This variance is given by (11.9) but with $\mathbf{S} = (1-k)\left(\begin{smallmatrix} 2 & 1 \\ 1 & 1-k \end{smallmatrix}\right) = 2\left(\begin{smallmatrix} 2 & 1 \\ 1 & 2 \end{smallmatrix}\right)$ (cf. e.g. Smith [10]).

11.4 The New Sampling Plan

Since we have established asymptotic normality with similar variances for the various underlying cdfs we may proceed in the same way as in Kössler [4] to determine a new sampling plan. Given $q > 0$ define $m = \lfloor nq \rfloor$, i.e. for the estimation of the fraction defective only the $m+1$ smallest observations are used.

For a discussion of the choice of the threshold values t_L we refer to Kössler [4]. Here we apply a slightly modified version

$$q = q(n_0) = p_2 + \frac{1}{\sqrt{n_0}},$$

where n_0 is an initial estimate of the sample size, $n_0 = \frac{n_V + n_A}{2}$, n_V and n_A are the sample sizes for the ordinary variable sampling and for the attribute sampling plan, respectively. This definition reflects the conditions $q \to 0$, $q > p$ and also the fact that the resulting sample size is expected to lie between n_V and n_A.

Since the number m is essential, the sampling plan is denoted by (n, m, c). An approximate OC of this sampling plan is given by the asymptotic distribution of $\hat{p}$.

To determine the numbers m and c meeting the two-point conditions (11.1) approximately we solve the system of equations

$$L^{n,c}(p_1) \approx \Phi\left(\sqrt{m}\frac{c - p_1}{p_1\sqrt{V(p_1)}}\right) = 1 - \alpha,$$
$$L^{n,c}(p_2) \approx \Phi\left(\sqrt{m}\frac{c - p_2}{p_2\sqrt{V(p_2)}}\right) = \beta.$$

An to integer values for m adjusted solution (m, c) of this system of equations is given by

$$m = \left\lceil \frac{1}{(p_1 - p_2)^2}\left(p_2\sqrt{V(p_2)}\Phi^{-1}(\beta) - p_1\sqrt{V(p_1)}\Phi^{-1}(1-\alpha)\right)^2 \right\rceil \quad (11.11)$$

$$c = p_1 + \Phi^{-1}(1-\alpha)\frac{p_1\sqrt{V(p_1)}}{\sqrt{m}}. \quad (11.12)$$

Given the numbers m and q the sample size n is determined by $m = \lfloor nq \rfloor$. In such a way a new sampling plan (n, m, c) is obtained. It is given by

$$n = \left\lceil \frac{m}{q} \right\rceil, \quad \text{where } q = p_2 + \frac{1}{\sqrt{n_0}}$$

and m and c are given by (11.11) and (11.12).

Note that $V(p)$ is also dependent on q, and since the definition of q is slightly modified, these variances and also the sample sizes are slightly different from that in Kössler [4].

Table 11.1 The new sampling plan (n, m, c_{SW}) together with the sample sizes n_V and n_A of the ordinary variable sampling plan and the attribute sampling plan, respectively

No.	Two-point condition				New sampling plan				
	p_1	$1-\alpha$	p_2	β	n	m	c_{SW}	n_V	n_A
1	0.0521	0.9500	0.1975	0.10	31	11	0.1053	27	45
2	0.0634	0.9000	0.1975	0.10	31	11	0.1072	27	45
3	0.0100	0.9000	0.0600	0.10	59	11	0.0237	36	88
4	0.0100	0.9743	0.0592	0.10	80	13	0.0280	54	133
5	0.0152	0.9000	0.0592	0.10	83	14	0.0292	54	111
6	0.0100	0.9900	0.0600	0.10	90	14	0.0303	64	153
7	0.0360	0.9500	0.0866	0.10	143	24	0.0576	106	189
8	0.0406	0.9000	0.0866	0.10	149	25	0.0581	107	189
9	0.0100	0.9900	0.0600	0.01	203	27	0.0237	111	263
10	0.0200	0.9500	0.0500	0.05	316	34	0.0309	186	410
11	0.0100	0.9900	0.0300	0.10	390	33	0.0198	217	590
12	0.0200	0.9900	0.0300	0.01	4609	213	0.0244	2241	5362

First simulations show that the OC estimates are slightly shifted to the right. Therefore, the acceptance number is empirically modified to $c_{SW} := c \cdot (1 - 1/n)$.

11.5 Comparison with Other Sampling Plans

In Table 11.1 the sampling plans (n, m, c_{SW}) for twelve different two-point conditions are presented. For comparison the corresponding sample sizes n_V and n_A of the ML-variable sampling plan and the attribute sampling plan, respectively, are given in the last two columns of Table 11.1. The sample sizes for the ordinary ML variable sampling plan are computed by the R program ExLiebeRes of Krumbholz and Steuer [7]. Since our new sampling plan can be used also in the case of two-sided specification limits the sample size n_V is computed for that case.

The Examples 1, 2, 4, 5, 7 and 8 are from Resnikoff [9], Example 10 is from Steland and Zähle [12]. From Table 11.1 it can be seen that the sample sizes for the new plan are considerably less than that for the attribute sampling plan.

11.6 Simulation Study

The method described to obtain variable sampling plans is based on the asymptotic normality of the estimates $\hat{p}$ with the variance $V(p)$. The reference cdf for computing $V(p)$ is the (reverse) Pareto with $k = -1$ (where ML estimates are used).

To investigate whether the sampling plans constructed can be applied for short tail densities as well as for moderate sample sizes simulation studies are carried out.

The OC is estimated for the same examples as in the previous section. Note that the examples 1–9, 11 are the same as in Kössler [4] but the necessary sample sizes may differ slightly since the definition of the used fraction of the sample is altered. To see whether the asymptotic theory works in practice we have included an example with very large sample sizes (Example 12).

The simulation size is $M = 2000$. The following cdf's are included in the simulation study: GPD, Weibull, Gamma, and Burr, all with $k = 0.25, 0.5, 0.75, 1$.

We obtain that for $k \geq 0.5$ and for most densities the OC is well estimated. To give an impression on the goodness of the estimated OC values we present only the worst cases. For β they are $\hat{\beta} = 0.13$ (instead of $\beta = 0.10$). For $1 - \alpha$ they are $1 - \hat{\alpha} = 0.97$ (instead of $1 - \alpha = 0.99$), $1 - \hat{\alpha} = 0.93$ (instead of $1 - \alpha = 0.95$), $1 - \hat{\alpha} = 0.86$ (instead of $1 - \alpha = 0.90$). For $k = 0.25$ the estimates are only slightly worse. Perhaps somewhat surprisingly, the latter happens also in Example 12 where we have very large sample sizes. Note that, for $k = 0.25$ a ML estimate is to be preferred.

11.7 Adaptive Procedure and Summary

In the short tail case the estimates of the fraction defective are different from that in the medium or long tail case. Since it is generally not known which case occurs, we suggest to apply an adaptive procedure. First the sample size is determined in the way described. Then, after the sample is drawn from the lot, the parameter k_L is estimated by the SW method. If $\hat{k}_L = \hat{k}_{L,SW} \leq 0.5$ we assume that we have a medium or long tail, estimate k_L, σ_L and the fraction defective p_L by the ML method and use the modified acceptance number c_{ML} from the ML plan (cf. Kössler [4]). If $\hat{k}_{L,SW} > 0.5$ we assume that we have a short tail, estimate k_L, σ_L and the fraction defective p_L by the SW method and use the modified acceptance number c_{SW}.

For normally distributed populations, of course, the ML-sampling plans are to be preferred. But usually, there is no exact information about the distribution of the underlying population in practice. Therefore, if the underlying c.d.f. is continuous the new variable sampling plan instead of an attribute plan should be applied. If it is known that we have short tails the sampling plan proposed here should be applied.

References

1. Beirlant J, Goegebeur Y, Segers J, Teugels J (2004) Statistics of extremes, theory and applications. Wiley, Chichester
2. Bruhn-Suhr M, Krumbholz W (1990) A new variable sampling plan for normally distributed lots with unknown standard deviation and double specification limits. Stat Hefte 31:195–207
3. Falk M (1989) Best attainable rate of joint convergence of extremes. In: Hüsler J, Reiss R-D (eds) Extreme value theory. Proceedings of a conference held in Oberwolfach, 6–12 Dec., 1987. Springer, Berlin, pp 1–9
4. Kössler W (1999) A new one-sided variable inspection plan for continuous distribution functions. Allg Stat Arch 83:416–433

5. Kössler W, Lenz H-J (1995) On the robustness of Lieberman-Resnikoff sampling plans by variables. J. Indian Assoc Product, Qual Reliability 20:93–105
6. Kössler W, Lenz H-J (1997) On the non-robustness of maximum-likelihood sampling plans by variables. In: Lenz H-J, Wilrich P-Th (eds) Frontiers in statistical quality control, vol 5. Physica, Heidelberg, pp 38–52.
7. Krumbholz W, Steuer D (2014) On exact and optimal single sampling plans by variables. AStA Adv Stat Anal 98:87–101
8. Pickands J (1975) Statistical inference using extreme order statistics. Ann Stat 3:119–135
9. Resnikoff GV (1952) A new two-sided acceptance region for sampling by variables. Technical report 8, Applied Mathematics, and Statistics Laboratory, Stanford University
10. Smith RL (1987) Estimating tails of probability distributions. Ann Stat 15:1174–1207
11. Smith RL, Weissman I (1985) Maximum likelihood estimation of the lower tail of a probability distribution. J R Stat Soc B 47:285–298
12. Steland A, Zähle H (2009) Sampling inspection by variables: nonparametric setting. Stat Neerl 63:101–123
13. Uhlmann W (1982) Statistische Qualitätskontrolle. Teubner, Stuttgart

Chapter 12
Goodness-of-Approximation of Copulas by a Parametric Family

Eckhard Liebscher

Abstract In the paper we introduce a measure for goodness of approximation based on the Cramér von Mises-statistic. In place of the unknown parameter of interest, a minimum-distance estimator of the parameter is plugged in. We prove asymptotic normality of this statistic and establish a test on goodness-of-approximation.

12.1 Introduction

Let $X = (X^{(1)}, \dots, X^{(d)})^T$ be a d-dimensional random vector. We denote the marginal density and the marginal distribution function of $X^{(m)}$ by f_m and F_m, respectively ($m = 1, \dots, d$). H denote the joint distribution function of X. According to Sklar's theorem (see Sklar [16]), we have

$$H(x_1, \dots, x_d) = C\big(F_1(x_1), \dots, F_d(x_d)\big) \quad \text{for } x_i \in \mathbb{R},$$

where $C : [0, 1]^d \to [0, 1]$ is the d-dimensional copula. The reader can find the detailed theory of copulas in the popular monographs by Joe [8] and by Nelsen [13]. In this paper we consider the parametric family $\mathscr{F} = (C_\theta)_{\theta \in \Theta}$ of copulas on $[0, 1]^d$ where $\Theta \subset \mathbb{R}^q$ is the parameter space. Let $\mathscr{D}(C, \mathscr{F})$ be a measure of discrepancy between the copula C of the sample and the family $\mathscr{F}$. The aim of this paper is to establish a test of the hypothesis

$$H_0\colon\ \mathscr{D}(C, \mathscr{F}) \le M, \qquad H_1\colon\ \mathscr{D}(C, \mathscr{F}) > M$$

and to show asymptotic normality of the test statistic. Here M is an appropriately given value. In this paper we focus on the Cramér-von-Mises divergence as measure of discrepancy. It describes how good the approximation of C by $\mathscr{F}$ is. A similar measure is considered in Tsukahara [17].

In a large variety of practical situations, it is hard to find an appropriate family of copulas which fits to a high precision the underlying copula of the sample. The reason is the complexity of the multivariate distribution especially in the situation of

E. Liebscher (✉)
Department of Computer Sciences and Communication Systems, University of Applied Sciences Merseburg, Geusaer Straße, 06217 Merseburg, Germany
e-mail: eckhard.liebscher@hs-merseburg.de

A. Steland et al. (eds.), *Stochastic Models, Statistics and Their Applications*,
Springer Proceedings in Mathematics & Statistics 122,
DOI 10.1007/978-3-319-13881-7_12

higher dimensions. Thus we cannot expect that C belongs to the family $\mathscr{F}$, and we will assume $C \notin \mathscr{F}$. The reader finds an extensive discussion about goodness-of-approximation in the one-dimensional case in Liebscher [12]. The consideration of approximate estimators is another aspect of this paper. Since as a rule there is no explicit formula for the estimators, we have to evaluate the estimator for the parameter θ by a numerical algorithm and receive the estimator as solution of an optimisation problem only at a certain (small) error.

In this paper the test statistic (the Cramér-von-Mises statistic) is actually an estimator for the measure $\mathscr{D}(C, \mathscr{F})$ of discrepancy. It is shown that the test statistic is asymptotically equivalent to an U-statistic. One advantage of our approach is that the asymptotic distribution of the test statistic is a normal one whose quantiles can be computed in the usual way. Observe that in the case $C \in \mathscr{F}$, the asymptotic distribution of the Cramér-von-Mises test statistic is not of standard type since it is asymptotically equivalent to a degenerate U-statistic, see Serfling [15, Theorem 5.5.2]. In this situation it is not an easy task to calculate (asymptotic) quantiles.

Concerning the estimation of the parameters of the copula, two types of estimators are studied in most of the literature: maximum pseudo-likelihood estimators and minimum distance estimators. In our approach minimum distance estimators on the basis of Cramér-von-Mises divergence are the appropriate choice. Minimum distance estimators for the parameters of copulas were examined in the papers by Tsukahara [17] and by the author [11]. The asymptotic behaviour of likelihood estimators were studied in papers by Genest and Rivest [4], Oakes [14], and Chen and Fan [2], among others. Joe [9] published results on the asymptotic behaviour of two-stage estimation procedures.

Goodness-of-fit tests correspond to the case $C \in \mathscr{F}$ and were studied in a lot of papers including those by Fermanian [3] and Genest et al. [5], see also the survey by Genest et al. [7]. In the paper by Genest and Rémillard [6] it is shown that the bootstrap works in the context of goodness-of-fit. Bücher and Dette consider in their paper [1] goodness-of-fit tests based on a kernel estimator for the L^2-distance of the densities.

The paper is organised as follows: In Sect. 12.2 we discuss the problem of goodness of approximation. Section 12.3 is devoted to minimum distance estimators. In Sect. 12.4 we provide the main results of the paper. The reader finds the proofs of the results in Sect. 12.5.

12.2 Goodness of Approximation

In this section we consider measures for the discrepancy between the copula C and the family $\mathscr{F} = (C_\theta)_{\theta \in \Theta}$ be a family of copulas where $\theta \rightsquigarrow C_\theta(u)$ is assumed to be continuous for all $u \in [0,1]^d$. Let $F(x) = (F_1(x_1), \ldots, F_d(x_d))^T$ for $x = (x_1, \ldots, x_d)^T \in \mathbb{R}^d$. In this paper we focus on the *Cramér-von-Mises divergence*:

$$\mathscr{D}(C,\mathscr{F}) = \inf_{\theta\in\Theta} \mathscr{D}(C, C_\theta), \quad \text{where}$$

$$\mathscr{D}(C, C_\theta) = \int_{[0,1]^d} \big(C(u) - C_\theta(u)\big)^2 \,\mathrm{d}C(u) = \int_{\mathbb{R}^d} \big(H(x) - C_\theta\big(F(x)\big)\big)^2 \,\mathrm{d}H(x).$$

Alternatively, one can consider L^p*-distance*

$$\mathscr{L}_p(C, C_\theta) = \int_{[0,1]^d} \big|C(u) - C_\theta(u)\big|^p \,\mathrm{d}u$$

or the *Kolmogorov–Smirnov distance*

$$\mathscr{K}(C, C_\theta) = \sup_{u\in[0,1]^d} \big|C(u) - C_\theta(u)\big|.$$

The Kolmogorov–Smirnov distance has the disadvantage that its estimator responds sensitively to outliers. The smaller the value of the divergence the better is the approximation.

As the next step we discuss the estimation of $\mathscr{D}(C, C_\theta)$. Let $X_1, \ldots, X_n$ be the sample of random vectors with distribution function H and copula C. We denote the empirical joint distribution function by $\hat{H}_n$. Let $\bar{F}_n(x) = (F_{1n}(x_1), \ldots, F_{dn}(x_d))^T$ be the vector of the marginal empirical distribution functions. We can construct the following estimator:

$$\widehat{\mathscr{D}}_n(C_\theta) = \frac{1}{n}\sum_{i=1}^{n} \big(\hat{H}_n(X_i) - C_\theta\big(\bar{F}_n(X_i)\big)\big)^2 \tag{12.1}$$

for $\theta \in \Theta$. The advantage of this estimator is that it is just a sum and no integral has to be computed. On the other hand, in case of estimators for the L^p-distance, an integral has to be evaluated. Moreover, Genest et al. [7] have found out that the use of Cramér-von-Mises statistic leads to more powerful goodness-of-fit tests in comparison to other test statistics like Kolmogorov–Smirnov one. The next section is devoted to the estimation of the parameter θ.

12.3 Parameter Estimation by the Minimum Distance Method

Let $X_1, \ldots, X_n$ be the sample as in the previous section. Throughout the paper we assume that $C \notin \mathscr{F}$. In this section we are interested in estimating the parameter θ_0 which gives the best approximation for the copula:

$$\theta_0 = \operatorname{argmin}_{\theta\in\Theta} \mathscr{D}(C, C_\theta).$$

It should be highlighted that in general, θ_0 depends on the choice of the discrepancy measure. There is no true parameter. The approximate minimum distance estimator $\hat{\theta}_n$ as introduced in Liebscher [11] is the object of our considerations in this section. This estimator is defined as an approximate minimiser of $\theta \rightsquigarrow \widehat{\mathscr{D}}_n(C_\theta)$:

$$\widehat{\mathscr{D}}_n(C_{\hat{\theta}_n}) \le \min_{\theta\in\Theta} \widehat{\mathscr{D}}_n(C_\theta) + \varepsilon_n,$$

where $\{\varepsilon_n\}$ is a sequence of random variables with $\varepsilon_n \to 0$ a.s. Concerning consistency and asymptotic normality of $\hat{\theta}_n$, we quote the main results of the paper by the author [11] which were obtained by utilising results from Lachout et al. [10]. The partial derivative $\frac{\partial}{\partial u_m} C_\theta(u_1, \dots, u_d)$ is denoted by $C_\theta^{(m)}(u)$.

Theorem 12.1 (*Theorem* 3.1 *of Liebscher* [11].) *Let Θ be compact, and $\theta \rightsquigarrow C_\theta(u)$ be continuous on Θ for all $u \in [0,1]^d$. Assume that $\mathscr{D}(C, C_\theta) > \mathscr{D}(C, C_{\theta_0})$ for all $\theta \in \Theta, \theta \neq \theta_0$. Then*

$$\lim_{n\to\infty} \hat{\theta}_n = \theta_0 \text{ a.s.}$$

Theorem 12.2 (*Theorem* 3.2 *of Liebscher* [11].) *Under certain regularity conditions,*

$$\sqrt{n}(\hat{\theta}_n - \theta_0) \xrightarrow{\mathscr{D}} \mathscr{N}(0, \Sigma).$$

Here $\Sigma = \Sigma_2^{-1} \Sigma_1 \Sigma_2^{-1}$, $\Sigma_1 = \operatorname{cov}(Z_i)$, $Z_i = (Z_{ij})_{j=1,\dots,q}$,

$$\begin{aligned}\gamma_{kj}(x \mid \theta_0) = \big(H(x) - C_\theta\big(F(x)\big)\big) \frac{\partial^2}{\partial\theta_j \partial u_k} C_\theta\big(F(x)\big) \\ - C_\theta^{(j)}\big(F(x)\big) C_\theta^{(k)}\big(F(x)\big)\Big|_{\theta=\theta_0},\end{aligned}$$

$$\begin{aligned}Z_{ij} = \sum_{j=1}^{d} \int_{\mathbb{R}^d} \Big(I\big(X_1^{(j)} \le x_j\big) \gamma_{kj}(x \mid \theta_0) \\ + I(X_1 \le x) \frac{\partial}{\partial\theta_k} C_\theta\big(F(x)\big)\Big|_{\theta=\theta_0} \Big) \mathrm{d}H(x) \\ + \big(H(X_1) - C_{\theta_0}\big(F(X_1)\big)\big) \frac{\partial}{\partial\theta_k} C_\theta\big(F(X_1)\big)\Big|_{\theta=\theta_0},\end{aligned}$$

$\Sigma_2 = (\mathscr{H}_{ij})_{i,j=1,\dots,q}$ *is a regular matrix with*

$$\begin{aligned}\mathscr{H}_{ij} = \int_{\mathbb{R}^d} \Big(\big(H(x) - C\big(F(x) \mid \theta_0\big)\big) \frac{\partial^2}{\partial\theta_i \partial\theta_j} C_\theta\big(F(x)\big)\Big|_{\theta=\theta_0} \\ + \frac{\partial}{\partial\theta_i} C_\theta\big(F(x)\big) \frac{\partial}{\partial\theta_j} C_\theta\big(F(x)\big)\Big|_{\theta=\theta_0} \Big) \mathrm{d}H(x).\end{aligned}$$

12.4 The Test

The approximate minimum value of $\widehat{\mathscr{D}}_n(C_\theta)$ defined in (12.1) can be used as the test statistic in the context of this section:

$$T_n = \widehat{\mathscr{D}}_n(C_{\hat{\theta}_n}) = \frac{1}{n} \sum_{i=1}^{n} \big(\hat{H}_n(X_i) - C_{\hat{\theta}_n}\big(\bar{F}_n(X_i)\big)\big)^2.$$

In the main result we need the following assumption:

Assumption $\mathscr{A}$ *Let Θ be compact, and $\theta \rightsquigarrow C_\theta(u)$ be continuous on Θ for all $u \in [0,1]^d$. Assume that $\mathscr{D}(C, C_\theta) > \mathscr{D}(C, C_{\theta_0})$ for all $\theta \in \Theta, \theta \neq \theta_0$. Let $U(\theta_0)$ be a neighbourhood of θ_0. Suppose that $\frac{\partial^2}{\partial u_i \partial u_j} C_\theta(u)$, $\frac{\partial}{\partial \theta_p} C_\theta$ and $\frac{\partial^2}{\partial \theta_p \partial \theta_q} C_\theta$ exist and are bounded on $U(\theta_0) \times [0,1]^d$.* □

Let

$$\rho_1(x) = \int_{\mathbb{R}^d} \big(I(x \le y) - C_{\theta_0}\big(F(y)\big)\big)\big(H(y) - C_{\theta_0}\big(F(y)\big)\big)\,\mathrm{d}H(y),$$

$$\rho_2(x) = \sum_{m=1}^{d} \int_{\mathbb{R}^d} C_{\theta_0}^{(m)}\big(F(y)\big)\big(I(x_m \le y_m) - F_m(y_m)\big) \times \big(H(y) - C_{\theta_0}\big(F(y)\big)\big)\,\mathrm{d}H(y),$$

and $\breve{\theta}_n := \arg\min_{\theta \in \Theta} \widehat{\mathscr{D}}_n(C_\theta)$. Now we provide the main result of the paper on asymptotic normality of T_n:

Theorem 12.3 *Assume that $\|\breve{\theta}_n - \theta_0\| = O_{\mathbb{P}}(n^{-1/2})$, and $\varepsilon_n = o_{\mathbb{P}}(n^{-1/2})$. Let Assumption $\mathscr{A}$ be satisfied. Then we have*

$$\sqrt{n}\big(T_n - \mathscr{D}(C, C_{\theta_0})\big) \xrightarrow{\mathscr{D}} \mathscr{N}\big(0, \sigma^2\big),$$

where $\sigma^2 := \mathrm{Var}(\lambda(X_1))$ and $\lambda(x) := (H(x) - C_{\theta_0}(F(x)))^2 + 2\rho_1(x) - 2\rho_2(x)$.

The validity of the condition $\|\breve{\theta}_n - \theta_0\| = O_{\mathbb{P}}(n^{-1/2})$ can be obtained by utilising Theorem 12.2, for example. It is easy to construct an estimator for the variance:

$$\hat{\sigma}^2 = \frac{1}{n-1} \sum_{i=1}^{n} \Big(\big(\hat{H}_n(X_i) - C_{\hat{\theta}_n}\big(\bar{F}_n(X_i)\big)\big)^2 + 2\hat{\rho}_1(X_i) - 2\hat{\rho}_2(X_i) - 3\mathscr{D}(C, C_{\hat{\theta}_n})\Big)^2,$$

$$\hat{\rho}_1(x) = \frac{1}{n} \sum_{j=1}^{n} \big(I(x \le X_j) - C_{\hat{\theta}_n}\big(\bar{F}_n(X_j)\big)\big) \times \big(\hat{H}_n(X_j) - C_{\hat{\theta}_n}\big(\bar{F}_n(X_j)\big)\big),$$

$$\hat{\rho}_2(x) = \frac{1}{n} \sum_{j=1}^{n} \sum_{m=1}^{d} C_{\hat{\theta}_n}^{(m)}\big(\bar{F}_n(X_j)\big)\big(I(x_m \le X_{jm}) - F_m(X_{jm})\big) \times \big(\hat{H}_n(X_j) - C_{\hat{\theta}_n}\big(\bar{F}_n(X_j)\big)\big),$$

$x = (x_1, \ldots, x_d)^T$. Let $M > 0$ be a given real number. Now we consider the test of the hypothesis H_0: $\mathscr{D}(C, \mathscr{F}) \le M$, H_1: $\mathscr{D}(C, \mathscr{F}) > M$. The null hypothesis

describes the situation where the approximation achieves the required quality. In this test the null hypothesis is rejected if

$$T_n > M + 2z(1-\alpha)n^{-1/2}\hat{\sigma}.$$

$z(1-\alpha)$ denotes the quantile of order $1-\alpha$ of the $\mathcal{N}(0,1)$-distribution. In applications, constant M has to be chosen appropriately. The values of T_n for a variety of models could be used as guideline for the choice of M.

Let $\mathcal{F}_0 = \{\tilde{C}_\xi, \xi \in \Xi\}$ be a comparative family of copulas. We propose the following *approximation coefficient*:

$$\rho = 1 - \frac{\mathcal{D}(C, \mathcal{F})}{\mathcal{D}(C, \mathcal{F}_0)}.$$

Obviously, $\rho \le 1$ holds, and $\rho \in [0,1]$ in the case $\mathcal{F}_0 \subset \mathcal{F}$. The interpretation is similar to correlation coefficients. Values of ρ close to 1 indicate that the approximation by $\mathcal{F}$ is good (see also Liebscher [12]). The coefficient ρ can be estimated by plugging in estimators for $\mathcal{D}(C, \mathcal{F})$ and $\mathcal{D}(C, \mathcal{F}_0)$ as introduced above.

12.5 Proofs

First we prove a central limit theorem for U-statistics of order 3:

Proposition 12.1 *Assume that the measurable function* $\Lambda : \mathbb{R}^3 \to \mathbb{R}$ *satisfies* $\mathbb{E}\Lambda^2(X_1, X_2, X_3) < +\infty$. *Let*

$$W_n = \frac{1}{n^3}\sum_{i=1}^n\sum_{j=1}^n\sum_{k=1}^n \Lambda(X_i, X_j, X_k), \qquad \Psi = \mathbb{E}\Lambda(X_1, X_2, X_3),$$

$$\bar{\lambda}(u) = \frac{1}{3}\big(\mathbb{E}\Lambda(u, X_1, X_2) + \mathbb{E}\Lambda(X_1, u, X_2) + \mathbb{E}\Lambda(X_1, X_2, u)\big).$$

Then

$$\sqrt{n}(W_n - \Psi) \xrightarrow{\mathcal{D}} \mathcal{N}\big(0, \sigma_1^2\big) \quad \text{with } \sigma_1^2 = 9\,\mathrm{Var}\big(\bar{\lambda}(X_1)\big).$$

Proof Let $K(u,v,w) = (\Lambda(u,v,w) + \Lambda(u,w,v) + \Lambda(v,u,w) + \Lambda(v,w,u) + \Lambda(w,u,v) + \Lambda(w,v,u))/6$. By the law of large numbers for U-statistics (see for example Serfling [15, Theorem 5.4.A]), we can deduce

$$\begin{aligned} W_n &= \frac{1}{n^3}\sum_{i=1}^n\sum_{j=i+1}^n\sum_{k=j+1}^n \big(\Lambda(X_i, X_j, X_k) + \Lambda(X_i, X_k, X_j) + \Lambda(X_j, X_i, X_k)\big) \\ &\quad + \Lambda(X_k, X_i, X_j) + \Lambda(X_j, X_k, X_i) + \Lambda(X_k, X_j, X_i)) + O_{\mathbb{P}}\big(n^{-1}\big) \\ &= \frac{6}{n^3}\sum_{i=1}^n\sum_{j=i+1}^n\sum_{k=j+1}^n K(X_i, X_j, X_k) + O_{\mathbb{P}}\big(n^{-1}\big). \end{aligned}$$

Note that $\bar{\lambda}(u) = \mathbb{E}(K(u, X_1, X_2))$, and $\mathbb{E}\bar{\lambda}(X_1) = \Psi$. An application of Theorem 5.5.1A in Serfling [15] leads to the assertion of the proposition. □

Proof of Theorem 12.3 Let $\mathscr{H}_n = (\mathscr{H}_{npq})_{p,q=1\ldots k}$ with $\mathscr{H}_{npq}(\theta) = \frac{\partial^2}{\partial\theta_p\partial\theta_q}\widehat{\mathscr{D}}_n(C_\theta)$ be the Hessian of $\widehat{\mathscr{D}}_n$. Since $\nabla_\theta \widehat{\mathscr{D}}_n(C_{\check{\theta}_n}) = 0$, we have

$$\widehat{\mathscr{D}}_n(C_{\check{\theta}_n}) = \widehat{\mathscr{D}}_n(C_{\theta_0}) - \frac{1}{2}(\check{\theta}_n - \theta_0)^T \mathscr{H}_n(\tilde{\theta}_n)(\check{\theta}_n - \theta_0)$$

where $\tilde{\theta}_{np} = \theta_0 + \bar{\eta}_p(\check{\theta}_n - \theta_0)$. Obviously, $\mathscr{H}_n(\tilde{\theta}_n) = O_{\mathbb{P}}(1)$. Hence $\widehat{\mathscr{D}}_n(C_{\check{\theta}_n}) - \widehat{\mathscr{D}}_n(C_{\theta_0}) = o_{\mathbb{P}}(n^{-1/2})$ and

$$\sqrt{n}\big(\widehat{\mathscr{D}}_n(C_{\check{\theta}_n}) - \mathscr{D}(C, C_{\theta_0})\big) = \sqrt{n}\big(\widehat{\mathscr{D}}_n(C_{\theta_0}) - \mathscr{D}(C, C_{\theta_0})\big) + o_{\mathbb{P}}(1).$$

We deduce

$$\begin{aligned}
&\sqrt{n}\big(\widehat{\mathscr{D}}_n(C_{\theta_0}) - \mathscr{D}(C, C_{\theta_0})\big) \\
&\quad = n^{-1/2}\sum_{i=1}^{n}\Big(\big(\hat{H}_n(X_i) - C_{\theta_0}\big(F(X_i)\big)\big)^2 - \mathscr{D}(C, C_{\theta_0})\Big) \\
&\qquad + n^{-1/2}\sum_{i=1}^{n}\big(C_{\theta_0}\big(F(X_i)\big) - C_{\theta_0}\big(\bar{F}_n(X_i)\big)\big) \\
&\qquad \times \big(2\hat{H}_n(X_i) - C_{\theta_0}\big(\bar{F}_n(X_i)\big) - C_{\theta_0}\big(F(X_i)\big)\big) \\
&\quad = A_n + B_{n1} + B_{n2}
\end{aligned}$$

where

$$\begin{aligned}
A_n &= n^{-1/2}\sum_{i=1}^{n}\Bigg(\big(\hat{H}_n(X_i) - C_{\theta_0}\big(F(X_i)\big)\big)^2 - \mathscr{D}(C, C_{\theta_0}) \\
&\qquad - 2\sum_{m=1}^{d} C_{\theta_0}^{(m)}\big(F(X_i)\big)\big(F_{nm}(X_{im}) - F_m(X_{im})\big)\big(H(X_i) - C_{\theta_0}\big(F(X_i)\big)\big)\Bigg) \\
B_{n1} &= n^{-1/2}\sum_{i=1}^{n}\Bigg(C_{\theta_0}\big(F(X_i)\big) - C_{\theta_0}\big(\bar{F}_n(X_i)\big) \\
&\qquad + \sum_{m=1}^{d} C_{\theta_0}^{(m)}\big(F(X_i)\big)\big(F_{nm}(X_{im}) - F_m(X_{im})\big)\Bigg) \\
&\qquad \times \big(2\hat{H}_n(X_i) - C_{\theta_0}\big(F(X_i)\big) - C_{\theta_0}\big(\bar{F}_n(X_i)\big)\big) \\
B_{n2} &= n^{-1/2}\sum_{i=1}^{n}\sum_{m=1}^{d} C_{\theta_0}^{(m)}\big(F(X_i)\big)\big(F_{nm}(X_{im}) - F_m(X_{im})\big) \\
&\qquad \times \big(2\big(H(X_i) - \hat{H}_n(X_i)\big) - C_{\theta_0}\big(F(X_i)\big) + C_{\theta_0}\big(\bar{F}_n(X_i)\big)\big).
\end{aligned}$$

Further we obtain

$$B_{n1} = o(1), \qquad B_{n2} = o(1) \text{ a.s.}$$

Observe that

$$\begin{aligned} A_n &= n^{-5/2} \sum_{i=1}^{n} \Bigg(\sum_{j=1}^{n} \sum_{l=1}^{n} \big(I(X_j \le X_i) - C_{\theta_0}\big(F(X_i)\big)\big)\big(I(X_l \le X_i) - C_{\theta_0}\big(F(X_i)\big)\big) \\ &\quad - n^2 \mathscr{D}(C, C_{\theta_0}) - 2n \sum_{j=1}^{n} \sum_{m=1}^{d} C_{\theta_0}^{(m)}\big(F(X_i)\big)\big(I(X_{jm} \le X_{im}) - F_m(X_{im})\big) \\ &\quad \times \big(H(X_i) - C_{\theta_0}\big(F(X_i)\big)\big)\Bigg) \\ &= \sqrt{n}\left(n^{-3} \sum_{i=1}^{n} \sum_{j=1}^{n} \sum_{l=1}^{n} \Lambda(X_i, X_j, X_l) - \mathscr{D}(C, C_{\theta_0}) \right) \end{aligned}$$

where $X_i = (X_{i1}, \ldots, X_{id})$,

$$\begin{aligned} \Lambda(X_i, X_j, X_l) &= \big(I(X_j \le X_i) - C_{\theta_0}\big(F(X_i)\big)\big)\big(I(X_l \le X_i) - C_{\theta_0}\big(F(X_i)\big)\big) \\ &\quad - 2 \sum_{m=1}^{d} C_{\theta_0}^{(m)}\big(F(X_i)\big)\big(I(X_{jm} \le X_{im}) - F_m(X_{im})\big) \\ &\quad \times \big(H(X_i) - C_{\theta_0}\big(F(X_i)\big)\big). \end{aligned}$$

We have

$$\begin{aligned} \lambda(x) &= \mathbb{E}\Lambda(x, X_1, X_2) + \mathbb{E}\Lambda(X_1, x, X_2) + \mathbb{E}\Lambda(X_1, X_2, x) \\ &= \big(H(x) - C_{\theta_0}\big(F(x)\big)\big)^2 + 2\rho_1(x) - 2\rho_2(x). \end{aligned}$$

An application of Proposition 12.1 ($\lambda = 3\bar{\lambda}$) leads to the theorem. □

References

1. Bücher A, Dette H (2010) Some comments on goodness-of-fit tests for the parametric form of the copula based on L^2-distances. J Multivar Anal 101:749–763
2. Chen X, Fan Y (2005) Pseudo-likelihood ratio tests for semiparametric multivariate copula model selection. Can J Stat 33:389–414
3. Fermanian J-D (2005) Goodness-of-fit tests for copulas. J Multivar Anal 95:119–152
4. Genest C, Rivest L-P (1993) Statistical inference procedures for bivariate Archimedian copulas. J Am Stat Assoc 88:1034–1043
5. Genest C, Quessy J-F, Rémillard B (2006) Goodness-of-fit procedures for copula models based on the probability integral transformation. Scand J Stat 33:337–366
6. Genest C, Rémillard B (2008) Validity of the parametric bootstrap for goodness-of-fit testing in semiparametric models. Ann Inst Henri Poincaré Probab Stat 44:1096–1127
7. Genest C, Rémillard B, Beaudoin D (2009) Goodness-of-fit tests for copulas: a review and a power study. Insur Math Econ 44:199–213

8. Joe H (1997) Multivariate models and dependence concepts. Chapman & Hall, London
9. Joe H (2005) Asymptotic efficiency of the two-stage estimation method for copula-based models. J Multivar Anal 94:401–419
10. Lachout P, Liebscher E, Vogel S (2005) Strong convergence of estimators as ε_n-minimisers of optimisation problems. Ann Inst Stat Math 57:291–313
11. Liebscher E (2009) Semiparametric estimation of the parameters of multivariate copulas. Kybernetika 6:972–991
12. Liebscher E (2014) Approximation of distributions by using the Anderson Darling statistic. To appear in Commun Stat Theory Methods
13. Nelsen RB (1999) An introduction to Copulas. Lecture notes in statistics, vol 139. Springer, Berlin
14. Oakes D (1994) Multivariate survival distributions. J Nonparametr Stat 3:343–354
15. Serfling R (1980) Approximation theorems of mathematical statistics. Wiley, New York
16. Sklar A (1959) Fonctions de répartition à n dimensions et leurs marges. Publ Inst Stat Univ Paris 8:229–231
17. Tsukahara H (2005) Semiparametric estimation in copula models. Can J Stat 33:357–375

Chapter 13
Selection Consistency of Generalized Information Criterion for Sparse Logistic Model

Jan Mielniczuk and Hubert Szymanowski

Abstract We consider selection rule for small-n-large-P logistic regression which consists in choosing a subset of predictors minimizing Generalized Information Criterion over all subsets of variables of size not exceeding k. We establish consistency of such rule under weak conditions and thus generalize results of Chen and Chen in Biometrika, 95:759-771, 2008 to much broader regression scenario which also allows for a more general criterion function than considered there and k depending on a sample size. The results are valid for number of predictors of exponential order of sample size.

13.1 Introduction

Let X be $n \times (P+1)$ design matrix with rows $x'_{i,.}$, columns $x_{.,j}$ and $Y = (y_1, \ldots, y_n)'$ a response vector. All elements of $x_{.,0}$ are equal to 1. We consider a standard logistic regression model in which response $y \in \{0, 1\}$ is related to explanatory variable $x \in \mathbb{R}^{P+1}$ by the equation

$$\mathscr{P}(y = 1|x) = \exp\big(x'\beta_0\big)/\big[1 + \exp\big(x'\beta_0\big)\big], \tag{13.1}$$

where vector $\beta_0 = (\beta_{0,0}, \ldots, \beta_{0,P})'$ is a vector of parameters. The first coordinate $\beta_{0,0}$ corresponds to the column of ones in design matrix. Remaining coordinates pertain to P explanatory variables. We assume that observations are either deterministic vectors in $\mathbb{R}^{P+1}$ or random variables distributed according to $\mathscr{P}_x$. Data consists of independent observations $(x'_{i,.}, y_i)$, $i = 1, \ldots, n$ and we assume that $x_{i,.}$

H. Szymanowski was supported by POKL research fellowship.

J. Mielniczuk (✉) · H. Szymanowski
Institute of Computer Sciences, Polish Academy of Sciences, Warsaw, Poland
e-mail: miel@ipipan.waw.pl

J. Mielniczuk
Warsaw University of Technology, Warsaw, Poland

H. Szymanowski
e-mail: h.szymanowski@ipipan.waw.pl

A. Steland et al. (eds.), *Stochastic Models, Statistics and Their Applications*,
Springer Proceedings in Mathematics & Statistics 122,
DOI 10.1007/978-3-319-13881-7_13

are either deterministic or $x_{i,\cdot} \sim \mathscr{P}_x$ and conditional distribution of y_i given $x_{i,\cdot} = x$ is specified by (13.1). In the paper we consider the problem of selecting unknown subset of relevant predictors with nonzero coefficients. Thus we want to estimate $s_0 = \{i \in \{1, 2, \ldots, P\}\colon\ \beta_{0,i} \neq 0\} \cup \{0\}$, where augmentation by 0 means that the fitted model always contains intercept. We assume that s_0 is fixed. From now on $\beta_0(s_0) = \beta_0$ will stand for the vector of true parameters in the model s_0 augmented by zeros to $(P+1)$-dimensional vector if necessary.

We consider the following Generalized Information Criterion GIC (cf. [8])

$$\mathrm{GIC}(s) = -2l(\hat{\beta}_s, Y|X_s) + a_n|s|, \tag{13.2}$$

where s is a given submodel containing $|s|$ explanatory variables and an intercept, l is defined in (13.4), $\hat{\beta}_s$ is a maximum likelihood estimator for model s (augmented by zeros to $(P+1)$-dimensional vector if necessary) and a_n is a chosen penalty. Observe that $a_n = \log(n)$ corresponds to BIC and $a_n = 2$ to AIC. Consideration of different penalties gained momentum after realization (cf. [2]) that BIC penalty, although significantly larger than AIC, can also lead to choice of too many variables e.g. in case of linear model with many predictors. Solutions to this problem such as modified BIC (MBIC) [1] and Extended BIC (EBIC) [3] were proposed. EBIC criterion stems from putting a certain non-uniform prior on family of models and corresponds to a_n in (13.2) equal $\log n + 2\gamma \log P$ for some $\gamma > 0$. We also mention extension to generalized linear models (GLMs) of three-stage procedure developed in [7]. For analysis of variable selection under sparsity in a general regression model we refer to [4]. Here, we consider the following selection method which looks for the minimum of GIC over a family of models with number of regressors bounded by a predetermined threshold. Namely, let $\mathscr{M} = \{s\colon\ |s| \leq k_n\}$ where k_n is certain nondecreasing sequence of integers and

$$\hat{s}_0 = \arg\min_{s \in \mathscr{M}} \mathrm{GIC}(s). \tag{13.3}$$

This selection method in the case of $k_n = k$ was introduced in [3] for the linear models and extended in [5] to the case of the generalized GLMs. Here, specializing GLM to the case of logistic regression we study behavior of general criterion function (13.2) under much weaker conditions on design and more general sequence k_n allowing in particular that it diverges to infinity.

In order to heuristically justify $\hat{s}_0$ we need to know that $k_n \geq |s_0|$. As such knowledge is usually unavailable when k_n is fixed, therefore it is natural to assume that k_n is a sequence tending slowly to infinity. This is a principal motivation to extend results in [5] in this direction. We study consistency of $\hat{s}_0$ defined in (13.3) under fairly general assumptions on design and sequences k_n and a_n. In particular we allow for random as well as deterministic predictors. As a byproduct we obtain a rate of consistency of maximum likelihood estimator which is uniform over supermodels of s_0.

The main technical improvement in comparison to [5] relies on application of exponential inequality for subgaussian random variables derived in [10]. This allows to circumvent Lemma 1 in [5] which seems unjustified under presented set

of assumptions (see line 7 on p. 586 of [5] in which condition that $(\sum_{i=1}^{n} a_{ni}^2)_n$ is bounded is tacitly used) and there is no obvious way to verify amended assumptions in the proof of their crucial Theorem 2. In particular, the condition on EBIC constant γ in their result is still a conjecture, see Remark 3 for a result in this direction.

13.2 Main Results

Under the logistic regression model (13.1) and letting $p(s) = 1/(1+e^{-s})$ the conditional log-likelihood function for the parameter $\beta \in \mathbb{R}^{P+1}$ is

$$l(\beta, Y|X) = \sum_{i=1}^{n} \{ y_i \log[p(x_{i,\cdot}'\beta)] + (1-y_i) \log[1 - p(x_{i,\cdot}'\beta)] \} \tag{13.4}$$

Maximum likelihood estimator (ML) of β_0 is denoted by $\hat{\beta}_0$. Note that the score function $S_n(\beta)$, derivative of $l(\beta, Y|X)$, equals $X'(Y - p(\beta))$, where $p(\beta) = (p(x_{1,\cdot}'\beta), \ldots, p(x_{n,\cdot}'\beta))'$. Negative Hessian $H_n(\beta)$ of loglikelihood, equals $X'\Pi(\beta)X$, where $\Pi(\beta) = \mathrm{diag}\{p(x_{1,\cdot}'\beta)(1-p(x_{1,\cdot}'\beta)), \ldots, p(x_{n,\cdot}'\beta)(1-p(x_{n,\cdot}'\beta))\}$.

All the results of the section are proved for the case of random observations $x_{i,\cdot}$, however (see Remark 13.1) they remain true under slightly modified assumptions for the case of deterministic $x_{i,\cdot}$ which is the scenario considered in [5] for constant k. The proof for the random case requires more care. The conditions we impose on $P = P_n$, k_n and penalty a_n are $k_n^2 \log P_n = o(n)$ and $k_n \log P_n = o(a_n)$. They reduce for constant k to $\log P_n = o(n)$ and $\log P_n = o(a_n)$. EBIC criterion corresponds to $a_n = \log n + 2\gamma \log P_n$ thus for $n \le P_n$ this is a boundary case of the condition $\log P_n = o(a_n)$. We indicate in Remark 13.3 that our results extend to the case of EBIC for large values of coefficient γ. Thus for constant k our results are extensions of the results in [5] for EBIC for large penalty constants proved under less demanding conditions. In their paper the case of $P_n = O(\exp(n^\kappa))$ is considered and $\kappa < 1/3$ is assumed whereas our conditions stipulate only that $\kappa < 1$. Then the condition corresponding the first condition on k_n is $k_n = o(n^{(1-\kappa)/2})$.

The lemma below is the main technical tool in proving GIC selection consistency.

It follows from Zhang [10] after noting that binary random variable satisfies $Ee^{t(\xi - E\xi)} \le e^{t^2/8}$ and taking $\sigma = 1/2$, $\varepsilon = \eta^{1/2} - \sigma$ in his Proposition 10.2.

Lemma 13.1 *Let $Y = (y_1, \ldots, y_n)'$ be a vector consisting of independent binary variables and $Z = Z(n \times n)$ be a fixed matrix. For any $\eta > 1/4$*

$$\mathscr{P}\big(\|Z(Y - EY)\|^2 \ge \mathrm{tr}(Z'Z)\eta\big) \le e^{-\eta/20}. \tag{13.5}$$

We apply the inequality to the case of logistic model when predictors are random. Let $Z = Z(X)$ be a random matrix. It is easily seen by conditioning that the following modification of the above inequality also holds. Namely

$$\mathscr{P}\big(\|Z\big(Y - E(Y|X)\big)\|^2 \ge \mathrm{tr}(Z'Z)\eta\big) = E_X \mathscr{P}\big(\|Z\big(Y - E(Y|X)\big)\|^2 \ge \mathrm{tr}(Z'Z)\eta|X\big) \le e^{-\eta/20}.$$

In the following we will always assume that $|s_0| \leq k_n$ which is automatically satisfied for large n if $k_n \to \infty$. We define two families of models: $A_0 = \{s\colon\ s_0 \subseteq s \wedge |s| \leq k_n\}$, i.e. family of true models consisting of at most k_n predictors and $A_1 = \{s\colon\ s_0 \nsubseteq s \wedge 0 \in s \wedge |s| \leq k_n\}$. Let $\beta_0(s)$ for $s_0 \subseteq s$ denote $\beta_0(s_0)$ augmented by zeros for coordinates belonging to $s \setminus s_0$. The following conditions will be imposed.

$C1$: For every $\eta > 0$ there exist constants $0 < C_1, C_2 < +\infty$ such that for all n

$$\mathscr{P}\left\{C_1 \leq \min_{s\in A_1} \lambda_{\min}\left(\frac{1}{n} H_n\big(\beta_0(s \cup s_0)\big)\right) \leq \max_{s\in A_1} \lambda_{\max}\left(\frac{1}{n} X'_{s\cup s_0} X_{s\cup s_0}\right) \leq C_2\right\} \geq 1 - \eta.$$

$C2$: For every $\varepsilon > 0$ there exists $\delta > 0$ such that for every $\eta > 0$ and every $n \geq n_0(\varepsilon, \delta, \eta)$, with $\leq_L$ denoting Loewner ordering

$$\mathscr{P}\big\{\forall_{s\colon\ |s|\leq k_n} \forall_{\|\beta(s\cup s_0) - \beta_0(s\cup s_0)\| \leq \delta} (1-\varepsilon) H_n\big(\beta_0(s \cup s_0)\big) \leq_L H_n\big(\beta(s \cup s_0)\big) \leq_L (1+\varepsilon) H_n\big(\beta_0(s \cup s_0)\big)\big\} \geq 1 - \eta.$$

Remark 13.1 Results of this section are valid for deterministic X with slightly modified but simpler proofs with the following changes of assumptions. Condition $C1$ is replaced by:

$C1'$: There exist constants $0 < C_1, C_2 < +\infty$ such that for all n

$$C_1 \leq \min_{s\in A_1} \lambda_{\min}\left(\frac{1}{n} H_n\big(\beta_0(s \cup s_0)\big)\right) \leq \max_{s\in A_1} \lambda_{\max}\left(\frac{1}{n} X'_{s\cup s_0} X_{s\cup s_0}\right) \leq C_2 \quad (13.6)$$

and $C2$ by:

$C2'$: For any $\varepsilon > 0$ there exists $\delta > 0$ such that for sufficiently large n

$$\forall_{s\colon\ |s|\leq k_n} \forall_{\|\beta(s\cup s_0) - \beta_0(s\cup s_0)\| \leq \delta} (1-\varepsilon) H_n\big(\beta_0(s \cup s_0)\big) \leq_L H_n\big(\beta(s \cup s_0)\big) \leq_L (1+\varepsilon) H_n\big(\beta_0(s \cup s_0)\big).$$

The first of this assumptions is a slight strengthening of Assumption A4 in [5] whereas the second one is the same as their A5. Note that since $X'\Pi X \leq_L X'X$ condition $C1'$ implies that all subsets of columns of X of size at most k_n are linearly independent. It is shown in [9] that condition $C1$ (with Hessian H_n replaced by moment matrix $X'X$) is satisfied for normal predictors under appropriate assumptions on their covariance matrices, p and k_n. Condition C_2' is analogous to condition (N) in [6] (cf. (3.4), p. 348 there). Moreover, note that the assumption $\max_{s\in A_1} \operatorname{tr}(X'_{s\cup s_0} X_{s\cup s_0}) = O_P(k_n n)$ used in Theorem 13.1 below follows from $C1$. Further on it is replaced by $C1$.

Theorem 13.1 *Let $X = (x_{ij})$ $i = 1, \ldots, n$; $j = 1, \ldots, k_n$ be a random matrix such that $\max_{s\in A_1} \operatorname{tr}(X'_{s\cup s_0} X_{s\cup s_0}) = O_P(k_n n)$. Then*

$$\max_{s\in A_1} \big\| S_n\big(\beta_0(s \cup s_0)\big)\big\| = O_P(k_n \sqrt{n \log P_n}). \quad (13.7)$$

Proof Intersecting set $\{\max_{s\in A_1}\|S_n(\beta_0(s\cup s_0))\|\geq M_1k_n\sqrt{n\log P_n}\}$ with an event $\{\max_{s\in A_1}\operatorname{tr}(X'_{s\cup s_0}X_{s\cup s_0})\leq M_2k_nn\}$ and its complement we see that probability of the second set can be made arbitrarily small by a choice of M_2 whereas the first can be bounded using (13.1) by

$$\mathscr{P}\left(\max_{s\in A_1}\left\|X'_{s\cup s_0}\big(Y-p\big(\beta(s\cup s_0)\big)\big)\right\|\geq\frac{M_1}{\sqrt{M_2}}\sqrt{k_n\log P_n\,tr\big(X'_{s\cup s_0}X_{s\cup s_0}\big)}\right)$$
$$\leq P_n^{k_n}\exp\left(-\frac{M_1^2}{20M_2}k_n\log P_n\right).$$

For sufficiently large constant M_1 the last expression is arbitrarily small. □

Lemma 13.2 *Let $k_n^2\log P_n=o(n)$. Then, under assumptions C1 and C2 we have*

$$\max_{s\in A_0}\left\|\hat\beta_0(s)-\beta_0(s)\right\|=O_P\left(k_n\sqrt{\frac{\log P_n}{n}}\right).\tag{13.8}$$

Proof Let $\beta_u(s)=\beta_0(s)+\gamma_nu$ for a vector u such that $\|u\|=1$ and $\gamma_n=C_0k_n\sqrt{\log P_n/n}$. For any $\delta>0$ and sufficiently large n in view of the condition on k_n we have $\|\beta_u(s)-\beta_0(s)\|\leq\delta$ and assumption $C2$ becomes applicable. We show that

$$\mathscr{P}\left\{\exists u\colon\|u\|=1,\ \max_{s\in A_0,s\neq s_0}\left\{l_n\big(\beta_u(s)\big)-l_n\big(\beta_0(s)\big)\right\}>0\right\}=o(1).\tag{13.9}$$

Let us fix $\varepsilon_0>0$ and let δ_0 be the value of δ corresponding to ε_0 in assumption $C2$. Denote by $\mathscr{A}_n$ the following event

$$\left\{C_1\leq\min_{s\in A_0}\lambda_{\min}\left(\frac{1}{n}H_n\big(\beta_0(s)\big)\right)\leq\max_{s\in A_0}\lambda_{\max}\left(\frac{1}{n}X'_sX_s\right)\leq C_2\right\}$$
$$\cap\left\{\forall_{s\colon|s|\leq k_n}\forall_{\|\beta(s\cup s_0)-\beta_0(s\cup s_0)\|\leq\delta}(1-\varepsilon)H_n\big(\beta_0(s\cup s_0)\big)\leq_L H_n\big(\beta(s\cup s_0)\big)\right.$$
$$\left.\leq_L(1+\varepsilon)H_n\big(\beta_0(s\cup s_0)\big)\right\}.$$

Moreover, β^* will stand for generic vector belonging to the line segment with endpoints $\beta_u(s)$ and $\beta_0(s)$ i.e. having the form $\lambda\beta_u(s)+(1-\lambda)\beta_0(s)$ for some $\lambda\in[0,1]$. It follows from assumptions $C1$ and $C2$ that $\mathscr{P}(\mathscr{A}_n)$ is arbitrarily close to 1 for large n and sufficiently small C_1 and C_2^{-1}.

We have on $\mathscr{A}_n$ with some β^*

$$\mathscr{P}\left\{\exists u\colon\|u\|=1,\ \max_{s\in A_0}\left\{l_n\big(\beta_u(s)\big)-l_n\big(\beta_0(s)\big)\right\}>0\right\}$$
$$\leq P_n^{k_n}\max_{s\in A_0}\mathscr{P}\left\{\exists u\colon\|u\|=1,\ u'S_n(\beta_0)>\frac{1}{2}\gamma_nu'H_n\big(\beta^*\big)u\right\}$$
$$\leq P_n^{k_n}\max_{s\in A_0}\mathscr{P}\left\{\exists u\colon\|u\|=1,\ u'S_n(\beta_0)>\frac{1}{2}(1-\varepsilon_0)\gamma_nu'H_n(\beta_0)u\right\}$$
$$\leq P_n^{k_n}\max_{s\in A_0}\mathscr{P}\left\{\left\|S_n(\beta_0)\right\|>\frac{C_1}{2}(1-\varepsilon_0)\gamma_nn\right\}$$

where the last inequality follows by taking $u = S_n(\beta_0)/\|S_n(\beta_0)\|$. Since $\mathscr{A}_n \subset \{\max_{s\in A_1\cup s_0} \mathrm{tr}(X_s' X_s) \le C_2 k_n n\}$, we have from (13.1) that the last expression tends to zero when constant C_1 is sufficiently large. As $l_n(\beta(s))$ is a concave function for any s, it follows that, with probability tending to 1, estimator $\hat{\beta}_0(s)$ exists and belongs to γ_n-neighborhood of $\beta_0(s)$ uniformly for all $s \in A_0$. □

Remark 13.2 Note that for $k_n = k$ and $P_n = O(\exp(n^\kappa))$ it follows from (13.8) that the uniform rate of convergence of $\hat{\beta}$ over supersets of s_0 is $k_n(\log P_n/n)^{1/2} = O(n^{\frac{\kappa-1}{2}})$, thus assuming $\kappa \in (0, 1/3)$ as in [5] we obtain better rate of convergence than $O_P(n^{-1/3})$ determined in their Theorem 1.

Theorem 13.2 *Let assumptions C1 and C2 hold. Moreover, assume $a_n = o(n)$ and $k_n^2 \log P_n = o(n)$. Then*

$$\mathscr{P}\Big(\min_{s\in A_1} \mathrm{GIC}(s) \le \mathrm{GIC}(s_0)\Big) \to 0. \tag{13.10}$$

Proof Let $\varepsilon_0 > 0$ and δ_0 corresponds to ε_0 in assumption $C2$. Moreover, $\tilde{s} = s \cup s_0$. Let us denote by $\breve{\beta}(\tilde{s})$ ML estimator $\hat{\beta}(s)$ augmented with zeros corresponding to the elements in $s_0 \setminus s$. Note that

$$\big\|\breve{\beta}(\tilde{s}) - \beta_0(\tilde{s})\big\| \ge \big\|\beta_0(s_0 \setminus s)\big\| \ge \beta_{\min} > 0 \tag{13.11}$$

for all $s \in A_1$ where $\beta_{\min} = \min_{i\in s_0\setminus s} |\beta_{0,i}|$.

Let us fix $s \in A_1$ and denote $B = \{\beta\colon \|\beta(\tilde{s}) - \beta_0(\tilde{s})\| = r\}$, where $r = \min\{\beta_{\min}/2, \delta_0/2\}$. We have from Schwarz inequality and assumptions $C1$ and $C2$ on event $\mathscr{A}_n$ defined in the proof of Lemma 13.2 that for all $\beta \in B$ and some β^* between $\beta(\tilde{s})$ and $\beta_0(\tilde{s})$ the difference $l_n(\beta(\tilde{s})) - l_n(\beta_0(\tilde{s}))$ equals

$$\begin{aligned}
&\big[\beta(\tilde{s}) - \beta_0(\tilde{s})\big]' S_n\big(\beta_0(\tilde{s})\big) - \frac{1}{2}\big[\beta(\tilde{s}) - \beta_0(\tilde{s})\big]' H_n\big(\beta^*\big)\big[\beta(\tilde{s}) - \beta_0(\tilde{s})\big] \\
&\quad\le \big\|\beta(\tilde{s}) - \beta_0(\tilde{s})\big\| \cdot \big\|S_n\big(\beta_0(\tilde{s})\big)\big\| \\
&\qquad - \frac{1}{2}(1-\varepsilon_0)\big[\beta(\tilde{s}) - \beta_0(\tilde{s})\big]' H_n\big(\beta_0(\tilde{s})\big)\big[\beta(\tilde{s}) - \beta_0(\tilde{s})\big] \\
&\quad\le \big\|\beta(\tilde{s}) - \beta_0(\tilde{s})\big\| \cdot \big\|S_n\big(\beta_0(\tilde{s})\big)\big\| - \frac{C_1}{2}(1-\varepsilon_0)\cdot n\big\|\beta_0(\tilde{s}) - \beta(\tilde{s})\big\|^2.
\end{aligned}$$

It follows from Theorem 13.1 and the definition of sphere B that the last expression is bounded from above on a set of arbitrarily large positive measure by $-M_2 n$ for some positive constant M_2. By a concavity of function l_n and a fact $\breve{\beta} \notin B$ on $\mathscr{A}_n$

$$\begin{aligned}
&l_n\big(\hat{\beta}(s)\big) - l_n\big(\hat{\beta}(s_0)\big) = l_n\big(\breve{\beta}(\tilde{s})\big) - l_n\big(\hat{\beta}(s_0)\big) \le l_n\big(\breve{\beta}(\tilde{s})\big) - l_n\big(\beta_0(\tilde{s})\big) \\
&\quad\le l_n\big(\beta^*(\tilde{s})\big) - l_n\big(\beta_0(\tilde{s})\big) \le -M_2 \cdot n,
\end{aligned}$$

where $\beta^*(\tilde{s})$ is any element of B. This and an assumption $a_n = o(n)$ yields that

$$\begin{aligned}
&\mathscr{P}\Big(\min_{s\in A_1}\mathrm{GIC}(s)\le \mathrm{GIC}(s_0)\Big)\\
&\quad=\mathscr{P}\Big(\Big\{\max_{s\in A_1}\big(l_n\big(\hat\beta(s)\big)-l_n\big(\hat\beta(s_0)\big)+a_n\big(|s_0|-|s|\big)\big)\ge 0\Big\}\cap\mathscr{A}_n\Big)+\mathscr{P}\big(\mathscr{A}_n^c\big)\\
&\quad\le \mathscr{P}\big(-M_2 n+a_n|s_0|\ge 0\big)+\mathscr{P}\big(\mathscr{A}_n^c\big)\to 0.
\end{aligned}$$

□

The next result states that with probability tending to 1 GIC choses the smallest true model among all true models. Note that for $P_n = O(n^\kappa)$ the second condition on k_n is implied by $k_n = O(n^{1/2-\varepsilon})$ for any $\varepsilon > 0$.

Theorem 13.3 *Under assumptions C1 and C2 for* $k_n \log P_n = o(a_n)$ *and* $k_n^2 \log P_n = o(n)$

$$\mathscr{P}\Big(\min_{s\in A_0, s\ne s_0}\mathrm{GIC}(s)\le \mathrm{GIC}(s_0)\Big)\to 0. \tag{13.12}$$

Proof Let $s \in A_0$ and $s \ne s_0$. We have on event $\mathscr{A}_n$ and for some β^*, β^{**} that

$$\begin{aligned}
&l_n\big(\hat\beta(s)\big)-l_n\big(\hat\beta(s_0)\big)\le l_n\big(\hat\beta(s)\big)-l_n\big(\beta_0(s)\big)\\
&\quad=\big[\hat\beta(s)-\beta_0(s)\big]' S_n\big(\beta_0(s)\big)-\frac{1}{2}\big[\hat\beta(s)-\beta_0(s)\big]' H_n\big(\beta^{**}\big)\big[\hat\beta(s)-\beta_0(s)\big].
\end{aligned}$$

Note that

$$S_n\big(\hat\beta(s)\big)-S_n\big(\beta_0(s)\big)=-H_n\big(\beta^*\big)\big[\hat\beta(s)-\beta_0(s)\big], \tag{13.13}$$

and in view of $C1$, $C2$ and Lemma 13.2 $H_n(\beta^*)$ is invertible. Thus

$$\hat\beta(s)-\beta_0(s)=H_n\big(\beta^*\big)^{-1}S_n\big(\beta_0(s)\big). \tag{13.14}$$

Therefore, the right side of inequality (13.13) can be rewritten as

$$\begin{aligned}
&\big[S_n\big(\beta_0(s)\big)\big]' H_n\big(\beta^*\big)^{-1}S_n\big(\beta_0(s)\big)\\
&\quad-\frac{1}{2}\big[S_n\big(\beta_0(s)\big)\big]' H_n\big(\beta^*\big)^{-1}H_n\big(\beta^{**}\big)H_n\big(\beta^*\big)^{-1}S_n\big(\beta_0(s)\big).
\end{aligned}$$

Assumption $C2$ and a fact that $A \le_L B \Rightarrow A^{-1} \le_L A^{-1}BA^{-1}$ yields

$$l_n\big(\hat\beta(s)\big)-l_n\big(\hat\beta(s_0)\big)\le c\big[S_n\big(\beta_0(s)\big)\big]' H_n\big(\beta_0(s)\big)^{-1}S_n\big(\beta_0(s)\big) \tag{13.15}$$

for some constant c independent of $s \in A_0$. Hence, on event $\mathscr{A}_n$ we have

$$\mathscr{P}\Big(\max_{s\in A_0, s\ne s_0}\big(l_n\big(\hat\beta(s)\big)-l_n\big(\hat\beta(s_0)\big)-\big(|s|-|s_0|\big)a_n\big)\ge 0\Big) \tag{13.16}$$

$$\le \max_{s\in A_0, s\ne s_0} P_n^{k_n}\,\mathscr{P}\big(cS_n\big(\beta_0(s)\big)' H_n\big(\beta_0(s)\big)^{-1}S_n\big(\beta_0(s)\big)\ge a_n\big(|s|-|s_0|\big)\big) \tag{13.17}$$

$$= \max_{s\in A_0, s\ne s_0} P_n^{k_n}\,\mathscr{P}\big(c\big\|Z_s\big(Y-p\big(\beta_0(s)\big)\big)\big\|^2\ge a_n\big(|s|-|s_0|\big)\big) \tag{13.18}$$

where $Z_s = (X_s' \Pi_s X_s)^{-\frac{1}{2}} X_s'$. It is seen that on $\mathscr{A}_n$ $\operatorname{tr}(Z_s' Z_s) \le M_1 |s|$. It follows now from Zhang's inequality that for fixed $s \in A_0$ on $\mathscr{A}_n$ with $M_2 = (20cM_1)^{-1}$

$$P_n^{k_n} \mathscr{P}\big(c \big\| Z_s(Y - EY)\big\|^2 \ge a_n\big(|s| - |s_0|\big)\big) \le P_n^{k_n} E\left[\exp\left(-\frac{a_n(|s| - |s_0|)}{20c \cdot \operatorname{tr}(Z_s' Z_s)}\right)\right]$$
$$\le P_n^{k_n} \exp\left(-M_2 \frac{(|s| - |s_0|)a_n}{|s|}\right) \le P_n^{k_n} \exp\left(-C \frac{(|s| - |s_0|)k_n \log P_n}{|s|}\right),$$

where C may be chosen arbitrarily large and independent of s. Finally, we have as $\min_{s \in \mathscr{A}_0} (|s| - |s_0|)/|s| = 1/(|s_0| + 1)$

$$\mathscr{P}\Big(\min_{s \in \mathscr{A}_0} \mathrm{GIC}(s) \le \mathrm{GIC}(s_0)\Big) \tag{13.19}$$
$$\le \mathscr{P}\Big(\Big\{\max_{s \in \mathscr{A}_0} \big(l_n\big(\hat{\beta}(s)\big) - l_n\big(\hat{\beta}(s_0)\big) + a_n\big(|s_0| - |s|\big)\big) \ge 0\Big\} \cap \mathscr{A}_n\Big) + \mathscr{P}\big(\mathscr{A}_n^c\big) \tag{13.20}$$
$$\le P_n^{k_n} \exp\left(-C \frac{k_n \log P_n}{|s_0| + 1}\right) + \mathcal{P}\big(\mathscr{A}_n^c\big) \to 0 \tag{13.21}$$

for sufficiently large constant C independent of s. □

Remark 13.3 Theorem 13.2 is applicable to EBIC as the sole condition on a_n there is $a_n = o(n)$. Moreover, Theorem 13.3 remains true for EBIC in the case when $n = o(P_n)$ and constant $k_n = k$ if penalty coefficient γ is large enough. Indeed, substitution $a_n = \log n + 2\gamma \log P_n$ in (13.19) leads to the inequality

$$P_n^k \mathscr{P}\big(c \big\| Z_s(Y - EY)\big\|^2 \ge a_n\big(|s| - |s_0|\big)\big) \le P_n^k \exp\left(-M_2 \frac{2\gamma \log P_n}{|s_0| + 1}\right). \tag{13.22}$$

Thus if $\gamma > 0.5k(|s_0| + 1)M_2^{-1}$ (13.12) holds.

References

1. Bogdan M, Doerge R, Ghosh J (2004) Modifying the Schwarz Bayesian information criterion to locate multiple interacting quantitative trait loci. Genetics 167:989–999
2. Broman K, Speed T (2002) A model selection approach for the identification of quantitative trait loci in experimental crosses. J Am Stat Assoc 64:641–656
3. Chen J, Chen Z (2008) Extended Bayesian information criteria for model selection with large model spaces. Biometrika 95:759–771
4. Comminges L, Dalalyan A (2012) Tight conditions for consistency of variable selection in the context of high dimensionality. Ann Stat 40:2667–2696
5. Chen J, Chen Z (2012) Extended BIC for small-n-large-p sparse GLM. Stat Sin 22:555–574
6. Fahrmeir L, Kaufmann H (1985) Consistency and asymptotic normality of the maximum likelihood estimator in generalized linear models. Ann Stat 1(13):342–368
7. Pokarowski P, Mielniczuk J (2014) Combined ℓ_1 and greedy ℓ_0 least squares for linear model selection. J Mach Learn Res, to appear
8. Sin C, White H (1996) Information criteria for selecting possibly misspecified parametric models. J Econom 71:207–225

9. Wang H (2009) Forward regression for ultra-high dimensional variable screening. J Am Stat Assoc 104:1512–1524
10. Zhang T (2009) Some sharp performance bounds for least squares regression with L_1 regularization. Ann Stat 37:2109–2144

Chapter 14
Kernel Estimation of Wiener–Hammerstein System Nonlinearity

Grzegorz Mzyk

Abstract The paper addresses the problem of non-parametric estimation of the static characteristic in Wiener–Hammerstein (sandwich) system excited and disturbed by random processes. Two kernel-based methods are presented and compared. The proposed estimates are consistent under small amount of a priori information. An IIR dynamics, non-invertible static non-linearity, and non-Gaussian excitations are admitted. The convergence of the estimates is proved for each continuity point of the static characteristic and the asymptotic rate of convergence is analysed. The results of computer simulation example are included to illustrate the behaviour of the estimates for moderate number of observations.

14.1 Introduction

In the paper we address the problem of nonlinearity recovering in the system of Wiener–Hammerstein structure (see Fig. 14.1). It consists of one static nonlinear block with the characteristic $\mu()$, surrounded by two linear dynamic components with the impulse responses $\{\lambda_j\}_{j=0}^{\infty}$ and $\{\gamma_j\}_{j=0}^{\infty}$, respectively. Such a structure, and its particular cases (Wiener systems and Hammerstein systems), are widely considered in the literature because of numerous potential applications in various domains of science and technology (see e.g. [2]). The Wiener and Wiener–Hammerstein models allow for a good approximation of many real processes [1, 6, 11–14]. It was noticed that the nonparametric algorithms proposed in [7–9] and [3] for a Wiener system, can be adopted, after slight modification, for a broad class of Wiener–Hammerstein (sandwich) systems. All the assumptions taken therein remain the same. The algorithms work under poor prior knowledge of subsystems and excitations and in contrast to earlier literature items concerning sandwich and Wiener system identification:

- the input sequence need not to be a Gaussian white noise,

G. Mzyk (✉)
Institute of Computer Engineering, Control and Robotics, Wrocław University of Technology, Janiszewskiego 11/17, 50-372 Wrocław, Poland
e-mail: Grzegorz.Mzyk@pwr.edu.pl

A. Steland et al. (eds.), *Stochastic Models, Statistics and Their Applications*,
Springer Proceedings in Mathematics & Statistics 122,
DOI 10.1007/978-3-319-13881-7_14

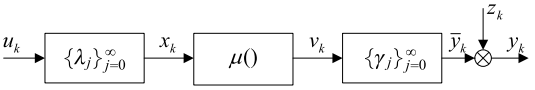

Fig. 14.1 Wiener–Hammerstein (sandwich) system

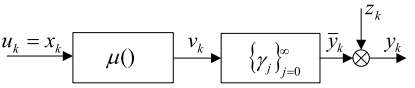

Fig. 14.2 Hammerstein system

- the nonlinear characteristic is not assumed to be invertible,
- the IIR linear dynamic blocks are admitted,
- the algorithms are of nonparametric nature (see e.g. [4]), i.e. it is not assumed that the subsystems can be described with the use of finite and known number of parameters. In consequence, the estimates are free of the possible approximation error, or this error can be made arbitrarily small by proper selection of tuning parameters.

Firstly, in Sect. 14.2, we show intuitively, why the censored algorithm (see [7]) proposed for Wiener system can be successfully applied for Hammerstein systems and Wiener–Hammerstein (sandwich) systems. Then, in Sect. 14.3, the problem is formulated in detail and the assumptions imposed on signals and system components are discussed. Finally, in Sect. 14.4 we present two nonparametric kernel-based estimates of the nonlinearity in Wiener–Hammerstein system, and analyse their properties.

14.2 Preliminaries

14.2.1 Hammerstein System

For the Hammerstein system (Fig. 14.2) described by

$$y_k = \sum_{j=0}^{\infty} \gamma_j \mu(x_{k-j}) + z_k, \tag{14.1}$$

we assume that the unknown impulse response $\{\gamma_j\}_{j=0}^{\infty}$ fulfils conditions $|\gamma_j| \leq c_1 \lambda^j$, and $G = \sum_{j=0}^{\infty} \gamma_j = 1$. For Lipschitz function $\mu()$ we simply get

$$\begin{aligned} &\left|\bar{y}_k - \mu(x)\right| \\ &= \left|\sum_{j=0}^{\infty} \gamma_j \mu(x_{k-j}) - \sum_{j=0}^{\infty} \gamma_j \mu(x)\right| = \left|\sum_{j=0}^{\infty} \gamma_j \big(\mu(x_{k-j}) - \mu(x)\big)\right| \\ &= \left|\sum_{j=0}^{k-1} \gamma_j \big(\mu(x_{k-j}) - \mu(x)\big) + \sum_{j=k}^{\infty} \gamma_j \big(\mu(x_{k-j}) - \mu(x)\big)\right| \end{aligned}$$

$$\leq \sum_{j=0}^{k-1} |\gamma_j| \left|\mu(x_{k-j}) - \mu(x)\right| + 2u_{\max} l \sum_{j=k}^{\infty} |\lambda_j| \leq l\delta_k(x) + \frac{l\lambda^k}{1-\lambda} = l\Delta_k(x),$$

which means that for a given x, the noise-free output $\overline{y}_k$ is located close to $\mu(x)$.

14.2.2 Wiener–Hammerstein System

Now, let us consider a tandem three-element connection shown in Fig. 14.1, where u_k and y_k is a measurable system input and output at time k respectively, z_k is a random noise, $\mu()$ is the unknown characteristic of the static nonlinearity and $\{\lambda_j\}_{j=0}^{\infty}$, $\{\gamma_j\}_{j=0}^{\infty}$ – the unknown impulse responses of the two linear dynamic components. By assumption, the interaction signals x_k and v_k are not available for measurements. The system is described as follows

$$y_k = \sum_{j=0}^{\infty} \gamma_j v_{k-j} + z_k, \qquad v_k = \mu\left(\sum_{j=0}^{\infty} \lambda_j u_{k-j}\right). \tag{14.2}$$

Similarly as for Hammerstein system, we get

$$\begin{aligned}
&\left|\overline{y}_k - \mu(x)\right| \\
&= \left|\sum_{i=0}^{\infty} \gamma_i \mu(x_{k-i}) - \sum_{i=0}^{\infty} \gamma_i \mu(x)\right| \\
&= \left|\sum_{i=0}^{\infty} \gamma_i \mu\left(\sum_{j=0}^{\infty} \lambda_j u_{k-i-j}\right) - \sum_{i=0}^{\infty} \gamma_i \mu\left(\sum_{j=0}^{\infty} \lambda_j x\right)\right| \\
&= \left|\sum_{i=0}^{\infty} \gamma_i \left[\mu\left(\sum_{j=0}^{\infty} \lambda_j u_{k-i-j}\right) - \mu\left(\sum_{j=0}^{\infty} \lambda_j x\right)\right]\right| \\
&\leq l \sum_{i=0}^{\infty} |\gamma_i| \left|\sum_{j=0}^{\infty} \lambda_j (u_{k-i-j} - x)\right| \\
&\leq l \sum_{i=0}^{\infty} |\gamma_i| \sum_{j=0}^{\infty} |\lambda_j| |u_{k-i-j} - x| = l \sum_{i=0}^{\infty} \kappa_i |u_{k-i} - x|,
\end{aligned}$$

where the sequence $\{\kappa_i\}_{i=0}^{\infty}$ is the convolution of $\{|\gamma_i|\}_{i=0}^{\infty}$ with $\{|\lambda_j|\}_{i=0}^{\infty}$, which obviously fulfils the condition $|\kappa_i| \leq \lambda^i$.

14.3 Assumptions

For a Wiener–Hammerstein system we assume that:

A1. The input $\{u_k\}$ is an i.i.d., bounded ($|u_k| < u_{\max}$; unknown $u_{\max} < \infty$) random process, and there exists a probability density of the input, say $\vartheta_u(u_k)$, which is a continuous and strictly positive function around the estimation point x, i.e., $\vartheta_u(x) \geq \varepsilon > 0$.

A2. The unknown impulse responses $\{\lambda_j\}_{j=0}^{\infty}$ and $\{\gamma_j\}_{j=0}^{\infty}$ of the linear IIR filters are both exponentially upper bounded, that is

$$|\lambda_j| \leq c_1 \lambda^j, \qquad |\gamma_j| \leq c_1 \lambda^j \tag{14.3}$$

some unknown $0 < c_1 < \infty$, where $0 < \lambda < 1$ is an a priori known constant.

A3. The nonlinear characteristic $\mu(x)$ is a Lipschitz function, i.e., it exists a positive constant $l < \infty$, such that for each $x_a, x_b \in R$ it holds that

$$\left|\mu(x_a) - \mu(x_b)\right| \leq l|x_a - x_b|.$$

A4. The output noise $\{z_k\}$ is a zero-mean stationary and ergodic process, which is independent of the input $\{u_k\}$.

A5. For simplicity of presentation we also let $L = \sum_{j=0}^{\infty} \lambda_j = 1$, $G = \sum_{j=0}^{\infty} \gamma_j = 1$, and $u_{\max} = \frac{1}{2}$.

The goal is to estimate the unknown characteristic of the nonlinearity $\mu(x)$ on the interval $x \in (-u_{\max}, u_{\max})$ on the basis of N input–output measurements $\{(u_k, y_k)\}_{k=1}^{N}$ of the whole Wiener–Hammerstein system. Similarly as for Wiener system from Assumptions A1 and A2 it holds that $|x_k| < x_{\max} < \infty$, where $x_{\max} = u_{\max} \sum_{j=0}^{\infty} |\lambda_j|$. The condition (14.3), with unknown c_1, is rather not restrictive, and characterises the class of stable objects. In particular case of FIR linear dynamic blocks, Assumption A2 is fulfilled for arbitrarily small $\lambda > 0$. As regards the Assumption A5, we note, that the class of Wiener–Hammerstein systems composed by series connection of linear filters with the impulse responses $\{\overline{\lambda}_j\} = \{\frac{\lambda_j}{\beta}\}_{j=0}^{\infty}$, $\{\overline{\gamma}_j\} = \{\frac{\gamma_j}{\alpha}\}_{j=0}^{\infty}$ and the nonlinearities $\overline{\mu}(x) = \alpha\mu(\beta x)$ are, for $\alpha, \beta \neq 0$, indistinguishable from the input–output point of view.

Remark 14.1 If the technical Assumption A5 is not fulfilled, i.e., the gains $L = \sum_{j=0}^{\infty} \lambda_j$ or $G = \sum_{j=0}^{\infty} \gamma_j$ are not unit, then only the scaled and dilated version $G\mu(Lx)$ of the true system characteristic $\mu(x)$ can be identified. The constants G and L are not identifiable, since the internal signals x_k and v_k cannot be measured.

14.4 The Algorithms

For a Wiener–Hammerstein system we apply and compare the following two nonparametric kernel-based estimates of the nonlinear characteristic $\mu()$, proposed before for a Wiener system in [7] and [3], respectively,

$$\widehat{\mu}_N^{(1)}(x) = \frac{\sum_{k=1}^{N} y_k \cdot K\left(\frac{\sum_{j=0}^{k} |u_{k-j} - x|\lambda^j}{h(N)}\right)}{\sum_{k=1}^{N} K\left(\frac{\sum_{j=0}^{k} |u_{k-j} - x|\lambda^j}{h(N)}\right)}, \tag{14.4}$$

$$\widehat{\mu}_N^{(2)}(x) = \frac{\sum_{k=1}^{N} y_k \prod_{i=0}^{p} K\left(\frac{x-u_{k-i}}{h(N)}\right)}{\sum_{k=1}^{N} \prod_{i=0}^{p} K\left(\frac{x-u_{k-i}}{h(N)}\right)}. \tag{14.5}$$

In (14.4) and (14.5) $K()$ is a bounded kernel function with compact support, i.e., it fulfils the following conditions

$$\int_{-\infty}^{\infty} K(x)dx = 1, \tag{14.6}$$

$$\sup_x \left|K(x)\right| < \infty, \tag{14.7}$$

$$K(x) = 0 \quad \text{for } |x| > x_0 \tag{14.8}$$

some $x_0 < \infty$. The sequence $h(N)$ (bandwidth parameter) is such that $h(N) \to 0$, as $N \to \infty$. The following theorem holds.

Theorem 14.1 *If* $h(N) = d(N)\log_\lambda d(N)$, *where* $d(N) = N^{-\gamma(N)}$, *and* $\gamma(N) = (\log_{1/\lambda} N)^{-w}$, *then for each* $w \in (\frac{1}{2}, 1)$ *the estimate* (14.4) *is consistent in the mean square sense*, *i.e.*, *it holds that*

$$\lim_{N\to\infty} E\left(\widehat{\mu}_N^{(1)}(x) - \mu(x)\right)^2 = 0. \tag{14.9}$$

Proof For the proof see [10]. □

In contrast to $\widehat{\mu}_N^{(1)}(x)$, the estimate $\widehat{\mu}_N^{(2)}(x)$ uses the FIR(p) approximation of the linear subsystems. We will show that since the linear blocks are asymptotically stable, the approximation of $\mu()$ can be made with arbitrary accuracy, i.e., by selecting p large enough. Let us introduce the following regression-based approximation of the true characteristic $\mu()$

$$m_p(x) = E\{y_k \mid u_k = u_{k-1} = \cdots = u_{k-2p+1} = x\} \tag{14.10}$$

and the constants $g_p = \sum_{i=0}^{p-1} \gamma_i$, $l_p = \sum_{j=0}^{p-1} \lambda_j$. The following theorem holds.

Theorem 14.2 *If* $K()$ *satisfy* (14.7) *then it holds that*

$$\widehat{\mu}_N^{(2)}(x) \to m_p(l_p x) \tag{14.11}$$

in probability, as $N \to \infty$, *at every point* x, *for which* $\vartheta_u(x) > 0$ *provided that* $Nh^{2p}(N) \to \infty$, *as* $N \to \infty$.

Proof The proof is a consequence of Theorem 1 in [3]. □

We obtain that $m_p(x) = E\{\sum_{i=0}^{p-1} \gamma_i \mu(x_{k-i}) + \varsigma | u_k = \cdots = u_{k-2p+1} = x\}$, where $\varsigma = \sum_{i=p}^{\infty} \gamma_i \mu(x_{k-i})$. Moreover, since $x_k = \sum_{j=0}^{p-1} \lambda_j u_{k-j} + \xi$, where $\xi = \sum_{j=p}^{\infty} \lambda_j u_{k-j}$ it holds that $|m_p(l_p x) - \mu(l_p x)| = |E\{g_p \mu(l_p x + \xi) + \varsigma\} - \mu(l_p x)| \le E|\{g_p \mu(l_p x + \xi) + \varsigma\} - \mu(l_p x)| \le |g_p - 1|(lEu_k + E\mu(x_k))$, and under

Table 14.1 The errors of the estimates (3) and (4) versus N

N	10^2	10^3	10^4	10^5	10^6
$ERR(\widehat{\mu}_N^1(x))$	16.4	12.4	8.1	6.0	4.8
$ERR(\widehat{\mu}_N^2(x))$	14.0	10.1	3.6	1.5	0.9

stability of linear components (see Assumptions A2 and A5) we have $|g_p - 1| \leq c_0^p$, some $|c_0| < 1$. Consequently,

$$\widehat{\mu}_N^{(2)}(x) \to \mu(l_p x) + \varepsilon_p$$

in probability, as $N \to \infty$, where $\varepsilon_p = c_0^p(lu_{\max} + v_{\max})\phi(x)$, and $|\phi(x)| \leq 1$. Since $\lim_{p\to\infty} l_p = 1$, and $\lim_{p\to\infty} \varepsilon_p = 0$ we conclude that (14.11) is constructive in the sense that the approximation model of $\mu()$ can have arbitrary accuracy by proper selection of p.

14.5 Numerical Example

To compare the proposed algorithms in practise we simulated Wiener–Hammerstein system with discontinuous nonlinearity $\mu(x) = \lfloor x \rfloor$ surrounded by two first-order IIR filters of the form

$$x_k = 0.5x_{k-1} + 0.5u_k, \quad \text{and} \quad \overline{y}_k = 0.5\overline{y}_{k-1} + 0.5v_k,$$

i.e. $\lambda_j = \gamma_j = 0.5^{j+1}$, $j = 0, 1, \ldots, \infty$. The system was excited by uniformly distributed i.i.d. input sequence $u_k \sim U[-10, 10]$ and the output noise $z_k \sim U[-1, 1]$. We assumed $\lambda = 0.8$ in (14.4), and we took $p = 3$ in (14.5). Both estimates were computed on the same simulated data $\{(u_k, y_k)\}_{k=1}^N$ and compared with respect to the following estimation error

$$ERR\big(\widehat{\mu}_N(x)\big) = \frac{1}{N_0}\sum_{i=1}^{N_0}\big(\widehat{\mu}_N\big(x^{(i)}\big) - \mu\big(x^{(i)}\big)\big)^2, \tag{14.12}$$

where $\{x^{(i)}\}_{i=1}^{N_0}$ is the grid of equidistant estimation points. The routine was repeated for various values of the tuning parameter h. As can be seen in Figs. 14.3 and 14.4, according to intuition, improper selection of h increases the variance or bias of the estimate. Table 14.1 shows the errors (14.12) of $\widehat{\mu}_N^1(x)$ and $\widehat{\mu}_N^2(x)$ versus number of measurements N. Since the linear component in the Wiener system has infinite impulse response (IIR), it illustrates advantages of $\widehat{\mu}_N^1(x)$ over $\widehat{\mu}_N^2(x)$, especially when the number of measurements tends to infinity. The bandwidth parameters was set (experimentally) according to $h(N) = N^{-(\log_{1/\lambda} N)^{-w}} \log_\lambda N^{-(\log_{1/\lambda} N)^{-w}}$, with $w = 0.75$ in (14.4), and $h(N) = cN^{-1/(2p+1)}$ with $p = 5$ and $c = 1.4$ in (14.5).

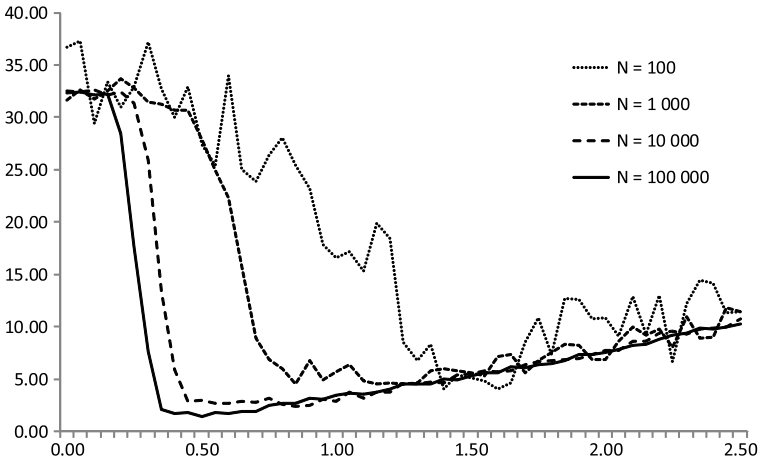

Fig. 14.3 Relationship between the estimation error $ERR(\widehat{\mu}_N^{(1)}(x))$ and the bandwidth parameter h

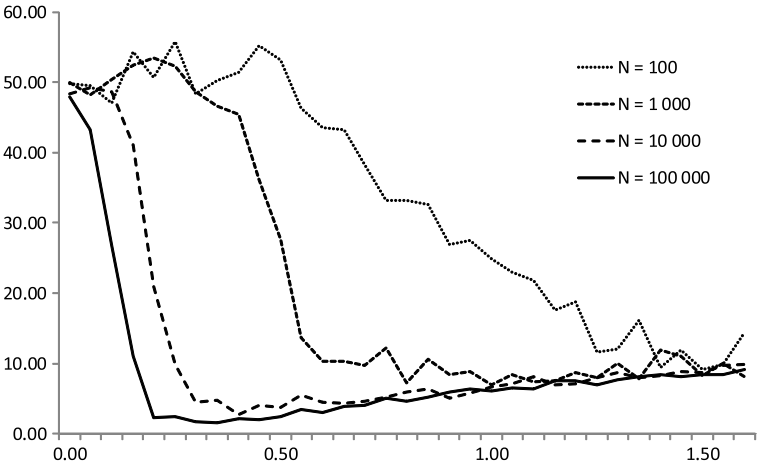

Fig. 14.4 Relationship between the estimation error $ERR(\widehat{\mu}_N^{(2)}(x))$ and the bandwidth parameter h

14.6 Final Remarks

The nonlinear characteristic of Wiener–Hammerstein system is successfully recovered from the input-output data under small amount of a priori information. The estimates work under IIR dynamic blocks, non-Gaussian input and for non-invertible characteristics. Since the Hammerstein systems and the Wiener systems are special cases of the sandwich system, the proposed approach is universal in the sense that it can be applied without the prior knowledge of the cascade system structure.

As regards the limit properties, the estimates $\widehat{\mu}_N^{(1)}(x)$ and $\widehat{\mu}_N^{(2)}(x)$ are not equivalent. First of them has slower rate of convergence (logarithmic), but it converges to

the true system characteristic, since the model becomes more complex as the number of observations tends to infinity. The main limitation is assumed knowledge of λ, i.e., the upper bound of the impulse response. On the other hand, the rate of convergence of the estimate $\widehat{\mu}_N^{(2)}(x)$ is faster (exponential), but the estimate is biased, even asymptotically. However, its bias can be made arbitrarily small by selecting the cut-off parameter p large enough.

As it was shown in [5], the nonparametric methods allow for decomposition of the identification task of block-oriented system and can support estimation of its parameters. Computing of both estimates $\widehat{\mu}_N^{(1)}(x)$, $\widehat{\mu}_N^{(2)}(x)$ and the distance $\delta_k(x)$ has the numerical complexity $O(N)$, and can be performed in recursive or semi-recursive version (see [4]).

References

1. Celka P, Bershad NJ, Vesin JM (2001) Stochastic gradient identification of polynomial Wiener systems: analysis and application. IEEE Trans Signal Process 49(2):301–313
2. Giannakis GB, Serpedin E (2001) A bibliography on nonlinear system identification. Signal Process 81(3):533–580
3. Greblicki W (2010) Nonparametric input density-free estimation of the nonlinearity in Wiener systems. IEEE Trans Inf Theory 56(7):3575–3580
4. Greblicki W, Pawlak M (2008) Nonparametric system identification. Cambridge University Press, Cambridge
5. Hasiewicz Z, Mzyk G (2009) Hammerstein system identification by non-parametric instrumental variables. Int J Control 82(3):440–455
6. Hunter IW, Korenberg MJ (1986) The identification of nonlinear biological systems: Wiener and Hammerstein cascade models. Biol Cybern 55(2):135–144
7. Mzyk G (2007) A censored sample mean approach to nonparametric identification of nonlinearities in Wiener systems. IEEE Trans Circuits Syst II, Express Briefs 54(10):897–901
8. Mzyk G (2010) Parametric versus nonparametric approach to Wiener systems identification. In: Lecture Notes in Control and Information Sciences, vol 404. Springer, Berlin, pp 111–125. Chapter 8
9. Mzyk G (2012) Nonparametric recovering of nonlinearity in Wiener–Hammerstein systems. In: Proceedings of the 9th international conference on informatics in control, automation and robotics, ICINCO, Rome, Italy. IEEE, New York, pp 439–445
10. Mzyk G (2014) Combined parametric–nonparametric identification of block-oriented systems. Lecture Notes in Control and Information Sciences, vol 454. Springer, Berlin
11. Vandersteen G, Schoukens J (1999) Measurement and identification of nonlinear systems consisting of linear dynamic blocks and one static nonlinearity. IEEE Trans Autom Control 44(6):1266–1271
12. Vörös J (2007) Parameter identification of Wiener systems with multisegment piecewise-linear nonlinearities. Syst Control Lett 56(2):99–105
13. Westwick D, Verhaegen M (1996) Identifying MIMO Wiener systems using subspace model identification methods. Signal Process 52(2):235–258
14. Westwick DT, Schoukens J (2012) Initial estimates of the linear subsystems of Wiener–Hammerstein models. Automatica 48(11):2931–2936

Chapter 15
Monitoring Changes in RCA Models

Zuzana Prášková

Abstract In the paper a sequential monitoring scheme is proposed to detect instability of parameters in a random coefficient autoregressive (RCA) time series model of general order p. A given set of historical stable observations is available that serves as a training sample. The proposed monitoring procedure is based on the quasi-likelihood scores and the quasi-maximum likelihood estimators of the respective parameters computed from the training sample, and it is designed so that the sequential test has a small probability of a false alarm and asymptotic power one as the size of the training sample is sufficiently large. The asymptotic distribution of the detector statistic is established under both the null hypothesis of no change as well as under the alternative that a change occurs.

15.1 Introduction

Random coefficient autoregressive models belong to a broad class of conditional heteroscedastic time series models because of their varying conditional variance and as such may be used in various applications.

Let us consider a random coefficient autoregressive model of order p, RCA(p),

$$X_t = \sum_{i=1}^{p}(\beta_{it} + B_{it})X_{t-i} + Y_t = (\boldsymbol{\beta}_t + \mathbf{B}_t)^T \mathbf{X}_{t-1} + Y_t, \quad t \in \mathbb{Z} \qquad (15.1)$$

where $\boldsymbol{\beta}_t = (\beta_{1t}, \ldots, \beta_{pt})^T$ are vectors of constants, $\mathbf{B}_t = (B_{1t}, \ldots, B_{pt})^T$ are random vectors with zero mean and the variance matrices $\boldsymbol{\Sigma}_t$, $\mathbf{X}_{t-1} = (X_{t-1}, \ldots, X_{t-p})^T$, and Y_t are random variables with zero mean and the variances σ_t^2. The superscript T denotes the transpose of a vector or a matrix. In the next we will assume that $\{\mathbf{B}_t\}, \{Y_t\}$ are mutually independent sequences. We assume that $\boldsymbol{\beta}_t$, $\boldsymbol{\Sigma}_t$ and σ_t^2 are unknown; let $\boldsymbol{\theta}_t = (\boldsymbol{\beta}_t^T, \boldsymbol{\omega}_t^T, \sigma_t^2)^T$ be the $(p+1)(p/2+1)$-dimensional column vectors of unknown parameters, where $\boldsymbol{\omega}_t = \text{vech}\, \boldsymbol{\Sigma}_t$. (Recall here that for

Z. Prášková (✉)
Faculty of Mathematics and Physics, Charles University in Prague, Sokolovská 83, 186 75 Prague, Czech Republic
e-mail: praskova@karlin.mff.cuni.cz

A. Steland et al. (eds.), *Stochastic Models, Statistics and Their Applications*, Springer Proceedings in Mathematics & Statistics 122,
DOI 10.1007/978-3-319-13881-7_15

any $p \times p$ symmetric matrix $\mathbf{A}$, vech $\mathbf{A}$ denotes the $p(p+1)/2$-dimensional column vector stacking parts of the columns of $\mathbf{A}$ on and below the main diagonal, one on top of the other in order from the left to the right.)

In this paper we are interested in sequential testing stability of parameters $\boldsymbol{\theta}_t$. For this we assume that a training sample of stable observations $X_1, \ldots, X_m$ is available that serves to the calibration of the model such that

$$\boldsymbol{\theta}_1 = \cdots = \boldsymbol{\theta}_m = \boldsymbol{\theta}_0.$$

New observations are arriving one after another; after each new observations arrives, we make a decision whether the condition of stability is violated (i.e., change occurs) or not.

The problem of the instability of parameters $\boldsymbol{\theta}_t$ is formulated as a sequential testing problem, that is, we test the null hypothesis of no change

$$H_0: \quad \boldsymbol{\theta}_i = \boldsymbol{\theta}_0, \quad i = 1, 2, \ldots, \tag{15.2}$$

against the alternative that a change occurs at a break point K, i.e.,

$$\begin{aligned} H_A: \quad & \text{there exists } K \geq 1, \\ & \boldsymbol{\theta}_i = \boldsymbol{\theta}_0, \quad 1 \leq i < m + K, \\ & \boldsymbol{\theta}_i = \boldsymbol{\theta}_0 + \boldsymbol{\delta}_m, \quad m + K \leq i < \infty, \ \boldsymbol{\delta}_m \neq \mathbf{0}, \end{aligned} \tag{15.3}$$

$\boldsymbol{\theta}_0, \boldsymbol{\delta}_m, K = K_m$ are unknown. The decision is based on a detector statistic constructed from all observations up to $m + k$, $k = 1, 2, \ldots$, and when it exceeds a critical level for the first time, we stop the monitoring.

Following the ideas of the seminal paper by Chu et al. [7], Horváth et al. [10] developed CUSUM monitoring procedures for testing stability in regression parameters in linear regression models. In a similar vein, Berkes et al. [4] proposed monitoring procedure for testing structural breaks in parameters of GARCH(p, q) models and Hušková and Koubková [12] monitoring procedures in autoregressive models. Other monitoring procedure in autoregression models was considered by Gombay and Serban [9]. A procedure for monitoring general time series can be found in Na et al. [15]. The list of references is not in any case complete, for other references concerning monitoring changes as well as other change point problems, see, e.g., the discussion paper [11].

Concerning RCA models, Aue [2] investigated monitoring breaks in the mean value of an RCA(1) process, Na et al. [14] proposed a monitoring procedure for detection of structural parameter changes in RCA(1) models. Li et al. [13] generalize results of [14] to monitoring changes in autoregressive parameters in RCA(p) models with diagonal matrices $\boldsymbol{\Sigma}_t$. All the mentioned papers work with the least squares estimators (LSE) of the respective parameters.

In this paper we deal with a general RCA(p) model and with quasi-maximum likelihood (QMLE) estimators.

The rest of the paper is organized as follows. In Sect. 15.2 we formulate the conditions of stationarity and summarize some asymptotic properties of QMLE. In Sect. 15.3 we formulate and prove the main results concerning monitoring procedure.

15.2 Preliminary Results

In this section we review basic properties of the RCA(p) models such as stationarity, and consistency and asymptotic normality of quasi-maximum likelihood estimators that we will use in our next considerations. For these purposes we assume here that $\boldsymbol{\beta}_t = \boldsymbol{\beta}$, $\boldsymbol{\Sigma}_t = \boldsymbol{\Sigma}$, $\sigma_t^2 = \sigma^2$ are constant for all $t \in \mathbb{Z}$, and $\mathbf{B}_t = \boldsymbol{\Sigma}^{1/2}\mathbf{b}_t$, $Y_t = \sigma y_t$, i.e., we consider model

$$X_t = (\boldsymbol{\beta} + \mathbf{B}_t)^T \mathbf{X}_{t-1} + Y_t = \left(\boldsymbol{\beta} + \boldsymbol{\Sigma}^{1/2}\mathbf{b}_t\right)^T \mathbf{X}_{t-1} + \sigma y_t, \quad t \in \mathbb{Z} \tag{15.4}$$

where $\mathbf{b}_t$ are zero mean random vectors with identity variance matrix and y_t are random variables with zero mean and unit variance.

Conditions of stationarity in this model were studied, e.g., by Anděl [1] and Nicholls and Quinn [16]; Aue et al. [3] stated minimal moment conditions for stationarity in RCA(1) models. Results of Aue et al. [3] can be generalized to any RCA(p) model as we will show below.

First, let us introduce some notation: let $\|\cdot\|$ be any norm in $\mathbb{R}^p$, and $\|\cdot\|_{\mathscr{M}}$ be an operator norm defined on the set $\mathscr{M}_p$ of real $p \times p$ matrices $\mathbf{A}$ by $\|\mathbf{A}\|_{\mathscr{M}} = \sup\{\|\mathbf{A}\mathbf{x}\|/\|\mathbf{x}\|, \mathbf{x} \in \mathbb{R}^p, \mathbf{x} \neq \mathbf{0}\}$. Further, for any real x, let $x^+ = \max(x, 0)$. In the sequel, $\|\cdot\|$ will be the Euclidean norm.

Assumption A1 *$(\mathbf{b}_t, y_t), t \in \mathbb{Z}$ are iid pairs and $\{\mathbf{b}_t\}$ and $\{y_t\}$ are mutually independent sequences.*

We see that under Assumption A1, $\{(\mathbf{b}_t, y_t), t \in \mathbb{Z}\}$ is strictly stationary end ergodic process. Further put for any $t \in \mathbb{Z}$

$$\mathbf{A}_t = \begin{pmatrix} \beta_1 + B_{t1}, \ldots, \beta_p + B_{tp} \\ \mathbf{I}_{p-1} \quad \mathbf{0}_{p-1} \end{pmatrix}, \qquad \mathbf{Y}_t = \begin{pmatrix} Y_t \\ \mathbf{0}_{p-1} \end{pmatrix} \tag{15.5}$$

with $\mathbf{I}_{p-1}$ and $\mathbf{0}_{p-1}$ denoting the $(p-1)$-dimensional identity matrix and the $(p-1)$-dimensional column zero vector, respectively. Then (15.4) can be written in a vector form $\mathbf{X}_t = \mathbf{A}_t\mathbf{X}_{t-1} + \mathbf{Y}_t$. Further, consider the top Lyapunov exponent of the sequence $\{\mathbf{A}_t\}$

$$\lambda = \inf_{t>0} \frac{1}{t} \mathsf{E} \log \|\mathbf{A}_t \cdots \mathbf{A}_1\|_{\mathscr{M}}. \tag{15.6}$$

Assumption A2 $\mathsf{E} \log^+ \|Y_0\| < \infty$, $\mathsf{E} \log^+ \|\mathbf{A}_0\|_{\mathscr{M}} < \infty$.

Lemma 15.1 *Under Assumptions A1–A2, and for $\lambda < 0$, $\{X_t, t \in \mathbf{Z}\}$ is strictly stationary process and*

$$\mathbf{X}_t = \sum_{k=0}^{\infty} \prod_{j=1}^{k} \mathbf{A}_{t-j}\mathbf{Y}_{t-k}. \tag{15.7}$$

Proof Since (15.4) has a vector representation $\mathbf{X}_t = \mathbf{A}_t\mathbf{X}_{t-1} + \mathbf{Y}_t$, the proof follows, e.g., from [6] or [5]. □

Nicholls and Quinn [16] studied both the LSE and QMLE of the parameters in model (15.4) under Assumption A1, and under some additional assumptions on the moments and the structure of random matrices proved their strong consistency and asymptotic normality. Aue et al. [3] proved the strong consistency and asymptotic normality of the QMLE in an RCA(1) model allowing a correlation between $\mathbf{b}_t$ and y_t under minimal moment conditions. Strong consistency and asymptotic normality of QMLE in an RCA(p) model assuming general correlation structure between random autoregression coefficients and the noise were established in [18].

Here we adapt the assumptions from [18] to model (15.4) satisfying assumptions of Lemma 15.1. We have

$$\mathsf{E}\mathbf{B}_t = \mathbf{0}, \qquad \mathsf{E}\big(\mathbf{B}_t\mathbf{B}_t^T\big) = \boldsymbol{\Sigma}; \qquad \mathsf{E}Y_t = 0, \qquad \mathsf{E}Y_t = \sigma^2; \qquad \mathsf{E}(\mathbf{B}_t Y_t) = \mathbf{0}$$

and with the σ-field $\mathscr{F}_t = \sigma\{(\mathbf{b}_s, y_s), s \le t\}$

$$\mathsf{E}X_t|\mathscr{F}_{t-1} = \boldsymbol{\beta}^T\mathbf{X}_{t-1}; \qquad \mathsf{Var}X_t|\mathscr{F}_{t-1} = \mathbf{X}_{t-1}^T\boldsymbol{\Sigma}\mathbf{X}_{t-1} + \sigma^2 = \boldsymbol{\omega}^T\mathbf{z}_{t-1} + \sigma^2 \tag{15.8}$$

where we denoted $\boldsymbol{\omega} = \mathrm{vech}\,\boldsymbol{\Sigma}$ and $\mathbf{z}_{t-1} = \mathbf{K}\,\mathrm{vec}(\mathbf{X}_{t-1}\mathbf{X}_{t-1}^T)$, vec is the operator that is stacking the columns of any matrix one on top of the other in order from left to right and $\mathbf{K}$ is so-called duplication matrix (see, e.g., [16], Chap. 1 for details).

In the next, we will assume that $\sigma^2 > 0$. If σ_{ij} are elements of $\boldsymbol{\Sigma}$, we put

$$\boldsymbol{\eta} = \big(\beta_1, \ldots, \beta_p, \sigma_{11}, \sigma_{22}, \ldots, \sigma_{pp}, \sigma_{21}, \ldots, \sigma_{p1}, \ldots, \sigma_{p,p-1}, \sigma^2\big)^T \tag{15.9}$$

and define the compact set

$$\begin{aligned}\boldsymbol{\Gamma}(a,b,c,d) = [-a,a]^p \times [1/b,b]^p \times [-c,c]^{p(p-1)/2} \\ \times [1/d,d] \subset \mathbb{R}^{(p+1)(1+p/2)}\end{aligned} \tag{15.10}$$

for some $a, b, c, d > 0$.

Obviously, $\boldsymbol{\theta} = (\boldsymbol{\beta}^T, \boldsymbol{\omega}^T, \sigma^2)^T$ is a continuous function of $\boldsymbol{\eta}$ and we define the parametric space $\boldsymbol{\Theta} = f(\boldsymbol{\Gamma})$ where f is a continuous function $f : \boldsymbol{\Gamma} \to \mathbb{R}^{(p+1)(1+p/2)}$ such that $\boldsymbol{\theta} = (\boldsymbol{\beta}^T, \boldsymbol{\omega}^T, \sigma^2)^T = f(\boldsymbol{\eta})$. We can see that $\boldsymbol{\Theta}$ is a compact subspace of $\mathbb{R}^{(p+1)(1+p/2)}$.

Given $X_0, X_{-1}, \ldots, X_{-p+1}$, the conditional log-likelihood function of $X_1, \ldots, X_n$ under joint normality of $(\mathbf{b}_t, y_t)$ is

$$L_n(\boldsymbol{\theta}) = -\frac{1}{2}\sum_{t=1}^{n}\left[\frac{(X_t - \boldsymbol{\beta}^T\mathbf{X}_{t-1})^2}{\boldsymbol{\omega}^T\mathbf{z}_{t-1} + \sigma^2} + \log\big(\boldsymbol{\omega}^T\mathbf{z}_{t-1} + \sigma^2\big)\right] \tag{15.11}$$

and without the normality assumption, the quasi-maximum likelihood estimator $\widehat{\boldsymbol{\theta}}_n$ of the parameter $\boldsymbol{\theta}$, if we use the transformed log-likelihood $l_n(\boldsymbol{\theta}) = -2L_n(\boldsymbol{\theta})/n$, is defined by

$$l_n(\widehat{\boldsymbol{\theta}}_n) = \inf_{\boldsymbol{\theta}\in\boldsymbol{\Theta}} l_n(\boldsymbol{\theta}). \tag{15.12}$$

Assumption A3 $\mathsf{E}\|(\mathbf{b}_0, y_0)\|^2 < \infty$.

Assumption A4 *For any real numbers* $a_1, \ldots, a_p, \phi, \psi$ *with* $a_j \neq 0$ *for* $j = 1, \ldots, p$,

$$P\left(\sum_{j=1}^{p} a_j b_{0j} + y_0 \in \{\phi, \psi\}\right) < 1.$$

Assumption A5 $\mathsf{E}\|(\mathbf{b}_0, y_0)\|^4 < \infty$.

Assumption A6 *True value* $\boldsymbol{\theta}_0$ *is an inner point of* $\boldsymbol{\Theta}$.

Note that

$$\begin{aligned} l_n(\boldsymbol{\theta}) &= \frac{1}{n}\sum_{t=1}^{n} g_t(\boldsymbol{\theta}), \\ g_t(\boldsymbol{\theta}) &= \frac{(X_t - \boldsymbol{\beta}^T \mathbf{X}_{t-1})^2}{\boldsymbol{\omega}^T \mathbf{z}_{t-1} + \sigma^2} + \log\left(\boldsymbol{\omega}^T \mathbf{z}_{t-1} + \sigma^2\right) \\ &:= \frac{(X_t - m_t(\boldsymbol{\theta}))^2}{V_t(\boldsymbol{\theta})} + \log\left(V_t(\boldsymbol{\theta})\right). \end{aligned} \tag{15.13}$$

Assumption $\sigma^2 > 0$ and the compactness of $\boldsymbol{\Theta}$ ensure that $\inf_{\theta \in \boldsymbol{\Theta}} V_t(\theta) \geq \delta > 0$ for some $\delta > 0$.

Let $g_t'(\boldsymbol{\theta})$ and $g_t''(\boldsymbol{\theta})$ denote the gradient vector and the Hessian matrix of $g_t(\boldsymbol{\theta})$, respectively. It follows from the stationarity and ergodicity of $\{X_t\}$ that $\{g_t'(\boldsymbol{\theta})\}, \{g_t''(\boldsymbol{\theta})\}$ are strictly stationary and ergodic sequences, that are continuous and bounded on $\boldsymbol{\Theta}$. Further, it can be shown that

$$\mathsf{E}\left\|g_1'(\boldsymbol{\theta}_0)\right\|^2 < \infty, \qquad \mathsf{E}\sup_{\boldsymbol{\theta} \in \boldsymbol{\Theta}} \left\|g_1''(\boldsymbol{\theta})\right\| < \infty \tag{15.14}$$

and according to [18], $\{g_t''(\boldsymbol{\theta})\}$ satisfies conditions of the uniform strong law of large numbers. Moreover, $\{g_t'(\boldsymbol{\theta}_0)\}$ is an $\mathscr{F}_t$-ergodic strictly stationary martingale difference sequence with finite variance.

Lemma 15.2 *Let Assumptions A1–A4 hold and* $\lambda < 0, \sigma^2 > 0$. *Then, for* $\boldsymbol{\theta}_0 \in \boldsymbol{\Theta}$, *as* $n \to \infty$,

$$\widehat{\boldsymbol{\theta}}_n \to \boldsymbol{\theta}_0 \quad \text{almost surely.} \tag{15.15}$$

Proof It is shown in [18] that Assumption A4 implies Assumption H3 there. Then the proof follows from Theorem 1 in [18]. □

Lemma 15.3 *Let Assumptions A1–A2, A4–A6 be satisfied, let* $\lambda < 0$, $\sigma^2 > 0$. *Then, as* $n \to \infty$,

$$\sqrt{n}(\widehat{\boldsymbol{\theta}}_n - \boldsymbol{\theta}_0) \to \mathcal{N}\big(\mathbf{0}, \mathbf{H}^{-1}\mathbf{D}\mathbf{H}^{-1}\big) \tag{15.16}$$

where $\mathbf{D} = \mathsf{E}g_1'(\boldsymbol{\theta}_0)g_1'(\boldsymbol{\theta}_0)^T$, $\mathbf{H} = \mathsf{E}g_1''(\boldsymbol{\theta}_0)$ *and* $\mathbf{D}$, $\mathbf{H}$ *are non-singular matrices.*

Proof See, e.g., [18], Theorem 2. □

15.3 Main Results

Now, let us consider model (15.1) and sequential testing of hypothesis (15.2) of no change in parameters against alternative (15.3) that a change occurs at time K after the monitoring was started. For this we introduce a stopping time

$$\tau(m) = \inf\big\{k \geq 1, \big|Q(m,k)\big| \geq c\, g(m,k)\big\}$$

(with $\inf(\emptyset) := +\infty$), where $Q(m,k)$ is a detector statistic and $q(m,k)$ is a boundary function, $c = c(\alpha) > 0$ is a constant such that $\lim_{m\to\infty} P(\tau(m) < \infty | H_0) = \alpha$ ($\alpha \in (0,1)$ is the prescribed probability of a false alarm), and $\lim_{m\to\infty} P(\tau(m) < \infty | H_1) = 1$ (the test procedure is consistent).

As a detector statistic we propose

$$Q(m,k) = \widehat{\mathbf{D}}_m^{-1/2} \frac{1}{\sqrt{m}} \sum_{i=m+1}^{m+k} g_i'(\widehat{\boldsymbol{\theta}}_m) \tag{15.17}$$

where $g_i'(\boldsymbol{\theta})$ is the gradient vector, $\widehat{\boldsymbol{\theta}}_m$ is the QMLE of $\boldsymbol{\theta}$ based on the training sample of size m and $\widehat{\mathbf{D}}_m$ is a consistent estimator of $\mathbf{D}$ as given in Lemma 15.3, based on the training sample. We can use, e.g., the estimator

$$\widehat{\mathbf{D}}_m = \frac{1}{m}\sum_{i=1}^{m} g_i'(\widehat{\boldsymbol{\theta}}_m)g_i'(\widehat{\boldsymbol{\theta}}_m)^T. \tag{15.18}$$

As a boundary function we choose, similarly as in [10]

$$q(t) = (1+t)(t/1+t)^{\gamma}, \quad \gamma \in [0, 1/2). \tag{15.19}$$

The tunning constant γ can affect the ability of the test procedure to detect change early (γ close to 1/2) or later ($\gamma = 0$).

Theorem 15.1 *Let Assumptions A1–A2, A4–A6 be satisfied, and* $\lambda < 0$, $\sigma^2 > 0$. *Let* $Q(m,k)$ *be statistic (15.17) and* $\widehat{\mathbf{D}}_m - \mathbf{D} = o_p(1)$. *Then under* H_0, *as* $m \to \infty$,

$$P\Big(\max_{1\leq k<\infty} \big|Q(m,k)\big|/q(k/m) \leq x\Big) \to P\Big(\sup_{0<t<1} \big|\boldsymbol{W}(t)\big|/t^{\gamma} \leq x\Big) \tag{15.20}$$

where $\boldsymbol{W}$ *is* d*-dimensional standard Wiener process with independent components,* $d = (p+1)(1+p/2)$ *and* $|\cdot|$ *denotes the maximum norm.*

Proof The proof consists from a few quite standard steps. First, we will show that

$$\sup_{1\le k<\infty} \frac{1}{m^{1/2}q(k/m)} \left| \sum_{i=m+1}^{m+k} g_i'(\widehat{\boldsymbol{\theta}}_m) - \left(\sum_{i=m+1}^{m+k} g_i'(\boldsymbol{\theta}_0) - \frac{k}{m} \sum_{i=1}^{m} g_i'(\boldsymbol{\theta}_0) \right) \right| = o_p(1). \tag{15.21}$$

But it follows quite easily if we recall that $\{g_i'(\boldsymbol{\theta}_0)\}$ is a martingale difference sequence with the variance matrix $\mathbf{D}$, use the Taylor expansion for $g_i'(\widehat{\boldsymbol{\theta}}_m)$ and apply the uniform strong law of large numbers to $\{g_i''(\boldsymbol{\theta})\}$, and the fact that $|\widehat{\boldsymbol{\theta}}_m - \boldsymbol{\theta}| = O_p(m^{-1/2})$, which follows from Lemma 15.3.

Next, according to Theorem 27.17 in [8], for any $T > 0$, as $m \to \infty$,

$$m^{-1/2} \sum_{i=1}^{\lfloor mt \rfloor} g_i'(\boldsymbol{\theta}_0) \xrightarrow{\mathscr{D}[0,T]} W_{\mathbf{D}}(t) \tag{15.22}$$

in the Skorokhod space $\mathscr{D}^d[0,T]$, where $\{W_{\mathbf{D}}(t), t \in [0,T]\}$ is a zero mean Gaussian process with $\mathsf{E} W_{\mathbf{D}}(t) W_{\mathbf{D}}(s)^T = \min(t,s)\mathbf{D}$, and

$$m^{-1/2}\mathbf{D}^{-1/2} \left(\sum_{i=m+1}^{m+\lfloor mt \rfloor} g_i'(\boldsymbol{\theta}_0) - t \sum_{i=1}^{m} g_i'(\boldsymbol{\theta}_0) \right) \xrightarrow{\mathscr{D}[0,T]} W_{\mathbf{I}}(1+t) - (1+t) W_{\mathbf{I}}(1). \tag{15.23}$$

It follows from the properties of the Wiener process that $W_{\mathbf{I}}(1+t) - (1+t)W_{\mathbf{I}}(1) \stackrel{\mathscr{D}}{=} (1+t)\mathbf{W}(t/1+t)$ with $\{\mathbf{W}(t), t > 0\}$ denoting the standard Brownian motion.

In the next step we use the Hájek–Rényi inequality as in Lemma 6.6 of [4] (with $b(t) = (\frac{t}{1+t})^\gamma$) and in combination with (15.21) and replacing $\mathbf{D}$ by $\widehat{\mathbf{D}}_m$ we conclude the proof after some careful computations. □

The critical values of the limiting process are known only for $\gamma = 0$ and are tabulated for some values of p, e.g., in [15] or in [13]; otherwise they should be approximated by simulations from the limiting process.

Now, let us consider the alternative hypothesis. We study the model

$$\begin{aligned} X_t &= \left(\boldsymbol{\beta_0} + \boldsymbol{\Sigma}_0^{1/2}\mathbf{b}_t\right)^T \mathbf{X}_{t-1} + \sigma_0 y_t, \quad t \le m+K \\ &= \left(\boldsymbol{\beta}_1 + \boldsymbol{\Sigma}_1^{1/2}\mathbf{b}_t\right)^T \mathbf{X}_{t-1} + \sigma_1 y_t, \quad t > m+K \end{aligned} \tag{15.24}$$

and parameters $\boldsymbol{\theta}_0 = (\boldsymbol{\beta}^T, \boldsymbol{\omega}^T, \sigma^2)^T$, and $\boldsymbol{\theta}_1 = (\boldsymbol{\beta}_1^T, \boldsymbol{\omega}_1^T, \sigma_1^2)^T$ before and after the change, respectively, with $\boldsymbol{\omega} = \operatorname{vech} \boldsymbol{\Sigma}$ as above and $\boldsymbol{\omega}_1 = \operatorname{vech} \boldsymbol{\Sigma}_1$. Define matrix $\mathbf{A}_t^1$ in the same way as in (15.5) with the components of $\boldsymbol{\beta}$ being replaced by those of $\boldsymbol{\beta}_1$. The top Lyapunov coefficient λ_1 is defined analogously. Assuming $\lambda_1 < 0$ together with A1 and A2 we have assured that the process after the change is stationary and can be written in the form

$$\mathbf{X}_t = \mathbf{A}_t^1 \mathbf{X}_{t-1} + \mathbf{Y}_t, \quad t > m+K. \tag{15.25}$$

Let $h_t(\boldsymbol{\theta})$ be the scores (15.13) defined with the parameters of the process (15.25), $\mathsf{E}h_t(\boldsymbol{\theta}) := \bar{h}(\boldsymbol{\theta})$ and $\bar{h}'(\boldsymbol{\theta}_0) \neq \mathbf{0}$. Let there is a neighborhood U of $\boldsymbol{\theta}_0$ such that $\bar{h}(\boldsymbol{\theta})$ and $\bar{h}'(\boldsymbol{\theta}), \bar{h}(''\boldsymbol{\theta})$ exist and are continuous for each $\boldsymbol{\theta} \in U$. Let $K = K_m$ and $\limsup K/m < \infty$ as $m \to \infty$.

Theorem 15.2 *Let us consider model* (15.24) *and suppose that Assumptions* A1–A2, A4–A6 *hold and* $\lambda < 0, \lambda_1 < 0, \sigma^2 > 0, \sigma_1^2 > 0$ *and the above regularity conditions for* $\bar{h}(\boldsymbol{\theta})$ *are satisfied. Then*

$$\max_{1 \le k < \infty} Q(m,k)/q(k/m) \to \infty \quad \text{in probability.} \tag{15.26}$$

Proof It follows in the same way as the proof of Theorem 3.2 in [4], utilizing representation (15.7), (15.25) and results from Lemma 2.4 in [17] applied to $\|\mathbf{A}_t\|$ and $\|\mathbf{A}_t^1\|$, respectively. □

Acknowledgements The work was supported by the Czech Science Foundation project No. P402/12/G097 DYME – Dynamic Models in Economics.

References

1. Anděl J (1976) Autoregressive series with random parameters. Math Operforsch Stat 7:735–741
2. Aue A (2004) Strong approximation for RCA(1) time series with applications. Stat Probab Lett 68:369–382
3. Aue A, Horváth L, Steinebach J (2006) Estimation in random coefficient autoregressive models. J Time Ser Anal 27:60–67
4. Berkes I, Gombay E, Horváth L, Kokoszka P (2004) Sequential change-point detection in GARCH(p,q) models. Econom Theory 20:1140–1167
5. Bougerol P, Picard N (1992) Strict stationarity of generalized autoregressive processes. Ann Probab 20:1714–1730
6. Brandt A (1986) The stochastic equation $Y_{n+1} = A_n Y_n + B_n$ with stationary coefficients. Adv Appl Probab 18:211–220
7. Chu C-SJ, Stinchcombe M, White H (1996) Monitoring structural change. Econometrica 64:1045–1065
8. Davidson J (1994) Stochastic limit theory. Advanced texts in econometrics. Oxford University Press, Oxford
9. Gombay E, Serban D (2009) Monitoring parameter change in AR(p) time series models. J Multivar Anal 100:715–725
10. Horváth L, Hušková M, Kokoszka P, Steinebach J (2004) Monitoring changes in linear models. J Stat Plan Inference 126:225–251
11. Horváth L, Rice G (2014) Extensions of some classical methods in change point analysis. Test 23:219–255
12. Hušková M, Koubková A (2006) Sequential procedures for detection of changes in autoregressive sequences. In: Hušková M, Janžura M (eds) Proceedings of Prague stochastics. MATFYZPRESS, Charles University, Prague, pp 437–447
13. Li F, Tian Z, Qi P (2014) Structural change monitoring for random coefficient autoregressive time series. Commun Stat, Simul Comput. doi:10.1080/03610918.2013.800205
14. Na O, Lee J, Lee S (2010) Monitoring parameter changes for random coefficient autoregressive models. J Korean Stat Soc 39:281–288

15. Na O, Lee Y, Lee S (2011) Monitoring parameter change in time series models. Stat Methods Appl 20:171–199
16. Nicholls DF, Quinn BG (1982) Random coefficient autoregressive models: an introduction. Lecture notes in statistics, vol 11. Springer, New York
17. Straumann D, Mikosch T (2006) Quasi-maximum-likelihood estimation in conditionally heteroscedastic time series: a stochastic recurrence equations approach. Ann Stat 34:2449–2495
18. Truquet L, Yao J (2012) On the quasi-likelihood estimation for random coefficient autoregressions. Statistics 46:505–512

Chapter 16
Detecting Changes in Spatial-Temporal Image Data Based on Quadratic Forms

Annabel Prause and Ansgar Steland

Abstract We consider the problem to monitor a sequence of images that may be affected by spatial as well as temporal dependencies. In order to detect a change, we consider a detector based on linear combinations of quadratic forms, thus allowing to consider linear contrasts of subimages in terms of their average grey value. We derive the asymptotic distribution of the proposed detector and the underlying empirical processes under the no-change null hypothesis and general alternatives.

16.1 Introduction

Suppose that we observe sequentially a sequence of images represented by two-dimensional matrices of grey values. In many areas of applications that use imaging technologies, those images represent both information about physical objects and information about the spatial distribution of a characteristic of interest.

The approach is motivated by the analysis of electroluminescence (EL) images of solar panels, which allow to investigate the physical properties of the photovoltaic effect on a microscopic scale, as they show the irradiance emitted by the solar cells when exposed to a voltage. In such an EL image, the boundaries of the cells and the grid fingers, which collect the electrons when the cell operates under sun light and cover a part of the cell, are usually visible. Only the cell areas between those grid fingers define the areas of interest, e.g. in order to detect change-points where suspicious areas or local defects and damages such as shunts, cell breaks, which lead to inactive cell areas, or micro cracks, which are visible but do not lead to inactive areas, grow or have to be classified as confirmed defects.

Motivated by a postfiltering smooth correction of the Shannon–Whittaker interpolation series, we propose a detection procedure based on quadratic forms of reconstructed images. It turns out that for image data with fixed spatial sampling

A. Prause · A. Steland (✉)
Institute of Statistics, RWTH Aachen University, Wuellnerstr. 3, Aachen, Germany
e-mail: steland@stochastik.rwth-aachen.de

A. Prause
e-mail: prause@stochastik.rwth-aachen.de

A. Steland et al. (eds.), *Stochastic Models, Statistics and Their Applications*,
Springer Proceedings in Mathematics & Statistics 122,
DOI 10.1007/978-3-319-13881-7_16

rates the asymptotics can be derived on the grounds of the results obtained by [3], provided that the spatial-temporal noise is φ-mixing. For monitoring schemes addressing general high-dimensional data, increasing sampling rates, more general pixel-wise weighting schemes and asymptotic results going beyond those discussed here, we refer to [6, 7] and [8].

16.2 Model and Assumptions

Let us consider a sequentially observed time series of images represented by $N_y \times N_x$-dimensional matrices

$$\mathbf{Y}_i = (Y_{i,\nu,\mu})_{1\le\nu\le N_y, 1\le\mu\le N_x}, \quad i = 1, \ldots, n,$$

obtained by discretely sampling a true image (signal) $\mathbf{f}\colon [0, \bar{\tau}] \to \mathbb{R}^{N_y \times N_x}$,

$$\mathbf{f}(t) = \left(f^{(\nu,\mu)}(t)\right)_{1\le\nu\le N_y, 1\le\mu\le N_x}, \quad t \in [0, \bar{\tau}],$$

at an equidistant grid $i\tau$, $1 \le i \le n$, where $\tau = \bar{\tau}/n$ is the sampling period. We assume that the image pixels at time $i\tau$ satisfy the model equation

$$Y_i = \mathbf{f}(i\tau) + \varepsilon_i, \quad i = 1, \ldots, n,\ n \ge 1,$$

where

$$\boldsymbol{\varepsilon}_i = (\varepsilon_{i,\nu,\mu})_{1\le\nu\le N_y, 1\le\mu\le N_x}, \quad i \ge 1,$$

are matrices of mean zero error terms modeling the spatial-temporal noise.

We are interested in detecting a change in the sequence of images and thus consider the change-point model

$$f^{(\nu,\mu)}(t) = f_0^{(\nu,\mu)}(t) + g^{(\nu,\mu)}(t)\mathbf{1}(t \ge q\tau), \quad t \in [0, \bar{\tau}],$$

for $\nu = 1, \ldots, N_y$ and $\mu = 1, \ldots, N_x$. Here $f_0 = (f_0^{(\nu,\mu)})_{\nu,\mu}$ is the reference image when no change is present and $(g^{(\nu,\mu)})_{\nu,\mu}$ models the departure from the reference model in case that $g^{(\nu,\mu)} \neq 0$. There is a change if $g \neq 0$, i.e. for at least one pair (ν, μ), $g^{(\nu,\mu)} \neq 0$ on $[0, \bar{\tau}]$, and that change occurs, by definition, at the time instant $q = \inf\{n_0 \le i\colon\ g(i\tau) \neq 0\} < \infty$. Clearly, if there is no change, then $q = \infty$, since $\inf \emptyset = \infty$. Notice that our change-point model covers jump alternatives as well as smooth transitions as special cases.

16.3 Image Estimation and Detection

Fixing a pixel location (ν, μ), we sequentially observe an equidistantly sampled discretized signal $f^{(\nu,\mu)}(t)$, $t \in [0, \bar{\tau}]$, as in [3]. Motivated by the Shannon/Whittaker cardinal series $\sum_{k\in\mathbb{Z}} f(k\tau)\mathrm{sinc}(\Omega(t - k\tau))$ for a bandlimited real-valued signal f

with bandwidth Ω (i.e. its Fourier transform is supported on $[-\Omega, \Omega]$), we consider the post-filtering reconstruction,

$$\widehat{f}_n^{(\nu,\mu)} = \tau \sum_{i=1}^{n} Y_{i,\nu,\mu} \varphi(t - i\tau),$$

where $\varphi(x) = \sin(x\Omega)/\pi x$, obtained by applying an ideal low pass filter with bandwidth Ω to the truncated series. This estimator is known to be consistent under certain assumptions, see [4] and [5]. In [3] it has been proposed to base change-point detectors on the empirical process

$$\mathscr{F}_n^{(\nu,\mu)}(s,t) = \sqrt{\tau} \sum_{i=1}^{\lfloor ns \rfloor} \big[Y_{i,\nu,\mu} - f_0^{(\nu,\mu)}(i\tau) \big] \varphi(t - i\tau), \quad s \in [0,1],\ t \in [0, \bar{\tau}],$$

by applying an appropriate norm $\| \bullet \|$ with respect to t and providing a signal at time instant $k \geq n_0$ if $\| \mathscr{F}_n^{(\nu,\mu)}(k/n, \bullet) \|$ exceeds a control limit c for the first time. Here $n_0 = \lfloor s_0 n \rfloor$, $0 < s_0 < 1$, is the start of monitoring and $Y_1, \ldots, Y_L$, is a learning sample of size $L = n_0 - 1$ assumed to satisfy the non-contamination hypothesis of no change.

To obtain a univariate detector from an image matrix $\mathbf{I} = (I_{\nu,\mu})_{\nu,\mu}$, we consider the quadratic form $Q(\mathbf{I}) = \mathbf{v}'\mathbf{I}\mathbf{w}$ for given weighting vectors $\mathbf{v} \in \mathbb{R}^{N_y}$ and $\mathbf{w} \in \mathbb{R}^{N_x}$. When using normalized binary vectors corresponding to the x- and y-coordinates of the pixels defining a rectangular subimage, $Q(\mathbf{I})$ is the average grey value of this *focus area*. More generally, we also study linear combinations of quadratic forms,

$$T(\mathbf{I}) = \sum_{j=1}^{J} \mathbf{v}^{(j)\prime} \mathbf{I} \mathbf{w}^{(j)}, \quad \mathbf{v}^{(j)} \in \mathbb{R}^{N_y},\ \mathbf{w}^{(j)} \in \mathbb{R}^{N_x},$$

which allows to consider linear contrasts of average grey values of J rectangular subimages.

Thus we are led to the associated process

$$G_n(s,t) = \mathbf{v}' \mathscr{F}_n(s,t) \mathbf{w}, \quad s \in [0,1],\ t \in [0, \bar{\tau}].$$

The proposed detector is now defined by the stopping time

$$M_n = \min \Big\{ n_0 \leq k \leq n \colon \max_{t \in [0, \bar{\tau} k/n]} \big| G_n(k/n, t) \big| > c_M \Big\},$$

where the control limit c_M is selected such that the type I error rate is controlled in the limit, i.e. $P_0(M_n < n) \to \alpha$, $n \to \infty$, for some preassigned $\alpha \in (0,1)$. The asymptotic limit theory below shows that the control limit c_M still depends on a constant σ summarizing the dependencies. Given some consistent estimate $\widehat{\sigma}_L^2$, one may use the estimated control limit $\widehat{c}_M = \widehat{\sigma}_L c_M(1)$, where $c_M(1)$ is obtained by simulation using the constraint $\sigma = 1$, as discussed in [3].

16.4 Main Results

Let us recall the following facts about random fields indexed by $\mathbb{Z}^3$. A random field $\{\xi_{(i,j,k)}\colon (i,j,k) \in \mathbb{Z}^3\}$ is stationary if its distribution is shift-invariant. Suppose that $E(\xi_{0,0,0}^2) < \infty$ and put $\mu_\xi = E(\xi_{0,0,0})$. Then the covariance function

$$c(\mathbf{i}, \mathbf{j}) = E(\xi_{\mathbf{i}} - \mu_\xi)(\xi_{\mathbf{j}} - \mu_\xi),$$

where $\mathbf{i} = (i_1, i_2, i_3)$, $\mathbf{j} = (j_1, j_2, j_3) \in \mathbb{Z}^3$, is a function of $\mathbf{i} - \mathbf{j}$. If it is a function of $\|\mathbf{i} - \mathbf{j}\|$, it is called isotropic, but our results also hold true for anisotropic fields. To quantify the degree of dependence present in such a stationary random field $\{\xi_{(i,j,k)}\colon (i,j,k) \in \mathbb{Z}^3\}$, it is convenient to work with the φ-mixing coefficient as defined in [2]. For $1 \le j \le 3$ the lag-k φ-mixing coefficient with respect to a split of coordinate j is defined as

$$\varphi(j,k) = \sup\big\{\big|P(B|A) - P(B)\big|\colon\ A \in \mathscr{A}^-(j,k),\ P(A) > 0,\ B \in \mathscr{A}^+(j,k)\big\},$$

where $\mathscr{A}^-(j,k) = \sigma(\{\xi_{(i_1,i_2,i_3)}\colon (i_1,i_2,i_3) \in \mathbb{Z}^3, i_j \le k\})$ and $\mathscr{A}^+(j,k)$ is defined as $\mathscr{A}^-(j,k)$ with $\le$ replaced by $\ge$. The stationary random field is called φ-mixing, if the sequence of φ-mixing coefficients

$$\varphi(k) = \max_{1 \le \ell \le 3} \varphi(\ell, k), \quad k \in \mathbb{N},$$

satisfies $\varphi(k) \to 0$, as $k \to \infty$. Our assumption on the random field is as follows.

Assumption (A) *$\{\boldsymbol{\varepsilon}_{i,\nu,\mu}\colon i \ge 1,\ 1 \le \nu \le N_y,\ 1 \le \mu \le N_x\}$ is the subarray corresponding to the index set $\mathbb{N} \times \{1, \ldots, N_y\} \times \{1, \ldots, N_x\}$ of a mean zero stationary second order φ-mixing random field $\{\varepsilon_{(i,\nu,\mu)}\colon (i,\nu,\mu) \in \mathbb{Z}^3\}$ with covariance function $\gamma_i(h,\ell) = E(\varepsilon_{0,0,0}\varepsilon_{i,h,\ell})$, $i, h, \ell \in \mathbb{Z}$, φ-mixing coefficients satisfying*

$$\sum_{k=1}^{\infty} \varphi^{1/2}(k) < \infty \tag{16.1}$$

and $0 < \sigma^2 = \sum_{(i,h,\ell) \in \mathbb{Z}^3} \gamma_i(h,\ell) < \infty$.

Proposition 16.1 *Under Assumption (A) the time series $\xi_n(\mathbf{v}, \mathbf{w}) = \mathbf{v}'\varepsilon_n\mathbf{w}$, $n \ge 1$, is strictly stationary with mean zero, $E|\xi_1(\mathbf{v},\mathbf{w})|^2 < \infty$ and autocovariance function*

$$\gamma_h = E\big(\xi_1(\mathbf{v},\mathbf{w})\xi_{1+|h|}(\mathbf{v},\mathbf{w})\big) = \sum_{k=1}^{N_y}\sum_{l=1}^{N_x}\sum_{s=1}^{N_y}\sum_{t=1}^{N_x} v_k w_l v_s w_t E(\varepsilon_{0,0,0}\varepsilon_{h,s-k,t-l})$$

for $h \in \mathbb{Z}$ satisfying $\sigma_\xi^2 = \sum_{h \in \mathbb{Z}} \gamma_h < \infty$. Further, $\xi_n(\mathbf{v},\mathbf{w})$, $n \ge 1$, is φ-mixing with mixing coefficients φ_k, $k \ge 1$, satisfying $\sum_{k=1}^{\infty} \varphi_k^{1/2} < \infty$.

Proof The elementary inequality $|\mathbf{v}'\mathbf{A}\mathbf{w}| \le \|\mathbf{v}\|_2\|\mathbf{w}\|_2\|\mathbf{A}\|_F$, where $\|\mathbf{A}\|_F$ denotes the Frobenius norm of a matrix $\mathbf{A}$ with entries a_{ij} given by $\|\mathbf{A}\|_F^2 = \sum_{i,j} a_{ij}^2$, shows that the second moments are finite, since $E|\mathbf{v}'\varepsilon_i\mathbf{w}|^2 \le \|\mathbf{v}\|_2^2\|\mathbf{w}\|_2^2 E\|\varepsilon_i\|_F^2$ leads to

$$E\left|\mathbf{v}'\varepsilon_i\mathbf{w}\right|^2 \le \|\mathbf{v}\|_2^2\|\mathbf{w}\|_2^2\sum_{\nu=1}^{N_y}\sum_{\mu=1}^{N_x}E\left(\varepsilon_{i,\nu,\mu}^2\right) = \|\mathbf{v}\|_2^2\|\mathbf{w}\|_2^2 N_x N_y \gamma_{1,0,0} < \infty,$$

for all $i \ge 1$. The formula for the covariance function follows by a straightforward calculation and one easily verifies that $\sum_{h\in\mathbb{Z}}|\gamma_h| < \infty$. Notice that $\mathscr{A}_k^+ = \sigma(\{\mathbf{v}'\varepsilon_i\mathbf{w}\colon\ i \ge k\}) \subset \sigma(\{\varepsilon_{\mathbf{i}}\colon\ \mathbf{i}\in\mathbb{Z}^3, i_1 \ge k\}) = \mathscr{A}^+(1,k)$, and analogously $\mathscr{A}_k^- = \sigma(\{\mathbf{v}'\varepsilon_i\mathbf{w}\colon\ i \le k\}) \subset \mathscr{A}^-(1,k)$, for all $k \ge 1$. Thus the sequence $\xi_n(\mathbf{v},\mathbf{w})$, $n \ge 1$, is φ-mixing with coefficients φ_k satisfying

$$\varphi_k = \sup_{A\in\mathscr{A}_0^-, P(A)>0, B\in\mathscr{A}_k^+}\left|P(B|A) - P(B)\right| \le \max_{1\le j\le 3}\varphi(j,k) = \varphi(k), \quad k \ge 1,$$

such that $\sum_{k=1}^{\infty}\varphi_k^{1/2} \le \sum_{k=1}^{\infty}\varphi(k)^{1/2} < \infty$. □

In what follows, $\{B(t)\colon\ t\in[0,1]\}$ denotes a standard Brownian motion. Our first result is as follows.

Theorem 16.1 *Suppose that Assumption* (*A*) *holds and* $\sigma_\xi^2 > 0$. *Under the no change null hypothesis, we have*

$$G_n(s,t) \Rightarrow \mathscr{F}(s,t), \quad \text{with } \mathscr{F}(s,t) = \sqrt{\bar\tau}\sigma_\xi\int_0^s \varphi(t-\bar\tau u)\,dB(u),$$

as $n\to\infty$, *where* σ_ξ^2 *is defined in Proposition* 16.1, *and*

$$M_n \xrightarrow{d} \inf\left\{s_0 \le s \le 1 : \sup_{t\in[0,s\bar\tau]}\left|\mathscr{F}(s,t)\right|\right\}, \quad n\to\infty.$$

Proof For $s\in[0,1]$ and $t\in[0,\bar\tau]$, $G_n(s,t) = \mathbf{v}'\mathscr{F}_n(s,t)\mathbf{w}$ attains the representation

$$G_n(s,t) = \sqrt{\tau}\sum_{i=1}^{\lfloor ns\rfloor}\mathbf{v}'\left[\mathbf{Y}_i - \mathbf{f}_0(i\tau)\right]\mathbf{w}\varphi(t-i\tau) = \sqrt{\tau}\sum_{i=1}^{\lfloor ns\rfloor}\mathbf{v}'\varepsilon_i\mathbf{w}\varphi(t-i\tau).$$

By Proposition 16.1 the sequence $\xi_i(\mathbf{v},\mathbf{w}) = \mathbf{v}'\varepsilon_i\mathbf{w}$, $i\ge 1$, is a stationary φ-mixing second order time series with mixing coefficients φ_k, $k\ge 1$, satisfying $\sum_{k=1}^{\infty}\varphi_k^{1/2} < \infty$. Hence, by virtue of [1, Th. 20.1], the univariate version of [2], it satisfies the invariance principle $\frac{1}{\sqrt{n}}\sum_{i=1}^{\lfloor nu\rfloor}\mathbf{v}'\varepsilon_i\mathbf{w} \Rightarrow \sigma_\xi B(u)$, as $n\to\infty$. Now one may argue as in [3]. □

The unknown long run variance parameter σ_ξ^2 can be estimated from the learning sample using an estimator similar to those proposed in [3] and [6]. For that, take a weighting function $w_m(h)$ with tuning parameter $m = m_n$. Define the estimator

$$\widehat{\sigma}_\xi^2 := \sum_{|h|\le m} w_m(h)\sum_{k=1}^{N_y}\sum_{l=1}^{N_x}\sum_{s=1}^{N_y}\sum_{t=1}^{N_x} v_k w_l v_s w_t\widehat{\gamma}(h, s-k, t-l),$$

where $\widehat{\gamma}(h, s-k, t-l)$ is the (consistent) estimator from [6] for the autocovariance $E(\varepsilon_{0,0,0}\varepsilon_{h,s-k,t-l})$. With similar techniques as those in [6] we can show that $\widehat{\sigma}_\xi^2$ is a consistent estimator for σ_ξ^2 under certain regularity conditions, including uniformly bounded weights with $w_m(j) \to 1$ as $m \to \infty$ as well as $m^3/n \to 0$.

Next, we also want to derive the limit distribution of G_n under local alternatives. To be more precise, we now assume that the image pixels at time $i\tau$ satisfy the model equation

$$Y_i = \mathbf{f}_n(i\tau) + \varepsilon_i, \quad i = 1, \ldots, n,\ n \geq 1,$$

where

$$f_n^{(\nu,\mu)}(t) = f_0^{(\nu,\mu)}(t) + \frac{\delta^{(\nu,\mu)}(t)}{n^\beta}, \quad t \in [0, \bar{\tau}].$$

for $\nu = 1, \ldots, N_y$ and $\mu = 1, \ldots, N_x$ and some $\beta > 0$. Here, f_n is the true signal tending to f_0 for $n \to \infty$. We impose the following assumption on δ.

Assumption (B) *Suppose that each entry of $\delta = (\delta^{(\nu,\mu)})_{\nu,\mu}$ is either*

(a) *continuous or*
(b) *of bounded variation.*

Theorem 16.2 *Suppose that Assumptions (A) and (B) hold. Under the local alternative with $\beta = 1/2$, we have*

$$G_n(s,t) \Rightarrow \mathscr{F}^\delta(s,t), \quad \text{with } \mathscr{F}^\delta(s,t) = \mathscr{F}(s,t) + \frac{1}{\sqrt{\bar{\tau}}} \int_0^{s\bar{\tau}} \varphi(t-u)\delta_{\mathbf{v},\mathbf{w}}(u)\,du,$$

as $n \to \infty$, for $\delta_{\mathbf{v},\mathbf{w}}(u) = \mathbf{v}'\delta(u)\mathbf{w}$.

Proof We have for $s \in [0,1]$ and $t \in [0, \bar{\tau}]$,

$$\begin{aligned} G_n(s,t) &= \sqrt{\tau} \sum_{i=1}^{\lfloor ns \rfloor} \mathbf{v}'\varepsilon_i \mathbf{w}\varphi(t - i\tau) + \sqrt{\tau} \sum_{i=1}^{\lfloor ns \rfloor} \mathbf{v}'\delta(i\tau)\mathbf{w}\varphi(t - i\tau) \\ &=: T_n^{(1)}(s,t) + T_n^{(2)}(s,t). \end{aligned}$$

Since an arbitrary linear combination of continuous functions (resp. functions of bounded variation) is also continuous (resp. of bounded variation), we have that $\delta_{\mathbf{v},\mathbf{w}}(u) = \mathbf{v}'\delta(u)\mathbf{w}$ is continuous (resp. of bounded variation) as well. Thus, we can argue as in [3] and the assertion follows. □

Remark 16.1 Similar as in [3] we have $T_n^{(2)}(s,t) \to 0$ (and thus $G_n(s,t) \Rightarrow \mathscr{F}(s,t)$) for $\beta > 1/2$ and $T_n^{(2)}(s,t) \to \infty$ for $\beta < 1/2$ as $n \to \infty$. This means that for $\beta > 1/2$ it is impossible to detect a change whereas it is rather simple for $\beta < 1/2$.

The above results help in identifying when the procedure works. First notice that it is clear that a time-constant alternative $\delta(u) = \delta$ that lies in a subspace $\text{span}\{\mathbf{b}_i\mathbf{c}_i' \colon 1 \le i \le m\}$ cannot be detected if $\mathbf{v} \perp \text{span}\{\mathbf{b}_i\}$ or $\mathbf{w}_i \perp \text{span}\{\mathbf{c}_i\}$. More subtle is the question whether there are situations where the change cancels out, i.e. where

$$\delta_{\mathbf{v},\mathbf{w}}(u) = \mathbf{v}'\delta(u)\mathbf{w} = \sum_{k=1}^{N_y}\sum_{l=1}^{N_x} v_k w_l \delta^{(k,l)} \equiv 0.$$

This can happen, for example, if the components of δ are linearly dependent functions. If, on the contrary, they are independent, we know that $\delta_{\mathbf{v},\mathbf{w}} \neq 0$ for all choices of $\mathbf{v}, \mathbf{w} \neq \mathbf{0}$. A simple criterion to check if a given set of (sufficiently smooth) functions $g_1, \ldots, g_n$ on the interval I is linearly independent is to consider the Wronski determinant which is defined as

$$W(g_1, \ldots, g_n)(t) = \det \begin{pmatrix} g_1(t) & g_2(t) & \ldots & g_n(t) \\ g_1^{(1)}(t) & g_2^{(1)}(t) & \ldots & g_n^{(1)}(t) \\ \vdots & & \ddots & \vdots \\ g_1^{(n-1)}(t) & g_2^{(n-1)}(t) & \ldots & g_n^{(n-1)}(t) \end{pmatrix}$$

for $t \in I$. Here, $g_i^{(n)}$ denotes the n-th derivative of the function g_i. If

$$W(g_1, \ldots, g_n)(t_0) \neq 0$$

for some $t_0 \in I$, the functions $g_1, \ldots, g_n$ are linearly independent on I. Note, however, that linearly independent functions can be linearly dependent on subintervals of I. For example, if $g_1(t) = \sin(t)\mathbf{1}_{[0,\pi]}(t)$ and $g_2(t) = \sin(t)\mathbf{1}_{(\pi,2\pi]}(t)$, the two functions are linearly independent on $[0, 2\pi]$, but linearly dependent on both $[0, \pi]$ and $(\pi, 2\pi]$.

Furthermore, the diagonal elements of δ cancel out in $\delta_{\mathbf{v},\mathbf{w}}$ if $\mathbf{v}$ and $\mathbf{w}$ are orthogonal, i.e. if $\mathbf{v}'\mathbf{w} = 0$.

Generalizing the process G_n let us now study the process G_n^J defined by

$$G_n^J(s,t) = \sum_{j=1}^{J} \mathbf{v}^{(j)'} \mathscr{F}_n(s,t)\mathbf{w}^{(j)}, \quad s \in [0,1],\ t \in [0,\bar{\tau}].$$

The question arises, whether this process still fulfills a functional limit theorem as in Theorem 16.1. Hence, we first establish a result similar to Proposition 16.1.

Proposition 16.2 *The time series* $\xi_n^J(\mathbf{v},\mathbf{w}) = \sum_{j=1}^{J} \mathbf{v}^{(j)'}\varepsilon_n\mathbf{w}^{(j)}$, $n \ge 1$, *is strictly stationary with mean zero,*

$$E\left|\xi_1^J(\mathbf{v},\mathbf{w})\right|^2 < \infty$$

and autocovariance function $\gamma_h^J = E(\xi_1(\mathbf{v},\mathbf{w})\xi_{1+|h|}(\mathbf{v},\mathbf{w}))$ *given by*

$$\gamma_h^J = \sum_{k=1}^{N_y}\sum_{l=1}^{N_x}\sum_{s=1}^{N_y}\sum_{t=1}^{N_x}\sum_{j=1}^{J}\sum_{m=1}^{J} v_k^{(j)} w_l^{(j)} v_s^{(m)} w_t^{(m)} E(\varepsilon_{0,0,0}\varepsilon_{h,s-k,t-l})$$

for $h \in \mathbb{Z}$ *satisfying* $(\sigma_\xi^J)^2 = \sum_{h\in\mathbb{Z}} \gamma_h^J < \infty$. *Further,* $\xi_n^J(\mathbf{v},\mathbf{w})$, $n \geq 1$, *is* φ*-mixing with mixing coefficients* φ_k, $k \geq 1$, *satisfying* $\sum_{k=1}^{\infty} \varphi_k^{1/2} < \infty$.

Proof Using an estimate as in the proof of Proposition 16.1 we obtain

$$E\left|\xi_1^J(\mathbf{v},\mathbf{w})\right|^2 \leq E\left(\sum_{j=1}^{J}\left|\mathbf{v}^{(j)'}\varepsilon_1\mathbf{w}^{(j)}\right|\right)^2 \leq \left(\sum_{j=1}^{J}\|v_j\|_2\|w_j\|_2\right)^2 E\left(\|\varepsilon_1\|_F^2\right)$$

with $E(\|\varepsilon_1\|_F^2) = N_x N_y \gamma_{0,0,0}$ such that the second moments are finite. The covariance function follows again by a straightforward calculation. Set $C = \max\{v_k^{(j)}, w_l^{(j)},\ j \in \{1,\ldots,J\},\ k \in \{1,\ldots,N_y\},\ l \in \{1,\ldots,N_x\}\}$. Then, $\sigma_\xi^2 < \infty$ follows, since

$$\begin{aligned}\sum_{h\in\mathbb{Z}}\left|\gamma_h^J\right| &\leq CJ^2 \sum_{h\in\mathbb{Z}} \sum_{k=-(N_y-1)}^{N_y-1} \sum_{l=-(N_x-1)}^{N_x-1} \left|E(\varepsilon_{0,0,0}\varepsilon_{h,k,l})\right| \\ &\leq CJ^2 \sum_{(h,k,l)\in\mathbb{Z}^3} \left|\gamma_h(k,l)\right| < \infty.\end{aligned}$$

The rest of the proof follows now along the lines of the proof of Proposition 16.1. □

Now, we directly obtain the following theorem.

Theorem 16.3 *Suppose that Assumption (A) holds. Under the no change null hypothesis, we have*

$$G_n^J(s,t) \Rightarrow \mathscr{F}(s,t), \quad n \to \infty, \quad \text{with } \mathscr{F}(s,t) = \sqrt{\bar{\tau}}\sigma_\xi^J \int_0^s \varphi(t-\bar{\tau}u)\,dB(u).$$

Acknowledgements The authors acknowledge the support of BMWi (Federal Ministry for Economic Affairs and Energy) under grant No. 0325588B, PV-Scan project.

References

1. Billingsley P (1968) Convergence of probability measures. Wiley, New York
2. Deo CM (1975) A functional central limit theorem for stationary random fields. Ann Probab 3(4):708–715
3. Pawlak M, Steland A (2013) Nonparametric sequential signal change detection under dependent noise. IEEE Trans Inf Theory 59(6):3514–3531
4. Pawlak M, Stadtmüller U (1996) Recovering band-limited signals under noise. IEEE Trans Inf Theory 42(5):1425–1438
5. Pawlak M, Stadtmüller U (2007) Signal sampling and recovery under dependent errors. IEEE Trans Inf Theory 53(7):2526–2541
6. Prause A, Steland A (2014) Sequential detection of three-dimensional signals under dependent noise. Preprint

7. Prause A, Steland A (2014) Sequential detection of three-dimensional signals under dependent noise – some simulation results. Preprint
8. Prause A, Steland A (2014) Sequential detection of vector-valued signals under dependent noise. Preprint

Chapter 17
Optimal Designs for Steady-State Kalman Filters

Guillaume Sagnol and Radoslav Harman

Abstract We consider a stationary discrete-time linear process that can be observed by a finite number of sensors. The experimental design for the observations consists of an allocation of available resources to these sensors. We formalize the problem of selecting a design that maximizes the information matrix of the steady-state of the Kalman filter, with respect to a standard optimality criterion, such as D- or A-optimality. This problem generalizes the optimal experimental design problem for a linear regression model with a finite design space and uncorrelated errors. Finally, we show that under natural assumptions, a steady-state optimal design can be computed by semidefinite programming.

17.1 Introduction

We consider a stationary discrete-time linear process with a state vector $\mathbf{x}_t \in \mathbb{R}^n$:

$$\mathbf{x}_t = F\mathbf{x}_{t-1} + L\,\nu_t \quad (t = 1, 2, \ldots) \tag{17.1}$$

where F is an $n \times n$ transition matrix, L is an $n \times \ell$ noise selection matrix, and $\nu_t \sim \mathcal{N}(\mathbf{0}, \mathbf{I}_\ell)$ is a process noise. In addition, we assume $\mathbf{x}_0 \sim \mathcal{N}(\hat{\mathbf{x}}_0, \Sigma_0)$. Uncorrelated observations $\mathbf{y}_t^{(1)}, \ldots, \mathbf{y}_t^{(s)}$ of the process are available at each time step:

$$\forall i = 1, \ldots, s, \quad \mathbf{y}_t^{(i)} = H_i\mathbf{x}_t + \mathbf{v}_t^{(i)}$$

Electronic supplementary material Supplementary material is available in the online version of this chapter at doi:10.1007/978-3-319-13881-7_17.

G. Sagnol (✉)
Dept. Optimization, Zuse Institut Berlin, Takustr. 7, 14195 Berlin, Germany
e-mail: sagnol@zib.de

R. Harman
Faculty of Mathematics, Physics and Informatics, Comenius University, Mlynská Dolina, 84248 Bratislava, Slovakia
e-mail: harman@fmph.uniba.sk

A. Steland et al. (eds.), *Stochastic Models, Statistics and Their Applications*,
Springer Proceedings in Mathematics & Statistics 122,
DOI 10.1007/978-3-319-13881-7_17

where the ith observation matrix H_i is $r_i \times n$ and the measurements errors satisfy $\mathbf{v}_t^{(i)} \sim \mathcal{N}(\mathbf{0}, \sigma_i^2 \mathbf{I}_{r_i})$. We can group the measurements at time t, which gives a multi-dimensional observation

$$\mathbf{y}_t = H\mathbf{x}_t + \mathbf{v}_t \tag{17.2}$$

of size $r = \sum_{i=1}^{s} r_i$, with $H = [H_1^T, \ldots, H_s^T]^T$, and $\mathbf{v}_t \sim \mathcal{N}(\mathbf{0}, R)$ where R is the $r \times r$ block diagonal matrix whose ith diagonal block is $\sigma_i^2 \mathbf{I}_{r_i}$. The random vectors $\{\mathbf{x_0}, \nu_1, \ldots, \nu_t, \ldots, \mathbf{v}_1, \ldots, \mathbf{v}_t, \ldots\}$ are assumed to be mutually independent.

In this article, we are concerned with the case where the variance σ_i^2 depends on the quantity w_i of resources dedicated to the ith observation. More precisely, we assume that $\sigma_i^2 = \frac{1}{\mu_i(w_i)}$, where μ_i is a nondecreasing, concave and continuous function mapping $\mathbb{R}_+$ onto itself, and such that $\mu_i(0) = 0$. The interpretation for $w_i = 0$ is that $\sigma_i^2 = +\infty$, meaning that $\mathbf{y}_t^{(i)}$ is unobserved if no resource is allocated to the ith observation point. The vector $\mathbf{w} = [w_1, \ldots, w_s] \in \mathbb{R}_+^s$ will be called a *measurement design*, or simply a *design* for the dynamic process (17.1)–(17.2).

The problem studied in this paper is the optimal allocation of resources to the s observation points, when the resources are limited and the design $\mathbf{w}$ must be selected within a compact set $\mathscr{W} \subset \mathbb{R}_+^s$ prior to the beginning of the dynamic process.

The process described by Eqs. (17.1)–(17.2) contains the natural ingredients to run a Kalman filter, cf. Eqs. (17.4)–(17.8), which yields at each time t an unbiased estimator $\hat{\mathbf{x}}_t$ of $\mathbf{x}_t$ that is linear with respect to the observations $\mathbf{y}_1, \ldots, \mathbf{y}_t$, and with Loewner-minimum covariance matrix in the class of all linear unbiased estimators of $\mathbf{x}_t$; see, e.g., [15, Sect. 5.2]. Under standard assumptions (see Sect. 17.2), the information matrix M_t, which is defined as the inverse of the variance-covariance matrix Σ_t of the error $(\hat{\mathbf{x}}_t - \mathbf{x}_t)$, converges to a constant matrix M_∞. This limit depends only on the design $\mathbf{w}$ (and not on the initial state $\mathbf{x}_0$ or the measurements $\mathbf{y}_1, \mathbf{y}_2, \ldots$), and is the unique positive definite solution X of the discrete algebraic Riccati equation (written here in information form):

$$X = \left(FX^{-1}F^T + LL^T\right)^{-1} + M(\mathbf{w}), \tag{17.3}$$

where $M(\mathbf{w}) := \sum_{i=1}^{s} \mu_i(w_i) H_i^T H_i$. To stress this dependency, we denote by $M_\infty(\mathbf{w})$ the unique positive definite solution X of (17.3). A natural approach hence consists in choosing $\mathbf{w} \in \mathscr{W}$ so as to maximize an appropriate scalarization $\Phi(M_\infty(\mathbf{w}))$ of the steady-state information matrix. The main result of this paper (Theorem 17.1) shows that under natural conditions on $\Phi()$, $\mu_i()$ and $\mathscr{W}$, this problem can be solved using semidefinite programming (SDP).

The problem of maximizing $\Phi(M_\infty(\mathbf{w}))$ over $\mathscr{W}$ is in fact a generalization of a classical problem which has been extensively studied by statisticians: in the *standard optimal experimental design problem*, the quality of a design $\mathbf{w}$ is measured by a function of the form $\mathbf{w} \to \Phi(M(\mathbf{w}))$, where $M(\mathbf{w}) = \sum_{i=1}^{s} w_i H_i^T H_i$. This corresponds to the expression of $M_\infty(\mathbf{w})$ when no information can be gained from the observation of a dynamic process (so "$LL^T \to +\infty$"), and $\mu_i(w_i) = w_i$ for all i. The approach presented in this paper thus extends the standard optimal design theory to deal with the situation where information can be gained from the knowledge

of the system dynamics. We refer the reader to Pukelsheim [11] for a comprehensive monograph on the theory of optimal experimental designs.

Related Work The results presented in this paper answer a question raised in [16] by Singhal and Michailidis, who have considered a problem applicable in telecommunications, where $F = \mathbf{I}_n$ and each H_i has a single nonzero entry per row. The authors propose to use Second-Order Cone Programming to maximize the smallest element of the diagonal steady-state information matrix, i.e., they use the criterion of E-optimality. In contrast, the semidefinite programming approach of the present paper allows one to handle non-diagonal covariance matrices.

Steady-state sensor optimization problems have been considered since the 70's, but almost all authors consider a continuous time model $\frac{d\mathbf{x}_t}{dt} = F\mathbf{x}_t + L\mathbf{v}_t$, and optimize the location of sensors over a continuous space, see e.g. [1, 5, 12]. A recent reference is [10], where the design weights w_i are interpreted as probabilities to activate the ith sensor at time t, and are optimized by semidefinite programming with respect to a specific criterion, which is in fact weighted A-optimality. One of the rare papers that considers a discrete time model is [7], where a gradient descent is used to minimize a bound of the steady-state covariance matrix.

Notation Throughout this article, we denote by $\mathbb{S}_n$ ($\mathbb{S}_n^+$, $\mathbb{S}_n^{++}$) the set of $n \times n$ symmetric (positive semidefinite, positive definite) matrices. The symbol $\preceq$ denotes the Löwner ordering ($A \preceq B \Longleftrightarrow B - A \in \mathbb{S}_n^+$), and $A \prec B$ means that $B - A \in \mathbb{S}_n^{++}$.

17.2 The Optimal Design Problem in a Filtering Context

Assume (temporarily) that $w_i > 0$ for all $i \in \{1, \ldots, s\}$, so that $R < +\infty$ and the Kalman filter equations read (see e.g. [15]):

$$\hat{\mathbf{x}}_{t+1|t} = F\hat{\mathbf{x}}_t, \tag{17.4}$$

$$\hat{\Sigma}_{t+1|t} = F\Sigma_t F^T + LL^T, \tag{17.5}$$

$$K_t = \hat{\Sigma}_{t+1|t} H^T \left(H\hat{\Sigma}_{t+1|t} H^T + R\right)^{-1}, \tag{17.6}$$

$$\hat{\mathbf{x}}_{t+1} = \hat{\mathbf{x}}_{t+1|t} + K_t(\mathbf{y}_{t+1} - H\hat{\mathbf{x}}_{t+1|t}), \tag{17.7}$$

$$\Sigma_{t+1} = (\mathbf{I}_n - K_t H)\hat{\Sigma}_{t+1|t}, \tag{17.8}$$

where $\hat{\mathbf{x}}_{t+1|t}$ is the *a-priori* estimator of $\mathbf{x}_{t+1}$ based on the observations up to the time t, $\hat{\Sigma}_{t+1|t}$ is the covariance matrix of $\hat{\mathbf{x}}_{t+1|t}$, the matrix K_t is the so-called optimal Kalman gain, $\hat{\mathbf{x}}_{t+1}$ is the *a-posteriori* estimator of $\mathbf{x}_{t+1}$ based on the observations up to the time $t+1$, and Σ_{t+1} is the covariance matrix of $\hat{\mathbf{x}}_{t+1}$.

Provided that (i) R is positive definite; (ii) the pair (F, L) is controllable [9, Sect. C3], i.e. $\text{rank}[L, FL, \ldots, F^{n-1}L] = n$; and (iii) the pair (F, H) is detectable [9, Sect. C4], that is, $\text{rank}[F^T - \lambda\mathbf{I}_n, H^T] = n$ for all $\lambda \in \mathbb{C}$ such that $|\lambda| \geq 1$, it is well known that the sequence of covariance matrices of the a-priori

estimator of the state $(\hat{\Sigma}_{t+1|t})_{t\in\mathbb{N}}$ converges to a constant matrix Σ_∞^-, that is the unique positive definite solution of the discrete algebraic Riccati equation (DARE), see [15, Sect. 7.3]. In this article, we work with information matrices rather than with covariance matrices, and so we shall consider an alternative Riccati equation in information form (17.3), which we call I-DARE. To derive it, note that the correction equation (17.8) of the Kalman filter is sometimes given under an alternative form, which can be obtained by using the Woodbury matrix identity: $\Sigma_{t+1} = (\hat{\Sigma}_{t+1|t}^{-1} + H^T R^{-1} H)^{-1}$. This gives a simple update formula for the *information matrix* $M_t := \Sigma_t^{-1}$ of the filter, which implies the I-DARE, see Eq. (17.3):

$$M_{t+1} = \hat{\Sigma}_{t+1|t}^{-1} + H^T R^{-1} H = \left(F M_t^{-1} F^T + L L^T\right)^{-1} + \underbrace{\sum_{i=1}^{s} \mu_i(w_i) H_i^T H_i}_{M(\mathbf{w})}.$$

Now, let us remove the assumption that $w_i > 0$ for all $i \in \{1,\dots,s\}$: Recall that $w_i = 0$ means that the sequence $(\mathbf{y}_t^{(i)})$ is unobserved. Hence we define the reduced observation matrix $H_{\mathbf{w}} = [H_{i_1}^T, \dots, H_{i_q}^T]^T$, where $\{i_1,\dots,i_q\} := \{i \in \{1,\dots,s\}\colon\ w_i > 0\}$. Similarly, $R_{\mathbf{w}}$ is the block diagonal matrix whose kth diagonal block is $\frac{1}{\mu_{i_k}(w_{i_k})}\mathbf{I}_{r_{i_k}}$. The equations of the Kalman filter are now obtained by substituting $H_{\mathbf{w}}$ for H and $R_{\mathbf{w}}$ for R in Eqs. (17.4)–(17.8). This leaves the I-DARE (17.3) unchanged, since $H_{\mathbf{w}}^T R_{\mathbf{w}}^{-1} H_{\mathbf{w}} = \sum_{i:\ w_i>0} \mu_i(w_i) H_i^T H_i = \sum_{i=1}^{s} \mu_i(w_i) H_i^T H_i = M(\mathbf{w})$.

Now, for the rest of this article we assume that

A1. The pair (F, L) is controllable.
A2. The subset of *detectable designs*, $\mathscr{W}^+ := \{\mathbf{w} \in \mathscr{W}\colon\ (F, H_{\mathbf{w}}) \text{ is detectable}\}$ is nonempty.
A3. The criterion $\Phi : \mathbb{S}_+^n \mapsto \mathbb{R}_+$ is isotonic (i.e., $A \succeq B \Longrightarrow \Phi(A) \geq \Phi(B)$), continuous, concave, and $\Phi(M) = 0$ if and only if M is singular.

Assumption A3 is satisfied by most common criteria used in optimal design, such as $\Phi_D : M \to \det M^{\frac{1}{n}}$, $\Phi_E : M \to \lambda_{\min}(M)$ or $\Phi_A : M \to n/\operatorname{trace} M^{-1}$, see [11]. An isotonic criterion Φ is said to be *strictly isotonic* if in addition it satisfies $A \neq B$, $A \succeq B \Longrightarrow \Phi(A) > \Phi(B)$. For example, Φ_E is isotonic but not strictly isotonic.

Assumptions A1 and A2 ensure that Eq. (17.3) has a unique positive definite solution, which we denote by $M_\infty(\mathbf{w})$, for all $\mathbf{w} \in \mathscr{W}^+$:

Lemma 17.1 *Equation (17.3) has a positive definite solution if and only if the design* $\mathbf{w}$ *is detectable, i.e.* $\mathbf{w} \in \mathscr{W}^+$. *Moreover, this solution is unique.*

We omit the proof of this result for the sake of length.[1] The idea is to show that there is a one-to-one correspondence between the positive definite solutions of the

[1] The proof is given in an Appendix of this article, available at http://dx.doi.org/10.1007/978-3-319-13881-7_17.

standard DARE and its counterpart in information form I-DARE; then we can use known results on the DARE (see e.g. [15, Theorems 23 and 25]).

So the problem of maximizing $\Phi(M_\infty(\mathbf{w}))$ over $\mathscr{W}^+$ is well defined, and can be rewritten as follows:

$$\begin{aligned} \sup_{\mathbf{w}\in\mathbb{R}^s,\ X\in\mathbb{S}_n} \quad & \Phi(X) \\ \text{s.t.} \quad & X = \left(FX^{-1}F^T + LL^T\right)^{-1} + \sum_{i=1}^{s} \mu_i(w_i) H_i^T H_i \\ & X \succ 0, \qquad \mathbf{w} \in \mathscr{W}^+. \end{aligned} \tag{17.9}$$

17.3 Semidefinite Programming Formulation

We next give a series of propositions that basically show that the Riccati equation in (17.9) may be replaced by a linear matrix inequality (LMI). In fact, Propositions 17.2 and 17.3 are similar to existing results concerning the inequality version of the standard DARE,[2] see e.g. Appendix E in [9]. However, our LMI representation of the closure of the set $\{X \succ 0 :\ X \preceq (FX^{-1}F^T + LL^T)^{-1} + M(\mathbf{w})\}$, cf. Proposition 17.1, is completely new. Its proof is inspired by the LMI representation of the harmonic mean of two matrices, cf. § 4.1 in [3], and is presented at the end of this section.

Let us first introduce the sets

$$\mathscr{X}(\mathbf{w}) := \left\{ X \succeq 0 : \quad \exists U \in \mathbb{S}_n : \quad (i)\colon X = U + M(\mathbf{w}) \right.$$
$$\left. (ii)\colon \begin{pmatrix} X - F^T U F & F^T U L \\ L^T U F & \mathbf{I}_\ell - L^T U L \end{pmatrix} \succeq 0 \right\}, \tag{17.10}$$

and

$$\mathscr{X}^+(\mathbf{w}) := \left\{ X \succ 0 :\ f(X, \mathbf{w}) \succeq 0 \right\},$$

where $f(X, \mathbf{w}) := (FX^{-1}F^T + LL^T)^{-1} + M(\mathbf{w}) - X$.

The first proposition of this series shows the relation between these two sets:

Proposition 17.1 *For all designs $\mathbf{w} \in \mathscr{W}$, we have $\mathscr{X}(\mathbf{w}) \cap \mathbb{S}_n^{++} = \mathscr{X}^+(\mathbf{w})$.*

Then, we shall see that $\mathscr{X}(\mathbf{w})$ is bounded, and hence $\mathscr{X}^+(\mathbf{w})$ is bounded as well:

[2] Proofs are given in an Appendix of this article, available at http://dx.doi.org/10.1007/978-3-319-13881-7_17.

Proposition 17.2 *For all designs* $\mathbf{w} \in \mathscr{W}$*, the set* $\mathscr{X}(\mathbf{w})$ *is bounded. Moreover, there exists a constant* $\alpha \geq 0$ *such that* $X \in \mathscr{X}(\mathbf{w}) \Longrightarrow \|X\|_2 \leq \alpha(1 + \sum_i \mu_i(w_i)\|H_i\|_2^2)$*, where* $\|M\|_2$ *denotes the spectral norm of* M*.*

This proposition will be useful to show that $\mathscr{X}^+(\mathbf{w})$ has a maximal element:

Proposition 17.3 *Assume that* $\mathscr{X}^+(\mathbf{w})$ *is nonempty. Then, there is a matrix* $X^*_{\mathbf{w}} \in \mathscr{X}^+(\mathbf{w})$ *such that*

$$X \in \mathscr{X}^+(\mathbf{w}) \Longrightarrow X \preceq X^*_{\mathbf{w}}.$$

Moreover, this maximal element necessarily satisfies $f(X^*_{\mathbf{w}}, \mathbf{w}) = 0$*, so that* $\mathbf{w}$ *is detectable and* $X^*_{\mathbf{w}} = M_\infty(\mathbf{w})$*.*

In consequence, we can deduce equivalent statements for a design $\mathbf{w}$ to be detectable:

Corollary 17.1 *The following statements are equivalent*:

(i) *The design* $\mathbf{w}$ *is detectable, i.e.* $\mathbf{w} \in \mathscr{W}^+$;
(ii) *The I-DARE equation* $f(X, \mathbf{w}) = 0$ *has a positive definite solution* $X \succ 0$;
(iii) *The LMI* $f(X, \mathbf{w}) \succeq 0$ *has a positive definite solution* $X \succ 0$;
(iv) *The set* $\mathscr{X}^+(\mathbf{w})$ *is nonempty*;
(v) *There is a pair* $(X, U) \in \mathbb{S}_n^{++} \times \mathbb{S}_n$ *satisfying the conditions* (*i*) *and* (*ii*) *of the definition* (17.10).

Proof The equivalence (i) $\Longleftrightarrow$ (ii) follows from Lemma 17.1 and (iii) $\Longleftrightarrow$ (iv) $\Longleftrightarrow$ (v) is clear from the definitions of $\mathscr{X}^+(\mathbf{w})$ and $\mathscr{X}(\mathbf{w})$ and Proposition 17.1. The implication (ii) $\Longrightarrow$ (iii) is trivial, and by Proposition 17.3 we have (iv) $\Longrightarrow$ (i). Hence the corollary is proved. □

The main result of this article follows. It shows that Problem (17.9) can be reformulated by using linear matrix inequalities. As a consequence, a solution $\mathbf{w}$ of the steady-state optimal design problem (17.9) can be computed by semidefinite programming (under natural assumptions on $\Phi, \mathscr{W}$ and the functions μ_i, see Remark 17.1):

Theorem 17.1 *Consider the following optimization problem*:

$$\max_{\substack{\mathbf{w} \in \mathbb{R}^s \\ X, U \in \mathbb{S}_n}} \quad \Phi(X) \tag{17.11a}$$

$$\text{s.t.} \quad \begin{pmatrix} X - F^T U F & F^T U L \\ L^T U F & \mathbf{I}_\ell - L^T U L \end{pmatrix} \succeq 0 \tag{17.11b}$$

$$X = U + \sum_{i=1}^{s} \mu_i(w_i) H_i^T H_i \tag{17.11c}$$

$$X \succeq 0 \tag{17.11d}$$

$$\mathbf{w} \in \mathscr{W}. \tag{17.11e}$$

This problem has a solution, i.e. the problem is bounded and the maximum is reached for a triple $(\mathbf{w}^*, X^*, U^*)$. *Moreover,* $\mathbf{w}^*$ *is a solution of the steady-state optimal design problem,* $\max\{\Phi(M_\infty(\mathbf{w})) : \mathbf{w} \in \mathscr{W}^+\}$. *If in addition* Φ *is strictly isotonic, then* X^* *coincides with the optimal steady-state information matrix* $M_\infty(\mathbf{w}^+)$.

Proof We will prove this theorem in three steps:

1. We observe that the feasibility set of Problem (17.11a)–(17.11e) is compact, which guarantees the existence of an optimal solution $(\mathbf{w}^*, X^*, U^*)$ by continuity of Φ. This is a direct consequence of the bound in Proposition 2, together with the compactness of $\mathscr{W}$ and the continuity of the μ_i.
2. We show that this solution necessarily satisfies $X^* \succ 0$. Indeed, by Assumption A2 there exists a detectable design $\mathbf{w}$, so that $M_\infty(\mathbf{w}) \succ 0$ and we know from Assumption A3 that $\Phi(M_\infty(\mathbf{w})) > 0$. Hence the optimal value of Problem (17.11a)–(17.11e) must be positive, which implies that the optimal X^* cannot be singular (Assumption A3).
3. To conclude, observe that Problem (17.11a)–(17.11e) can be rewritten as

$$\max_{\mathbf{w}\in\mathscr{W}} \max_{X\in\mathscr{X}(\mathbf{w})} \Phi(X),$$

and by point 2, we can replace $X \in \mathscr{X}(\mathbf{w})$ by $X \in \mathscr{X}^+(\mathbf{w})$, see Proposition 17.1. Moreover by Corollary 17.1 the optimal design $\mathbf{w}^*$ is necessarily detectable (otherwise the maximization over X goes over the empty set and so it takes the value $-\infty$). Let $X^*(\mathbf{w})$ denote an optimal variable X of the inner problem, for a fixed $\mathbf{w} \in \mathscr{W}^+$. Since Φ preserves the Löwner ordering, the value $\Phi(X^*(\mathbf{w}))$ is necessarily equal to $\Phi(M_\infty(\mathbf{w}))$, because $M_\infty(\mathbf{w})$ is the maximal element of $\mathscr{X}^+(\mathbf{w})$, see Proposition 17.3. If moreover Φ is strictly isotonic, then the optimizer must be the maximal element: $X^*(\mathbf{w}) = M_\infty(\mathbf{w})$. This proves the theorem. □

Remark 17.1 Assume that $\mathscr{W}, \Phi$ and the μ_i $(i \in \{1, \ldots, s\})$ are *semidefinite-representable*: a precise definition can be found in [2], but basically it means that the constraint $\mathbf{w} \in \mathscr{W}$ can be replaced by an LMI, as well as constraints of the form $\Phi(M) \geq t$ and $\mu_i(w_i) \geq u_i$. (For example, it is known that the most common criteria Φ_A, Φ_D, and Φ_E are semidefinite representable [4], as well as all Kiefer's Φ_p-criteria for a value of $p \in \mathbb{Q}$ [14]; Concerning the scalar functions μ_i, every concave rational function is semidefinite representable [8].) Then, it is straightforward to reformulate Problem (17.11a)–(17.11e) as a semidefinite program (SDP). Note that interfaces such as CVX [6] or PICOS [13] allows one to easily pass Problem (17.11a)–(17.11e) to modern interior-point solvers, without further reformulations.

Proof of Proposition 17.1 Let $X \succ 0$. Let $[V_1^T, V_2^T]^T$ be a base of $\mathrm{Ker}([F, L])$, i.e., $FV_1 + LV_2 = 0$. The matrix $[V_1^T, V_2^T]^T$ has full rank by rank-nullity theorem and controllability of (F, L). So the matrix $(V_1^T V_1 + V_2^T V_2)$ is invertible.

The matrix $\Delta := \left(\begin{smallmatrix} FX^{-1} & -L \\ V_1^T & -V_2^T \end{smallmatrix}\right)$ is invertible. Indeed we can check by direct calculation that its inverse is $\left(\begin{smallmatrix} F^T T & A_1 \\ -L^T T & -A_2 \end{smallmatrix}\right)$, where

$$\begin{aligned} T &= \big(FX^{-1}F^T + LL^T\big)^{-1}, \\ A_1 &= \big(V_1 - F^T T\big(FX^{-1}V_1 + LV_2\big)\big)\big(V_1^T V_1 + V_2^T V_2\big)^{-1}, \\ A_2 &= \big(V_2 - L^T T\big(FX^{-1}V_1 + LV_2\big)\big)\big(V_1^T V_1 + V_2^T V_2\big)^{-1}. \end{aligned}$$

So, $\left(\begin{smallmatrix} X - F^T U F & F^T U L \\ L^T U F & \mathbf{I}_\ell - L^T U L \end{smallmatrix}\right) \succeq 0$ if and only if

$$\begin{aligned} &\Delta \begin{pmatrix} X - F^T U F & F^T U L \\ L^T U F & \mathbf{I}_\ell - L^T U L \end{pmatrix} \Delta^T \succeq 0 \\ \iff \quad &\Delta \begin{pmatrix} X & 0 \\ 0 & \mathbf{I}_\ell \end{pmatrix} \Delta^T \succeq \Delta(F, -L)^T U (F, -L) \Delta^T. \end{aligned}$$

We can simplify the last expression by using the relation $FV_1 + LV_2 = 0$. This yields a block diagonal LMI with following expressions on the two diagonal blocks:

$$FX^{-1}F^T + LL^T \succeq \big(FX^{-1}F^T + LL^T\big)U\big(FX^{-1}F^T + LL^T\big); \quad (17.12)$$

$$V_1^T X V_1 + V_2^T V_2 \succeq 0. \quad (17.13)$$

The LMI (17.13) is always satisfied, and LMI (17.12) reduces to $U \preceq (FX^{-1}F^T + LL^T)^{-1}$ (after pre- and post-multiplication by $(FX^{-1}F^T + LL^T)^{-1}$).

So, we have shown that $(X, U) \in \mathbb{S}_n^{++} \times \mathbb{S}_n$ satisfies the condition (ii) of Definition (17.10) if and only if $U \preceq (FX^{-1}F^T + LL^T)^{-1}$. The rest of the proof is easy. Let $(X, U) \in \mathbb{S}_n^{++} \times \mathbb{S}_n$ satisfy conditions (i) and (ii) of the definition of $\mathscr{X}(\mathbf{w})$. We have $X \preceq (FX^{-1}F^T + LL^T)^{-1} + M(\mathbf{w})$, that is, $f(X, \mathbf{w}) \geq 0$, and hence $X \in \mathscr{X}^+(\mathbf{w})$. Conversely, assume that $X \succ 0$, $f(X, \mathbf{w}) \geq 0$ and set $U' := (FX^{-1}F^T + LL^T)^{-1}$, $U := X - M(\mathbf{w})$. We know that (X, U') satisfies condition (ii) of (17.10), and since we have $f(X, \mathbf{w}) \geq 0 \iff U' \succeq U$, the pair (X, U) satisfies both conditions (i) and (ii), that is, $X \in \mathscr{X}(w) \cap \mathbb{S}_n^{++}$. □

Acknowledgements The research of the second author was supported by the VEGA 1/0163/13 grant of the Slovak Scientific Grant Agency.

References

1. Amouroux M, Babary JP, Malandrakis C (1978) Optimal location of sensors for linear stochastic distributed parameter systems. In: Distributed parameter systems: modelling and identification. Springer, Berlin, pp 92–113
2. Ben-Tal A, Nemirovski A (1987) Lectures on modern convex optimization: analysis, algorithms, and engineering applications. Society for industrial mathematics, vol 2
3. Bhatia R (2008) Positive definite matrices. Princeton University Press, Princeton
4. Boyd S, Vandenberghe L (2004) Convex optimization. Cambridge University Press, Cambridge

5. Curtain RF, Ichikawa A (1978) Optimal location of sensors for filtering for distributed systems. In: Distributed parameter systems: modelling and identification. Springer, Berlin, pp 236–255
6. Grant M, Boyd S (2010) CVX: Matlab software for disciplined convex programming, version 1.21. http://cvxr.com/cvx
7. Gupta V, Chung TH, Hassibi B, Murray RM (2006) On a stochastic sensor selection algorithm with applications in sensor scheduling and sensor coverage. Automatica 42(2):251–260
8. Henrion D (2011) Semidefinite representation of convex hulls of rational varieties. Acta Appl Math 115(3):319–327
9. Kailath T, Sayed AH, Hassibi B (2000) Linear estimation. Prentice Hall, New York
10. Mourikis AI, Roumeliotis SI (2006) Optimal sensor scheduling for resource-constrained localization of mobile robot formations. IEEE Trans Robot 22(5):917–931
11. Pukelsheim F (1993) Optimal design of experiments. Wiley, New York
12. Rafajłowicz E (1984) Optimization of measurements for state estimation in parabolic distributed systems. Kybernetika 20(5):413–422
13. Sagnol G (2012) Picos, a python interface to conic optimization solvers. Technical report 12-48, ZIB. http://picos.zib.de
14. Sagnol G (2013) On the semidefinite representation of real functions applied to symmetric matrices. Linear Algebra Appl 439(10):2829–2843
15. Simon D (2006) Optimal state estimation: Kalman, H_∞, and nonlinear approaches. Wiley, New York
16. Singhal H, Michailidis G (2010) Optimal experiment design in a filtering context with application to sampled network data. Ann Appl Stat 4(1):78–93

Chapter 18
On the Impact of Correlation on the Optimality of Product-Type Designs in SUR Models

Moudar Soumaya and Rainer Schwabe

Abstract For multivariate observations with seemingly unrelated variables product-type designs often turn out to be optimal which are generated by their univariate optimal counterparts. This is, in particular, the case when all variables contain an intercept term. If these intercepts are missing, the product-type designs may lose their optimality when the correlation between the components becomes stronger.

18.1 Introduction

In many applications two or more variables are observed at the same observational units. These observations will be typically correlated, even if the variables are observed at different time points and under different experimental conditions. When additionally each observational variable is influenced by a separate set of explanatory variables one might be tempted to perform univariate analyses for each variable separately. Such models of a seemingly unrelated regression (SUR) type have been introduced by Zellner [8] in the context of economic data, who showed that a joint analysis, which accounts for the correlation of the variables, will improve the precision of estimates and tests.

Such models also occur in many scientific fields when problems or phenomena are investigated in pharmacology, toxicology, process engineering etc. at different time points or input variables. For example, when we are interested in the pharmacokinetic measurement of the concentration of two or more drugs or the toxicity with different dissolution times, then the problem can be adequately described by a SUR model.

M. Soumaya (✉)
Institute of Process Engineering, Otto-von-Guericke University, PF 4120, 39 016 Magdeburg, Germany
e-mail: moudar.soumaya@gmail.com

R. Schwabe
Institute for Mathematical Stochastics, Otto-von-Guericke University, PF 4120, 39 016 Magdeburg, Germany
e-mail: rainer.schwabe@ovgu.de

A. Steland et al. (eds.), *Stochastic Models, Statistics and Their Applications*,
Springer Proceedings in Mathematics & Statistics 122,
DOI 10.1007/978-3-319-13881-7_18

To be more specific consider the univariate regression model of concentration of a substance, hormone, drug or of the toxicity with response function $\eta(t) = Ae^{-t\theta}$, where A and θ are the initial concentration and reaction rate (see Atkinson et al. [1]). When we observe two such relations at the same observational units but potentially at different time points, we obtain multivariate data with correlated components and marginal response functions $\eta_1(t_1) = A_1 e^{-t_1\theta_1}$ and $\eta_2(t_2) = A_2 e^{-t_2\theta_2}$, respectively. We will distinguish between two cases, where either the initial concentrations A_1 and A_2 are known or not depending on the experimental situation. Moreover, we assume that the data are appropriately modeled on a logarithmic scale which leads to a linear model formulation for the components $Y_{ij} = \beta_{j1} + \beta_{j2}x_{ij} + \varepsilon_{ij}$ with $\beta_{j1} = \ln A_j$, $\beta_{j2} = \theta_j$ and $x_{ij} = t_{ij}$. If the initial concentrations A_1 and A_2 are known, the marginal models can be reduced to $Y_{ij} = \beta_{j2}x_{ij} + \varepsilon_{ij}$. In any case the SUR structure comes in when we admit that the observations are correlated ($\mathrm{Cov}(Y_{i1}, Y_{i2}) = \mathrm{Cov}(\varepsilon_{i1}, \varepsilon_{i2}) \neq 0$) within the observational units.

While the data analysis has been widely investigated in such models, hardly anything has been done in the design of such experiments. This is partly due to the fact that these models are mainly considered in economic applications, where there are only data available from observational studies, but this is also caused by a widespread opinion that everything is clear about optimal design for multivariate observations. In particular, it seems to be obvious that designs, which are optimal in the univariate settings, will also be optimal in the multivariate case. This is definitely true for MANOVA or multivariate regression settings, where the univariate models depend on the same (values of the) explanatory variables and all univariate models coincide (see e.g. Kurotschka and Schwabe [4]). For various design criteria the corresponding proofs are based on multivariate equivalence theorems by Fedorov [2].

In the situation of SUR models techniques concerning product-type designs have to be employed, which were developed in Schwabe [5]. Soumaya and Schwabe [7] established that in the presence of intercept terms the D-optimal design can be generated as a product of the D-optimal counterparts in the corresponding univariate models for the single components irrespectively of the underlying covariance structure. These results were widely extended to other design criteria by Soumaya [6]. In the absence of intercept terms the product-type design may lose its optimality when the correlation becomes large.

It should be mentioned that against common believe even in the case of identical models for all components the MANOVA-type design, in which the settings of the explanatory variables are the same for all components, turns out to be not optimal, in general, when the observations are correlated.

The paper is organized as follows: In Sect. 18.2 we specify the model, and we characterize optimal designs in Sect. 18.3. In Sect. 18.4 the results are illustrated by means of an example in the bivariate case and some conclusions are drawn in Sect. 18.5.

18.2 Model Specification

In general for the m components the m-dimensional observations are described by m model equations. The components of the multivariate observations can be heterogeneous, which means that the response can be specified by different regression functions and different experimental settings, which may be chosen from different experimental regions.

The observation of the jth component of individual i can be described by

$$Y_{ij} = \mathbf{f}_j(x_{ij})^\top \boldsymbol{\beta}_j + \varepsilon_{ij} = f_{j1}(x_{ij})\beta_{j1} + \cdots + f_{jp_j}(x_{ij})\beta_{jp_j} + \varepsilon_{ij}, \quad (18.1)$$

where $\mathbf{f}_j = (f_{j1}, \ldots, f_{jp_j})^\top$ are known regression functions, $\boldsymbol{\beta}_j = (\beta_{j1}, \ldots, \beta_{jp_j})^\top$ are the unknown parameter vectors and the experimental settings x_{ij} may be chosen from experimental regions $\mathscr{X}_j$.

Denote by $\mathbf{Y}_i = (Y_{i1}, \ldots, Y_{im})^\top$ and $\boldsymbol{\varepsilon}_i = (\varepsilon_{i1}, \ldots, \varepsilon_{im})^\top$ the multivariate vectors of observations and error terms for individual i. The multivariate regression function is block diagonal $\mathbf{f}(\mathbf{x}) = \operatorname{diag}(\mathbf{f}_j(x_j))_{j=1,\ldots,m}$ for the multivariate experimental setting $\mathbf{x} = (x_1, \ldots, x_m) \in \mathscr{X} = \bigtimes_{j=1}^m \mathscr{X}_j$. For the introductory examples the regression functions are

$$\mathbf{f}(\mathbf{x}) = \begin{pmatrix} 1 & x_1 & 0 & 0 \\ 0 & 0 & 1 & x_2 \end{pmatrix}^\top \quad \text{resp.} \quad \mathbf{f}(\mathbf{x}) = \begin{pmatrix} x_1 & 0 \\ 0 & x_2 \end{pmatrix}.$$

The individual observation vector can be written as $\mathbf{Y}_i = \mathbf{f}(\mathbf{x}_i)^\top \boldsymbol{\beta} + \boldsymbol{\varepsilon}_i$, where $\boldsymbol{\beta} = (\boldsymbol{\beta}_1^\top, \ldots, \boldsymbol{\beta}_m^\top)^\top$ is the stacked parameter vector of dimension $p = \sum_{j=1}^m p_j$ for all components. For the error vectors $\boldsymbol{\varepsilon}_i$ it is assumed that they have zero mean and have a common positive definite covariance matrix $\operatorname{Cov}(\boldsymbol{\varepsilon}_i) = \boldsymbol{\Sigma}$ within the observational units, while they are uncorrelated across the observational units.

Finally, denote by $\mathbf{Y} = (\mathbf{Y}_1^\top, \ldots, \mathbf{Y}_n^\top)^\top$ and $\boldsymbol{\varepsilon} = (\boldsymbol{\varepsilon}_1^\top, \ldots, \boldsymbol{\varepsilon}_n^\top)^\top$ the stacked vectors of all observations and all error terms, respectively. Then we can write the overall observation vector as

$$\mathbf{Y} = \mathbf{F}\boldsymbol{\beta} + \varepsilon, \quad (18.2)$$

where $\mathbf{F} = (\mathbf{f}(\mathbf{x}_1), \ldots, \mathbf{f}(\mathbf{x}_n))^\top$ is the overall design matrix. The full observational error vector $\boldsymbol{\varepsilon}$ then has the covariance matrix $\mathbf{V} = \operatorname{Cov}(\boldsymbol{\varepsilon}) = \mathbf{I}_n \otimes \boldsymbol{\Sigma}$, where $\mathbf{I}_n$ is the $n \times n$ identity matrix and "$\otimes$" denotes the Kronecker product.

If we assume that the covariance matrix $\boldsymbol{\Sigma}$ and, hence, $\mathbf{V}$ is known, we can estimate the parameter $\boldsymbol{\beta}$ by the Gauss–Markov estimator $\hat{\boldsymbol{\beta}}_{\mathrm{GM}} = (\mathbf{F}^\top \mathbf{V}^{-1} \mathbf{F})^{-1} \mathbf{F}^\top \mathbf{V}^{-1} \mathbf{Y}$, Its covariance matrix is equal to the inverse of the corresponding information matrix

$$\mathbf{M} = \mathbf{F}^\top \mathbf{V}^{-1} \mathbf{F} = \sum_{i=1}^n \mathbf{f}(\mathbf{x}_i) \boldsymbol{\Sigma}^{-1} \mathbf{f}(\mathbf{x}_i)^\top, \quad (18.3)$$

which is the sum of the individual informations, $\mathbf{M}(\mathbf{x}_i) = \mathbf{f}(\mathbf{x}_i) \boldsymbol{\Sigma}^{-1} \mathbf{f}(\mathbf{x}_i)^\top$.

Note that the univariate marginal models of the components are of the form

$$\mathbf{Y}^{(j)} = \mathbf{F}^{(j)} \boldsymbol{\beta}_j + \boldsymbol{\varepsilon}^{(j)}, \quad (18.4)$$

where $\mathbf{Y}^{(j)} = (Y_{1j}, \ldots, Y_{nj})^\top$ and $\boldsymbol{\varepsilon}^{(j)} = (\varepsilon_{1j}, \ldots, \varepsilon_{nj})^\top$ are the vectors of observations and errors for the jth component, respectively, and $\mathbf{F}^{(j)} = (\mathbf{f}_j(x_{1j}), \ldots, \mathbf{f}_j(x_{nj}))^\top$ is the design matrix for the jth marginal model. The corresponding error terms are uncorrelated and homoscedastic, $\mathrm{Cov}(\boldsymbol{\varepsilon}^{(j)}) = \sigma_j^2 \mathbf{I}_n$, where $\sigma_j^2 = \sigma_{jj}$ is the jth diagonal entry of $\boldsymbol{\Sigma}$.

18.3 Optimal Designs

We can define an experimental design in the multivariate case

$$\xi = \begin{pmatrix} \mathbf{x}_1 & \ldots & \mathbf{x}_k \\ w_1 & \ldots & w_k \end{pmatrix} \tag{18.5}$$

by the set of all different experimental settings $\mathbf{x}_i = (x_{i1}, \ldots, x_{im})$, $i = 1, \ldots, k$, which belong to the design region $\mathscr{X} = \bigtimes_{j=1}^m \mathscr{X}_j$, with the corresponding relative frequencies $w_i = \frac{n_i}{n}$, where n_i is the number of replications at $\mathbf{x}_i$. Then the standardized information matrix for the GM-estimator is $\mathbf{M}(\xi) = \sum_{i=1}^k w_i \mathbf{f}(\mathbf{x}_i) \boldsymbol{\Sigma}^{-1} \mathbf{f}(\mathbf{x}_i)^\top$. For analytical purposes we consider approximate designs, see for example Kiefer [3], for which the weights $w_i \geq 0$ need not be multiples of $\frac{1}{n}$, but only have to satisfy $\sum_{i=1}^k w_i = 1$. As information matrices are not necessarily comparable, we have to consider some real-valued criterion function of the information matrix. In this paper we will adopt the most popular criterion $-\ln\det(\mathbf{M}(\xi))$ of D-optimality and some linear criteria $\mathrm{trace}(\mathbf{L}\mathbf{M}(\xi)^{-1})$ like A- and IMSE-optimality, where $\mathbf{L}$ is a positive definite weight matrix.

An approximate design ξ_D^* is called D-optimal if it minimizes the determinant of the variance covariance matrix, i.e. it minimizes the volume of the confidence ellipsoid under the assumption of Gaussian errors. An approximate design ξ_A^* is called A-optimal if it minimizes the trace $\mathrm{trace}(\mathbf{M}(\xi)^{-1})$ of the variance covariance matrix, i.e. it minimizes the average of the variances of the parameter estimates. Hence, the A-criterion is linear with $\mathbf{L}$ equal to the identity matrix $\mathbf{I}_p$.

The integrated mean squared error is the integrated predictive covariance with respect to the uniform measure $\mu(\mathrm{d}\mathbf{x})$ on the design region $\mathscr{X}$ and is defined as

$$\mathrm{IMSE} = \int_{\mathscr{X}} \mathrm{E}\big(\big\|\mathbf{f}(\mathbf{x})^\top(\hat{\boldsymbol{\beta}} - \boldsymbol{\beta})\big\|^2\big)\mu(\mathrm{d}\mathbf{x}) = \int_{\mathscr{X}} \mathrm{trace}\big(\mathrm{Cov}\big(\mathbf{f}(\mathbf{x})^\top \hat{\boldsymbol{\beta}}\big)\big)\mu(\mathrm{d}\mathbf{x}),$$

where $\|.\|$ denotes the Euclidean norm. Then an approximate design ξ_{IMSE}^* is called IMSE-optimal in the multivariate case, if it minimizes the averaged predictive variance $\mathrm{E}(\|\mathbf{f}(\mathbf{x})^\top(\hat{\boldsymbol{\beta}} - \boldsymbol{\beta})\|^2)$. After rearranging terms the IMSE-criterion is equivalent to a linear criterion with $\mathbf{L} = \int_{\mathscr{X}} \mathbf{f}(\mathbf{x})\mathbf{f}(\mathbf{x})^\top \mu(\mathrm{d}\mathbf{x})$.

Useful tools for checking the optimality of given candidate designs are the following multivariate versions of the equivalence theorems for the above mentioned criteria (see Fedorov [2, Theorems 5.2.1 and 5.3.1]).

Theorem 18.1 *The approximate design ξ_D^* is D-optimal in the multivariate linear model if and only if*

$$\varphi_D\big(\mathbf{x};\xi_D^*\big) := \operatorname{trace}\big(\boldsymbol{\Sigma}^{-1}\mathbf{f}(\mathbf{x})^\top \mathbf{M}\big(\xi_D^*\big)^{-1}\mathbf{f}(\mathbf{x})\big) \le p, \tag{18.6}$$

for all $x \in \mathscr{X}$, *where* $p = \sum_{j=1}^m p_j$ *is the number of parameters in the model.*

Theorem 18.2 *The approximate design* ξ_L^* *is linear optimal in the multivariate linear model if and only if*

$$\varphi_L\big(\mathbf{x};\xi_L^*\big) := \frac{\operatorname{trace}(\boldsymbol{\Sigma}^{-1}\mathbf{f}(\mathbf{x})^\top \mathbf{M}(\xi_L^*)^{-1}\mathbf{L}\mathbf{M}(\xi_L^*)^{-1}\mathbf{f}(\mathbf{x}))}{\operatorname{trace}(\mathbf{L}\mathbf{M}(\xi_L^*)^{-1})} \le 1, \tag{18.7}$$

for all $x \in \mathscr{X}$.

Note that the linear optimality criteria considered here (A and IMSE) result in a block-diagonal weight matrix $\mathbf{L} = \operatorname{diag}(\mathbf{L}_j)_{j=1,\dots,m}$, where the diagonal blocks $\mathbf{L}_j$ are the weight matrices for the corresponding linear criteria in the marginal components: $\mathbf{I}_p = \operatorname{diag}(\mathbf{I}_{p_j})_{j=1,\dots,m}$ for the A-criterion and $\int_{\mathscr{X}} \mathbf{f}(\mathbf{x})\mathbf{f}(\mathbf{x})^\top \mu(\mathrm{d}\mathbf{x}) = \operatorname{diag}(\int_{\mathscr{X}_j} \mathbf{f}(x_j)\mathbf{f}(x_j)^\top \mu_j(\mathrm{d}x_j))_{j=1,\dots,m}$ for the IMSE-criterion, where μ_j is the uniform distribution on $\mathscr{X}_j$.

In the case that all marginal models contain an intercept term the following result has been established by Soumaya [6].

Theorem 18.3 *Let* ξ_j^* *be* Φ*-optimal for the* j*th marginal component* (18.4) *with an intercept on the marginal design region* $\mathscr{X}_j$, *then the product-type design* $\xi^* = \bigotimes_{j=1}^m \xi_j^*$ *is* Φ*-optimal for the multivariate SUR model* (18.2) *on the design region* $\mathscr{X} = \bigtimes_{j=1}^m \mathscr{X}_j$.

Φ *can be either the* D*-criterion or a linear criterion with block-diagonal* $\mathbf{L}$.

For the D*-criterion* φ_D *does not depend on the covariance matrix* $\boldsymbol{\Sigma}$.

This theorem states that the D-, A- or IMSE-optimal designs can be obtained as the product of their corresponding counterparts in the marginal models.

To retain the optimality of product-type designs also in the case that all or some of the marginal models are lacking an intercept term additional orthogonality conditions have to be imposed similarly to results for additive models (see Schwabe [5, Sect. 5.2]).

Theorem 18.4 *Let* ξ_j^* *be* Φ*-optimal for the* j*th marginal component* (18.4) *without intercept on the marginal design region* $\mathscr{X}_j$. *If the marginal components are uncorrelated* ($\boldsymbol{\Sigma} = \operatorname{diag}(\sigma_j^2)_{j=1,\dots,m}$) *or the regression functions are orthogonal to a constant with respect to the* Φ*-optimal designs* ξ_j^*, *i.e.* $\int_{\mathscr{X}_j} \mathbf{f}_j(x_j)\xi_j^*(\mathrm{d}x_j) = \mathbf{0}$, *then the product-type design* $\xi^* = \bigotimes_{j=1}^m \xi_j^*$ *is* Φ*-optimal for the multivariate SUR model* (18.2) *on the design region* $\mathscr{X} = \bigtimes_{j=1}^m \mathscr{X}_j$.

Φ *can be either the* D*-criterion or a linear criterion with block-diagonal* $\mathbf{L}$.

For the D*-criterion* φ_D *does not depend on the covariance matrix* $\boldsymbol{\Sigma}$.

The conditions of the above theorem guarantee that the information matrix of the product-type design ξ^* is block-diagonal such that the considered criteria as well as the associated sensitivity functions decompose.

If these conditions are violated, the overall optimality of the product-type designs can fail. The sensitivity function may depend crucially on the correlation. While for small correlations the product-type designs may be still optimal, they will lose their optimality for stronger correlations. In particular, we will exhibit by an example that the product-type designs are D-optimal for SUR models without intercepts for a restricted range of correlations around 0. For large correlations the D-optimal designs have weights related to the size of the correlation. In the present example the optimal weights tend to those for an additive model without intercept as considered in Schwabe [5, Sect. 5.2].

For linear criteria the situation is even worse, as the optimal weights also depend on the ratio of the variances for the single components. If the variances differ by a large factor, the product-type design may not be optimal even for very small correlation.

18.4 Example

To illustrate the behavior for SUR models without intercepts in the marginal models we consider the introductory example $Y_{ij} = \beta_{j2} x_{ij} + \varepsilon_{ij}$ of linear regression on the unit intervals $\mathscr{X}_j = [0, 1]$ as experimental regions. Then a setting $x_{ij} = 0$ results in a measurement at baseline for the jth component.

It is well-known that in the marginal models the optimal designs are all concentrated on the setting $x_j^* = 1$ with maximal response. The resulting product-type design $\xi_\otimes = \xi_1^* \otimes \xi_2^*$ is also a one-point design concentrated on $\mathbf{x}^* = (1, 1)$. The information matrix for a one-point design $\xi_{\mathbf{x}}$, i.e. a single observation at $\mathbf{x} = (x_1, x_2)$, equals

$$\mathbf{M}(\xi_{\mathbf{x}}) = \mathbf{M}(x_1, x_2) = \frac{1}{1-\rho^2} \begin{pmatrix} x_1/\sigma_1^2 & -\rho x_1 x_2/\sigma_1\sigma_2 \\ -\rho x_1 x_2/\sigma_1\sigma_2 & x_2/\sigma_2^2 \end{pmatrix},$$

where ρ is the correlation. In particular, $\mathbf{M}(\xi_\otimes) = \boldsymbol{\Sigma}^{-1}$ for the product-type design $\xi_\otimes$ with optimal marginals. In this model the weight matrix $\mathbf{L}$ for the IMSE-criterion equals $\frac{1}{3}\mathbf{I}_2$. Hence, A- and IMSE-optimality coincide. For the uncorrelated case ($\rho = 0$) the product-type design $\xi_\otimes$ is D-, A- and IMSE-optimal by Theorem 18.4.

In general, for the D-criterion the sensitivity function φ_D of the product-type design $\xi_\otimes$ equals

$$\varphi_D(\mathbf{x}; \xi_\otimes) = \frac{1}{1-\rho^2}\left(x_1^2 + x_2^2 - 2\rho^2 x_1 x_2\right), \tag{18.8}$$

which is bounded by $p = 2$ as long as $|\rho| \le 1/\sqrt{2} \approx 0.7071$. This sensitivity function is plotted in Figs. 18.1 and 18.2 for the values $\rho = 0$ and $\rho = 1/\sqrt{2}$, respectively. Note that in the last case the sensitivity function equals $p = 2$ at the support

Fig. 18.1 $\varphi_D(\xi_\otimes)$, $\rho = 0$

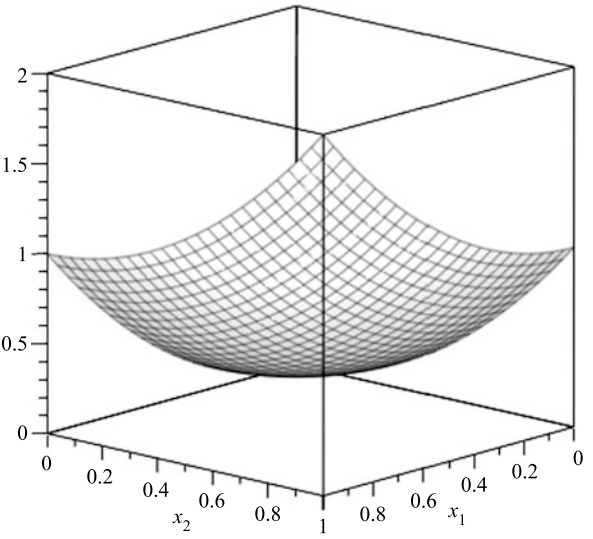

Fig. 18.2 $\varphi_D(\xi_D^*)$, $\rho \geq 1/\sqrt{2}$

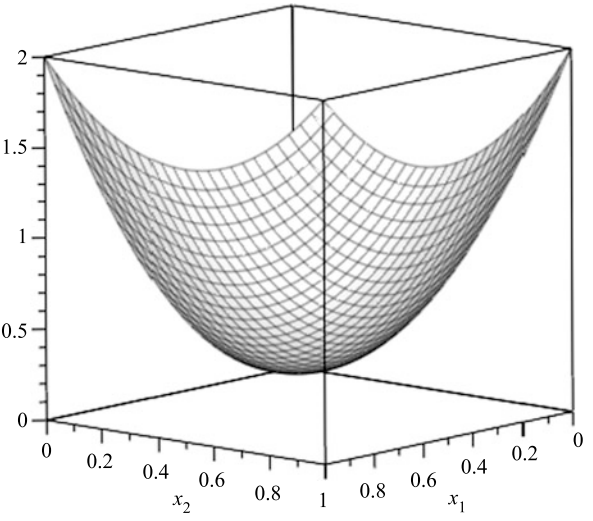

point $\mathbf{x}^* = (1, 1)$ and additionally at the settings $(0, 1)$ and $(1, 0)$, where one of the components is observed at baseline.

For larger values of the correlation, $|\rho| > 1/\sqrt{2}$, the D-optimal design ξ^* also contains these additional points with weights increasing in $|\rho|$,

$$\xi_D^* = \begin{pmatrix} (1,1) & (1,0) & (0,1) \\ 1-2w^* & w^* & w^* \end{pmatrix} \quad \text{with } w^* = \frac{2\rho^2 - 1}{4\rho^2 - 1}$$

The sensitivity function $\varphi_D(\mathbf{x}; \xi_D^*) = 2(x_1^2 + x_2^2 - x_1 x_2)$ is bounded by $p = 2$. This sensitivity function coincides with φ_D for $\xi_\otimes$ in the boundary case $\rho = 1/\sqrt{2}$.

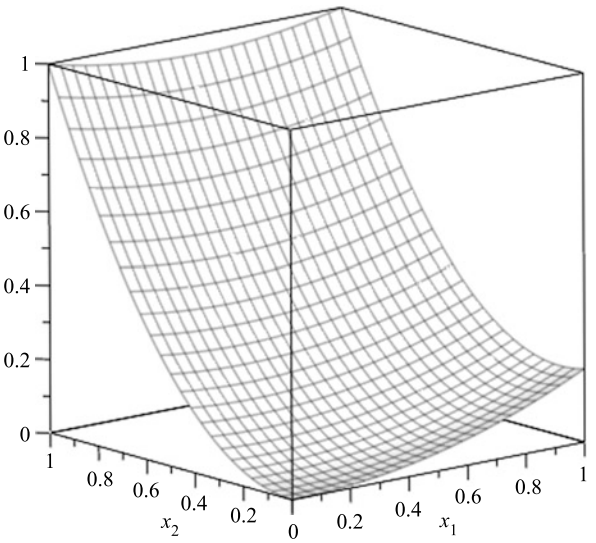

Fig. 18.3 $\varphi_A(\xi_\otimes)$, $\tau = 3$, $\rho = 0.3$

For the linear criteria the standardized sensitivity function $\varphi_A = \varphi_{\text{IMSE}}$ for the product-type design $\xi_\otimes$ is

$$\varphi_A(\mathbf{x}; \xi_\otimes) = \frac{(1+\rho^2)x_1^2 + \tau^2(1+\rho^2)x_2^2 - 2(1+\tau^2)\rho^2 x_1 x_2}{(1+\tau^2)(1-\rho^2)}, \qquad (18.9)$$

where $\tau^2 = \sigma_2^2/\sigma_1^2$ is the variance ratio.

For $\rho = 0.3$ and $\tau = 3$ the sensitivity function φ_A is plotted in Fig. 18.3. In this case the product-type design $\xi_\otimes$ appear to be optimal.

For $\sigma_1 = 0.1$, $\sigma_2 = 10$ and $\tau^2 = 10000$ the maximum of the sensitivity function φ_A is attained at $\mathbf{x} = (0, 1)$ and exceeds 1 even for ρ close to 0. Therefor the product-type designs cannot be A-optimal for extremely different variances.

Numerical calculations indicate that for every variance ratio τ^2 there is an interval for the correlations ρ centered at 0, for which the product-type design $\xi_\otimes$ is A-optimal, while it loses its optimality for larger values of $|\rho|$. If τ^2 increases, these intervals may become arbitrarily small. Note that for symmetry reasons the same intervals are valid for τ^2 replaced by $1/\tau^2$.

For equal variances ($\tau^2 = 1$) the product-type design $\xi_\otimes$ is A-optimal as long as $|\rho| \le 1/\sqrt{3}$, while for stronger correlations, $|\rho| > 1/\sqrt{3}$, the A-optimal design is

$$\xi_A^* = \begin{pmatrix} (1,1) & (1,0) & (0,1) \\ 1-2w^* & w^* & w^* \end{pmatrix} \quad \text{with } w^* = 1 - \sqrt{\rho^2/(4\rho^2-1)}.$$

For $\rho = 1/\sqrt{3}$ the standardized sensitivity function $\varphi_A(\mathbf{x}; \xi_A^*) = x_1^2 + x_2^2 - x_1 x_2$ is plotted in Fig. 18.4.

Fig. 18.4 $\varphi_A(\xi_A^*)$, $\tau = 1$

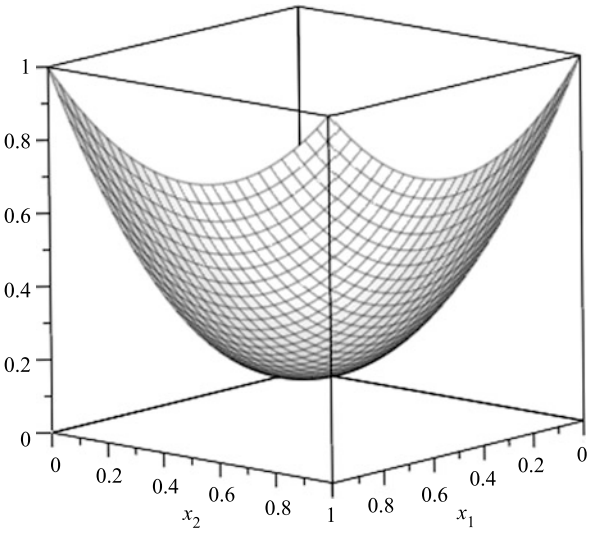

18.5 Conclusions

In the presence of intercept terms the variance covariance structure does not affect the optimality of product-type designs, which are generated by the corresponding optimal counterparts. But their optimality reaches its limits for SUR models without intercepts, when the information matrix is not block-diagonal. Then product-type designs are optimal only for weak to moderate correlation. For stronger correlation the optimal designs depend on the size of the correlation and eventually on the variance ratio. These results may be extended to higher dimensions, when a homogeneous correlation structure is assumed.

References

1. Atkinson AC, Donev AN, Tobias RD (2007) Optimum experimental design, with SAS. Oxford University Press, Oxford
2. Fedorov VV (1972) Theory of optimal experiments. Academic Press, New York
3. Kiefer J (1974) General equivalence theory for optimum designs (approximate theory). Ann Appl Stat 2:849–879
4. Kurotschka VG, Schwabe R (1996) The reduction of design problems for multivariate experiments to univariate possibilities and their limitations. In: Brunner E, Denker M (eds) Research developments in probability and statistics. VSP, Utrecht, pp 193–204
5. Schwabe R (1996) Optimum designs for multi-factor models. Springer, New York
6. Soumaya M (2013) Optimal designs for multivariate linear models. Dissertation, Otto-von-Guericke University Magdeburg, Faculty of Mathematics
7. Soumaya M, Schwabe R (2011) *D*-optimal design for a seemingly unrelated linear model. In: Melas V, Nachtmann G, Rasch D (eds) Optimal design of experiments – theory and application. University of Natural Resources and Life Sciences, Vienna, pp 170–174.
8. Zellner A (1962) An efficient method of estimating seemingly unrelated regression equations and tests for aggregation bias. J Am Stat Assoc 57:348–368

Chapter 19
On the Time-Reversibility of Integer-Valued Autoregressive Processes of General Order

Sebastian Schweer

Abstract Integer-valued autoregressive processes of a general order $p \geq 1$ (INAR(p) processes) are considered, and the focus is put on the time-reversibility of these processes. It is shown that for the case $p = 1$ the time-reversibility of such a process already implies that the innovations are Poisson distributed. For the case of a general $p \geq 2$, two competing formulations for the INAR(p) process of Alzaid and Al-Osh (in J. Appl. Prob. 27(2):314–324, 1990) and Du and Li (in J. Time Ser. Anal. 12(2):129–142, 1991) are considered. While the INAR(p) process as defined by Alzaid and Al-Osh behaves analogously to the INAR(1) process, the INAR(p) process of Du and Li is shown to be time-irreversible in general.

19.1 Introduction

In recent years, the study of count data time series has gained a significant amount of attention. One of the most popular models for such time series is the integer-valued autoregressive model (or INAR model), introduced in [1] and [5]. Especially the INAR(1) model has been studied intensively in the literature, and it has been applied in a wide range of varying applications. For instance, the model was used to analyze the monthly number of workers in the heavy manufacturing industry collecting benefits due to a burn related injury (see [7]).

The INAR(1) model can be seen as an integer-valued analogy to the continuous AR(1) model, and it is therefore not surprising that the modeling of higher order autoregressive structures has been considered in the literature. However, the two most prominent attempts defining an INAR(p) process, given by [2] and [4], differ substantially so that there exists no canonical extension of the INAR(1) process. Both definitions have their advantages and disadvantages, yet the autocorrelation function of the INAR(p) process as defined in [2] behaves like that of an ARMA(p, $p-1$) process, which is an obvious drawback for modeling purposes.

S. Schweer (✉)
Institute of Applied Mathematics, University of Heidelberg, Im Neuenheimer Feld 294, 69120 Heidelberg, Germany
e-mail: schweer@uni-heidelberg.de

A. Steland et al. (eds.), *Stochastic Models, Statistics and Their Applications*,
Springer Proceedings in Mathematics & Statistics 122,
DOI 10.1007/978-3-319-13881-7_19

The INAR(p) process as defined in [4] on the other hand has the same correlation structure as that of the continuous AR(p) model.

A notable characteristic of the continuous AR(p) process is that it is time-reversible if and only if the error distribution is Gaussian, cf. [12], Theorem 2. For INAR(1) processes, the Poisson distribution takes on a similar role as that of the Gaussian distribution in the continuous AR(1) process, i.e. if the innovation distribution is Poisson, then the stationary distribution is Poisson; it is the only infinitely divisible distribution to have this property, cf. Theorem 3.2.1 in [7]. Further, in [10] it was shown that if the innovations are Poisson distributed, then the process is time-reversible. For a detailed discussion concerning the time-reversibility of integer-valued ARMA processes the reader is referred to [6] and [8], the latter of which considered time-reversibility for the special case of Compound Poisson INAR(1) processes.

This paper is organized as follows. In Sect. 19.2, the INAR(1) model is introduced and it is shown that these processes are time-reversible if and only if the innovations' distribution is Poisson. An analogous result is shown in the next section for the INAR(p) processes as defined in [2], whereas in Sect. 19.4 the proof is provided that the INAR(p) processes in the formulation of Du and Li in [4] are only time-reversible in trivial cases.

Concerning notation, denote $\mathbb{N} = \{1, 2, 3, \ldots\}$ and $\mathbb{N}_0 = \{0, 1, 2, 3, \ldots\}$, the latter coincides with the state space of all processes considered in this article. For a parameter $p \in [0, 1]$, define $\overline{p} := 1 - p$. Often, sequences of states for a given stationary stochastic process $(Y_t)_{t\in\mathbb{Z}}$ will be considered and will be written in a shorthand notation; the event $\{Y_t = a_0, Y_{t+1} = a_1, Y_{t+2} = a_2 \ldots Y_{t+r} = a_r\}$ is written $\overline{a_0, a_1, a_2, \ldots, a_r}$ for any $r \in \mathbb{N}$. For any stationary process $(Y_t)_{t\in\mathbb{Z}}$, denote the transition probabilities of the process for sequences by $p_Y(a_r|a_{r-1}, \ldots, a_1) := \mathbb{P}(\overline{a_0, a_1, a_2, \ldots, a_r})/\mathbb{P}(\overline{a_0, a_1, a_2, \ldots, a_{r-1}})$. Consequently, the stationary distribution of the process $(Y_t)_{t\in\mathbb{Z}}$ is given by $p_Y(\cdot)$, i.e. $p_Y(a) = \mathbb{P}(Y_t = a)$ for $a \in \mathbb{N}_0$. Notice the suppressed time index t as the processes considered in this article are generally stationary.

19.2 Time-Reversibility for the INAR(1) Model

In order to introduce the INAR(1) model it is necessary to first define *binomial thinning*: If X is a discrete random variable with range $\mathbb{N}_0 = \{0, 1, \ldots\}$ and if $\alpha \in (0; 1)$, then the random variable $\alpha \circ X := \sum_{i=1}^{X} Z_i$ is said to arise from X by binomial thinning, and the Z_i's are referred to as the *counting series*. They are independent and identically distributed (i.i.d.) binary random variables with $\mathbb{P}(Z_i = 1) = \alpha$, which are also independent of X. The operator "$\circ$" was first introduced in [9] and allows for the following definition of the INAR(1) model:

Definition 19.1 Let $(\varepsilon_t)_{t\in\mathbb{Z}}$ be an i.i.d. process with range $\mathbb{N}_0 = \{0, 1, \ldots\}$, denote $\mathbb{E}[\varepsilon_0] = \mu_\varepsilon$, $\mathrm{Var}[\varepsilon_0] = \sigma_\varepsilon^2$. Let $\alpha \in (0; 1)$. A process $(Y_t)_{t\in\mathbb{Z}}$ following the recursion

$$Y_t = \alpha \circ Y_{t-1} + \varepsilon_t$$

for all $t \in \mathbb{Z}$ is said to be an *INAR(1) process* if all thinning operations are performed independently of each other and of $(\varepsilon_t)_{t\in\mathbb{Z}}$, and if the thinning operations at each time t as well as ε_t are independent of $(Y_s)_{s<t}$.

For an INAR(1) process $(Y_t)_{t\in\mathbb{Z}}$ the transition probabilities are given by

$$p_Y(a|b) = \sum_{l=0}^{\min(a,b)} \mathbb{P}(\varepsilon_0 = a - l)\binom{b}{l}\overline{\alpha}^{b-l}\alpha^l \quad \text{for } a, b \in \mathbb{N}_0. \tag{19.1}$$

The following result has been shown to hold in the special case of Compound Poisson INAR(1) processes in [8]. Here, a different proof is presented which holds for general INAR(1) processes.

Theorem 19.1 *Let $(Y_t)_{t\in\mathbb{Z}}$ be a stationary INAR(1) process and let $\mathbb{P}(\varepsilon_0 = 0) \in (0, 1)$. Then $(Y_t)_{t\in\mathbb{Z}}$ is time-reversible if and only if $\varepsilon_0 \sim \text{Poi}(\lambda)$ for some $\lambda > 0$.*

Proof For the necessity of the statement see [10], who showed this result by verifying the detailed balance equations $p_Y(i)p_Y(j|i) = p_Y(j)p_Y(i|j)$.

Now, let $(Y_t)_{t\in\mathbb{Z}}$ be time reversible. Then $\mathbb{P}(\overline{0, 1, i, 0}) = \mathbb{P}(\overline{0, i, 1, 0})$ holds for all $i \in \mathbb{N}_0$. By the Markov property this yields $p_Y(1|0)p_Y(i|1)p_Y(0|i)p_Y(0) = p_Y(i|0)p_Y(1|i)p_Y(0|1)p_Y(0)$. Now, $p_Y(0) > 0$ follows by elementary properties of stationary Markov chains and $\overline{\alpha} > 0$ by definition, thus, with (19.1), this is equivalent to

$$\mathbb{P}(\varepsilon_0 = 1)\mathbb{P}(\varepsilon_0 = i - 1) = i\mathbb{P}(\varepsilon_0 = i)\mathbb{P}(\varepsilon_0 = 0) \quad \text{for } i > 0. \tag{19.2}$$

Summation over i on both sides leads to $\mathbb{P}(\varepsilon_0 = 1) = \mu_\varepsilon \mathbb{P}(\varepsilon_0 = 0)$. Since $0 < \mathbb{P}(\varepsilon_0 = 0) < 1$ it holds that $\mu_\varepsilon > 0$ and therefore that $\mathbb{P}(\varepsilon_0 = 1) > 0$. Applying (19.2) recursively,

$$\mathbb{P}(\varepsilon_0 = i) = \frac{1}{i}\mu_\varepsilon \mathbb{P}(\varepsilon_0 = i - 1) = \cdots = \frac{1}{i!}\mu_\varepsilon^i \mathbb{P}(\varepsilon_0 = 0).$$

Normalization yields $\mathbb{P}(\varepsilon_0 = 0)^{-1} = \sum_{l=0}^{\infty} \frac{1}{l!}\mu_\varepsilon^l$, concluding the proof. □

19.3 Time-Reversibility for the INAR(p) Model of Al-Osh and Alzaid

In this section and the following one, higher order autoregressive structures are considered, starting with the INAR(p) process formulation given by [2].

Definition 19.2 Let $(\varepsilon_t)_{t\in\mathbb{Z}}$ be an i.i.d. process with range $\mathbb{N}_0 = \{0, 1 \ldots\}$, denote $\mathbb{E}[\varepsilon_0] = \mu_\varepsilon$, $\text{Var}(\varepsilon_0) = \sigma_\varepsilon^2$. Let $p \in \mathbb{N}, \alpha_1, \ldots, \alpha_p \in [0, 1)$ with $\sum_{i=1}^p \alpha_i < 1$. A process $(Y_t)_{t\in\mathbb{Z}}$, which follows the recursion

$$Y_t = \sum_{i=1}^{p} \alpha_i \circ Y_{t-i} + \varepsilon_t \tag{19.3}$$

for all $t \in \mathbb{Z}$ is said to be an *INAR(p) process* in Al-Osh's and Alzaid's formulation, or *AAINAR(p) process*, if the conditional distribution of the vector $(\alpha_1 \circ Y_t, \alpha_2 \circ Y_t, \ldots, \alpha_p \circ Y_t)$ given $Y_t = y_t$ is multinomial with parameters $(\alpha_1, \alpha_2, \ldots, \alpha_p, y_t)$ and if, given $Y_t = y_t$, the random variables $a_i \circ Y_t$ and ε_t are independent of Y_{t-k} and its survivals (and the thinning operations) $a_j \circ Y_{t-k}$ for $i, j = 1, 2, \ldots, p$ and $k > 0$.

In Sect. 5.2 of [2], the time-reversibility of the AAINAR(2) process with Poisson innovations is shown and it is indicated how this result may be established in higher-order autoregressive structures. In the next Theorem it is shown that the approach of Theorem 19.1 can be extended to AAINAR(p) process of a general order.

Theorem 19.2 *Let $(Y_t)_{t\in\mathbb{Z}}$ be a time-reversible AAINAR(p) process with $p > 1$ and let $\mathbb{P}(\varepsilon_0 = 0) \in (0, 1)$. Then $(Y_t)_{t\in\mathbb{Z}}$ is time-reversible if and only if $\varepsilon_0 \sim \text{Poi}(\lambda)$ for some $\lambda > 0$.*

Proof Sufficiency of the assertion remains to be shown. First, let $p = 2$, and define the vector-valued process $\mathbf{Y}_t := (Y_t, \alpha_2 \circ Y_{t-1})$. As shown in Section 4 of [2], this process is Markovian. Denote the transition probabilities of this process by $\mathbb{P}(\mathbf{Y}_t = (a_1, a_2)|\mathbf{Y}_{t-1} = (b_1, b_2)) := p_{\mathbf{Y}}((a_1, a_2)|(b_1, b_2))$ for $a_1, a_2, b_1, b_2 \in \mathbb{N}_0$. Now, the event $\{Y_t = 0\}$ implies that $\{\alpha_j \circ Y_t = 0\}$ for $j = 1, 2$ and any $t \in \mathbb{Z}$ by the definition of the thinning operation. Further, $\{Y_t = 0\}$ implies that $\{\alpha_2 \circ Y_{t-2} = 0\}$ for any $t \in \mathbb{Z}$, since by Definition 19.2, $Y_t = \alpha_1 \circ Y_{t-1} + \alpha_2 \circ Y_{t-2} + \varepsilon_t$ and all random variables are assumed to be nonnegative. Therefore, for any $i \in \mathbb{N}_0$,

$$\begin{aligned}
&\mathbb{P}\big(\{Y_{-1} = 0, Y_0 = 0, Y_1 = 1, Y_2 = i, Y_3 = 0, Y_4 = 0,\\
&\qquad \alpha_2 \circ Y_t = 0 | t = -2, -1, \ldots, 3\}\big)\\
&= \mathbb{P}(Y_{-1} = 0, Y_0 = 0, Y_1 = 1, Y_2 = i, Y_3 = 0, Y_4 = 0)
\end{aligned}$$

Using the time-reversibility of $(Y_t)_{t\in\mathbb{Z}}$ and the Markovian structure of $(\mathbf{Y}_t)_{t\in\mathbb{Z}}$, the argumentation above implies for every $i \in \mathbb{N}_0$ that

$$\begin{aligned}
&\mathbb{P}\big(\mathbf{Y}_{-1} = (0,0), \mathbf{Y}_0 = (0,0), \mathbf{Y}_1 = (1,0), \mathbf{Y}_2 = (i,0), \mathbf{Y}_3 = (0,0), \mathbf{Y}_4 = (0,0)\big)\\
&= \mathbb{P}\big(\mathbf{Y}_{-1} = (0,0), \mathbf{Y}_0 = (0,0), \mathbf{Y}_1 = (i,0), \mathbf{Y}_2 = (1,0), \mathbf{Y}_3 = (0,0),\\
&\qquad \mathbf{Y}_4 = (0,0)\big).
\end{aligned} \tag{19.4}$$

Further, by Definition 19.2, it holds that

$$p_{\mathbf{Y}}\big((a,0)|(b,0)\big) = \sum_{l=0}^{\min(a,b)} \mathbb{P}(\varepsilon_0 = a - l) \frac{b!}{l!(b-l)!} \overline{\alpha_1 + \alpha_2}^{b-l} \alpha_1^l \quad \text{for } a, b \in \mathbb{N}_0,$$

implying $p_{\mathbf{Y}}((0,0)|(0,0)) > 0$. Following the argumentation of [2], the process $(\mathbf{Y}_t)_{t\in\mathbb{Z}}$ is a stationary Markov process on the state space $\mathbb{N}_0^2$, under the assumption $\mathbb{P}(\varepsilon_0 = 0) > 0$ it follows that it is both irreducible and aperiodic. Hence, each state $(a, b) \in \mathbb{N}_0$ is positive recurrent and, in particular, $p_{\mathbf{Y}}((0,0)) > 0$.

This argumentation shows that (19.4) is equivalent to

$$\begin{aligned}&\mathbb{P}(\varepsilon_0 = 1)\big[\mathbb{P}(\varepsilon_0 = i)\overline{\alpha_1+\alpha_2} + \mathbb{P}(\varepsilon_0 = i-1)\alpha_1\big]\mathbb{P}(\varepsilon_0 = 0)\overline{\alpha_1+\alpha_2}^{\,i}\\ &\quad = \mathbb{P}(\varepsilon_0 = i)\big[\mathbb{P}(\varepsilon_0 = 1)\overline{\alpha_1+\alpha_2}^{\,i} + \mathbb{P}(\varepsilon_0 = 0)i\overline{\alpha_1+\alpha_2}^{\,i-1}\alpha_1\big]\overline{\alpha_1+\alpha_2}\mathbb{P}(\varepsilon_0 = 0).\end{aligned}$$

This last expression is easily seen to be equivalent to (19.2), as $\overline{\alpha_1+\alpha_2} > 0$. Thus, the argumentation of Theorem 19.1 holds again, proving the assertion for $p = 2$.

Now, let $p > 2$. Replace the process $(\mathbf{Y}_t)_{t\in\mathbb{Z}}$ with the process (see Sect. 4 in [2])

$$\mathbf{Y}_t^* = \left(Y_t, \sum_{i=2}^{p}\alpha_i Y_{t+1-i}, \sum_{i=3}^{p} Y_{t+2-i}, \ldots, \alpha_p \circ Y_{t-1}\right).$$

For the sequence of events $\mathbf{Y}_{-p+1}^* = (0,0,\ldots,0) = \mathbf{Y}_{-p+2}^* = \cdots = \mathbf{Y}_0^*$, $\mathbf{Y}_3^* = (0,0,\ldots,0) = \mathbf{Y}_4^* = \cdots = \mathbf{Y}_{p+2}^*$ and $\mathbf{Y}_1^* = (1,0,\ldots,0)$ as well as $\mathbf{Y}_2^* = (i,0,\ldots,0)$, a short moment of reflection should convince the reader that an extension of (19.4) holds. Similar to the argumentation above, this relation can be shown to be equivalent to (19.2), concluding the proof. □

19.4 Time-Irreversibility for the INAR(p) Model of Du and Li

In this section a competing formulation for an INAR(p) process given in [4] is considered.

Definition 19.3 Let $(\varepsilon_t)_{t\in\mathbb{Z}}$ be an i.i.d. process with range $\mathbb{N}_0 = \{0, 1\ldots\}$, denote $\mathbb{E}[\varepsilon_0] = \mu_\varepsilon$, $\mathrm{Var}(\varepsilon_0) = \sigma_\varepsilon^2$. Let $p \in \mathbb{N}$, $\alpha_1, \ldots, \alpha_p \in [0, 1)$ with $\sum_{i=1}^{p}\alpha_i < 1$. A process $(Y_t)_{t\in\mathbb{Z}}$, which follows the recursion (19.3) for all $t \in \mathbb{Z}$ is said to be an INAR(p) *process* as defined by Du and Li, or DLINAR(p) *process*, if all thinning operations are mutually independent and if the $(\varepsilon_t)_{t\in\mathbb{Z}}$ are independent of all thinning operations and the random variable ε_t is independent of Y_{t-k} and its survivals (and the thinning operations) $a_j \circ Y_{t-k}$ for $j = 1, 2, \ldots, p$ and $k > 0$.

For the transition probabilities, this definition implies (cf. [3], (2))

$$p_Y(a|b_1,\ldots,b_p) = \sum \mathbb{P}\Big(\varepsilon_0 = a - \sum l_i\Big)\binom{b_1}{l_1}\alpha_1^{l_1}\overline{\alpha_1}^{b_1-l_1}\cdots\binom{b_p}{l_p}\alpha_p^{l_p}\overline{\alpha_p}^{b_p-l_p} \tag{19.5}$$

for $a, b_i \in \mathbb{N}_0$, where sum extends over all l_i's satisfying the restrictions $l_k \le b_k$ for all $k = 1, \ldots, p$ and $\sum l_k \le a$. Thus, in contrast to the AAINAR(p) process of Definition 19.2, the DLINAR(p) process is a pth order Markov chain. This allows us to show the following analogue of Theorem 19.2.

Lemma 19.1 *Let $(Y_t)_{t\in\mathbb{Z}}$ be a time-reversible DLINAR(p) process with $p > 1$ and let $\mathbb{P}(\varepsilon_0 = 0) \in (0, 1)$. Then there exists a $\lambda > 0$ such that $\varepsilon_0 \sim \text{Poi}(\lambda)$.*

Proof First, let $p = 2$. By the time-reversibility of the process $(Y_t)_{t\in\mathbb{Z}}$, it follows that for any $i \in \mathbb{N}_0$, $\mathbb{P}(\overline{0, 0, 1, i, 0, 0}) = \mathbb{P}(\overline{0, 0, i, 1, 0, 0})$. Due to the Markovian structure of $(Y_t)_{t\in\mathbb{Z}}$ and the fact that $p_Y(0) > 0$ as well as $p_Y(0|0) > 0$ (which is deduced analogously to the argumentation in Theorem 19.2), this is equivalent to

$$\begin{aligned} &p_Y(0|0, i)\, p_Y(0|i, 1)\, p_Y(i|1, 0)\, p_Y(1|0, 0) \\ &\quad = p_Y(0|0, 1)\, p_Y(0|1, i)\, p_Y(1|i, 0)\, p_Y(i|0, 0). \end{aligned}$$

Using (19.5) and simple manipulations, this is equivalent to (19.2) as $\overline{\alpha_2} > 0$ by Definition 19.3. For a general $p > 2$, consideration of the sequence $\overline{0, 0, \ldots, 0, 1, i, 0, \ldots, 0}$ and its inverse where the dots represent p zeroes, yields an equivalent relation as above, as $\overline{\alpha_k} > 0$ holds for all $k = 3, \ldots, p$. The assertion follows analogously to Theorem 19.1. □

At first glance, since the result of Lemma 19.1 is exactly analogous to that of Theorem 19.2 there doesn't seem to be a difference in the characteristics of DLINAR(p) processes and AAINAR(p) processes with respect to time-reversibility. However, the following result shows that a DLINAR(p) process is time-reversible only if the parameters take on degenerate values, i.e. if it is in fact an INAR(1) process.

Theorem 19.3 *Let $(Y_t)_{t\in\mathbb{Z}}$ be a time-reversible DLINAR(p) process with $p > 1$ and $\alpha_1 > 0$ and let $0 < \mathbb{P}(\varepsilon = 0) < 1$. Then $\alpha_j = 0$ for $j = 2, \ldots, p$.*

Proof Let $p = 2$. Since $(Y_t)_{t\in\mathbb{Z}}$ is time-reversible, the transition probabilities necessarily satisfy $\mathbb{P}(\overline{0, 0, 1, 3, 2, 0, 0}) = \mathbb{P}(\overline{0, 0, 2, 3, 1, 0, 0})$. By (19.5) and the fact that $p_Y(0|0)$, $p_Y(0) > 0$, this is equivalent to

$$\begin{aligned} &\overline{\alpha_2}^5\overline{\alpha_1}^2\lambda\Bigg[\sum_{\substack{l_1\le 3, l_2\le 1\\ l_1+l_2\le 2}} \frac{\lambda^{2-l_1-l_2}}{(2-l_1-l_2)!}\binom{3}{l_1}\alpha_1^{l_1}\overline{\alpha_1}^{3-l_1}\alpha_2^{l_2}\overline{\alpha_1}^{1-l_2}\Bigg]\left(\frac{\lambda^3}{6}\overline{\alpha_1} + \frac{\lambda^2}{2}\alpha_1\right) \\ &\quad = \overline{\alpha_2}^4\overline{\alpha_1}\frac{\lambda^2}{2}\left[\lambda\overline{\alpha_1}^3\overline{\alpha_2}^2 + 2\overline{\alpha_1}^3\overline{\alpha_2}\alpha_2 + 3\overline{\alpha_1}^2\alpha_1\overline{\alpha_2}^2\right]\left(\frac{\lambda^3}{6}\overline{\alpha_1}^2 + \lambda^2\overline{\alpha_1}\alpha_1 + \lambda\alpha_1^2\right). \end{aligned} \tag{19.6}$$

This, in turn (recall that $\lambda > 0$ and $\overline{\alpha_1}, \overline{\alpha_2} > 0$ by Definition 19.3), is equivalent to $\frac{1}{2}\overline{\alpha_1}\alpha_1^2\alpha_2 = 0$. Since $\overline{\alpha_1} > 0$, this implies the assertion for $p = 2$.

Now, let $p > 2$ be arbitrary but fixed. It remains to be seen that $\alpha_j = 0$ for $j = 2, \ldots, p$ which is done by first showing that $\alpha_2 = 0$ and then proceeding inductively. An appeal to (19.5) reveals that the relations considered in the first part of this proof hold similarly for the sequence $\overline{0, 0, \ldots, 0, 1, 3, 2, 0, \ldots, 0}$ and its inverse, here the first and last p entries are 0. Since there are at most three consecutive non-null states in these sequences, the relation of the transition probabilities is equivalent to that of (19.6) save for the factors of the form $e^{-k\lambda}$ for some k, $p_Y(0|0, 0)$, $p_Y(0|0, 0, 0)$

and so forth and $\prod_{i=3}^{p} \overline{\alpha_i}^6$. By (19.5), $p_Y(0|0,0)$, $p_Y(0|0,0,0)$ etc. are all larger than zero, and $\overline{\alpha_i}, e^{-\lambda} > 0$ by definition. Thus, time-reversibility of the process and $\alpha_1 > 0$ implies $\alpha_2 = 0$.

Now, let $2 < k \leq p$, and let $\alpha_i = 0$ for $1 < i < k$, it is shown that this implies $\alpha_k = 0$. Consider the sequence of states

$$\overline{\underbrace{0,0,\ldots,0}_{p \text{ times}},1,3,\underbrace{0,\ldots,0}_{k-2 \text{ times}},2,\underbrace{0,\ldots,0,0}_{p \text{ times}}}$$

and its inverse. For a time-reversible process, the transition probabilities for this sequence has to equal the transition probability of its inverse. With (19.5) and recalling that $\overline{\alpha_i}, e^{-\lambda}, p_Y(0|0,0), p_Y(0|0,0,0)$ etc. are all larger than zero, this relation is equivalent to

$$\begin{aligned}&\overline{\alpha_1}^3\overline{\alpha_k}^4\left(\lambda\overline{\alpha_1}^3\overline{\alpha_k}^2 + 3\alpha_1\overline{\alpha_1}^2\overline{\alpha_k}^2 + 2\overline{\alpha_1}^3\alpha_k\overline{\alpha_k}\right)\frac{\lambda^5}{12}\\ &= \overline{\alpha_1}^5\overline{\alpha_k}^5\left(\frac{\lambda^2}{2}\overline{\alpha_k} + \lambda\alpha_k\right)\left(\frac{\lambda^3}{6}\overline{\alpha_1} + \frac{\lambda^2}{2}\alpha_1\right)\lambda.\end{aligned}$$

This relation can be simplified to yield $0 = \frac{1}{2}\alpha_1\alpha_k$. The assertion thus follows by induction over k. □

It may be pointed out that the result of Theorem 19.3 is only partial in the sense that $\alpha_1 > 0$ was assumed. In the author's opinion, this is a quite natural assumption for DLINAR(p) processes, and the investigation is stopped at this point. However, given the previous result, the author conjectures the following assertion to be true:

Conjecture 19.1 *Let $(Y_t)_{t\in\mathbb{Z}}$ be a DLINAR(p) process with $p > 1$ and $\alpha_j > 0$ for some $j \in \{1,\ldots,p\}$ and let $0 < \mathbb{P}(\varepsilon = 0) < 1$. Then $(Y_t)_{t\in\mathbb{Z}}$ is time-reversible if and only if $\alpha_l = 0$ for $l \in \{1,\ldots,p\}, l \neq j$.*

To illustrate why the conjecture contains the reverse implication as well, consider the result of Lemma 19.1 for the case $p = 2$. It shows that for time-reversibility of the process, either $\alpha_1 = 0$ or $\alpha_2 = 0$ has to hold. The case $\alpha_1 = 0$ is clearly a degenerate case, and it can indeed be shown quite easily that it has the same stationary distribution as that of the corresponding INAR(1) process (i.e. with $\alpha = \alpha_2$) and that it is time-reversible. Similar argumentation applies to higher order autoregressive structures.

19.5 Discussion and Conclusion

At first sight, the results presented in this article might seem surprising, as on the one hand, the AAINAR(p) process behaves in complete analogy to the INAR(1) process when considering time-reversibility, on the other hand, the DLINAR(p) process is

only time-reversible in trivial cases. However, the author would like to point out that there seems to be a connection between the time-reversibility behaviour of autoregressive processes and an invariance principle between the marginal distribution and the innovations' distribution of the process which also extends to the continuous AR(p) case. To be more precise, for an INAR(1) process or an AAINAR(p) process with Poisson innovations it can be shown that the marginal distribution of these processes is Poisson distributed again (cf. [1] and [2, Sect. 5.1]), corresponding to the Gaussian distribution in the continuous AR(p) model. In all of these instances, time-reversibility of the process implies the error distribution to be Poisson or Gaussian, respectively (for the latter result, see Theorem 2 in [12]).

For the DLINAR(p) process however, the assumption of Poisson innovations does not imply a Poisson marginal distribution. This can be seen (for the case $p = 2$) in the discussion following (30) in [11], which shows that a DLINAR(2) process with $\alpha_2 > 0$ always exhibits overdispersion and can thus never be Poisson distributed.

The results presented in this article warrant further research concerning the question whether there exists an integer-valued autoregressive model of order p which has the same autocorrelation structure as the continuous AR(p) model and which is time-reversible given a certain type of innovation (or error) distribution.

Acknowledgements The author is grateful to Prof. Christian Weiß for carefully reading the paper and for helpful suggestions which greatly improved the paper.

The author's research has been supported by the *Deutsche Forschungsgemeinschaft* (German Research Foundation) within the programme "Statistical Modeling of Complex Systems and Processes – Advanced Nonparametric Approaches", grant GRK 1953.

References

1. Al-Osh M, Alzaid A (1987) First-order integer-valued autoregressive INAR(1) processes. J Time Ser Anal 8(3):261–275
2. Alzaid A, Al-Osh M (1990) An integer-valued pth-order autoregressive structure (INAR(p)) process. J Appl Probab 27(2):314–324
3. Bu R, McCabe B (2008) Model selection, estimation and forecasting in INAR(p) models: a likelihood-based Markov chain approach. Int J Forecast 24(1):151–162
4. Du JG, Li Y (1991) The integer-valued autoregressive (INAR(p)) model. J Time Ser Anal 12(2):129–142
5. McKenzie E (1985) Some simple models for discrete variate time series. Water Resour Bull 21(4):645–650
6. McKenzie E (1988) Some ARMA models for dependent sequences of Poisson counts. Adv Appl Probab 20(4):822–835
7. Schweer S, Weiß CH (2014) Compound Poisson INAR(1) processes: stochastic properties and testing for overdispersion. Comput Stat Data Anal 77:267–284
8. Schweer S, Wichelhaus C (2014) Queueing systems of INAR(1) processes with compound Poisson arrival distributions. Submitted
9. Steutel FW, Van Harn K (1979) Discrete analogues of self-decomposability and stability. Ann Probab 7(5):893–899
10. Walrand J (1983) A discrete-time queueing network. J Appl Probab 20(4):903–909

11. Weiß CH (2013) Integer-valued autoregressive models for counts showing underdispersion. J Appl Stat 40(9):1931–1948
12. Weiss G (1975) Time-reversibility of linear stochastic processes. J Appl Probab 12(4):831–836

Chapter 20
Change-Point Detection of the Mean Vector with Fewer Observations than the Dimension Using Instantaneous Normal Random Projections

Ewa Skubalska-Rafajłowicz

Abstract Our aim in this paper is to propose a simple method of a change-point detection of mean vector when the number of samples (historical data set) is smaller than the dimension. We restrict here our attention to the problem of monitoring independent individual observations under normality assumption. The presented approach is based on the Hotelling statistic. This statistic is applied to the data set projected onto a randomly chosen subspace of a sufficiently smaller dimension. We propose the procedure of normal random projection of data (historical data set and a new observation) instantaneously, just after a new observation appears. Next, we provide a model of the changes in the mean vector and derive the distribution of noncentrality parameter values. Further, a non-local power of the Hotelling test performed on projected samples is defined, which is the criterion for selecting the dimensionality of a projection subspace. Finally, simulation results are provided.

20.1 Introduction

It often happens that the dimension of observed data vectors is larger than the sample size and this case is referred to as small sample size, high dimensional data. Microarrays, medical imaging, text recognition, finance and chemometrics data analysis leads to such problems [4, 9, 21]. Statistical decision problems with fewer observations than the dimension of the data have been studied by many authors and in different contexts (see [1, 5, 9, 11, 12, 17–21] among many others). Control charts based on the Hotelling statistic [6, 7, 16] are the most popular methods for handling changes of multivariate process data [10, 13, 22, 24].

We restrict here our attention to the problem of monitoring independent individual observations under normality assumption [13, 22, 24]. Although control charts based on the Hotelling statistic are very popular method for identifying a change in a multivariate normal process, their use is restricted to low dimensional problems and sufficiently large number of historical data samples. We propose a new

E. Skubalska-Rafajłowicz (✉)
Institute of Computer Engineering, Control and Robotics, Wrocław University of Technology, Wrocław, Poland
e-mail: ewa.rafajlowicz@pwr.edu.pl

A. Steland et al. (eds.), *Stochastic Models, Statistics and Their Applications*,
Springer Proceedings in Mathematics & Statistics 122,
DOI 10.1007/978-3-319-13881-7_20

approach for change-point detection of a mean vector when the number of observations is smaller than the dimension. A dimension of the problem is diminished by a linear singular projection onto a randomly chosen subspace of a sufficiently smaller dimension. Random projections [3, 8, 15, 23] are considered to be one of the most potential methods of dimensionality reduction. Random projection based approaches have been widly used in computer science and machine learning applications. The use of random projection was also considered to two-sample testing [11] and to identify probability distributions belonging to parametric families [2]. It is important to stress that this approach is different than the method proposed previously by the author in [17] and [18], where the projection matrix was generated only once as a starting point of the dimensionality reduction procedure. Here we propose to perform the procedure of random projection of data (historical data set and a new observation) instantaneously, just after a new observation appears. This means that Phase I and Phase II of the control chart design [13] is repeated consecutively. This approach, though more time-consuming, is also more efficient, because there is no direction in the observation space where changes cannot be detected. The paper is organized as follows. In the next section we describe the new version of a Hotelling control chart based on instantaneous normal random projections. Next, in Sect. 20.3 we provide a model of the changes in the mean vector and the distribution of noncentrality parameter values. Under assumption of this model we then define non-local power of the Hotelling test performed on projected samples. As a consequence we propose a method of optimal selecting the dimensionality of projection subspace which minimizes the non-local power of the test. An illustrative example is given in Sect. 20.5.

20.2 The Algorithm of Mean Change Detection with Fewer Observations than the Dimension

We start by defining a historical dataset (HDS) consisting of N independent vectors of dimension d observed over time, where d is the dimension of these vectors. We consider the case where the in-control observation vectors, X_i, $i = 1, \ldots, N$, are iid random vectors with common mean vector μ and covariance matrix Σ, having Gaussian distribution $X_i \sim N_d(\mu_0, \Sigma)$. Both, μ_0 and Σ are not known and should be estimated on the bases of the HDS.

If the distribution mean changes from μ_0 to μ_1 we should be able to detect this event with possibly the highest probability. We assume that the sample size $N < d$, so the sample covariance matrix, based on iid HDS,

$$S = \sum_{i=1}^{N} (X_i - \bar{X})(X_i - \bar{X})^T / (N - 1), \tag{20.1}$$

is singular, so S^{-1} does not exists and $|S| = 0$.

We propose to use the Hotelling control chart based on individual observations and to apply it to multidimensional Gaussian data projected onto random k dimensional subspace of $\mathscr{R}^d$, where $k \ll d$.

Let $R \in \mathscr{R}^{k\times d}$ be a matrix of projection with iid normal entries, i.e., $r_{ij} \sim \mathscr{N}(0,1)$. For a new observation matrix R is generated and applied to it as well as to HDS.

Conditioning on R the projected HDS are iid normal:

$$V_i = RX_i, \quad V_i|R \sim \mathscr{N}_k\big(R\mu_0, R\Sigma R^T\big),\ i = 1,\ldots,N. \tag{20.2}$$

If $k < N$, the projected sample covariance matrix

$$S_R = \frac{1}{N-1}\sum_{i=1}^{N}(V_i - \bar{V})(V_i - \bar{V})^T, \tag{20.3}$$

where $\bar{V} = \sum_{i=1}^{N} V_i/N$, is non-singular with probability 1.

Let X denote a current observation in the monitoring sequence. For change-point detection of the mean vector we shall use the following statistic:

$$T_R^2 = (RX - \bar{V})^T S_R^{-1}(RX - \bar{V})\big|R \sim \frac{k(N+1)(N-1)}{(N-k)N}F(k, N-k), \tag{20.4}$$

where F is the F-Snedecor distribution with k and $N-k$ degrees of freedom. Notice that T_R^2 depends on k and N; it does not depend on d.

When change in the mean occurred and $\mu_1 = \mu_0 + m$, $m \neq 0$. $V = RX|R \sim \mathscr{N}_k(R\mu_1, R\Sigma R^T)$.

$$T_R^2 \sim \frac{k(N+1)(N-1)}{(N-k)N}F\big(k, N-k, \lambda^2\big), \tag{20.5}$$

where $F(k, N-k, \lambda^2)$ is a noncentral F-Snedecor distribution with non-centrality parameter $\lambda^2 = (Rm)^T(R\Sigma R^T)^{-1}Rm$ and with the degrees of freedom k and $N-k$, respectively. The general idea is to test (based on individual observations): H_0: $\mu = \mu_0$ versus H_1: $\mu = \mu_1 \neq \mu_0$.

If $T_R^2 < h_\alpha(k) = \frac{k(N+1)(N-1)}{(N-k)N}F_\alpha^{-1}(k, N-k)$, where α is a significance level, we decide that the process is in-control (no change in the mean is supposed). In other words, $h_\alpha(k)$ is the upper control limit.

We propose here to use the following algorithm:

For given HDS $X_1,\ldots,X_N$ and α choose k and compute $h_\alpha(k)$. For a given new observation X

1. Generate R. Compute RX S_R and T_R^2.
2. If $T_R^2 > h_\alpha(k)$ decide that the process is not in control. Otherwise, wait for the next observation.

Notice that for every new observation we should generate randomly a new projection matrix. This is very important, because there are no directions in $\mathscr{R}^d$ where changes cannot be detected. More precisely, for any orthogonal matrix $Q \in O(d)$ it can be shown that RQ is also a normal random projection matrix.

Thus, although the test statistics T_R^2 value depends on R and is not rotation invariant, its expected value with respect to R is invariant under the rotation group $O(d)$.

20.3 Model of the Changes in the Mean Vector and the Distribution of Noncentrality Parameter Values

Let

$$\delta = m^T \Sigma m, \quad m \in \mathscr{R}^d, \tag{20.6}$$

where m is a change in the mean vector.

Define a vector random variable $Z \sim \mathscr{N}_d(0, I)$ and let $Y = \Sigma^{1/2} Z$. Recall that we have assumed that Σ is a nonsingular positive definite symmetric matrix. $E\{Z^T Z\} = d$ since $Z^T Z \sim \chi_d^2$. Similarly, $Y^T \Sigma^{-1} Y \sim \chi_d^2$ and $E\{Y^T \Sigma^{-1} Y\} = d$. Random vector $M = \sqrt{\frac{\delta}{d}} Y$ is a random model of the changes in the mean vector with Mahalanobis distance which is close to δ. It is easy to show that

$$(RM)^T \left(R \Sigma R^T\right)^{-1} MY = \frac{\delta}{d} Z^T R^T \left(RR^T\right)^{-1} RZ. \tag{20.7}$$

Although RR^T follows the Wishart distribution $W_k(d, I)$ and $U = RZ|Z = z \sim N_k(0, \|x\|^2 I)$, the Gaussian random vector $U = RZ|Z = z$ and the random matrix RR^T are dependent.

Let u be an eigenvector of $R^T(RR^T)^{-1}R$, and let v denote the eigenvalue corresponding to that eigenvector. Rank of the matrix R is k (with probability 1). Furthermore,

$$R^T \left(RR^T\right)^{-1} Ru = vu, \qquad RR^T \left(RR^T\right)^{-1} Ru = vRu, \quad Ru = vRu. \tag{20.8}$$

Thus, eigenvalues of matrix $R^T(RR^T)^{-1}R$ are 1 or 0, with only k eigenvalues equal to 1 (with probability 1). Further,

$$R^T \left(RR^T\right)^{-1} R = Q^T A Q, \tag{20.9}$$

where $Q \in O(d)$ is an appropriately chosen orthogonal matrix, and

$$A = \begin{bmatrix} I_k & 0 \\ 0 & 0 \end{bmatrix}. \tag{20.10}$$

It can be shown that the diagonal elements of $R^T(RR^T)^{-1}R$ follow beta distribution $\beta(k/2, (d-k)/2)$ and expected values of out-of diagonal elements of this matrix are zero. So,

$$E_R\left[R^T \left(RR^T\right)^{-1} R\right] = E_Q\left\{Q^T A Q\right\} = \frac{k}{d} I$$

and

$$E_Z E_R\left\{\frac{\delta}{d} Z^T R^T \left(RR^T\right)^{-1} RZ | Z = z\right\} = \frac{\delta k}{d^2} E_Z\left(\|Z\|^2\right) = \frac{\delta k}{d}. \quad (20.11)$$

Furthermore, we can easily obtain that the random variable defined in (20.7) follows $\frac{\delta}{d}\chi^2_k$ distribution. Notice that for any $Q \in O(d)$ vector AQZ is a k-dimensional orthogonal projection of normal random vector $Z \sim \mathcal{N}_d(0, I)$ and using normal random projections we obtain a k-dimensional orthogonal vector basis according to a unique rotation-invariant probability measure (Haar measure) on compact Stiefel manifold (see for example [14]). Power of the test T^2_R for individual observation X and given mean shift vector m, denoted as $P_l(m)$ depends on dimension k of the normal random projection, noncentrality parameter $\delta(k, R, m) = m^T R^T (R\Sigma R^T)^{-1} Rm$ value obtained after projection and Type I error α (recall that in our case $ARL_0 = 1/\alpha$). Thus, conditionally on R, we obtain the following formula

$$P_l(m) = \int_{h(k)}^{\infty} f\left(k, N-k, \delta(k, R, m), x\right) dx, \quad (20.12)$$

where $f(k, N-k, \delta(k, R, m), x)$ is the probability density of noncentral distribution $F(k, N-k, \delta(k, R, m))$ and $h(k)$ is the critical value of the test for a given α. The new noncentrality parameter $\delta(k, R, m)$ depends strongly on Σ which is unknown and in fact non-estimable due to small N. Thus, assuming model (20.7) we shall concentrate on non-local power defined as:

$$P_{nl}(\delta, k, N) = E_{M,R}\left\{\int_{h(k)}^{\infty} f\left(k, N-k, \delta(k, R, M), x\right) dx\right\} \quad (20.13)$$

$$= E_{Z,R}\left\{\int_{h(k)}^{\infty} f\left(k, N-k, \frac{\delta}{d} Z^T R^T \left(RR^T\right)^{-1} RZ, x\right) dx\right\} \quad (20.14)$$

$$= \int_0^{\infty} f_{\chi^2}(k)(y)\left[\int_{h(k)}^{\infty} f\left(k, N-k, \frac{\delta}{d} y, x\right) dx\right] dy. \quad (20.15)$$

20.4 Choosing Dimension of Random Projection k

It is well known that Hotelling type control charts perform better in low dimension [24]. On the other hand the noncentrality parameter of the appropriate F-Snedecor distribution is larger in higher dimensions. Thus, the optimal choice of k is a compromise between both opposite tendencies.

Under assumption of model (20.7) we have to solve the following optimization problem:

$$\text{maximise } P_{nl}(\delta, k, N) \quad \text{with respect to } k \leq N-2. \quad (20.16)$$

For moderate N values the problem can be solved numerically. Figure 20.1 shows $P_{nl}(\delta, k, N)$ for $k = 1, \ldots, 18$ and false alarm rate 0.005, i.e. $\alpha = 0.005$, $N = 20$, $d = 100$ and $\delta = 1000, 300, 200, 100$ respectively. It is important to indicate, that function (20.15) is very flat with respect to k and the proposed method of selecting k is robust to small and moderate changes of α and δ.

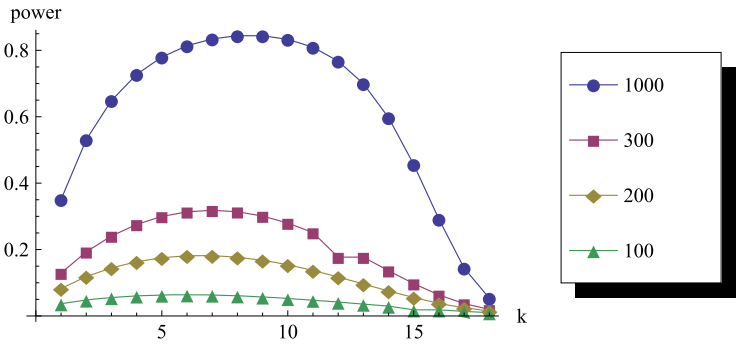

Fig. 20.1 Non-local power values of the test obtained numerically according to the formula (20.15) for $\alpha = 0.005$ ($d = 100$, $N = 20$, $\delta = 1000, 300, 200, 100$ and $k = 1, \ldots, 18$)

20.5 Numerical Experiments

We perform some experiments for multivariate normal distributions with population covariance matrix with compound symmetry structure [4, 9]: $\Sigma = (1-\rho)I_d + \rho \mathbf{1}\mathbf{1}^T$, where $\mathbf{1}_d$ is the column vector with all entries one, $\rho \in (0, 1)$ is a common correlation factor. The trace of Σ is d, independently of ρ value. Notice that the eigenvalues of the compound symmetry structure are $\lambda_1 = 1 + (d-1)\rho$ and $\lambda_2 = \cdots = \lambda_d = 1 - \rho$. Without loss of generality we can assume that the true covariance matrix is diagonal since the proposed approach is rotation invariant in the mean (see Sect. 20.2 for explanations).

In our study $N = 20$, $d = 100$ and $\rho = 0.6$, 0.4 and 0.1 are selected. We fix the nominal significance level $\alpha = 0.005$. This significance level is equivalent to the average run length ARL in an in-control state, i.e., nominal $ARL_0 = 1/\alpha = 200$. Numerical experiments are performed for 10 different HDS. Each experiment consists of 10 000 replications. We select dimension of the projection according to (20.16) (see also Fig. 20.1).

In Table 20.1 the averages over 10 HDS of ARL to detection are shown for 6 different m and the corresponding $\delta = m^T \Sigma^{-1} m$. As one can observe, ARL's to detection strongly depend on a direction of the change vector m, e.g., changes in the direction of the largest eigenvalue of Σ are the easiest to detect. In contrary, the most difficult to disclose is vector m_6, where the change is in the direction of the smallest eigenvalue.

The above simulations were repeated for non-optimal k and in every case ARL's to detection were larger than those reported in Table 20.1. However, the results are not too sensitive to small inaccuracies in selecting optimal k. Furthermore, k selected according to (20.16), i.e., averaged with respect to (20.7), performed very well in each particular case listed in Table 20.1.

Table 20.1 ARL's for $d = 100$, $N = 20$, $k = 7$ and $m_0 = (0, \ldots, 0)$, $m_1 = (10.99, 0, \ldots, 0)$, $m_2 = (5.495, 0, \ldots, 0)$, $m_3 = (0.0899, \ldots, 0.0899)$, $m_4 = (0, 0.6324, 0.6324, 0.6324, 0, \ldots, 0)$, $m_5 = (0, 0.6324, 0.6324, 0, \ldots, 0)$, $m_6 = (0, 0.6324, 0, \ldots, 0)$

m	$\rho = 0.6$		$\rho = 0.4$		$\rho = 0.1$	
	δ	ARL	δ	ARL	δ	ARL
m_0	0	208.3	0	217.4	0	217.4
m_1	200.0	1.00	297.5	1.00	1108.0	1.00
m_2	50.0	1.30	74.4	1.11	277.0	1.02
m_3	200.03	6.78	133.34	12.35	88.9	20.81
m_4	300.0	3.97	200.0	6.99	133.3	12.27
m_5	200	7.23	133.3	13.14	88.9	22.52
m_6	100.0	21.87	66.7	37.11	44.4	56.95

20.6 Concluding Remarks

In this paper a new method of using the Hotelling control chart is proposed for change-point detection of a mean vector with fewer observations than the dimension. We concentrate on finite sample problems. The method performs well, when a population covariance matrix has a compound symmetry structure. Due to the known distribution of the test statistic the control level of the chart is data independent, what is important in a small sample case. The proposed method of selecting the dimension of the normal projection provides accurate values when the number of samples is moderate. If the average change of the mean vector is it assumed to be proportional to the dimension, the power of the test for a given projection dimension depends only on the number of samples and a significance level.

References

1. Ahn J, Marron JS, Muller KE, Chi Y-Y (2007) The high dimension, low sample size geometric representation holds under mild conditions. Biometrika 94:760–766
2. Cuesta-Albertos JA, del Barrio E, Fraiman R, Matran C (2007) The random projection method in goodness of fit for functional data. Comput Stat Data Anal 51(10):4814–4831
3. Frankl P, Maehara H (1990) Some geometric applications of the beta distribution. Ann Inst Stat Math 42(3):463–474
4. Fridley BL, Jenkins GD, Biernacka JM (2010) Self-contained gene-set analysis of expression data: an evaluation of existing and novel methods. PLoS One 5(9), e12693
5. Hall P, Marron JS, Neeman A (2005) Geometric representation of high dimension, low sample size data. J R Stat Soc B 67:427–444
6. Hotelling H (1931) The generalization of student's ratio. Ann Math Stat 2(3):360–378
7. Hotelling H (1947) Multivariate quality control-illustrated by the air testing of sample bombsights. In: Eisenhart C, Hastay MW, Wallis WA (eds) Techniques of statistical analysis. McGraw-Hill, New York, pp 111–184
8. Johnson WB, Lindenstrauss J (1984) Extensions of Lipshitz mapping into Hilbert space. Contemp Math 26:189–206

9. Katayamaa S, Kanoa Y, Srivastava MS (2013) Asymptotic distributions of some test criteria for the mean vector with fewer observations than the dimension. J Multivar Anal 116:410–421
10. Liu R (1995) Control charts for multivariate processes. J Am Stat Assoc 90:1380–1387
11. Lopes M, Jacob L, Wainwright M (2011) A more powerful two-sample test in high dimensions using random projection. In: Advances in neural information processing systems (NIPS) vol 24
12. Marzetta TL, Tucci GH, Simon SH (2011) A random matrix-theoretic approach to handling singular covariance estimates. IEEE Trans Inf Theory 57(9):6256–6271
13. Mason RL, Young JC (2002) Multivariate statistical process control with industrial application. SIAM, Philadelphia
14. Meckes E (2012) Approximation of projections of random vectors. J Theor Probab 25(2):333–352
15. Milman V (1971) A new proof of the theorem of A. Dvoretzky on sections of convex bodies. Funct Anal Appl 5(4):28–37 (English translation)
16. Rao CR (1973) Linear statistical inference and its applications, wyd. II. Wiley, New York
17. Skubalska-Rafajłowicz E (2011) Fast and efficient method of change detection in statistically monitored high-dimensional data streams. In: Proceedings of the 10th international science and technology conference on diagnostics of processes and systems, Zamość, Poland, pp 256–260
18. Skubalska-Rafajłowicz E (2013) Random projections and Hotelling's T^2 statistics for change detection in high-dimensional data streams. Int J Appl Math Comput Sci 23(2):447–461
19. Srivastava MS (2006) Minimum distance classification rules for high dimensional data. J Multivar Anal 97(9):2057–2070
20. Srivastava MS, Du M (2008) A test for the mean vector with fewer observations than the dimension. J Multivar Anal 99:386–402
21. Srivastava MS (2009) A review of multivariate theory for high dimensional data with fewer observations. In: SenGupta A (ed) Advances in multivariate statistical methods, vol 9. World Scientific, Singapore, pp 25–52
22. Sullivan JH, Woodall WH (2000) Change-point detection of mean vector or covariance matrix shifts using multivariate individual observations. IIE Trans 32(6):537–549
23. Vempala S (2004) The random projection method. American Mathematical Society, Providence
24. Wang K, Jiang W (2009) High-dimensional process monitoring and fault isolation via variable selection. J Qual Technol 41(3):247–258

Chapter 21
On Some Distributed Disorder Detection

Krzysztof Szajowski

Abstract Multivariate data sources with components of different information value seem to appear frequently in practice. Models in which the components change their homogeneity at different times are of significant importance. The fact whether any changes are influential for the whole process is determined not only by the moments of the change, but also depends on which coordinates. This is particularly important in issues such as reliability analysis of complex systems and the location of an intruder in surveillance systems. In this paper we developed a mathematical model for such sources of signals with discrete time having the Markov property given the times of change. The research also comprises a multivariate detection of the transition probabilities changes at certain sensitivity level in the multidimensional process. Additionally, the observation of the random vector is depicted. Each chosen coordinate forms the Markov process with different transition probabilities before and after some unknown moment. The aim of statisticians is to estimate the moments based on the observation of the process. The Bayesian approach is used with the risk function depending on measure of chance of a false alarm and some cost of overestimation. The moment of the system's disorder is determined by the detection of transition probabilities changes at some coordinates. The overall modeling of the critical coordinates is based on the simple game.

21.1 Introduction

The aim of the study is to investigate the mathematical model of a multivariate surveillance system introduced in [17]. In the model there is net $\mathfrak{N}$ of p nodes. At each node the state is the signal at moment $n \in \mathbb{N}$ which is at least one coordinate of the vector $\vec{x}_n \in \mathbb{E} \subset \Re^m$. The distribution of the signal at each node has two forms that depends on the state of surrounding. The state of the system changes dynamically. We consider the discrete time signal observed as $m \geq p$ dimensional process on the probability space $(\Omega, \mathscr{F}, \mathbf{P})$. The Markov processes, which are observed at

K. Szajowski (✉)
Inst. of Math. and CS, Wrocław Univ. of Tech., Wyb. Wyspiańskiego 27, 50-370 Wrocław, Poland
e-mail: Krzysztof.Szajowski@pwr.edu.pl
url: http://im.pwr.edu.pl/~szajow

A. Steland et al. (eds.), *Stochastic Models, Statistics and Their Applications*,
Springer Proceedings in Mathematics & Statistics 122,
DOI 10.1007/978-3-319-13881-7_21

each node, are non homogeneous with two homogeneous segments as they have different transition probabilities (see [12] for details). The visual consequence of the transition distribution changes at moment θ_i, $i \in \mathfrak{N}$ is a change of its character. In order to avoid false alarm the confirmation from other nodes is needed. The family of subsets (coalitions) of nodes is defined in such a way that the decision of all members of a given coalition is equivalent to the claim that the disorder appeared in the net. It is not certain, however that the disorder has taken place. The aim is to define the rules of nodes and a construction of the net decision based on individual nodes claims. Various approaches can be found in the recent research that refer to the description of such systems (see e.g. [11, 19]). The problem is quite similar to a pattern recognition with multiple algorithm when the results of fusions of individual algorithms are unified to a final decision. In the study two different approaches are proposed. Both are based on the simple game defined on the nodes. The naïve methods determine the system disordering by fusion individual node strategies. This construction of the individual decisions is based on the observation at each node separately.

The advanced solution of Bayesian version of the multivariate detection with a common fusion center is based on a stopping game defined by a simple game related to the observed signals. The individual decisions are based on the analysis of the processes observed at all nodes and knowledge of nodes' interaction (the simple game). The sensors' strategies are constructed as an equilibrium strategy in a non-cooperative stopping game with a logical function defined by a simple game (which aggregates their decision).

The general description of such multivariate stopping games has been formulated by Kurano, Yasuda and Nakagami in the case when the aggregation function is defined by the voting majority rule [5] and the observed sequences of the random variables are independent, identically distributed. It was Ferguson [3] who substituted the voting aggregation rules by a simple game. The Markov sequences have been investigated by the author and Yasuda [16].

The model of detection of the disorders at each sensor is presented in the next section. It allows to define the individual payoffs of the players (sensors). The final decision based on the state of the sensors is given by the fusion center and it is described in Sect. 21.5. The natural direction of further research is formulated in the same section.

21.2 Detection of Disorder at Sensors

Following the consideration presented in Sect. 21.1, let us suppose that the process $\{\vec{X}_n, n \in \mathbb{N}\}$, $\mathbb{N} = \{0, 1, 2, \ldots\}$, is observed sequentially in such a way that each sensor, *e.g.* rth one gets its coordinates in the vector $\vec{X}_n$ at moment n. By assumption, it is a stochastic sequence that has the Markovian structure which is given random moment θ_r in such a way that the process after θ_r starts from state $\vec{X}_{\theta_r - 1}$. The objective is to detect these moments based on the observation of $\vec{X}_n$ at each sensor separately. There are some results on the discrete time case of such disorder

detection which generalize the basic problem stated by Shiryaev in [13] (see e.g. Brodsky and Darkhovsky [2], Bojdecki [1]) in various directions. In the early papers the observed sequence has independent elements given disorder moment. The sequences with dependent observations are subject of investigation by Yoshida [21], Szajowski [15], Yakir [20], Moustakides [7] and Mei [6].

The application of the model for the detection of traffic anomalies in networks was discussed by Tartakovsky et al. [18]. The version of the problem when the moment of disorder is detected with given precision will be used here (see [12]).

21.2.1 Formulation of the Problem

The observable random variables $\{\vec{X}_n\}_{n\in\mathbb{N}}$ are consistent with the filtration $\mathscr{F}_n$ (or $\mathscr{F}_n = \sigma(\vec{X}_0, \vec{X}_1, \ldots, \vec{X}_n)$). The random vectors $\vec{X}_n$ take values in $(\mathbb{E}, \mathscr{B})$, where $\mathbb{E} \subset \Re^m$. On the same probability space there are defined unobservable (hence not measurable with respect to $\mathscr{F}_n$) random variables $\{\theta_r\}_{r=1}^m$ which have the following geometric distributions:

$$\mathbf{P}(\theta_r = j) = \pi_r \mathbb{I}_{\{j=0\}}(j) + \big(1 - \mathbb{I}_{\{j=0\}}(j)\big)(1-\pi_r) p_r^{j-1} q_r,$$

where $\pi_r, q_r = 1 - p_r \in (0,1)$, $j = 0, 1, 2, \ldots$.

The sensor r follows the process which is based on switching between two, time homogeneous and independent the Markov processes $\{X_{rn}^i\}_{n\in\mathbb{N}}$, $i = 0, 1$, $r \in \mathfrak{N}$ with the state space $(\mathbb{E}, \mathscr{B})$. These are both independent of $\{\theta_r\}_{r=1}^m$. Moreover, the processes $\{X_{rn}^i\}_{n\in\mathbb{N}}$ have transition densities

$$\mathbf{P}_x^i\big(X_{r1}^i \in B\big) = \mathbf{P}\big(X_{r1}^i \in B | X_{r0}^i = x\big) = \int_B f_x^{ri}(y)\mu(dy).$$

The random processes $\{X_{rn}\}$, $\{X_{rn}^0\}$, $\{X_{rn}^1\}$ and the random variables θ_r are connected via the rule: $X_{rn} = X_{rn}^0 \mathbb{I}_{\{n:\, n<k\}}(n) + X_{r\,n+1-k}^1 \mathbb{I}_{\{n:\, n\le k\}}(n)$ on $\theta_r = k$, where $\{X_{rn}^1\}$ starts from $X_{r\,k-1}^0$ (but is otherwise independent of $X_{r\,\cdot}^0$).

For any $x \in \mathbb{E}$, $\pi_r \in [0,1]$, $c \in \Re_+$ and $\tau_r \in \mathfrak{S}^X$, where $\mathfrak{S}^X$ denotes the set of all stopping times with respect to the filtration $\{\mathscr{F}_n\}_{n\in\mathbb{N}}$, the risk associated with τ_r is defined as follows $\rho_r(x, \pi_r, \tau_r) = \mathbf{P}_{x\,\pi_r}(\tau_r < \theta_r) + c\mathbf{E}_{x\,\pi_r} \max\{\tau_r - \theta_r, 0\}$, where $\mathbf{P}_{x\,\pi_r}(\tau_r < \theta_r)$ is the probability of false alarm and $\mathbf{E}_{x\,\pi_r} \max\{\tau_r - \theta_r, 0\}$ is the average delay of detecting correctly the occurrence of disruption.

Every sensor is looking for the stopping time $\tau_r^* \in \mathfrak{S}^X$ such that for every $(x; \pi_r) \in \mathbb{E} \times [0,1]$

$$\rho^\star(x, \pi_r) = \rho_r\big(x, \pi_r, \tau_r^\star\big) = \inf_{\tau_r \in \mathfrak{S}^X} \rho_r(x, \pi_r, \tau_r). \tag{21.1}$$

21.2.2 The Optimal Detection Problem as an Optimal Stopping Problem

In case of the independent sequence given the disorder moment the construction of τ^* through the transformation of the problem to the optimal stopping problem for the Markov process $(X_n, \Pi_{r\,n}^{\pi_r})$ can be made, where $\Pi_{r\,n}^{\pi_r}$ is the posterior process (see e.g. [14]). It is stated that $\Pi_{r0}^{\pi_r} = \pi_r$, $\Pi_{rn}^{\pi_r} = \mathbf{P}^{\pi_r}(\theta_r \le n \mid \mathscr{F}_n)$, for $n = 1, 2, \ldots$, is designed as information about the distribution of the disorder instant θ_r. Moreover,

$$\rho_r(x, \pi_r, \tau_r) = \mathbf{E}^{x,\pi_r}\left\{\left(1 - \Pi_{r\tau_r}^{\pi_r}\right) + c\sum_{k=0}^{\tau_r - 1}\Pi_{r\,k}^{\pi_r}\right\}. \tag{21.2}$$

The family of the Markov random functions $\{\Pi^{\pi_r}, \pi_r \in [0, 1]\}$ can be associated with a Markov process with discrete time $\Pi = (\pi_n, \mathscr{F}_n, \mathbf{P}^{\pi_r})$, for $n \ge 0$, having the same transition probabilities as each Markov random function is presented as Π^{π_r}, $\pi_r \in [0, 1]$.

21.2.3 The Optimal Stopping Problem with Observation Costs

The problem of minimization of the risk (21.2) can be solved as the special optimal stopping problem. As it is shown in [10], pp. 22–23, the problem can be transformed to the optimal stopping problem for the time-homogeneous two dimensional Markov chain without observation costs. The Wald–Bellman equation which solves (21.1) takes the form:

$$\rho^\star(x, \pi_r) = \min\left\{1 - \pi_r, c\pi_r + \mathbf{E}_{x,\pi_r}\rho^\star(x_1, \pi_1)\right\}. \tag{21.3}$$

21.3 The Aggregated Decision via the Cooperative Game

There are various methods combining the decisions of several classifiers or sensors. The methods based on winning coalitions in the simple game presented in [17] will be used. The obvious changes are the consequence that in the model considered now the aim is to minimize the risk. We apply two methods of decision aggregation. In the first one, based on the optimal disorder detection strategies, we apply the aggregation method. This approach does not guarantee that the obtained system disorder detection will have certain stability or equilibrium properties.

In the second approach each ensemble member contributes to some degree to the decision at any point of the sequentially delivered states. The fusion algorithm takes into account all the decision outputs from each ensemble member and comes up with an ensemble decision in such a way that the solution is an equilibrium point in an antagonistic, no-zero sum game.

21.3.1 A Simple Game

Let us assume that there are many nodes which absorb information and make decisions if the disorder has appeared or not. The final decision is made in the fusion center which aggregates the information from all sensors.

The voting decision is made according to the rules of *a simple game*. Let us recall that a coalition is a subset of the players. Let $\mathscr{C} = \{C\colon\ C \subset \mathfrak{N}\}$ denote the class of all coalitions. *A simple game* (see [3, 9]) is a coalition game having the characteristic function of $\phi(\cdot)\colon \mathscr{C} \to \{0, 1\}$.

Let us denote $\mathscr{W} = \{C \subset \mathfrak{N}\colon\ \phi(C) = 1\}$ and $\mathscr{L} = \{C \subset \mathfrak{N}\colon\ \phi(C) = 0\}$. The coalitions in $\mathscr{W}$ are called the winning coalitions, and those from $\mathscr{L}$ are called the losing coalitions. By assumption, the characteristic function satisfies the properties: $\mathfrak{N} \in \mathscr{W}$; $\emptyset \in \mathscr{L}$; (the monotonicity): $T \subset S \in \mathscr{L}$ implies $T \in \mathscr{L}$.

21.3.2 The Aggregated Decision Rule

When the simple game is defined and the players can vote presence or absence, $x_i = 1$ or $x_i = 0$, $i \in \mathfrak{N}$ of the local disorder then the aggregated decision is given by the logical function

$$\delta(x_1, x_2, \ldots, x_p) = \sum_{C \in \mathscr{W}} \prod_{i \in C} x_i \prod_{i \notin C} (1 - x_i). \tag{21.4}$$

For the logical function δ we have (cf. [5])

$$\delta\big(x^1, \ldots, x^p\big) = x^i \cdot \delta\big(x^1, \ldots, \overset{i}{\breve{1}}, \ldots, x^p\big) + \overline{x}^i \cdot \delta\big(x^1, \ldots, \overset{i}{\breve{0}}, \ldots, x^p\big),$$
$$\text{where} \quad \overline{x}^i = 1 - x^i.$$

21.3.3 Aggregated Sensors Strategies

For any stopping times $\{\tau_i\}_{i=1}^p$ with respect of the filtration $\{\mathscr{F}_n\}_{n \in \mathbb{N}}$ we have the representation by the individual stopping strategies $\sigma_n^i(\tau) = \mathbb{I}_{\{\omega\colon\ \tau_i \geq n\}}$. The aggregate function applied to the individual stopping times will construct the detection strategy σ_n of the system disorder. The stopping time from the individual stopping strategy is constructed as $\tau = \inf\{0 \leq n \leq N\colon\ \sigma_n \prod_{k=1}^{n-1}(1 - \sigma_k) = 1\}$.

This aggregation method is the basement of both constructions. In the *naive* algorithm it is applied to the optimal individual strategies of the sensors constructed as the solution of the optimal stopping problem (21.1).

In the multivariate stopping game approach the aggregation of the individual decision is used to construct the set of admissible strategies. The details are the subject of the next section.

21.4 A Non-cooperative Detection Problem

Following the results of the author and Yasuda [16] the multilateral stopping of a Markov chain problem can be described in the terms of the notation used in the non-cooperative game theory (see [8, 9]). This approach can be applied to the distributed disorder detection by reformulation of the problem to the multilateral stopping problem. The important issue is the representation of the expected risk in the disorder detection problem for one sensor given in (21.2).

Let us denote $\sigma^i = (\sigma_1^i, \ldots, \sigma_N^i)$ and let $\mathfrak{S}^i$ be the set of ISSs of player i, $i = 1, 2, \ldots, p$ (see [5]). Define $\mathfrak{S} = \mathfrak{S}^1 \times \cdots \times \mathfrak{S}^p$ the set of the stopping strategy (SS). The factual stopping of the observation process (the estimate of the system disorder moment), and the players realization of the payoffs are defined by the stopping strategy exploiting p-variate logical function $\delta : \{0, 1\}^p \to \{0, 1\}$. Since δ is fixed during the analysis we write $\mathfrak{t}(\sigma) = \mathfrak{t}_\delta(\sigma)$.

We have $\{\omega \in \Omega\colon\ \mathfrak{t}_\delta(\sigma) = n\} = \bigcap_{k=1}^{n-1}\{\omega \in \Omega\colon\ \delta(\sigma_k^1, \sigma_k^2, \ldots, \sigma_k^p) = 0\} \cap \{\omega \in \Omega\colon\ \delta(\sigma_n^1, \sigma_n^2, \ldots, \sigma_n^p) = 1\} \in \mathfrak{F}_n$, then the random variable $\mathfrak{t}_\delta(\sigma)$ is the stopping time with respect to $\{\mathfrak{F}_n\}_{n=1}^N$. For any stopping time $\mathfrak{t}_\delta(\sigma)$ and $i \in \{1, 2, \ldots, p\}$, let $\rho_i(X_{\mathfrak{t}_\delta(\sigma)}, \Pi_{\mathfrak{t}_\delta(\sigma)}, \delta(\sigma)) = \rho_i(X_n, \Pi_n, n)\mathbb{I}_{\{\mathfrak{t}_\delta(\sigma)=n\}} + \limsup_{n\to\infty} \rho_i(X_n, \Pi_n, n)\mathbb{I}_{\{\mathfrak{t}_\delta(\sigma)=\infty\}}$. (cf. [14, 16]). If players use SS $\sigma \in \mathfrak{S}$ and the individual preferences are converted to the effective stopping time by the aggregate rule δ, then player i gets $\rho_i(X_{\mathfrak{t}_\delta(\sigma)}, \Pi_{\mathfrak{t}_\delta(\sigma)})$.

Let ${}^*\sigma = ({}^*\sigma^1, \ldots, {}^*\sigma^p)^T \in \mathfrak{S}$ and ${}^*\sigma(i) = ({}^*\sigma^1, \ldots, {}^*\sigma^{i-1}, \sigma^i, {}^*\sigma^{i+1}, \ldots, {}^*\sigma^p)^T$.

Definition 21.1 (Cf. [16].) For the fixed aggregate rule δ the strategy ${}^*\sigma \in \mathfrak{S}$ is an equilibrium strategy if for each $i \in \{1, 2, \ldots, p\}$ and any $\sigma^i \in \mathfrak{S}^i$ we have

$$\rho_i\big(x, \pi_i, \mathfrak{t}_\delta({}^*\sigma)\big) \le \rho_i\big(x, \pi_i, \mathfrak{t}_\delta({}^*\sigma(i))\big). \tag{21.5}$$

The set $\mathfrak{S}$, the vector of the utility functions $f = (f_1, f_2, \ldots, f_p)$ and the monotone rule δ define the non-cooperative game $\mathcal{G} = (\mathfrak{S}, f, \delta)$. The construction of the equilibrium strategy ${}^*\sigma \in \mathfrak{S}$ in $\mathcal{G}$ is provided in [16]. In the case of the considered distributed disorder detection problem we have $f_i(x, \pi) = 1 - \pi$.

With each ISS of player i the sequence of stopping events $D_n^i = \{\omega\colon\ \sigma_n^i = 1\}$ is associated. For each aggregate rule δ there exists the corresponding set value function $\Delta : \mathfrak{F} \to \mathfrak{F}$ such that $\delta(\sigma_n^1, \ldots, \sigma_n^p) = \delta\{\mathbb{I}_{D_n^1}, \ldots, \mathbb{I}_{D_n^p}\} = \mathbb{I}_{\Delta(D_n^1, \ldots, D_n^p)}$. For the solution of the considered game the important class of ISS and the stopping events can be defined by subsets $C^i \in \mathscr{B}$ of the state space $\mathbb{E}$. A given set $C^i \in \mathscr{B}$ will be called the stopping set for player i at moment n if $D_n^i = \{\omega\colon\ X_n \in C^i\}$ is the stopping event.

Let g_i be the real, integrable functions defined on $\mathbb{E} \times [0, 1]$ and $C^i \in \mathscr{B}$. Let ${}^iD_1(A) = \Delta(D_1^1, \ldots, D_1^{i-1}, A, D_1^{i+1}, \ldots, D_1^p)$. For fixed $D_n^j = \{\omega\colon\ X_n \in C^i\}$, $j = 1, \ldots, p$, $j \ne i$ define $\psi(C^i) = \mathbf{E}_x[(1 - \Pi_1^i)\mathbb{I}_{{}^iD_1(D_1^i)} + g_i(X_1, \Pi_1)\mathbb{I}_{\overline{{}^iD_1(D_1^i)}}]$.

Lemma 21.1 *Let $C^j \in \mathscr{B}$, $j = 1, 2, \dots, p$, $j \neq i$, be fixed. Then the set ${}^*C^i = \{x \in \mathbb{E}\colon\ \rho_i(x) - g_i(x) \le 0\} \in \mathscr{B}$ is such that $\psi({}^*C^i) = \inf_{C^i \in \mathscr{B}} \psi(C^i)$ and*

$$\psi\big({}^*C^i\big) = \mathbf{E}_{x,\pi}\big(1 - \Pi_1^i - g_i(X_1, \Pi_1)\big)^+ \mathbb{I}_{iD_1(\emptyset)} - \mathbf{E}_{x,\pi}\big(1 - \Pi_1^i - g_i(X_1, \Pi_1)\big)^- \mathbb{I}_{iD_1(\Omega)} + \mathbf{E}_{x,\pi} g_i(X_1, \Pi_1). \quad (21.6)$$

Based on Lemma 21.1 we derive the recursive formulae defining the equilibrium point and the equilibrium payoff for the finite horizon detection problem.

21.4.1 The Finite Horizon Detection Problem

Let horizon N be finite and the equilibrium strategy ${}^*\sigma$ exist. We denote $\rho_{i,N}(x, \pi) = \mathbf{E}_{x,\pi}\rho_i(X_{t({}^*\sigma)}, \Pi_{t({}^*\sigma)})$ the equilibrium payoff of ith player when $X_0 = x$. Let $\mathfrak{S}_n^i = \{\{\sigma_k^i\}, k = n, \dots, N\}$ and $\mathfrak{S}_n = \mathfrak{S}_n^1 \times \mathfrak{S}_n^2 \times \cdots \times \mathfrak{S}_n^p$.

Denote $t_n = t_n(\sigma) = t({}^n\sigma) = \inf\{n \le k \le N\colon\ \delta(\sigma_k^1, \sigma_k^2, \dots, \sigma_k^p) = 1\}$ to be the stopping time not earlier than n. Let $\rho_{i,N-n+1}(X_{n-1}, \Pi_{n-1}) = \rho_i(X_{t_n({}^*\sigma)}, \Pi_{t_n({}^*\sigma)}, t_n({}^*\sigma))$. At $n = N$ we have $\rho_{i,0}(x, \pi) = \rho_i(x, \pi, N)$. Let us assume that the process is not stopped up to moment n and the players are using the equilibrium strategies ${}^*\sigma_k^i$, $i = 1, 2, \dots, p$, at $k = n+1, \dots, N$. Choose player i and assume that other players are using the equilibrium strategies ${}^*\sigma_n^j$, $j \neq i$, and player i is using strategy σ_n^i defined by the stopping set C^i. Then the expected payoff $\varphi_{N-n}(X_{n-1}, C^i)$ of player i in the game starting at n, when the state of a Markov chain at $n-1$ is X_{n-1}, is equal to

$$\varphi_{N-n}\big(X_{n-1}, \Pi_{n-1}, C^i\big) = \mathbf{E}_{X_{n-1},\Pi_{n-1}}\big[\big(1 - \Pi_n^i\big)\mathbb{I}_{i{}^*D_n(D_n^i)} + \rho_{i,N-n}(X_n, \Pi_n)\mathbb{I}_{\overline{i{}^*D_n(D_n^i)}}\big],$$

where ${}^i{}^*D_n(A) = \Delta({}^*D_n^1, \dots, {}^*D_n^{i-1}, A, {}^*D_n^{i+1}, \dots, {}^*D_n^p)$.

By Lemma 21.1 the conditional expected gain $\varphi_{N-n}(X_{N-n}, C^i)$ attains the maximum on the stopping set ${}^*C_n^i = \{x \in \mathbb{E}\colon\ f_i(x) - v_{i,N-n}(x) \le 0\}$ and

$$\begin{aligned} &v_{i,N-n+1}(X_{n-1}, \Pi_{n-1}) - c_i\Pi_{n-1}^i \\ &\quad = \mathbf{E}_x\big[\big(1 - \Pi_n^i - v_{i,N-n}(X_n, \Pi_n)\big)^+ \mathbb{I}_{i{}^*D_n(\emptyset)} | \mathfrak{F}_{n-1}\big] \\ &\qquad - \mathbf{E}_x\big[\big(1 - \Pi_n^i - v_{i,N-n}(X_n)\big)^- \mathbb{I}_{i{}^*D_n(\Omega)} | \mathfrak{F}_{n-1}\big] + \mathbf{E}_x\big[v_{i,N-n}(X_n, \Pi_n) | \mathfrak{F}_{n-1}\big] \end{aligned}$$

$\mathbf{P}_x-$a.e. This reasoning allows to formulate the following construction of the equilibrium strategy and the equilibrium value for the game $\mathscr{G}$.

Theorem 21.1 *In the game $\mathscr{G}$ with finite horizon N we have the following solution.*

(i) *The equilibrium value $v_i(x, \pi)$, $i = 1, 2, \dots, p$, of the game $\mathscr{G}$ can be calculated recursively as follows*: $v_{i,0}(x, \pi) = 1 - \pi_i$ *and for $n = 1, 2, \dots, N$, $i = 1, 2, \dots, p$ we have $\mathbf{P}_x-a.e.$*

$$
\begin{aligned}
&v_{i,n}(X_{N-n}, \Pi_{N-n}) - c_i \Pi^i_{N-n} \\
&\quad = \mathbf{E}_{x,\pi}\left[v_{i,n-1}(X_{N-n+1}, \Pi_{N-n+1})|\mathfrak{F}_{N-n}\right] \\
&\qquad + \mathbf{E}_{x,\pi}\left[\left(1 - \Pi^i_{N-n+1}\right) - v_{i,n-1}(X_{N-n+1}, \Pi_{N-n+1})^+\right. \\
&\qquad \left. \times \mathbb{I}_{i*_{D_{N-n+1}(\Omega)}}|\mathfrak{F}_{N-n}\right] \\
&\qquad - \mathbf{E}_{x,\pi}\left[\left(\left(1 - \Pi^i_{N-n+1}\right) - v_{i,n-1}(X_{N-n+1}, \Pi_{N-n+1})\right)^-\right. \\
&\qquad \left. \times \mathbb{I}_{i*_{D_{N-n+1}(\emptyset)}}|\mathfrak{F}_{N-n}\right].
\end{aligned}
$$

(ii) *The equilibrium strategy* ${}^*\sigma \in \mathfrak{S}$ *is defined by the SS of the players* ${}^*\sigma^i_n$, *where* ${}^*\sigma^i_n = 1$ *if* $X_n \in {}^*C^i_n$, *and* ${}^*C^i_n = \{x \in \mathbb{E}\colon\ f_i(x) - v_{i,N-n}(x) \le 0\}$, $n = 0, 1, \ldots, N$.

We have $v_i(x, \pi) = v_{i,N}(x, \pi)$, *and* $\mathbf{E}_{x,\pi}(1 - \Pi^i_{t({}^*\sigma)}) = v_{i,N}(x)$, $i = 1, 2, \ldots, p$.

21.5 Determining the Strategies of Sensors

Based on the model constructed in Sects. 21.2–21.4 for the net of sensors with the fusion center determined by a simple game, one can determine the rational decisions of each nodes. The rationality of such a construction refers to the individual aspiration for the highest sensitivity to detect the disorder without a false alarm. The Nash equilibrium fulfills the requirement that nobody deviates from the equilibrium strategy, otherwise its expected risk will be higher.

The proposed model disregards the correlation of the signals. It is also assumed that the fusion center has complete information about the signals and that the information is available at each node. The method of a cooperative game was used in [4] to find the best coalition of sensors in the problem of the target localization. The approach which is proposed in the study shows the possibility of modeling the detection problem by multiple agents at a general level.

Acknowledgements The author would like to thank the Isaac Newton Institute for Mathematical Sciences, Cambridge, for support and hospitality during the programme "Inference for Change-Point and Related Processes", where a part of the work on this paper was undertaken.

References

1. Bojdecki T (1979) Probability maximizing approach to optimal stopping and its application to a disorder problem. Stochastics 3:61–71
2. Brodsky B, Darkhovsky B (1993) Nonparametric methods in change-point problems. Mathematics and its applications, vol 243. Kluwer Academic, Dordrecht
3. Ferguson TS (2005) Selection by committee. In: Nowak A, Szajowski K (eds) Advances in dynamic games. Ann Internat Soc Dynam Games, vol 7. Birkhäuser, Boston, pp 203–209
4. Gharehshiran ON, Krishnamurthy V (2010) Coalition formation for bearings-only localization in sensor networks—a cooperative game approach. IEEE Trans Signal Process 58(8):4322–4338

5. Kurano M, Yasuda M, Nakagami J (1980) Multi-variate stopping problem with a majority rule. J Oper Res Soc Jpn 23:205–223
6. Mei Y (2006) Comments on: "A note on optimal detection of a change in distribution", by Benjamin Yakir. Ann Stat 34(3):1570–1576
7. Moustakides GV (1998) Quickest detection of abrupt changes for a class of random processes. IEEE Trans Inf Theory 44(5):1965–1968
8. Nash J (1951) Non-cooperative game. Ann Math 54(2):286–295
9. Owen G (1995) Game theory, 3rd edn. Academic Press, San Diego
10. Peskir G, Shiryaev A (2006) Optimal stopping and free-boundary problems. Lectures in mathematics. ETH, Zürich
11. Raghavan V, Veeravalli VV (2010) Quickest change detection of a Markov process across a sensor array. IEEE Trans Inf Theory 56(4):1961–1981
12. Sarnowski W, Szajowski K (2011) Optimal detection of transition probability change in random sequence. Stochastics 83(4–6):569–581
13. Shiryaev A (1961) The detection of spontaneous effects. Sov Math Dokl 2:740–743. Translation from Dokl Akad Nauk SSSR 138:799–801 (1961)
14. Shiryaev A (1978) Optimal stopping rules. Springer, New York
15. Szajowski K (1992) Optimal on-line detection of outside observations. J Stat Plan Inference 30:413–422
16. Szajowski K, Yasuda M (1996) Voting procedure on stopping games of Markov chain. In: Christer AH, Osaki S, Thomas LC (eds) UK-Japanese res workshop on stoch. Modelling in innovative manufacturing, Moller Centre, Churchill College, Univ. Cambridge, UK, 21–22 July, 1995. LN in Econ and Math Sys, vol 445. Springer, Cambridge, pp 68–80
17. Szajowski K (2011) Multi-variate quickest detection of significant change process. In: Baras JS, Katz J, Altman E (eds) Decision and game theory for security. Second int conf, GameSec 2011, College Park, MD, USA, 14–15 Nov., 2011. LN in comp sci, vol 7037. Springer, Berlin, pp 56–66
18. Tartakovsky AG, Rozovskii BL, Blažek RB, Kim H (2006) Detection of intrusions in information systems by sequential change-point methods. Stat Methodol 3(3):252–293
19. Tartakovsky AG, Veeravalli VV (2008) Asymptotically optimal quickest change detection in distributed sensor systems. Seq Anal 27(4):441–475
20. Yakir B (1992) Optimal detection of a change in distribution when the observations form a Markov chain with a finite state space. In: Carlstein E, Müller HG, Siegmund D (eds) Change-point problems. IMS LN-monograph series, vol 23. Papers from the AMS-IMS-SIAM Summer Res Conf held at Mt Holyoke College, South Hadley, MA, USA, 11–16 July, 1992. IMS, Hayward, pp 346–358
21. Yoshida M (1983) Probability maximizing approach for a quickest detection problem with complocated Markov chain. J Inf Optim Sci 4:127–145

Chapter 22
Changepoint Inference for Erdős–Rényi Random Graphs

Elena Yudovina, Moulinath Banerjee, and George Michailidis

Abstract We formulate a model for the off-line estimation of a changepoint in a network setting. The framework naturally allows the parameter space (network size) to grow with the number of observations. We compute the signal-to-noise ratio detectability threshold, and establish the dependence of the rate of convergence and asymptotic distribution on the network size and parameters. In addition, we show that inference can be adaptive, i.e. asymptotically correct confidence intervals can be computed based on the data. We apply the method to the question of whether US Congress has abruptly become more polarized at some point in recent history.

22.1 Introduction

The problem of estimating the location of a jump discontinuity (*changepoint*) has been extensively studied in the statistics literature. There are two versions of the problem. The *on-line* version is concerned with the quickest detection of a changepoint in the parameters of a dynamic stochastic system, and is closely related to classical problems in sequential analysis; for a comprehensive treatment, together with a discussion of important applications, see the books by Siegmund [18], Basseville and Nikiforov [1], and the review article by Lai [12] and references therein. In the *off-line* version, data are available for n covariate-response pairs, and one is interested in estimating the location of the changepoint as accurately as possible

E. Yudovina (✉)
Department of Mathematics, University of Minnesota, 127 Vincent Hall, 206 Church St. S.E., Minneapolis, MN 55455, USA
e-mail: eyudovin@umn.edu

M. Banerjee · G. Michailidis
Department of Statistics, University of Michigan, 439 West Hall, 1085 South University, Ann Arbor, MI 48109, USA

M. Banerjee
e-mail: moulib@umich.edu

G. Michailidis
e-mail: gmichail@umich.edu

A. Steland et al. (eds.), *Stochastic Models, Statistics and Their Applications*,
Springer Proceedings in Mathematics & Statistics 122,
DOI 10.1007/978-3-319-13881-7_22

(see Ritov [17], Müller [15], Loader [13], Gijbels, Hall and Kneip [6], Hall and Molchanov [7], Kosorok and Song [11], and the book by Csörgő and Horváth [4]). The on-line version is also closely related to many developments in statistical process control (Hawkins et al. [8]) and associated control charts (e.g. Cumulative Sums (CUSUM), Exponential Weighted Moving Average (EWMA), etc.). However, both versions of the problem have dealt primarily with low- (usually one-) dimensional problems. Although there have been some extensions to multivariate data, they are usually obtained under an assumption of multivariate normality that gives rise to Hotelling's T^2 test.

In this paper, we consider the off-line version in a high-dimensional network setting. Data are indexed by the edges of a graph; in the simplest case, binary data indicate whether the edge is present. We consider edges which evolve independently, so that at each point in time the network looks like an Erdős–Rényi random graph. This is a fundamental problem in changepoint analysis on networks, and already presents technical challenges. As graph size grows, we acquire more data about the changepoint, but have to deal with a higher-dimensional nuisance parameter space; this interaction is the main technical focus of the paper. We obtain the limiting distributions of the maximum likelihood estimates of both the changepoint and the remaining model parameters; although the asymptotic distribution for the changepoint estimate depends on the (unknown) signal-to-noise ratio, we develop an adaptive inference framework that does not require prior information about the limiting regime. Many of our results generalize those known for finite-dimensional models, although to our knowledge the focus on adaptive inference is new.

As a motivating application, we consider the question of whether the US Congress has abruptly become more polarized at some point in recent history. This question has raised a lot of interest in the political science literature; see for example [14, 16]. These works were primarily exploratory in nature, and no attempt was made to make inferences regarding the polarization process. Within the framework of our network-based approach, we use roll call vote data to generate a sequence of graphs, with vertices corresponding to congressmen and edges corresponding to whether they voted in the same way on a particular issue. We are then able to make inference about any changepoints in voting pattern.

Due to space constraints, we skip most of the details. A more extensive version of the paper is in preparation.

22.2 Network Changepoint Model and Estimators

Consider a sequence of random graphs indexed by n. Each graph has $m = m(n)$ potential edges; we allow $m(n)$ to grow with n. Each edge has a *state* $\alpha \in \mathscr{S}$; for simplicity, in this note we take $\mathscr{S} = \{0, 1\}$, but the model readily extends to arbitrary common finite state space. We assume that the underlying graphs are embedded into each other, so that it makes sense to speak of "edge 1 of system n". The edges evolve in discrete time; each edge evolves as a Markov chain with its own transition kernel,

independently of all the other edges. Consequently, at each time point the state of the system is an Erdős–Rényi random graph (with different, time-varying, probabilities for each edge). We assume that edges transition according to one set of transition kernels $\{P_k^*,\ 1 \le k \le m(n)\}$ before a time t^*, the *changepoint*, and according to another set of transition kernels $\{Q_k^*,\ 1 \le k \le m(n)\}$ after t^*. The changepoint t^*, as well as the matrices P_k^* and Q_k^*, may depend on n; but note that t^* is the same for all the edges. We may also have $P_k^* = Q_k^*$ for some edges, i.e. the changepoint may only affect a subset of the edges in the graph. For convenience, we will rescale time so that $t^* \in [0, 1]$.

We make n observations of the graph indexed by n, at times $\{\frac{i}{n},\ i = 1, \ldots, n\}$. This means that in the nth experiment, $t^* = t^*(n) \in \{\frac{i}{n}\},\ i = 1, \ldots, n$. We will assume $t^*(n) \to t^0$ as $n \to \infty$, as well as $P_k^* \to P_k^0$ and $Q_k^* \to Q_k^0$ for each k. Below, we will frequently omit the dependence on n.

Let $\mathbf{1}_{k,\alpha\to\beta}(s)$ be the indicator of the event that edge k was in state α at time s and in state β at time $s+1$. The log-likelihood function for this model is

$$l_n^M(P, Q, t) = n^{-1}\left(\sum_{k=1}^{m}\sum_{\alpha,\beta\in\mathscr{S}}\left(\sum_{s=0}^{nt-1}\left(\mathbf{1}_{k,\alpha\to\beta}(s)\log(P_k)_{\alpha\beta}\right)\right.\right.$$
$$\left.\left.+\sum_{s=nt}^{n-1}\left(\mathbf{1}_{k,\alpha\to\beta}(s)\log(Q_k)_{\alpha\beta}\right)\right)\right). \tag{22.1}$$

If the changepoint were at t, we could write down the MLEs $\hat{P} = \hat{P}(t)$ and $\hat{Q} = \hat{Q}(t)$:

$$\left(\hat{P}_k(t)\right)_{\alpha\beta} = \frac{\sum_{s=0}^{nt-1}\mathbf{1}_{k,\alpha\to\beta}(s)}{\sum_{s=0}^{nt-1}\sum_{\gamma\in\mathscr{S}}\mathbf{1}_{k,\alpha\to\gamma}(s)},$$
$$\left(\hat{Q}_k(t)\right)_{\alpha\beta} = \frac{\sum_{s=nt}^{n-1}\mathbf{1}_{k,\alpha\to\beta}(s)}{\sum_{s=nt}^{n-1}\sum_{\gamma\in\mathscr{S}}\mathbf{1}_{k,\alpha\to\gamma}(s)}. \tag{22.2}$$

The MLE $\hat{t}$ can be obtained by iterating over $t \in [0, 1]$ (on the grid of discrete observation times), using the above form for $\hat{P}$ and $\hat{Q}$; in case of ties, we take the smallest maximizer.

Our main results will concern the asymptotic behavior of $\hat{P}$, $\hat{Q}$, and $\hat{t}$ as $n \to \infty$. Below, we describe the necessary assumptions on the behavior of the dimension $m(n)$, the "signal" $\sum_k \|P^* - Q^*\|_F$, and the values of true parameters. Here, $\|A\|_F = (\sum_{i,j} A_{ij}^2)^{1/2}$ is the Frobenius, or Hilbert–Schmidt, norm of the matrix A; and we write $\|P^* - Q^*\|_F^2 = \sum_k \|P_k^* - Q_k^*\|_F^2$.

Assumption 22.1

1. *The underlying parameters converge as follows.*
   a. *$m(n)$ is either constant $m(n) = m^0$ or else monotonically increasing to infinity.*

   b. $t^*(n) \to t^0$ *as* $n \to \infty$. (*For example, we could have* $t^*(n) = n^{-1}\lfloor nt^0 \rfloor$.)
   c. $P_k^*(n) \to P_k^0$ *and* $Q_k^*(n) \to Q_k^0$ *uniformly in* k.
2. *There exists a constant* $\varepsilon > 0$ (*which we need not know*) *such that, for each* k, *one of the following holds*: *either* $\|Q_k^0 - P_k^0\|_F > \varepsilon$, *or else* $Q_k^0 = P_k^0$.
3. *For each* n *and* k, *the transition matrices* $P_k^*(n)$ *and* $Q_k^*(n)$ *correspond to irreducible, aperiodic Markov chains with state space* $\mathscr{S}$. *There exists some known constant* $c > 0$ *such that* $t^* \in (c, 1-c)$, *and all entries of* P_k^* *and* Q_k^* *belong to* $(c, 1-c)$. (*The same is then true of* t^0, P_k^0, *and* Q_k^0.) *We will only consider estimates of the changepoint that fall within* $(c, 1-c)$.
4. *The number of edges* m *satisfies* $n^{-1/2}\log m(n) \to 0$.
5. *The signal-to-noise ratio satisfies* $\frac{n}{m}\sum_{k=1}^m \|P_k^* - Q_k^*\|_F^2 \to \infty$.

Remark 22.1 Assumption 22.1.3 implies that the Markov chains with transition kernels P_k^* and Q_k^* have uniformly bounded mixing times; in particular, observations $\mathbf{1}_{k,\alpha\to\beta}(\cdot)$ form a mixing sequence, with mixing coefficients bounded uniformly in k. For discussion of variants of the changepoint problem where the changepoint is very close to the edge of the interval, see for example [4, Theorem 1.5.3].

Assumption 22.1.4 implies that with high probability, all estimates $\hat{P}_k(t)$ and $\hat{Q}_k(t)$ will satisfy Assumption 22.1.3; and together with Assumption 22.1.2, it means that we will correctly identify which of the edges experienced a change at t^*. The requirement $n^{-1/2}\log m(n) \to 0$ still allows quite large graphs, e.g. we may have $m(n) = \exp(n^{1/4})$.

Assumption 22.1.5 asserts that the "average" per-edge signal $\|P_k^* - Q_k^*\|_F^2 \gg n^{-1}$. With finitely many edges ($m(n) = m^0$), this is necessary for detectability; when $m(n) \to \infty$, the necessary condition is very slightly weaker.

22.3 Results

We now present our main results. Theorem 22.1 addresses the rates of convergence of the estimators and their asymptotic distributions. Finally, Theorem 22.2 addresses the question of adaptive inference, that is, inferring the parameters of the asymptotic distribution from the data.

Because the exact formulae below get somewhat involved, we state only the qualitative form of the limiting processes and distributions. Full expressions for the parameters will be found in our forthcoming longer paper on the subject. The form of the result is qualitatively similar to finite-dimensional models, cf. [4, Chap. 1], although our model is considerably more general.

Theorem 22.1 (Rates of convergence and asymptotic distribution.) *Under Assumptions* 22.1.1 *through* 22.1.5, $n\|Q^* - P^*\|_F^2|\hat{t} - t^*| = O_P(1)$.

For any finite set of edges K *and simultaneously for all* $k \in K$, $n\|\hat{P}_k - P_k^*\|_F^2 = O_P(1)$ *and* $n\|\hat{Q}_k - Q_k^*\|_F^2 = O_P(1)$.

Define the local parameters $h_k^P = \sqrt{n}(P_k - P_k^*)$, $h_k^Q = \sqrt{n}(Q_k - Q_k^*)$. *For each* k, h_k^P *and* h_k^Q *are asymptotically normal*:

$$\big(h_k^P\big) \Longrightarrow N\big(0, \big(t^0\big)^{-1} V_k^P\big), \qquad h_k^Q \Longrightarrow N\big(0, \big(t^0\big)^{-1} V_k^Q\big),$$

where the $S^2 \times S^2$ *covariance matrices* V_k^P, V_k^Q *depend on* P_k^0, *respectively* Q_k^0. *For any fixed finite set* K *of edges, the estimates* $\{\hat{h}_k^P, \hat{h}_k^Q, \hat{t}\colon\ k \in K\}$ *are asymptotically independent.*

For the limiting distribution of $(\hat{t} - t^*)$, *we distinguish three cases, one of which is further subdivided*:

1. *If* $\|P^* - Q^*\|_F^2 \to \infty$, *then* $n(\hat{t} - t^*) \to 0$ *in probability. That is, asymptotically we precisely identify the index of the transition where the transition probability matrix changed.*
2. *If* $\|P^* - Q^*\|_F^2 \to 0$, *then*

$$n \sum_{k=1}^{m} \sum_{\alpha,\beta \in \mathscr{S}} \frac{(\pi_k^0)_\alpha}{(P_k^0)_{\alpha\beta}} \big((P_k^* - Q_k^*)_{\alpha\beta}\big)^2 \big(\hat{t} - t^*\big) \to \sigma^{-1} \arg\max_{h \in \mathbb{R}} \left(B(h) - \frac{1}{2}|h| \right),$$

   where $B(h)$ *is a standard Brownian motion, and* σ^2 *comes from the Markov chain central limit theorem* (*cf.* [10, *Case* 1 *of Theorem* 5]).
3. *If* $\|P^* - Q^*\|^2 \to C \in (0, \infty)$, *then* $n(\hat{t} - t^*)$ *converges to the* (*smallest*) *maximizer of a limiting jump process supported on* $\mathbb{Z}$: $n(\hat{t} - t^*) \to \arg\max_{h \in \mathbb{Z}} [M(h) + G(h) - D(h)]$. *Here,* D *is a deterministic triangular drift,* G *is a random walk with correlated Gaussian step sizes, and* M *is a functional of the Markov chain trajectories of some of the edges. Let* $\mathscr{I}_+ = \{k\colon\ P_k^0 \neq Q_k^0\}$ (*necessarily finite*); $M(\cdot)$ *depends only on the edges in* $\mathscr{I}_+$, *and* $D(\cdot)$ *and* $G(\cdot)$ *depend only on the remaining edges.*

Interestingly, the network size m does not appear in the scaling of $\hat{t} - t^*$; however, Assumption 22.1.5 places a lower bound on $\|Q^* - P^*\|_F^2$ that scales with m.

The proofs follow the approach of [20, Theorem 3.4.1], making extensive use of Doob's martingale maximal inequality (the use for Markov chains is somewhat unusual). The continuity of the argmax functional in Case 22.1.3 is non-standard. The high-dimensional nuisance parameter space makes it hard to apply many classical changepoint techniques, such as those in [4].

Lastly, we present a result which allows adaptive inference of the limiting distribution from the data, irrespective of the limiting regime that applies. This means that we can provide asymptotically correct quantile estimation of the distribution based only on the data, without knowledge of the true parameters. The adaptive process is essentially the one that appears in case 3 of Theorem 22.1 when $|\mathscr{I}_+| = m$.

Theorem 22.2 (Adaptive inference.) *Define the process* $\widetilde{M}(h)$ *as follows. Let* $\tilde{X}_k(h), h \geq 0$ *be the* reversed *Markov chain with initial distribution* $\hat{\pi}_k$ *and transition kernel* $\hat{\mathscr{P}}_k$, $(\hat{\mathscr{P}}_k)_{\alpha\beta} = \frac{(\hat{\pi}_k)_\beta}{(\hat{\pi}_k)_\alpha} (\hat{P}_k)_{\beta\alpha}$. *Here,* $(\hat{\pi}_k)_\alpha := \sum_{s=0}^{n\hat{t}-1} \sum_{\beta \in \mathscr{S}} \mathbf{1}_{k,\alpha\to\beta}(s)$

is the empirical proportion of time that edge k spends in state α up to time $\hat{t}$. Let $\tilde{Y}_k(h), h \geq 0$ be the (ordinary) Markov chain with initial distribution $\hat{\pi}_k$ and transition kernel $\hat{Q}_k$. For different values of k, let the Markov chains be independent; moreover, let $X_k(0) = Y_k(0)$ and let their transitions be independent otherwise. Define

$$\widetilde{M}(h+1) - \widetilde{M}(h) = \begin{cases} \sum_{k=1}^{m} \sum_{\alpha,\beta \in \mathscr{S}} \mathbf{1}_{\tilde{Y}_k, \alpha \to \beta}(h) \log \frac{(\hat{P}_k)_{\alpha\beta}}{(\hat{Q}_k)_{\alpha\beta}}, & h \geq 0, \\ \sum_{k=1}^{m} \sum_{\alpha,\beta \in \mathscr{S}} \mathbf{1}_{\tilde{X}_k, \beta \to \alpha}(|h|-1) \log \frac{(\hat{P}_k)_{\alpha\beta}}{(\hat{Q}_k)_{\alpha\beta}}, & h < 0. \end{cases}$$

Let $\tilde{h}$ be the smallest maximizer of $\widetilde{M}(\cdot)$. Then $\tilde{h}$ has the same asymptotic distribution as $n(\hat{t} - t^*)$, in the following sense:

1. *If $\|Q^* - P^*\|_F^2 \to \infty$, then both $\tilde{h} \to 0$ and $n(\hat{t} - t^*)$ in probability.*
2. *If $\|Q^* - P^*\|_F^2 \to 0$, then we have convergence in distribution for the renormalized estimate*:

$$\sum_{k=1}^{m} \sum_{\alpha,\beta \in \mathscr{S}} \frac{(\pi_k^0)_\alpha}{(P_k^0)_{\alpha\beta}} \left(\left(P_k^* - Q_k^*\right)_{\alpha\beta} \right)^2 \tilde{h} \to \sigma^{-1} \arg\max_{h \in \mathbb{R}} B(h) - \frac{1}{2}|h|,$$

   where $B(h)$ is a standard Brownian motion, and σ^2 is as in Theorem 22.1.
3. *If $\|Q^* - P^*\|_F^2 \to C \in (0, \infty)$, then $\tilde{h} \to \arg\max_{h \in \mathbb{Z}} [M(h) + G(h) - \frac{1}{2} D(h)]$, where $M(\cdot)$, $G(\cdot)$, and $D(\cdot)$ are as in Theorem 22.1.*

22.4 Application: Polarization in US Congress

We consider the question of whether the dynamics of discussion in the US Senate have experienced a changepoint in recent past. To construct the sequence of graphs as above, we identify the senators with senate seats (two per state, e.g. Michigan 1 and Michigan 2). We then consider 7949 roll call votes on bills during the years 1979–2012. The state of the edges of the (complete) graph on 100 vertices is then 1 if the corresponding senators voted in the same way on the issue, and 0 if they voted differently. The Markovian structure is, of course, an approximation of this data, but represents the fact that a particular pair of senators will tend to either agree or disagree on most issues. We note that while the occupants of a particular seat can change, this does not occur very often in practice, so the assumption that the parameters of the model are time-independent aside from the changepoint is not unreasonable.

In Fig. 22.1, we present the (profile) log-likelihood function for the location of the changepoint. We see broadly that the log-likelihood function reaches its maximum somewhere between the 104th and 107th Congresses, i.e. 1995–2003. (2003 corresponds to the Iraq war.) Within this interval, there are several local maxima; as the table to the right of Fig. 22.1 shows, which changepoint is dominant depends in particular on when data analysis starts. We can also examine the nature of the change

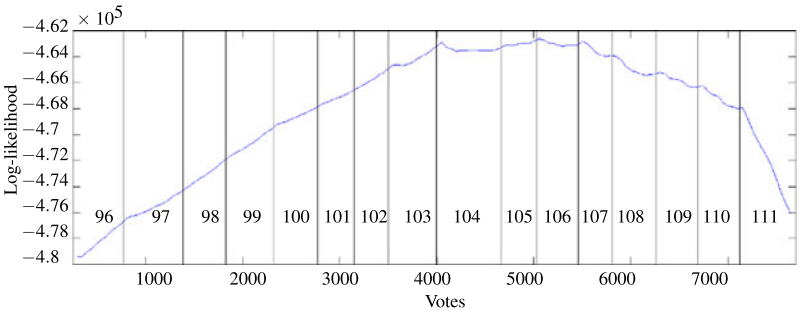

Year	Estimate	CI
1995	4025	(3995, 4152)
1999	5100	(5000, 5225)
2001	5850	(5775, 5875)

Fig. 22.1 Log-likelihood function for the senate roll call data. The *horizontal axis* is labelled with the index of the roll call vote; *vertical bands* identify the Congress, i.e. the two-year inter-election period. The table to the right presents the dominant changepoint as a function of the year when data collection begins

by examining the estimated transition parameters before and after the changepoint (in this case, before the 104th and after the 107th Congress). We do not show the graphs due to space constraints, but the average probability of changing the status of an edge decreases by almost a factor of 2, from approximately 0.2 to approximately 0.1, leading to longer negotiation times until a compromise is reached.

22.5 Discussion and Simulation Issues

We have presented a model which can address questions of changepoint inference in a networked setting. We begin by discussing several extensions of the model assumptions, and then discuss the computational complexity of the estimation.

Vertex Labels and Dependent Edges A natural extension to community structures is to add labels to the vertices (e.g. political party affiliation for the US Congress), and allow dependence among the edges. There are many possibilities for such extensions; some are the subject of future work.

Multiple Changepoints Although our research is only directly applicable under the assumption of exactly one changepoint, we may use techniques similar to the binary segmentation method of [3, 21] to find multiple changepoints. The basic idea is to locate the dominant changepoint, and keep looking in the two smaller subintervals around it; an extra elimination step may reduce the probability of finding too many changepoints. In general, estimating multiple changepoints is a challenging issue; we refer to the survey article [9] for a discussion of current approaches.

Computational Complexity When the signal-to-noise ratio is either quite large or quite small (Cases 22.1 and 22.2 of Theorem 22.1), computing $\hat{t}$ is the main computational challenge; the distribution of the maximizer of a Brownian motion with triangular drift, which appears in Case 22.2, can be computed precisely [2, 19]. In Case 22.3, which corresponds to the adaptive regime, the limiting process is easily simulated if $P^0 = Q^0$; see also Fotopoulos et al. [5] for computing the maximizer. However, even in the case of Gaussian jumps, there is not a universal scaling that can relate different examples to each other, in part due to the non-stationarity of the process. For the generalized binomial component of the limiting random process, it seems necessary to simulate the trajectories of all m Markov chains in order to estimate the maximizer; the computation is, however, parallelizable, and can scale up to fairly large networks.

Acknowledgements E.Y.'s research was partially supported by US NSF grant DMS-1204311. M.B.'s research was partially supported by US NSF DMS-1007751, US NSA H98230-11-1-0166, and a Sokol Faculty Award, University of Michigan. G.M.'s research was partially supported by US NSF DMS-1228164 and US NSA H98230-13-1-0241. The authors thank the referees for helpful comments.

References

1. Basseville M, Nikiforov IV (1993) Detection of abrupt changes: theory and application. Prentice Hall, Englewood Cliffs
2. Bhattacharya PK, Brockwell PJ (1976) The minimum of an additive process with applications to signal estimation and storage theory. Probab Theory Relat Fields 37(1):51–75
3. Cho H, Fryzlewicz P (2012) Multiple change-point detection for high-dimensional time series via sparsified binary segmentation. Preprint
4. Csörgő M, Horváth L (1997) Limit theorems in change-point analysis. Wiley, New York
5. Fotopoulos SB, Jandhyala VK, Khapalova E (2010) Exact asymptotic distribution of change-point MLE for change in the mean of Gaussian sequences. Ann Appl Stat 4(2):1081–1104
6. Gijbels I, Hall P, Kneip A (1999) On the estimation of jump points in smooth curves. Ann Inst Stat Math 51(2):231–251
7. Hall P, Molchanov I (2003) Sequential methods for design-adaptive estimation of discontinuities in regression curves and surfaces. Ann Stat 31(3):921–941
8. Hawkins DM, Qiu P, Kang CW (2003) The changepoint model for statistical process control. J Qual Technol 35(4):355–366
9. Jandhyala V, Fotopoulos S, MacNeill I, Liu P (2013) Inference for single and multiple change-points in time series. J Time Ser Anal 34(4):423–446
10. Jones GL (2004) On the Markov chain central limit theorem. Probab Surv 1:299–320
11. Kosorok MR, Song R (2007) Inference under right censoring for transformation models with a change-point based on a covariate threshold. Ann Stat 35(3):957–989
12. Lai TL (2001) Sequential analysis: some classical problems and new challenges. Stat Sin 11(2):303–350
13. Loader CR (1996) Change point estimation using nonparametric regression. Ann Stat 24(4):1667–1678
14. Moody J, Mucha PJ (2013) Portrait of political party polarization. Netw Sci 1(01):119–121
15. Müller HG (1992) Change-points in nonparametric regression analysis. Ann Stat 20(2):737–761

16. Poole KT, Rosenthal H (1997) Congress: a political-economic history of roll call voting. Oxford University Press, Oxford
17. Ritov Y (1990) Asymptotic efficient estimation of the change point with unknown distributions. Ann Stat 18(4):1829–1839
18. Sigmund D (1985) Sequential analysis: tests and confidence intervals. Springer, New York
19. Stryhn H (1996) The location of the maximum of asymmetric two-sided Brownian motion with triangular drift. Stat Probab Lett 29(3):279–284
20. van der Vaart AW, Wellner JA (1996) Weak convergence and empirical processes. Springer, New York
21. Yu VL (1981) Detecting disorder in multidimensional random processes. Sov Math Dokl 23:55–59

Chapter 23
Quasi-maximum Likelihood Estimation of Periodic Autoregressive, Conditionally Heteroscedastic Time Series

Florian Ziel

Abstract We consider a general multivariate periodically stationary and ergodic causal time series model. We prove consistency and asymptotic normality of the quasi-maximum likelihood (QML) estimator of it. Applications to the multivariate nonlinear periodic AR(∞)–ARCH(∞) process are shown.

23.1 Introduction

We introduce a very general multivariate causal periodic time series model that is based on the model from [1]. It is completely nested into their model and can be seen as a periodic generalisation. Moreover, it provides a lot of relevant special cases, such as the multivariate periodic nonlinear-AR(∞)–ARCH(∞) process, which includes a lot of important special cases such as the periodic versions the ARMA-GARCH model. As [1] or [4] we consider the conditional Gaussian qausi-likelihood estimation, as it provides a powerful technique even if the underlying residuals are non-normally distributed.

The main result of this paper is the consistency and asymptotic normality of the QML estimator. We even relax the conditions for the asymptotic normality in comparison to the non-periodic case of [1]. Then we discuss applications to the multivariate, periodic non-linear AR(∞)–ARCH(∞) process.

23.2 Considered Time Series Model and Likelihood

Let a multivariate time series $Y := (Y_t)_{t\in\mathbb{Z}}$ taking values in $(\mathbb{R}^m)^{\mathbb{Z}}$ be given and denote by $\mathscr{Y}_t := (Y_t, Y_{t-1}, \ldots)$ the full past of the time series Y at t. Moreover, we introduce an $S \in \mathbb{N}$, that refers to the periodicity of Y, and define $\tilde{s}(t) = t \bmod S$ with mod as modulo operation. Note that for each t the function $\tilde{s}(t)$ provides the corresponding season at time t. We denote the set of all seasons $\{0, \ldots, S-1\}$ by $\mathbb{S}$.

F. Ziel (✉)
Europa-Universität Viadrina, Frankfurt (Oder), Germany
e-mail: ziel@europa-uni.de

A. Steland et al. (eds.), *Stochastic Models, Statistics and Their Applications*,
Springer Proceedings in Mathematics & Statistics 122,
DOI 10.1007/978-3-319-13881-7_23

Now assume that Y is a causal S-periodically stationary solution of

$$Y_t = f_\theta^{\tilde{s}(t)}(\mathscr{Y}_{t-1}) + M_\theta^{\tilde{s}(t)}(\mathscr{Y}_{t-1})Z_t, \tag{23.1}$$

where $f_\theta^s(\mathscr{Y}_{t-1}) \in \mathbb{R}^m$ is a mean vector and $M_\theta^s(\mathscr{Y}_{t-1}) \in \mathbb{R}^{m\times p}$ a variance matrix with almost surely full rank m for all $s \in \mathbb{S}$. Note that in the functions f_θ^s and M_θ^s we use the θ and s as index. Further we assume that the parameter vector θ is d-dimensional and the innovations sequence $(Z_t)_{t\in\mathbb{Z}} \in (\mathbb{R}^p)^{\mathbb{Z}}$ is i.i.d. with $\mathbb{E}Z_t = 0$ and $\mathbb{E}Z_t Z_t^\top = \operatorname{cov}(Z_t, Z_t) = I_p$.

We can simplify our notation, as for all $t \in \mathbb{Z}$ there only $\tilde{s}(t) = s \in \mathbb{S}$ influences Y_t depending on $\mathscr{Y}_{t-1}$. Thus we can define f_θ and M_θ dependent on $\mathscr{Y}_{t-1}$ by $f_\theta(\mathscr{Y}_{t-1}) := f_\theta^s(\mathscr{Y}_{t-1})$ if $\tilde{s}(t) = s$ and $M_\theta(\mathscr{Y}_{t-1}) := M_\theta^s(\mathscr{Y}_{t-1})$ if $\tilde{s}(t) = s$.

Note that in this notation f_θ and M_θ are functions of t as well. Now model (23.1) turns to

$$Y_t = f_\theta(\mathscr{Y}_{t-1}) + M_\theta(\mathscr{Y}_{t-1})Z_t, \tag{23.2}$$

without explicit denoting of the periodic dependency structure. This matches exactly the notation as used in [1]. We use the definition of periodic stationary and ergodicity in the strict sense, for more details see e.g. [2] for a recent summary. For us it is important that a process $(X_t)_{t\in\mathbb{Z}}$ is periodically stationary with periodicity S if all its subsequences $(X_{k+sS})_{k\in\mathbb{Z}}$ with $s \in \mathbb{S}$ are stationary. Additionally periodic stationarity and periodic ergodicity is preserved under measurable periodic mappings.

Now we consider the conditional quasi-maximum likelihood (QML) estimation for the unknown parameter vector θ. Henceforth denote Θ the parameter space of θ and define $H_\theta := M_\theta M_\theta^\top$. Then under normality assumption to $(Z_t)_{t\in\mathbb{Z}}$ the conditional Gaussian QML is given by

$$\begin{aligned} L_n(\theta, \mathscr{Y}_{n-1}) &:= \frac{-1}{2}\sum_{t=0}^{n-1} \ell(\theta; \mathscr{Y}_t) \quad \text{with} \\ \ell(\theta, \mathscr{Y}_t) &:= \log\big(\det\big(H_\theta(\mathscr{Y}_{t-1})\big)\big) + \big(Y_t - f_\theta(\mathscr{Y}_{t-1})\big)^\top \\ &\quad \times H_\theta(\mathscr{Y}_{t-1})^{-1}\big(Y_t - f_\theta(\mathscr{Y}_{t-1})\big) \end{aligned} \tag{23.3}$$

for $\theta \in \Theta$ up to an additional constant. Note that L_n depends on $\mathscr{Y}_{n-1}$, not on $\mathscr{Y}_n$. Anyway L_n in (23.3) is a sum over n summands as we start indexing by 0. Thus Y_0 is in the first season 0, which will be our first observable random variable.

Now let a sequence $y = (y_t)_{t\in\mathbb{N}} \in (\mathbb{R}^m)^{\mathbb{N}}$ be given such that $y_t = 0$ for all sufficiently large t. Then we denote $\widetilde{\mathscr{Y}}_t := (Y_t, \ldots, Y_0, y)$ by the sequence $\mathscr{Y}_t = (Y_t, Y_{t-1}, \ldots)$ where we replace the unobservable past $(Y_{-1}, Y_{-2}, \ldots)$ by the given initial sequence y. Using the plug-in principle we define the (conditional) QML estimator of θ by $\widehat{\theta}_n := \widehat{\theta}_n(\widetilde{\mathscr{Y}}_{n-1}) := \operatorname{argmax}_{\theta\in\Theta} L_n(\theta, \widetilde{\mathscr{Y}}_{n-1})$. Note that $\widehat{\theta}_n(\mathscr{Y}_{n-1})$ would provide the exact conditional maximum likelihood. In the next section we analyse the asymptotic behaviour of the QML estimator $\widehat{\theta}_n$.

23.2.1 Consistency and Asymptotic Normality of the QML Estimator

From [1] we know the conditions of a general class of causal processes for receiving consistency and asymptotic normality of the QML estimator. We can adjust their results so that we can apply them to the given seasonal model. Therefore let $\Theta \subseteq \mathbb{R}^d$ be a compact and denote $\|\cdot\|_\Theta$ denotes the Euclidean uniform norm restricted to Θ. We require the following conditions for the strong consistency and asymptotic normality:

(C1(Θ)) For all $s \in \mathbb{S}$, $x, y \in (\mathbb{R}^m)^{\mathbb{N}_0}$ we assume a Lipschitz condition in f_θ and M_θ

$$\begin{cases} \left\| f_\theta^s(x) - f_\theta^s(y) \right\|_\Theta \le \sum_{j=1}^{\infty} \alpha_j^s(f, \Theta) \|x_j - y_j\|, \\ \left\| M_\theta^s(x) - M_\theta^s(y) \right\|_\Theta \le \sum_{j=1}^{\infty} \alpha_j^s(M, \Theta) \|x_j - y_j\|, \end{cases}$$

with $\sum_{j=1}^{\infty} \alpha_j^s(f, \Theta) < \infty$ and $\sum_{j=1}^{\infty} \alpha_j^s(M, \Theta) < \infty$ for all $s \in \mathbb{S}$.

(C2) Additionally define the set of parameters $\Theta(r) := \bigcap_{s\in\mathbb{S}} \Theta_s(r)$ with

$$\Theta_s(r) := \Bigg\{ \theta \in \mathbb{R}^d \Big| \mathbf{C1}\big(\{\theta\}\big) \text{ holds}, \\ \sum_{j=1}^{\infty} \alpha_j^s\big(f, \{\theta\}\big) + \big(\mathbb{E}\|Z_0\|^r\big)^{\frac{1}{r}} \sum_{j=1}^{\infty} \alpha_j^s\big(M, \{\theta\}\big) < 1 \Bigg\}.$$

(C3(Θ)) There exists $\underline{H} > 0$ such that $\inf_{\theta\in\Theta} \det(H_\theta^s(x)) > \underline{H}$ for all $s \in \mathbb{S}$ and $x \in (\mathbb{R}^m)^{\mathbb{N}_0}$.

(C4(Θ)) We need an identification condition for the true parameter θ_0. So for all $\theta \in \Theta$ we have:

$$\big(\forall s \in \mathbb{S}\colon\ f_\theta^s(\mathscr{Y}_t) = f_{\theta_0}^s(\mathscr{Y}_t) \text{ and } H_\theta^s(\mathscr{Y}_t) = H_{\theta_0}^s(\mathscr{Y}_t)\big) \quad \Rightarrow \quad \theta = \theta_0.$$

(AN1(Θ)) The functions $\theta \in \Theta \mapsto f_\theta(x)$ and $\theta \in \Theta \mapsto M_\theta(x)$ are twice continuously differentiable for all $x \in (\mathbb{R}^m)^{\mathbb{N}_0}$ with

$$\left\| \frac{\partial f_\theta^s}{\partial\theta}(0) \right\|_\Theta + \left\| \frac{\partial^2 f_\theta^s}{\partial\theta\partial\theta}(0) \right\|_\Theta + \left\| \frac{\partial M_\theta^s}{\partial\theta}(0) \right\|_\Theta + \left\| \frac{\partial^2 M_\theta^s}{\partial\theta\partial\theta}(0) \right\|_\Theta < \infty$$

for all $s \in \mathbb{S}$. Moreover we have Lipschitz conditions to the derivatives of f_θ^s and M_θ^s. So for $s \in \mathbb{S}$, $g_\theta \in \{f_\theta^s, M_\theta^s\}$ and $i \in \{1, 2\}$ there are sequences $\{\alpha_j^{(i)}(g_\theta, \Theta)\}_{j\in\mathbb{N}_0}$ such that for all $x, y \in (\mathbb{R}^m)^{\mathbb{N}_0}$

$$\left\| \frac{\partial^i g_\theta}{\partial^i \theta}(x) - \frac{\partial^i g_\theta}{\partial^i \theta}(y) \right\|_\Theta \le \sum_{j=1}^{\infty} \alpha_j^{(i)}(g_\theta, \Theta) \|x_j - y_j\|.$$

(AN2) Either $\left(\frac{\partial f_{\theta_0}(\mathscr{Y}_t)}{\partial \theta_i}\right)_{i\in\{1,\dots,d\}}$ or $\left(\frac{\partial H_{\theta_0}(\mathscr{Y}_t)}{\partial \theta_i}\right)_{i\in\{1,\dots,d\}}$ is almost everywhere linearly independent.

Note that **(C2)** defines directly the set $\Theta(r)$ for a given r if **(C1(Θ))** is satisfied for some Θ. Now similarly to [1] we get with these conditions the unique existence of a solution to Y of (23.1), such as consistency and asymptotic normality of the QML estimator $\widehat{\theta}_n$:

Theorem 23.1 *Let* **(C1(Θ))** *to* **(C4(Θ))** *be satisfied for $r \geq 2$ and let $\Theta \subseteq \mathbb{R}^d$ be compact. Further let $\theta_0 \in \Theta(r) \cap \Theta$. If*

$$\sum_{s\in\mathbb{S}} \alpha_j^s(f,\Theta) + \alpha_j^s(M,\Theta) = \mathscr{O}\left(j^{-l}\right) \quad \text{for some } l > \gamma_r \text{ where } \gamma_r := \max\left\{3r^{-1}, 1\right\} \tag{23.4}$$

holds then we have that there is a unique S-periodically stationary and periodically ergodic solution $Y = (Y_t)_{t\in\mathbb{Z}}$ of model (23.1) with $\mathbb{E}\|Y_0\|^r < \infty$ and $\widehat{\theta}_n$ is strongly consistent, so $\widehat{\theta}_n \to \theta_0$ a.s.

If additionally $r \geq 4$, $\theta_0 \in$ interior$(\Theta) \cap \Theta(r)$, **(AN1(Θ))** *and* **(AN2)** *hold with*

$$\alpha_j^{(1)}(f,\Theta) + \alpha_j^{(1)}(M,\Theta) = \mathscr{O}\left(j^{-l_1}\right) \quad \text{for some } l_1 > 1 \tag{23.5}$$

then $\sqrt{n}(\widehat{\theta}_n - \theta_0) \to N(0, A(\theta_0)^{-1}B(\theta_0)A(\theta_0)^{-1})$ holds in distribution. The matrices $A(\theta_0)$ and $B(\theta_0)$ are defined in Eqs. (23.9) and (23.10), respectively.

Note that for $r = 2$ and $S = 1$ (which implies $l > \frac{3}{2}$) Theorem 23.1 is exactly the same as in [1] regarding the consistency. For $r > 2$ we relaxed the condition (23.4). So for example for all $r \geq 3$ we need only $l > 1$ for the consistency. This holds as well for the corresponding condition for the asymptotic normality. Here [1] required $l_1 > \frac{3}{2}$, too.

Proof We may follow [1] and [3]. The proof consists of three steps. First we show the existence of a periodically stationary and ergodically stationary solution in the sense of [2]. Then we establish the consistency. Lastly, a proof of the asymptotic normality is given.

Similarly to [1] we represent the model (23.1) by

$$Y_t = F^{\tilde{s}(t)}(\mathscr{Y}_{t-1}, Z_t) = f_\theta^{\tilde{s}(t)}(\mathscr{Y}_{t-1}) + M_\theta^{\tilde{s}(t)}(\mathscr{Y}_{t-1})Z_t$$

for all $t \in \mathbb{Z}$. Similarly as for f_θ and M_θ we can define F dependent on $\mathscr{Y}_{t-1}$ by

$$F(\mathscr{Y}_{t-1}) := \left\{F^s(\mathscr{Y}_{t-1}), \quad \tilde{s}(t) = s\right.$$

We want to apply a modification of Theorem 3.1 in [3]:

Lemma 23.1 *Assume that the following statements hold for $r \geq 2$:*

1. $\mathbb{E}\|F^s(\mathbf{0}, Z_0)\|^r < \infty$ *for all* $s \in \mathbb{S}$

2. $(\mathbb{E}\|F^s(x,Z_0)-F^s(y,Z_0)\|^r)^{\frac{1}{r}} < \sum_{j=1}^{\infty} a_j^s \|x_j - y_j\|$ *with* $\sum_{j=1}^{\infty} a_j^s < 1$ *for all* $s \in \mathbb{S}$, $x, y \in (\mathbb{R}^m)^{\mathbb{N}_0}$.

Then there exist a periodically stationary and ergodic solution $(Y_t)_{t\in\mathbb{Z}}$ *of* (23.1).

The proof of this lemma is skiped here, but uses similar methods as [3]. Furthermore it is clear that $\mathbb{E}\|F^s(0,Z_0)\| < \infty$ as $\mathbb{E}\|Z_0\|^r < \infty$.

The main problem for showing the consistency of the QLME estimator is to show that $\frac{1}{n}\|L_n(\cdot,\widetilde{\mathscr{Y}}_{n-1}) - L_n(\cdot,\mathscr{Y}_{n-1})\|_\Theta$ converges almost surely to 0 as $n\to\infty$. Hence denote $\widehat{L}_n := L_n(\cdot,\widetilde{\mathscr{Y}}_{n-1})$ and $L_n := L_n(\cdot,\mathscr{Y}_{n-1})$.

Given the existence of a periodically stationary and periodically ergodic solution $Y = (Y_t)_{t\in\mathbb{Z}}$ to model (23.1) we know that $(\ell(\theta,\mathscr{Y}_t))_{t\in\mathbb{Z}}$ is periodically stationary and periodically ergodic as well. Further note that $\ell^s(\theta) := (\ell(\theta,\mathscr{Y}_{kS+s}))_{k\in\mathbb{Z}}$ is stationary ergodic for $s\in\mathbb{S}$. Now we want to apply the uniform strong law of large numbers as in [5] to ℓ respectively their subsequences. From **(C3(Θ))** and $\log(x) \le x-1$ for $x>0$ we get immediately that for $s\in\mathbb{S}$

$$\begin{aligned}\left|\ell(\theta,\mathscr{Y}_{t-1})\right| &\le \left|\log\left(\left\|H_\theta^{\tilde{s}(t)}(\mathscr{Y}_{t-1})\right\|^m\right)\right| + \underline{H}^{\frac{-1}{m}}\left\|Y_t - f_\theta^{\tilde{s}(t)}(\mathscr{Y}_{t-1})\right\|^2 \\ &\le m\left|\max_{s\in\mathbb{S}}\left\|H_\theta^s(\mathscr{Y}_{t-1})\right\| - 1\right| + \underline{H}^{\frac{-1}{m}}\max_{s\in\mathbb{S}}\left\|Y_t - f_\theta^s(\mathscr{Y}_{t-1})\right\|^2\end{aligned}$$

holds for all $\theta\in\Theta$. So we can deduce that

$$\left\|\ell(\theta,\mathscr{Y}_{t-1})\right\|_\Theta \le m\max_{s\in\mathbb{S}}\left\|H_\theta^s(\mathscr{Y}_{t-1})\right\|_\Theta + m + \underline{H}^{\frac{-1}{m}}\max_{s\in\mathbb{S}}\left\|Y_t - f_\theta^s(\mathscr{Y}_{t-1})\right\|_\Theta^2 < \infty$$

as with **(C1(Θ))** and Lemma 1 from [1] we have that $\mathbb{E}\|f_\theta^s\|_\Theta^2 < \infty$ and $\mathbb{E}\|H_\theta^s\|_\Theta < \infty$ for all $s\in\mathbb{S}$. Hence we have $\mathbb{E}\|\ell(\theta,\mathscr{Y}_{t-1})\|_\Theta < \infty$. Consequently the we can apply the uniform strong law of large numbers on the subsequences ℓ^s of ℓ.

$$\begin{aligned}L_{nS}(\cdot,\mathscr{Y}_{nS-1}) &= \frac{1}{nS}\sum_{t=0}^{nS-1}\ell(\cdot,\mathscr{Y}_{t-1}) = \frac{1}{S}\sum_{s\in\mathbb{S}}\frac{1}{n}\sum_{k=0}^{n-1}\ell(\cdot,\mathscr{Y}_{kS+s-1}) \\ &\to \quad \frac{1}{S}\sum_{s\in\mathbb{S}} L^s \text{ a.s. as } n\to\infty\end{aligned}$$

with respect to $\|\cdot\|_\Theta$ where $L^s(\theta) := \frac{-1}{2}\mathbb{E}\ell(\theta,\mathscr{Y}_s)$. If we denote $L(\theta) := \frac{1}{S}\times\sum_{s\in\mathbb{S}} L^s(\theta)$, we have $\|L_n(\theta,\mathscr{Y}_{n-1}) - L(\theta)\|_\Theta \to 0$ almost surely as $n\to\infty$. Now we want to show that $\frac{1}{n}\|\widehat{L}_n - L_n\|_\Theta \to 0$ almost surely. The beginning of this part to prove you can copy almost one to one from the corresponding part of the proof of Theorem 1 in [1] until we receive

$$\left\|\ell(\theta,\widetilde{\mathscr{Y}}_{t-1}) - \ell(\theta,\mathscr{Y}_{t-1})\right\|_\Theta \le C\,A_\theta(\mathscr{Y}_{t-1},\widetilde{\mathscr{Y}}_t)B_\theta(\mathscr{Y}_{t-1},\widetilde{\mathscr{Y}}_t)$$

where $A_\theta(\mathscr{Y}_{t-1},\widetilde{\mathscr{Y}}_t) := \|X_t\| + \|f_\theta(\widetilde{\mathscr{Y}}_t)\|_\Theta + \|f_\theta(\mathscr{Y}_t)\|_\Theta$ and $B_\theta(\mathscr{Y}_{t-1},\widetilde{\mathscr{Y}}_t) := \|H_\theta(\widetilde{\mathscr{Y}}_t) - H_\theta(\mathscr{Y}_t)\|_\Theta + \|f_\theta(\widetilde{\mathscr{Y}}_t) - f_\theta(\mathscr{Y}_t)\|_\Theta$. Now let $\delta\in(0,\frac{1}{3})$ and define now $\lambda_r(\delta) := \min\{\frac{r}{3}, 1-\delta\}$. With Hölder inequality applied to $p=3$ and $q=\frac{3}{2}$ and the previous inequality we get

$$\mathbb{E}\left\|\ell(\theta,\widetilde{\mathscr{Y}}_{t-1})-\ell(\theta,\mathscr{Y}_{t-1})\right\|_{\Theta}^{\lambda_r(\delta)}$$
$$\leq C\left(\mathbb{E}\left|A_\theta(\mathscr{Y}_{t-1},\widetilde{\mathscr{Y}}_t)\right|^{3\lambda_r(\delta)}\right)^{\frac{1}{3}}\left(\mathbb{E}\left|B_\theta(\mathscr{Y}_{t-1},\widetilde{\mathscr{Y}}_t)\right|^{\frac{3\lambda_r(\delta)}{2}}\right)^{\frac{2}{3}}$$

Now note that because of the definition of $\lambda_r(\delta)$ we have $3\lambda_r(\delta)\leq r$ resp. $\frac{3\lambda_r(\delta)}{2}\leq \frac{r}{2}$. Thus with Minkowski inequality, assumption **(C1(Θ))**, and Lemma 1 from [1] we obtain directly that

$$\mathbb{E}\left\|\ell(\theta,\widetilde{\mathscr{Y}}_{t-1})-\ell(\theta,\mathscr{Y}_{t-1})\right\|_{\Theta}^{\lambda_r(\delta)}\leq \tilde{C}\left(\sum_{t=j}^{\infty}\sum_{s\in\mathbb{S}}\alpha_j^s(f,\Theta)+\alpha_j^s(M,\Theta)\right)^{\lambda_r(\delta)} \tag{23.6}$$

for some $\tilde{C}>0$. Now we choose $\delta\in(0,\frac{1}{3})$ small enough such that $l>\lambda_r(\delta)^{-1}$ holds. Then with inequality (23.6) and condition (23.4) there exists a $C_0>0$ such that

$$t^{-\lambda_r(\delta)}\mathbb{E}\left\|\ell(\theta,\widetilde{\mathscr{Y}}_{t-1})-\ell(\theta,\mathscr{Y}_{t-1})\right\|_{\Theta}^{\lambda_r(\delta)}\leq C_0 t^{-l\lambda_r(\delta)}. \tag{23.7}$$

Now similarly to [1] we want to apply Kronecker's lemma on the sum $S_n:=\sum_{t=1}^n\frac{1}{t}\|\ell(\theta,\widetilde{\mathscr{Y}}_{t-1})-\ell(\theta,\mathscr{Y}_{t-1})\|_\Theta$ to deduce $\frac{1}{n}\|\widehat{L}_n-L_n\|_\Theta\to 0$ almost surely as $n\to\infty$. Therefore we have to show that $\lim_{n\to\infty}S_n<\infty$. Hence it is sufficient to show that for all $\varepsilon>0$ $P(A)=0$ holds where $A:=\bigcap_{n\in\mathbb{N}}\bigcup_{m\geq n}A_{m,n}$ with $A_{m,n}:=\{|S_m-S_n|>\varepsilon\}$. As $(A_{m,n})_{m>n}$ is increasing and $(\bigcup_{m\geq n}A_{m,n})_{n\in\mathbb{N}}$ is decreasing it follows that $\lim_{n\to\infty}\lim_{m\to\infty}P(A_{m,n})=\lim_{n\to\infty}P(\bigcup_{m\geq n}A_{m,n})=P(A)$. With the Markov inequality we receive

$$P(A_{m,n})=P\left(\sum_{t=n+1}^{m}\frac{1}{t}\left\|\ell(\theta,\widetilde{\mathscr{Y}}_{t-1})-\ell(\theta,\mathscr{Y}_{t-1})\right\|_\Theta>\varepsilon\right)$$
$$\leq\frac{1}{\varepsilon^{\lambda_r(\delta)}}\sum_{t=n+1}^{m}t^{-\lambda_r(\delta)}\mathbb{E}\left\|\ell(\theta,\widetilde{\mathscr{Y}}_{t-1})-\ell(\theta,\mathscr{Y}_{t-1})\right\|_{\Theta}^{\lambda_r(\delta)}$$

Hence with inequality (23.7) and the fact that $l\lambda_r(\delta)>1$ we can deduce that

$$\frac{1}{\varepsilon^{\lambda_r(\delta)}}\sum_{t=1}^{\infty}t^{-\lambda_r(\delta)}\mathbb{E}\left\|\ell(\theta,\widetilde{\mathscr{Y}}_{t-1})-\ell(\theta,\mathscr{Y}_{t-1})\right\|_{\Theta}^{\lambda_r(\delta)}<\frac{C_0}{\varepsilon^{\lambda_r(\delta)}}\sum_{t=n+1}^{m}t^{-\lambda_r(\delta)l}<\infty.$$

So we get that $\lim_{n\to\infty}\lim_{m\to\infty}P(A_{m,n})=0$, thus by Kronecker $\frac{1}{n}\|\widehat{L}_n-L_n\|_\Theta\to 0$ almost surely as $n\to\infty$. To show the consistency of $\widehat{\theta}_n$ it remains to show that L defined by $L(\theta)=\frac{-1}{2S}\sum_{s\in\mathbb{S}}\mathbb{E}\ell(\theta,\mathscr{Y}_s)$ has a unique maximum in θ_0. We can state that

$$L(\theta)-L(\theta_0)=\frac{-1}{2S}\sum_{s\in\mathbb{S}}\mathbb{E}\ell(\theta,\mathscr{Y}_s)-\mathbb{E}\ell(\theta_0,\mathscr{Y}_s) \tag{23.8}$$

From Proposition 2.1 in [6] and **(C4(Θ))** we can deduce that for all $s\in\mathbb{S}$ the function $\mathbb{E}\ell(\cdot,\mathscr{Y}_s)$, as limit of the stationary ergodic process $(L_{kS+s}(\theta,\mathscr{Y}_{kS+s-1}))_{k\in\mathbb{Z}}$, has a unique maximum in θ_0. Thus it follows immediately from Eq. (23.8) that L has its maximum in θ_0. So finally the strong consistency of $\widehat{\theta}_n$ is proved.

The proof of the asymptotic normality of $\widehat{\theta}_n$ is very similar to the case with $S = 1$ as in [1]. The main difference is that the martingale central limit theorem that has to be applied to the processes $(\frac{\partial \ell(\cdot, \mathscr{Y}_{kS+s})}{\partial \theta_j}(\theta_0))_{k\in\mathbb{Z}}$ for all $s \in \mathbb{S}$ with respect to the S-difference to receive that $(kS+s)^{-\frac{1}{2}} \frac{\partial L_{kS+s}(\cdot, \mathscr{Y}_{kS+s})}{\partial \theta}(\theta_0) \xrightarrow{d} N(0, B_s)$ with $B_s = (\mathbb{E}\frac{\partial \ell(\cdot, \mathscr{Y}_s)}{\partial \theta_i}(\theta_0)\frac{\partial \ell(\cdot, \mathscr{Y}_s)}{\partial \theta_j}(\theta_0))_{(i,j)\in\{1,\ldots,d\}^2}$ as $k \to \infty$. Moreover the relaxed conditions to the Lipschitz-conditions (see (23.5)) in comparison to [1] work with similar arguments as in the proof for the consistency as well for this proof. The parameters for the matrices $A(\theta) = (A(\theta)_{i,j})_{(i,j)\in\{1,\ldots,d\}^2}$ and $B(\theta) = (B(\theta)_{i,j})_{(i,j)\in\{1,\ldots,d\}^2}$ are given by

$$A(\theta)_{i,j} = \frac{1}{S}\sum_{s\in\mathbb{S}} \mathbb{E}\Bigg(2\bigg(\frac{\partial f_{\theta_0}^{s,s}}{\partial \theta_j}\bigg)^{\top}\big(H_{\theta_0}^{s,s}\big)^{-1}\frac{\partial f_{\theta_0}^{s,s}}{\partial \theta_j} + \operatorname{trace}\bigg(\big(H_{\theta_0}^{s,s}\big)^{-2}\frac{\partial H_{\theta_0}^{s,s}}{\partial \theta_i}\frac{\partial H_{\theta_0}^{s,s}}{\partial \theta_j}\bigg)\Bigg) \tag{23.9}$$

$$B(\theta)_{i,j} = \frac{1}{S}\sum_{s\in\mathbb{S}} \mathbb{E}\frac{\partial \ell(\cdot, \mathscr{Y}_s)}{\partial \theta_i}(\theta)\frac{\partial \ell(\cdot, \mathscr{Y}_s)}{\partial \theta_j}(\theta) \tag{23.10}$$

with

$$\begin{aligned}\frac{\ell(\cdot, \mathscr{Y}_s)}{\partial \theta_k}(\theta) = &-2\bigg(\frac{\partial f_{\theta_0}^{s,s}}{\partial \theta_k}\bigg)^{\top}\big(H_{\theta_0}^{s,s}\big)^{-1}\big(Y_t - f_{\theta}^{s,s}\big)\\ &+\big(Y_t - f_{\theta}^{s,s}\big)^{\top}\frac{\partial (H_{\theta_0}^{s,s})^{-1}}{\partial \theta_k}\big(Y_t - f_{\theta}^{s,s}\big) + \operatorname{trace}\bigg(\big(H_{\theta_0}^{s,s}\big)^{-1}\frac{\partial H_{\theta_0}^{s,s}}{\partial \theta_k}\bigg)\end{aligned}$$

where $f_{\theta}^{s,t} := f_{\theta}^{s}(\mathscr{Y}_t)$, $M_{\theta}^{s,t} := M_{\theta}^{s}(\mathscr{Y}_t)$ and $H_{\theta}^{s,t} := H_{\theta}^{s}(\mathscr{Y}_t)$.

□

23.3 Applications

Various time series models are of the form as given in Eq. (23.1). We can use the non-periodic results from [1] to apply the theory to their S-periodic equivalent. Therefore we have to remark that for all $s \in \mathbb{S}$ a non-periodic time series model is given by

$$Y_t = f_{\theta}^{s}(\mathscr{Y}_{t-1}) + M_{\theta}^{s}(\mathscr{Y}_{t-1})Z_t \tag{23.11}$$

with a periodicity of 1. The corresponding set of parameters from **(C2)** is $\Theta_s(r)$.

If we show that the models (23.11) satisfy all conditions of Theorem 23.1 for $\Theta_s(r)$ for all $s \in \mathbb{S}$, then we can deduce that the corresponding (pure) periodic model as in Eq. (23.1) satisfies all conditions of Theorem 23.1 for $\Theta(r)$. In [1] there are some examples of models given that satisfy the conditions of model (23.11), such

as the TARCH(∞), multivariate NLARCH(∞), multivariate GARCH or the multivariate non-linear AR(∞) model. So the corresponding periodic models satisfy the conditions of Theorem 23.1 as well.

There is an important general class of models that can be expressed as in Eq. (23.1), the periodic non-linear AR(∞)–ARCH(∞) processes. They are given by

$$Y_t = f_\theta^{\tilde{s}(t)}(\mathscr{Y}_{t-1}) + \varepsilon_t \quad \text{where } \varepsilon_t = \widetilde{M}_\theta^{\tilde{s}(t)}(\varepsilon_{t-1}, \varepsilon_{t-2}, \ldots) Z_t \tag{23.12}$$

for $\widetilde{M}_\theta^s(\varepsilon_{t-1}, \varepsilon_{t-2}, \ldots) \in \mathbb{R}^{m \times p}$ for $s \in \mathbb{S}$. Many models can be represented by (23.12), such as the periodic ARMA-GARCH models. They can be rewritten as in (23.1) by

$$Y_t = f_\theta^{\tilde{s}(t)}(\mathscr{Y}_{t-1}) + \widetilde{M}_\theta^{\tilde{s}(t)}\big(Y_{t-1} - f_\theta^{\tilde{s}(t)}(\mathscr{Y}_{t-2})\big) Z_t.$$

Assuming that the Lipschitz condition from **(C2)** holds for f_θ^s and $\widetilde{M}_\theta^s$ for all $s \in \mathbb{S}$, then we can conclude with the inverse triangle inequality that

$$\big\| M_\theta^s(x) - M_\theta^s(y) \big\|_\Theta \leq \sum_{j=1}^{\infty} \left(\alpha_j^s(\widetilde{M}, \Theta) + \sum_{k=1}^{\infty} \alpha_{j-k}^s(\widetilde{M}, \Theta) \alpha_k^s(f, \Theta) \right) \|x_j - y_j\|$$

holds for $x, y \in (\mathbb{R}^m)^{\mathbb{N}_0}$. So $\Theta(r)$ can be estimated by

$$\Theta(r) \supseteq \bigcap_{s \in \mathbb{S}} \left\{ \theta \in \mathbb{R}^d \,\middle|\, \sum_{j=1}^{\infty} \alpha_j^s\big(f, \{\theta\}\big) + \big(\mathbb{E}|Z_0|^r\big)^{\frac{1}{r}} \times \sum_{j=1}^{\infty} \left(\alpha_j^s\big(\widetilde{M}, \{\theta\}\big) + \sum_{k=1}^{\infty} \alpha_{j-k}^s\big(\widetilde{M}, \{\theta\}\big) \alpha_k^s\big(f, \{\theta\}\big) \right) < 1 \right\},$$

where we use only the Lipschitz constants of f_θ^s and $\widetilde{M}_\theta^s$. The theorem also generalises QML estimation results of [4] for the univariate ARMA-GARCH model, as they require $r \geq 2$ for consistency and $r \geq 4$ for asymptotic normality, as we do.

References

1. Bardet J-M, Wintenberger O (2009) Asymptotic normality of the quasi-maximum likelihood estimator for multidimensional causal processes. Ann Stat 37(5):2730–2759
2. Aknouche A, Al-Eid E (2012) Asymptotic inference of unstable periodic ARCH processes. Stat Inference Stoch Process 15:61–79
3. Doukhan P, Wintenberger O (2008) Weakly dependent chains with infinite memory. Stoch Process Appl 118(11):1997–2013
4. Aknouche A, Bibi A (2009) Quasi-maximum likelihood estimation of periodic GARCH and periodic ARMA-GARCH processes. J Time Ser Anal 40(1):19–46
5. Straumann D, Mikosch T (2009) Quasi-maximum likelihood estimation in conditionally heteroscedastic time series: a stochastic recurrence equations approach. Ann Stat 34(5):2449–2495
6. Jeantheau T (1998) Strong consistency of estimators for multivariate ARCH models. Econ Theory 14(1):70–86

Part III
Stochastic Models, Methods and Simulations

Chapter 24
Mixture and Non-mixture Cure Rate Model Considering the Burr XII Distribution

Emílio Augusto Coelho-Barros, Jorge Alberto Achcar, and Josmar Mazucheli

Abstract This paper presents estimates for the parameters included in long-term mixture and non-mixture lifetime models, applied to analyze survival data when some individuals may never experience the event of interest. We consider the case where the lifetime data have a three-parameter Burr XII distribution, which includes the popular Weibull mixture model as a special case.

24.1 Introduction

A long-term survivor mixture model, also known as standard cure rate model, assumes that the studied population is a mixture of susceptible individuals, who experience the event of interest and non susceptible individuals that will never experience it. These individuals are not at risk with respect to the event of interest and are considered immune, non susceptible or cured [9]. Following Maller and Zhou [9], the standard cure rate model assumes that a certain fraction p in the population is cured or never fail with respect to the specific cause of death or failure, while the remaining $(1 - p)$ fraction of the individuals is not cured, leading to the survival function for the entire population written as:

$$S(t) = p + (1 - p)S_0(t), \tag{24.1}$$

where $p \in (0, 1)$ is the mixing parameter and $S_0(t)$ denotes a proper survival function for the non cured group in the population. Considering a random sample of

E.A. Coelho-Barros
COMAT, Universidade Tecnológica Federal do Paraná, Cornélio Procópio, PR, Brazil
e-mail: eabarros@utfpr.edu.br

J.A. Achcar (✉)
DMS/FMRP, Universidade de São Paulo, Ribeirão Preto, SP, Brazil
e-mail: achcar@fmrp.usp.br

J. Mazucheli
DES, Universidade Estadual de Maringá, Maringá, PR, Brazil
e-mail: jmazucheli@uem.br

A. Steland et al. (eds.), *Stochastic Models, Statistics and Their Applications*,
Springer Proceedings in Mathematics & Statistics 122,
DOI 10.1007/978-3-319-13881-7_24

lifetimes $(t_i, \delta_i, i = 1, \ldots, n)$, under the assumption of right censored lifetime, the contribution of the ith individual for the likelihood function is:

$$L_i = \left[f(t_i)\right]^{\delta_i}\left[S(t_i)\right]^{1-\delta_i}, \tag{24.2}$$

where δ_i is a censoring indicator variable, that is, $\delta_i = 1$ for an observed lifetime and $\delta_i = 0$ for a censored lifetime.

From the mixture survival function, (24.1), the probability density function is obtained from $f(t_i) = -\frac{d}{dt}S(t_i)$ and given by:

$$f(t_i) = (1 - p) f_0(t_i), \tag{24.3}$$

where $f_0(t_i)$ is the probability density function for the susceptible individuals.

An alternative to a long-term survivor mixture model is the long-term survivor non-mixture model suggested by [7, 12, 13] which defines an asymptote for the cumulative hazard and hence for the cure fraction. The survival function for a non-mixture cure rate model is defined as:

$$S(t) = p^{1-S_0(t)}, \tag{24.4}$$

where, like in (24.1), $p \in (0, 1)$ is the mixing parameter and $S_0(t)$ denotes a proper survival function for the non cured group. Observe that if the probability of cure is large, then the intrinsic survival function $S(t)$ is large – $S_0(t)$ will be large which implies in $F_0(t) = 1 - S_0(t)$ small. Larger values of $F_0(t)$ at a fixed time t imply lower values of $S(t)$. This model was derived under the threshold model for tumor resistance (cancer research) where, $F_0(t)$ refers to the distribution of division time for each cell in a homogeneous clone of cells. The non-mixture model (24.4) or the promotion time cure fraction has been used by Lambert et al. [7, 8] to estimate the probability of cure fraction in cancer lifetime data.

From (24.4), the survival and hazard function for the non-mixture cure rate model can be written, respectively, as:

$$S(t_i) = \exp\left[\log(p) F_0(t_i)\right] \tag{24.5}$$

and

$$h(t_i) = -\log(p) f_0(t_i). \tag{24.6}$$

Since $f(t) = h(t)S(t)$, the contribution of the ith individual for the likelihood function is given by:

$$L_i = h(t_i)^{\delta_i} S(t_i) \tag{24.7}$$

that is:

$$L_i = \left[-\log(p) f_0(t_i)\right]^{\delta_i} \exp\left[\log(p) F_0(t_i)\right]. \tag{24.8}$$

A Bayesian formulation of the non-mixture cure rate model is given in Chen et al. [2]. A model which includes a standard mixture model for cure rate was considered in Yin and Ibrahim [14]. Rodrigues et al. [10] extended the long-term survival model proposed by Chen et al. [2].

In this paper, considering the Burr XII distribution, we compare the performance of the mixture and non-mixture cure fraction formulation when the scale and shape parameters are dependent of covariates. The Burr XII distribution provides more flexibility than the Weibull distribution which could be a special case of the Burr XII distribution if its parameters are extended to a limiting case. It is also important to point out that the Burr XII distribution is mathematically tractable with a closed form for its cumulative distribution function.

24.2 The Burr XII Distribution Cure Model

Burr [1] suggested a number of cumulative distributions, where the most popular one is the so-called Burr XII distribution, whose three-parameter probability density function is given by:

$$f_0(t \mid \mu, \alpha, \lambda) = \frac{\alpha}{\mu^{\alpha}} t^{\alpha-1} \left[1 + \lambda \left(\frac{t}{\mu}\right)^{\alpha}\right]^{-(1+\frac{1}{\lambda})}, \tag{24.9}$$

where $\mu > 0$ is the scale parameter; $\alpha > 0$ and $\lambda > 0$ are shape parameters. For $\lambda \to +0$ we have the Weibull distribution as a particular case. The hazard function of a Burr XII distribution is decreasing if $\alpha \leq 1$ and is unimodal with the mode at $t = \frac{(\alpha-1)^{1/\alpha}}{\mu^{-1}\lambda^{1/\alpha}}$ when $\alpha > 1$. The three-parameter Burr XII distribution is much more flexible than the standard two-parameter Weibull distribution.

From (24.9), the survival function is written by:

$$S_0(t \mid \mu, \alpha, \lambda) = \left[1 + \lambda \left(\frac{t}{\mu}\right)^{\alpha}\right]^{-\frac{1}{\lambda}}. \tag{24.10}$$

From (24.10), the Burr XII model in the presence of long-term survivors or immunes has a probability density function and a survival function given, respectively, as follows:

$$f(t \mid \theta) = (1-p) \frac{\alpha}{\mu^{\alpha}} t^{\alpha-1} \left[1 + \lambda \left(\frac{t}{\mu}\right)^{\alpha}\right]^{-(1+\frac{1}{\lambda})}, \tag{24.11}$$

$$S(t \mid \theta) = p + (1-p) \left[1 + \lambda \left(\frac{t}{\mu}\right)^{\alpha}\right]^{-\frac{1}{\lambda}}, \tag{24.12}$$

where $\theta = (\mu, \alpha, \lambda, p)$, μ is the scale parameter, α and λ are shape parameters and p is the proportion of immunes or non susceptible.

Under the non-mixture formulation and using (24.10), the probability density function and the survival function are given respectively by:

$$f(t \mid \theta) = -\log(p) \frac{\alpha}{\mu^{\alpha}} t^{\alpha-1} \left[1 + \lambda \left(\frac{t}{\mu}\right)^{\alpha}\right]^{-(1+\frac{1}{\lambda})} p^{\{1-[1+\lambda(\frac{t}{\mu})^{\alpha}]^{-\frac{1}{\lambda}}\}} \tag{24.13}$$

$$S(t \mid \theta) = p^{\{1-[1+\lambda(\frac{t}{\mu})^{\alpha}]^{-\frac{1}{\lambda}}\}}. \tag{24.14}$$

In the presence of one covariate x_i, $i = 1, \ldots, n$, we can assume a link function for μ, α, λ and p, that is, $\log(\mu_i) = \beta_0 + \beta_1 x_i$, $\log(\alpha_i) = \alpha_0 + \alpha_1 x_i$, $\log(\lambda_i) = \gamma_0 + \gamma_1 x_i$ and $\log(\frac{p_i}{1-p_i}) = \eta_0 + \eta_1 x_i$, where x_i, for example, taking the value 0 if individual i is in the treatment group 1 or the value 1 if individual i is in the treatment group 2. In this way, we can have interest in test the following hypothesis: H_0: $\beta_1 = 0$ (no treatment effect in the susceptible patients), H_0: $\alpha_1 = 0$ (no treatment effect in the shape of the lifetime distribution), H_0: $\gamma_1 = 0$ (no treatment effect in the shape of the lifetime distribution) or H_0: $\eta_1 = 0$ (no treatment effect in the proportion of cured individuals).

24.3 A Bayesian Analysis

For a Bayesian analysis of the mixture and non-mixture models introduced in Sect. 24.1, we assume an prior uniform distribution defined in the interval $(0, 1)$, $U(0, 1)$, for the probability of cure p and $Gamma(0.001, 0.001)$ prior distributions for the scale parameter μ and shape parameters α and λ, where $Gamma(a, b)$ denotes a gamma distribution with mean a/b and variance a/b^2. We further assume prior independence among p, μ, α and λ. Observe that we are using approximately non-informative priors for the parameters of the models.

Assuming the mixture and non-mixture models introduced in Sect. 24.1, let us consider a gamma prior distribution $Gamma(0.001, 0.001)$ for the regression parameters β_0 and α_0 and a normal prior distribution $N(0, 100)$ for the regression parameters β_l and α_l, $l = 1, \ldots, k$, where $N(\mu, \sigma^2)$ denotes a normal distribution with mean μ and variance σ^2. We also assume prior independence among the parameters.

Posterior summaries of interest are obtained from simulated samples for the joint posterior distribution using standard Markov Chain Monte Carlo (MCMC) methods as the Gibbs sampling algorithm [4] or the Metropolis–Hastings algorithm [3].

24.4 An Application

In this section we analyze a leukaemia data set consisting of 90 observations introduced by Kersey et al. [6] and reproduced by Maller and Zhou [9]. In this data 46 patients were treated by allogeneic transplant (Group I) and the other 44 by autologous transplant (Group II). The survival time refers to the number of days to recurrence of leukaemia for patients after one of the two treatments. The medical problems of interest include: the existence of "cured" patients (who will never suffer a recurrence of leukaemia) and the estimation of their proportion; the failure distributions of susceptible patients; and comparison between the effects of the two treatments.

In Tables 24.1 and 24.2, we have the inference results considering the Bayesian approach for mixture and non-mixture models, respectively. We also have the Monte

Table 24.1 Posterior means (standard deviation) for μ, α, λ and p in each group—mixture model

Group	$\widehat{\mu}$	$\widehat{\alpha}$	$\widehat{\lambda}$	$\widehat{p}$	DIC
I	170.2	1.3224	1.5235	0.2046	495.3
	(15.5727)	(0.3386)	(1.2280)	(0.0984)	
II	114.4	3.2585	1.8328	0.2073	457.3
	(22.5142)	(1.1278)	(1.3489)	(0.0622)	

Table 24.2 Posterior means (standard deviation) for μ, α, λ and p in each group — non-mixture model

Group	$\widehat{\mu}$	$\widehat{\alpha}$	$\widehat{\lambda}$	$\widehat{p}$	DIC
I	302.0	1.3200	1.1538	0.2497	494.0
	(60.1777)	(0.2091)	(0.5350)	(0.0673)	
II	158.4	2.7506	1.3057	0.2141	455.8
	(25.4148)	(0.5098)	(0.4480)	(0.0603)	

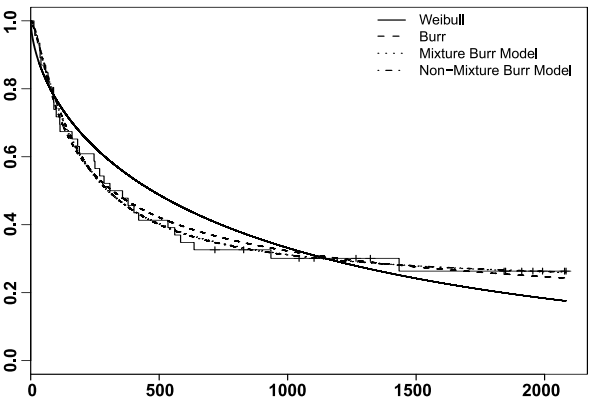

(a) Group I

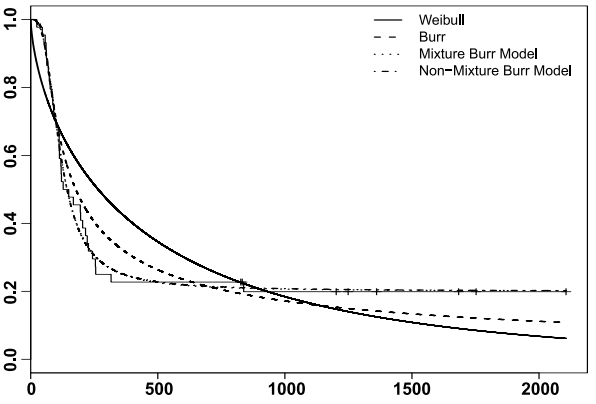

(b) Group II

Fig. 24.1 Fitted models for the data

Table 24.3 Posterior Means (PM) and Standard Deviation (SD) for regression models — mixture model

Model	Parameter	*PM*	*SD*	Credible Interval
Model 1	$\widehat{\mu}$	122.6	28.7453	(77.2546; 194.9)
	$\widehat{\alpha}$	2.1934	0.5451	(1.2602; 3.4459)
	$\widehat{\lambda}$	2.2280	1.3879	(0.3819; 5.9824)
	$\widehat{p}$	0.2009	0.0632	(0.0646; 0.3176)
Model 2	$\widehat{\alpha}$	1.8272	0.4815	(1.0778; 2.9824)
	$\widehat{\lambda}$	1.3434	1.1575	(0.0332; 4.5494)
	$\widehat{p}$	0.2173	0.0593	(0.0851; 0.3261)
	$\widehat{\beta}_0$	174.9	52.0182	(81.5222; 277.9)
	$\widehat{\beta}_1$	−0.3018	0.2916	(−0.8292; 0.3199)
Model 3	$\widehat{\lambda}$	1.7100	1.0094	(0.3734; 4.1672)
	$\widehat{p}$	0.2005	0.0528	(0.0997; 0.3093)
	$\widehat{\beta}_0$	175.8	52.2661	(88.4162; 298.2)
	$\widehat{\beta}_1$	−0.4070	0.2806	(−0.9384; 0.1674)
	$\widehat{\alpha}_0$	1.4214	0.3461	(0.8879; 2.2550)
	$\widehat{\alpha}_1$	0.8004	0.2449	(0.3295; 1.2986)

Carlo estimates of DIC (Deviance Information Criterion) used as a discrimination criterion for different models. Smaller values of DIC indicates better models.

To obtain the Bayesian estimates we have used MCMC (Markov Chain Monte Carlo) methods available in *SAS* software 9.2, *SAS/MCMC* [11]. A single chain has been used in the simulation of samples for each parameter of both models considering a "burn-in-sample" of size 15,000 to eliminate the possible effect of the initial values. After this "burn-in" period, we simulated other 200,000 Gibbs samples taking every 100th sample, to get approximated uncorrelated values which result in a final chain of size 2,000. Usual existing convergence diagnostics available in the literature for a single chain using the *SAS/MCMC* procedure indicated convergence for all parameters.

In Fig. 24.1, we have the plots of the estimated survival functions considering mixture and non-mixture models in presence of cure fraction and the plot of the non-parametric Kaplan–Meier estimate for the survival function [5]. We also have in Fig. 24.1, the plot of the estimated survival function based on the Weibull and Burr XII distributions not considering the cure fraction modeling.

From the fitted survival models (see Fig. 24.1), we conclude that the survival times are very well fitted by the mixture and non mixture cure fraction models. From the results of Tables 24.1 and 24.2, the obtained DIC discrimination values from both models also give similar results.

We can also consider a binary variable related to the different groups where $x_{1i} = 1$ for Group II and 0 for the Group I. Then we consider three cases: model without covariates (Model 1), regression model for μ (Model 2) and regression model for μ and α (Model 3).

Table 24.4 Posterior Means (PM) and Standard Deviation (SD) for regression models — non-mixture model

Model	Parameter	*PM*	*SD*	Credible Interval
Model 1	$\widehat{\mu}$	191.3	47.1324	(118.4; 309.2)
	$\widehat{\alpha}$	2.0741	0.4720	(1.2757; 3.0983)
	$\widehat{\lambda}$	3.4496	3.0633	(0.2589; 12.2087)
	$\widehat{p}$	0.1879	0.0668	(0.0432; 0.3062)
Model 2	$\widehat{\alpha}$	1.6350	0.2545	(1.1474; 2.1417)
	$\widehat{\lambda}$	1.3797	1.8359	(0.00255; 7.8565)
	$\widehat{p}$	0.2170	0.0674	(0.0482; 0.3320)
	$\widehat{\beta}_0$	295.4	9.5409	(276.6; 313.4)
	$\widehat{\beta}_1$	−0.3886	0.1929	(−0.7404; 0.0111)
Model 3	$\widehat{\lambda}$	1.6695	1.1204	(0.1919; 4.6356)
	$\widehat{p}$	0.2044	0.0499	(0.1049; 0.3055)
	$\widehat{\beta}_0$	338.9	15.2548	(308.1; 356.9)
	$\widehat{\beta}_1$	−0.7833	0.1830	(−1.1088; −0.4185)
	$\widehat{\alpha}_0$	1.2762	0.2040	(0.9006; 1.7011)
	$\widehat{\alpha}_1$	0.7752	0.2432	(0.2887; 1.2575)

Table 24.5 Deviance Information Criterion (DIC)

Model	Mixture model	Non-mixture model
Model 1	959.5	958.2
Model 2	959.8	958.7
Model 3	949.5	948.7

In Tables 24.3 and 24.4, we have the inference results considering the Bayesian approach for regression models considering mixture and non-mixture models, respectively.

In Bayesian context using MCMC methods, we have used the DIC given automatically by the SAS software (see, Table 24.5).

From the results of Table 24.5, we conclude that Model 3 (regression model for μ and α) is better fitted by the data. Since DIC is a little bit smaller considering the non-mixture Model 3 when compared to the other models, we use this model to get our final inferences of interest. From Table 24.4 and using the non-mixture Model 3, we conclude that the parameters β_1 and α_1 have significative treatment effect in the ratio of susceptible patients.

References

1. Burr IW (1942) Cumulative frequency functions. Ann Math Stat 13:215–232
2. Chen MH, Ibrahim JG, Sinha D (1999) A new Bayesian model for survival data with a surviving fraction. J Am Stat Assoc 94(447):909–919

3. Chib S, Greenberg E (1995) Undestanding the Metropolis-Hastings algorithm. Am Stat 49(4):327–335
4. Gelfand AE, Smith AFM (1990) Sampling-based approaches to calculating marginal densities. J Am Stat Assoc 85(410):398–409
5. Kaplan EL, Meier P (1958) Nonparametric estimation from incomplete observations. J Am Stat Assoc 53:457–481
6. Kersey JH, Weisdorf D, Nesbit ME, LeBien TW, Woods WG, McGlave PB, Kim T, Vallera DA, Goldman AI, Bostrom B (1987) Comparison of autologous and allogeneic bone marrow transplantation for treatment of high-risk refractory acute lymphoblastic leukemia. N Engl J Med 317(8):461–467
7. Lambert PC, Dickman PW, Weston CL, Thompson JR (2010) Estimating the cure fraction in population-based cancer studies by using finite mixture models. J R Stat Soc, Ser C, Appl Stat 59(1):35–55
8. Lambert PC, Thompson JR, Weston CL, Dickman PW (2007) Estimating and modeling the cure fraction in population-based cancer survival analysis. Biostatistics 8(3):576–594
9. Maller RA, Zhou X (1996) Survival analysis with long-term survivors. Wiley series in probability and statistics: applied probability and statistics. Wiley, Chichester
10. Rodrigues J, Cancho VG, de Castro M, Louzada-Neto F (2009) On the unification of long-term survival models. Stat Probab Lett 79(6):753–759
11. SAS (2010) The MCMC procedure, SAS/STAT® user's guide, version 9.22. SAS Institute Inc., Cary, NC
12. Tsodikov AD, Ibrahim JG, Yakovlev AY (2003) Estimating cure rates from survival data: an alternative to two-component mixture models. J Am Stat Assoc 98(464):1063–1078
13. Yakovlev AY, Tsodikov AD, Asselain B (1996) Stochastic models of tumor latency and their biostatistical applications. World Scientific, Singapore
14. Yin G, Ibrahim JG (2005) Cure rate models: a unified approach. Can J Stat 33(4):559–570

Chapter 25
Obtaining Superior Wind Power Predictions from a Periodic and Heteroscedastic Wind Power Prediction Tool

Daniel Ambach and Carsten Croonenbroeck

Abstract The Wind Power Prediction Tool (WPPT) has successfully been used for accurate wind power forecasts in the short to medium term scenario (up to 12 hours ahead). Since its development about a decade ago, a lot of additional stochastic modeling has been applied to the interdependency of wind power and wind speed. We improve the model in three ways: First, we replace the rather simple Fourier series of the basic model by more general and flexible periodic Basis splines (B-splines). Second, we model conditional heteroscedasticity by a threshold-GARCH (TGARCH) model, one aspect that is entirely left out by the underlying model. Third, we evaluate several distributional forms of the model's error term. While the original WPPT assumes gaussian errors only, we also investigate whether the errors may follow a Student's t-distribution as well as a skew t-distribution. In this article we show that our periodic WPPT-CH model is able to improve forecasts' accuracy significantly, when compared to the plain WPPT model.

25.1 Introduction

Compensation systems for renewable energy like wind energy are pluralistic through several countries. Many differences aside, accurate wind power forecasts are essential to the energy producer.

Research on wind power forecasting has been manifold. Lei et al. [5] and, more recently, Giebel et al. [3] provide an overview. There are models based on the physics of wind speed and power, models based on machine learning, wavelet models and others. Simple, yet accurate stochastic models like the Wind Power Prediction Tool (WPPT), as introduced by Nielsen et al. [6], are quite successful. WPPT is put to wide usage, especially in Denmark, the world leader in wind energy harvesting, as Giebel et al. [3] point out. However, WPPT disregards several characteristics

D. Ambach · C. Croonenbroeck (✉)
European University Viadrina, Große Scharrnstraße 59, 15230 Frankfurt(Oder), Germany
e-mail: croonenbroeck@europa-uni.de

D. Ambach
e-mail: ambach@europa-uni.de

A. Steland et al. (eds.), *Stochastic Models, Statistics and Their Applications*,
Springer Proceedings in Mathematics & Statistics 122,
DOI 10.1007/978-3-319-13881-7_25

of the wind speed against wind power relationship. First, WPPT uses a Fourier series to capture diurnal periodicity. This is a straightforward way to model periodic effects, but replacing the Fourier terms by periodic B-spline functions introduces more flexibility. The idea to use periodic B-splines is inspired by Harvey and Koopman [4], who use these functions to forecast the hourly electricity demand. These functions enable the model to follow the diurnal periodic structure independently from seasonal or yearly periodicity that may be present. Second, the residuals of the WPPT show a strongly heteroscedastic behavior, which also seems to be askew. We capture the skew (or: leveraged) heteroscedastic variance by modeling the error term as a TGARCH process, as introduced by Rabemananjara and Zakoïan [7]. Finally, the WPPT model's assumption of gaussian errors may be violated.[1] As the residual's density exhibits fat tails (particularly on its left-hand side), we investigate alternative distributional assumptions. After all, we show that our periodic WPPT-CH model generates forecasts that perform significantly more accurate than those obtained by the plain WPPT model.

This article is organized as follows. In Sect. 25.2, we describe the analyzed data. Section 25.3 introduces the underlying WPPT model and our new periodic wind power prediction model with TGARCH effects. The results of the in-sample fit and out-of-sample predictions are presented in Sect. 25.4 and Sect. 25.5 provides a short conclusion.

25.2 Description of the Wind Power Data

The data used in this study are collected from a Fuhrländer FL MD 77 Turbine in Germany. Due to a non-disclosure agreement, the specific location cannot be revealed. Wind speed, wind direction and wind power is recorded at a frequency of 10 minutes. This Turbine exhibits a power range of [0; 1500] kW. The observed time frame for the training data set spans from October 31, 2010 to August 19, 2011 (40 000 observations).

25.3 A New Wind Power Forecasting Method

WPPT, as given by Nielsen et al. [6], models wind power P_t as a dynamic regression approach. It includes lagged wind speed and diurnal periodicity as regressors. The periodic behavior is captured by a Fourier series. Clearly, the important wind speed forecasts are not deterministic. They may stem from numerical weather predictions (NWP) or could be predicted from statistical model approaches. In this article, we use the recently developed predictions from a periodic ARFIMA–APARCH model with time varying regressors, as discussed by Ambach and Schmid [1]. As

[1] Shapiro–Wilk-Tests generally reject the hypothesis of gaussian WPPT errors.

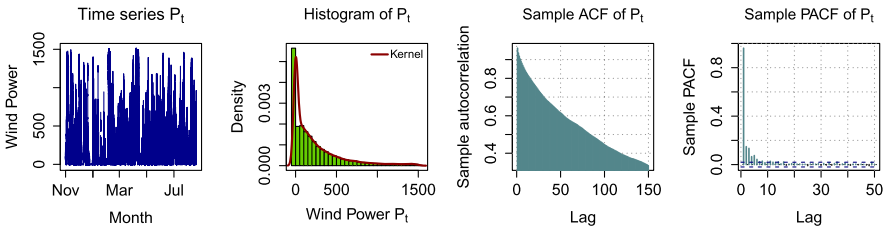

Fig. 25.1 Time series of wind power P_t (*first* panel), histogram of wind power (*second* panel), ACF and PACF for wind power (*third* and *fourth* panels), time frame October 31, 2010 to August 19, 2011

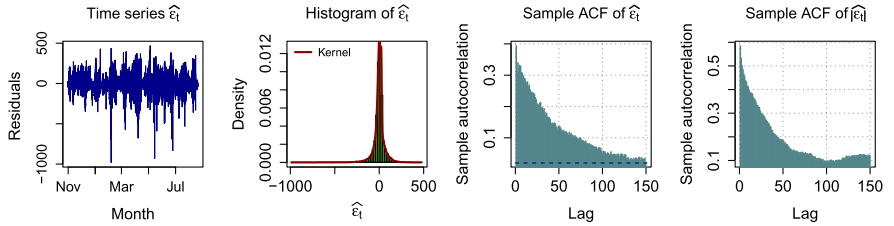

Fig. 25.2 WPPT residuals $\widehat{\varepsilon_t}$ (*first* panel), histogram of $\widehat{\varepsilon_t}$ (*second* panel), ACF of $\widehat{\varepsilon_t}$ (*third* panel) and ACF of $\widehat{|\varepsilon_t|}$ (*fourth* panel), time frame October 31, 2010 to August 19, 2011

WPPT includes only two lags of wind speed in addition to periodicity as explanatory variables, it is not flexible enough to capture important features of wind power. The high-frequency data investigated here clearly show a strong presence of autocorrelation, see Fig. 25.1. The autoregressive model order should be extended and include multiple lags. Furthermore, the variance structure shows heteroscedastic disturbance, see Fig. 25.2. Therefore, we model the conditional standard deviation by a TGARCH model.

Furthermore, we include wind direction as an additional explanatory variable, as due to the Turbine's uneven surroundings, local wind speed may depend on wind direction. Wind power shows a correlation structure that suggests that it may very well be dependent on wind direction. Figure 25.3 provides evidence on that assumption.

Our new wind power prediction model uses B-splines to model the periodic structure, instead of the Fourier series used in WPPT. The considered periodic basis functions are inspired by Harvey and Koopman [4]. The B-spline approach uses local basis functions to provide more flexibility, especially when modeling time series with nonstationary impacts such as wind power. After all, our new model suggestion is

$$P_t = \vartheta_0 + \sum_{j=1}^{m} \theta_j P_{t-j} + \theta_{144} P_{t-144} + b_1 W_t + b_2 (W_t)^2 + \sin(A_t) + \cos(A_t) + \sum_{k=2}^{K-1} \delta_k \widetilde{B}_k(t) + \sum_{r=1}^{o} \phi_r \varepsilon_{t-r}, \tag{25.1}$$

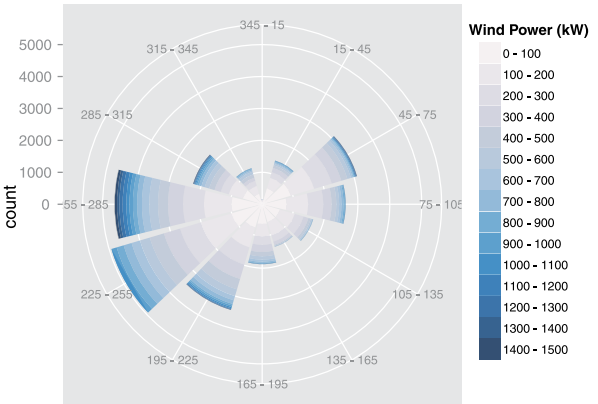

Fig. 25.3 Absolute number of wind power observations and the perceived wind directions

where $m \in \mathbb{Z} \setminus \{144\}$, W_t is the wind speed (in m/s) and A_t is the wind direction (Azimuth). Wind direction is measured in degrees. To avoid numerical problems resulting from that, we split the wind direction information into two components $\cos(A_t)$ and $\sin(A_t)$. The autoregressive coefficients θ provide a stationary solution if and only if $P(z) = 1 - (\sum_j^m \theta_j z^j + \theta_{144} z^{144}) \neq 0$ for $|z| \leq 1$. ϕ represents the moving average components. We include MA coefficients to reduce the parameters of the model and to capture the strongly persistent behavior of the dependent variable. The essential model enhancements are the periodic B-splines $\widetilde{B}_k(t)$. For our definition of these splines, we follow Ziel and Steinert [8]. The basis functions of the wind power series are given by

$$\widetilde{B}_k(t) = \sum_{l \in \mathbb{Z}} B_{lS,d_\kappa}(t) = \sum_{l \in \mathbb{Z}} B_{lS,d_\kappa}\big(t; \kappa(d_\kappa, T, D), D\big), \tag{25.2}$$

where κ is a set of equidistant knots which we choose directly, T depicts the central point of this set of knots, S represents the periodicity and D is the degree of the spline. The distance of the equidistant knots is given by d_κ. As the data frequency is 10 minutes, the diurnal periodicity for the wind power is $S = 144$. It is reasonable to choose the number of included basis functions to be a common denominator of S. Thus, we decide to use $\lambda = 6$ basis functions. Hence, we obtain a distance d_κ of $S/\lambda = 24$. Finally, we are able to iteratively define the complete set of basis functions $\widetilde{B}_k(t) = \widetilde{B}_{k-1}(t - 24)$, where $k \in \{2, \ldots, 6\}$. Besides, we choose $D = 3$, to get the popular cubic splines, which are twice continuously differentiable. Furthermore, we have to remark that the sum of all basis functions is constant. Hence, the first component is omitted to avoid singularities. Finally, all parameters for the B-spline function are exogenously determined. Henceforth, we have to introduce the TGARCH model described by Rabemananjara and Zakoïan [7]

$$\varepsilon_t = \sigma_t \eta_t, \tag{25.3}$$

$$\begin{aligned}\sigma_t &= \alpha_0 + \sum_{l=1}^{q} \alpha_l \big(|\varepsilon_{t-l}| - \gamma_l \varepsilon_{t-l}\big) + \sum_{i=1}^{p} \beta_i \sigma_{t-i} \\ &= \alpha_0 + \sum_{l=1}^{q} \alpha_l (1-\gamma_l)\varepsilon_t^+ - \sum_{l=1}^{q} \alpha_l (1+\gamma_l)\varepsilon_t^- + \sum_{i=1}^{p} \beta_i \sigma_{t-i}, \end{aligned} \tag{25.4}$$

where $\{\eta_t\}_{t\in\mathbb{Z}} \sim F$ is i.i.d. with $E[\eta_t] = 0$ and $Var[\eta_t] = 1$. Specifically, the error term $\{\eta_t\}$ is assumed to be either standard normally distributed, standardized t-distributed or skewed t-distributed. The TGARCH parameter γ_l are the asymmetry parameters with $|\gamma_l| \leq 1$ for $l = 1, \ldots, q$. This parameter depicts the asymmetry within the conditional variance. Furthermore, $\alpha_0 > 0$, $\alpha_l \geq 0$ $\forall l = 1, \ldots, q$ and $\beta_i \geq 0$ $\forall i = 1, \ldots, p$ are the classical GARCH parameters. Rabemananjara and Zakoïan [7] discuss the existence of a stationary solution of the TGARCH process. One definition of the skewed t-distribution is given by Fernandez and Steel [2]. This approach combines two halves of a symmetric base distribution, which are differently scaled. The subsequential equation provides the density function

$$\begin{aligned} f_x(x) = &\frac{2\xi}{(\xi^2+1)} \frac{\Gamma(\frac{\nu+1}{2})}{\Gamma(\frac{\nu}{2})\sqrt{\pi}\sqrt{\nu}\sigma} \\ &\times \left[1 + \frac{(\frac{x-\mu}{\sigma})^2}{\nu}\left(\frac{1}{\xi^2} I(x \geq \mu) + \xi^2 I(x < \mu)\right)\right]^{-\frac{\nu+1}{2}} \end{aligned} \tag{25.5}$$

with ν degrees of freedom, $I(\cdot)$ the indicator function, expectation μ and variance $\sigma^2 = \nu/(\nu-2)$. Moreover, ξ is the skewness parameter with $\xi > 0$. It reduces f to the noncentral t-distribution if $\xi = 1$.

25.4 Comparison of the Forecasting Performance

We want to produce wind power forecasts that are significantly better than those computed by previous models. In contrast to WPPT, which is estimated by a least-squares approach, we use the maximum likelihood method for our periodic WPPT-CH model. We apply our method to three different distributional assumptions. Figure 25.2 provides the histogram of the WPPT residual process, $\{\widehat{\varepsilon_t}\}$. This histogram and the Shapiro–Wilk-Test reject the assumption of normally distributed residuals. Implying normality, the ACF of $\{\widehat{\varepsilon_t}\}$ and the ACF of $\{|\widehat{\varepsilon_t}|\}$ suggest the presence of strong autocorrelation.

We use Akaike/Bayesian information criteria to select the best model for the residuals $\{\widehat{\varepsilon_t}\}$. Hence, for the autoregressive order, we choose $m = 5$ and $o = 4$ for the moving average part. Moreover, for the TGARCH model, we choose $q = 2$ and $p = 4$. For a comparison of the underlying distribution, we choose the same model order for each model. Figure 25.4 provides ACF of $\widehat{\varepsilon_t}$ and $|\widehat{\varepsilon_t}|$. This figure depicts a clear model improvement over normality. A huge amount of autocorrelation vanishes. The Ljung–Box-Test supports the assumption of no remaining autocorrelation

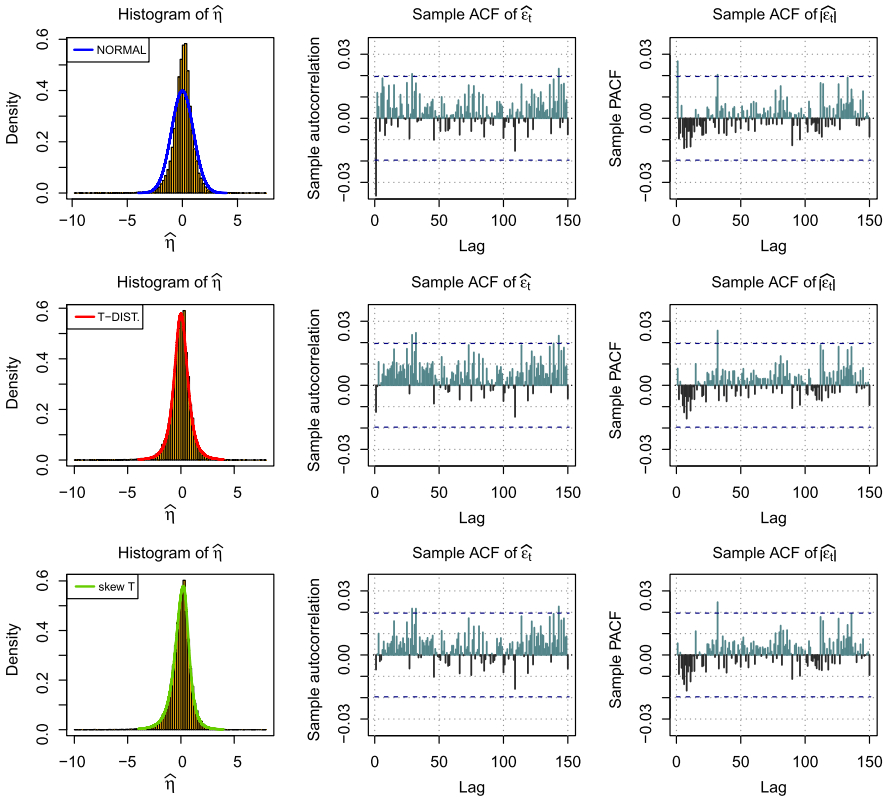

Fig. 25.4 Histogram of $\widehat{\eta}_t$ (*first* column), ACF of $\widehat{\varepsilon}_t$ (*second* column) and ACF of $|\widehat{\varepsilon_t}|$ (*third* column), time frame October 31, 2010 to August 19, 2011 for the pWPPT-CH and all distributions

for each distribution. Furthermore, we use the Kolmogorow–Smirnow-Test to test for the underlying distribution. Only the assumption of the skew t-distribution is not rejected.

Regarding the in-sample fit, we conclude that the periodic WPPT-CH with skew t-distributed residuals provides the best fit. Therefore, we expect that this model outperforms the other models concerning the out-of-sample forecasts. We use the first 40 000 observations as a training data set. The following week from August 19, 2011 to August 26, 2011 is used for out-of-sample forecasts. Here, we consider forecasts up to a maximum of half a day. Using a rolling window technique, we re-estimate each model for each forecast with a part of the information set available at the period t, namely $P_{t-10\,000+1}, \ldots, P_t$. Subsequently, we derive $\widehat{P}_{t+\tau|t}$, where $\tau \in \{1, \ldots, 72\}$. This procedure is repeated 1.000 times. We evaluate the out-of-sample forecasts for the classical WPPT and the periodic WPPT-CH model with normally, t-distributed and skew t-distributed errors. Besides, we take the persistence predictor $\widehat{P}_{t+\tau} = P_t$ and an AR(p) model as benchmark. Table 25.1 presents

Table 25.1 RMSE for all models, time frame August 19, 2011 to August 26, 2011, 10 minutes, 3 hours, 6 hours and 12 hours ahead

	1 step	18 steps	36 steps	72 steps
Persistence	110.77	258.04	281.11	282.45
AR	112.08	207.38	213.11	**204.18**
WPPT	**101.97**	208.48	211.41	205.93
pWPPT-CH-n	102.53	**202.89**	**206.85**	204.60
pWPPT-CH-t	102.85	204.10	208.05	204.58
pWPPT-CH-st	102.04	203.60	207.61	205.06

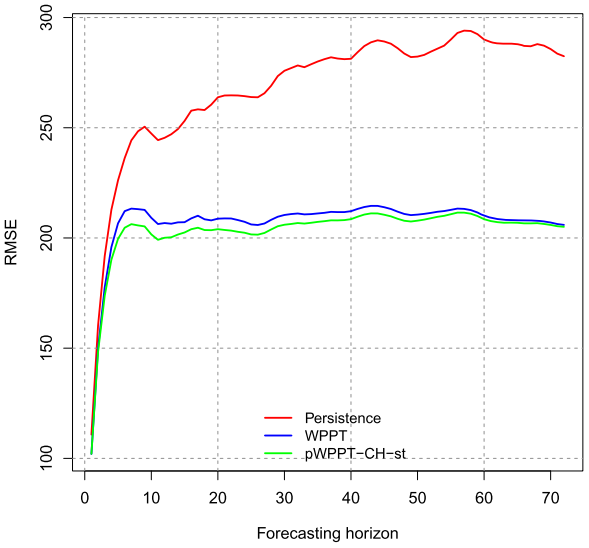

Fig. 25.5 RMSE for all models and all forecasting horizons, time frame August 19, 2011 to August 26, 2011

aggregated root mean square errors (RMSE)[2] for all models and forecasting horizons of $\tau \in \{1, 18, 36, 72\}$. The best (smallest) values are bolded.

In almost all cases, the periodic WPPT-CH model provides the lowest forecasting errors. Figure 25.5 visualizes the RMSE inflation paths of the models by forecasting horizons. The figure emphasizes the findings presented in Table 25.1.[3] Thus, we conclude that the best in-sample model also provides the best predictions.

[2]We also calculate MAE. Results are quite similar and omitted here to conserve space. Tables and figures are available upon request.

[3]For lucidity, the figure depicts only the worst (persistence), best (pWPPT-CH) and the WPPT benchmark model. All other curves lie inside the spanned range. According to Diebold–Mariano-Tests, the pWPPT-CH family models are not significantly different from each other.

25.5 Conclusion

We provide a new class of models that replace the Fourier series utilized by WPPT by more appropriate and more flexible periodic B-splines. Beyond, we capture conditional heteroscedasticity by modeling the error term as a TGARCH process. Finally, different error distributions are used. The skew t-distribution seems to capture the residuals' empirical properties quite better than the normal distribution. Our models improve the in-sample features quite well, when compared to the classical WPPT model. Clearly, there are further improvements possible, for example, using a multivariate model. Here, Ziel and Steinert [8] propose a multivariate periodic AR-TARCH model. This approach might be extended and applied to the wind power data set. Nevertheless, the new wind power prediction model derived here does improve forecasts over WPPT already.

References

1. Ambach D, Schmid W (2014) Periodic and long range dependent models for high frequency wind speed data. Viadrina Discussion Papers 2014, No 357
2. Fernandez C, Steel M (1998) On Bayesian modelling of fat tails and skewness. J Am Stat Assoc 93:359–371
3. Giebel G, Brownsword R, Kariniotakis G, Denhard M, Draxl C (2011) The state-of-the-art in short-term prediction of wind power. Tech rep, ANEMOS.plus, Riso DTU, Wind Energy Division
4. Harvey A, Koopman SJ (1993) Forecasting hourly electricity demand using timevarying splines. J Am Stat Assoc 88(424):1228–1236
5. Lei M, Shiyan L, Chuanwen J, Hongling L, Zhang Y (2009) A review on the forecasting of wind speed and generated power Renew Sustain Energy Rev 13:915–920
6. Nielsen H, Pinson P, Christiansen L, Nielsen T, Madsen H, Badger J, Giebel G, Ravn H (2007) Improvement and automation of tools for short term wind power forecasting. Tech rep, scientific proceedings of the European wind energy conference and exhibition, Milan, Italy
7. Rabemananjara R, Zakoïan JM (1993) Threshold arch models and asymmetries in volatility. J Appl Econom 8(1):31–49
8. Ziel F, Steinert R (2014) Efficient modeling and forecasting of the electricity spot price. arXiv:1402.7027

Chapter 26
Stochastic Dynamics of G-Protein-Coupled Cell-Surface Receptors

Michał Balcerek and Aleksander Weron

Abstract The field of bio-medicine has seen immense increase in single particle tracking techniques and experimental results. We analyze here the data obtained from experiment described by D. Calebiro et al. in Proc. Natl. Acad. Sci. 110: 743–748, 2013 describing the motion of fluorescently labeled G-protein-coupled cell-surface receptors. Our study revealed that some proteins' trajectories do not have Gaussian increments. We tried to determine distribution of such increments. Also, by using various techniques like: p-variation analysis (Burnecki and Weron in Phys. Rev. E 82:021130, 2010; Magdziarz et al. in Phys. Rev. Lett. 103:180602, 2009), dynamical functional analysis (Burnecki et al. in Biophys. J. 103:1839–1847, 2012; Magdziarz and Weron in Ann. Phys. 326:2431–2443, 2011; Magdziarz and Weron in Phys. Rev. E 84:051138, 2011), MSD analysis (Burnecki and Weron in Phys. Rev. E 82:021130, 2010; Burnecki et al. in Biophys. J. 103:1839–1847, 2012; Burnecki et al. in Phys. Rev. E 86:041912, 2012), we attempt to narrow down possible models of particles in biological system. For more methods used in analysis (and their description), yet not included in this paper, see Burnecki and Weron in J. Stat. Mech., 2014, to appear.

26.1 Introduction

Activation of G protein-coupled receptors (GPCRs) is presumably the most important and also most diverse mode of regulating cell and organ functions. Activation means that receptors become capable of coupling to their downstream effector pathways [2], such as G proteins. In this paper we try to analyze the movement of aforementioned GPCRs, during their activation time, on the surface of a cell.

M. Balcerek (✉) · A. Weron
Institute of Mathematics and Computer Science, Wrocław University of Technology, Hugo Steinhaus Center, ul. Wyspianskiego 27, 50-370 Wrocław, Poland
e-mail: michal.balcerek@pwr.edu.pl

A. Weron
e-mail: aleksander.weron@pwr.edu.pl

A. Steland et al. (eds.), *Stochastic Models, Statistics and Their Applications*,
Springer Proceedings in Mathematics & Statistics 122,
DOI 10.1007/978-3-319-13881-7_26

26.2 General Information

In this paper we discuss results for two data sets containing single molecule coordinates of fluorescently labeled G-protein-coupled receptors.

While the first data set consisted of 4111 trajectories measured in 400 time frames, the second data set consists of 6345 trajectories, also measured in 400 time frames (we will mostly focus on the first data set, though the second data set is quite similar). Both data sets are highly irregular, due to fluorescence blinking and fading out the measured trajectories have gaps, they are of uneven length and usually they are very short (more information about the experiment itself can be found in [1]).

Our study revealed that some of scrutinized trajectories' one-dimensional increments (i.e. $dX_t = X_t - X_{t-1}$ and $dY_t = Y_t - Y_{t-1},\ t = 1, \ldots, 400$) did not present Gaussian behavior. This is typical for anomalous subdiffusion in biological cells, see for example [3, 5]. In [1] authors claimed that the trajectories have Gaussian distributions. We focused mostly on those trajectories, and due to statistical purposes we analyzed only those trajectories which were measured in over 70 continuous (without gaps) time frames; those are referred to as the "longer trajectories". Unfortunately there are only 102 such trajectories in the first data set and 99 in the second data set. All trajectories' increments show stationary behavior (e.g. by plotting quantile lines), a property which is essential for further presented analysis.

Behavior of all trajectories and those trajectories that increments do not follow Gaussian law can be seen in the left and the right part of Fig. 26.1 respectively.

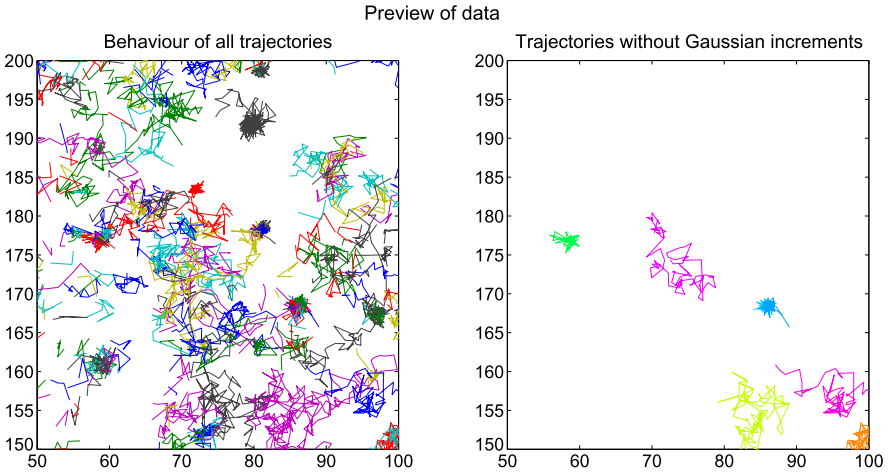

Fig. 26.1 Behavior of all trajectories in the first data set (*left* panel) compared to behavior of trajectories without Gaussian increments (*right* panel)

Table 26.1 Table presenting the percentage of trajectories for which the null hypothesis that the increments have Gaussian distribution is rejected. Both tests: Jarque–Bera (JB) and Anderson–Darling (AD) respectively, were used at 0.05 significance level

Test	First data set		Second data set	
	dX	dY	dX	dY
JB	0.1313	0.2020	0.1176	0.1471
AD	0.0808	0.1414	0.0980	0.1078

Table 26.2 Table presenting the estimated α parameters (using regression method) of longer trajectories which increments do not follow Gaussian law. Such trajectories were found using tests presented in Table 26.1

Statistic	First data set		Second data set	
	dX	dY	dX	dY
Min	1.3704	1.5551	1.5074	1.4590
Mean	1.8637	1.8607	1.8734	1.8223
Median	1.8856	1.8901	1.9105	1.8464
Max	2.0000	2.0000	2.0000	2.0000

26.3 Data Testing

To determine which trajectories (of those longer ones) had non-Gaussian increments we used some statistical tests such as: Jarque–Bera (JB) and Anderson–Darling (AD) applied to one-dimensional increments of the data. Results are presented in Table 26.1. Jarque–Bera test being more strict one for both data sets. Each of those tests reject about 0.05 of trajectories in case where all of them were tested, which is close to the significance level. Those trajectories that were rejected by either of those tests (for either coordinate) can be seen on the right panel of Fig. 26.1.

In order to find proper distribution of those increments (specifically, for increments that the null hypothesis of normality was rejected in either test, see Table 26.1) we tested whether they follow stable law, as it is fairly common in inter-cellular biological data. Anderson–Darling test (detailed description in [7]) results suggested then we can assume that increments of each of the examined trajectories can be considered as realizations from stable distribution. By stable distribution (symmetric case) we have in mind a random variable X having distribution with characteristic function as follows:

$$\varphi_X(t) = \exp\left\{-|ct|^\alpha\right\}, \quad c > 0,\ \alpha \in (0, 2]. \tag{26.1}$$

For more general case see [12]. The stable distributions, in contrast to Gaussian case ($\alpha = 2$), have heavy tails. This property is responsible for subdiffusion effects. Moreover, the trajectories of α-stable processes have jumps.

Furthermore we used regression method to determine α parameters of those stable distributions for each trajectory. Results are presented in Table 26.2. Note that despite maximum estimated parameter α is 2 (as in normal distribution) it did not occur simultaneously in both coordinates for single trajectory.

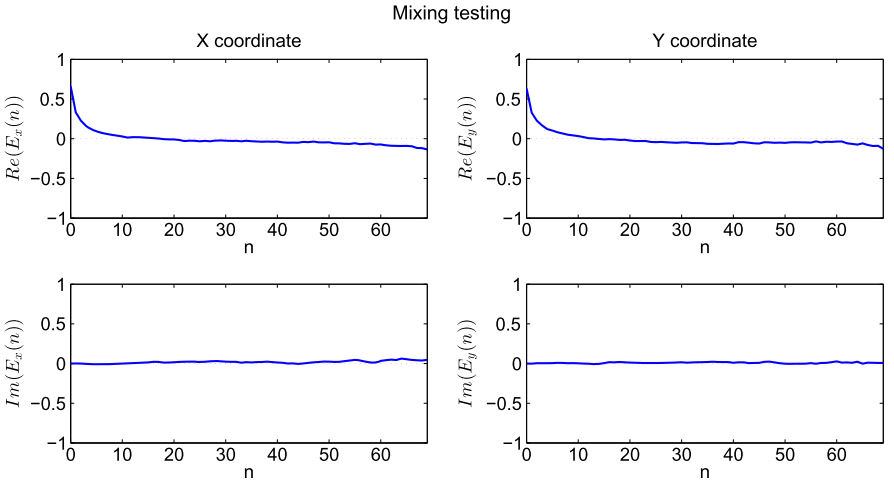

Fig. 26.2 Verification of mixing property of increments in longer trajectories which increments do not have Gaussian distribution (in the first data set). *Right* panel presents X coordinate, *left* panel presents Y coordinate, on top – real part of examined functional, on bottom – its imaginary part

We also would like to present test of some fundamental properties of the data. Both mixing and ergodicity are such fundamental and desired properties. Specifically, ergodicity of the stationary process $Z(n)$ (in case of this work – process of increments) means that the phase space cannot be divided into two nontrivial sets such that a point starting in one set will never get to the second set [4]. Another fundamental property is mixing, i.e., the asymptotic independence of the random variables $Z(n)$ and $Z(0)$ as $n \to \infty$. It is well known that mixing is a stronger property than ergodicity [11]. Thus, to show ergodicity it is enough to prove mixing, which is easier in many cases.

To test whether our data has those properties we use dynamical functional test developed in [10]. It is based on dynamical functional [12]:

$$D(n) = \left\langle \exp\left\{ i\left(Z(n) - Z(0)\right)\right\}\right\rangle. \tag{26.2}$$

By denoting $E(n) = D(n) - |\langle \exp\{iZ(0)\}\rangle|^2$, it turns out that:

$$\text{Stationary process } Z(n) \text{ is mixing} \iff \lim_{n\to\infty} E(n) = 0, \tag{26.3}$$

$$\text{Stationary process } Z(n) \text{ is ergodic} \iff \lim_{n\to\infty} \frac{1}{n}\sum_{k=1}^{n} E(k) = 0. \tag{26.4}$$

Figures 26.2 and 26.3 visualize calculated $E(n)$ and $\frac{1}{n}\sum_{k=1}^{n} E(k)$ with regard to their real and imaginary parts.

Figures 26.2 and 26.3 show that even trajectories with non-Gaussian increments in that experiment have desired characteristics. Same results also occur in the second data set. The real and imaginary part of $E(n)$ functional converge to zero, thus

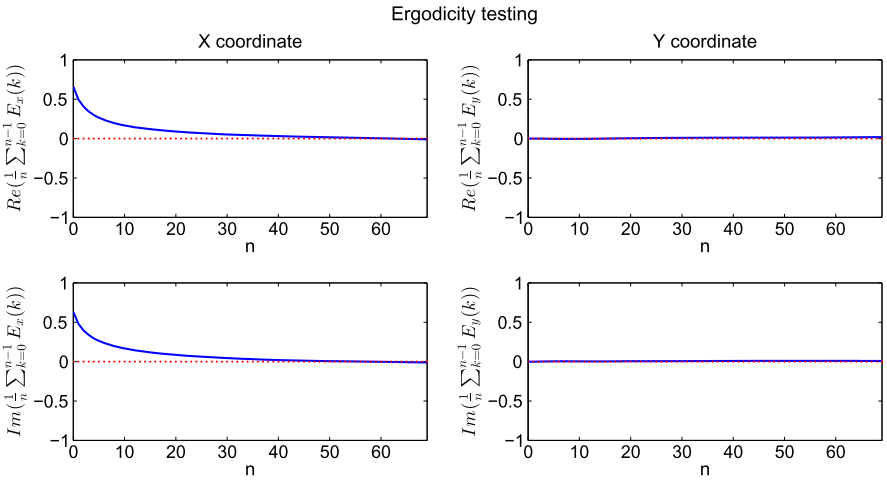

Fig. 26.3 Verification of ergodicity property of increments in longer trajectories (which increments do not have Gaussian distribution) of the first data set. *Left* panel presents X coordinate, *right* panel presents Y coordinate, on *top* – real part of examined functional, on *bottom* – its imaginary part

condition needed for mixing property (see Eq. (26.3)) is satisfied; it is also that $\lim_{n\to\infty} \frac{1}{n}\sum_{k=0}^{n} E(k) = 0$ which suggests ergodic property (see Eq. (26.4)).

Another way of approaching the data is using sample mean square displacement analysis. In particular: let $\{X_k,\ k = 1, \ldots, N\}$ be a sample of length N. The sample MSD was introduced in [3] as:

$$\mathrm{MSD}_N(\tau) = \frac{1}{N-\tau}\sum_{k=1}^{N-\tau}(X_{k+\tau} - X_k)^2. \tag{26.5}$$

Notice that the sample MSD is a time average MSD on a finite sample regarded as a function of difference τ between observations.

If the sample comes from an H-self-similar process with stationary increments belonging to the domain of attraction of the Lévy α-stable law, then for large N we have [3]:

$$\mathrm{MSD}_N(\tau) \sim \tau^{2d+1} S_{\alpha/2}, \tag{26.6}$$

where $\sim$ means similarity in distribution, $d = H - 1/\alpha$, and $S_{\alpha/2}$ is a totally skewed $\alpha/2$-stable random variable. In particular, if $\alpha = 2$, i.e. the data follows Gaussian law or has second moment, then for large N and small τ we have [3]:

$$\mathrm{MSD}_N(\tau) \sim \tau^{2H}\langle X_1^2\rangle. \tag{26.7}$$

Most of estimated α parameters (see Table 26.2) are quite close to $\alpha = 2$. Since we focused on case with stable increments, we analyze sample MSD by using Eq. (26.6).

Table 26.3 Summary of MSD exponent parameter: mean, standard deviation and confidence bounds (of levels 0.025 and 0.975)

	First data set		Second data set	
	X	Y	X	Y
MSD exponent a				
mean	0.7667	0.8075	0.6231	0.6337
std	0.4654	0.4818	0.5130	0.5249
$CB_{0.025}$	0.0075	0.0065	0.0018	0.0028
$CB_{0.975}$	1.4062	1.4921	1.4457	1.6133

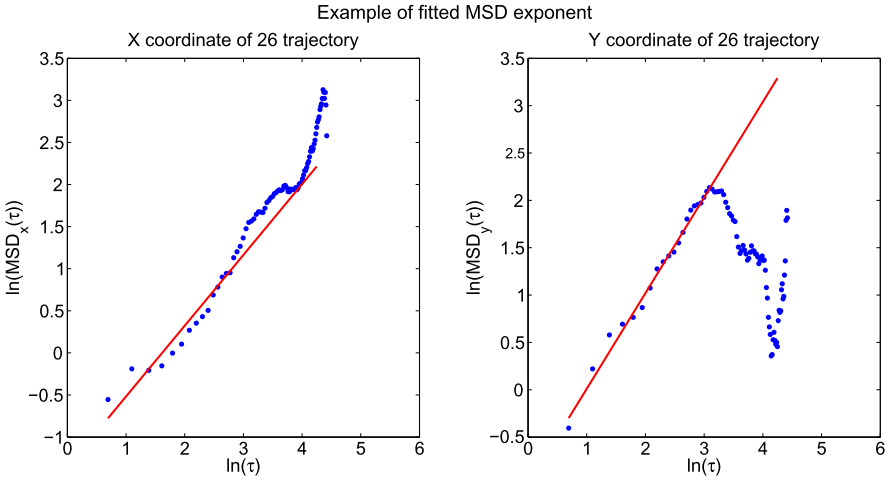

Fig. 26.4 Log–log plot of mean square displacement for 26th trajectory (*blue* dots), which has non-Gaussian increments, of the first data set with fitted slope line (*red* line), so that $\mathrm{MSD}(\tau) \sim \tau^a$ for small τ, where $a = 2H - \frac{2}{\alpha} + 1$ (as in Eq. (26.6)). *Left* panel presents MSD of X coordinate with $a = 0.84$, while *right* panel presents MSD of Y coordinate with fitted $a = 1.01$

The discrepancy of the MSD exponent in Table 26.3 might be caused by biological effects. Observed particles can occur as monomers (they tend to move fastest) but also they can join in bigger polymers. In such cases they move slower and thus the smaller MSD exponents. Furthermore, as the cell membrane is rather irregular, some "traps" might exist on it. This also can limit the particles from moving freely.

To validate our results on the self-similarity index H we can use sample p-variation. The idea was presented e.g. in [3] and [8]. Having $\{X_k,\ k = 1, \ldots, N\}$, we calculate sample p-variation by using Formula (26.8):

$$V_m^{(p)} = \sum_{k=0}^{N/m-1} |X_{(k+1)m} - X_{km}|^p. \tag{26.8}$$

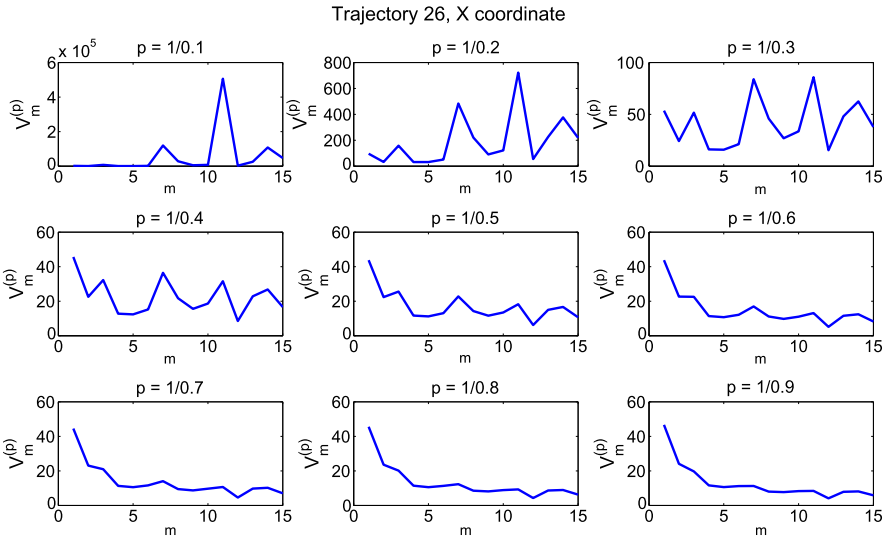

Fig. 26.5 Plot of p-variation for 26th trajectory (which has non-Gaussian increments). Notice the change of $V_m^{(p)}$ behavior: for $p = \frac{1}{0.1}, \frac{1}{0.2}, \frac{1}{0.3}$ it tends to increase, while for $p = \frac{1}{0.5}, \ldots, \frac{1}{0.9}$ it tends to decrease

The value where $p = \frac{1}{2H}$ where the change of $V_m^{(p)}$ regime appears (from increasing to decreasing or vice versa) might indicate the value of self-similarity parameter H.

In Fig. 26.5 we plotted sample p-variation with respect to m for $p = \frac{1}{H}$, $H = 0.1, 0.2, \ldots, 0.9$ for the X coordinate 26th trajectory. In Fig. 26.5 we can see that the behavior of the p-variation changes depending on parameter p (equivalently parameter H). Namely, the functions show an increasing trend for $p < \frac{1}{0.4}$ (that is, for small H), become flat around the value $p \approx \frac{1}{0.4}$, and for $p > \frac{1}{0.4}$ they result in increasing functions. This also indicates that the self-similarity index $H \approx 0.4$, which coincides with result in Fig. 26.4, where the slope of MSD_X function was equal approximately 0.84, which would equal $2H - \frac{2}{\alpha} + 1$ (by Eq. (26.6)).

26.4 Conclusion

The fluorescently labeled G-protein-coupled cell-surface receptors turned out to represent a very complex system. As we focused only on trajectories that increments do not follow Gaussian law, we wanted to present a survey of few techniques applied to those trajectories, and also to one specific trajectory. The data proved to have both, so much desired, ergodic and mixing properties. The complexity of this system appeared in mean square displacement analysis, specifically some biological effects, such as grouping of particles or falling into "traps", probably underlies the discrepancy of MSD exponent. Even on the stage of data preparation it is quite difficult to distinguish separate particles which also might cause some problems. We

found that increments of some G-protein-coupled cell-surface receptors movements follow strictly stable law, and also that the motion itself appears to be subdiffusive. Lastly, we presented another manner to obtain self-similarity index H and then we compared it to results obtained from MSD analysis.

Acknowledgements We would like to thank Davide Calebiro and his research team for providing the single particle tracking empirical data and great biological insight into the experiment.

The research of A.W. was partially supported by NCN Maestro Grant No. 2012/06/A/ST1/00258.

References

1. Calebiro D et al (2013) Proc Natl Acad Sci 110(2):743–748
2. Calebiro D et al (2014) Curr Opin Cell Biol 27:87–93. doi:10.1016/j.ceb.2013.11.009
3. Burnecki K, Weron A (2010) Phys Rev E 82:021130
4. Burnecki K et al (2012) Biophys J 103:1839–1847
5. Burnecki K, Sikora G, Weron A (2012) Phys Rev E 86:041912
6. Burnecki K, Weron A (2014) Algorithms for testing of fractional dynamics: a practical guide to ARFIMA modelling. J Stat Mech, doi:10.1088/1742-5468/2014/10/P10036
7. Burnecki K, Wyłomańska A et al (2012) Phys Rev E 85:056711
8. Magdziarz M, Weron A, Burnecki K, Klafter J (2009) Phys Rev Lett 103:180602
9. Magdziarz M, Weron A (2011) Ann Phys 326:2431–2443
10. Magdziarz M, Weron A (2011) Phys Rev E 84:051138
11. Lasota A, Mackey MC (1994) Chaos, fractals and noise: stochastic aspects of dynamics. Springer, New York
12. Janicki A, Weron A (1994) Simulation and chaotic behavior of α-stable stochastic processes. Dekker, New York

Chapter 27
Novel Methodology of Change-Points Detection for Time Series with Arbitrary Generating Mechanisms

Boris Darkhovsky and Alexandra Piryatinska

Abstract A novel approach to the change-point detection problem is proposed. This approach is based on the concept of the ε-complexity of continuous functions introduced recently by the authors, and the non-parametric change-point detection methodology. We show that, for a function satisfying Hölder condition, the ε-complexity can be characterized by a pair of real numbers called here the ε-complexity coefficients. These coefficients are used as diagnostic sequences to detect changes in the generating mechanism. The proposed methodology is model-free and does not depend on the data generating mechanisms. The results of simulations, and application to stock market data, demonstrate the efficiency of the proposed methodology.

27.1 Introduction

In this paper we propose a novel methodology for segmentation of time series of an arbitrary nature into homogeneous increments. We call a segment homogeneous if it is generated by a single mechanism. This mechanism can be stochastic, deterministic (in particular, chaotic) or mixed. Once the series is separated into homogeneous increments it is possible to model them and make inferences about parameters of the models.

If the time series is generated by a stochastic mechanism the segmentation problem is known as the change-point detection problem. For the review on recent developments on change-points detection in time series, see, e.g. [1, 10]. Models with change-points are used in econometrics [8], climatology [9] and etc.

To the best of our knowledge, the only segmentation procedures we are aware of in the literature are performed in the case of stochastic data generating mecha-

B. Darkhovsky
Institute for Systems Analysis, RAS 9 pr. 60-letiya Oktyabrya, Moscow 117312, Russia
e-mail: darbor2004@mail.ru

A. Piryatinska (✉)
San Francisco State University, 1600 Holloway Ave, San Francisco, CA 94132, USA
e-mail: alpiryat@sfsu.edu

A. Steland et al. (eds.), *Stochastic Models, Statistics and Their Applications*,
Springer Proceedings in Mathematics & Statistics 122,
DOI 10.1007/978-3-319-13881-7_27

nisms. This assumption allows the researcher to use different change-point detection methodologies. In practice, time series *are not always generated by probabilistic mechanisms*. If data are generated by *unknown* deterministic or mixed mechanism there are no methodologies which are applicable to the segmentation procedures. In this paper we propose to use the ε-complexity of a continuous function as an "intrinsic" characteristic of a time series, which on the one hand allows us to perform segmentation into homogeneous increments and on the other hand doesn't depend on the type of data generating mechanism. Our definition of the ε-complexity is in line with the Kolmogorov complexity [7].

The idea of a quantitative estimation of the complexity of a continuous function was first proposed in [3]. In [4] *an effective characterization of the ε-complexity for class of functions satisfying Hölder condition* was given. This concept was successfully applied in analysis of human EEG data [5] and for the sequential detection of changes in time series [4]. In this paper we present a result about characterization of the ε-complexity for an *individual function* satisfying Hölder condition. This result was published first in [6]. Then we apply the concept of the ε-complexity of continuous functions for the detection of changes in data generating mechanisms.

The paper is organized as follows. In Sect. 27.2.1 the definition and characterization of the ε-complexity of an individual continuous function satisfying Hölder condition are given. In Sect. 27.2.2 an algorithm for the time series segmentation of an arbitrary nature is presented. In Sect. 27.3.1 we present results of the simulations to show the efficiency of our new methodology for the "off-line" detection of multiple changes in generating mechanism for different types of processes. In Sect. 27.3.2 results on segmentation of high frequency stock market data are presented.

27.2 Methodology

27.2.1 On the ε-Complexity of a Continuous Function

Let $x(\cdot)$ be a real-valued continuous function, defined on a unit cube $\mathbb{I} \subset \mathbb{R}^k$. Let $\mathbb{Z}_h$ be a uniform grid of size $0 < h < 1$ and $\mathbb{I}_h = \mathbb{I} \cap \mathbb{Z}_h$. Suppose that values of the function $x(\cdot)$ are known only on the grid $\mathbb{I}_h$ and let $\mathscr{F}$ be a set of approximation methods for the function reconstruction from its values on the grid.

Suppose that $\|x(\cdot)\| = R > 0$ (where $\|x(\cdot)\| = \sup_{t\in\mathbb{I}} |x(t)|$). Let $\hat{x}(\cdot)$ be an approximation of the function $x(\cdot)$ using its values on the grid $\mathbb{I}_h$ by some method from the set $\mathscr{F}$. Denote

$$\delta_x^{\mathscr{F}}(h) \stackrel{\text{def}}{=} \inf_{\hat{x}(\cdot)\in\mathscr{F}} \left\| x(\cdot) - \hat{x}(\cdot) \right\| \tag{27.1}$$

The function $\delta_x^{\mathscr{F}}(h)$ will be called *absolute error of the reconstruction of $x(\cdot)$ by methods from the set $\mathscr{F}$*.

A continuous function $x(\cdot)$ is called *$\mathscr{F}$-trivial* if $\inf_{h_0\le h<1} \delta_x^{\mathscr{F}}(h) = 0$ for some $h_0 > 0$. Otherwise it is called *$\mathscr{F}$-nontrivial*.

For any $\varepsilon \geq 0$ let

$$h_x^*(\varepsilon, \mathscr{F}) = \begin{cases} \inf\{h \leq 1 : \delta_x^{\mathscr{F}}(h) > \varepsilon R\}, & \text{if } x(\cdot) \text{ is } \mathscr{F}\text{-nontrivial function} \\ 1, & \text{otherwise} \end{cases} \tag{27.2}$$

Definition 27.1 The value $\mathbb{S}_x(\varepsilon, \mathscr{F}) \stackrel{\text{def}}{=} \log \frac{1}{h_x^*(\varepsilon, \mathscr{F})}$ is called the $(\varepsilon, \mathscr{F})$-*complexity* of the function $x(\cdot)$.

In other words, the $(\varepsilon, \mathscr{F})$-complexity of an individual continuous function is a logarithm of the minimal number of function values which should be retained to reconstruct the function $x(\cdot)$ from its values on the grid using set of approximation methods $\mathscr{F}$ with an error not larger then ε.

Similarly to (27.1), we define $\delta_x(h) \stackrel{\text{def}}{=} \inf_{\hat{x}(\cdot)} \|x(\cdot) - \hat{x}(\cdot)\|$, where $\hat{x}(\cdot)$ is an arbitrary (computable) estimate of the function $x(\cdot)$ by its values on a uniform grid of size h.

A continuous function $x(\cdot)$ is called *totally trivial* if $\inf_{h_0 \leq h < 1} \delta_x(h) = 0$ for some $h_0 > 0$. Otherwise it is called *totally nontrivial*.

In majority of applications, we deal with functions given by their values at a discrete set of points (i.e., by a finite sample). Here, we will assume that our time series is the projection of a continuous function on a uniform grid of the unit cube. Let us consider how the definition of the ε-complexity has to be adjusted to this situation.

Let N be the number of function values of a continuous function $x(\cdot)$ on some uniform grid of the unit cube. We choose $0 < S < 1$ and discard $[(1 - S)N]$ function values from the sample (where $[\cdot]$ is an integer part of a number). Using the remaining values of the function we approximate its values at the discarded points by the set of approximation methods $\mathscr{F}$ (due to the finite dimension the choice of the norm for measurement of an approximation error is inessential).

Consider value $h_x^*(\varepsilon, \mathscr{F})$ which was introduced in (27.1) and assume that $[h_x^*(\varepsilon, \mathscr{F})N] \gg 1$.

In that case the number of function values which should be retained to reconstruct the function with an error less of equal εR on the cube with side $h_x^*(\varepsilon, \mathscr{F})$ is equal $n^* = [N/[h_x^*(\varepsilon, \mathscr{F})N]]$. Therefore, the definition of the ε-complexity for the discrete set of points is as follows.

Definition 27.2 The value

$$\mathscr{S}_N\big(x(\cdot), \varepsilon, \mathscr{F}\big) = \log \frac{N}{[h_x^*(\varepsilon, \mathscr{F})N]} \tag{27.3}$$

is called the $(\varepsilon, \mathscr{F})$-complexity of an individual function $x(\cdot)$ given by its values on a uniform grid.

It is easy to see that the following relation follows from (27.3)

Proposition 27.1

$$\mathscr{S}_N\big(x(\cdot), \varepsilon, \mathscr{F}\big) \to \mathbb{S}_x(\varepsilon, \mathscr{F}) \tag{27.4}$$

as $N \to \infty$.

Now let us formulate the main theorem (see [6]) which gives us a characterization of the ε-complexity of an individual function satisfying Hölder condition.

Theorem 27.1 *For any* $x(\cdot)$ *from some dense subset of the set of totally nontrivial Hölder functions, for any sufficiently small* $\kappa > 0, \delta > 0$, *and* $N \geq n_0(x(\cdot))$ *there exist set of approximation methods* $\mathscr{F}^*$, *numbers* $0 < \alpha(N, x(\cdot)) < \beta(N, x(\cdot)) < 1$, *functions* $\rho(S)$, $\xi(S)$ *and set* $M \subset Q = [\alpha(\cdot), \beta(\cdot)]$, $\mu(M) > \mu(Q) - \delta$ (*where* $\mu(\cdot)$ *is Lebesgue measure*) *such that under* $\mathscr{F} \supseteq \mathscr{F}^*$ *for* $S \in M$ *the following relations hold*:

$$\begin{aligned} &\log \varepsilon = A + B \log S + \rho(S) \log S + \xi(S), \\ &\sup_{S \in M} \max\big(\big|\rho(S)\big|, \big|\xi(S)\big|\big) \leq \kappa. \end{aligned} \tag{27.5}$$

Therefore the ε-complexity of a time series which is a projection of an individual Hölder function is completely characterized by pair of real numbers (A, B). This pair of numbers will be called the *ε-complexity coefficients.*

27.2.2 Algorithm for Segmentation of Time Series

Let $X = \{x(t)\}_{t=1}^{N}$ be a time series with unknown moments of changes in generating mechanism (MCGM) t_i, $i = 2, \ldots, k$ (it is unknown if there are changes or not). The type of generating mechanism is also unknown and can be stochastic, deterministic or mixed.

Any segment $[t_i, t_{i+1}]$, $t_1 = 1, \ldots, t_{k+1} = N$, which is generated by the same mechanisms is called *homogeneous*. We assume that homogeneous segments are sufficiently long. Due to our Theorem 27.1 the ε-complexity is uniquely characterized by a pair of parameters $\mathbb{R} = (A, B)$. For a given time series let us choose a window of size n (we assume that $n \ll \min_i(t_{i+1} - t_i)$). We can separate time series into disjoint intervals of length n or consider a sliding window of size n. In case of disjoint intervals we calculate the ε-complexity coefficients $\mathbb{R}(j)$ for $\{x(t)\}_{t=1+(j-1)n}^{jn}$, $j = 1, 2 \ldots, p$ (for a simplicity we suppose that $N/n = p$ and p is an integer). As a result we obtain a new *diagnostic vector sequence* $\{\mathbb{R}(j)\}_{j=1}^{[N/n]}$. Similar vector sequence of the ε-complexity coefficients can be also calculated for sliding window.

The keystone of the proposed methodology for segmentation of time series into homogeneous increments is a following Conjecture:

Conjecture 27.1 *At i-st segment of homogeneity $[t_i, t_{i+1}]$ of the time series X for $t_i \le t$, $(t+n) < t_{i+1}$ the corresponding ε-complexity coefficients $\mathbb{R}(j)$ satisfy the relation*

$$\mathbb{R}(j) = \mathbb{R}_i + \xi_i(j), \tag{27.6}$$

where $\xi_i(j)$ is a random process with zero expectation.

In other words, Conjecture 27.1 implies that the expected values of the ε-complexity coefficients of a time series are constant within segments of homogeneity. For the justification of the conjecture see [6].

Notice that in case of a sliding window, several windows will cover MCGM. Then (assuming Conjecture 27.1 is true) the mathematical expectation of the sequence $\mathbb{R}$ will change according to some transitional process from one constant to another. However, we assume that the size of the window is small compared to the length of homogeneous segments therefore such transitional process will not significantly affect the estimation of MCGM.

Thus, assuming the Conjecture 27.1 is true, the problem of a time series segmentation is reduced to the detection of changes in mathematical expectation of the vector diagnostic sequence $\mathbb{R}$.

To solve this problem we propose to use the following family of the statistics, which was introduced by Brodsky and Darkhovsky, see [2].

$$Y(n,\delta) = \left((\mathbb{N}-r)r/\mathbb{N}^2\right)^{\delta}\left(r^{-1}\sum_{k=1}^{r} z(k) - (\mathbb{N}-r)^{-1}\sum_{k=r+1}^{\mathbb{N}} z(k)\right), \tag{27.7}$$

where $0 \le \delta \le 1$, $1 \le r \le \mathbb{N}-1$, $\mathbb{N} = [N/n]$, $Z = \{z(s)\}_{s=1}^{\mathbb{N}}$ is a diagnostic sequence. It can be shown (for details, see [2]) that the estimates of the change-points parameter $\vartheta = (\vartheta_2, \ldots, \vartheta_k)$, $t_i = [\vartheta_i N]$, $i = 2, \ldots, k$, $0 < \theta_1 < \theta_2 < \cdots < \theta_k < 1$ by using the family of statistics (27.7) under mild conditions are asymptotically minimax as $N \to \infty$ (here we apply the change-point detection procedure for each component of vector diagnostic sequence $\mathbb{R}$ separately).

27.3 Results of Simulation and Applications to the Stock Market Data

27.3.1 Results of Simulations

To estimate the ε-complexity coefficients, as a family $\mathscr{F}$ of approximation methods we choose piecewise polynomial functions up to 5th degree. For each simulated time series we choose S_i (in %): 50, 33, 29, 25, 22.5, 20. For each S_i we estimate reconstruction error ε_i. Then the least square method is used for pairs $(\log(S_i), \log(\varepsilon_i))$ to estimate the ε-complexity coefficients. For the detailed algorithm for the practical estimation of the ε-complexity see [4].

Simulations to Demonstrate Efficiency of Our Segmentation Methodology

Example 27.1 In this example we generate four ARIMA$(2, d, 1)$ processes

$$\left(1 - \sum_{i=1}^{2} \phi_r^i L^i\right)(1-L)^{d_r} X_t = \left(1 - \sum_{i=1}^{2} \theta_r^i L^i\right)\varepsilon_t, \quad r = 1, \ldots, 4, \; L^k X_t = X_{t-k} \tag{27.8}$$

of length 18 000 with the following coefficients: $\phi_1 = (-0.1, 0.002)$, $d_1 = 0$, $\theta_1 = (0.1, 0.01)$; $\phi_2 = (0.2, 0.4)$, $d_2 = 0$, $\theta_2 = (-0.1, 0.02)$; $\phi_3 = \phi_2$, $d_3 = 1$, $\theta_3 = \theta_2$; $\phi_4 = \phi_1$, $d_4 = 1$, $\theta_4 = \theta_1$. Here the first two process are just ARMA ($d = 0$), stationary processes, and the third and fourth processes are non-stationary ARIMA processes. Then we concatenate them. After concatenation, we separate each time series into non-overlapping intervals of length 100, and estimate the ε-complexity coefficients for each interval. That creates our vector diagnostic sequence. For each component of diagnostic sequence the non-parametric change-point detection procedure is applied. The example of such simulation is presented in Fig. 27.1 (upper). To insure the stability of the results, 1000 replications were performed. In 84 % of the cases all three MCGM points by both coefficients A and B were detected. Using coefficient A we never missed MCGM points in this example. Using coefficient B in 1 % of the simulations we missed one MCGM point. In 16 % (15 %) of the cases one or two extra MCGM points were detected by coefficients $A(B)$ (Fig. 27.1) (middle and lower).

Example 27.2 Change from the stochastic process to the deterministic one and change in deterministic process We generate ARMA(2,1) process with uniformly distributed noise

$$\left(1 - \sum_{i=1}^{2} \phi^i L^i\right) X_t = (1 - \theta L)\varepsilon_t, \qquad L^k X_t = X_{t-k} \tag{27.9}$$

where $\phi = (0.0001, 0.1)$, $\theta = 0.001$ and $\varepsilon \sim Uniform(-1, 1)$.

Then we generate three Logistic Maps processes $x(t) = \alpha_i x(t-1)(1 - x(t-1))$ with $\alpha_2 = 3.97$, $\alpha_3 = 3.92$ $\alpha_3 = 3.87$. To have Logistic Map process on the same scale as uniform ARMA process the liner transformation $2(x(t) - 0.5)$ is performed. After that we concatenate these four processes and repeat procedure from the previous example. The example of such simulation is presented in Fig. 27.2 (upper). After performing 1000 replications we found that 83 % (84 %) of the cases we detected three change points using coefficients A (B). We didn't miss MCGM points in this example. In 17 % (16 %) of the cases one, two or three extra MCGM points were detected (Fig. 27.2 (middle and lower)).

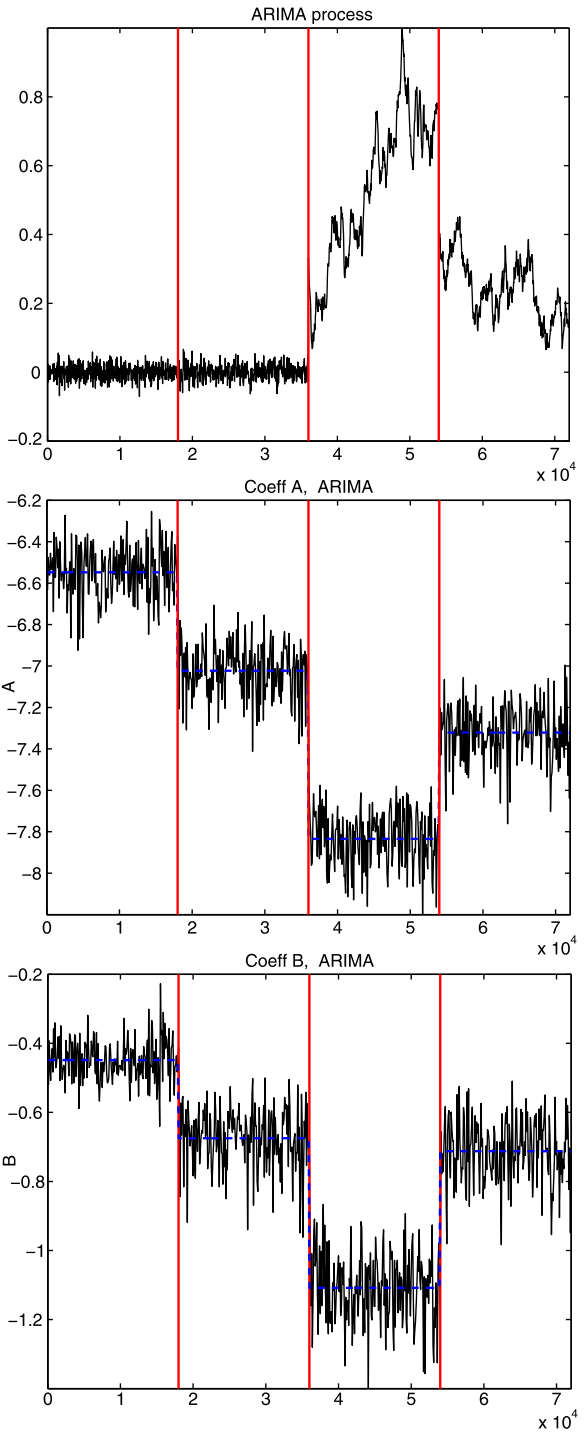

Fig. 27.1 Segmentation of ARIMA processes: (A) Simulated process, (B) Coefficient $A(t)$, (C) Coefficient $B(t)$. The *red vertical* lines correspond to the true MCGM, the *blue dash* lines correspond to the local means inside of the homogeneous increments

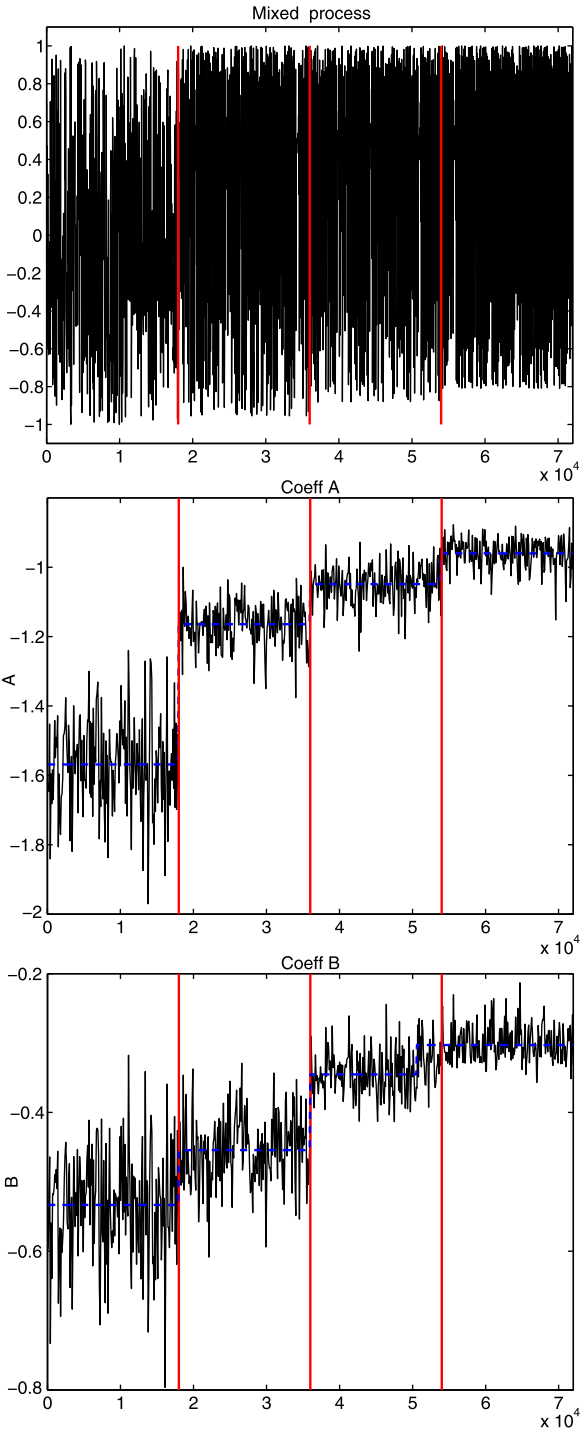

Fig. 27.2 Detection of MCGM, change from stochastic process to deterministic one. (A) Simulated process, (B) Coefficient $A(t)$, (C) Coefficient $B(t)$. The *red vertical* lines correspond to the true MCGM, the *blue dash* lines correspond to the local means between the detected MCGM

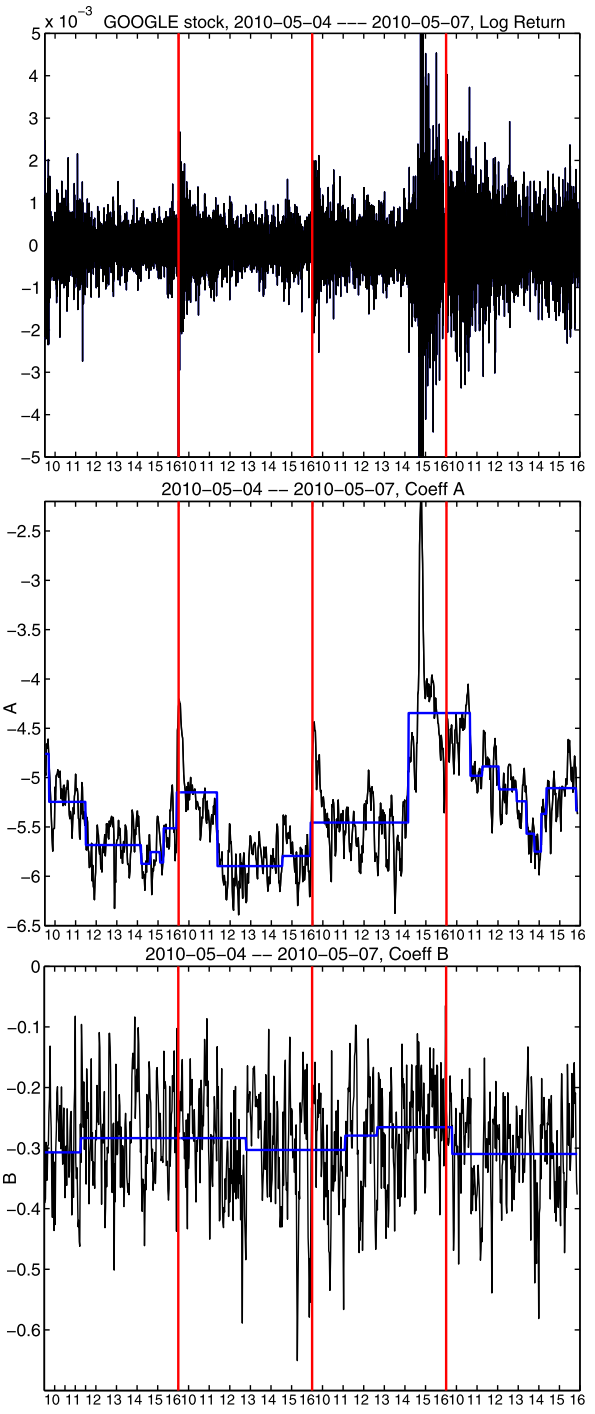

Fig. 27.3 *Upper*: Log return of GOOGLE stock price, *Middle*: Coefficient $A(t)$, *Lower*: Coefficient $B(t)$. *Red vertical* line separate days, *horizontal blue* lines correspond to the local means between detected MCGM

27.3.2 Applications to the Stock Market Data

Application to Stock Market Data We tested our approach on the high frequency GOOGLE stock price data during the Flash crash. Data were provided by nanex.net. The data were recorded every five seconds. In this analysis median between bid, ask, last trade price values at each time point was used. Figure 27.3 (upper) presents the log-returns data (difference of the log of the original data). We considered the overlapping window of size 100 with the step 20. For each such interval we found the ε-complexity coefficients and used them as diagnostic sequences for the non-parametric change-point detection procedure discussed in Sect. 27.2.2.

The results are presented in Fig. 27.3 (middle and lower). We observe that parameter A is useful for the detection of the flash crash. We also observe different dynamics before the flash crash. It seems that there are many change points on a typical morning, but we do not observe as many changes the day of the flash crash. This observation needs further studying.

27.4 Conclusions

In this paper we proposed a new methodology for the detection of moments of changes in a data generating mechanism. This methodology is based on the novel concept of the ε-complexity of a continuous function recently proposed by the authors [6] and the non-parametric change-point detection procedure [2]. Our novel methodology is designed to detect MCGM using only the "intrinsic" characteristics of a function (i.e., the ε-complexity coefficients) and *does not require any knowledge about the model or type* of the process.

We demonstrated the efficiency of our methodology on simulated data as well as on example of high frequency stock market data. Our simulations and application to real data suggest that the proposed methodology can be widely used.

References

1. Aue A, Horváth L (2013) Structural breaks in time series. J Time Ser Anal 34(1):1–16
2. Brodsky BE, Darkhovsky BS (2000) Non-parametric statistical diagnosis: problems and methods. Kluwer, Dordrecht
3. Darkhovsky BS, Kaplan AYa, Shishkin SL (2002) On an approach to the complexity estimation of curves (based on example of human encephalogram). Autom Remote Control 63(3):468–474
4. Darkhovsky B, Piryatinska A (2014) Quickest detection of changes in the generating mechanism of a time series via the ε-complexity of continuous functions. Seq Anal 33(2):231–250
5. Darkhovsky B, Piryatinska A (2012) A new complexity-based algorithmic procedures for electroencephalogram (EEG) segmentation. In: Conf proc IEEE signal proc med biol symp (SPMB) 2012. doi:10.1109/SPMB.2012.6469462
6. Darkhovsky B, Piryatinska A (2014) A new approach to the problem of segmentation of time series of arbitrary nature. Proc Steklov Inst Math, vol 288 pp 54–67

7. Kolmogorov A (1983) Combinatorial foundations of information theory and the calculus of probability. Russ Math Surv 38(4):29–40
8. Perron P (2006) Dealing with structural breaks. In: Patterson K, Mills TS (eds) Palgrave handbook of econometrics, vol 1. Palgrave Macmillan, Basingstoke, pp 278–352
9. Reeves J, Chen J, Wang XL, Lund R, Lu QQ (2007) A review and comparison of change-point detection techniques for climate data. J Appl Meteorol Climatol 46(6):900–915
10. Shiryaev AN (2010) Quickest detection problems: fifty years later. Seq Anal 29(4):345–385

Chapter 28
Self-concordant Profile Empirical Likelihood Ratio Tests for the Population Correlation Coefficient: A Simulation Study

Thorsten Dickhaus

Abstract We present results of a simulation study regarding the finite-sample type I error behavior of the self-concordant profile empirical likelihood ratio (ELR) test for the population correlation coefficient. Three different families of bivariate elliptical distributions are taken into account. Uniformly over all considered models and parameter configurations, the self-concordant profile ELR test does not keep the significance level for finite sample sizes, albeit the level exceedance monotonously decreases to zero as the sample size increases. We discuss some potential modifications to address this problem.

28.1 Introduction

Empirical likelihood ratio (ELR) tests for multivariate means were introduced in [11]. Although ELR tests are nonparametric tests for statistical functionals, they share an important property with parametric likelihood ratio tests. Namely, under regularity assumptions, the asymptotic distribution of twice the negative logarithmic (empirical) likelihood ratio statistic is chi-squared under the null, with degrees of freedom determined by the dimensionality of the parameter (functional) of interest. This result is commonly referred to as the "Wilks phenomenon", see [18].

ELR tests for the population correlation coefficient ρ of a bivariate distribution constitute a particularly challenging application example, because the evaluation of the ELR in this case requires a nested optimization. In the inner level, optimization has to be performed with respect to a five-dimensional Lagrange multiplier, and in the outer level four nuisance parameters have to be profiled out. We will provide more details in Sect. 28.2.

As reported for instance in Table 1 of [9], the original ELR test for ρ often does not keep the significance level accurately for finite sample sizes. Recently, several novel strategies have been proposed to address this problem. In particular, in [15–17, 19] it has been proposed to extend the parameter space over which the ELR is maximized beyond the convex hull of the observations. Another recent development

T. Dickhaus (✉)
Weierstrass Institute for Applied Analysis and Stochastics, Mohrenstr. 39, 10117 Berlin, Germany
e-mail: Thorsten.Dickhaus@wias-berlin.de

A. Steland et al. (eds.), *Stochastic Models, Statistics and Their Applications*,
Springer Proceedings in Mathematics & Statistics 122,
DOI 10.1007/978-3-319-13881-7_28

is [13] which is centered on an alternative algorithm for the empirical likelihood calculation in order to avoid known issues of earlier approaches. Although not derived from this perspective, the algorithm proposed in [13] also leads to a relaxation of the convex hull constraint; cf. the discussion around Fig. 2 in [13]. While the authors of [16] assess the accuracy of their "extended empirical likelihood" method for multivariate means rather systematically in their Sect. 4, [13] does not contain numerical results.

In this work, we assess the type I error accuracy of the self-concordant profile ELR test for ρ according to [13] by means of computer simulations. We consider three families of multivariate elliptical distributions (see [8] for a comprehensive overview of such distributions). The choice of elliptical models is motivated by the fact that ρ is a meaningful measure of dependency only in such models. Elliptical models play an important role in many applications from the life sciences (cf., e.g., Part II of [5]) and in portfolio theory in finance (see Part IV of [8]). ELR methods are particularly attractive in such a context, because the type of elliptical distribution can often not be specified exactly. For example, there may be lacking information about the degrees of freedom of a multivariate Student's t distribution, see Sect. 28.3 for a definition.

The rest of the paper is structured as follows. In Sect. 28.2.1, we briefly summarize the statistical methodology of ELR tests for ρ. Section 28.2.2 contains some remarks on the computational strategies employed. Our main contribution is Sect. 28.3, where simulation results under three different elliptical models are presented. We conclude with a discussion in Sect. 28.4.

28.2 Statistical Methodology and Implementation

28.2.1 Statistical Methodology

Let $(X_1, Y_1), \ldots, (X_n, Y_n)$ denote an independent and identically distributed (i.i.d.) sample from a bivariate distribution, where (X_1, Y_1) is in distribution equal to (X, Y). Assume that the second moment of the joint distribution of (X, Y) (denoted by $\mathscr{L}(X, Y)$) exists. Let $\mathbf{Z} = (X, Y, X^2, Y^2, XY)^\top$ denote a random vector with values in $\mathbb{R}^5$. For the expectation of $\mathbf{Z}$, it holds that

$$\mathbb{E}[\mathbf{Z}] = \left(\mu_X, \mu_Y, \mu_X^2 + \sigma_X^2, \mu_Y^2 + \sigma_Y^2, \rho\sigma_X\sigma_Y + \mu_X\mu_Y\right)^\top. \tag{28.1}$$

In (28.1) and throughout the remainder, μ_W (σ_W^2) denotes the mean (variance) of the random variable W, and $\rho = \rho(X, Y)$ is Pearson's product-moment correlation coefficient of X and Y. We denote by $\theta = (\mu_X, \mu_Y, \sigma_X^2, \sigma_Y^2, \rho)^\top \in \Theta \subset \mathbb{R}^5$ the five-dimensional vector of the first two population moments of interest and define $h : \Theta \to \mathbb{R}^5$ as the function which maps θ onto $\mathbb{E}[\mathbf{Z}]$. Obviously, h possesses (partial) derivatives of any order.

The ELR for a given parameter value θ^* is given by

$$\mathscr{R}(\theta^*) = \max\left\{\prod_{i=1}^{n} np_i \mid 0 \le p_i \le 1,\ \sum_{i=1}^{n} p_i = 1,\ \sum_{i=1}^{n} p_i \mathbf{Z}_i = h(\theta^*)\right\}, \qquad (28.2)$$

where $\mathbf{Z}_i$ is calculated from (X_i, Y_i) as $\mathbf{Z}$ from (X, Y), for $1 \le i \le n$. The (asymptotic) ELR test for the null hypothesis $H_0' : \theta = \theta^*$ rejects H_0' at significance level $\alpha \in (0, 1)$, if $\ell(\theta^*) = -2\log(\mathscr{R}(\theta^*))$ exceeds $\chi^2_{5;1-\alpha}$, where $\chi^2_{\nu;1-\alpha}$ denotes the $(1-\alpha)$-quantile of the central chi-square distribution with ν degrees of freedom.

In this work, we are concerned with the more general hypothesis H_0: $\{\rho = \rho^*\}$ for a given value $\rho^* \in [-1, 1]$. For testing H_0, we profile out the nuisance parameters μ_X, μ_Y, σ_X^2, and σ_Y^2. More specifically, let $\Theta(\rho^*) = \{\theta \in \Theta\colon\ \rho = \rho^*\}$. The test for H_0 can then be described by the following algorithm.

Algorithm 28.1

1. *Maximize $\mathscr{R}$ over $\theta^* \in \Theta(\rho^*)$. Denote the maximizer by $\theta(\rho^*)$.*
2. *Reject H_0 at significance level α, if $\ell(\rho^*) = -2\log(\mathscr{R}(\theta(\rho^*))) > \chi^2_{1;1-\alpha}$.*

Remark 28.1 The testing method based on $\mathbf{Z}$ has been outlined in Sect. 3.4 of [12]. It appears more convenient than the method originally proposed in Sect. 6.2 of [11], because it avoids iterated re-centering of the observations when step 1 of Algorithm 28.1 is performed.

28.2.2 Implementation

Notice that Algorithm 28.1 involves a nested double optimization. Namely, the inner optimization is given by the maximization in (28.2) for given θ^*, and the outer optimization is given by the maximization over the nuisance parameters μ_X, μ_Y, σ_X^2, σ_Y^2 as described in the first step of Algorithm 28.1.

For the outer optimization, a general-purpose (constrained) optimizer can be employed. For the simulations in Sect. 28.3, we utilized the `optim` function in `R` with method `"L-BFGS-B"`. This routine implements the box-constrained optimization algorithm from [3]. Constraints are required in our context, because σ_X^2 and σ_Y^2 are necessarily non-negative.

More crucial is the inner optimization problem (28.2). To this end, in [13] an algorithm based on self-concordance has been introduced. In a nutshell, the negative empirical log-likelihood ratio is approximated by a quartic polynomial, leading to a convex constrained optimization problem which can be solved by the method of Lagrange multipliers. Art B. Owen, the author of [13], also contributed the `R` program `scel.R` on which our simulations in Sect. 28.3 rely.

28.3 Simulation Results

In this section, we present simulation results under three different elliptical models for $\mathscr{L}(X, Y)$. In general, the probability density function (pdf) of an elliptically contoured distribution on $\mathbb{R}^d$ is of the form

$$f(\mathbf{t}) = C_d |\det \Sigma|^{-1/2} g\left(\mathbf{t}^\top \Sigma^{-1} \mathbf{t}\right), \quad \mathbf{t} \in \mathbb{R}^d,$$

where C_d is a normalizing constant which depends on d. The positive definite matrix $\Sigma \in \mathbb{R}^{d \times d}$ is called the dispersion matrix. It captures the (elliptical) dependencies among the components of a random vector with pdf f. The scalar function g is called the density generator of the elliptical distribution. Three well-known families of elliptical distributions are

(a) normal distributions on $\mathbb{R}^d$ with $g(u) = \exp(-u/2)$,
(b) Student's t distributions on $\mathbb{R}^d$ with $g(u) = (1 + u/\nu)^{-(d+\nu)/2}$, $\nu \in \mathbb{N}$,
(c) double-exponential (Laplace) distributions on $\mathbb{R}^d$ with $g(u) = \exp(-|u|)$.

We will consider these three distributional families in the remainder of this section.

28.3.1 Bivariate Normal Distribution

We assume that $\mathscr{L}(X, Y) = \mathscr{N}_2(0, \Sigma)$, where $\sigma_X^2 = \sigma_Y^2 = 1$ without loss of generality. The off-diagonal element of $\Sigma \in [-1, 1]^{2\times 2}$ is the parameter ρ of interest. Pseudo-random samples were generated by utilizing the routine `rmvnorm` from the `R` package `mvtnorm`, cf. [7]. Table 28.1 summarizes our simulation results under this Gaussian model for $\mathscr{L}(X, Y)$.

28.3.2 Bivariate Student's t Distribution

In this section, we assume that $\mathscr{L}(X, Y)$ is a centered bivariate Student's t distribution with $\nu > 2$ degrees of freedom and dispersion matrix $\Sigma \in \mathbb{R}^{2\times 2}$, denoted as $t_2(\nu, \Sigma)$. In analogy to Sect. 28.3.1, we may without loss of generality assume that $\Sigma_{11} = \Sigma_{22} = 1$. In this case, Σ is the correlation matrix of (X, Y) (see Sect. 1.7 of [10]); hence, its off-diagonal element equals again the parameter ρ. Pseudo-random samples were generated by utilizing the routine `rmvt` from the `R` package `mvtnorm`. Since it is well-known that $t_2(\nu, \Sigma)$ converges weakly to $\mathscr{N}_2(0, \Sigma)$ with increasing degrees of freedom ν, we restrict our attention to small values $\nu \in \{5, 10\}$ in Table 28.2.

Table 28.1 Relative rejection frequencies of the self-concordant profile empirical likelihood ratio test for the population correlation coefficient in case of bivariate Gaussian data. The nominal significance level was set to $\alpha = 5$ % in all simulations. Results are based on 10,000 Monte Carlo repetitions for each parameter configuration (ρ: true underlying correlation coefficient, n: sample size).

ρ	n	Relative rejection frequency
−0.9	10	0.1669
−0.9	20	0.1030
−0.9	50	0.0681
−0.9	100	0.0593
−0.75	10	0.1668
−0.75	20	0.1069
−0.75	50	0.0758
−0.75	100	0.0588
−0.5	10	0.1645
−0.5	20	0.1089
−0.5	50	0.0688
−0.5	100	0.0624
−0.25	10	0.1655
−0.25	20	0.1102
−0.25	50	0.0737
−0.25	100	0.0593
0	10	0.1669
0	20	0.1106
0	50	0.0697
0	100	0.0623
0.25	10	0.1612
0.25	20	0.1085
0.25	50	0.0716
0.25	100	0.0558
0.5	10	0.1705
0.5	20	0.1066
0.5	50	0.0743
0.5	100	0.0586
0.75	10	0.1649
0.75	20	0.1077
0.75	50	0.0737
0.75	100	0.0605
0.9	10	0.1662
0.9	20	0.1015
0.9	50	0.0716
0.9	100	0.0625

28.3.3 Bivariate Double-Exponential Distribution

Here, we consider centered bivariate double-exponential (Laplace) distributions for $\mathscr{L}(X, Y)$. To this end, it is convenient to notice that in this case (X, Y) possesses the stochastic representation

$$\begin{pmatrix} X \\ Y \end{pmatrix} \stackrel{d}{=} \sqrt{E}\mathbf{G}, \tag{28.3}$$

where E follows a univariate exponential distribution with intensity parameter $\lambda > 0$, and $\mathbf{G}$ denotes a centered bivariate Gaussian random vector which is independent of E and has covariance matrix Σ; see, e.g., Eq. (6) in [6]. Letting $\Sigma_{11} = \Sigma_{22} = 1$, we again obtain that $\rho(X, Y) = \Sigma_{12}$. Since the latter property holds regardless of the value of λ, we can restrict our attention to $\lambda = 1$. Based on (28.3), pseudo-random samples were generated by generating independent realizations of E with the `R` function `rexp` and independent realizations of $\mathbf{G}$ with the `rmvnorm`

Table 28.2 Relative rejection frequencies of the self-concordant profile empirical likelihood ratio test for the population correlation coefficient in case of bivariate Student's t data. The nominal significance level was set to $\alpha = 5\ \%$ in all simulations. Results are based on 10,000 Monte Carlo repetitions for each parameter configuration (ρ: true underlying correlation coefficient, ν: degrees of freedom, n: sample size)

ρ	ν	n	Relative rejection freq.
−0.9	5	10	0.2069
−0.9	5	20	0.1481
−0.9	5	50	0.1091
−0.9	5	100	0.0974
−0.9	10	10	0.1762
−0.9	10	20	0.1157
−0.9	10	50	0.0869
−0.9	10	100	0.0763
−0.75	5	10	0.2088
−0.75	5	20	0.1459
−0.75	5	50	0.1080
−0.75	5	100	0.0919
−0.75	10	10	0.1741
−0.75	10	20	0.1271
−0.75	10	50	0.0838
−0.75	10	100	0.0722
−0.5	5	10	0.2083
−0.5	5	20	0.1482
−0.5	5	50	0.1068
−0.5	5	100	0.0871
−0.5	10	10	0.1856
−0.5	10	20	0.1307
−0.5	10	50	0.0853
−0.5	10	100	0.0690
−0.25	5	10	0.2094
−0.25	5	20	0.1530
−0.25	5	50	0.1053
−0.25	5	100	0.0904
−0.25	10	10	0.1888
−0.25	10	20	0.1282
−0.25	10	50	0.0835
−0.25	10	100	0.0707
0	5	10	0.2089
0	5	20	0.1468
0	5	50	0.1065
0	5	100	0.0887
0	10	10	0.1835
0	10	20	0.1327
0	10	50	0.0844
0	10	100	0.0738
0.25	5	10	0.2163
0.25	5	20	0.1561
0.25	5	50	0.1112
0.25	5	100	0.0888
0.25	10	10	0.1803
0.25	10	20	0.1215
0.25	10	50	0.0867
0.25	10	100	0.0699
0.5	5	10	0.2131
0.5	5	20	0.1492
0.5	5	50	0.1092
0.5	5	100	0.0916
0.5	10	10	0.1955
0.5	10	20	0.1248
0.5	10	50	0.0851
0.5	10	100	0.0692
0.75	5	10	0.2106
0.75	5	20	0.1425
0.75	5	50	0.1110
0.75	5	100	0.0884
0.75	10	10	0.1844
0.75	10	20	0.1224
0.75	10	50	0.0865
0.75	10	100	0.0639
0.9	5	10	0.2022
0.9	5	20	0.1478
0.9	5	50	0.1039
0.9	5	100	0.0942
0.9	10	10	0.1830
0.9	10	20	0.1220
0.9	10	50	0.0825
0.9	10	100	0.0679

Table 28.3 Relative rejection frequencies of the self-concordant profile empirical likelihood ratio test for the population correlation coefficient in case of bivariate double-exponential data. The nominal significance level was set to $\alpha = 5$ % in all simulations. Results are based on 10,000 Monte Carlo repetitions for each parameter configuration (ρ: true underlying correlation coefficient, n: sample size)

ρ	n	Relative rejection frequency
−0.9	10	0.2262
−0.9	20	0.1585
−0.9	50	0.1017
−0.9	100	0.0823
−0.75	10	0.2273
−0.75	20	0.1575
−0.75	50	0.1004
−0.75	100	0.0840
−0.5	10	0.2417
−0.5	20	0.1603
−0.5	50	0.1059
−0.5	100	0.0812
−0.25	10	0.2362
−0.25	20	0.1632
−0.25	50	0.1021
−0.25	100	0.0846
0	10	0.2351
0	20	0.1644
0	50	0.1022
0	100	0.0848
0.25	10	0.2363
0.25	20	0.1570
0.25	50	0.1045
0.25	100	0.0833
0.5	10	0.2281
0.5	20	0.1565
0.5	50	0.1067
0.5	100	0.0856
0.75	10	0.2293
0.75	20	0.1578
0.75	50	0.1005
0.75	100	0.0824
0.9	10	0.2279
0.9	20	0.1494
0.9	50	0.1023
0.9	100	0.0822

function as described in Sect. 28.3.1. Simulation results for this model are presented in Table 28.3.

28.4 Concluding Remarks

Summarizing our findings we observe that the relative rejection frequencies obtained under joint normality of (X, Y) are very close to those reported in Table 1 of [9]. The ELR test does not keep the significance level accurately for finite sample sizes, but the level exceedance monotonously decreases to zero as the sample size increases. Qualitatively, this behavior of the ELR test is also reflected in our Tables 28.2 and 28.3 which correspond to two other elliptical models for $\mathscr{L}(X, Y)$.

Thus, if Gaussianity of (X, Y) can be assumed, it seems recommendable to carry out a parametric test as explained, e.g., in Sect. 4.2 of [2]. In the nonparametric setting, future research will consider Bartlett-corrected critical values (see [4]) in

order to overcome the reported anti-conservativity of the considered ELR tests. On a more fundamental level, an interesting and challenging research direction would be to analyze the finite-sample properties of ELR-based inference by providing concentration inequalities in the spirit of [14].

Finally, let us mention that our restriction to point hypotheses of the form H_{ρ^*}: $\{\rho = \rho^*\}$ is not a severe limitation. Namely, by duality of tests and confidence regions, a composite null hypothesis $H_{\text{comp.}}$ (associated with a subset of $[-1, 1] \ni \rho$) can be tested on the basis of a family of point hypothesis tests. Following [1], a $(1-\alpha)$-confidence region $\mathscr{C}_\alpha$ is constituted by the set of all parameter values ρ^* for which H_{ρ^*} is not rejected. Then, $H_{\text{comp.}}$ can be rejected at level α if $H_{\text{comp.}} \cap \mathscr{C}_\alpha = \emptyset$. It is clear that the type I error accuracy of this test for $H_{\text{comp.}}$ depends on that of the tests for the H_{ρ^*}.

References

1. Aitchison J (1964) Confidence-region tests. J R Stat Soc B 26:462–476
2. Anderson TW (1984) An introduction to multivariate statistical analysis, 2nd edn. Wiley series in probability and mathematical statistics. Wiley, New York
3. Byrd RH, Lu P, Nocedal J, Zhu C (1995) A limited memory algorithm for bound constrained optimization. SIAM J Sci Comput 16(5):1190–1208
4. DiCiccio T, Hall P, Romano J (1991) Empirical likelihood is Bartlett-correctable. Ann Stat 19(2):1053–1061
5. Dickhaus T (2014) Simultaneous statistical inference with applications in the life sciences. Springer, Berlin
6. Eltoft T (2006) On the multivariate Laplace distribution. IEEE Signal Process Lett 13(5):300–303
7. Genz A, Bretz F (2009) Computation of multivariate normal and t probabilities. Lecture notes in statistics, vol 195. Springer, Berlin
8. Gupta AK, Varga T, Bodnar T (2013) Elliptically contoured models in statistics and portfolio theory, 2nd edn. Springer, New York
9. Hall P, La Scala B (1990) Methodology and algorithms of empirical likelihood. Int Stat Rev 58(2):109–127
10. Kotz S, Nadarajah S (2004) Multivariate t distributions and their applications. Cambridge University Press, Cambridge
11. Owen AB (1990) Empirical likelihood ratio confidence regions. Ann Stat 18(1):90–120
12. Owen AB (2001) Empirical likelihood. Chapman & Hall/ CRC, Boca Raton
13. Owen AB (2013) Self-concordance for empirical likelihood. Can J Stat 41(3):387–397
14. Spokoiny V (2012) Parametric estimation. Finite sample theory. Ann Stat 40(6):2877–2909
15. Tsao M (2013) Extending the empirical likelihood by domain expansion. Can J Stat 41(2):257–274
16. Tsao M, Wu F (2013) Empirical likelihood on the full parameter space. Ann Stat 41(4):2176–2196
17. Tsao M, Wu F (2014) Extended empirical likelihood for estimating equations. Biometrika 101(3):703–710, doi:10.1093/biomet/asu014
18. Wilks SS (1938) The large-sample distribution of the likelihood ratio for testing composite hypotheses. Ann Math Stat 9:60–62
19. Wu F, Tsao M (2014) Two-sample extended empirical likelihood. Stat Probab Lett 84:81–87

Chapter 29
Risk-Averse Equilibrium Modeling and Social Optimality of Cap-and-Trade Mechanisms

Paolo Falbo, Juri Hinz, and Cristian Pelizzari

Abstract We present and explore a link between social optimality and risk-neutral dynamics satisfied in the equilibrium of emission markets. Our contribution addresses market modeling in the setting of risk-averse market players and goes beyond all existing models in this field, which neglect risk-aversion aspects at the cost of having a wide range of singularities.

29.1 Introduction

According to theoretical arguments, a properly designed emission trading system should help pollution reduction with low social costs. Originated from this idea, and based on the theoretical work of environmental economists, cap-and-trade systems have been put into operations all over the world. However, the practice from emission trading yields a real stress test for the underlying theory and reveals a number of its weak points. This paper aims to fill this gap. For proofs, additional insides, and an extensive literature overview, we refer the reader to Falbo et al. [7].

Before we start, let us mention the contributions which are related to our analysis. The efficiency properties of environmental markets have been first addressed in Dales [6] and Montgomery [10], which first advanced the principle that the "environment" is a good that cannot be "consumed" for free. Subsequent research has also considered stochastic and multi-period modeling. We refer the interested reader to Taschini [13], which provides an extensive literature review, though it is far from

P. Falbo (✉) · C. Pelizzari
Department of Economics and Management, University of Brescia, Contrada S. Chiara, 50–25122 Brescia BS, Italy
e-mail: paolo.falbo@unibs.it

C. Pelizzari
e-mail: cristian.pelizzari@unibs.it

J. Hinz
School of Mathematics, University of Technology, Sydney, 15 Broadway – ULTIMO NSW 2007, Sydney, Australia
e-mail: juri.hinz@uts.edu.au

A. Steland et al. (eds.), *Stochastic Models, Statistics and Their Applications*,
Springer Proceedings in Mathematics & Statistics 122,
DOI 10.1007/978-3-319-13881-7_29

being complete. A majority of relatively recent papers (see, in particular, Stevens and Rose [12]; Chesney and Taschini [5]; Seifert et al. [11]; Carmona et al. [3, 4]; Hinz and Novikov [8]; Kijima et al. [9]; Barrieu and Fehr [1]; Carmona and Fehr, [2]) are related to equilibrium models, where risk-neutral individuals optimize the expected value of their profits.

29.2 Model

To explain the emission trading mechanism, we present a market model where a finite number of agents, indexed by the set I, are confronted with abatement of their pollution. The key assumptions are:

- We consider a trading scheme in isolation, within a time horizon $[0, T]$, without credit transfer from and to other markets. That is, unused allowances expire worthless.
- There is no production strategy adjustment within the compliance period $[0, T]$. This means that the agents schedule their production plans for the entire period $[0, T]$ at the beginning. Allowances can be traded twice: at time $t = 0$ at the beginning and at time $t = T$ immediately before emission reports are surrendered to the regulator.
- For the sake of simplicity, we set the interest rate to zero.
- Each agent decides how much of a polluting good to produce and how many allowances to trade (we focus on electricity, which will also be called energy).

This one-period model is best suited for our needs of explaining the core mechanism of market operation and to discuss its properties.

Allowance allocation: We assume that the administrator allocates a pre-determined number $\gamma_0^i \in \mathbb{R}_+$ of allowances to each agent i.

Production costs and volume: The ith agent is specified by the set Ξ^i of feasible production plans for the generation of energy within one time period from $t = 0$ to $t = T$. At time $t = 0$, each agent $i \in I$ faces the energy demand $D_0 \in \mathbb{R}_+$ of the entire market, the realized electricity price $P_0 \in \mathbb{R}_+$, and the allowance price $A_0 \in \mathbb{R}_+$. Based on this information, each agent decides on its production plan $\xi_0^i \in \Xi^i$. Given $\xi_0^i \in \Xi^i$, the agent realizes at the decision time $t = 0$ the production volume $V_0^i(\xi_0^i) \in \mathbb{R}$ and the production costs $C_0^i(\xi_0^i) \in \mathbb{R}$, which are described by functions

$$\xi_0^i : \Xi^i \to \mathbb{R}, \qquad \xi_0^i \mapsto V_0^i\big(\xi_0^i\big), \qquad \xi_0^i \mapsto C_0^i\big(\xi_0^i\big), \quad i \in I.$$

That is, the revenue of the production plan is known at time $t = 0$ and is given by $P_0 V_0^i(\xi_0^i)$. Let us now turn to the uncertainties, which will be modeled by random variables defined on an appropriate probability space $(\Omega, \mathscr{F}, \mathbb{P})$.

Emission from production: Following the production plan ξ_0^i, the total pollution of agent i is expressed as $E_T^i(\xi_0^i)$. It is natural to assume that, although the production plan ξ_0^i is deterministically scheduled at time $t = 0$, the total emissions associated with this production cannot be predicted with certainty at $t = 0$, when the

production and trading decisions are made. In fact, in practice the producers have to manage diverse sources of randomness while following production (demand fluctuation, outages of generators), which usually yield small but unpredictable deviations N^i from the nominal emission $E_0^i(\xi_0^i)$ associated with production plan ξ_0^i. Thus, let us agree that $E_T^i(\xi_0^i)$ is modeled as a random variable expressed as a sum $E_T^i(\xi_0^i) = E_0^i(\xi_0^i) + N^i$, $\xi_0^i \in \Xi^i$, $i \in I$, with the deterministic function $E_0^i : \Xi^i \to \mathbb{R}$, $i \in I$, describing the dependence of nominal emissions $E_0^i(\xi_0^i)$ on production plan ξ_0^i and with the random variable N^i standing for the deviation from nominal emissions. Note that the random emissions $E_T^i(\xi_0^i)$, $i \in I$, will be the only source of uncertainty in our model.

Assumption: To ease our analysis, let us agree that for the production plans $\xi_0^i \in \Xi_i$, $i \in I$, the total market emissions $\sum_{i\in I} E_T^i(\xi_0^i)$ possess no point masses, which is ensured by $\mathbb{P}(\sum_{i\in I} N^i = z) = 0$ for all $z \in \mathbb{R}$.

Allowance trading: At times $t = 0, T$, the allowances can be exchanged between agents by trading at the prices A_0 and A_T, respectively. Denote by ϑ_0^i, ϑ_T^i the change at times $t = 0, T$ of the allowance number held by agent $i \in I$. Such trading yields a revenue, which is $-\vartheta_0^i A_0 - \vartheta_T^i A_T$. Note that ϑ_0^i and A_0 are deterministic, whereas ϑ_T^i and A_T are modeled as random variables. Observe that sales are described by negative values of ϑ_0^i and ϑ_T^i, therefore the result is a non-negative random variable if allowances are sold.

Penalty payment: A penalty $\pi \in \mathbb{R}_+$ must be paid at maturity T for each unit of pollutant not covered by allowances. Given the changes at times $t = 0, T$ due to allowance trading, i.e. ϑ_0^i and ϑ_T^i, the production plan ξ_0^i, and the total number γ_0^i of allowances allocated to agent $i \in I$, the loss of agent i due to a potential penalty payment is given by $\pi(E_T^i(\xi_T^i) - \vartheta_0^i - \vartheta_T^i - \gamma_0^i)^+$.

Individual profit: The profit of agent $i \in I$ following trading and production strategy $(\vartheta^i, \xi^i) = (\vartheta_0^i, \vartheta_T^i, \xi_0^i)$ depends on the market prices $(A, P) = (A_0, A_T, P_0)$ of allowances and energy and is given by

$$L^{A,P,i}\big(\vartheta^i, \xi^i\big) = -\vartheta_0^i A_0 - \vartheta_T^i A_T - C_0^i\big(\xi_0^i\big) + P_0 V_0^i\big(\xi_0^i\big) - \pi\big(E_T^i\big(\xi_0^i\big) - \vartheta_0^i - \vartheta_T^i - \gamma_0^i\big)^+.$$

Risk-aversion and rational behavior: Suppose that the risk attitudes of each agent $i \in I$ are described by a pre-specified strictly increasing utility function $U^i : \mathbb{R} \to \mathbb{R}$. With this, the rational behavior of agent i is targeted on the maximization of the functional $(\vartheta^i, \xi^i) \mapsto \mathbb{E}(U^i(L^{A,P,i}(\vartheta^i, \xi^i)))$ over all the possible trading and production strategies $(\vartheta^i, \xi^i) = (\vartheta_0^i, \vartheta_T^i, \xi_0^i)$.

Energy demand: Suppose that at time $t = 0$ the agents observe the total energy demand, which is described by $D_0 \in \mathbb{R}_+$. Let us agree that the demand must be covered.

Market equilibrium: Following standard apprehension, a realistic market state is described by the so-called equilibrium—a situation where allowance prices, allowance positions, and production decisions are such that each agent is satisfied by the own policy and, at the same time, natural restrictions are fulfilled.

Definition 29.1 Given energy demand $D_0 \in \mathbb{R}_+$, the prices $(A^*, P^*) = (A_0^*, A_T^*, P_0^*)$ are called equilibrium prices if for each agent $i \in I$ there exists a strategy $(\vartheta^{i*}, \xi^{i*}) = (\vartheta_0^{i*}, \vartheta_T^{i*}, \xi_0^{i*})$ such that:

(i) The energy demand is covered: $\sum_{i\in I} V_0^i(\xi_0^{i*}) = D_0$,
(ii) The emission certificates are in zero net supply:

$$\sum_{i\in I} \vartheta_t^{i*} = 0 \quad \text{almost surely for } t = 0 \text{ and } t = T,$$

(iii) Each agent $i \in I$ is satisfied by the own policy, in the sense that

$$\mathbb{E}\big(U^i\big(L^{A^*,P^*,i}\big(\vartheta^{i*}, \xi^{i*}\big)\big)\big) \geq \mathbb{E}\big(U^i\big(L^{A^*,P^*,i}\big(\vartheta^{i}, \xi^{i}\big)\big)\big)$$

holds for any alternative strategy (ϑ^i, ξ^i).

Given production plans $\xi_0^i \in \Xi^i$, $i \in I$, we denote the market production schedule by $\xi_0 = (\xi_0^i)_{i\in I} \in \bigtimes_{i\in I} \Xi^i$ and introduce the total production costs C_0, the total production volume V_0, the total carbon dioxide emission E_T, the total nominal carbon dioxide emission E_0, and the overall unpredictable emission fluctuations N as defined by

$$C_0(\xi_0) = \sum_{i\in I} C_0^i\big(\xi_0^i\big), \qquad V(\xi_0) = \sum_{i\in I} V_0^i\big(\xi_0^i\big), \qquad E_T(\xi_0) = \sum_{i\in I} E_T^i\big(\xi_0^i\big),$$
$$E_0(\xi_0) = \sum_{i\in I} E_0^i\big(\xi_0^i\big), \qquad N = \sum_{i\in I} N^i.$$

It turns out that there is no arbitrage allowance trading and that the terminal allowance price is digital.

Proposition 29.1 *Given energy demand $D_0 \in \mathbb{R}_+$, let $(A^*, P^*) = (A_0^*, A_T^*, P_0^*)$ be the equilibrium prices with the corresponding strategies $(\vartheta^{i*}, \xi^{i*})$, $i \in I$. It holds*:

(i) *There exists a risk-neutral measure $\mathbb{Q}^* \sim \mathbb{P}$ such that $A^* = (A_0^*, A_T^*)$ follows a martingale with respect to $\mathbb{Q}^*$.*
(ii) *The terminal allowance price in equilibrium is digital*:

$$A_T^* = \pi 1_{\{E_T(\xi_0^*) - \gamma_0 \geq 0\}}, \tag{29.1}$$

where $\xi_0^* = (\xi_0^{i*})_{i\in I} \in \times_{i\in I} \Xi^i$ is the equilibrium market production schedule.
(iii) *For each market production schedule $\xi_0 = (\xi_0^i)_{i\in I} \in \bigtimes_{i\in I} \Xi^i$ which covers the demand, i.e. $V_0(\xi_0) \geq V_0(\xi_0^*) = D_0$, it holds that*

$$C_0\big(\xi_0^*\big) + A_0^* E_0\big(\xi_0^*\big) \leq C_0(\xi_0) + A_0^* E_0(\xi_0). \tag{29.2}$$

To formulate social optimality, we require additional notations. Having in mind that $C_0(\xi_0)$ stands for the social costs of the market production schedule and interpreting $\pi(E_T(\xi_0) - \gamma_0)^+$ as a proxy of the environmental impact of the market

production schedule ξ_0, let us agree that $B(\xi_0) = C_0(\xi_0) + \pi(E_T(\xi_0) - \gamma_0)^+$ expresses the social burden caused by the market production schedule ξ_0. It turns out that the equilibrium market production schedule minimizes the social burden among all the market production schedules which cover a given demand.

Proposition 29.2 *Given energy demand $D_0 \in \mathbb{R}_+$, let $(A^*, P^*) = (A_0^*, A_T^*, P_0^*)$ be the equilibrium prices with the corresponding strategies $(\vartheta^{i*}, \xi^{i*})$, $i \in I$. Let $\mathbb{Q}^*$ be a risk-neutral measure whose existence is shown in Proposition 29.1. Then*

$$\mathbb{E}^{\mathbb{Q}^*}\big(B(\xi_0^*)\big) \le \mathbb{E}^{\mathbb{Q}^*}\big(B(\xi_0)\big)$$

holds for each market production schedule $\xi_0 = (\xi_0^i)_{i\in I} \in \bigtimes_{i\in I} \Xi^i$ which yields at least the same production volume of the equilibrium market production schedule $\xi_0^* = (\xi_0^{i*})_{i\in I} \in \bigtimes_{i\in I} \Xi^i$, i.e. $V_0(\xi_0) \ge V_0(\xi_0^*) = D_0$.

In Proposition 29.2, the equilibrium market production schedule ξ_0^* (which coincides with that resulting in Proposition 29.1) was characterized as a solution of the minimization problem

$$\text{minimize } \mathbb{E}^{\mathbb{Q}^*}\big(B(\xi_0)\big) \text{ over } \xi_0 \in \bigtimes_{i\in I} \Xi^i, \quad \text{subject to } V_0(\xi_0) \ge D_0. \tag{29.3}$$

Although this fact is about minimization of social burden, it should not be interpreted as one of the classical welfare results, which typically follow from equilibrium considerations. A critical point here is that this type of cost-optimality needs to be taken with great care: due to the opportunity cost-pass-through, even though society overall reduces emissions at the lowest cost, an (inappropriately designed) cap-and-trade could end up with distributing that cost all (or the largest part of it) to consumers.

An interesting observation from Proposition 29.2 is that the expectation $\mathbb{E}^{\mathbb{Q}^*}(B(\xi_0))$ of the social burden $B(\xi_0)$ is minimized with respect to a risk-neutral measure $\mathbb{Q}^*$, which in general differs from the objective measure $\mathbb{P}$. The measure $\mathbb{Q}^*$ is an outcome of the equilibrium, and, as such, it depends heavily on the many model components, such as risk-aversions, allowance endowments, and production technologies of the agents. However, it is surprising that, once the measure $\mathbb{Q}^*$ is known, other important equilibrium outcomes can be obtained from aggregated quantities only. In particular, given $\mathbb{Q}^*$, the equilibrium market production schedule ξ_0^* can be obtained as the solution of optimization problem (29.3). Such solution is determined by aggregated quantities, since the social burden is by definition $B(\xi_0) = C_0(\xi_0) + \pi(E_T(\xi_0) - \gamma_0)^+$ and, apart the quantities γ_0 and π decided by the authority, it depends only on technologies present in the market. Having obtained the equilibrium market production schedule ξ_0^* as the solution of optimization problem (29.3), the equilibrium allowance price A_0^* is calculated by applying martingale pricing: $A_0^* = \pi\mathbb{E}^{\mathbb{Q}^*}(1_{\{E_T(\xi_0^*)-\gamma_0\ge 0\}})$. Finally, given the market production schedule ξ_0^* and the allowance price A_0^*, the electricity price P_0^* can be obtained as the marginal price of the most expensive technology, active in the schedule ξ_0^*. Bottom line, given $\mathbb{Q}^*$, merely aggregated market parameters are needed to obtain ξ_0^*, A_0^*, and P_0^*. This observation can be used to establish and analyze realistic equilibrium-like emission market models.

29.3 Market Equilibrium in Terms of Risk-Neutral Measure

In view of this, we suggest an alternative way to quantitatively assess the equilibrium state of an emission market, starting from aggregated quantities and using an exogenously specified proxy for a risk-neutral measure $\mathbb{Q}^*$. This general approach follows the standard methodology of financial mathematics, which describes the stochastic evolution of equilibrium prices in financial markets under a risk-neutral measure:

(0) Determine a risk-neutral measure $\mathbb{Q}$, which corresponds to an equilibrium situation of the emission market in the sense of (ii) of Proposition 29.1.

(1) Observe that, because of (29.2), the equilibrium market production schedule ξ_0^* must be a solution of the following *deterministic optimization problem*

$$\text{minimize } C_0(\xi_0) + A_0 E_0(\xi_0) \text{ over } \xi_0 \in \times_{i\in I} \Xi^i, \quad \text{subject to } V_0(\xi_0) \geq D_0, \tag{29.4}$$

where the parameter A_0 equals the equilibrium allowance price A_0^*, which will be determined in the next steps.

(2) To proceed, assume that

$$\text{for each } A_0 \in [0, \pi] \text{ there exists a unique solution } \xi_0^*(A_0) \text{ of (29.4)}, \tag{29.5}$$

to define the following function of A_0:

$$E_0^*(A_0) = E_0\big(\xi_0^*(A_0)\big), \quad A_0 \in [0, \pi].$$

(3) Having assumed (29.5), because of (29.1), the equilibrium emission price must be a solution of the following fixed point problem:

$$A_0 = \pi \mathbb{E}^{\mathbb{Q}}(1_{\{E_0^*(A_0)+N-\gamma_0 \geq 0\}}), \quad \text{subject to } A_0 \in [0, \pi]. \tag{29.6}$$

Further, suppose that problem (29.6) admits a unique solution A_0^*.

(4) Determine the solution A_0^* of (29.6) and calculate $\xi_0^* = \xi_0^*(A_0^*)$ from (29.5).

(5) Having calculated the equilibrium market production schedule $\xi_0^* = \xi_0(A_0^*)$, determine the equilibrium production costs $C_0(\xi_0^*)$, the equilibrium nominal emissions $E_0(\xi_0^*)$, and the equilibrium energy price P_0^* to assess the performance in the emission reduction of the proposed market architecture.

Such risk-neutral equilibrium-like modeling requires specification of few aggregated quantities. Furthermore, a risk-neutral measure $\mathbb{Q}^*$ must be determined. One only needs to specify $N = \sum_{i\in I} N^i$, i.e. the overall unpredictable emission fluctuations, under a risk-neutral measure. This distribution can be described in a parameter-dependent way, which adds a desirable flexibility to the model. As one of the central questions in quantitative finance, the connection between risk-neutral and objective measures has been successfully addressed over the recent decades.

29.4 Energy Mix Model

Let us show how a realization of the above program can be carried out within a realistic situation, where an energy market is given in terms of production capacities allocated along diverse technologies with their specific cost structure, usually referred to as the *energy mix model*.

Let us agree that the space of energy production technologies is described by the set $[0,\infty[^2$ such that each point $(c,e)\in[0,\infty[^2$ represents a production technology with production costs c (euros per megawatt hour) and emission rate e (tonnes of carbon dioxide per megawatt hour). We describe the energy mix as *production capacity distribution, modeled in terms of a measure q on* $[0,\infty[^2$. The set $R\subset[0,\infty[^2$ describes a range of technologies (c,e), which are chosen for consideration. Having specified the technology range $R\subset[0,\infty[^2$, the production capacity, the production costs and the emissions of R can be obtained by integration, and are, respectively, $\int_R q(\mathrm{d}c,\mathrm{d}e)$, $\int_R c\cdot q(\mathrm{d}c,\mathrm{d}e)$, and $\int_R e\cdot q(\mathrm{d}c,\mathrm{d}e)$. Now, we introduce the equilibrium production which is always scheduled in the merit order, according to the production costs. Thereby, the production costs account for the actual emission rate, because of opportunity cost arguments (see Falbo et al. [7]). Given the energy demand $D_0\in\mathbb{R}_+$, it is shown in Falbo et al. [7] that the range $R(P_0,A_0)$ of technologies, active in energy production, is given in terms on the energy price $P_0\in\mathbb{R}_+$ and the emission price $A_0\in[0,\pi]$ by $R(P_0,A_0)=\{(c,e)\in[0,\infty[^2\colon\ c+A_0e\le P_0\}$. In other words, given the emission price A_0, the relevant costs of production technology (c,e) consist of the true production costs c in addition to the opportunity costs $e\cdot A_0$, which describe the forgone profit of using emission rights to cover production instead of selling them to the market. Given prices (P_0,A_0), each technology (c,e) with $c+A_0e\le P_0$ participates in the production. Thus, let us define the volume $V(P_0,A_0)$, the costs $C(P_0,A_0)$, and the emissions $E(P_0,A_0)$ at the prices (P_0,A_0) as the corresponding quantities from the production schedule $R(P_0,A_0)$ by $V(P_0,A_0)=\int_{R(P_0,A_0)}q(\mathrm{d}c,\mathrm{d}e)$, $C(P_0,A_0)=\int_{R(P_0,A_0)}c\cdot q(\mathrm{d}c,\mathrm{d}e)$, and $E(P_0,A_0)=\int_{R(P_0,A_0)}e\cdot q(\mathrm{d}c,\mathrm{d}e)$. By definition, the equilibrium production must satisfy the energy demand D_0, thus we define the energy price $P^*(D_0,A_0)$, the emissions $E^*(D_0,A_0)$, and the production costs $C^*(D_0,A_0)$, at demand D_0 and emission price A_0, as

$$\begin{aligned}
P^*(D_0,A_0)&=\inf\bigl\{P_0\ge 0\colon\ V(P_0,A_0)\ge D_0\ge 0\bigr\},\\
E^*(D_0,A_0)&=E\bigl(P^*(D_0,A_0),A_0\bigr),\\
C^*(D_0,A_0)&=C\bigl(P^*(D_0,A_0),A_0\bigr).
\end{aligned}$$

For the penalty size $\pi\in\mathbb{R}_+$, we introduce the expected penalty payment $\Pi^*(D_0,A_0)$ at demand D_0 and emission price A_0 as

$$\begin{aligned}
\Pi^*(D_0,A_0)&=\pi\mathbb{E}^{\mathbb{Q}}\bigl(\bigl(E^*(D_0,A_0)+N-\gamma_0\bigr)^+\bigr)\\
&=\pi\int_{\mathbb{R}}\bigl(E^*(D_0,A_0)+n-\gamma_0\bigr)^+\nu(n)dn,
\end{aligned}$$

where we assume that,

$$\left.\begin{array}{c}\text{with respect to the risk-neutral measure } \mathbb{Q},\\ \text{the overall unpredictable emission fluctuations } N\\ \text{follow a distribution with pre-specified density } \nu : \mathbb{R} \to \mathbb{R}_+.\end{array}\right\}$$

In the next step, the equilibrium allowance price $A_0^*(D_0)$ at demand D_0 will be determined as the solution of the fixed point problem (29.6) as $A_0 = \Pi(D_0, A_0)$, $A_0 \in [0, \pi]$. Having obtained the equilibrium allowance price at demand D_0, the market performance can be assessed in terms of the consumer's burden $B^{*c}(D_0)$, the producer's burden $B^{*p}(D_0)$, and the environmental burden $B^{*e}(D_0)$, calculated at demand D_0, which we define by

$$\begin{aligned}
B^{*c}(D_0) &= D_0 P^*\big(D_0, A_0^*(D_0)\big),\\
B^{*p}(D_0) &= -D_0 P^*\big(D_0, A_0^*(D_0)\big) + C^*\big(D_0, A_0^*(D_0)\big) + \Pi^*\big(D_0, A_0^*(D_0)\big),\\
B^{*e}(D_0) &= E^*\big(D_0, A_0^*(D_0)\big).
\end{aligned}$$

Summarizing, we shall emphasize that the energy mix model provides a simple framework, which merely requires a specification of few parameters (capacity allocation q and emission uncertainty ν) to overcome the ambiguity originated from unobserved model variables, to obtain a full quantitative and qualitative picture of the energy market response to a proposed emission regulation.

References

1. Barrieu P, Fehr M (2011) Integrated EUA and CER price modeling and application for spread option pricing. Centre for Climate Change Economics and Policy Working Papers 50, Centre for Climate Change Economics and Policy, London, UK.
2. Carmona R, Fehr M (2011) The clean development mechanism and joint price formation for allowances and CERs. In: Dalang R, Dozzi M, Russo F (eds) Seminar on stochastic analysis, random fields and applications, vol VI. Springer, Basel, pp 341–383
3. Carmona R, Fehr M, Hinz J (2009) Optimal stochastic control and carbon price formation. SIAM J Control 48(4):2168–2190
4. Carmona R, Fehr M, Hinz J, Porchet A (2010) Market design for emission trading schemes. SIAM Rev 52(3):403–452
5. Chesney M, Taschini L (2008) The endogenous price dynamics of the emission allowances and an application to CO_2 option pricing. Swiss Finance Institute Research Papers 08-02, Swiss Finance Institute, Zurich, Switzerland
6. Dales JH (1968) Land, water, and ownership. Can J Econ 1(4):791–804
7. Falbo P, Hinz J, Pelizzari C (2014) Risk-neutral equilibrium modeling of cap-and-trade mechanisms. Department of Economics and Management of the University of Brescia Working Papers, Università degli Studi di Brescia, Brescia, Italy
8. Hinz J, Novikov A (2010) On fair pricing of emission-related derivatives. Bernoulli 16(4):1240–1261
9. Kijima M, Maeda A, Nishide K (2010) Equilibrium pricing of contingent claims in tradable permit markets. J Futures Mark 30(6):559–589
10. Montgomery WD (1972) Markets in licenses and efficient pollution control programs. J Econ Theory 5(3):395–418

11. Seifert J, Uhrig-Homburg M, Wagner M (2008) Dynamic behavior of CO_2 spot prices. J Environ Econ Manag 56(2):180–194
12. Stevens B, Rose A (2002) A dynamic analysis of the marketable permits approach to global warming policy: A comparison of spatial and temporal flexibility. J Environ Econ Manag 44(1):45–69
13. Taschini L (2010) Environmental economics and modeling marketable permits. Asia-Pac Financ Markets 17(4):325–343

Chapter 30
Simultaneous Surveillance of Means and Covariances of Spatial Models

Robert Garthoff and Philipp Otto

Abstract This paper deals with the problem of statistical process control applied to multivariate spatial models. After introducing the target process that coincides with the spatial white noise, we concentrate on the out-of-control behavior taking into account both changes in means and covariances. Moreover, we propose conventional multivariate control charts either based on exponential smoothing or cumulative sums to monitor means and covariances simultaneously. Via Monte Carlo simulation the proposed control schemes are calibrated. Moreover, their out-of-control behavior is studied for specific mean shifts and scale transformation.

30.1 Introduction

Modeling spatial dependence is of potential interest in diverse statistical fields like econometrics and environmetrics. In statistical process control (SPC), we sequentially check whether there is any deviation of the observed process, available data, from the predefined target process. Basically, we extend conventional control charts consisting of the control statistic and the control limit. The run length of the process is the point of time when the control statistic exceeds the control limit. As a consequence, the surveillance of the process is stopped. At this certain point of time we expect the change point. Eventually, the process is called in control for those points of time before the change point occurs. Afterwards, the process is said to be out of control. Initially, control limits are calibrated for the previously specified expected run length. After the calibration the control procedures are applied to the observed process. In contrast to the conventional approach, we focus on changes occurring at a certain point in the multidimensional space. Hence, the run length is not anymore a point of time but a distance in space.

In [7] the conventional methods of (SPC) are transferred to conditional autoregressive models (cf. [16]) or simultaneous autoregressive models (cf. [2]) that are

R. Garthoff · P. Otto (✉)
European University Viadrina, Große Scharrnstraße 59, Frankfurt (Oder), Germany
e-mail: potto@europa-uni.de

R. Garthoff
e-mail: garthoff@europa-uni.de

A. Steland et al. (eds.), *Stochastic Models, Statistics and Their Applications*,
Springer Proceedings in Mathematics & Statistics 122,
DOI 10.1007/978-3-319-13881-7_30

defined as target process. Assuming that the change point may occur at a certain point in the multidimensional space, the common approach of SPC is extended. In particular, the focus is on changes at points with equal distance from some predefined center.

The aim of this paper is the simultaneous surveillance of both means and covariances based on the residuals of spatial processes. The procedures are constructed for spatial models. The considered process has a previously specified center square of the whole grid of squares, the origin of the target process. Accordingly, the spatial process spreads from this initial point. Since we take into account the monitoring of both means and covariances, the procedures we propose are multivariate. They are based on either cumulative sums (cf. [6, 8, 11] and [13]) or exponential smoothing (cf. [10]). The sample mean vector of each ring of squares is the respective characteristic quantity. Contrary to [7], the in-control process is assumed to be independent. We implement a Monte Carlo simulation to study the out-of-control behavior using the average run length (ARL) as performance measure.

We choose the following structure. In Sect. 30.2 the multivariate spatial model, the target process, and the respective relation to the observed process are introduced. Moreover, we propose a suitable characteristic quantity for the simultaneous surveillance. In Sect. 30.3 we focus on multivariate CUSUM and EWMA type charts. Section 30.4 includes the Monte Carlo simulation. Finally, Sect. 30.5 concludes.

30.2 Simultaneous Monitoring of Spatial Models

Subsequently, we define the target process that is a specific spatial model. Afterwards, we concentrate on the relation to the observed process. Finally, we propose a suitable characteristic quantity for the spatial surveillance.

30.2.1 Target and Observed Process

The target process is the p-dimensional stochastic process $\{Y(s)\colon\ s \in \mathbb{Z}^q\}$. More precisely, s denotes the location in the q-dimensional spatial unit grid. Every component of $Y(s)$ denoted by $Y_i(s)$ is defined as spatial white noise. Below, $(Y_i(s_j))_{j=1,\ldots,n}$ represents the vector of all observations. Thus, the process equals

$$Y_i = \mu_i 1_n + \varepsilon_i, \quad i = 1, \ldots, p. \tag{30.1}$$

In (30.1) μ_i denotes the individual mean referring to the observation $Y_i(s)$ multiplied by the n-dimensional vector of ones 1_n. Furthermore, the number of locations $n(d)$ is a function of distance. Let I_n be the identity matrix of dimension n. Moreover, the variance of homoscedastic errors is denoted by $\sigma^2_{\varepsilon_i}$. Since $\varepsilon_i \sim N_n(0, \sigma^2_{\varepsilon_i}\mathrm{I}_n)$, it holds that $Y_i \sim N_n(\mu_i 1_n, \sigma^2_{\varepsilon_i}\mathrm{I}_n)$. The elements of the vector $Y(s)$ following the identical spatial process are independent, i.e. $Y(s) \sim$

$N_p(\mu, \operatorname{diag}((\sigma^2_{\varepsilon_i})_{i=1,\dots,p}))$, where $\mu = (\mu_1, \dots, \mu_p)$. Basically, $Y(s)$ has $\gamma(q,d) \in \mathbb{N}$ observations at each d. We define $\varsigma_=(d) = \{s \in \mathbb{Z}^q\colon\ D(s) = d\}$ and $\varsigma_<(d) = \{s \in \mathbb{Z}^q\colon\ D(s) < d\}$ as the sets of locations.

Generally, spatial models that are monitored depend only on the distance d from the q-dimensional initial location $s_0 = 0$. We differ between the queen setting where the distance equals the maximum norm $D(s) = \|s\|_\infty = \max_{i=1,\dots,q} |s_i|$ and the rook setting where the distance $D(s)$ is given by $D(s) = \|s\|_1 = \sum_{i=1}^q |s_i|$ (cf. [7]). For the surveillance of the spatial process we use the mean $\{\bar{Y}(d)\colon\ d \in \mathbb{N}\}$ of all observations with equal distance from the origin, i.e.

$$\bar{Y}(d) = \frac{1}{\gamma(q,d)} \sum_{s \in \varsigma_=(d)} Y(s), \quad q \in \mathbb{N}. \tag{30.2}$$

Since we assume normal distribution, it holds that $\bar{Y}(d) \sim N_p(\mu, \Sigma(d))$, where

$$\Sigma(d) = \frac{1}{\gamma(q,d)} \operatorname{diag}\big((\sigma^2_{\varepsilon_i})_{i=1,\dots,p}\big). \tag{30.3}$$

Eventually, we choose the constant $\gamma(q,d) \equiv \tilde{\gamma}$ to avoid that the respective variances decrease with increasing d.

As mentioned previously, the aim is simultaneous monitoring, i.e. we check for changes in both means or covariances. Therefore, the following sequential testing problem is considered for each d.

$$\begin{aligned} H_{0,d}\colon\ & E\big[\bar{X}(d)\big] = \mu \quad \wedge \quad Cov\big[\bar{X}(d)\big] = \Sigma(d) \\ & \text{versus} \\ H_{1,d}\colon\ & E\big[\bar{X}(d)\big] \neq \mu \quad \vee \quad Cov\big[\bar{X}(d)\big] \neq \Sigma(d) \end{aligned} \tag{30.4}$$

The relation between the target process $\{Y(s) : s \in \mathbb{Z}^q\}$ and the observed process $\{X(s) : s \in \mathbb{Z}^q\}$ has to be formulated. Let $\delta \in \mathbb{N} \cup \{\infty\}$ denote the change point. Further, the vector of mean changes $a \in \mathbb{R}^p \setminus \{0\}$ and the scale transformation $\Upsilon = \operatorname{diag}(\upsilon_1, \upsilon_2, \dots, \upsilon_p) \neq \mathrm{I}_p$ with $\upsilon_i \in \mathbb{R}$ for $i \in \{1, \dots, p\}$ are unknown parameters. Eventually, simultaneous changes of both means and covariances are modeled in the following way.

$$X(s) = \begin{cases} Y(s) & \text{for } s \in \varsigma_<(\delta) \\ \mu + a + \Upsilon(Y(s) - \mu) & \text{for } s \in \mathbb{Z}^p \setminus \varsigma_<(\delta) \end{cases} \tag{30.5}$$

The process is said to be in control for any s where $D(s) < \delta$. Otherwise, the process is called out of control. The focus is on the ring of squares with the distance d from the predefined initial location $s_0 = 0$. The respective mean of $\gamma(q,d)$ observations is given by

$$\bar{X}(d) = \frac{1}{\gamma(q,d)} \sum_{s \in \varsigma_=(d)} X(s). \tag{30.6}$$

30.2.2 Characteristic Quantity for Spatial Surveillance

Initially, the effectively observed process is transformed, and we monitor means and covariances of the respective transformed process. The characteristic quantity is based on these residuals. Therefore, we propose the quantity

$$T^{(q)}(d) = \begin{pmatrix} \Sigma(d)^{-1/2}(\bar{X}(d) - \mu) \\ vech(\Sigma(d)^{-1/2}(\bar{X}(d) - \mu)(\bar{X}(d) - \mu)'\Sigma(d)^{-1/2}) \end{pmatrix}. \quad (30.7)$$

We use the *vech*-operator to transfer the symmetric $p \times p$-dimensional matrix $\Sigma(d)^{-1/2}(\bar{X}(d) - \mu)(\bar{X}(d) - \mu)'\Sigma(d)^{-1/2}$ to a vector of dimension $p(p+1)/2$. The elements above the diagonal are excluded. Let $\mathrm{O}_{k\times l}$ be the zero matrix of dimension $k \times l$, and $\iota_{ij} = 1$ for $i = j$ and 0, otherwise. Regarding the in-control state it holds that $\bar{X}(d) \sim N_p(\mu, \Sigma(d))$. Therefore, the in-control mean vector as well as the in-control covariance matrix are given by

$$E_{\delta=\infty}\big(T^{(q)}(d)\big) = \begin{pmatrix} 0 \\ vech(\mathrm{I}_p) \end{pmatrix} \quad (30.8)$$

and

$$Cov_{\delta=\infty}\big(T^{(q)}(d)\big) = \begin{pmatrix} \mathrm{I}_p & \mathrm{O}_{p\times p(p+1)/2} \\ \mathrm{O}_{p(p+1)/2\times p} & \Omega \end{pmatrix}, \quad (30.9)$$

where $\Omega = (\omega_{rs})_{r,s=1,\ldots,p(p+1)/2}$ with $\omega_{rs} = \iota_{il}\iota_{jk} + \iota_{ik}\iota_{jl}$.

30.3 Multivariate CUSUM and EWMA Charts

The following procedures are defined for $d \in \mathbb{N}$. Subsequently, both multivariate CUSUM type charts proposed by [13] are modified, so that the schemes can be applied to spatial processes. The cumulative sum of the first multivariate CUSUM (MC1) scheme is given by

$$S_{d-n_d,d} = \sum_{i=d-n_d+1}^{d} \big(T^{(q)}(i) - E_{\delta=\infty}\big(T^{(q)}(i)\big)\big). \quad (30.10)$$

The control statistic equals the difference of the norm of (30.10) and a quantity said to be the reference value including the reference parameter $k \geq 0$, i.e.

$$MC1_d = \max\Big\{0, \sqrt{S'_{d-n_d,d}Cov_{\delta=\infty}\big(T^{(q)}(d)\big)^{-1}S_{d-n_d,d}} - kn_d\Big\}. \quad (30.11)$$

Further, $n_d = n_{d-1} + 1$ if $MC1_{d-1} > 0$, and $n_d = 1$, otherwise.

The second multivariate CUSUM (MC2) procedure is based on the following Mahalanobis distance

$$\begin{aligned} T_d = &\big(T^{(q)}(d) - E_{\delta=\infty}\big(T^{(q)}(d)\big)\big)'Cov_{\delta=\infty}\big(T^{(q)}(d)\big)^{-1} \\ &\times \big(T^{(q)}(d) - E_{\delta=\infty}\big(T^{(q)}(d)\big)\big). \end{aligned} \quad (30.12)$$

Therefore, the control statistic of MC2 equals

$$MC2_d = \max\{0, MC2_{d-1} + T_d - p - 2k^2\}. \tag{30.13}$$

For both multivariate CUSUM procedures the starting value is equal to $MC1_0 = MC2_0 = 0$.

In [14] and [15] EWMA schemes for multivariate time series are introduced. We propose modifications to apply them to spatial models. Let $\lambda \in (0, 1]$ denote the weighting parameter. The first multivariate EWMA (ME1) chart is based on the linear combination

$$Z^{(q)}(d) = (1 - \lambda)Z^{(q)}(d - 1) + \lambda T^{(q)}(d). \tag{30.14}$$

The starting value is equal to the target value such that $Z^{(q)}(0) = E_{\delta=\infty}(T^{(q)}(d))$. Consequently, we can easily derive $E_{\delta=\infty}(Z^{(q)}(d)) = E_{\delta=\infty}(T^{(q)}(d))$. As mentioned previously, we assume independent random variables. Thus, for $h \neq 0$ it holds that $Cov_{\delta=\infty}(T^{(q)}(d), T^{(q)}(d + h)) = \mathrm{O}_{p\times p}$. Eventually, the in-control covariance matrix of $Z^{(q)}(d)$ equals

$$Cov_{\delta=\infty}\big(Z^{(q)}(d)\big) = \frac{\lambda(1 - (1 - \lambda)^{2d})}{(2 - \lambda)\gamma(q, d)} \begin{pmatrix} \mathrm{I}_p & \mathrm{O}_{p\times p(p+1)/2} \\ \mathrm{O}_{p(p+1)/2\times p} & \Omega \end{pmatrix}. \tag{30.15}$$

The control statistic of ME1 is given by the distance

$$\begin{aligned} ME1_d = &\big(Z^{(q)}(d) - E_{\delta=\infty}\big(Z^{(q)}(d)\big)\big)' \big(Cov_{\delta=\infty}\big(Z^{(q)}(d)\big)\big)^{-1} \\ &\times \big(Z^{(q)}(d) - E_{\delta=\infty}\big(Z^{(q)}(d)\big)\big). \end{aligned} \tag{30.16}$$

The second procedure proposed in [14] and [15] is called Mahalanobis EWMA (ME2) chart. The control statistic equals the recursion

$$ME2_d = (1 - \lambda)ME2_{d-1} + \lambda T_d, \tag{30.17}$$

where T_d is already defined in (30.12). Moreover, $ME2_0 = E_{\delta=\infty}(T_d) = p$ is the starting value. For $\lambda = 1.0$ both ME1 and ME2 coincide with the control chart proposed in [9].

30.4 Comparative Study

First, we present several examples of spatial white noise with implemented shifts in mean. Second, the focus is on the calibration of the introduced multivariate CUSUM and multivariate EWMA type charts. Finally, the out-of-control behavior of the introduced procedures is studied using the out-of-control ARL as suitable measure of performance.

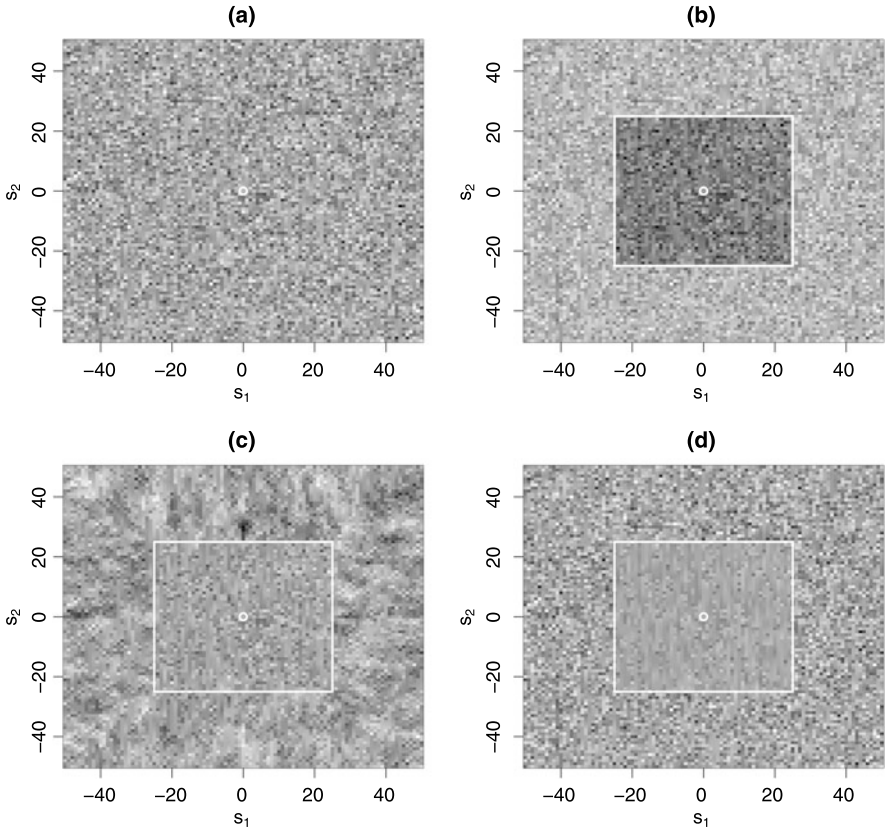

Fig. 30.1 Graphical representation of changes in mean **(b)**, autocorrelation **(c)** and variance **(d)** for $p = 1$ and $q = 2$ (overhead view) and a simulated process without any changes **(a)**

30.4.1 Simulation of Spatial Models

Possible mean or covariance changes of the spatial white noise introduced in Sect. 30.2.1 are now simulated. The aim is to visualize possible structural changes. In Fig. 30.1 graphical representations of changes in mean or covariance as well as autocorrelation for $p = 1$ and $q = 2$ are shown. Further, a simulated process without any changes is presented as benchmark. The simulated process is a two-dimensional spatial white noise for $d < 25$. After the change point has occurred at $d = \delta = 25$, one of the following processes is implemented. First, we consider an uncorrelated process with the covariance matrix I_n and the mean $\mu = 2$. Second, a spatial autoregressive process with the starting point $(0, 0)$ is implemented, where $\mu = 0$ and the autocorrelation equals 0.8. Hence, the off-diagonal elements differ from 0. Third, we implement an uncorrelated process with $\mu = 0$ and the covariance matrix $2\mathrm{I}_n$. The higher the simulated value, the brighter the location is drawn and vice versa.

Table 30.1 UCLs of the introduced multivariate control charts referring to simultaneous changes in means and covariances; in-control ARL is equal to $\mathscr{A} = 200$ ($m = 10^6$, $p = 2$, $q = 2$)

k	MC1	MC2	λ	ME1	ME2
0.0	30.8533	587.176			
0.1	16.9886	583.344	0.1	20.3113	10.5626
0.2	12.1077	571.253	0.2	28.1363	15.7509
0.3	9.89577	551.301	0.3	34.7905	20.8785
0.4	8.7788	523.531	0.4	40.5414	26.0134
0.5	8.11572	487.768	0.5	45.4506	31.1596
0.6	7.67371	444.281	0.6	49.5895	36.3049
0.7	7.36178	393.421	0.7	52.8311	41.4990
0.8	7.15216	335.399	0.8	55.2046	46.7018
0.9	6.96663	271.449	0.9	56.6490	51.9240
1.0	6.79988	204.342	1.0	57.1513	57.1473
1.1	6.73338	144.642			
1.2	6.59684	107.582			
1.3	6.45955	88.1625			
1.4	6.32323	77.0334			
1.5	6.19376	69.8739			
1.6	6.06575	64.8183			
1.7	5.9437	61.0405			
1.8	5.82528	58.0577			
1.9	5.70803	55.5682			
2.0	5.59463	53.4515			

To sum up, changes in the process cause either changes in the gray scale or in the pattern.

30.4.2 Calibration of Control Charts and Implementation of Changes

The introduced control procedures referring to the queen setting with $q = 2$ are calibrated, such that the in-control ARL equals the predefined value $\mathscr{A}$. To put it another way, we expect deviations from spatial white noise after $\mathscr{A} = 200$ steps from the center. For the proposed control procedures we have to compute upper control limits (UCL). The UCLs depend on the respective parameters of the multivariate EWMA or CUSUM charts. Hence, we have to calibrate for different values of λ and k. More precisely, $\lambda \in \{0.1, 0.2, \ldots, 1.0\}$ and $k \in \{0.0, 0.1, \ldots, 2.0\}$. In Table 30.1 the UCLs of the Monte Carlo simulation with $m = 10^6$ repetitions are shown. Obvi-

Table 30.2 Out-of-control ARL of the spatial model based on in-control ARL equal to $\mathscr{A} = 200$; ARLs refer to different shifts in means and covariances ($m = 10^6$, $p = 2$, $q = 2$)

a	d								
	1.00	1.10	1.20	1.30	1.50	1.75	2.00	2.25	2.50
−1.00	1.20 (2.0)	1.22 (1.9)	1.24 (1.9)	1.26 (2.0)	1.29 (1.8)	1.32 (1.6)	1.32 (1.8)	1.32 (2.0)	1.33 (2.0)
	1.24 (2.0)	1.26 (2.0)	1.28 (2.0)	1.29 (2.0)	1.32 (2.0)	1.34 (2.0)	1.34 (2.0)	1.34 (2.0)	1.34 (2.0)
	1.05 (0.1)	**1.06** (0.1)	**1.08** (0.1)	**1.09** (0.1)	**1.12** (0.1)	**1.14** (0.1)	**1.16** (0.1)	**1.17** (0.1)	**1.17** (0.1)
	1.21 (0.3)	1.24 (0.3)	1.26 (0.3)	1.27 (0.2)	1.30 (0.3)	1.32 (0.3)	1.32 (0.3)	1.32 (0.3)	1.32 (0.3)
−0.75	1.74 (1.0)	1.75 (1.0)	1.75 (1.0)	1.74 (1.0)	1.73 (1.0)	1.69 (1.0)	1.59 (1.0)	1.54 (0.9)	1.55 (2.0)
	1.98 (2.0)	1.95 (2.0)	1.92 (2.0)	1.89 (2.0)	1.83 (2.0)	1.76 (2.0)	1.69 (2.0)	1.62 (2.0)	1.56 (2.0)
	1.30 (0.1)	**1.32** (0.1)	**1.34** (0.1)	**1.35** (0.1)	**1.37** (0.1)	**1.37** (0.1)	**1.35** (0.1)	**1.33** (0.1)	**1.30** (0.1)
	1.91 (0.1)	1.89 (0.1)	1.87 (0.1)	1.84 (0.1)	1.79 (0.2)	1.72 (0.2)	1.66 (0.2)	1.59 (0.2)	1.53 (0.2)
−0.50	3.30 (0.7)	3.20 (0.7)	3.08 (0.7)	2.96 (0.7)	2.72 (0.7)	2.44 (0.7)	2.19 (0.7)	1.99 (0.9)	1.82 (0.9)
	4.94 (1.8)	4.37 (1.8)	3.93 (1.9)	3.57 (1.9)	3.04 (2.0)	2.58 (2.0)	2.26 (2.0)	2.03 (2.0)	1.85 (2.0)
	2.39 (0.1)	**2.32** (0.1)	**2.25** (0.1)	**2.17** (0.1)	**2.02** (0.1)	**1.85** (0.1)	**1.70** (0.1)	**1.57** (0.1)	**1.48** (0.1)
	4.58 (0.1)	4.09 (0.1)	3.70 (0.1)	3.39 (0.1)	2.91 (0.1)	2.50 (0.1)	2.20 (0.1)	1.98 (0.1)	1.82 (0.1)
−0.25	10.17 (0.4)	9.06 (0.4)	7.89 (0.4)	6.81 (0.5)	5.10 (0.5)	3.74 (0.6)	2.94 (0.6)	2.44 (0.7)	2.11 (0.8)
	25.09 (1.4)	16.25 (1.5)	11.54 (1.5)	8.76 (1.6)	5.74 (1.8)	3.94 (1.9)	3.02 (1.9)	2.48 (2.0)	2.13 (2.0)
	9.56 (0.1)	**7.78** (0.1)	**6.34** (0.1)	**5.23** (0.1)	**3.74** (0.1)	**2.73** (0.1)	**2.18** (0.1)	**1.86** (0.1)	**1.65** (0.1)
	25.33 (0.1)	15.56 (0.1)	10.86 (0.1)	8.20 (0.1)	5.40 (0.1)	3.76 (0.1)	2.91 (0.1)	2.41 (0.1)	2.09 (0.1)
0.00	MC1	60.64 (0.3)	27.22 (0.3)	16.00 (0.3)	8.01 (0.4)	4.75 (0.6)	3.38 (0.6)	2.66 (0.7)	2.24 (0.7)
	MC2	55.96 (1.3)	26.95 (1.4)	16.29 (1.5)	8.29 (1.6)	4.88 (1.8)	3.44 (1.9)	2.70 (2.0)	2.26 (2.0)
	ME1	**54.85** (0.1)	**23.08** (0.1)	**12.64** (0.1)	**5.90** (0.1)	**3.42** (0.1)	**2.47** (0.1)	**2.00** (0.1)	**1.73** (0.1)
	ME2	59.58 (0.1)	26.89 (0.1)	15.59 (0.1)	7.76 (0.1)	4.61 (0.1)	3.30 (0.1)	2.62 (0.1)	2.21 (0.1)

Table 30.2 (*continued*)

a	*d*								
	1.00	1.10	1.20	1.30	1.50	1.75	2.00	2.25	2.50
0.25	10.18 (0.4)	9.05 (0.4)	7.89 (0.4)	6.82 (0.5)	5.09 (0.5)	3.73 (0.6)	2.94 (0.7)	2.43 (0.7)	2.11 (0.8)
	25.08 (1.4)	16.24 (1.5)	11.56 (1.5)	8.77 (1.6)	5.74 (1.7)	3.95 (1.9)	3.02 (2.0)	2.48 (2.0)	2.13 (2.0)
	9.57 (0.1)	**7.79** (0.1)	**6.35** (0.1)	**5.24** (0.1)	**3.74** (0.1)	**2.73** (0.1)	**2.18** (0.1)	**1.85** (0.1)	**1.65** (0.1)
	25.33 (0.1)	15.58 (0.1)	10.86 (0.1)	8.19 (0.1)	5.40 (0.1)	3.76 (0.1)	2.92 (0.1)	2.41 (0.1)	2.09 (0.1)
0.50	3.30 (0.6)	3.20 (0.7)	3.08 (0.7)	2.96 (0.7)	2.72 (0.7)	2.44 (0.7)	2.19 (0.8)	1.98 (0.9)	1.82 (0.9)
	4.93 (1.8)	4.38 (1.8)	3.93 (1.9)	3.57 (1.9)	3.04 (2.0)	2.58 (2.0)	2.26 (2.0)	2.02 (2.0)	1.85 (2.0)
	2.39 (0.1)	**2.32** (0.1)	**2.25** (0.1)	**2.17** (0.1)	**2.02** (0.1)	**1.84** (0.1)	**1.69** (0.1)	**1.57** (0.1)	**1.48** (0.1)
	4.58 (0.1)	4.09 (0.1)	3.70 (0.1)	3.39 (0.1)	2.91 (0.1)	2.50 (0.1)	2.20 (0.1)	1.98 (0.2)	1.82 (0.2)
0.75	1.75 (1.0)	1.75 (1.0)	1.75 (1.0)	1.74 (1.0)	1.73 (0.9)	1.69 (1.0)	1.64 (1.0)	1.59 (1.0)	1.54 (1.0)
	1.98 (2.0)	1.95 (2.0)	1.92 (2.0)	1.89 (2.0)	1.83 (2.0)	1.75 (2.0)	1.68 (2.0)	1.62 (2.0)	1.56 (2.0)
	1.30 (0.1)	**1.32** (0.1)	**1.34** (0.1)	**1.35** (0.1)	**1.36** (0.1)	**1.37** (0.1)	**1.35** (0.1)	**1.33** (0.1)	**1.30** (0.1)
	1.91 (0.1)	1.89 (0.1)	1.87 (0.1)	1.84 (0.1)	1.79 (0.1)	1.72 (0.2)	1.65 (0.2)	1.59 (0.2)	1.53 (0.2)
1.00	1.20 (1.9)	1.22 (1.9)	1.24 (2.0)	1.26 (2.0)	1.29 (1.8)	1.31 (1.7)	1.32 (1.5)	1.32 (1.8)	1.32 (1.7)
	1.24 (2.0)	1.26 (2.0)	1.28 (2.0)	1.29 (2.0)	1.32 (2.0)	1.34 (2.0)	1.34 (2.0)	1.34 (2.0)	1.33 (2.0)
	1.05 (0.1)	**1.06** (0.1)	**1.08** (0.1)	**1.09** (0.1)	**1.12** (0.1)	**1.14** (0.1)	**1.16** (0.1)	**1.17** (0.1)	**1.17** (0.1)
	1.22 (0.3)	1.24 (0.4)	1.26 (0.3)	1.27 (0.3)	1.30 (0.2)	1.32 (0.3)	1.32 (0.3)	1.32 (0.3)	1.32 (0.3)

ously, for multivariate CUSUM charts the UCLs decline with growing k. However, for multivariate EWMA procedures the UCLs increase with growing λ.

Subsequently, we concentrate on the out-of-control behavior to identify dominating as well as dominated control procedures. Assuming $a_1 = a_2 = a$ and $\upsilon_1 = \upsilon_2 = \upsilon$, the mean shifts and the scale transformation taken into account are equal to $a \in \{-1.0, -0.75, \ldots, 1.0\}$ and $\upsilon \in \{1.0, 1.1, 1.2, 1.3, 1.5, 1.75, \ldots, 2.5\}$. The out-of-control ARLs are presented in Table 30.2. The ARLs are minimized by the respective smoothing parameter λ or the reference parameter k given in brackets. The lowest ARLs for a specific mean shift or scale transformation are bold. Apparently, ME1 is the best control procedure for both small and large changes using the out-of-control ARL as measure of performance. It is worth noting that for ME1 the optimal λ is constantly 0.1. Therefore, smaller values may provide even better performance.

30.5 Conclusions

The simultaneous surveillance of means and covariances of spatial models is the main purpose of this paper. The target process is assumed to be spatial white noise. Accordingly, the proposed CUSUM and EWMA type charts are calibrated. The out-of-control behavior is studied for possible shifts in means and covariance changes. ME1 seems to have the best performance using the ARL as measure of detection speed. However, since we focus on the ARL as performance measure, the explicit dominance of ME1 should be checked again using different measures, e.g. the expected delay.

Moreover, the focus of future research should be on the out-of-control behavior of spatial autoregressive models introduced in [1, 4], and [5]. The main problem is the implementation of the matrix of weights and the respective row-standardized matrix. The choice of these matrices is discussed in [1, 3, 4] and [5]. [1, 3] and [12] propose the maximum-likelihood method to estimate the correlation coefficient, the parameter of interest. Eventually, the dimension of these matrices extensively increases with the distance from the origin of the process. Consequently, the curse of dimensionality complicates the simulation with $m = 10^6$ repetitions. Nevertheless, the implementation of a comparative study focusing on spatial autoregressive models will be an interesting question in future.

References

1. Anselin L (1988) Spatial econometrics: methods and models, vol 1. Kluwer Academic, Dordrecht
2. Besag J (1974) Spatial interaction and the statistical analysis of lattice systems (with discussion). J R Stat Soc B 36:192–236
3. Cliff AD, Ord JK (1973) Spatial autocorrelation. Pion, London
4. Cliff AD, Ord JK (1981) Spatial processes: models & applications, vol 44. Pion, London

5. Cressie N (1993) Statistics for spatial data. Wiley, New York
6. Crosier R (1988) Multivariate generalizations of cumulative sum quality control schemes. Technometrics 30:291–303
7. Garthoff R, Otto P (2014) Control charts for multivariate spatial autoregressive models. European University Viadrina. Department of Business Administration and Economics. Discussion Paper
8. Golosnoy V, Ragulin S, Schmid W (2009) Multivariate CUSUM chart: properties and enhancements. AStA Adv Stat Anal 93:263–279
9. Hotelling H (1947) Multivariate quality control. In: Eisenhart C, Hastay MW, Wallis MA (eds) Techniques of statistical analysis. McGraw–Hill, New York
10. Lowry C, Woodall W, Champ C, Rigdon S (1992) A multivariate exponentially weighted moving average control chart. Technometrics 34:46–53
11. Ngai H-M, Zhang J (2001) Multivariate cumulative sum control charts based on projection pursuit. Stat Sin 11:747–766
12. Ord JK (1975) Estimation methods for models of spatial interaction. J Am Stat Assoc 70(349):120–126
13. Pignatiello J, Runger G (1990) Comparison of multivariate CUSUM charts. J Qual Technol 22:173–186
14. Śliwa P, Schmid W (2005) Monitoring the cross-covariances of a multivariate time series. Metrika 61:89–115
15. Śliwa P, Schmid W (2005) Surveillance of the covariance matrix of multivariate nonlinear time series. Statistics 39:221–246
16. Whittle P (1954) On stationary processes in the plane. Biometrika 41:434–449

Chapter 31
Risk Modelling of Energy Futures: A Comparison of RiskMetrics, Historical Simulation, Filtered Historical Simulation, and Quantile Regression

Kai Erik Dahlen, Ronald Huisman, and Sjur Westgaard

Abstract Prices of energy commodity futures often display high volatility and changes in return distribution over time, making accurate risk modelling both important and challenging. Non-complex risk measuring methods that work quite well for financial assets perform worse when applied to energy commodities. More advanced approaches have been developed to deal with these issues, but either are too complex for practitioners or do not perform consistently as they work for one commodity but not for another. The goal of this paper is to examine, from the viewpoint of a European energy practitioner, whether some non-estimation complex methods for calculating Value-at-Risk can be found to provide consistent results for different energy commodity futures. We compare RiskMetrics™, historical simulation, filtered historical simulation and quantile regression applied to crude oil, gas oil, natural gas, coal, carbon and electricity futures.

We find that historical simulation filtered with an exponential weighted moving average (EWMA) for recent trends and volatility performs best and most consistent among the commodities in this paper.

31.1 Introduction

Energy commodity prices have different risk characteristics than those from financial assets such as stocks, bonds and currencies. The physical aspect of energy com-

K.E. Dahlen (✉) · S. Westgaard
Department of Industrial Economics and Technology Management, Norwegian University of Science and Technology, Trondheim, Norway
e-mail: kai.e.dahlen@himolde.no

S. Westgaard
e-mail: sjur.westgaard@iot.ntnu.no

R. Huisman
Erasmus School of Economics, Rotterdam, The Netherlands
e-mail: rhuisman@ese.eur.nl

R. Huisman
IEB (Institut d'Economia de Barcelona), Barcelona, Spain

A. Steland et al. (eds.), *Stochastic Models, Statistics and Their Applications*,
Springer Proceedings in Mathematics & Statistics 122,
DOI 10.1007/978-3-319-13881-7_31

modities make prices vulnerable to short and long term demand and supply frictions and limited storage capacity.[1] This manifests into complex stochastic price dynamics such as time-varying volatility and (expected) return distributions that are skewed, exhibit kurtosis and with empirical quantiles that vary over time. These characteristics of price dynamics differ over energy commodities as well as electricity which is not (yet) storable in an economic sense while other energy commodities such as gas and oil are. Some energy commodity distributions are highly volatile, while others are not. Some distributions are skewed to the left and some to the right, in both cases generating an asymmetrical tail risk. Others have low/high kurtosis and hence, low/high tail risk. Energy commodity return distributions also change over time because of changing market regimes, changes in commodity-specific business cycles, weather conditions, etc. For those reasons, it is not obvious that standard risk models from financial markets, such as RiskMetrics™ and historical simulation, can be applied to energy commodities. One problem with existing standard risk models such as RiskMetrics™ and historical simulation is that the former does not necessarily capture the correct (conditional) return distribution. The latter has the opposite problem by capturing the empirical return distribution but not making it conditional upon volatility.

Although few, there are some attempts to model the risk in energy markets. Giot and Laurent [7] investigate market risk in various commodity markets, including Brent Crude Oil and WTI Crude Oil, assessing the performance of various GARCH type models. They find that an asymmetric GARCH model with skewed-t error distribution performs best regarding out of sample Value at Risk forecast. A more extended research of energy commodities is found in Hung et al. [13] including heating oil, propane, and gasoline in addition to Crude Oil. Again, the results indicate that heavy tailed GARCH models are suitable regarding Value at Risk calculation. Similar results are also found in Aloui [2] investigating Crude Oil and gasoline. In addition, Aloui [2] also argue for GARCH models capturing long-run dependencies in volatility. Füss et al. [10] extend the analysis of energy and other commodities, also looking at risk assessment using CAViaR[2] type of models. They look at Goldman Sachs indices for agricultural, industry metals, precious metals, livestock, and energy. The semi-parametric CAViaR methodology is recommended for all commodities, including energy. In a recent study, Mabrouk [17] investigates both Value at Risk and Expected Shortfall (Conditional Value at Risk) forecasts using a rich set of GARCH models for WTI, Brent, New York Harbour conventional gasoline regular, and Los Angeles gas. In accordance to other studies, he finds long-memory features and heavy tail distribution performs best. The new result is also that Expected Shortfall can be predicted using these models. Veka et al. [27] is one of the few attempts to model energy markets using multivariate GARCH. They investigate the extent to which the price of Nordic electricity derivatives correlates with electricity futures at EEX and ICE. They also look at the correlation of the electricity

[1] We refer to [22] and [12] for an overview of energy price and market characteristics.

[2] As GARCH models are ways of modelling conditional volatility as an auto regressive process, CaViaR models model the conditional quantiles as an autoregressive processes.

contract with Crude Oil, Natural Gas, coal, and carbon emission contracts. They find significant time-varying relationships between all of the energy commodities included in the analysis, with the exception of oil. This suggests that pricing models based on constant correlation may be misleading. Another reference investigating multivariate volatility and correlations is Pen and Sevi [21]. They analyse volatility transmission between European electricity markets. More insights are also found in Marzo and Zagaglia [19] and Solibakke [23, 24]. A weakness of these studies is that the authors do not test their models for VaR and CVaR assessment of energy commodity portfolios.

In a recent study, Hanly [8] compares the hedging effectiveness of decisions based on various risk models for different energy commodities and finds that hedging effectiveness differs over energy commodities. An approach that works well for one commodity does not necessarily deliver the same performance for another. Chang et al. [5] examine the effectiveness of various GARCH [3] type methods applied to crude oil contracts and find that the performance of methods differ over types of crude oil. Brinkmann and Rabinovitch [4] focus on natural gas futures and find that hedging effectiveness differs over geographical regions. These studies are among several that find that hedging effectiveness and the performance of risk measures varies over different energy commodities and markets. This heterogeneity in performance is a nightmare for practitioners as they prefer one model to be applied to all commodities for reasons of understanding, acceptance and credibility. More advanced risk models such as GARCH with different error distributions and Conditional Autoregressive Value at Risk (CAViaR) [11] that models quantiles as an autoregressive process typically improve the fit but are not widely adopted by market participants because of estimation complexity.[3] For that reason, we examine to what extent several non-estimation complex risk methods make proper risk assessments. We focus on the viewpoint of a European practitioner (which determines the choice of contracts to be examined) and use value-at-risk as a risk measure as it is widely adopted. We then examine to what extent filtered historical volatility and quantile estimates provide good risk assessments consistently over different energy commodities.

The rest of the paper is organized as follows. Section 31.2 describes the various Value-at-Risk models, backtesting procedures for VaR models and gives an introduction to the data used in the empirical study in this paper. Section 31.3 presents the empirical findings with backtesting of the different VaR models used in this paper before we conclude and discuss our results.

31.2 Data and VaR Models

We use data from the most important energy exchanges for European contracts. The Inter-Continental Exchange (ICE) covers a wide range of commodity and financial

[3] This argument is based on many discussions with market participants.

futures and options. Energy products includes North sea crude oil and refined oil products, UK and Dutch natural gas and electricity, coal delivered in Amsterdam–Rotterdam–Antwerp, and European emission contracts. In our analysis we will investigate the nearest front month future contracts of crude oil, gas oil, natural gas, and coal. From ICE we also collect front month and quarter base load electricity contracts for UK and the Netherlands. Finally we cover Phase II Carbon emission contracts. The European Energy Exchange (EEX) is located in Leipzig, Germany and is the leading exchange for electricity in Central Europe. Financial contracts for power futures and options, gas futures, coal futures and EU emission allowances are traded (similar to coal and emission contracts at ICE). In the paper we will investigate the nearest front month and quarter future baseload contracts based on the EEX system electricity price. Nasdaq OMX covers a wide range of financial product including electricity futures in the Nordpool area (Norway, Sweden, Denmark, Finland, and the Baltic states). In our analysis we will investigate the nearest front month and quarter future baseload contracts of Nord Pool system electricity price. The data covers the period 10.13.2008 to 09.30.2013 covering 1171 observations, after the returns associated with contract rollovers are removed. We also include a equally weighted portfolio of all 13 future contracts considered. For more details of the delivery conditions, roll-overs of contracts, trading hours etc., see [9, 26] and [20]. Summary statistics for all the time series are presented in Table 31.1. From the table of summary statistics we observe that the daily returns are close to zero, which is expected. The daily standard deviations, on the other hand, differ. We observe that it is the monthly electricity contract in the Nordic market which display the largest volatility with a daily volatility of 3.06 %. The least volatile contracts are quarterly German electricity future (1.28 %) and coal (1.45 %). Further we can summarize up the summary statistics as follows:

- Distributional properties vary across different energy commodities.
- Distribution properties vary over time.

RiskMetrics™ and historical simulation are the most common models used for VaR estimation in financial institutions [1]. We apply and analyze the performance of 4 different VaR models. These are the RiskMetrics™ VaR model [18], historical simulation, filtered historical simulation and quantile regression [14, 15].

Note that all of these measures do not require complicated estimation procedures and all (except historical distribution) use RiskMetrics™ like measures for mean and variances. We choose for these as the RiskMetrics™ measures are well-known among practitioners and are easy to calculate.

To evaluate our out-of-sample forecasts we will be using the unconditional coverage test of [16] and the conditional coverage test of [6].[4]

[4]We are aware that these are two simple methods and that more advanced one exist such the ones discussed in [25].

Table 31.1 Summary statistics on percentage daily price changes

Contract	Mean	Std	Skew	Kurt	Max	Min	0.05VaR	0.95VaR
Crude oil	0.02 %	2.15 %	0.00	3.28	11.13 %	−8.96 %	−3.47 %	3.17 %
Gas oil	0.01 %	1.87 %	0.17	3.56	11.26 %	−9.44 %	−3.16 %	2.77 %
Natural gas	−0.06 %	2.57 %	0.54	6.24	19.97 %	−10.88 %	−4.11 %	4.02 %
Coal	−0.05 %	1.45 %	0.50	15.68	14.72 %	−9.60 %	−1.99 %	1.77%
Carbon	−0.10 %	3.13 %	0.31	4.66	20.16 %	−15.87 %	−5.21 %	4.64 %
El-UK-M	−0.05 %	1.77 %	0.47	10.79	14.42 %	−11.93 %	−2.48 %	2.52 %
El-UK-Q	−0.03 %	1.53 %	1.49	11.10	12.02 %	−7.40 %	−2.07 %	2.22 %
El-Ned-M	−0.02 %	2.04 %	1.07	14.49	15.07 %	−15.65 %	−2.68 %	2.61 %
El-Ned-Q	−0.06 %	1.52 %	1.86	20.72	13.71 %	−10.13 %	−1.95 %	1.71 %
El-Ger-M	−0.08 %	1.81 %	0.53	8.42	11.61 %	−9.04 %	−2.72 %	2.33 %
El-Ger-Q	−0.09 %	1.28 %	0.38	6.63	8.11 %	−8.50 %	−1.87 %	1.94 %
El-Nor-M	−0.07 %	3.06 %	−0.16	2.44	12.22 %	−16.71 %	−4.88 %	5.09 %
El-Nor-Q	−0.04 %	2.30 %	−0.06	0.99	8.48 %	−9.92 %	−3.93 %	3.68 %
Portfolio	−0.04 %	2.57 %	0.54	0.96	8.50 %	−9.90 %	−3.90 %	3.71 %

31.3 Empirical Results

For the empirical test, we use the methods described in Sect. 31.2 to make out of sample estimates of one-day ahead Value-at-Risk measures for each of the futures contracts in our sample. Considering the changing distributions of the energy commodity returns the out of sample is done with a rolling window approach. For the rolling window the 600 previous observations are used in order to estimate the models and predict the VaR for the next day. An EWMA process is also estimated for several of the methods presented, leading to the first 30 observations of each time series being discarded as a burn-in period. Hence we have 541 out of sample observations for each of the time series, with the VaR estimated at six different levels ($\alpha = 0.01, 0.025, 0.05, 0.95, 0.975, 0.99$) each day.

Comparing the performance of the methods are done with the use of the Kupiec and Christoffersen tests. The p-values for the Kupiec test for all commodity futures are presented in Table 31.2, and H_0 (correct unconditional coverage) should be rejected if the value is below 0.05 (5 % significance). The p-values for the Christoffersen test for all commodity futures are presented in Table 31.3, and H_0 (correct conditional coverage) should be rejected if the value is below 0.05. The total number of rejections of H_0 for both the Kupiec and Christoffersen test can be found in Table 31.4. From these results we observe that VaR predictions from RiskMetrics™ seem to perform relatively well for the 5 % and 95 % quantile, at least when we consider the results from the Kupiec test. For the more extreme quantiles, however, the RiskMetrics™ does not seem to be an adequate model for describing the dynamics of the left and right tails of the distribution. Considering that RiskMetrics™ is based on the normal distribution this is no surprise. Considering the Christoffersen test the RiskMetrics™ seem to perform even worse. This is consistent with the findings of

Table 31.2 p-values for the Kupiec test for all commodities and methods

Commodity	RM	HS	FHS	QR	RM	HS	FHS	QR	RM	HS	FHS	QR
	Q0.01				Q0.025				Q0.05			
Crude oil	0.005	0.001	0.802	0.858	0.002	0.309	0.057	0.690	0.010	0.146	0.187	0.256
Gas oil	0.076	0.019	0.802	0.523	0.096	0.020	0.690	0.185	0.187	0.019	0.256	0.852
Natural gas	0.523	0.001	0.802	0.255	0.309	0.000	0.240	0.669	0.094	0.000	0.704	0.146
Coal	0.076	0.019	0.858	0.523	0.357	0.000	0.508	0.884	0.256	0.000	0.992	0.146
Carbon	0.076	0.000	0.296	0.076	0.096	0.000	0.357	0.240	0.342	0.000	0.852	0.133
el.UK M	0.858	0.802	0.157	0.014	0.185	0.100	0.897	0.240	0.010	0.058	0.540	0.682
el. UK Q	0.091	0.523	0.296	0.802	0.309	0.100	0.096	0.357	0.034	0.034	0.852	0.852
el. NL M	0.157	0.858	0.802	0.858	0.669	0.897	0.057	0.240	0.094	0.304	0.852	0.852
el. NL Q	0.005	0.511	0.076	0.014	0.240	0.669	0.155	0.155	0.682	0.058	0.852	0.540
el. Ger M	0.014	0.802	0.296	0.858	0.690	0.669	0.690	0.669	0.094	0.992	0.992	0.852
el. Ger Q	0.802	0.523	0.802	0.296	0.897	0.185	0.897	0.690	0.215	0.094	0.133	0.567
el. Nor M	0.014	0.511	0.802	0.296	0.240	0.897	0.897	0.508	0.682	0.567	0.992	0.540
el. Nor M	0.157	0.091	0.858	0.858	0.690	0.020	0.897	0.884	0.446	0.010	0.704	0.540
Port.	0.511	0.523	0.523	0.802	0.897	0.0201	0.884	0.309	0.413	0.010	0.835	0.215
	Q0.95				Q0.975				Q0.99			
Crude oil	0.002	0.000	0.540	0.019	0.020	0.000	0.100	0.185	0.523	0.091	0.523	0.523
Gas oil	0.835	0.002	0.446	0.540	0.508	0.020	0.357	0.884	0.296	0.019	0.157	0.802
Natural gas	0.835	0.000	0.992	0.215	0.057	0.002	0.884	0.309	0.014	0.019	0.802	0.858
Coal	0.005	0.000	0.215	0.010	0.007	0.000	0.473	0.002	0.091	0.019	0.802	0.255
Carbon	0.413	0.000	0.342	0.187	0.690	0.000	0.897	0.357	0.157	0.000	0.157	0.296
el. UK M	0.852	0.146	0.852	0.215	0.032	0.669	0.897	0.309	0.002	0.858	0.802	0.523
el. UK Q	0.215	0.005	0.215	0.058	0.508	0.100	0.884	0.100	0.076	0.858	0.802	0.802
el. NL M	0.094	0.146	0.704	0.682	0.897	0.669	0.897	0.884	0.034	0.523	0.511	0.255
el. NL Q	0.215	0.058	0.682	0.058	0.897	0.020	0.897	0.669	0.511	0.255	0.523	0.255
el. Ger M	0.540	0.256	0.187	0.187	0.155	0.669	0.690	0.669	0.005	0.523	0.858	0.255
el. Ger Q	0.215	0.019	0.446	0.304	0.690	0.048	0.508	0.048	0.076	0.255	0.802	0.255
el. Nor N	0.540	0.146	0.413	0.304	0.357	0.669	0.884	0.897	0.157	0.296	0.511	0.296
el. Nor Q	0.413	0.005	0.342	0.682	0.669	0.020	0.690	0.669	0.511	0.523	0.296	0.802
Portfolio	0.567	0.010	0.852	0.992	0.690	0.020	0.669	0.884	0.296	0.019	0.256	0.858

[7]. The historical simulation perform even worse than RiskMetrics™. The filtered historical simulation perform considerably better than both the previous models, and slightly better than the quantile regression approach. We have no rejects of unconditional coverage for the filtered historical simulation and only 2 (of 84 tests) rejects of conditional coverage from the Christoffersen test. This means that the filtered historical simulation gives an almost perfect fit when it comes to the number of exceedances over the predicted VaR levels, and satisfies the condition of independent

Table 31.3 p-values for the Christoffersen test for all commodities and methods

Commodity	RM	HS	FHS	QR	RM	HS	FHS	QR	RM	HS	FHS	QR
	Q0.01				Q0.025				Q0.05			
Crude oil	0.015	0.004	0.906	0.939	0.003	0.494	0.069	0.601	0.004	0.332	0.196	0.215
Gas oil	0.172	0.064	0.906	0.791	0.027	0.063	0.673	0.357	0.196	0.039	0.215	0.477
Natural gas	0.791	0.004	0.906	0.515	0.494	0.000	0.270	0.695	0.123	0.000	0.179	0.332
Coal	0.172	0.064	0.939	0.791	0.550	0.000	0.632	0.718	0.200	0.000	0.395	0.154
Carbon	0.081	0.000	0.150	0.081	0.024	0.000	0.025	0.031	0.015	0.000	0.005	0.019
el. UK M	0.939	0.906	0.315	0.038	0.357	0.229	0.683	0.445	0.023	0.089	0.827	0.693
el. UK Q	0.237	0.791	0.514	0.906	0.494	0.229	0.239	0.377	0.061	0.061	0.901	0.901
el. NL M	0.315	0.939	0.906	0.939	0.695	0.683	0.069	0.270	0.123	0.231	0.901	0.901
el. NL Q	0.015	0.735	0.172	0.038	0.270	0.695	0.189	0.189	0.287	0.089	0.225	0.285
el. Ger M	0.038	0.906	0.514	0.939	0.619	0.695	0.619	0.695	0.087	0.027	0.122	0.151
el. Ger Q	0.906	0.791	0.906	0.514	0.660	0.357	0.627	0.673	0.065	0.223	0.152	0.795
el. Nor M	0.038	0.160	0.906	0.514	0.445	0.136	0.683	0.493	0.908	0.064	0.424	0.827
el. Nor Q	0.315	0.237	0.939	0.939	0.601	0.063	0.683	0.718	0.597	0.023	0.820	0.271
Port.	0.726	0.786	0.786	0.890	0.665	0.062	0.701	0.485	0.148	0.022	0.753	0.436
	Q0.95				Q0.975				Q0.99			
Crude oil	0.005	0.000	0.827	0.050	0.063	0.002	0.229	0.134	0.791	0.237	0.791	0.791
Gas oil	0.263	0.007	0.113	0.271	0.493	0.063	0.377	0.718	0.514	0.064	0.315	0.906
Natural gas	0.093	0.000	0.395	0.220	0.077	0.009	0.736	0.503	0.038	0.064	0.916	0.948
Coal	0.013	0.000	0.198	0.023	0.026	0.000	0.615	0.009	0.237	0.064	0.906	0.515
Carbon	0.453	0.000	0.465	0.416	0.673	0.000	0.683	0.550	0.315	0.000	0.315	0.514
el. UK M	0.886	0.332	0.901	0.454	0.040	0.695	0.683	0.494	0.006	0.939	0.906	0.791
el. UK Q	0.454	0.013	0.454	0.089	0.493	0.229	0.718	0.229	0.172	0.939	0.906	0.906
el. NL M	0.020	0.154	0.509	0.287	0.660	0.483	0.660	0.592	0.049	0.791	0.735	0.515
el. NL Q	0.454	0.147	0.908	0.147	0.660	0.063	0.660	0.483	0.735	0.515	0.791	0.515
el. Ger M	0.217	0.023	0.080	0.006	0.337	0.483	0.673	0.483	0.013	0.791	0.939	0.515
el. Ger Q	0.454	0.014	0.502	0.336	0.601	0.129	0.493	0.129	0.172	0.515	0.906	0.515
el. Nor M	0.827	0.332	0.715	0.586	0.377	0.483	0.718	0.683	0.315	0.514	0.735	0.514
el. Nor Q	0.154	0.013	0.465	0.287	0.695	0.063	0.673	0.695	0.735	0.791	0.514	0.906
Portfolio	0.675	0.022	0.840	0.229	0.585	0.062	0.679	0.701	0.506	0.064	0.512	0.930

exceedances for most of the energy commodity futures considered. This does not necessarily mean, however, that the FHS-implied VaR levels are optimal. Kupiec [16] and Christoffersen [6] tests are not measures of fit, since they do not rank the distance from the expected number of exceedances. The Winkler (or interval) score or the Lopez score would be more appropriate in this context, see e.g. Weron [28] and Žiković and Aktan [29].

Table 31.4 Rejections of H_0 by method and test.

	RiskMetrics	Historical simulation	Filtered HS	Quantile regression
Kupiec test				
Total Tests	84	84	84	84
Total Rejections	17	41	0	6
Percentage Rejected	20.2 %	48.8 %	0.0 %	7.1 %
Christoffersen test				
Total Tests	84	84	84	84
Total Rejections	19	28	2	8
Percentage Rejected	22.6 %	33.3 %	2.4 %	9.5 %

31.4 Conclusion

Correct modeling and forecasting of risk is obviously of great importance to energy commodity traders, investors and hedgers. We have shown with our empirical study that standard risk models such as RiskMetrics™ and historical simulation have important weaknesses when they are used to measure the risk faced from changes in prices of energy futures contracts. Where does methods work quite well in financial markets, they perform worse when apply to energy contracts as energy commodity prices behave differently due to physical demand, supply and storage constraints in energy markets. The RiskMetrics™ assumes normal distributed returns, a simplification that does not work well with the heavy-tailed and skewed returns observed in these energy commodity futures data, while the historical simulation is unable to capture the changing volatility.

Focusing on European energy futures contracts, we have backtested the performance of four different models to measure Value-at-Risk and we show that filtered historical simulation is an accurate and easy model that provides consistent results over both the energy futures contracts in our sample and a portfolio of energy futures. From this we conclude that a European energy company, that searches for non-estimation complex method, is best off using the filtered historical simulation method for measuring the VaR of individual energy commodity positions.

References

1. Alexander C (2009) Market risk analysis, vol IV. West sussex, Wiley
2. Aloui C (2008) Value-at-risk analysis for energy commodities: long-range dependencies at fat tails in return innovations. J Energy Mark 1(1):31–63
3. Bollerslev T (1986) Generalized autoregressive conditional heteroskedasticity. J Econom 31(3):27–39
4. Brinkmann E, Rabinovitch R (1995) Regional limitations on the hedging effectiveness of natural gas futures. Energy J 16:113–124
5. Chang C, MacAleer W, Tansuchat R (2011) Crude oil hedging strategies using dynamic multivariate GARCH. Energy Econ 33:912–933

6. Christoffersen PF (1998) Evaluating interval forecasts. Int Econ Rev 39:817–840
7. Giot P, Laurent S (2003) Market risk in commodity markets: a VaR approach. Energy Econ 25(5):435–457
8. Hanly J (2014) Managing energy risk: a comparative analysis. Dublin Institute of Technology working paper
9. European energy exchange (2014). http://www.eex.com
10. Füss R, Adams Z, Kaiser DG (2010) The predictive power of Value-at-Risk Models in commodity futures markets. Working paper. Department of Empirical Research and Econometrics – University of Freiburg.
11. Engle RF, Manganelli S (2004) CAViaR: conditional autoregressive value at risk by regression quantiles. J Bus Econ Stat 22(4):367–381
12. Eydeland A, Wolyniec K (2002) Energy and power risk management: new developments in modeling, pricing, and hedging. Wiley, New York
13. Hung JC, Lee MC, Liu HC (2008) Estimation of value-at-risk for energy commodities via fat-tailed GARCH models. Energy Econ 30:1173–1191
14. Koeker R, Basset G (1978) Regression quantiles. Econometrica 46(1):33–55
15. Koeker R (2005) Quantile regression. Cambridge University Press, Cambridge
16. Kupiec P (1995) Techniques for verifying the accuracy of risk measurement models. J Deriv 2:183–184
17. Mabrouk S (2011) Value-at-risk and expected shortfall estimations based on GARCH-type models: evidence from energy commodities. J Energy Dev 35:279–314
18. Longerstaey J (1996) RiskMetrics™– technical document. Morgan
19. Marzo M, Zagaglia P (2007) Conditional leptokurtosis in energy prices: multivariate evidence from futures markets. Università degli Studie, Dipartimento di Scienze Economiche
20. Nasdaq OMX (2014). http://www.nasdaqomx.com/commodities
21. Pen YL, Sevi B (2010) Volatility transmission and volatility impulse response functions in European electricity forward markets. Energy Econ 32:758–770
22. Pilipovic D (2007) Energy risk: valuing and managing energy derivatives, 2nd edn. McGraw–Hill, New York
23. Solibakke PB (2008) Efficiency and transmission in European energy markets: a semi non-parametric approach. J Energy Mark 1(2):35–59
24. Solibakke PB (2010) Corporate risk management in European energy markets. J Energy Mark 3(1):93–131
25. Stavroyiannis S, Zarangas L (2013) Out of sample value-at-risk and backtesting with the standardized peason type-IV skewed distribution. Panoeconomicus 2:231–247
26. The Intercontinental Exchange (2014). http://www.theice.com
27. Veka S, Lien G, Westgaard S, Higgs H (2012) Time-varying dependency in European energy markets: an analysis of Nord Pool, European energy exchange and intercontinental exchange energy commodities. J Energy Mark 5(2):1–30
28. Weron R (2014) Electricity price forecasting: a review of the state-of-the-art with a look into the future. Int J Forecast 30(4):1030–1081
29. Žiković S, Aktan B (2011) Decay factor optimisation in time weighted simulation – evaluating VaR performance. Int J Forecast 27(4):1147–1159

Chapter 32
Periodic Models for Hydrological Storage Reservoir Levels. Case Study of New Zealand

Matylda Jabłońska-Sabuka and Agnieszka Wyłomańska

Abstract Many electricity markets across the world are strongly hydro-generation-dependent, and ability to predict hydrological storage levels is of key importance in generation planning and risk management. The purpose of this work is to introduce models reproducing periodic and irregular behavior of reservoir levels in New Zealand. The case study covers the period from January 2002 until July 2008. Two approaches are proposed here, namely, continuous time random walk with periodic probability of jumps and periodic autoregressive model. Results show that both models are capable of reproducing statistical features of the original data and provide a supporting tool for market analysts and generation planners.

32.1 Introduction

Ever since the electricity market deregulation, which has by now been carried out in many countries across the world, electricity prices became very volatile and heavily dependent on some deterministic and stochastic factors. A lot of studies have been carried out to model the price behavior, either based just on the price history, or including some explanatory variables having influence price dynamics.

For instance, an important factor which contributes to the high volatility in most markets is the large variations in the demand and supply of electricity, which are very uncertain in deregulated markets [4]. In particular, temperature strongly affects the demand; in total, the demand varies between 50–100 %. Thus, as some say, forecasting demand is almost equivalent to forecasting weather [18]. Next to any climatic factors, hydrological balance, demand and base load supply [22] can be considered with equal importance as the key spot price drivers.

M. Jabłońska-Sabuka (✉)
Department of Mathematics and Physics, Lappeenranta University of Technology, Skinnarilankatu 34, 53850 Lappeenranta, Finland
e-mail: matylda.jablonska-sabuka@lut.fi

A. Wyłomańska
Institute of Mathematics and Computer Science, Wrocław University of Technology, Wybrzeże Wyspiańskiego 27, 50-370 Wrocław, Poland
e-mail: agnieszka.wylomanska@pwr.wroc.pl

A. Steland et al. (eds.), *Stochastic Models, Statistics and Their Applications*, Springer Proceedings in Mathematics & Statistics 122,
DOI 10.1007/978-3-319-13881-7_32

We argue, that along with proper skills of modelling the price itself, it is equally important to be able to understand and predict the dynamics of the explanatory variables. One of these, having a long-term and sometimes more prominent than any other factor influence on the prices, is hydrological storage reservoir level. Hydro power is the cheapest source of energy, and can provide significant safety and sustainable development of country's energy sector. Some of the example regions blessed with good proportion of hydro power production are, for instance, Scandinavia and New Zealand. However, inability to predict the reservoir levels and their deviations from the mean annual levels can have disastrous influence on electricity spot prices [11].

In this work we present two mathematical approaches for predicting hydro storage dynamics. One of the models is a continuous time random walk with periodic probability of jumps and the second one is a periodic autoregressive time series model. Both approaches consider the daily historical data from the New Zealand Electricity Market (NZEM) covering the period from 1st of January 2002 until 31st of July 2008, as the New Zealand electricity market is heavily hydro-dependent and the information on country's hydrological information is of key importance to price modeling. The models are trained on part of the data set and perform out-of-sample simulations for the remaining period of over 9 months. The results show high goodness of fit between the original and simulated data.

32.2 Data and Methodology

32.2.1 Data

The data used in this study comes from the New Zealand electricity market. It has been retrieved from the Centralized Dataset CD provided by the New Zealand Electricity Commission free of charge. The data consists of daily centralized (aggregated for the entire country) values of hydrological storage reservoir levels covering the period from 1st of January, 2002 up to 31st of July, 2008. The data has been graphically introduced in Fig. 32.1 (red line) together with the daily mean electricity prices.

32.2.2 Model 1 – Continuous Time Random Walk with Periodic Probability of Jumps

The first proposed model that can be useful to describe data with seasonal behavior is based on the continuous time random walk (CTRW) methodology [15]. In the classical approach, the CTRW process is defined as:

$$Y_t = \sum_{i=1}^{T_t} X_i, \tag{32.1}$$

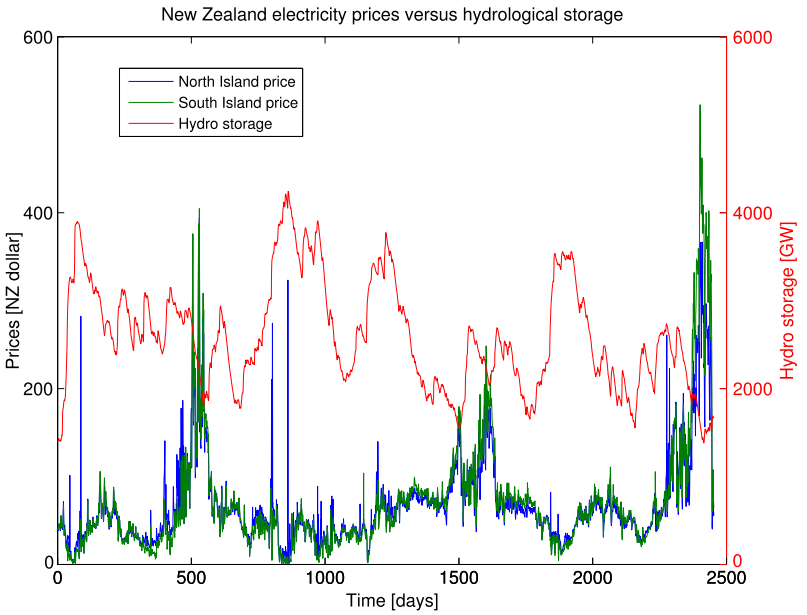

Fig. 32.1 New Zealand daily mean electricity prices from North and South Island versus the daily hydrological storage levels

where the process $\{T_t\}_{t\geq 0}$ is given by

$$T_t = \max\left\{n \in N\colon \sum_{i=1}^{n} S_i \leq t\right\} \tag{32.2}$$

with the sequence $\{S_n\}_{n=1}^{\infty}$ of nonnegative independent identically distributed (i.i.d.) random variables representing the waiting times. The sequence $\{X_n\}_{n=1}^{\infty}$ represents the jumps. The process $\{T_t\}$ is often referred to as the renewal process or, alternatively, as the counting process [14]. Moreover the sequences $\{S_n\}$ and $\{X_n\}$ are assumed to be independent.

One of the most popular distributions of sequence $\{S_n\}$ is the non-negative α-stable. Let us recall, the random variable S has α-stable distribution if there exist parameters $\alpha \in (0, 2]$, $\sigma > 0$, $-1 \leq \beta \leq 1$ and $\mu \in R$ such that the characteristic function of S takes the form [19]:

$$\boldsymbol{E}e^{ixS} = \begin{cases} e^{-\sigma^{\alpha}|x|^{\alpha}(1-i\beta\,\mathrm{sign}(x)\tan(\pi\alpha/2))+i\mu x}, & \text{for } \alpha \neq 1 \\ e^{-\sigma|x|(1+i\beta(2/\pi)\,\mathrm{sign}(x)\log(|x|))+i\mu x}, & \text{for } \alpha = 1. \end{cases} \tag{32.3}$$

The stability index α, scale parameter σ, skewness parameter β and shift parameter μ in a unique way define the distribution of a random variable S.

Since the analyzed data set exhibits seasonal behavior which corresponds to year changing of hydro storage, in this paper we propose using a modification of the classical CTRW scenario, in which the distribution of the jump sizes depends on the

actual time of the jump. The similar model was proposed in [13], where the extended CTRW system was used to describe indoor air quality data. From the theoretical point of view, the model was studied in [20].

Let us emphasize the second property of the data set, namely, the jumps of the process take only two values a and $-a$. Therefore, we consider a binomial model with a particle jumping between two sites, where a jump length is equal to a. The probability of the jump is governed by a periodic function that depends on the actual time t and, therefore, the jumps X_t for each t have the following form:

$$X_t = \begin{cases} a & \text{with probability } p_t, \\ -a & \text{with probability } 1 - p_t. \end{cases} \tag{32.4}$$

Such specification is an analogy to the field induced CTRW, analyzed in [20], with $p_t = \frac{1}{2}(1 + f(t))$ for f being a periodic function.

In the last decade the CTRW models have become very popular especially because of their simple form. They are also connected with the so-called subordinated processes, that are treated as limiting processes of CTRW systems. Some interesting applications of CTRW models can be found, for instance, in [5, 6, 9, 12]. According to our knowledge the CTRW system was never used in the hydrological context but there are papers where it is considered as a proper model to environmental data, see for instance [13, 23]. The procedure of estimating the parameters of CTRW and subordinated processes is presented, for instance, in [23].

32.2.3 Model 2 – Periodic Autoregressive Model

The second proposed model is based on an extended classical autoregressive model (AR) presented in [2]. The model is called periodic autoregressive time series and for order p it is defined as follows:

$$X_i - \sum_{j=1}^{p} a_j(i) X_{i-j} = b(i)\varepsilon_i, \tag{32.5}$$

where $\{\varepsilon_i\}$ is a white noise time series and the coefficients $a_1(i), \ldots, a_p(i)$ and $b(i)$ are periodic in i with the same period T. Usually, it is assumed that the time series $\{\varepsilon_i\}$ is Gaussian white noise.

The periodic autoregressive time series (PAR) is a special case of PARMA sequence (periodic autoregressive moving average), i.e. a time series which is defined as [8]:

$$X_i - \sum_{j=1}^{p} a_j(i) X_{i-j} = b(i)\varepsilon_i + \sum_{j=1}^{q} b_j(i)\varepsilon_{i-j}. \tag{32.6}$$

In the above definition the sequence coefficients are also periodic with the same period T and the series $\{\varepsilon_i\}$ is white noise.

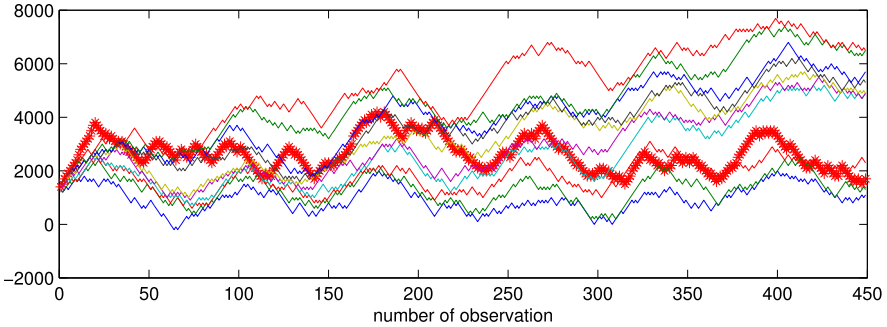

Fig. 32.2 Quantile lines of level 10 %, 20 %, ..., 90 % for Model 1 and the measured hydro storage jumps (*red thick line*)

The PARMA sequence is one of the main time series which can be used as a model for periodically correlated (or cyclostationary) processes. Generally, periodically correlated (PC) random processes of second order are random systems in which there exists a periodic rhythm in the structure that is generally more complicated than periodicity in the mean function [10].

Due to their interesting properties, periodically correlated time series have received much attention in the literature because they provide an alternative to the conventional stationary time series for periodically nonstationary phenomena. Examples occur in hydrology [21], meteorology [1], economics [3, 17] and electrical engineering [7]. The PARMA system was also considered in case of infinite variance, see [16].

There are many methods that can be used to estimate PAR coefficients. One of the methods is called Yule–Walker method [2], which is a consequence of the method of moments. This method is very often used in practice because of the simple form of estimators. More details according to estimation procedure one can find in [24].

32.3 Results of Real Data Analysis

32.3.1 Model 1

In order to prove the proposed model based on CTRW scenario is appropriate, in Fig. 32.2 we show the vector of observations and the constructed quartile lines by using the model and parameters estimated from the real data. Moreover, in Fig. 32.3 we present the analyzed data set and forecast for the next 293 days by using the continuous time random walk model described above. Here, we use the Monte Carlo method to construct the confidence intervals for the forecast. The number of Monte Carlo simulations is 1000.

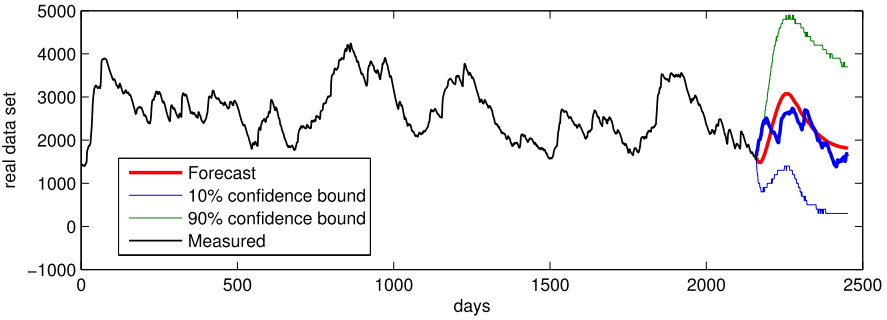

Fig. 32.3 Measured values of hydro storage together with the forecast for the next 293 days (Model 1). Additionally, the 10 % and 90 % confidence bounds are given

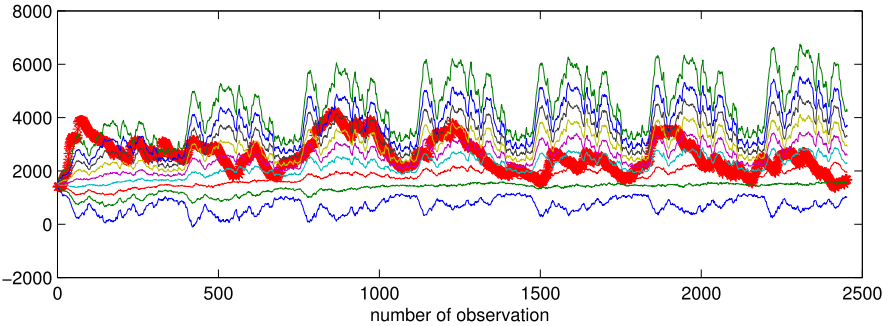

Fig. 32.4 Quantile lines of level 10 %, 20 %, ..., 90 % for Model 2 and the measured hydro storage (*red thick line*)

32.3.2 Model 2

The second proposed model for hydro storage data is a periodic autoregressive one described in Sect. 32.2.3. Since in the hydro storage data we observe the period equal to 360, we propose to use model PAR with period corresponding to year changes in the data.

In order to show the proposed model is appropriate to examined dataset on the basis of Monte Carlo simulations with 1000 repetitions, we simulate the samples of obtained PAR(1) model with period 360 with the assumption that the residuals come from Gaussian distribution. In Fig. 32.4 we present the constructed quantile lines on levels 10 %, ..., 90 %. As we observe, the measured hydro storage corresponds to the simulated model.

In order to show how beneficial the model may be, we construct the one-day prediction of the hydro storage data by using Model 2. In each step we update the observed data to the model. In Fig. 32.5 we present the obtained result. Let us mention, in the first approach where we use the CTRW model we presented the forecast which means, on the basis of simulated model we constructed the values of pro-

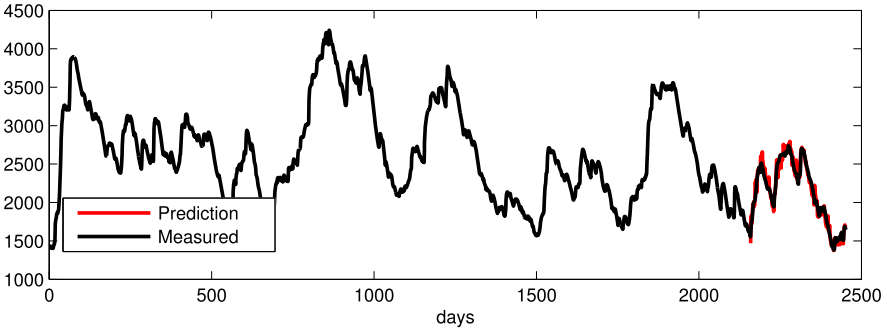

Fig. 32.5 Measured values of hydro storage together with the forecast for the next 293 days (Model 2)

cess by using Monte Carlo simulations. Actually the forecast was equal to the mean of simulated trajectories. In the second approach we present the prediction, which means, on the basis of the estimated model we show the predicted values. Here the Monte Carlo simulations are not needed.

32.4 Conclusion

In this work we have studied the behavior of historical measurements of New Zealand's hydrological storage reservoir levels. We have identified some characteristic features in the original time series and proposed two alternative models for reconstructing the behavior of the data. One of them is continuous time random walk with periodic probability of jumps. The model is an extension of the classical continuous time random walk by an additional skill of capturing seasonal behavior. The second approach is the periodic autoregressive model which uses the time series historical values and periodic patterns to model future values.

The results of the study give an important feedback in two aspects. Firstly, the mathematical approaches used here confirm their applicability to environment-related time series. Secondly, we can see that the models can produce high confidence forecasts which combined with other tools and information can support market analysts in planning. The model is replicable for any hydro-dominated electricity market, especially because it provided good-accuracy forecast on relatively difficult hydro data from the New Zealand market.

In future line of research, the hydrological storage data could be studied in multidimensional analysis together with other storage-related information like rainfall, lake inflows and snowpack data, to improve forecast accuracy. Moreover, a model forecasting seasonal trends of electricity prices related to changes in hydro storage levels should be built.

References

1. Bloomfield P, Hurd H, Lund R (1994) Periodic correlation in stratospheric ozone data. J Time Ser Anal 12:127–150
2. Brockwell P, Davis R (1996) Introduction to time series and forecasting. Springer, New-York
3. Broszkiewicz-Suwaj E, Makagon A, Weron R, Wyłomańska A (2004) On detecting and modeling periodic correlation in financial data. Physica A 336:196–205
4. Burger M, Klar B, Müller A, Schindlmayr G (2004) A spot market model for pricing derivatives in electricity markets. Quant Finance 4:109–122
5. Gajda J, Wyłomańska A (2012) Geometric Brownian motion with tempered stable waiting times. J Stat Phys 148:296–305
6. Gajda J, Wyłomańska A (2013) Tempered stable Lévy motion driven by stable subordinator. Physica A 392:3168–3176
7. Gardner W, Franks L (1975) Characterisation of cyclostationary random signal processes. IEEE Trans Inf Theory 21:4–14
8. Gladyshev E (1961) Periodically correlated random sequences. Sov Math 2:385–388
9. Golding I, Cox E (2006) Physical nature of bacterial cytoplasm. Phys Rev Lett 96:098102
10. Hurd H, Miamee E (2007) Periodically correlated random sequences. Spectral theory and practice. Wiley, New Jersey
11. Jabłońska M, Viljainen S, Partanen J, Kauranne T (2012) The impact of emissions trading on electricity spot market price behavior. Int J Energy Sector Manag 6(3):343–364
12. Jeon J, Tejedor V, Burov S, Barkai E, Selhuber-Unkel C, Berg-Sorensen K, Oddershede L, Metzler R (2011) In vivo anomalous diffusion and weak ergodicity breaking of lipid granules. Phys Rev Lett 106:048103
13. Maciejewska M, Szczurek A, Janczura J, Wyłomańska A (2013) Stochastic modeling of indoor air temperature. J Stat Phys 152:979–994
14. Magdziarz M, Weron K (2006) Anomalous diffusion schemes underlying the cole–cole relaxation. the role of the inverse-time. Physica A 367:1–6
15. Montroll E, Weiss G (1965) Random walks on lattices. II. J Math Phys 6:167–181
16. Nowicka-Zagrajek J, Wyłomańska A (2006) The dependence structure for parma models with a-stable innovations. Acta Phys Pol B 37:3071–3081
17. Parzen E, Pagano M (1979) An approach to modeling seasonaly stationary time-series. J Econom 9:137–153
18. Podraza E (2006) Challenges in forecasting electric load in deregulated markets. J Bus Forecast 25(3):31–35
19. Samorodnitsky G, Taqqu M (1994) Stable non-Gaussian random processes. Chapman & Hall, New York
20. Sokolov I, Klafter J (2006) Field-induced dispersion in subdiffusion. Phys Rev Lett 97:140602
21. Vecchia A (1985) Periodic autoregressive-moving average (parma) modeling with applications to water resources. Water Resour Bull 21:730
22. Vehviläinen I, Pyykkönen T (2005) Stochastic factor model for electricity spot price – the case of the Nordic market. Energy Econ 27:351–367
23. Wyłomańska A (2012) Arithmetic Brownian motion subordinated by tempered stable and inverse tempered stable processes. Physica A 391(22):5685–5696
24. Wyłomańska A, Obuchowski J, Zimroz R, Hurd H (2014) Periodic autoregressive modeling of vibration time series from planetary gearbox used in bucket wheel excavator. In: Chaari F et al (eds) Theory and methods lecture notes in mechanical engineering, pp 171–186

Chapter 33
Dynamic Price Linkage and Volatility Structure Model Between Carbon Markets

Takashi Kanamura

Abstract This paper investigates the dynamic price linkage and volatility structure between two leading carbon markets of EU allowance (EUA) and secondary certified emission reduction (sCER). We propose a correlation model between EUA and sCER price returns using the marginal abatement cost (MAC) curve and the emission reduction volume. The model reflects twohold market observations: financial players' EUA-sCER swap transaction in carbon price boom periods and stronger energy price impacts on EUA prices than sCER prices. The model demonstrates that the volatilities are affected by the MAC curve shape and the emission reduction volume while the correlations are indifferent from the MAC curve shape and affected by the emission reduction behavior. The model also suggests that the EUA-sCER price correlations increase when the swap transaction increases or energy prices fall, translated into the opposite EUA price movements of EUA price rise or fall, respectively.

33.1 Introduction

Carbon markets are interrelated with one another due to the political linkage between the two or more markets. For example, the EU emission trading scheme (EU-ETS) which allocates and exchanges EU allowances (EUAs)[1] enables the scheme participants to import the certified emission reductions (CERs) generated as carbon credits from clean development mechanism (CDM) projects to maintain the trading scheme in health. By using the linkage between EUAs and secondary CERs,[2] the market players may conduct arbitrage trading of sell-high and buy-low strategy between the two carbon markets, referred to as EUA-sCER swap. To this end, the political linkage between the two markets will affect the correlation structure

T. Kanamura (✉)
Graduate School of Advanced Integrated Studies in Human Survivability (GSAIS), Kyoto University, 69–2F, Yoshida–Konoe–cho, Sakyo–ku, Kyoto 606-8501, Japan
e-mail: tkanamura@gmail.com

[1] EUAs are carbon credits traded in the EU-ETS.

[2] The CER issued by the CDM executive board is referred to as the secondary CER (sCER).

A. Steland et al. (eds.), *Stochastic Models, Statistics and Their Applications*,
Springer Proceedings in Mathematics & Statistics 122,
DOI 10.1007/978-3-319-13881-7_33

of carbon prices. It is well-known that EUA and secondary CER (sCER) futures prices delivered in December 2009 seem to move together with one another as an empirical evidence of the linkage. Energy prices affect carbon prices in a different way depending on the carbon market structure of energy related and unrelated emission reduction technologies. The compositions of the emission reduction, i.e., carbon dioxide or other equivalent greenhouse gas emission reduction, technologies regarding energy in the carbon markets determine the shapes of the marginal abatement cost curves, affecting the price comovements and changes. Energy prices will also characterize the correlation structure accompanied by the volatility structure.

The recent evolution of carbon markets draws the strong attentions from academic researchers. Fehr and Hinz [1] propose an equilibrium price model for EUA prices taking into account the fuel switching between natural gas and coal fired power plants. Benz and Trück [2] employ AR-GARCH Markov switching price return model to capture the regime shifts between different phases of EU-ETS and the heteroskedasticity. Daskalakis et al. [3] compare existing popular diffusion and jump diffusion models, resulting in the favor of the Geometric Brownian motion with jumps to fit historical EUA spot price data other than mean-reverting processes often used for commodity price modeling. Moreover Seifert et al. [4] propose a stochastic price model where CO_2 prices do not have any seasonal pattern often observed in commodity markets. Paolella and Taschini [5] also propose the mixed normal and mixed stable GARCH models to capture the heavy tail and volatility clustering in the U.S. SO_2 permits and EUA price returns where the price returns are not represented using any mean-reversion and seasonality. Uhrig-Homburg and Wagner [6] examine the relationship between the carbon spot and futures prices traded on the Powernext and the European Climate Exchange. Borak et al. [7] conduct the empirical analyses of EUA convenience yields using the spot and futures prices traded on the EEX and offer a convenience yield model based on the spot price and the volatility. Kanamura [8] also investigated the characteristics of carbon asset prices, resulting in the possibility of the classification of carbon assets into non commodity asset class. While these empirical studies are keen on carbon price models and their empirical analyses for a single carbon market, they seem to pay no attention to the characteristics of the correlations between carbon markets. Grüell and Taschini [9] assessed the linkage between emission trading schemes by focusing on the price convergence, but unfortunately not using the carbon price model. Chevallier [10] provides evidence of time-varying correlations between EUAs and CERs; Mansanet-Bataller et al. [11] and Medina et al. [12] show that the spread between the two markets is driven by EUA prices; finally, Mizrach [13] notes the lack of convergence between EUA and CER prices. The studies are quite important to understand EUA-sCER price spreads empirically. But they employ existing econometric models, not supply-demand based models for carbon credits. To this end, the investigation of the two carbon markets linkage may not be conducted so far using the supply-demand based carbon price model. Since sCERs are allowed for the offset to meet their emission reduction target inside the EU-ETS, the two carbon markets may have strong relationship each other regarding the prices. In addition, carbon price correlation and volatility structures are strongly affected by the market marginal abatement cost curve with various energy price related and unrelated

emission reduction technologies. But these carbon market structures do not seem to be employed so far to examine the carbon price correlations and volatilities.

We propose a correlation model between EUA and sCER price returns using the supply-demand relationship between two carbon markets, i.e., marginal abatement cost curve and emission reduction volume. In particular, the role of financial players in carbon markets is built in the model by representing EUA and sCER swap in carbon price boom. The influence of energy prices on the EUA market contrary to the sCER market is also incorporated into the model by reflecting the different emission reduction measures between more energy-related EU-ETS and less energy-related CDM projects. The model demonstrates that the volatilities are affected by both of the MAC curve shape and the emission reduction volume while the correlations are indifferent from the MAC curve shape and affected by the emission reduction behavior. The model also suggests that the EUA-sCER price correlations increase when the swap transaction increases or energy prices fall, translated into the opposite EUA price movements of EUA price rise or fall, respectively.

33.2 The Correlation Model for EUA and sCER Prices

Carbon prices are strongly affected by the supply-demand relationship based on the marginal abatement cost and emission reduction in carbon markets. In addition, a certain amount of the credits or allowances in one carbon market can be used in the other carbon market, resulting in the volumetric linkage between the carbon markets due to the carbon products swap transactions. Furthermore, it is observed that energy prices affect the carbon prices via the MAC curve in particular EUA markets. It is well known that EUA and sCER are frequently traded in the carbon markets and considered as two leading carbon prices. The paper tries to model the EUA-sCER price correlation and volatility using the supply-demand relationship based on the volumetric linkage including EUA-sCER swap transaction and both carbon markets' characteristics including energy price impacts.

For baseline and credit type assets such as sCERs, the credits are generated along with the upward sloping marginal abatement cost (MAC) curve in the order of the low cost emission reduction technologies until the credit volume meets the emission reduction volume needed by the emission reduction entities for their compliance fulfillment. The price is determined by the intersection between the MAC curve and the emission reduction volume. For cap and trade system such as the EU-ETS, the pricing structure is taken in the same way. The market participants with emission reduction obligation possess the upward sloping MAC curve. Then, the emission reductions are represented by the differences between the emissions and capped allowances for the companies. The equilibrium prices for EUAs are also obtained from the intersection between the MAC curve and the emission reduction volume.[3]

[3]Thus in our model, the oversupply of EUAs occurred in year 2006 is expressed by low emission reduction volume taking into account the amount of allocated EUAs.

We start with the modeling of the emission reduction volume needed in whole EUA and sCER markets, respectively. It is assumed that the emission reduction amounts are stochastically fluctuated due to CO_2 or GHG emissions. We define by V_t and D_t the emission reduction volume for EUA and sCER, respectively[4]

$$dV_t = \mu_V dt + \sigma_V dw_t, \tag{33.1}$$

$$dD_t = \mu_D dt + \sigma_D dv_t, \tag{33.2}$$

where μ_V, σ_V, μ_D, and σ_D are constant for simplicity.

As the market observation of the carbon market linkage, we focus on the role of financial players in carbon markets regarding EUA-sCER swap transaction. sCER can be used for EUA in the EU-ETS due to the EU-ETS linking directive. sCER will be attractive in the EU-ETS and the sCER swap volume, i.e., the CER volume used for EUA-sCER swap, will increase if the EUA-sCER price spread becomes wide. It is generally observed as in Fig. 33.1 that the price spread becomes wide when EUA price rises, i.e., the emission reduction in the EU-ETS becomes large.[5] sCER swap volume will be positively correlated with the EU-ETS emission reduction volume. The swap transaction volume for the sCER is defined by B_t[6]

$$dB_t = \mu_B dt + \sigma_B dz_t, \tag{33.3}$$

where μ_B and σ_B are constant for simplicity.

$$E[dz_t dw_t] = \rho_{BV}(V)dt, \tag{33.4}$$

$$\text{where } 0 \leq \rho_{BV}(V) \leq 1. \tag{33.5}$$

More importantly when EUA price, i.e., EUA demand, is high, it is also considered that the market participants may try to obtain the EUA-sCER swap arbitrage opportunity more, resulting in the high correlation between the EUA and sCER volume. That is why the correlation is characterized by $\frac{\partial \rho_{BV}}{\partial V} > 0$. We assume $E[dv_t dz_t] = \phi dt$ with a constant value ϕ and $E[dw_t dv_t] = \varphi dt$ with a constant φ for simplicity.

We assume that the sCER trading volume for arbitragers does not affect the EUA pricing. That is, as the leading carbon market, EUA prices are robustly and independently determined by the emission reductions in the EU-ETS and marginal abatement cost in that area, especially for the EU-ETS covered entities, in order to fulfill their reduction obligation. This is because the EU-ETS market is more independently developed than sCER markets and sCER imports do not affect the EUA pricing. Hence the total demand for EUA X_t is set to be V_t irrelevant to B_t.

[4] We basically suppose that V_t and D_t are positive value. But emission reduction volume is calculated as emission minus emission reduction target. Thus it allows for negative emission reduction volume as in overallocation of EUAs.

[5] This may suggest that the model of sCER swap volume be affected by EUA prices, not EUA-sCER price spreads.

[6] B_t takes both of positive and negative value when sCER is purchased from and sold to the Kyoto market, respectively.

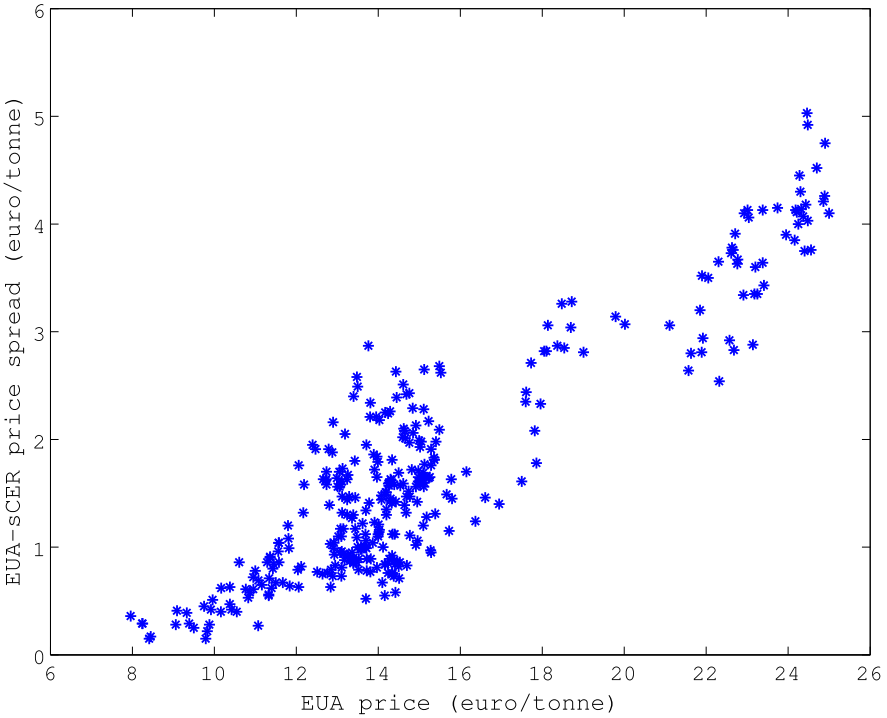

Fig. 33.1 Scatter plots between EUA spot prices and EUA-sCER spot price spreads

sCER prices are determined by the sCER volume other than the EU-ETS (D_t) plus the additional swap transaction volume from the arbitragers (B_t). Hence the total volume for sCERs Y_t is represented by $D_t + B_t$. This is consistent with the market participation of financial players, aggressively entering into sCER markets. Total emission reductions for EUA and sCER denoted by X_t and Y_t are assumed by

$$X_t = V_t, \tag{33.6}$$

$$Y_t = D_t + B_t. \tag{33.7}$$

We model the MAC curves for EUA and sCER to obtain the equilibrium prices of EUA and sCER, respectively. The emission reductions are conducted in the order of the technologies with cheaper emission reduction costs. In carbon markets, the MAC curves are modeled by increasing functions. Then we are interested in the ingredient of the MAC curve. When we consider the relationship between carbon prices and energy prices, it is assumed that EUA prices seem to comove with energy prices more than sCER prices. This is because EUA prices are strongly affected by the fuel switching costs, via the MAC curve, which generally increases in energy prices although sCER prices are determined by the other risk factors such as emission reduction project type and the certificate delivery, which are not relevant to energy prices. That is, since the internal emissions reductions for the EU-ETS covered enti-

ties are mainly conducted by fossil fuel-related activities such as fuel switching, the MAC curve for EUA is relevant to energy prices. In contrast, the emission reductions using the CDM are made by a variety of activities such as renewable energies and methane recovery which have different certificate delivery schedule. The impact of energy prices on sCER MAC curve will be restrictive contrary to EUA MAC curve.

We define by $f(\cdot)$ the second order differentiable, monotone, and increasing MAC curve for EUA which is positively affected by energy prices E_t. Here we consider how energy prices affect the MAC curve. When energy prices are up, the order of the emission reduction measure changes in the direction of the horizontal axis because the impact of energy prices on each technology marginal abatement cost is different. The influence of energy prices on the MAC curve is observed as the horizontal shift of the MAC curve.

$$P_t = f(x_t + kE_t), \tag{33.8}$$

where P_t represents EUA prices for the supply x_t, $\frac{\partial f}{\partial E} > 0$, and k is a constant. If k is positive, the MAC curve horizontal shift due to energy prices results in the increase of the marginal costs, i.e., carbon prices. Here we set energy prices as follows:

$$dE_t = \mu_E dt + \sigma_E d\eta_t, \tag{33.9}$$

where $\frac{\partial \sigma_E}{\partial E} \geq 0$[7] and $d\eta_t$ only possesses a positive correlation with dw_t, i.e., $E[d\eta_t dw_t] = \omega dt$ with $\omega \geq 0$ and $E[d\eta_t dv_t] = E[d\eta_t dz_t] = 0$ for simplicity because the energy price influence on emission reduction volume may be highlighted only in the fuel switching in the EU-ETS.[8] Then we define by $g(\cdot)$ the second order differentiable, monotone, and increasing MAC curve of sCER.

$$S_t = g(y_t), \tag{33.10}$$

where S_t represents sCER prices for supply y_t. The sCER MAC curve is different in the characteristics from EUA in the sense that the other risk factors than energy determine sCER prices. Taking $x_t = X_t$ and $y_t = Y_t$ on the assumption of emission reduction inelasticity to prices in a short period of time, we have the equilibrium prices of EUA and sCER. Employing Ito's Lemma and taking into account that EUA prices are the increasing MAC curve function for EUAs, we recover the correlation model between EUA and sCER price returns

$$\frac{dP_t}{P_t} = \mu_P dt + \sigma_P d\xi_t, \tag{33.11}$$

$$\frac{dS_t}{S_t} = \mu_S dt + \sigma_S du_t, \tag{33.12}$$

$$\rho_{PS} = \frac{(\varphi\sigma_D + \rho_{BV}(V)\sigma_B)\sigma_V}{\sqrt{\sigma_D^2 + \sigma_B^2 + 2\sigma_B\sigma_D\phi}\sqrt{k^2\sigma_E^2 + \sigma_V^2 + 2k\sigma_E\sigma_V\omega}}, \tag{33.13}$$

[7]The volatility-price dependence can be related to the inverse leverage effect, e.g., Knittel and Roberts [14].

[8]To secure the positive energy prices, we can take e.g., $\mu_E = \hat{\kappa}_E(\hat{\mu}_E - \log E_t)E_t$, $\sigma_E = \hat{\sigma}_E E_t$ where $\hat{\kappa}_E$, $\hat{\mu}_E$ and $\hat{\sigma}_E \geq 0$ are constants.

$$\mu_P = \frac{f'}{f}(k\mu_E + \mu_V) + \frac{1}{2}\frac{f''}{f}\left(k^2\sigma_E^2 + \sigma_V^2 + 2k\sigma_E\sigma_V\omega\right), \tag{33.14}$$

$$\sigma_P = \frac{f'}{f}\sqrt{k^2\sigma_E^2 + \sigma_V^2 + 2k\sigma_E\sigma_V\omega}, \tag{33.15}$$

$$d\xi_t = \frac{1}{\sqrt{k^2\sigma_E^2 + \sigma_V^2 + 2k\sigma_E\sigma_V\omega}}(k\sigma_E d\eta_t + \sigma_V dw_t), \tag{33.16}$$

$$\mu_S = \frac{g'}{g}(\mu_D + \mu_B) + \frac{1}{2}\frac{g''}{g}\left(\sigma_D^2 + \sigma_B^2 + 2\sigma_B\sigma_D\phi\right), \tag{33.17}$$

$$\sigma_S = \frac{g'}{g}\sqrt{\sigma_D^2 + \sigma_B^2 + 2\sigma_B\sigma_D\phi}, \tag{33.18}$$

$$du_t = \frac{1}{\sqrt{\sigma_D^2 + \sigma_B^2 + 2\sigma_B\sigma_D\phi}}(\sigma_D dv_t + \sigma_B dz_t). \tag{33.19}$$

Note that $f' = \frac{\partial f}{\partial X}$, $f'' = \frac{\partial^2 f}{\partial X^2}$, $g' = \frac{\partial g}{\partial Y}$, and $g'' = \frac{\partial^2 g}{\partial Y^2}$, respectively. It is found that EUA and sCER price return volatilities are affected by both of the MAC curve shapes and emission reduction behavior as in Eqs. (33.15) and (33.18), respectively. In contrast from Eq. (33.13), we found that the correlations between EUA and sCER price returns are not dependent of the MAC curve shapes f and g but dependent of both the correlation and volatility structures regarding carbon reduction behavior (ρ_{BV}, ϕ, and φ and σ_V, σ_D, and σ_B, resp.) in addition to the associated energy price model parameters (k, σ_E, and ω). Note that ρ_{PS} is assumed to be positive because of the market observation, implying that $\varphi\sigma_D + \rho_{BV}(V)\sigma_B > 0$.

We try to investigate the influence of EUA-sCER swap transaction and energy prices on the correlation between EUA and sCER prices. It is notable to say that the model characterizes the EUA-sCER swap transaction using the EUA-sCER swap volume correlation ρ_{BV} which is represented by a function of V. To this end, the impact of the EUA-sCER swap transaction on the EUA-sCER price correlations can be measured by the sensitivity of ρ_{PS} with respect to V. We examine the sign of the derivative of ρ_{PS} with respect to V and E for the investigations. Regarding V,

$$\frac{\partial\rho_{PS}}{\partial V} = \frac{\sigma_B\sigma_V}{\sqrt{\sigma_D^2 + \sigma_B^2 + 2\sigma_B\sigma_D\phi}\sqrt{k^2\sigma_E^2 + \sigma_V^2 + 2k\sigma_E\sigma_V\omega}}\frac{\partial\rho_{BV}}{\partial V}. \tag{33.20}$$

Taking into account $\frac{\partial\rho_{BV}}{\partial V} > 0$ due to the characteristics of EUA-sCER swap transaction, $\frac{\partial\rho_{PS}}{\partial V}$ has a positive value. It suggests that when EUA prices are high because of EUA emission reduction volume increase, the market participants may try to obtain the EUA-sCER swap arbitrage opportunity more, resulting in the high correlation between EUA and sCER volume from Eq. (33.20). Then we think of the impact of energy prices on the EUA-sCER price correlations. Regarding E,

$$\frac{\partial\rho_{PS}}{\partial E} = -\frac{(k\sigma_E + \sigma_V\omega)(\varphi\sigma_D + \rho_{BV}(V)\sigma_B)k\sigma_V}{\sqrt{\sigma_D^2 + \sigma_B^2 + 2\sigma_B\sigma_D\phi}(\sqrt{k^2\sigma_E^2 + \sigma_V^2 + 2k\sigma_E\sigma_V\omega})^3}\frac{\partial\sigma_E}{\partial E}. \tag{33.21}$$

Note $\varphi\sigma_D + \rho_{BV}(V)\sigma_B > 0$ from ρ_{PS} positive and $\frac{\partial\sigma_E}{\partial E} \geq 0$ by definition. When k is positive implying that the MAC curve horizontal shift due to energy prices causes the increase of the marginal costs, i.e., carbon prices, Eq. (33.21) demonstrates a negative value, implying that EUA-sCER price correlations decrease in line with energy prices. The model in Eq. (33.20) suggests that high EUA-sCER price correlations under high EUA prices come from the large EUA-sCER swap transaction volume during high EUA price periods. In contrast from Eq. (33.21), the high correlations between EUA and sCER price returns under low EUA prices stem from energy price plunge, which is translated into a description of contagion between the two carbon markets.

References

1. Fehr M, Hinz J (2006) A quantitative approach to carbon price risk modeling. Working paper, Institute of operations research, ETZ
2. Benz E, Trück S (2009) Modeling the price dynamics of CO2 emission allowances. Energy Econ 31:4–15
3. Daskalakis G, Psychoyios D, Markellos RN (2009) Modeling CO2 emissions allowance prices and derivatives: evidence from the European trading scheme. J Bank Finance 33:1230–1241
4. Seifert J, Uhrig-Homburg M, Wagner M (2008) Dynamic behavior of CO2 spot prices. J Environ Econ Manag 56:180–194
5. Paolella M, Taschini L (2008) An econometric analysis of emission allowance prices. J Bank Finance 32:2022–2032
6. Uhrig-Homburg M, Wagner M (2009) Futures price dynamics of CO2 emission allowances – an empirical analysis of the trial period. J Deriv 17:73–88. Winter 2009
7. Borak S, Härdle W, Trück S, Weron R (2006) Convenience yields for CO2 emission allowance futures contracts. Working paper, Humboldt-University of Berlin
8. Kanamura T (2009) A classification study of carbon assets into commodities. Working paper, SSRN
9. Grüell G, Taschini L (2012) Linking emission trading schemes: a short note. Econ Energy & Environ Policy 1:31–38
10. Chevallier J (2011) Anticipating correlations between EUAs and CERs: a dynamic conditional correlation GARCH model. Econ Bull 31(1):255–272
11. Mansanet-Bataller M, Chevallier J, Hervé-Mignucci M, Alberola E (2011) EUA and sCER phase II price drivers: unveiling the reasons for the existence of the EUA–sCER spread. Energy Policy 39(3):1056–1069
12. Medina V, Pardo A, Pascual R (2013) Carbon credits: who is the leader of the pack? Int J Energy Econ Policy 3(3):210–220
13. Mizrach B (2012) Integration of the global carbon markets. Energy Econ 34(1):335–349
14. Knittel CR, Roberts MR (2005) An empirical examination of restructured electricity prices. Energy Econ 27(5):791–817

Chapter 34
Combining Time Series Forecasting Methods for Internet Traffic

C. Katris and S. Daskalaki

Abstract The aim of this work is to explore whether forecasts from individual forecasting models can be improved with the use of combination rules. Working with Internet traffic data, first we use FARIMA, FARIMA with student-t innovations and Artificial Neural Networks as individual forecasting models, since each one of them explains some statistical characteristic of our data, and next we combine the forecasts using three different combination rules. Based on our experimental work simple combination rules may improve individual models. Finally, we consider a scheme where the selection of the model is based on the White's Neural Network test for non-linearity and compare with the results from the combination of forecasts.

34.1 Introduction

It is widely accepted that Internet traffic carries properties such as Self-Similarity and Long Range Dependence (LRD) [2, 15], while it sometimes displays non-linear structures [13]. Recent measurements have shown that Short Range Dependence (SRD) also appears in Internet traffic. A class of forecasting models which can describe both LRD and SRD are the FARIMA models [9, 11], which have become very popular for Internet traffic modeling [18]. While constructing a FARIMA model, the estimation of the fractional parameter d is an important issue and many methods have been developed for it. In this paper, we use the Geweke and Porter-Hudak method [7]. Lastly, since Internet traffic almost always exhibits heavy tails and is leptokurtic, it seems reasonable using FARIMA with heavy-tailed, instead of Normal, innovations [12]. In this paper we experiment with both FARIMA models, i.e. with Normal and student-t innovations, as traffic forecasting models.

Another issue addressed here is non-linearity in time series. FARIMA are linear models and their ability for prediction is limited when the traffic data require non-

C. Katris (✉) · S. Daskalaki
Department of Electrical & Computer Engineering, University of Patras, Patras, Greece
e-mail: chriskatris@upatras.gr

S. Daskalaki
e-mail: sdask@upatras.gr

A. Steland et al. (eds.), *Stochastic Models, Statistics and Their Applications*,
Springer Proceedings in Mathematics & Statistics 122,
DOI 10.1007/978-3-319-13881-7_34

linear structures. The approach mostly used for modeling non-linear time series involves Artificial Neural Networks (ANN), such as in Cortez et al. [4]. For our work we used the Multilayer Perceptron (MLP) feed-forward neural network as model but in order to optimally design its architecture for our experiments we also used certain concepts from dynamical systems.

The three forecasting approaches mentioned previously are quite promising but none of them may capture all characteristics of the Internet traffic at once, therefore in order to further improve forecasting accuracy we create combination schemes of different models. There are many methods of combining forecasts and a good description of several of them can be found in Menezes et al. [17]. We adopt three static combinations; the simple average, which is fair, robust and gives promising results; a weighted average, where the weights depend on the RMSE of the individual methods achieved during training; and an unconstrained linear regression approach. Finally, we compare the performance of the combination schemes with an approach where at first we apply a hypothesis test, the White neural network test, in order to detect non-linearity. If the test is significant we select an ANN model, otherwise we use the classical FARIMA model with normal innovations. This approach aims to assign the most appropriate individual forecasting model for each trace.

The rest of the paper is organized as follows. Section 34.2 reviews the individual models and their building procedures. Section 34.3 describes the combining schemes and the alternative approach of model selection according to the White test. Section 34.4 presents the application of all described methods to several Internet traffic data sets, while Sect. 34.5 concludes with a brief discussion on the experimental results.

34.2 Forecasting Models of Internet Traffic

In this section we present forecasting models which are quite suitable for Internet traffic. FARIMA models with normal or student-t innovations capture the LRD and SRD characteristics, while ANN models capture non-linearity. For each model type the fitting procedure is discussed briefly.

34.2.1 FARIMA Model Building

FARIMA models, as opposed to ARIMA, are suitable when SRD and LRD co-exist in a time series. LRD is detected when there is a very slow decrease of the autocorrelation function, in practice with a power-law rate. This implies that observations from the far past can affect future observations. On the other hand SRD is present when the decay of the autocorrelation function is exponential, and this means that only recent observations affect future observations.

A FARIMA model is an extension of the ARIMA (p, d, q) model, when the parameter d is allowed to take real (not only integer) values, and describes a time series using Eq. (34.1).

$$\Phi_p(L)(1-L)^d(X_t) = \Theta_q(L)\varepsilon_t \tag{34.1}$$

where $\Phi_p(L) = 1 - \phi_1 L - \cdots - \phi_p L^P$ and $\Theta_q(L) = 1 + \theta_1 L + \cdots + \theta_q L^q$. L is the lag operator, $(1-L)^d = \sum_{j=0}^{\infty} \binom{d}{j} (-1)^j L^j$, and $\binom{d}{j}(-1) = \frac{\Gamma(-d+j)}{\Gamma(-d)\Gamma(j+1)}$. The error terms ε_t follow normal distribution with mean zero and variance σ^2.

Alternatively, we consider a model where the error terms ε_t follow a student-t distribution $t(0, \sigma, v)$, where $v > 2$. The pdf in its location-scale version is:

$$f(x; \alpha, \beta, v) = \frac{\Gamma(\frac{v+1}{2})}{\sqrt{\beta v \pi}\,\Gamma(\frac{v}{2})} \left[1 + \frac{(x-\alpha)^2}{\beta v}\right]^{(-\frac{v+1}{2})} \tag{34.2}$$

with location parameter α, scale parameter β and shape parameter v. The mean equals to α and here is 0, while the variance is $\frac{\beta v}{(v-2)}$.

In order to fit a FARIMA model to traffic traces, a procedure similar to the one described in Liu et al. [16] is used. The first step is to *convert the data to a zero mean series* by subtracting the sample mean from the trace. The next step is to *specify the order of the model*. We restrict the auto-regressive and moving average order to be less than or equal to 5 (i.e. $0 \leq p, q \leq 5$). Then we consider all possible ARIMA models and choose the one with the lowest Bayesian Information Criterion (BIC). The final step is to *estimate the remaining parameters* of the model. The fractional parameter d is estimated via the Geweke and Porter-Hudak (GPH) estimator [7], while the parameters ϕ_i, θ_i are specified using Maximum Likelihood (ML) methodology. Note that if GPH fails to estimate $d \in (0, 0.5)$ then the fractional parameter is also estimated using the ML methodology. All computations for this procedure are performed using the R software [8].

34.2.2 ANN Model Building

FARIMA models, described previously, assume linearity in mean and this assumption can be a serious limitation in cases where the time series indicate non-linear structures. It is very important to detect whether a time series trace follows some non-linear structure. Fortunately there are some statistical procedures which can provide this information. In this work we use the White neural network test [14]. The test is based on an ANN structure and its null hypothesis is that the time series model that creates the dataset is linear. The alternative hypothesis is arbitrary non-linearity. The statistic of the test is assumed to follow Chi-square distribution.

Appropriate models for describing non-linearity in time series and for gaining additional accuracy in forecasting are the ANNs. An overview about them can be found in [19]. The most widely used architecture is that of the Multilayer Perceptron (MLP), which is a feed-forward NN comprising an input layer, one or more hidden

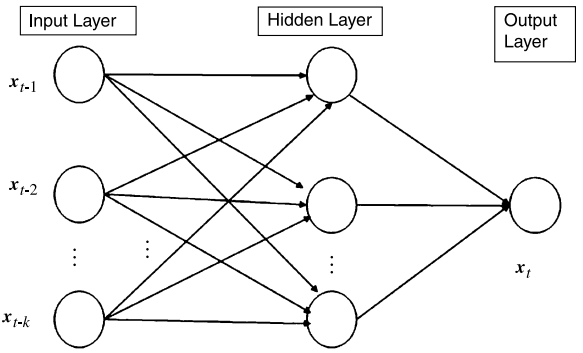

Fig. 34.1 Multilayer perceptron ANN with 1 hidden layer

layers and an output layer. An application of ANN on Internet traffic forecasting can be found in [4]. In this paper, we use a monotone multilayer perceptron network with one hidden layer (Fig. 34.1).

For the determination of the ANN architecture we have to specify the input variables, i.e. the lagged variables, the number of hidden layers and the number of nodes to each layer. For the input variables we borrow concepts from dynamical systems, the relation between inputs and outputs is determined by the activation function with the most popular selection to be the logistic function, while for the output, a linear function is a popular choice. For the training of the ANN, the algorithm that was used is the adaptive gradient descent.

We now briefly discuss some concepts from dynamical systems which are necessary for the construction of the ANN. Each time series is considered to be a dynamical system for which the next state is expressed as a function of its current state. Especially for a discrete time series, this is expressed as: $x(t+1) = F(x(t))$. The goal is to identify a simpler system from which the data could have come from. The embedding theorem states that the space of time lagged vectors with sufficiently large dimension will capture the original time series. This dimension is called embedding dimension and gives the number of lagged variables that are needed to reconstruct satisfactorily the original time series. In order to determine the embedding dimension the False Nearest Neighbors (FNN) method is used. Another important issue is the determination of the time lag k. When $k > 1$ the time series is considered as over-sampled, and a sampling with rate k must take place. The time lag has to be chosen in a way that keeps a balance between small value and great independence. Mutual information can help us decide whether resampling is needed [5].

In order to construct an ANN, at first we *decide whether resampling is needed*, using mutual information. In our case all time series we examined did not require any resampling. Next we *select input variables* (i.e. lagged variables) according to the FNN method and finally we *decide about the hidden layer nodes and the training epochs*. Specifically, we consider one hidden layer and decide for 1, 2, 10, 20, or 50 nodes based on a minimum RMSE for the 1000 most recent observations of the training sample. The training is performed using back-propagation with the adaptive gradient descent algorithm and for 500 epochs of training. The activation function is sigmoid for the hidden layer and linear for the output.

34.3 Combination Methods of Forecasting Models

Combining forecasts is a known procedure for improving forecasting accuracy and is supported by many researchers and practitioners [3]. The initial proposal for combining forecasts came from Bates and Granger [1] and after this work, a large number of articles referred to combinations of forecasts. Some well established methods are discussed and analyzed in Menezes et al. [17]. In this paper, we consider 3 methods of forecast combinations:

- *Simple Average*: This method has the advantages of impartiality and robustness, while provide good results generally [17]. The formula for this method is given as:

$$\hat{f} = \frac{\sum_{i=1}^{n} f_i}{n} \tag{34.3}$$

- *Weighted Average*: Instead of the simple average, we may weight the forecasts according to their performance in the training set. Here as criterion for each model's performance we consider the RMSE, which in general is more popular as an index. The formula used for this method is:

$$\hat{f} = \sum_{i=1}^{n} w_i f_i, \quad \text{where } w_i = \frac{(\frac{1}{RMSE_i})}{\sum_{i=1}^{n}(\frac{1}{RMSE_i})} \quad \text{and} \quad \sum_{i=1}^{n} w_i = 1 \tag{34.4}$$

- *Regression*: In this method the individual forecasts are used as regressors in an ordinary least squares regression with the inclusion of a constant term. An unbiased combined forecast is produced regardless of whether the constituent forecasts are biased [10].

Model Selection According to White Neural Network Test Except from the individual forecasting methods and the combination methods, we also consider a model selection according to the White neural network test. The procedure performs the test and if non-linearity is detected ANN is the indicated model for forecasting, otherwise, the FARIMA model with Normal innovations is the choice. This procedure identifies the best individual model for each trace. Basically if the White test is successful, then the procedure can lead to a successful individual model.

34.4 Data Analysis

We apply the aforementioned procedure to traces from Ethernet and video traffic at different levels of aggregation. All traces are publicly available, either from the Internet Traffic archive (http://ita.ee.lbl.gov/) or from TU-Berlin [6]. Table 34.1 gives overview information for each trace and specifically its source, type, level of aggregation (unit of measure and time scale) and volumes of data for the training and test set, respectively. The analysis that was described previously was performed on each dataset using separate packages from the R environment and specifically AMORE,

Table 34.1 Overview of traces

Trace	Source	Type	Unit	Aggregation time	Training (test) set
August89	Bellcore	LAN	Mbytes	10 seconds	264 (50)
Oct89	Bellcore	LAN	Mbytes	second	1260 (500)
LBL PK4	Bellcore	WAN	Mbytes	10 seconds	300 (60)
Dusk till Down	TU-Berlin	MPEG4	Kbytes	frame	4000 (1000)
Die Hard III	TU-Berlin	MPEG4	Kbytes	frame	4000 (1000)
Jurassic Park	TU-Berlin	MPEG4	Mbytes	second	3000 (600)
Star Wars IV	TU-Berlin	MPEG4	Mbytes	second	3000 (600)
The Firm	TU-Berlin	VBR	Kbytes	frame	4000 (1000)
Mr. Bean	TU-Berlin	VBR	Kbytes	frame	4000 (1000)

Table 34.2 Details on the forecasting models and approaches

Trace	FARIMA order	d	ANN model	White test	Model selection
August89	(1, 1)	0.3961873	(4, 20, 1)	Linearity	(FARIMA)
Oct89	(1, 1)	0.440625	(9, 50, 1)	Non-linearity	(ANN)
LBL PK4	(0, 4)	0.3955	(7, 50, 1)	Non-linearity	(ANN)
Dusk till Down	(4, 2)	0.00000001	(6, 10, 1)	Non-linearity	(ANN)
Die Hard III	(5, 2)	0.00000001	(10, 20, 1)	Non-linearity	(ANN)
Jurassic Park	(1, 2)	0.2732444	(10, 20, 1)	Linearity	(FARIMA)
Star Wars IV	(2, 3)	0.1785253	(10, 50, 1)	Linearity	(FARIMA)
The Firm	(0, 1)	0.5	(6, 10, 1)	Linearity	(FARIMA)
Mr. Bean	(2, 2)	0.3777264	(10, 10, 1)	Non-linearity	(ANN)

rugarch, tseries, forecast, fNonLinear. Table 34.2 displays information regarding the selected FARIMA models and ANN architectures, as well as the model suggested by the White NN test. Table 34.3 presents the performance of each individual model and that of the combination procedures using RMSE and MAE as metrics. Moreover, for each forecasting procedure we consider its ranking according to RMSE and MAE on each dataset and then report its average ranking over all datasets.

From Table 34.3 we can observe that from individual models the ANN is the most successful approach according to RMSE average position but worse than FARIMA with student t innovations according to MAE average ranking. From the combination methods, both the simple and weighted mean gave better results than the individual models according to average rankings. On the contrary, the regression combination scheme gave the worst average results. It is worth pointing out however that this method was found to be more efficient only for the Video data with higher levels of aggregation (i.e. seconds). Finally, the selection of a model according to the White criterion displayed the best results compared to all methods with the RMSE criterion and slightly worse only than the weighted mean combination

Table 34.3 Comparison of forecasting procedures

Trace	Metric	FARIMA	FARIMA student-*t*	ANN	Simple mean	Weighted mean	Regression	Model based on White test
August89	RMSE	0.42745	0.42439	0.44603	0.43109	0.43659	0.43651	0.42745
	MAE	0.32107	0.31916	0.34183	0.32689	0.33311	0.34183	0.32107
Oct89	RMSE	0.10872	0.10633	0.10772	0.10595	0.10599	0.11004	0.10772
	MAE	0.08822	0.08572	0.08515	0.08502	0.08447	0.08887	0.08515
LBL PK4	RMSE	0.20588	0.22208	0.1892	0.20090	0.19636	0.23841	0.1892
	MAE	0.14676	0.14908	0.1425	0.14434	0.14298	0.15509	0.1425
Dusk till Down	RMSE	1.02592	1.12627	1.01465	0.97032	0.95461	1.1256	1.01465
	MAE	0.70243	0.64089	0.58987	0.57569	0.54823	0.82759	0.58987
Die Hard III	RMSE	0.75444	0.73559	0.51354	0.59840	0.53200	0.73520	0.51354
	MAE	0.52896	0.46036	0.30446	0.38844	0.33303	0.55976	0.30446
Jurassic Park	RMSE	0.01753	0.01795	0.03295	0.01900	0.02808	0.01763	0.01753
	MAE	0.01231	0.01227	0.02275	0.01372	0.02398	0.01240	0.01231
Star Wars IV	RMSE	0.00874	0.00896	0.01214	0.00877	0.00961	0.00874	0.00874
	MAE	0.00532	0.00527	0.00910	0.00584	0.00682	0.00529	0.00532
The Firm	RMSE	0.39615	0.43023	0.37118	0.38593	0.37506	0.40065	0.39615
	MAE	0.18699	0.18655	0.17513	0.17744	0.17442	0.25994	0.18699
Mr. Bean	RMSE	0.91556	0.99696	0.89372	0.89963	0.88843	0.95909	0.89372
	MAE	0.46315	0.43446	0.42484	0.41759	0.41405	0.64611	0.42484
Average	**RMSE**	**3.61**	**4.22**	**3.33**	**2.78**	**2.78**	**4.28**	**2.28**
Ranking	**MAE**	**4**	**3.11**	**3.56**	**2.78**	**2.56**	**5**	**2.67**

approach according to MAE. In our study, the White test was found to be efficient in detecting non-linearity and led to a successful model selection.

34.5 Conclusions

In this work we considered FARIMA models with normal and student-t innovations along with ANN models to be used for Internet traffic forecasting. For each model we discussed its construction and fitting procedure and applied them to nine different datasets. In order to improve forecasting performance we applied combination methods based on a simple and a weighted mean of the individual forecasts and also regression of them. Finally, we proposed the selection of an individual model according to the White neural network test. From the experimental analysis that was performed it is shown that selection of a model according to White test led to better results on the average, while from the combinations both the simple and weighted means of forecasts reach to better forecasting performance compared to individual models.

References

1. Bates J, Granger C (1969) The combination of forecasts. 4OR 20:451–468
2. Beran J, Sherman R, Taqqu MS, Willinger W (1995) Variable bit-rate video traffic and long range dependence. IEEE Trans Commun 43(2–4):1566–1579
3. Bunn DW (1989) Forecasting with more than one model. J Forecast 8:161–166
4. Cortez P, Rio M, Rocha M, Sousa P (2012) Multi-scale Internet traffic forecasting using neural networks and time series methods. Expert Syst 29(2):143–155
5. Frank RJ, Davey N, Hunt SP (2001) Time series predictions and neural networks. J Intell Robot Syst 31(1-3):91–103
6. Fitzek FHP, Reisslein M (2001) MPEG-4 and H.263 Video Traces for Network Performance Evaluation. IEEE Netw 15(6):40–54
7. Geweke G, Porter-Hudak S (1983) The estimation and application of long memory time series models. J Time Ser Anal 4(4):221–238
8. Ghalanos A (2013) rugarch: Univariate GARCH models. R package version 1.2-7
9. Granger CWJ, Joyeux R (1980) An introduction to long-memory time series models and fractional differencing. J Time Ser Anal 1:15–30
10. Granger CWJ, Ramanathan R (1984) Improved methods of forecasting. J Forecast 3:197–204
11. Hosking JRM (1981) Fractional differencing. Biometrika 68:165–176
12. Ilow J (2000) Forecasting network traffic using FARIMA models with heavy tailed innovations. In: Proceedings of IEEE International Conference on Acoustics, Speech, and Signal Processing (ICASSP '00), vol 6, pp 3814–3817
13. Katris C, Daskalaki S (2014) Prediction of Internet traffic using time series and neural networks. In: Proceedings of International Work-Conference on Time Series Analysis (ITISE 2014), vol 1, pp 594–605
14. Lee TH, White H, Granger CWJ (1993) Testing for neglected nonlinearity in time series models. J Econom 56:269–290
15. Leland WE, Taqqu MS, Willinger W, Wilson D (1994) On the self-similar nature of Ethernet traffic (extended version). IEEE/ACM Trans Netw 2:1–15

16. Liu J, Shu Y, Zhang L, Xue F, Oliver W, Yang W (1999) Traffic modeling based on FARIMA models. In: Canadian conference on electrical and computer engineering – CCECE, vol 1, pp 162–167
17. de Menezes LM, Bunn DW, Taylor JW (2000) Review of guidelines for the use of combined forecasts. Eur J Oper Res 120(1):190–204
18. Shu Y, Jin Z, Zhang L, Wang L, Oliver W, Yang W (1999) Traffic prediction using FARIMA models. IEEE Int Conf Commun 2:891–895
19. Zhang G, Patuwo BE, Hu MY (1998) Forecasting with artificial neural networks: the state of the art. Int J Forecast 14(1):35–62

Chapter 35
Stochastic Model of Cognitive Agents Learning to Cross a Highway

Anna T. Lawniczak, Bruno N. Di Stefano, and Jason B. Ernst

Abstract We describe a stochastic model of simple cognitive agents ("creatures") learning to cross a highway. The creatures are capable of experiencing fear and/or desire to cross and they use an observational learning mechanism. Our simulation results are consistent with real life observations and are affected by the creatures' fears and desires, and the conditions of the environment. The transfer of the knowledge base acquired by creatures in one environment to the creatures operating in another one improves creatures' success of crossing a highway.

35.1 Introduction

Unmanned vehicles used in space and underwater exploration should be autonomous because remote operation is impractical & unreliable and the outcome cannot be guaranteed, [1]. The functional complexity of these robots results in reliability problems and increased development & operational costs, which may be improved by replacing complex robots with swarms of micro-bots, but still collectively exhibiting some learning & decision making ability. An advantage of micro-bots is that their behaviour can easily be verified because they can be modelled with cognitive agents, [2–6], which in turn can be implemented with object oriented design methodologies. We study what is a minimal requirement of micro-bots intelligence. We adopt "*biomimicry*" as modelling philosophy and experiment with very primitive creatures. Our agents make their crossing decision by adopting "*observational learning*", a type of "*social learning*" ("*imitate what works and don't do what*

A.T. Lawniczak (✉)
Department of Mathematics and Statistics, University of Guelph, Guelph, Ontario, Canada
e-mail: alawnicz@uoguelph.ca

B.N. Di Stefano
Nuptek Systems Ltd, Toronto, Ontario, Canada
e-mail: bruno.distefano@nupteksystems.com

J.B. Ernst
School of Computer Science, University of Guelph, Guelph, Ontario, Canada
e-mail: jernst@uoguelph.ca

A. Steland et al. (eds.), *Stochastic Models, Statistics and Their Applications*,
Springer Proceedings in Mathematics & Statistics 122,
DOI 10.1007/978-3-319-13881-7_35

doesn't work"), [5]. Using the simulator of the stochastic model that we developed, we conducted various experiments to evaluate the impact of the learning algorithm for the population of cognitive agents learning to cross the highway, [7]. This paper is structured as follows. In Sect. 35.2 we briefly describe the model and in Sect. 35.3 we report selected simulation results. In Sect. 35.4 we provide our conclusions and outline future work.

35.2 Stochastic Model of Creature Learning to Cross a Highway

Our model of cognitive agent is described in [8]. Here we provide its brief description and focus on the effects of knowledge base transfer on the creatures learning outcomes. Our model consists of an environment, creatures and their learning algorithms. We summarise our model as follows. The creatures' environment is a vehicular traffic highway, either single lane or multi-lane, either unidirectional or bidirectional, without any intersection. The highway traffic is modelled by means of the Nagel–Schreckenberg model, [9]. For our investigation its implementation requires to modify the Cellular Automata (CA) paradigm and to make the evolution of the CA not only dependent on the state of the neighbourhood but also on the current velocity of each vehicle. This implies that each cell is characterised not only by presence or absence of a vehicle but also by a pointer to a data structure containing the current velocity of the vehicle. As customary in discrete traffic modelling, we model each lane of unidirectional traffic of a highway as a large number of adjacent cells, with each cell representing a segment of highway of 7.5 m in length, [9, 10]. At each time step in the simulation, for each lane, a new car may be generated with a probability specified in the configuration file as car creation probability p. If there is already a car in the first cell because it has not sped up enough, or traffic is congested, the generated car is added to a queue of cars waiting to enter the highway. The entrance point is always cell zero of each lane. Cars accelerate by one until they reach their maximum speed, which is specified in the configuration file.

The creatures are born on one side of the highway. They are generated similarly to the cars and as cars they also use queues. The creatures want to cross the highway to get to its opposite side. If a creature at a top of the queue has not yet crossed the highway then the newly created creatures will line up behind it. The creatures are generated randomly (with a creation probability and fear and/or desire probabilities specified in the configuration file) at each time step at a crossing point selected at the initialisation step. The motion of the creature is modelled similarly to the motion of the vehicle; i.e. with a CA-like approach. The creatures have a strong instinct to survive when crossing a highway, which may or may not be successful. If the crossing is successful the creature remains on opposite side of the highway and never crosses it again. If it was not, it means the creature was struck by a vehicle and died. The creatures have ability to see what happened to other creatures that have previously crossed and if under similar conditions the crossing was not successful they will avoid crossing and wait. If a creature cannot cross the highway at its current

location, due to unsafe conditions, it may move to a different potential crossing point to cross at, either up stream or down stream traffic. This feature of the model may be enabled at the software initialisation.

We assume that the creatures are not capable of evaluating precisely distance and velocity, similarly as most humans who are not capable of evaluating precisely distance and velocity of moving vehicles. Each creature is able to rank the position of the vehicle with respect to its crossing locations according to a discrete number of categories (e.g., {far, mid range, close} or, alternatively, {very far, far, mid range, close, very close}, etc.). In the presented simulations we are using these categories. However, the simulation software allows selecting other numbers of categories. By increasing the number of categories we increase the precision of the estimates but also the computational cost increases, unfortunately, and the cost of potential hardware implementation. Information whether a creature crossed the highway successfully or not is recorded into the knowledge base of all the creatures. The columns of the knowledge base table store information about verbal descriptions of velocity and the rows of the table store information about verbal descriptions of the distance. The knowledge base table is initialised as "*tabula rasa*"; i.e. a "*blank slate*", represented with "*0*" at each location in the assumption that all possible (distance, velocity) combinations allow crossing. If a creature successfully crosses the highway the perceived (distance, velocity) score in the knowledge base table is increased by one point. If the creature was killed, it is decreased by one point. When a new creature arrives at the top of the queue, the creature consults the knowledge base table to decide if it is safe or not to cross. The decision is based on the naïve creature with fear and/or desire implemented intelligence/learning algorithm.

We impose a special initial condition for each (distance, velocity) pair to encourage creatures crossing the highway: (1) creatures pay no attention to their knowledge base table or to their fear and/or desire at the start of the simulation; (2) this lasts until the first successful crossing of a creature, or five consecutive unsuccessful crossing of the creatures, whichever comes first. After this initialisation, each randomly generated creature makes its decision to cross or not to cross the highway for a given (distance, velocity) pair by combining the "*success ratio*" of crossing the highway for this (distance, velocity) pair with the creature's fear and/or desire probabilities, as follows: (1) if a creature has both fear and desire, then it will base its decision on the following formula: "*success ratio* + *probability of desire* − *probability of fear*"; (2) if a creature has only fear then it will base its decision on the formula: "*success ratio* − *probability of fear*"; (3) if a creature has only desire then it will base its decision on the formula: "*success ratio* + *probability of desire*". If for a creature and a given (distance, velocity) combination the value of the respective formula is: (1) non-negative, then the creature will attempt to cross the highway; (2) less than zero, then the creature will not attempt to cross the highway under this condition and it will wait for a configuration for which the value of the formula is non-negative. For each (distance, velocity) pair at each time step the numerator in the "*success ratio*" is the number of "*successful crossings*" minus the number of "*unsuccessful crossings*" for this (distance, velocity) pair up to this time; i.e. it is the value from the knowledge base table corresponding to this (distance, velocity)

pair at this time. The denominator is the total number of creatures who have crossed successfully the highway regardless of the (distance, velocity) combination up to this time; i.e. it is the number describing the creatures' entire population success up to this time. If for some (distance, velocity) configuration at the start, all creatures are killed then the ratio becomes "$-5/0$". In this case, we set the "*success ratio*" to zero.

After the initialisation of the simulator the main loop of the simulator is executed once for every time step in the simulation and it consists of the following tasks: (1) generate cars at each lane of the highway using the car creation probability p; (2) generate creatures at each predefined cross point, as specified in the configuration file, using the creature creation probability; (3) update the car speeds. This accelerates the cars according the Nagel–Schreckenberg model; (4) move the creatures from the cross point queues into the highway (if the decision algorithm indicates this should occur); (5) move the cars on the highway including passing other cars and the logic to check if any creature has been hit; (6) advance the current time step. After the simulation has completed, the results are written to output files.

35.3 Selected Simulation Results

The selected simulation results show learning performance of a population of naïve creatures using naïve learning algorithm with fear and/or desire for various values of fear and desire probabilities p_f and p_d (listed in the first columns of the figures) when the creatures are learning to cross a one lane unidirectional highway under various traffic conditions characterised by car creation probability p and without "*erratic drivers*". The creatures' learning performance is measured by "*throughput of creatures crossing successfully the highway*".

The considered throughput is a time dependent function defined for every time t as follows: it is "*the average over the number of simulation runs of the number of creatures that crossed successfully the highway up to time t divided by time t*". For each considered experimental set up we performed 5 simulation runs with different random seed values. The experimental set up is defined by highway type, value of car creation probability, values of fear and desire probabilities, knowledge base transfer or not, selection of a crossing point, creatures ability to leave or not to leave the initial crossing point, the number and range of distances each creature can observe and the number and ranges of speeds each creature can perceive. In the presented simulation results the distances are classified as {close, midrange, far} and the speeds are classified a {slow, medium, fast}.

The graphs of the throughput functions (solid graphs) and theirs' one standard deviations (dotted graphs) are displayed in the plots of Figs. 35.1 and 35.2. On each plot they correspond, respectively, to various levels of car traffic density as measured by car creation probability p. We consider $p = 0.1, 0.3, 0.5, 0.7, 0.9$, and the corresponding colour coding of the graphs is consistent through all the plots of Figs. 35.1 and 35.2, and their explanation is provided in the legend box of each plot. In the

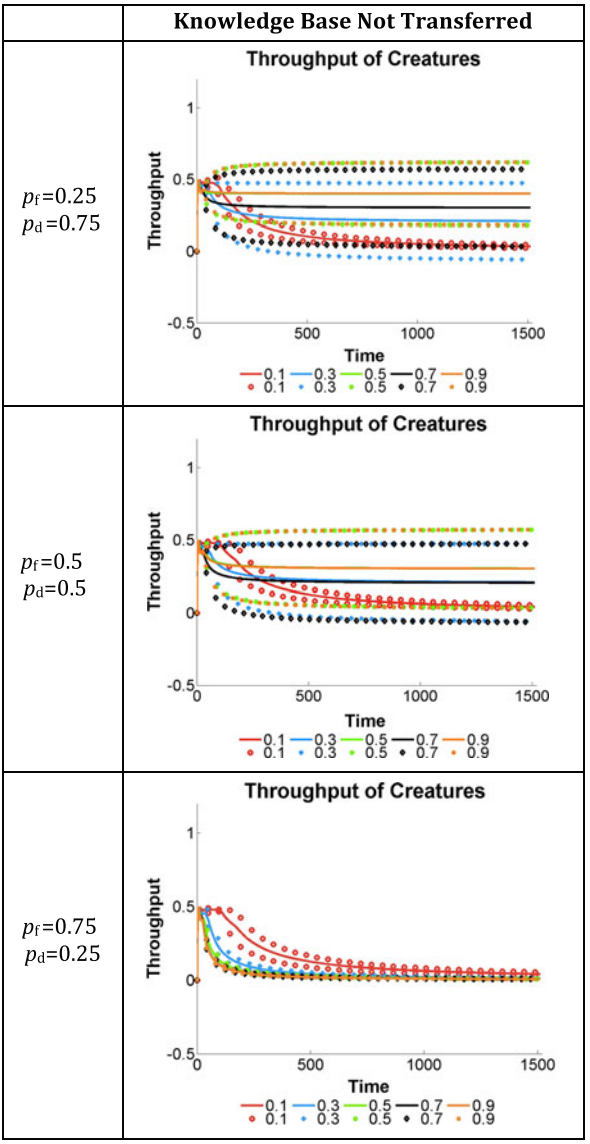

Fig. 35.1 Plots of throughput (*solid* graphs) and one standard deviations (*dotted* graphs) of number of creatures successfully crossing a one lane unidirectional traffic highway, respectively with car creation probability $p = 0.1, 0.3, 0.5, 0.7, 0.9$. The cars are not allowed to drive erratically. The creatures are not allowed to change the initial crossing point set at cell number 90 to another crossing point to cross from. The results in *rows* correspond to creatures' fear and desire probabilities (p_f and p_d) listed in the *first column*. The *second column* represents the results when knowledge base is not transferred from one environment to another one

discussed experiments we consider only one crossing point at each initialisation of the simulator that is the same for all simulation runs. This crossing point is at cell number 90 and creatures are not allowed to leave this crossing point.

In Fig. 35.1 the second column displays results when the knowledge base is not transferred from creatures learning to cross a highway from one experiment to the next one, indexed by car creation probability p; i.e. in each of these experiments the creatures are born "*tabula rasa*" and they have to build their knowledge base as the simulation progresses. In Fig. 35.2 the second and third columns display results

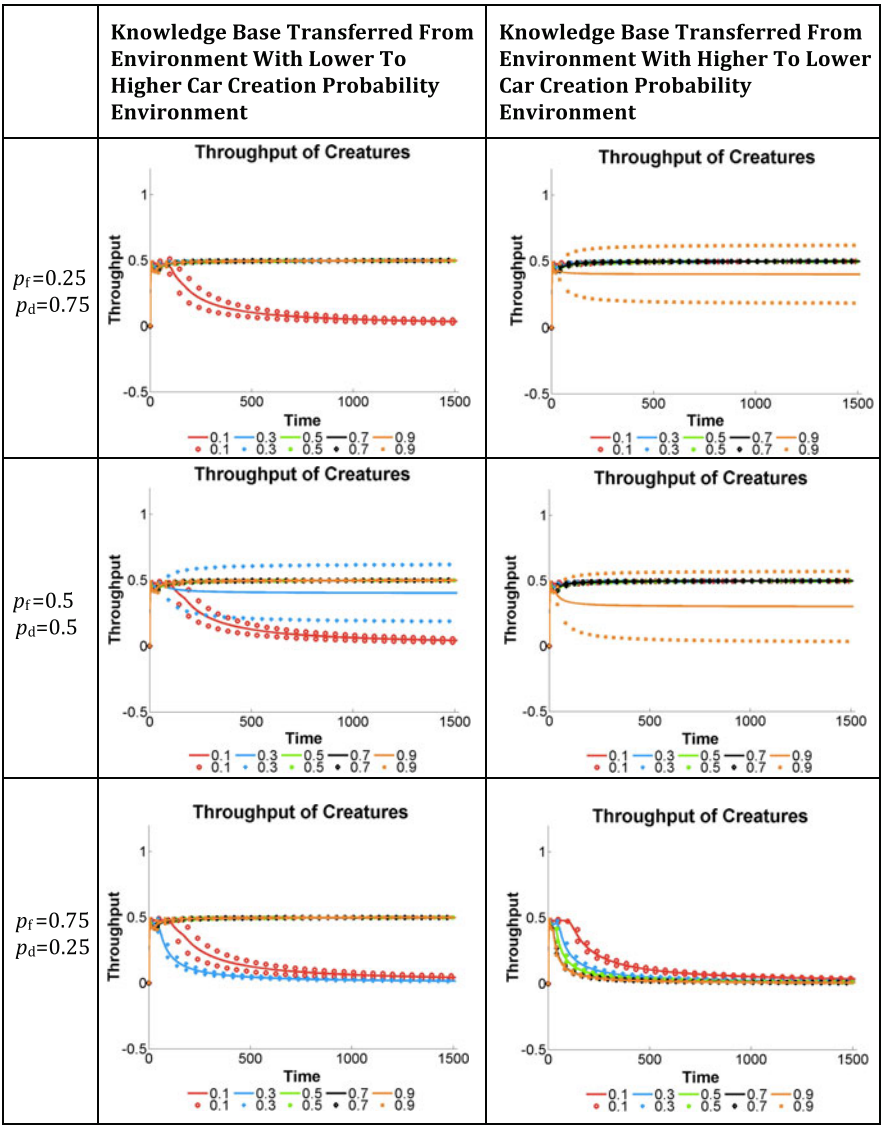

	Knowledge Base Transferred From Environment With Lower To Higher Car Creation Probability Environment	**Knowledge Base Transferred From Environment With Higher To Lower Car Creation Probability Environment**
p_f=0.25 p_d=0.75		
p_f=0.5 p_d=0.5		
p_f=0.75 p_d=0.25		

Fig. 35.2 Plots of throughput (*solid* graphs) and one standard deviations (*dotted* graphs) of number of creatures successfully crossing a one lane unidirectional traffic highway, respectively with car creation probability $p = 0.1, 0.3, 0.5, 0.7, 0.9$. The cars are not allowed to drive erratically. The creatures are not allowed to change the initial crossing point set at cell number 90 to another crossing point to cross from. The results in *rows* correspond to creatures' fear and desire probabilities (p_f and p_d) listed in the *first* column. The *second* column represents the results when knowledge base is transferred from an environment with lower to higher car creation probability, while the third one when it is transferred in opposite direction

when at the beginning of a simulation the knowledge base is transferred from the end of the preceding experiment, index by car creation probability p, to the next one, except of the first experiment. The plots of the second column of Fig. 35.2 correspond to the simulations when the first experiment was conducted for car creation probability $p = 0.1$. In this case creatures are born "*tabula rasa*" and they have to build their knowledge base as the simulation progresses. At the end of this simulation the knowledge base is transferred to the creatures created at the beginning of the next experiment; i.e. with car creation probability $p = 0.3$. This process is repeated for the subsequent experiments; i.e. the ones with car creation probability $p = 0.5$, 0.7, and 0.9. The plots of the third column of Fig. 35.2 correspond to the simulations when first experiment was conducted for car creation probability $p = 0.9$. Again, in this case creatures are born "*tabula rasa*" and they have to build their knowledge base as the simulation progresses. At the end of this simulation the knowledge base is transferred to the creatures created at the beginning of the next experiment, this time with car creation probability $p = 0.7$. This process is repeated for the subsequent experiments; i.e. the ones with car creation probability $p = 0.5$, 0.3, and 0.1. Thus, the second column of Fig. 35.2 displays results of experiments when the knowledge base is transferred from creatures learning to cross a highway in environment with lower car creation probability to the creatures learning to cross the highway in the environment with higher car creation probability. While the third column of Fig. 35.2 displays the results of experiments when this transfer of knowledge base is in opposite direction, i.e. from the learning environment with more dense traffic to the one with less dense traffic.

The presented simulation results show that with the increase of fear probability the fluctuations decrease and that with the increase of desire probability the throughput values increase, see Fig. 35.1. By comparing the corresponding results for fear and desire probabilities of Fig. 35.1 with those of Fig. 35.2 we observe that transfer of knowledge base built by creatures in one learning environment to creatures in another environment has significant effect of the creatures throughput, the throughput fluctuations and the creatures' learning outcomes. Regardless, of the direction in which the knowledge transfer took place. We observe that almost always the transfer of knowledge base improves creatures' throughput and reduces the throughput fluctuations. Furthermore, we notice that this improvement is better when the knowledge base is transferred from creatures in environment with more dense traffic to creatures in environment with less dense traffic.

35.4 Conclusions and Future Work

In this paper we described a model of simple cognitive agent, a "*creature*', capable of: (1) examining its environment; (2) learning from it; (3) adapting to it. The creature is capable on deciding on an action based on the evaluation of the outcomes of previous crossings of a highway by other creatures and the examination of the current environmental conditions. The creatures try to imitate the successful crossings.

The creatures ("*imitate what works and don't do what doesn't work*"), [5], i.e. they try to avoid crossing in the situations when they were not successful. The results of the simulations show that the creatures learning success improves when knowledge base built by the creatures in one learning environment is transferred to the creatures in another learning environment. We reported selected simulation results, while more extensive results will their detailed statistical analysis will be reported elsewhere.

Acknowledgements A.T.L. and B.N.Di S. acknowledge hospitality of The Fields Institute for Research in Mathematical Sciences where part of this research was conducted. A.T.L. acknowledges partial financial support from the NSERC of Canada. B.N.Di S. acknowledges full financial support from Nuptek Systems Ltd., J.E. acknowledges full financial support from a SHARCNET Research Fellowship provided by A.T.L.

References

1. Bajracharya M, Maimone MW, Helmick D (2008) Autonomy for mars rovers: past, present, and future. IEEE Comput 41(12):44–50
2. Ferber J (1999) Multi-agent systems. An introduction to distributed artificial intelligence. Addison–Wesley, London
3. Wooldridge M (2009) An introduction to MultiAgent systems. Wiley, Chichester
4. Uhrmacher AM, Weyns D (2009) Multi-agent systems simulation and applications. CRC Press, Boca Raton
5. Alonso E, d'Inverno M, Kudenko D, Luck M, Noble J (2001) Learning in multi-agent systems. Knowl Eng Rev 16(3):277–284
6. Lawniczak AT, Di Stefano BN (2010) Computational intelligence based architecture for cognitive agents. Proc Comput Sci 1(1):2227–2235
7. Lawniczak AT, Ernst JB, Di Stefano BN (2013) Simulated naïve creature crossing a highway. Proc Comput Sci 18:2611–2614
8. Lawniczak AT, Ernst JB, Di Stefano BN (2014) Improved performance of naïve creature learning to cross a highway. In: Proc. of IEEE CCECE 2014, 4–7 May, pp 1269–1274
9. Nagel K, Schreckenberg M (1992) A cellular automaton model for freeway traffic. J Phys I 2:2221–2229
10. Lawniczak AT, Di Stefano BN (2010) Digital laboratory of agent-based highway traffic model. Acta Phys Pol B, Proc Suppl 3(2):479–493

Chapter 36
Threshold Models for Integer-Valued Time Series with Infinite or Finite Range

Tobias Möller and Christian H. Weiß

Abstract Threshold models are very popular in research and application. We survey threshold models for integer-valued time series with an infinite range and compare two of them in a real data example. In particular, we propose and briefly discuss two new models for count data time series with a finite range.

36.1 Introduction

Threshold models as proposed by [11] have become very popular in research and application. Due to their attractive interpretability and ability to handle the nonlinearity found in real world data, these models arouse great interest especially in economics and finance, see [4] and [1], but also in other contexts like epidemiology, see [13]. For a long time, only threshold models for time series with a continuous state space have been in the focus of researchers, but recent developments also consider models for time series with a discrete state space. This article presents a brief survey of threshold models for integer-valued time series with an infinite range, and it introduces two new models for the case of a finite range.

The article is organized as follows. Section 36.2 gives a short presentation of the most famous threshold autoregressive models for time series with a continuous state space. Section 36.3 deals with models for time series with an infinite range and demonstrates their usefulness with a real data example of annual counts of heavy earthquakes. Section 36.4 introduces new models for integer-valued time series with a finite range. A short discussion of integer-valued threshold models as well as perspectives for future research conclude the article in Sect. 36.5.

T. Möller (✉) · C.H. Weiß
Department of Mathematics and Statistics, Helmut Schmidt University, 22008 Hamburg, Germany
e-mail: moellert@hsu-hh.de

C.H. Weiß
e-mail: weissc@hsu-hh.de

A. Steland et al. (eds.), *Stochastic Models, Statistics and Their Applications*,
Springer Proceedings in Mathematics & Statistics 122,
DOI 10.1007/978-3-319-13881-7_36

36.2 Threshold Autoregressive Models with Continuous State Space

A threshold autoregressive (TAR) model of order p is defined as follows:

$$X_t = a_0^{(J_t)} + \sum_{i=1}^{p} a_i^{(J_t)} X_{t-i} + b^{(J_t)} \varepsilon_t, \tag{36.1}$$

where the ε_t are i.i.d. with mean 0 and variance σ_ε^2 and (J_t) is an (indicator) time series taking values in $\{1, 2, \ldots, J\}$, see [10]. This basic model can be extended in many different ways for example with a moving average component to get TARMA models or with a smooth transition between regimes to get the class of STAR models, see also [10] for these and other extensions. The most famous subclass of TAR models is the class of self-exciting threshold autoregressive (SETAR) models. In this class of TAR models, the indicators J_t depend on $(X_s)_{s<t}$. Often a SETAR model of order one with two regimes is used. Let R be the threshold value and d the so-called delay parameter in this model. Then the model is defined as:

$$X_t = \begin{cases} \alpha_1 + \beta_1 X_{t-1} + \varepsilon_t & \text{if } X_{t-d} \leq R \\ \alpha_2 + \beta_2 X_{t-1} + \phi \varepsilon_t & \text{if } X_{t-d} > R, \end{cases} \tag{36.2}$$

where $\alpha_1, \alpha_2, \beta_1, \beta_2$ and ϕ are real constants [10]. Possible modifications to integer-valued threshold models are presented in the next sections.

36.3 Threshold Models with a Discrete State Space and Infinite Range

In this and the following section, some threshold models for integer-valued time series are discussed. The present section concentrates on three models for count data time series with an *infinite* range, while new models for time series with a *finite* range are proposed in Sect. 36.4.

36.3.1 SETINAR(2, 1) Model

The first model to mention is the self-exciting threshold integer-valued autoregressive model with 2 regimes of order 1, abbreviated as SETINAR(2,1) model. First introduced by [9] and later for the consideration of statistical properties taken up by [6], the SETINAR(2,1) process can be defined as

$$X_t = \begin{cases} \alpha_1 \circ X_{t-1} + \varepsilon_t & \text{if } X_{t-1} \leq R \\ \alpha_2 \circ X_{t-1} + \varepsilon_t & \text{if } X_{t-1} > R, \end{cases} \tag{36.3}$$

where $\alpha \circ X$ is the binomial thinning operation for $\alpha \in (0, 1)$ and $X \in \mathbb{N}_0$ introduced by [8], $\alpha_{1/2} \in (0, 1)$ and $(\varepsilon_t)_{t\in\mathbb{Z}}$ is an i.i.d. sequence of Poisson(λ)-distributed random variables. In terms of the definition of the threshold, the version of [6] is used with a delay of $d = 1$ and a dependence on X_{t-1}, while [9] have used a sum of two previous values of the sequence (X_t). For statistical properties, we refer the reader to [6].

Remark 36.1 A simple modification of model (36.3) is used in Example 36.1 by allowing different means λ_1 and λ_2 for the innovations in each regime. This approach has been used in [9], and it is also related to the branching process model by [7], where immigration is possible at time t only if $X_{t-1} = 0$. Adapted to model (36.3), this corresponds to $R = 0$ and $\lambda_2 = 0$.

The SETINAR model can also be extended by considering orders $p \geq 2$, more than two regimes and the introduction of a delay $d \geq 2$ and other ways, which are taken into consideration for future research.

36.3.2 SETPAR Model

The self-exciting[1] threshold integer-valued Poisson autoregression (SETPAR) model with two regimes as proposed by [12] is defined as follows: A sequence of random observations $(X_t)_{t\in\mathbb{Z}}$ is said to follow the SETPAR model, if

$$X_t | \mathscr{F}_{t-1} \sim \text{Poisson}(\lambda_t), \tag{36.4}$$

where $\mathscr{F}_t = \sigma\{X_s, s \leq t\}$ is the information at the time t, and

$$\lambda_t = \begin{cases} d_1 + a_1\lambda_{t-1} + b_1 X_{t-1} & \text{if } X_{t-1} \leq R \\ d_2 + a_2\lambda_{t-1} + b_2 X_{t-1} & \text{if } X_{t-1} > R, \end{cases} \tag{36.5}$$

with $d_i > 0$, $a_i > 0$ and $b_i > 0$ for $i \in \{1, 2\}$ and $R \in \mathbb{N}$. For further details, like conditions for a unique stationary marginal distribution, we refer the reader to [12].

The authors of [12] state that the process is also known in the literature as Poisson threshold model, see [15] and [2]. The model without consideration of a threshold can also be found under the name INGARCH model, see [3].

Example 36.1 We consider the annual number of earthquakes with a magnitude of 7 or higher for the period 1900–2010, and compute estimates for the SETPAR and versions of the SETINAR model. This time series has already been considered by [12], where also an estimation for the SETPAR model has been made. As in [12], the data are arranged as follows: the years 1900 to 2006 are taken from [17], and the years 2007 to 2010 are added with data of the US Geological Survey website (namely: 18, 12, 17, 24 at Sept. 1st 2014). A plot of the data is given in Fig. 36.1. The

[1] The authors call their model self-excited, but to have a consistent notation the name is changed.

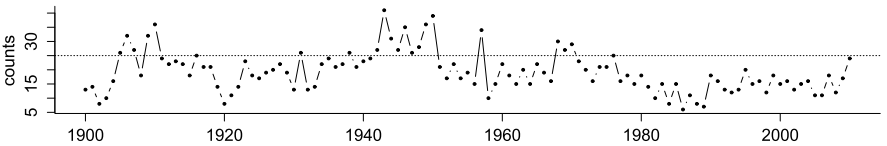

Fig. 36.1 Plot of the annual number of earthquakes with a magnitude of 7.0 or higher. The *dotted line* shows the possible threshold with value 25

Table 36.1 Estimates (standard errors) for the SETPAR model compared to the results of [12]

Model	R	d_1	a_1	b_1	d_2	a_2	b_2	$-\ell_{\max}$	AIC	BIC
SETPAR$^{\mathrm{W}}$	25	3.27 (1.36)	0.49 (0.12)	0.33 (0.10)	14.30 (7.45)	0.52 (0.20)	0.001 (0.26)	–	–	–
SETPAR	25	3.16 (1.39)	0.51 (0.14)	0.32 (0.11)	14.65 (8.13)	0.50 (0.22)	0.001 (0.30)	343.23	698.46	714.72
$b_2 = 0$:										
SETPAR$^{\mathrm{W}}$	25	3.27 (1.36)	0.49 (0.12)	0.33 (0.10)	14.33 (7.45)	0.52 (0.20)	–	–	–	–
SETPAR	25	3.14 (1.34)	0.51 (0.13)	0.32 (0.11)	14.65 (4.78)	0.50 (0.19)	–	343.22	696.44	709.99

$^{\mathrm{W}}$ Results of [12]

empirical mean of the earthquakes time series is 19.31 and the empirical variance is 50.45. Both values slightly differ from [12] which seems to be due to the value of the last year (23 vs. 24, see Fig. 2 in [12]): we achieve the same mean and variance, when we change the last value to 23. Since the classification of the magnitude on the Richter scale can sometimes change during the review process, we will continue with using the latest data. This already explains a part of the differences in the estimates compared to [12].

The estimation procedure is executed as follows: We set a range of possible threshold values in $\mathbb{N}_0$. For each of these values, the parameters are estimated via maximum likelihood estimation. Then we choose the threshold value which shows the maximum value in the log-likelihood function. To initialize the SETPAR model, we choose the first data point as the value for λ_1. Starting with the SETPAR model as proposed by [12], we get the values in Table 36.1. The threshold value is 25 for both considered modifications of the model. The estimates slightly differ from those in [12], which is partially explained by the different data basis as stated above. But the most conspicuous difference is the standard error of the parameter d_2 in the second model. A possible explanation could be that [12] still have considered a 6-parameter-model while this estimation considers a 5-parameter-model. The values of the log-likelihood and the AIC, BIC of [12] are not given here due to missing comparability caused by different calculation methods.

For the case of the SETINAR model some modifications are considered. The results can be found in Table 36.2. First an estimation for the SETINAR(2,1) model (36.3) is made. The results show a different threshold value compared to the SETPAR model, namely 20. The parameter α_1 has a high standard error compared to

Table 36.2 Estimates and standard errors in brackets for modifications of the SETINAR model

Model	R	α_1	α_2	λ_1	λ_2	$-\ell_{\max}$	AIC	BIC
SETINAR(2,1)	20	0.17 (0.08)	0.36 (0.05)	14.12 (1.27)	–	360.52	727.03	735.16
$\text{SETINAR}_{\lambda_2}(2,1)$	26	0.36 (0.06)	0.001 (0.17)	11.71 (1.14)	28.09 (5.67)	354.63	717.26	728.10
$\text{SETINAR}_{(\alpha_2=0)}$	26	0.36 (0.06)	–	11.71 (1.14)	28.12 (1.33)	354.63	715.25	723.38

its own value, which indicates possible insignificance. Therefore, modifications of the model are introduced. First, the sequence $(\varepsilon_t)_{t\in\mathbb{Z}}$ is split into two Poisson-distributed sequences with means λ_1 and λ_2 depending on the regime, see Remark 36.1. The estimation for this model shows that the threshold value changes to 26 and that α_2 becomes insignificant. Consequently, α_2 is deleted from this model and a new estimation is made. This version of the SETINAR(2,1) model shows a decline in the standard error of the parameter λ_2 compared to the second estimation.

For both models, the two regimes show significantly different parameter values, which supports the choice of a threshold model. Note that there is no autoregressive part in the upper regime, which indicates that there is no significant 'survival' of high counts of earthquakes. When we compare the results regarding the AIC and BIC, the SETPAR model fits the data better than the SETINAR(2,1) model.

36.3.3 INMASC(1) Model

Another model is the integer-valued moving average model with structural changes (INMASC) by [16]. Let $\alpha_i \in (0,1)$ for $i = 1,\dots,m$ and $\tau_i \in \mathbb{N}$ for $i = 1,\dots,m-1$. A process (X_t) is called an INMASC(1) process if X_t satisfies the equation

$$X_t = \begin{cases} \alpha_1 \circ \varepsilon_{t-1} + \varepsilon_t & \text{if } 0 \le \varepsilon_{t-1} \le \tau_1 \\ \alpha_2 \circ \varepsilon_{t-1} + \varepsilon_t & \text{if } \tau_1 < \varepsilon_{t-1} \le \tau_2 \\ \quad\vdots & \\ \alpha_m \circ \varepsilon_{t-1} + \varepsilon_t & \text{if } \tau_{m-1} < \varepsilon_{t-1} < \infty, \end{cases} \tag{36.6}$$

where (ε_t) is a sequence of i.i.d. Poisson(λ)-distributed random variables. For statistical properties of the model, we refer the interested reader to the article [16].

36.4 Integer-Valued Threshold Model with Finite Range

SET autoregressive models for counts with the finite range $\{0,\dots,N\}$ have not been considered in the literature so far. Motivated by the above models, two approaches for a threshold version of known binomial models are presented.

36.4.1 SET Binomial AR(1) Model

The newly proposed SET binomial AR(1) model is an extension of the binomial AR(1) model by [5]. It is defined as follows: Let $N \in \mathbb{N}$, $\pi_i \in (0,1)$ and $r_i \in (\max\{-\frac{\pi_i}{1-\pi_i}, -\frac{1-\pi_i}{\pi_i}\}; 1)$, define $\beta_i := \pi_i \cdot (1-r_i)$ and $\alpha_i := \beta_i + r_i$ for $i \in \{1,2\}$. A process $(X_t)_{t\in\mathbb{Z}}$ is called a SET binomial AR(1) process if it follows the recursion

$$X_t = \begin{cases} \alpha_1 \circ X_{t-1} + \beta_1 \circ (N - X_{t-1}) & \text{if } X_{t-1} \le R \\ \alpha_2 \circ X_{t-1} + \beta_2 \circ (N - X_{t-1}) & \text{if } X_{t-1} > R. \end{cases} \tag{36.7}$$

The SET binomial AR(1) model is a special case of a density-dependent binomial AR(1) model as proposed by [14]. Hence, we can use their results to derive some properties of the SET binomial AR(1) model. The process is a homogeneous Markov chain. The transition probabilities $p_{k|l} := P(X_t = k | X_{t-1} = l)$ are

$$p_{k|l} = \sum_{m=\max\{0,k+l-N\}}^{\min\{k,l\}} \binom{l}{m}\binom{N-l}{k-m} \phi_t^m (1-\phi_t)^{l-m} \eta_t^{k-m} (1-\eta_t)^{N-l+m-k} > 0,$$

where $\phi_t := I_{t-1}\alpha_1 + (1-I_{t-1})\alpha_2$ and $\eta_t := I_{t-1}\beta_1 + (1-I_{t-1})\beta_2$ with $I_{t-1} := 1_{\{X_{t-1}\le R\}}$ as the indicator variable. Conditional moments of the process are

$$\begin{aligned} E[X_t|X_{t-1}] &= I_{t-1}\big(r_1 X_{t-1} + (1-r_1)\pi_1 N\big) + (1-I_{t-1})\big(r_2 X_{t-1} + (1-r_2)\pi_2 N\big), \\ V[X_t|X_{t-1}] &= I_{t-1}\big(r_1(1-r_1)(1-2\pi_1)X_{t-1} + N(1-r_1)\pi_1\big(1-(1-r_1)\pi_1\big)\big) \\ &\quad + (1-I_{t-1})\big(r_2(1-r_2)(1-2\pi_2)X_{t-1} \\ &\quad + N(1-r_2)\pi_2\big(1-(1-r_2)\pi_2\big)\big). \end{aligned}$$

Unconditional moments, modifications and parameter estimations for the SET binomial AR(1) model are part of current research.

36.4.2 SET Binomial INARCH(1) Model

For the boundary case $r \to 0$ in the density-dependent binomial AR(1) model, [14] propose the binomial INARCH(1) model. We consider integrating a threshold into the model and call a process $(X_t)_{t\in\mathbb{Z}}$ a SET binomial INARCH(1) process if

$$X_t \overset{d}{=} \begin{cases} \text{Bin}(N, a_1 + b_1 \frac{X_{t-1}}{N}) & \text{if } X_{t-1} \le R \\ \text{Bin}(N, a_2 + b_2 \frac{X_{t-1}}{N}) & \text{if } X_{t-1} > R, \end{cases} \tag{36.8}$$

where a_i, $a_i + b_i \in (0;1)$ for $i \in \{1,2\}$ and $N \in \mathbb{N}$.

Obviously, the process is a homogeneous Markov chain. From the conditional binomial distribution in (36.8), the transition probabilities $p_{k|l} := P(X_t = k | X_{t-1} = l)$ follow as

$$p_{k|l} = \binom{N}{k} \pi_{t,l}^{k} (1 - \pi_{t,l})^{N-k} > 0,$$

where $\pi_{t,l} := I_{t-1}(a_1 + b_1 \frac{l}{N}) + (1 - I_{t-1})(a_2 + b_2 \frac{l}{N})$ with $I_{t-1} := 1_{\{X_{t-1} \le R\}}$ as the indicator variable. Conditional moments of the process are

$$\begin{aligned} E[X_t|X_{t-1}] &= I_{t-1}(b_1 X_{t-1} + N a_1) + (1 - I_{t-1})(b_2 X_{t-1} + N a_2), \\ V[X_t|X_{t-1}] &= I_{t-1}\left(N a_1(1 - a_1) - \frac{b_1^2}{N} X_{t-1}^2 + (1 - 2a_1) b_1 X_{t-1} \right) \\ &\quad + (1 - I_{t-1})\left(N a_2(1 - a_2) - \frac{b_2^2}{N} X_{t-1}^2 + (1 - 2a_2) b_2 X_{t-1} \right). \end{aligned}$$

Unconditional moments, modifications and parameter estimations for the SET binomial INARCH(1) model will be considered in a future research.

36.5 Conclusive Remarks

We gave an overview over recent developments concerning integer-valued threshold models. In particular, we introduced the new models SET binomial AR(1) and SET binomial INARCH(1), which will be examined in more details in a future research.

Integer-valued threshold models are able to describe time series of counts with nonlinear structures. For example, they can explain bimodality and level jumps in real data time series. Other types of state-dependent models might be able to give a comparable fit of the nonlinearity, but perhaps at the cost of using more parameters. Tests will be needed whether to use, e.g., a linear or a threshold state-dependent model.

References

1. Chen CWS, So MKP, Liu F-C (2011) A review of threshold time series models in finance. Stat Interface 4:167–181
2. Douc R, Doukhan P, Moulines E (2012) Ergodicity of observation-driven time series models and consistency of the maximum likelihood estimator. Stoch Process Appl 123(7):2473–2920
3. Ferland R, Latour A, Oraichi D (2006) Integer-valued GARCH process. J Time Ser Anal 27(6):923–942
4. Hansen BE (2011) Threshold autoregression in economics. Stat Interface 4:123–127
5. McKenzie E (1985) Some simple models for discrete variate time series. J Am Water Resour Assoc 21(4):645–650
6. Monteiro M, Scotto MG, Pereira I (2012) Integer-valued self-exciting threshold autoregressive processes. Commun Stat, Theory Methods 41(15):2717–2737
7. Pakes AG (1971) A branching process with a state dependent immigration component. Adv Appl Probab 3(2):301–314
8. Steutel FW, van Harn K (1979) Discrete analogues of self-decomposability and stability. Ann Probab 7(5):893–899

9. Thyregod P, Carstensen J, Madsen H, Arnbjerg-Nielsen K (1999) Integer valued autoregressive models for tipping bucket rainfall measurements. Environmetrics 10:395–411
10. Tong H (2011) Threshold models in time series analysis – 30 years on. Stat Interface 4:107–118
11. Tong H, Lim KS (1980) Threshold autoregression, limit cycles and cyclical data. J R Stat Soc, Ser B, Stat Methodol 42(3):245–292
12. Wang C, Liu H, Yao JF, Davis RA, Li WK (2014) Self-excited threshold Poisson autoregression. J Am Stat Assoc 109(506):777–787
13. Watier L, Richardson S (1995) Modelling of an epidemiological time series by a threshold autoregressive model. Statistician 44(3):353–364
14. Weiß CH, Pollett PK (2014) Binomial autoregressive processes with density-dependent thinning. J Time Ser Anal 35(2):115–132
15. Woodard DB, Matteson DS, Henderson SG (2011) Stationarity of generalized autoregressive moving average models. Electron J Stat 5:800–828
16. Yu K, Zou H, Shi D (2014) Integer-valued moving average models with structural changes. Mathematical problems in engineering 2014
17. Zucchini W, MacDonald IL (2009) Hidden Markov models for time series: an introduction using R. CRC Press, Boca Raton

Chapter 37
A Study on Robustness in the Optimal Design of Experiments for Copula Models

Elisa Perrone

Abstract Copulas are a very flexible tool to highlight structural properties of the design for a wide range of dependence structures. In this work we introduce a procedure for checking the robustness of the D-optimal design with respect to slight changes of the marginal distributions in the case of copula models. To this end, we first provide a clear insight for the concept of "robustness" in our domain. Then, we define a stepwise method for the investigation of the design robustness. Finally, by reporting an example focused on comparison between the use of logistic margins and Gaussian margins, we put the usefulness of the analysis up.

37.1 Introduction

In many areas of applied statistics, copula functions are largely employed as a flexible tool to describe the behavior of the dependence between random variables. Roughly speaking, a d-dimensional copula is the restriction of a joint distribution with Uniform margins to the unit d-hypercube.

The use of such functions is well known in insurance [19], econometrics [18], medicine [11], spatial extreme events [20], time series analysis [12] and [5], finance [1] as well as in environmental applications [14]. However, the study of the design of the related experiment is still a neglected aspect.

A first step in this direction was made in the work of Denman et al. [4], where a brute-force simulated annealing optimization was employed for the solution of a specific problem. A more complete and formal framework for copula models was described in our previous work [13], where a Kiefer–Wolfowitz type equivalence theorem was also provided. Despite the tools reported in [13] allow one to find the D-optimal design for any copula models, the computational complexity of the Fisher Information Matrix could represent a practical limitation. More precisely, the computational complexity could rapidly become an issue because of the presence in the copula model of particular marginal distributions for the random variables involved

E. Perrone (✉)
Department of Applied Statistics, Johannes Kepler University Linz, 4040 Linz, Austria
e-mail: elisa.perrone@jku.at

A. Steland et al. (eds.), *Stochastic Models, Statistics and Their Applications*,
Springer Proceedings in Mathematics & Statistics 122,
DOI 10.1007/978-3-319-13881-7_37

in the problem. Conversely, fixing a family of copula functions means assuming a class of model dependence structures. As a matter of fact, the interesting part of designing experiments by employing copula models is the investigation of the design behavior for different dependence structures and for different values of the copula parameter in the same dependence class. Therefore, a natural question is whether the assumptions on the margins can be relaxed to gain in computational power with a consequently better understanding of the role of the dependence structure itself in the design.

This question motivates this paper: we suggest a procedure for comparing two models with the same assumptions on the copula but slightly different margins. The aim of the work is to provide a way to check whether a candidate auxiliary model with the same dependence structure could be used to avoid some computational problems and to enlarge some evidences in the design robustness comparing to different copula functions.

This paper is organized as follows. In Sect. 37.2 we provide a theoretical framework based on Copula Theory and Optimal Design Theory where to embed the issue. In Sect. 37.3 we introduce a motivating example for this work. In Sect. 37.4 we present the procedure and point out to the usefulness of the study through a classical example. Finally, in Sect. 37.5, we draw some conclusions.

37.2 The General Framework

First, we need to define the abstract framework. We shall consider a vector $\mathbf{x}^T = (x_1, \ldots, x_r) \in \mathcal{X}$ of control variables, where $\mathcal{X} \subset \Re^r$ is a compact set. We focus directly on the bivariate case, while a general framework in arbitrary dimension can be found in [13]. The results of the observations and of the expectations in a regression experiment are the vectors:

$$\begin{aligned} \mathbf{y}(\mathbf{x}) &= \big(y_1(\mathbf{x}), y_2(\mathbf{x})\big), \\ \mathbf{E}\big[\mathbf{Y}(x)\big] &= \mathbf{E}\big[(Y_1, Y_2)\big] = \boldsymbol{\eta}(\mathbf{x}, \boldsymbol{\beta}) = \big(\eta_1(\mathbf{x}, \boldsymbol{\beta}), \eta_2(\mathbf{x}, \boldsymbol{\beta})\big), \end{aligned}$$

where $\boldsymbol{\beta} = (\beta_1, \ldots, \beta_k)$ is a certain unknown (trend) parameter vector to be estimated and η_i $(i = 1, 2)$ are known functions. Let us call $F_{Y_i}(y_i(\mathbf{x}, \boldsymbol{\beta}))$ the margins of each Y_i for all $i = 1, 2$ and $c_{\mathbf{Y}}(\mathbf{y}(\mathbf{x}, \boldsymbol{\beta}), \boldsymbol{\alpha})$ the joint probability density function of the random vector $\mathbf{Y}$, where $\boldsymbol{\alpha}$ is an unknown (copula) parameter.

According to Sklar's theorem (see [17] and [10]), let us assume that the dependence between Y_1 and Y_2 is modeled by a copula function

$$C_\alpha\big(F_{Y_1}\big(y_1(\mathbf{x}, \boldsymbol{\beta})\big), F_{Y_2}\big(y_2(\mathbf{x}, \boldsymbol{\beta})\big)\big).$$

The Fisher Information Matrix for a single observation is a $(k + 1) \times (k + 1)$ matrix whose elements are

$$\mathbf{E}\left(-\frac{\partial^2}{\partial\gamma_i \partial\gamma_j} \log\left[\frac{\partial^2}{\partial y_1 \partial y_2} C_\alpha\big(F_{Y_1}\big(y_1(\mathbf{x}, \boldsymbol{\beta})\big), F_{Y_2}\big(y_2(\mathbf{x}, \boldsymbol{\beta})\big)\big)\right]\right) \tag{37.1}$$

where $\boldsymbol{\gamma} = \{\boldsymbol{\gamma}_1, \ldots, \boldsymbol{\gamma}_{k+1}\} = \{\boldsymbol{\beta}_1, \ldots, \boldsymbol{\beta}_k, \boldsymbol{\alpha}\}$. The aim of design theory is to quantify the amount of information on both sets of parameters α and β, respectively, from the regression experiment embodied in the Fisher Information Matrix.

For r independent observations at $x_1, \ldots, x_r$, the corresponding Information matrix is

$$\mathbf{M}(\xi, \gamma) = \sum_{i=1}^{r} w_i m(x_i, \gamma), \qquad \sum_{i=1}^{r} w_i = 1 \quad \text{and} \quad \xi = \begin{Bmatrix} x_1 & \ldots & x_n \\ w_1 & \ldots & w_n \end{Bmatrix}.$$

The approximate design theory is concerned with finding $\xi^*(\gamma)$ such that it maximizes some scalar function $\phi(M(\xi, \gamma))$, i.e., the so-called design criterion. Hereinafter, we consider only *D-optimality*, i.e., the criterion $\phi(M) = \log\det M$, if M is nonsingular.

The formulation of a Kiefer–Wolfowitz type equivalence relation (see [8]) is the cornerstone of a theoretical investigation into optimal design. The following theorem of such type is a generalized version of a theorem given without proof in [7] and follows from a multivariate version of the basic theorem given in [16]. A complete proof can be found in [13].

Theorem 37.1 *For a local parameter vector* $(\bar{\gamma})$, *the following properties are equivalent*:

- ξ^* *is D-optimal*;
- $\mathrm{tr}[M(\xi^*, \bar{\gamma})^{-1} m(x, \bar{\gamma})] \leq (k+1), \forall x \in \mathcal{X}$;
- ξ^* *minimize* $\max_{x \in \mathcal{X}} \mathrm{tr}[M(\xi^*, \bar{\gamma})^{-1} m(x, \bar{\gamma})]$, *over all* $\xi \in \Xi$.

Theorem 37.1 allows one to implement standard design algorithms such as of the Fedorov–Wynn type (see [6, 21]). It also provides simple checks for D-optimality through the maxima of $d(x, \xi^*) = \mathrm{tr}[M(\xi^*, \bar{\gamma})^{-1} m(x, \bar{\gamma})]$, which is usually called *sensitivity function*.

The next definition is important for the comparison of two different designs.

Definition 37.1 Let $(k+1)$ be the number of the model parameters. The ratio

$$D(\xi, \xi') = \left(\frac{|M(\xi, \gamma)|}{|M(\xi', \gamma)|} \right)^{1/(k+1)} \tag{37.2}$$

is called *D-efficiency* of the design ξ with respect to the design ξ'.

Evidently, the resulting optimal designs depend upon the chosen copula, not only upon the trend model structure. Additionally, such designs might also be influenced by the unknown parameter values for γ through the induced nonlinearities. Thence, we are resorting to localized designs around the values $\bar{\gamma}$.

37.3 A Motivating Example

In this section, we clarify the paper motivations by displaying an example taken from [6] and reported in [13]. For each design point x, we may observe an independent pair of random variables Y_1 and Y_2, such that

$$E\big[Y_1(x)\big] = \beta_0 + \beta_1 x + \beta_2 x^2$$
$$E\big[Y_2(x)\big] = \beta_3 x + \beta_4 x^3 + \beta_5 x^4,$$

with $0 \leq x \leq 1$. This case is covered by Theorem 37.1, by employing the product copula with Gaussian margins.

In [13], several dependence structures with the use of other copulas were assumed and the corresponding optimal designs were found. Remarkably, the designs found relate to the following joint distribution function:

$$F_{\mathbf{Y}}(y_1, y_2) = C_\alpha\big(\Phi\big(y_1 - \eta_1(x, \beta)\big), \Phi\big(y_2 - \eta_2(x, \beta)\big)\big). \tag{37.3}$$

Mathematica (version 9.0.1.0) was used to compute the integrals. The computations were carried out by using some local adaptive strategies that seemed to perform better for our problem.

Even so, numerically unstable results were displayed by several warnings regarding the nonconvergence of the prescribed numerical method. Hence, some elements of the Fisher Information Matrix could not be computed for several instances corresponding to the interesting cases with large association measures. Such problems might be due to the error functions in the Gaussian margins and motivated this paper. The idea of this work is the following: avoiding such problems by finding a misspecified model, which might reduce the problematic instances; enlarging the range of the association measure for the dependence structures.

The contribution of this work is a stepwise procedure composed of two parts: first, check the goodness (in the sense of D-efficiency) of the D-optimal designs found for a misspecified model with respect to the initial one; second, use the misspecified model to conduct a robustness study on the designs for a wider range of the association measure.

The robustness study presented in this work differs from other approaches that can be found in the literature. In particular, in [2] and [9], robust designs with respect to misspecifications of the model assumptions were provided. To the contrary, we rather fix a model and find the corresponding D-optimal design with the standard criterion of D-optimality. Then, we analyze the goodness of the design in the sense of D-efficiency by considering different copulas.

Essentially, the robustness study in this paper concerns the impact of the dependence structure on the designs, whereas in [2] and [9] new robustness optimality criteria were introduced. To evidence the impact of the margins on the design, the analysis is carried out by slightly modifying the initial model. The new misspecified model has the same fixed dependence structure of the initial model, with different distributions of the random variables.

37.4 Robustness Issues

In this section, we explain the details of the stepwise method. To underline the advantages of the procedure, an example is given.

37.4.1 The Procedure

Let Y_1 and Y_2 be two random variables whose dependence is described by the copula C_α. We assume the "Model 1" being the true design model with margins $F_1(Y_1(x))$, $F_2(Y_2(x))$. We define for the vector (Y_1, Y_2) a second model, named "Model 2", whose margins are $G_1(Y_1(x))$ and $G_2(Y_2(x))$. With the goal of evaluating the goodness of D-optimal designs of the Model 2 with respect to the Model 1, we can introduce the following stepwise procedure:

1. Find the pure impact of the marginals on the design by considering the product copula for the two models.
2. Find the optimal design by using the Fedorov–Wynn algorithm for both models. Calculate the D-efficiency by assuming that the Model 1 is the correct one.
3. Fix a copula $\tilde{C}_\alpha$. Select a set of parameters where the optimal designs for the Model 1 can be computed.
4. Find the optimal design for both models for the selected parameter set. Calculate the D-efficiencies of the designs found by assuming the Model 1 as true model.
5. If the losses in the D-efficiencies in percent are lower than a given threshold (0.5, in our case) fix another set of the parameters where the optimals could not be reached for the Model 1. Then, investigate the robustness of the design (in the sense of the copula) for the new parameter space by using the Model 2.

Practically, in the first four steps we check how far the two models are. If the two models are almost alike (in the sense of designs produced), we carry out further investigations. Particularly, the behavior of the design for different dependence structures as well as for different copula parameter is analyzed by using the misspecified model.

37.4.2 The Example

To discuss some practical issues of the method described in the previous paragraph, we focus on the example introduced in Sect. 37.3.

The margins of the true model (Model 1) are

$$F_1\big(Y_1(x)\big) = \Phi\big(y_1 - \eta_1(x,\beta)\big) \quad \text{and} \quad F_2\big(Y_2(x)\big) = \Phi\big(y_2 - \eta_2(x,\beta)\big).$$

In order to define a misspecified model, a computationally more treatable approximation of the margins is needed. With the presence of the Gaussian margins, using the logistic margins as approximation is a very natural choice.

Table 37.1 Losses in D-efficiency in percent

τ	FGM		Clayton		Frank	
	α	D-eff.	α	D-eff.	α	D-eff.
−0.10	−0.45	0.16	n.d.	–	−0.9	0.63*
+0.10	+0.45	0.28	0.22	0.28	0.9	0.69*
+0.35	n.d.	–	1.08	0.01	3.51	0.56*
+0.75	n.d.	–	6	0.01	14.13	0.01

The issue of finding the appropriate scale parameter in such a way that the curve of the logistic distribution better approximates the Gaussian bell, has been treated largely in literature (see e.g. [3] and [15]). However, in our case, the little differences between the various scale parameters proposed have no impact on the model. Thus, according to [3], we chose the following distributions as marginals of Y_1 and Y_2 for the Model 2:

$$G_1\big(Y_1(x)\big) = \frac{1}{1+e^{-1.8138(y_1-\eta_1(x,\beta))}}$$
$$G_2\big(Y_2(x)\big) = \frac{1}{1+e^{-1.8138(y_2-\eta_2(x,\beta))}}$$

To implement the procedure proposed in the previous part of the section, we first consider the product copula. We find ξ_1 and ξ_2 respectively the optimal designs for the Model 1 and the Model 2. The loss in the D-efficiency of ξ_2 with respect to ξ_1 is in percent 0.001: for both models, the design found in the independence case is almost the same. Evidently, the changes to the model of the margins have no impact on the design obtained.

To check whether for other dependence structures the Model 2 provides "good" designs (in terms of D-efficiency) for the Model 1, we go to the next step. The copula functions chosen as well as the initial values of α are the ones reported in [13]. The results in comparison deserve attention.

Let ξ_1s and ξ_2s be, respectively, the optimal designs for the models Model 1 and Model 2. The values of the determinant for the Fisher Information Matrix for the designs ξ_2s are, for some instances, slightly higher than the values of the determinant for ξ_1s. Surprisingly, the Model 2 provides designs which are slightly "more optimal" than the ones obtained directly from the Model 1.

The losses in D-efficiencies $D(\xi_1, \xi_2)$ in percent are reported in Table 37.1. The results marked by asterisks are the losses for $1/D$.

In the approximate theory, with discrete designs, we are not able in general to find the continuous optimal design, but only an approximation of it. Nevertheless, by evaluating the maximum of the sensitivity function, the distance between the approximate optimal design and the continuous optimal design can always be measured. For instance, by looking at the losses reported in Table 37.1, the models yield the same optimal designs. As a matter of fact, the maxima of the corresponding sensitivity function lie under a fixed threshold value (7.001), that is, the stopping rule for the Fedorov–Wynn algorithm. This means that all the designs belong to the

Table 37.2 Losses in D-efficiency in percent

τ	Clayton		Frank	
	α	D-eff.	α	D-eff.
+0.80	8	0.18	18.19	0.50
+0.85	11.33	0.23	24.9	0.15
+0.89	16.18	0.24	34.64	0.09

approximate optimal design class. However, it has to be emphasized that a different but well chosen model might become a good support in finding optimal designs for another supposed true model.

The Model 2 is a good candidate in describing the phenomena drawn by the Model 1 as well as the optima found for the Model 2 are also reliable for the Model 1. We enlarge the interval of the association measure, in the case of Frank and Clayton. The new parameter space includes associations τ until the level of 0.89. A comparison, in terms of losses of D-Efficiencies, between the design reported in [6] and the optima computed by using the Model 2, is reported in Table 37.2. As clearly depicted in the table, the design found in the case of independence is a good design also when a dependence structure with a high association measure is assumed.

37.5 Conclusion

In this work we presented a new procedure based on the usage of misspecified models to address all the cases in which an initial (true) model has inacceptable computational cost. To avoid some numerical problems due to particular complex dependence structures or marginal distributions, a misspecified model might be preferred over a true one. By using the steps illustrated in this work, the goodness of the misspecified model is checked. We gain an increase in the robustness investigations related to the design. Apparently, in the particular example reported there is no impact on the design by changing the dependence structure. In spite of that, the procedure proposed in this work can be applied to different design models. By expanding the classical concept of robustness, the strength of copulas models for designing is highlighted. Different behaviors of the phenomenon are analyzed in a very flexible and complete way. Moreover, the new approach not only helps in reducing the computational complexity for some problems, but might also provide increased flexibility for certain classes of applications by enabling a more precise control over the model assumptions. In the future, we will try to apply our approach to other case studies.

Acknowledgements This work was funded by the joint ANR/FWF project DESIRE. I would like to thank Werner Müller for the supervision on my PhD research and Fabrizio Durante, Gianfausto Salvadori and Helga Wagner for the fruitful discussions.

References

1. Cherubini U, Luciano E, Vecchiato W (2004) Copula methods in finance. Wiley, New York
2. Biedermann S, Dette H, Pepelyshev A (2006) Some robust design strategies for percentile estimation in binary response models. Can J Stat 34(4):603–622
3. Bowling SR, Khasawneh MT (2009) A logistic approximation to the cumulative normal distribution. JIEM 2(1):114–127
4. Denman NG, McGree JM, Eccleston JA, Duffull SB (2011) Design of experiments for bivariate binary responses modelled by Copula functions. Comput Stat Data Anal 55(4):1509–1520
5. Durante F, Pappadà R (2015) Cluster analysis of time series via Kendall distribution. In: Grzegorzewski P, Gagolewski M, Hryniewicz O, Gil MA (eds) Strengthening links between data analysis and soft computing. AISC, vol 315. Springer, Berlin, pp 209–216
6. Fedorov VV (1971) The design of experiments in the multiresponse case. Theory Probab Appl 16(2):323–332
7. Heise MA, Myers RH (1996) Optimal designs for bivariate logistic regression. Biometrics 52(2):613–624
8. Kiefer J, Wolfowitz J (1960) The equivalence of two extremum problems. Can J Math 12:363–366
9. Kitsos CP, Müller C (1995) Robust linear calibration. Statistics 27:93–106
10. Nelsen RB (2006) An introduction to Copulas. SSST, 2nd edn.
11. Nikoloulopoulos AK, Karlis D (2008) Multivariate logit copula model with an application to dental data. Stat Med 27(30):6393–6406
12. Patton AJ (2012) A review of copula models for economic time series. J Multivar Anal 110:4–18
13. Perrone E, Müller WG (2014) Optimal designs for Copula models. Preprint. arXiv:1406.2933
14. Salvadori G, De Michele C, Kottegoda NT, Rosso R (2008) Extremes in nature. An approach using Copulas. Water sci technol libr, vol. 56. Springer, Berlin
15. Savalei V (2006) Logistic approximation to the normal: the KL rationale. Psychometrika 71(4):763–767
16. Silvey SD (1980) Optimal design (Science paperbacks). Chapman & Hall, London
17. Sklar A (1959) Fonctions de repartition a n dimensions et leurs marges. Publ Inst Stat Univ Paris 8:229–231
18. Trivedi PK, Zimmer DM (2006) Copula modeling: an introduction for practitioners. Found Trends Econ 1(1):1–111
19. Valdez EA (1998) Understanding relationships using copulas. N Am Actuar J 2(1):1–25
20. Wadsworth JL, Tawn JA (2012) Dependence modelling for spatial extremes. Biometrika 99(2):253–272
21. Wynn HP (1970) The sequential generation of d-optimum experimental designs. Ann Math Stat 41(5):1655–1664

Chapter 38
Use of a Generalized Multivariate Gamma Distribution Based on Copula Functions in the Average Bioequivalence

Roberto Molina de Souza, Jorge Alberto Achcar, Edson Zangiacomi Martinez, and Josmar Mazucheli

Abstract Bioequivalence studies have been generally used to compare a test formulation with a reference, in order to validate the interchangeability between them. Some pharmacokinetic (PK) parameters are compared in this type of study, typically using a model which assumes independence among PK parameters, the same variance for the different formulations, logarithmic transformation for the data and normal distribution for the residuals. We propose an alternative model based on a generalized gamma distribution, which permits the presence of positive asymmetry for the data and possible differences in the variances for the different formulations which could have more flexibility in this case. For the multivariate structure, we use a Gaussian copula function to capture the possible dependence between the PK parameters. We use Bayesian inference methods to obtain the results of interest. We also introduce a real data example from where we observe a good fit of the proposed model for the dataset. From this study, we conclude that the proposed model could be a good alternative in some applications where the distribution of the bioequivalence data presents a positive asymmetric distribution.

R.M. de Souza (✉) · J.A. Achcar · E. Zangiacomi Martinez
Faculty of Medicine of Ribeirão Preto, Department of Social Medicine, University of São Paulo, 3900, Bandeirantes Avenue, Ribeirão Preto, SP 14040-900, Brazil
e-mail: rmolinasouza@utfpr.edu.br

J.A. Achcar
e-mail: achcar@fmrp.usp.br

E. Zangiacomi Martinez
e-mail: edson@fmrp.usp.br

R.M. de Souza
Department of Mathematics, Federal Technological University of Paraná, 1640, Alberto Carazzai Avenue, Cornélio Procópio, PR 86300-000, Brazil

J. Mazucheli
Department of Statistics, State University of Maringá, 5790, Colombo Avenue, Maringá, PR 87020-900, Brazil
e-mail: jmazucheli@uem.br

A. Steland et al. (eds.), *Stochastic Models, Statistics and Their Applications*,
Springer Proceedings in Mathematics & Statistics 122,
DOI 10.1007/978-3-319-13881-7_38

38.1 Introduction

To evaluate the exchangeability of two or more drug formulations it is recommended the use of bioequivalence trials. Following a FDA (Food and Drug Administration) published guideline [2], bioequivalence is defined as "absence of a significant difference in the rate and extent to which the active ingredient in pharmaceutical equivalents or pharmaceutical alternatives become available at the site of drug action when administered at the same molar dose under similar conditions in an appropriately designed study". Bioavailability is defined by the FDA as the speed and extend of the absorption of an active principle in the form of a dosage, measured from the concentration/systemic circulation time curve. Usually, a generic drug can be marketed when it presents relative bioequivalence to the reference drug.

In a bioequivalence test, generally three pharmacokinetic parameters are obtained for each individual under each formulation in study: Maximum concentration ($C_{\max}$), Time when the $C_{\max}$ occurs ($T_{\max}$) and Area under the curve from blood concentration from time 0 to the last observed time point (AUC_{0-t}).

For most of the formulations, the pharmacokinetic parameters AUC_{0-t} and $C_{\max}$ are used for the bioequivalence decision where 90 % confidence intervals are obtained for each pharmacokinetic parameter considering the difference between a reference formulation and a test formulation. These intervals should be totally included in prespecified intervals (bioequivalence limits). This procedure is known as average bioequivalence [11]. If μ_R is the mean of a pharmacokinetic parameter to formulation reference and μ_T to formulation in test, the usual FDA criterion is $0.80 < \{\mu_T\}/\{\mu_R\} < 1.25$ which may be stated in terms of fractions of μ_R as $-0.25\mu_R < \mu_T - \mu_R < 0.20\mu_R$.

Although the pharmacokinetic parameters are obtained for the same individuals, usually the statistical analysis assume independence among them. Alternatively, multivariate statistical models also has been considered to analyse the pharmacokinetic parameters but they are limited to the assumption of normality for the data or residuals, as well as constant variance for the groups. Another existing limitation of this standard modeling approach is the need of a transformation of the data (generally logarithmic), since these parameters are positive.

As an alternative, we consider a new modeling approach. We assume an asymmetrical distribution defined for positive real numbers given by the generalized gamma distribution [9] from where some existing known probability distributions are given as special cases of this supermodel which could contemplate the specificities of the pharmacokinetic parameters $C_{\max}$ and AUC_{0-t} with positive asymmetry in their original scale. To capture a possible existing dependence between the pharmacokinetic parameters, we propose the use of copula function (see for example, [6]).

In this way, maximum likelihood estimators for the parameters of the models could present numerical difficulties and standard inferences based on asymptotical results could be not accurate, especially for small sample sizes. As a good alternative for this situation, we could use Bayesian methods, especially using MCMC (Markov Chain Monte Carlo) methods and available existing free softwares like the BUGS or JAGS to simulate samples of the joint posterior distribution of interest.

38.2 Methods

Let Y be a random variable with a generalized gamma distribution denoted by $GG(\beta, \eta, r)$ with probability density function

$$f(Y = y) = \frac{\beta}{\Gamma(r)} \eta^{\beta r} y^{\beta r - 1} \exp\left[-(\eta y)^{\beta}\right] \tag{38.1}$$

where $y \geq 0$, β, η and r are positive parameters and $\Gamma(r) = \int_0^{\infty} \exp(-t) t^{r-1} dt$ (gamma function). The expected mean of Y is given by $E(Y) = \Gamma(\frac{1}{\beta} + r)/\eta\Gamma(r)$.

The crossover design is more appropriate in a bioequivalence study since we have the same individual receiving both formulations in different periods. In this way, the individuals are randomized by the sequences and this effect should be introduced in the model. The period effect also is introduced.

Considering $k = 1, 2$ pharmacokinetic parameters (generally $C_{\max}$ and AUC_{0-t}); J formulations ($j = 1, \ldots, J$) (generally $J = 2$, reference (R) and test (T)) and n individuals ($i = 1, \ldots, n$), let us assume

$$Y_{kji} \sim GG(\beta_{kj}, \eta_{kji}, r_{kj}) \tag{38.2}$$

where y_{kji} is the value of the response variable provided by the ith individual, related to the kth pharmacokinetic parameter and jth formulation following a generalized gamma distribution with density (38.1). In a usual situation ($j = 1, 2$), we have a crossover model given by:

$$\eta_{kji} = \exp\left(\gamma_k^{(0)} + \gamma_k^{(1)} X_{1i} + \gamma_k^{(2)} X_{2i} + \gamma_k^{(3)} X_{3i} + \omega_{ki}\right) \tag{38.3}$$

where $\gamma_k^{(0)}$ is the intercept of this model; $\gamma_k^{(1)}$ is the effect of formulation; $\gamma_k^{(2)}$ is the effect of period and $\gamma_k^{(3)}$ is the effect of sequence for the kth pharmacokinetic parameter. In this way, X_{3i} denotes the sequence where the subject was randomized ($X_3 = 0$ if sequence RT and $X_3 = 1$ if sequence TR); X_{2i} denotes the period where the subject received a formulation ($X_{2i} = 0$ if period 1 and $X_{2i} = 1$ if period 2) and X_{1i} denotes the formulation received by the subject in each period ($X_{1i} = 0$ if formulation R and $X_{1i} = 1$ if formulation T); ω_{ki} is a random effect introduced to capture the dependence among the repeated measures. This effect is assumed to have a multivariate normal distribution with a mean vector of values equal to zero and a covariance matrix $\mathbf{S}$.

In the following, we consider a Gaussian copula function [5] that is a robust copula function since it is defined to model any degree of positive or negative dependence. For two random variables, its bivariate density function is given by [10]:

$$\begin{aligned} f(y_1, y_2; \theta) = {} & f_1(y_1) f_2(y_2) \frac{1}{\sqrt{(1-\theta^2)}} \\ & \times \exp\left\{\left[-\frac{1}{2(1-\theta^2)}\left(u^2 + z^2 - 2\theta u z\right)\right] + \frac{1}{2}\left(u^2 + z^2\right)\right\} \end{aligned} \tag{38.4}$$

where $u = \Phi^{-1}[F_1(y_1)]$; $z = \Phi^{-1}[F_2(y_2)]$ and $-1 < \theta < 1$.

The likelihood function for $\psi = (\beta_{kj}, r_{kj}, \gamma_k^{(l)}, \omega_{ki}, \tau_1^2, \tau_2^2, \rho, \theta)$, for $l = 0, 1, 2, 3$ is given by:

$$p(\mathbf{y} \mid \psi) = \prod_{k=1}^{2}\prod_{j=1}^{2}\prod_{i=1}^{n} \frac{\beta_{kj}}{\Gamma(r_{kj})} \eta_{kji}^{\beta_{kj} r_{kj}} y_{kji}^{\beta_{kj} r_{kj} - 1} \exp\left[-(\eta_{kji} y_{kji})^{\beta_{kj}}\right]$$
$$\times \frac{1}{\sqrt{(1-\theta^2)}} \prod_{j=1}^{2}\prod_{i=1}^{n} \exp\left\{-\frac{1}{2}\left(1-\theta^2\right)\left(u_{ji}^2 + z_{ji}^2 - 2\theta u_{ji} z_{ji}\right)\right.$$
$$\left. + \frac{1}{2}\left(u_{ji}^2 + z_{ji}^2\right)\right\} \tag{38.5}$$

where η_{kji} is given by (38.3) and $u_{ji} = \Phi^{-1}[F_{1ji}(y_{ji})]$; $z_{ji} = \Phi^{-1}[F_{2ji}(y_{ji})]$.

For the first stage of the Bayesian analysis, assuming the likelihood function defined in (38.5), we consider $\gamma^{(l)} \sim MN(\mathbf{a}^{(l)}; \Sigma_\gamma^{(l)})$, $\beta_{kj} \sim G(c_{kj}; d_{kj})$ and $r_{kj} \sim G(e_{kj}; f_{kj})$ for $j = 1, 2$; $k = 1, 2$ and $l = 0, 1, 2, 3$; $MN(\mathbf{a}^{(l)}; \Sigma_\gamma^{(l)})$ denotes a multivariate normal distribution with mean vector $\mathbf{a}^{(l)}$ and covariance matrix $\Sigma_\gamma^{(l)}$, $G(c, d)$ denotes a gamma distribution with mean c/d and variance c/d^2. In our case, we have $\mathbf{a}^{(l)} = (a_1^{(l)}, a_2^{(l)})$ and $\Sigma_\gamma^{(l)} = \begin{pmatrix} (b_1^{(l)})^2 & 0 \\ 0 & (b_2^{(l)})^2 \end{pmatrix}$. Also assume $\theta \sim U(-1; 1)$ where $U(-1; 1)$ denotes a uniform distribution in the interval $[-1; 1]$.

For the second stage of the hierarchical Bayesian analysis, we assume that ω_{ki} has a multivariate normal distribution with mean vector $\mathbf{0}$ and covariance matrix $\mathbf{S} = \begin{pmatrix} \tau_1^2 & \rho\tau_1\tau_2 \\ \rho\tau_1\tau_2 & \tau_2^2 \end{pmatrix}$. In this way, we assume $\tau_1^{-2} \sim G(s_1; s_2)$, $\tau_2^{-2} \sim G(t_1; t_2)$ and $\rho \sim U(-1; 1)$.

Observe that the effects of the covariates are evaluated by observing $(1-\alpha)$ HPD intervals for the associated regression parameters. If zero is included in the credible interval the associated covariate is not significative on the response of interest.

In the construction of HPD intervals for the differences (or ratios) of the pharmacokinetic parameters of the formulations, which are decisive in the evaluation of the bioequivalence, we should obtain Monte Carlo estimates based on the simulated Gibbs samples for the posterior means $E(y_{kji}) = \Gamma(\frac{1}{\beta_{kj}} + r_{kj})/\eta_{kji}\Gamma(r_{kj})$, for $k = 1, 2$ and $j = 1, 2$. Following, for each fixed kth pharmacokinetic parameter of interest, we construct $(1-\alpha)$ HPD intervals for the differences (or ratios) between the means of the formulations. If these intervals are entirely included in the bioequivalence limits, there is evidence of the exchangeability of the formulations.

Note that in addition to η, $E(y_{kji})$ depends of r and β. In this way, we consider different values of r and β for each pharmacokinetic parameter in each formulation (see (38.2)).

38.3 Results and Discussion

To apply the proposed methodology, we consider a data set introduced by [1]. This data set represents a bioequivalence study of a 2×2 crossover design with 23 in-

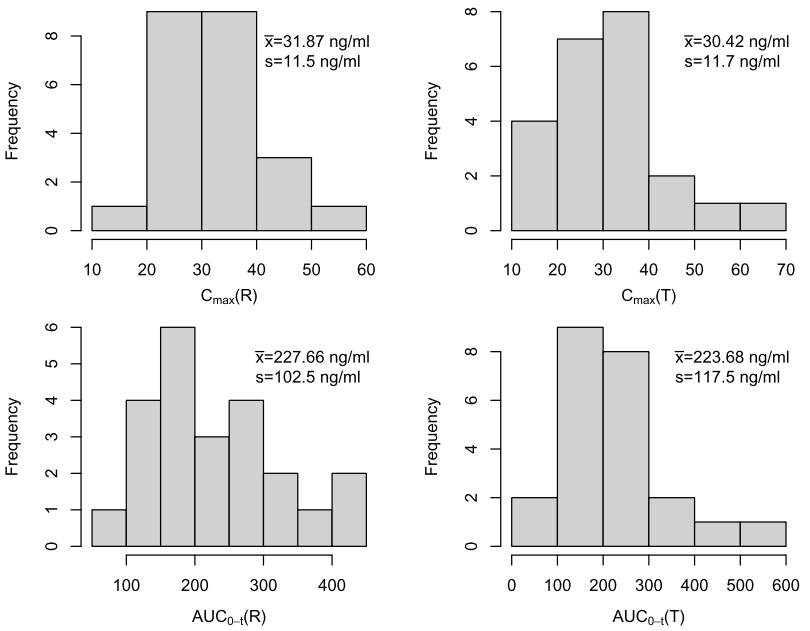

Fig. 38.1 Histograms by formulations and pharmacokinetic parameters

dividuals. The main goal of this study is to compare the relative biodisponibility of 8 mg ondansetron, one in the conventional release tablet, and another one in oral disintegration tablet produced by different laboratories. The reference formulation (R) was made by Zofran® and the test formulations (T) by Vonau® flash. A summary of the data set considered for the example is given in Fig. 38.1.

For the prior distributions related to (38.5) we choose hyperparameters values to have approximately non-informative prior distributions. In this case, $\mathbf{a}^{(l)} = \mathbf{0}$; $\Sigma_{\gamma}^{(l)} = \begin{pmatrix} 100^2 & 0 \\ 0 & 100^2 \end{pmatrix}$; for $l = 0, 1, 2, 3$ and $c_{kj} = d_{kj} = e_{kj} = f_{kj} = 1$ for $k = 1, 2$; $j = 1, 2$; Also, we have $s_1 = s_2 = t_1 = t_2 = 0.1$.

We simulated 150,000 Gibbs samples for each parameter using the JAGS software under the R software (library R2JAGS). In the simulation procedure, we choosed every 50th generated value to have approximately uncorrelated samples after deleting the first 50,000 generated Gibbs samples ("burn-in-sample") to eliminate the possible effect of the initial values for the Markov Chain. The convergence of the algorithm was verified from temporal traceplots, histograms of the simulated samples and from autocorrelation graphs.

In Table 38.1, we have the HPD intervals of the estimated correlation, values of DIC [8] and LPML [3] for the proposed model and assuming independence between the pharmacokinetic parameters. We observe that the correlation coefficients are relevant (the value 0 is not included in the 90 % HPD interval). In this way, we observe that this model captures the existing correlation between the pharmacokinetic parameters. The values of DIC and LPML also help us to reject the univariate

Table 38.1 Comparison between copula function and independence

Copula function	Correlation parameters 90 % *HPD*	DIC	LPML
Gaussian	$\widehat{\theta} = [0.86; 0.93]$	733.7	−316.9
Independent	–	859.9	−362.5

Table 38.2 HPD intervals for the pharmacokinetic parameters

Pharmacokinetic parameters	Copula function	$E(y_{k2.}) - E(y_{k1.})$		
		Mean (*sd*)	HPD (90 %)	Range
$C_{\max}$	Independent	−1.49(1.92)	−4.82; 1.38	6.20
	Gaussian	−1.78(1.74)	−4.50; 1.01	5.51
AUC_{0-t}	Independent	−5.06(14.14)	−27.17; 17.28	44.45
	Gaussian	−5.96(13.45)	−28.16; 14.22	42.38

sd: standard deviation

(or no dependence) models. In this way, we observe in Table 38.2, that the HPD intervals for the difference between the formulations assuming dependence between the pharmacokinetic parameters are shorter when compared to the HPD intervals assuming independence between the pharmacokinetic parameters.

For the bioequivalence decision, the bioequivalence limits for $C_{\max}$ and AUC_{0-t} are given, respectively, by $[-0.25 \times 31.87; 0.20 \times 31.87] = [-7.97; 6.37]$ and $[-0.25 \times 227.66; 0.20 \times 227.66] = [-56.92; 45.53]$. In Table 38.2, we observe that for this example, we do not have problems to accept bioequivalence between the two formulations in study. The HPD intervals are fully included in the bioequivalence limits. We observe in Fig. 38.2, a good fit of the proposed model for the bioequivalence data.

38.4 Conclusion and Remarks

It is well known that bioequivalence tests are regulated by regulatory agencies around the world and the statistical steps to analyse the data are standardized by these agencies. This procedure is important to guide the bioequivalence studies but in many situations we could have datasets where the standard model is not the best choice to analyze the bioequivalence data. In the introduced example, we have observed that the usual standard model assumption given by regulatory agencies could be not appropriate as observed in the preliminary data analysis using the popular Shapiro non-parametric test for normality [7]; in our case, we reject the normality assumption for the residuals considering the pharmacokinetic parameter AUC_{0-t} ($p < 0.02$).

In this sense, we believe that it is important to search for the best model in each application, since this is justified and guided by common sense and ethics of the

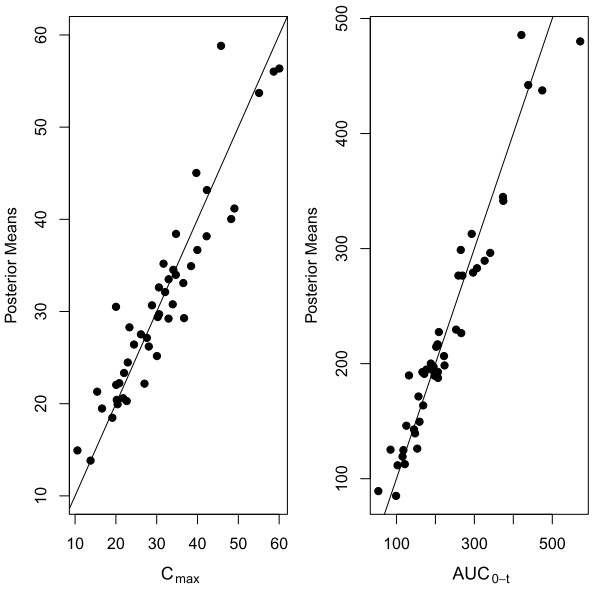

Fig. 38.2 Posterior means against observed values by pharmacokinetic parameters

involved statisticians. The literature also presents some other studies with different methodologies for bioequivalence studies (see for example, [4]). Other models also could be fitted by the dataset introduced in the example presented in this paper leading to better results, but we credit our work to be a good alternative in the context of bioequivalence studies. Observe that we did not need to transform the data as commonly used in bioequivalence studies to get a good fit of the proposed model for the data set.

Observe that using the Bayesian approach, our final BE decision (Table 38.2) is based on separately computing HPDs for each pharmacokinetic parameter. It is interesting to observe that in this context we could alternatively to obtain a bivariate joint HPD region (whose projections on each axis not necessarily would coincide with the univariate HPDs) and base the final decision (in a single step) on this joint posterior probability region, coping with the possible dependency and avoiding the multitesting problem of separately deciding with respect to each pharmacokinetic parameter (goal of a future work).

Alternatively for the use of a Bayesian inference approach, we also could use a standard classical inference approach based on MLE (Maximum Likelihood Estimation) methods, but these methods usually depends on good initial values in the iterative numerical algorithm to be used to find the point estimates, a difficulty in many applications.

In summary, in situations where the researcher is not sure with the standard distribution assumption used in bioequivalence studies, especially with positive asymmetric data sets (see Fig. 38.1), we suggest the use of the proposed model introduced in this paper. These results could be of great interest in bioequivalence studies.

Acknowledgements We are using resources of the LCCA-Laboratory of Advanced Scientific Computation of the University of São Paulo.

References

1. Armando YP (2008) Evaluation of bioequivalence of conventional tablet and orally disintegrating tablet containing 8 mg ondansetron. http://www.teses.usp.br/teses/disponiveis/9/9139/tde-08102009-190008/pt-br.php. Cited 01 Jun 2014
2. FDA (2003) Guidance for industry: bioavailability and bioequivalence studies for orally administered drug products – general considerations. http://www.fda.gov/downloads/Drugs/Guidances/ucm070124.pdf. Cited 01 Jun 2014
3. Gelfand AE (1996) Model determination using sampling-based methods. In: Gilks WR, Richardson S, Spiegelhalter DJ (eds) Markov chain Monte Carlo in practice. Chapman & Hall, London, pp 145–161
4. Ghosh P, Gönen M (2008) Bayesian modeling of multivariate average bioequivalence. Stat Med 27(13):2402–2419
5. Lee L (1983) Generalized econometric models with selectivity. Econometrica 51(2):507–512
6. Nelsen R (2006) An introduction to copulas. Springer, New York
7. Shapiro SS (1965) An analysis of variance test for normality (complete samples). Biometrika 52(3-4):591–611
8. Spiegelhalter DJ, Best NG, Carlin NP, van Der Linde A (2002) Bayesian measures of model complexity and fit. J R Stat Soc B 64(4):583–639
9. Stacy EW (1962) A generalization of the gamma distribution. Ann Math Stat 33(3):1187–1192
10. Trivedi PK, Zimmer DM (2005) Copula modeling: an introduction for practitioners. Found Trends Econ 1(1):1–111
11. Westlake WJ (1972) Use of confidence intervals in analysis of comparative bioavailability trials. J Pharm Sci 61(8):1340–1341

Chapter 39
The Marginal Distribution of Compound Poisson INAR(1) Processes

Christian H. Weiß and Pedro Puig

Abstract A compound Poisson distribution is a natural choice for the innovations of an INAR(1) model. If the support of the compounding distribution is finite (Hermite-type distributions), the observations' marginal distribution belongs to the same family and it can be computed exactly. In the infinite case, however, which includes the popular choice of negative binomial innovations, this is not so simple. We propose two types of Hermite approximations for this case and investigate their quality in a numerical study.

39.1 Introduction: Compound Poisson Distribution

Definition 39.1 (Compound Poisson distribution.) Let $Z_1, Z_2, \ldots$ be independent and identically distributed (i.i.d.) count random variables defined over $\{1, 2, \ldots, \nu\}$, where the case $\nu = \infty$ is allowed. The common distribution of the random variables $Z_i \sim Z$ is called the *compounding distribution*, and let $H(z)$ denote its probability generating function (pgf).

Let $N \sim \text{Poi}(\lambda)$ be Poisson-distributed with mean $\lambda > 0$, independently of $Z_1, Z_2, \ldots$

Then $\varepsilon := Z_1 + \cdots + Z_N$ is said to be *compound Poisson distributed*, and we denote $\varepsilon \sim \text{CP}_\nu(\lambda, H)$. [4, Chapter XII]

The distribution of Definition 39.1 has also been referred to as Poisson-stopped sum distribution, stuttering Poisson distribution or multiple Poisson distribution [5, Sects. 4.11 and 9.3]. In the particular case $\nu < \infty$, also the names extended Poisson

C.H. Weiß (✉)
Department of Mathematics and Statistics, Helmut Schmidt University, 22008 Hamburg, Germany
e-mail: weissc@hsu-hh.de

P. Puig
Department of Mathematics, Universitat Autònoma de Barcelona, 08193 Cerdanyola del Vallés (Barcelona), Spain
e-mail: ppuig@mat.uab.cat

A. Steland et al. (eds.), *Stochastic Models, Statistics and Their Applications*,
Springer Proceedings in Mathematics & Statistics 122,
DOI 10.1007/978-3-319-13881-7_39

distribution of order ν [1] or *Hermite distribution* of order ν [10] are common, and the pgf of the compounding distribution then becomes a polynomial of degree ν, that is $H(z) = h_1 z + \cdots + h_\nu z^\nu$.

The pgf of ε is given by [4, 7]

$$\mathrm{pgf}_\varepsilon(z) = \exp\big(\lambda\big(H(z) - 1\big)\big). \tag{39.1}$$

So the factorial cumulant generating function (fcgf) of ε follows as

$$\mathrm{fcgf}_\varepsilon(z) := \ln\big(\mathrm{pgf}_\varepsilon(1+z)\big) = \lambda\big(H(1+z) - 1\big) =: \sum_{r=1}^{\nu} \frac{\kappa_{(r),\varepsilon}}{r!} \cdot z^r, \tag{39.2}$$

where the coefficients $\kappa_{(r),\varepsilon}$ of the series expansion of $\mathrm{fcgf}_\varepsilon(z)$ are referred to as the factorial cumulants of ε [3, p. 449]. Since $H(1+z)$ is just the factorial moment generating function (fmgf) of the compounding distribution, it follows that

$$\kappa_{(r),\varepsilon} = \lambda \cdot \mu_{(r),Z}, \quad \text{where } \mu_{(r),Z} := E\big[Z \cdots (Z - r + 1)\big] \tag{39.3}$$

are the factorial moments of the compounding distribution. Note that in the case $\nu < \infty$, we have $\mu_{(r),Z} = 0$ for $r > \nu$, and hence $\kappa_{(r),\varepsilon} = 0$ for $r > \nu$. Relations for transforming factorial cumulants into usual cumulants or (factorial) moments are provided in the book by [3], also see Appendix 1 in [14]. In particular,

$$\sigma_\varepsilon^2 - \mu_\varepsilon = \kappa_{(2),\varepsilon} = \lambda \cdot \mu_{(2),Z} = \lambda \cdot \big(E\big[Z^2\big] - E[Z]\big).$$

If $\nu < \infty$, then $E[Z^2] \le \nu \cdot E[Z]$. But we also have $E[Z^2] \ge E[Z]$, so

$$\frac{\sigma_\varepsilon^2}{\mu_\varepsilon} \quad \begin{cases} = 1 & \text{iff } \nu = 1, \\ \in (1;\, \nu] & \text{iff } \nu > 1. \end{cases} \tag{39.4}$$

So the CP_ν-distributions are overdispersed with a maximal index of dispersion equal to ν.

Example 39.1 (Special cases.) The CP_ν-family includes several well-known distributions as a special case [5, Chapter 9]. $\nu = 1$ corresponds to the Poisson distribution, i.e., $\mathrm{CP}_1(\lambda, H) = \mathrm{Poi}(\lambda)$. For $\nu = 2$, this is just the Hermite distribution introduced in [7]. For $\nu < \infty$ and the compounding distribution being uniform on $\{1, \ldots, \nu\}$, we have the *Poisson distribution of order* ν.

The case $\nu = \infty$ includes, among others, *Consul's generalized Poisson* distribution, the *Neyman type A* distribution and the *Polya-Aeppli* distribution. In particular, if

$$\lambda = -n \ln \pi, \qquad H(z) = \sum_{k=1}^{\infty} \frac{(1-\pi)^k}{-k \ln \pi} z^k \quad \text{(logarithmic series distribution)}, \tag{39.5}$$

then we obtain the *negative binomial* distribution $\mathrm{NB}(n, \pi)$ with $n > 0$ and $\pi \in (0; 1)$ [5, Chapter 5]. Its fcgf is given by $\mathrm{fcgf}_\varepsilon(z) = -n \cdot \ln(1 - \frac{1-\pi}{\pi} z)$.

So the factorial cumulants follow as $\kappa_{(r),\varepsilon} = n(r-1)!(\frac{1-\pi}{\pi})^r$. In particular, the mean equals $\mu_\varepsilon = n(1-\pi)/\pi$ and the dispersion index $\sigma_\varepsilon^2/\mu_\varepsilon = 1/\pi$.

In Sect. 39.2, we shall argue that the CP_ν-family is a natural choice for the *in*teger-valued *a*uto*r*egressive model of order 1 (INAR(1) model) as introduced by [2, 8]. Marginal moments or cumulants are easily calculated for the resulting CP_ν-INAR(1) process, and if $\nu < \infty$, also the exact computation of the corresponding probability mass function (pmf) is easily possible. If $\nu = \infty$, however, no simple solution seems to be available to evaluate the pmf. Therefore, in Sect. 39.3, we develop ways of approximating the marginal distribution of a CP_∞-INAR(1) process.

39.2 The Compound Poisson INAR(1) Model

The INAR(1) model, a counterpart to the Gaussian AR(1) model but for counts, is based on the random operator called *binomial thinning* (sometimes also "binomial subsampling" [10]) as introduced by [12] and denoted by the symbol "$\circ$": If X has range $\mathbb{N}_0$ and if $\alpha \in (0;1)$, then the random variable $\alpha \circ X := \sum_{i=1}^{X} Y_i$ arises from X by binomial thinning. The counting series Y_i are i.i.d. Bernoulli random variables with $P(Y_i = 1) = \alpha$, which are also independent of X. So $\alpha \circ X | X = x \sim \mathrm{B}(x, \alpha)$, where $\mathrm{B}(n, \pi)$ abbreviates the binomial distribution with parameters $n \in \mathbb{N}$ and $\pi \in (0;1)$. Refs. [2, 8] now defined the *INAR(1) process* in the following way:

Definition 39.2 (INAR(1) Model.) The innovations $(\varepsilon_t)_\mathbb{Z}$ are an i.i.d. process with range $\mathbb{N}_0$. Let $\alpha \in (0;1)$, a process $(X_t)_\mathbb{Z}$, which follows the recursion

$$X_t = \alpha \circ X_{t-1} + \varepsilon_t, \tag{39.6}$$

is said to be an *INAR(1) process* if all thinning operations are performed independently of each other and of $(\varepsilon_t)_\mathbb{Z}$, and if the thinning operations at each time t as well as ε_t are independent of $(X_s)_{s<t}$.

The INAR(1) process is a homogeneous Markov chain, which has a unique stationary solution under weak conditions [11]. If the INAR(1) process is stationary, and if we have given the innovations' distribution (in terms of the pgf, $\mathrm{pgf}_\varepsilon(z)$), then the pgf of the stationary marginal distribution of X_t, say $\mathrm{pgf}_X(z)$, has to satisfy the equation $\mathrm{pgf}_X(z) = \mathrm{pgf}_X(1-\alpha+\alpha z) \cdot \mathrm{pgf}_\varepsilon(z)$, see [2]. This leads to a simple relation for the factorial cumulants [14]:

$$\mathrm{fcgf}_X(z) = \mathrm{fcgf}_X(\alpha z) + \mathrm{fcgf}_\varepsilon(z), \qquad \kappa_{(n),X} = \frac{\kappa_{(n),\varepsilon}}{1-\alpha^n}. \tag{39.7}$$

In particular, if $\mu_\varepsilon, \sigma_\varepsilon < \infty$, mean and variance are given by

$$\mu_X = \frac{\mu_\varepsilon}{1-\alpha}, \qquad \frac{\sigma_X^2}{\mu_X} = \frac{\frac{\sigma_\varepsilon^2}{\mu_\varepsilon} + \alpha}{1+\alpha}, \tag{39.8}$$

i.e., the observations X_t are overdispersed iff the innovations ε_t are overdispersed. The autocorrelation function is of AR(1)-type, given as $\rho(k) = \alpha^k$. For further properties and references, see [2, 11].

For the innovations' distribution, one may select, e.g., a particular underdispersed count data model [14] such that the resulting INAR(1) process produces underdispersed counts, see (39.8). However, the most natural approach is to assume the innovations to be CP_ν-distributed: As it was shown in Theorem 1 of [10], a count data model being parametrized by its ν first factorial cumulants $\kappa_{(1)}, \ldots, \kappa_{(\nu)}$ is closed under addition and under binomial thinning *iff* it has a CP_ν-distribution according to Definitions (39.1) and (39.2). In view of the INAR(1) recursion (39.6), this implies that observations and innovations stem from the same ν-th order family *iff* these are CP_ν-distributed. We refer to an INAR(1) process $(X_t)_\mathbb{Z}$ with $\mathrm{CP}_\nu(\lambda, H)$-distributed innovations $(\varepsilon_t)_\mathbb{Z}$ as a *compound Poisson INAR(1) process*. Because of the cited Theorem 1 by [10], such a CP_ν-INAR(1) process also has marginal CP_ν-distributed observations. In particular, the case $\nu = 1$ leads to the well-known Poisson INAR(1) model, where both the innovations and observations are Poisson-distributed.

In Theorem 3.2.1 in [11], the unique stationary marginal distribution of a CP_ν-INAR(1) process was shown to be the $\mathrm{CP}_\nu(\eta, G)$-distribution with

$$\eta\big(G(z) - 1\big) = \lambda \sum_{i=0}^{\infty} \big(H\big(1 - \alpha^i + \alpha^i z\big) - 1\big) \quad \text{for all } z \in [0; 1]; \tag{39.9}$$

the coefficients of $G(z)$ are denoted as $g_1, g_2, \ldots$ Unfortunately, formula (39.9) allows to evaluate the pmf of the observations X_t only in special cases. Besides the trivial case $\nu = 1$, the pmf of X_t can always be computed numerically exactly if $\nu < \infty$:

Scheme 39.1 (pmf of CP_ν-INAR(1) process.)

1. Given the pgf of the innovations' CP_ν-distribution, compute the pgf (39.9) of the marginal distribution by extracting the parameters η and $g_1, \ldots, g_\nu$.

   a. If the parameters λ and $h_1, \ldots, h_\nu$ are readily available, solve the linear equations presented in Example 3.2.2 of [11] to compute η and $g_1, \ldots, g_\nu$:

   $$g_1 + \cdots + g_\nu = 1, \qquad \frac{\lambda}{\eta} - (1-\alpha) \cdot g_1 - \cdots - (1-\alpha)^\nu \cdot g_\nu = 0,$$

   $$h_k \cdot \frac{\lambda}{\eta} - (1 - \alpha^k) \cdot g_k + \alpha^k \sum_{i=k+1}^{\nu} \binom{i}{k} (1-\alpha)^{i-k} \cdot g_i = 0 \quad \textit{for } k = \nu, \ldots, 2.$$

   b. If the innovations' CP_ν-distribution is specified in terms of its factorial cumulants $\kappa_{(1),\varepsilon}, \ldots, \kappa_{(\nu),\varepsilon}$, then first compute $\kappa_{(1),X}, \ldots, \kappa_{(\nu),X}$ according to (39.7), afterwards compute η and $g_1, \ldots, g_\nu$ by expanding

   $$\eta\big(G(z) - 1\big) := \sum_{r=1}^{\nu} \frac{\kappa_{(r),X}}{r!} \cdot (z-1)^r, \quad \textit{see (39.2)}.$$

2. Apply the recursive scheme by [6] for the computation of the pmf of the marginal distribution $P(X = k)$:

$$P(X=0)=e^{-\eta}, \qquad P(X=k)=\frac{\eta}{k}\cdot\sum_{j=1}^{\min\{k,\nu\}} j g_j \cdot P(X=k-j) \quad \text{for } k\geq 1.$$

Note that the recursive scheme in step 2, which is an instance of the Panjer recursion [9], also holds if $\nu=\infty$. But to be able to apply this, it would be necessary to know the *observations*' compounding probabilities $g_1, g_2, \ldots$, which is usually not the case if $\nu=\infty$. So step 1 of Scheme 39.1 is the crucial point in view of a numerically exact computation of the observations' pmf. Since the case $\nu=\infty$ is very important for practice, including the popular INAR(1) model with negative binomial innovations (see Example 39.1), approximate solutions are developed in Sect. 39.3.

39.3 Approximating the Marginal Distribution

Let $(X_t)_{\mathbb{Z}}$ be a stationary CP_∞-INAR(1) process. In general, a closed-form expression for the observations' pmf is not available, so numerical approaches are required. In the sequel, we propose and investigate two approximations for the observations' pmf, which replace the original infinite compounding structure by a finite one (also see the discussion in [7]) and then continue with Scheme 39.1. To simplify writing, let us refer to these approximations as *Hermite-ν approximations*, also see the discussion before Example 39.1. As the benchmark for the performance comparisons, we use a (computationally demanding) *Markov approximation* (see [13] for the details).

We consider two types of Hermite approximations of order ν; note that the approximations with $\nu=1$ are just Poisson approximations.

Scheme 39.2 (Hermite-ν approximation, type 1.) For the CP_∞-INAR(1) process $(X_t)_{\mathbb{Z}}$, let the innovations ε_t be $\mathrm{CP}_\infty(\lambda, H)$-distributed.

Define the νth order approximation $\mathrm{CP}_\nu(\tilde{\lambda}, \tilde{H})$ by

$$\tilde{\lambda}:=\lambda, \qquad \tilde{h}_1:=h_1,\ldots,\tilde{h}_{\nu-1}:=h_{\nu-1}, \qquad \tilde{h}_\nu:=1-\sum_{k=1}^{\nu-1}h_k.$$

Then proceed according to steps 1(a) and 2 of Scheme 39.1.

From the recursive scheme by [6], see step 2 of Scheme 39.1, it becomes clear that Scheme 39.2 preserves the first ν innovations' probabilities, $P(\varepsilon=0),\ldots,P(\varepsilon=\nu-1)$, and only approximates the remaining ones. This feature, however, does in general not carry over to the observations' probabilities. Furthermore, the innovations' mean and, hence, the observations' mean are usually not preserved exactly. For the latter reason, we consider an alternative type of Hermite approximation, where the mean μ_X is always met exactly.

Table 39.1 Model parameterizations with corresponding mean, dispersion index and skewness of the marginal distribution of the observations X_t

π	α	$n=1$			$n=2$		
		mean	disp.	skew.	mean	disp.	skew.
0.75	0.25	0.444	1.267	2.072	0.889	1.267	1.465
	0.50	0.667	1.222	1.626	1.333	1.222	1.150
	0.75	1.333	1.190	1.112	2.667	1.190	0.786
0.50	0.25	1.333	1.800	1.766	2.667	1.800	1.249
	0.50	2.000	1.667	1.361	4.000	1.667	0.963
	0.75	4.000	1.571	0.908	8.000	1.571	0.642
0.25	0.25	4.000	3.400	1.748	8.000	3.400	1.236
	0.50	6.000	3.000	1.358	12.000	3.000	0.960
	0.75	12.000	2.714	0.899	24.000	2.714	0.636

Scheme 39.3 (Hermite-ν approximation, type 2.) For the CP_∞-INAR(1) process $(X_t)_{\mathbb{Z}}$, let the innovations ε_t be $\mathrm{CP}_\infty(\lambda, H)$-distributed with mean μ_ε.

Define the νth order approximation $\mathrm{CP}_\nu(\tilde{\lambda}, \tilde{H})$ by

$$\tilde{h}_1 := \frac{h_1}{\sum_{k=1}^{\nu} h_k}, \ \ldots, \ \tilde{h}_\nu := \frac{h_\nu}{\sum_{k=1}^{\nu} h_k}, \qquad \tilde{\lambda} := \frac{\mu_\varepsilon}{\sum_{k=1}^{\nu} k\,\tilde{h}_k}.$$

Then proceed according to steps 1(a) and 2 of Scheme 39.1.

To evaluate the performance of approximations 39.2 and 39.3, we consider the NB-INAR(1) model with $\mathrm{NB}(n, \pi)$-distributed innovations, see (39.5) in Example 39.1 for the true compounding distribution of ε_t. For different levels of the mean parameter n, the dispersion parameter π and the autocorrelation parameter α (see the overview in Table 39.1), we compute the marginal distribution approximately via Schemes 39.2 and 39.3. We compare the result with the numerically exact Markov chain approach ("MC") [13] in terms of the *Kullback–Leibler divergence*,

$$d_{\mathrm{KL}}(P_{\mathrm{MC}}, P_{\mathrm{approx}}) := \sum_k P_{\mathrm{MC}}(k)\ \ln\left(\frac{P_{\mathrm{MC}}(k)}{P_{\mathrm{approx}}(k)}\right), \tag{39.10}$$

and by comparing the respective values for the mean, dispersion index and skewness. While the computing time for the approximations was always < 0.1 s, the MC approach was much more demanding and required 70–100 s.

Consider first the obtained results based on the Kullback–Leibler divergence, which measures the overall quality of approximation. Some illustrative graphs are plotted in Fig. 39.1. With increasing approximation order ν, the divergence decreases nearly exponentially (note the log scale of the Y axis). Without exception (see (a) for illustration), the Hermite approximation of type 1 ("HA1") becomes superior when ν increases (although the difference is small). Therefore, plots (b)–(d) only refer to "HA1". It can be seen that the mean parameter n (see (b)) and

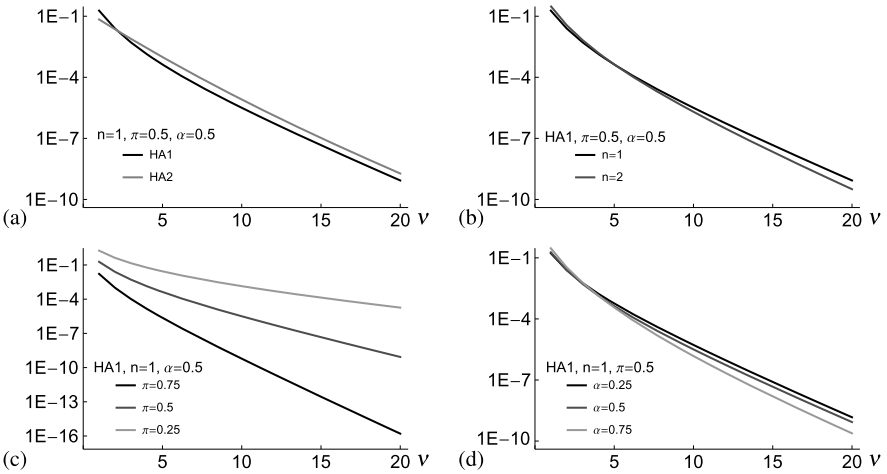

Fig. 39.1 Plot of Kullback–Leibler divergences against approximation order ν

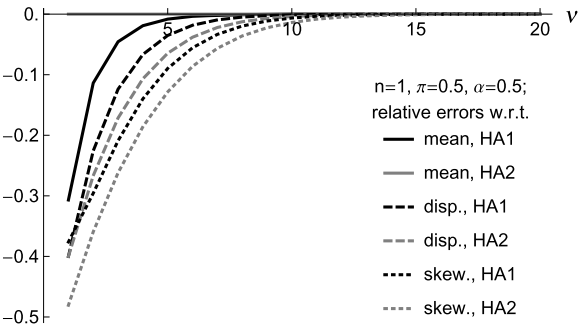

Fig. 39.2 Plot of relative errors against approximation order ν. Relative errors $\frac{\text{approx}-\text{true}}{\text{true}}$ computed for mean, dispersion index and skewness (also see Table 39.1), and for approximations of both types 1 and 2

autocorrelation parameter α (see (d)) have only little effect on the quality of approximation, while a decreasing π (= increasing overdispersion, see (c)) leads to a severe degradation. So the approximation order has to be increased with increasing overdispersion.

Overally, HA1 performs best, but if it is important to reproduce the mean exactly, then HA2 is the method of choice. Looking at Fig. 39.2, we see that at least for $\nu \geq 10$, also HA1 represents the mean nearly exactly. In particular, HA1 is always the better choice when considering the dispersion index or the skewness. If one chooses $\nu \geq 15$, the difference between the exact distribution and HA1 appears to be practically negligible.

39.4 Discussion

To approximate the marginal distribution of a CP_∞-INAR(1) process, the Hermite-ν approximation of type 1 appears as the method of choice. It gives the best overall approximation of the marginal pmf of X_t, and it also better reflects skewness and dispersion index. Only if it is essential to exactly reproduce the mean, then the type 2 approximation should be used. The order ν of (any) approximation has to be carefully adapted in order to be compatible with the actual dispersion index (increasing overdispersion requires increasing ν), while mean and autocorrelation level are nearly without effect on the approximation's quality, at least in the explored ranges.

The present work is focused on the case of a *given* CP_ν-INAR(1) model, which is important, e.g., for simulations and theoretical analyses. Future research should develop also an empirical version of the Hermite approximation approach, where a marginal approximation could be computed based on appropriate empirical characteristics (e.g., based on the first ν empirical factorial cumulants in view of step 1(b) in Scheme 39.1). In a sense, this would lead to some kind of semi-parametric estimation of the INAR(1)'s marginal distribution.

Acknowledgements The first author is grateful to Sebastian Schweer (Heidelberg University) for many valuable discussions about CP-INAR(1) processes. This work was partially funded by the grant MTM2012-31118 from the Ministry of Economy and Competitiveness of Spain.

References

1. Aki S (1985) Discrete distributions of order k on a binary sequence. Ann Inst Stat Math 37(1):205–224
2. Al-Osh MA, Alzaid AA (1987) First-order integer-valued autoregressive INAR(1) processes. J Time Ser Anal 8:261–275
3. Douglas JB (1980) Analysis with standard contagious distributions. Int. Co-operative Publishing House, Fairland
4. Feller W (1968) An introduction to probability theory and its applications – vol I, 3rd edn. Wiley, New York
5. Johnson NL, Kemp AW, Kotz S (2005) Univariate discrete distributions, 3rd edn. Wiley, Hoboken
6. Kemp CD (1967) 'Stuttering-Poisson' distributions. J Stat Soc Inquiry Soc Ireland 21(5):151–157
7. Kemp CD, Kemp AW (1965) Some properties of the 'Hermite' distribution. Biometrika 52(3):381–394
8. McKenzie E (1985) Some simple models for discrete variate time series. Water Resour Bull 21(4):645–650
9. Panjer HH (1981) Recursive evaluation of a family of compound distributions. ASTIN Bull 12(1):22–26
10. Puig P, Valero J (2007) Characterization of count data distributions involving additivity and binomial subsampling. Bernoulli 13(2):544–555
11. Schweer S, Weiß CH (2014) Compound Poisson INAR(1) processes: stochastic properties and testing for overdispersion. Comput Stat Data Anal 77:267–284
12. Steutel FW, van Harn K (1979) Discrete analogues of self-decomposability and stability. Ann Probab 7(5):893–899

13. Weiß CH (2010) The INARCH(1) model for overdispersed time series of counts. Commun Stat, Simul Comput 39(6):1269–1291
14. Weiß CH (2013) Integer-valued autoregressive models for counts showing underdispersion. J Appl Stat 40(9):1931–1948

Part IV
Algorithms and Applications

Chapter 40
Monitoring Euro Area Real Exchange Rates

Philipp Aschersleben, Martin Wagner, and Dominik Wied

Abstract We apply the stationarity and cointegration monitoring procedure of Wagner and Wied in (Monitoring stationarity and cointegration. SFB823 Discussion Paper 23/14. http://hdl.handle.net/2003/33430, 2014) to monthly real exchange rate indices, vis-*à*-vis Germany, of the first round Euro area member states. For all countries except Portugal structural breaks are detected prior to the onset of the Euro area crisis triggered in turn by the global financial crisis. The results indicate that a more detailed investigation of RER behavior in the Euro area may be useful for understanding the unfolding of the deep crisis currently plaguing many countries in the Euro area.

40.1 Introduction

An issue that has received a lot of attention in particular since the onset of the Euro crisis, or to be more precise, the deep economic crisis in many – often peripheral – Euro area countries, is the question whether persistent real exchange rate (RER) misalignment is one of the factors responsible for Euro area disequilibria. Clearly, given that nominal exchange rates across Euro area member states are by construction fixed at one, the nominal exchange rate is not available anymore as an instrument for readjusting RERs. Sizeable nominal exchange rate adjustments, often devaluations with respect to the "hard currencies" like the DM, have occurred almost regularly for some European countries in the decades before monetary unification. Shutting down the currency devaluation channel may have contributed to persistent RER misalignments when institutional and price rigidities prevent smooth re-establishment of external equilibrium.

P. Aschersleben · M. Wagner (✉) · D. Wied
Faculty of Statistics, Technical University Dortmund, Vogelpothsweg 87, 44227 Dortmund, Germany
e-mail: mwagner@statistik.tu-dortmund.de

P. Aschersleben
e-mail: aschersleben@statistik.tu-dortmund.de

D. Wied
e-mail: wied@statistik.tu-dortmund.de

A. Steland et al. (eds.), *Stochastic Models, Statistics and Their Applications*,
Springer Proceedings in Mathematics & Statistics 122,
DOI 10.1007/978-3-319-13881-7_40

A simple, empirical cornerstone in the analysis of international equilibrium is the concept of purchasing power parity (PPP). Loosely speaking PPP states that when expressed in common currency similar baskets of goods should have similar prices across countries. To fix concepts, denote with E_t the nominal exchange rate of the country considered vis-*à*-vis Germany at time t in DM per unit of local currency, with P_t the consumer price index (CPI) of the considered country at time t and with P_t^* the CPI of Germany at time t, i.e., we consider Germany as the base country in our empirical analysis. The real exchange rate *index* Q_t with respect to the base country Germany is then defined as

$$Q_t := \frac{E_t P_t}{P_t^*}. \tag{40.1}$$

Taking logarithms, indicated by lower cases letters, leads to

$$q_t = e_t + p_t - p_t^*. \tag{40.2}$$

Given that (logarithms of) price indices and (flexible) nominal exchange rates are often modeled as integrated processes, the empirical analysis of *weak* PPP is often phrased as a unit root or cointegration testing problem, see, e.g., Wagner [9]. In this setting PPP is said to hold in its weak form, if q_t is stationary. Clearly, the value of a RER *index* that corresponds to strong purchasing power parity is undetermined when price indices rather than actual price data are used.[1]

When considering countries with different levels of development, often in addition a linear trend is included to proxy for trend RER appreciation in catching-up economies, via, e.g., the Balassa–Samuelson effect. The Balassa–Samuelson effect has been shown to be sizeably present also in Europe, see, e.g., Wagner [8]. Typically, trend stationary log RERs are interpreted as being consistent with structural ("catching-up" or convergence) processes towards PPP.

The definition (40.2) of the log RER is often used as a basis for a cointegrating relationship between the prices indices and the nominal exchange rate of the form

$$p_t = c + \delta t + \beta_1 e_t + \beta_2 p_t^* + u_t, \tag{40.3}$$

where $\{u_t\}$ is a stationary process and where – obviously – a trend stationary log RER corresponds to the restrictions $\beta_1 = -1$, $\beta_2 = 1$.[2]

Given that RER misalignments are, as mentioned at the beginning, seen by many observers as a contributing factor to the crisis in some Euro area economies it is a natural question to ask whether a monitoring procedure detects structural changes in

[1] Strong PPP is typically defined as a RER equal to one and thus its logarithm equal to zero. Typically, however, due to the lack of actual price data empirical analysis is confined to work with RER indices where the "level information" is lost.

[2] It is natural to normalize the potential cointegrating relationship on the price index p_t – or p_t^* – rather than on the nominal exchange rate, which may have been fixed or almost fixed even before monetary unification (e.g., the exchange rate between the Austrian Schilling and the DM) and which is in that case almost by construction not an integrated process.

RERs away from trend stationarity respectively cointegration in the looser formulation (40.3). This is the question we analyze for the "first round" Euro area member states.[3] In the present situation there is, of course, some extra information concerning important dates available, most notably the fixing of the final nominal exchange rates between the 12 first round member states on December 31, 1998 and the introduction of the Euro as a virtual currency on January 1, 1999.[4] Consequently, we consider as the so-called calibration period for the monitoring procedure (see the description in the following section) a period until December 1998 for which trend stationarity of the log RER prevails. For all countries except Austria, where the calibration period is set to begin in January 1991 this means that the calibration period is set to begin in either February 1994 or February 1996. Subsequently, we monitor the behavior of the log RER from the beginning of the Euro area in January 1999 until July 2014 with the procedure described in the following section. The resulting *detection times*, if a break is detected, are the estimated break points at which a structural break in the considered RER indices has occurred.

40.2 A Brief Description of the Monitoring Procedure

The monitoring procedure used in this contribution has been developed in Wagner and Wied [10], where detailed descriptions as well as a detailed analysis of the asymptotic and finite sample properties of the procedure and tables with critical values are contained.

We consider, under the null hypothesis, a cointegrated system in triangular form:

$$y_t = D_t'\theta + X_t'\beta + u_t \tag{40.4}$$

$$X_t = X_{t-1} + v_t, \tag{40.5}$$

with observations available for $t = 1, \ldots, T$. Here D_t is a deterministic trend function, in our application given by constant and linear trend. The joint vector process $\{[u_t, v_t']'\}$ is, under the null hypothesis of a cointegrating relationship, an I(0) vector process, i.e.,

$$\frac{1}{\sqrt{T}} \sum_{t=1}^{\lfloor sT \rfloor} \begin{pmatrix} u_t \\ v_t \end{pmatrix} \Rightarrow_d \Omega^{1/2} W(s), \quad 0 \le s \le 1, \tag{40.6}$$

[3] These are Austria, Belgium, Finland, France, Germany, Greece, Ireland, Italy, Luxembourg, Netherlands, Portugal and Spain. Here it has to be noted that Luxembourg used the Belgian Franc prior to using the Euro and Greece was scheduled to join the Euro area in 2001 only. Thus, effectively we use the data for 11 countries as Luxembourg has to be excluded. As indicated in the main text we consider RERs with base country Germany. This is a natural choice given that Germany is the largest Euro area economy and the DM was the European anchor currency at the time. Alternatively, it is possible to calculate for each country its RER index with respect to the Euro area.

[4] The first quotation of the Euro was on January 4, 1999 and the physical introduction occurred at the beginning of 2002.

where $W(s)$ is a vector of standard Wiener processes, Ω is the so-called long-run variance matrix of $\{[u_t, v_t']'\}$ and $\lfloor z \rfloor$ denotes the integer part of a real number z. Throughout we assume that the long-run variance matrix of $\{v_t\}$ is positive definite, to exclude cointegration amongst the components of $\{X_t\}$. This implies that the relationship (40.4) is the only cointegrating relationship for the vector process $\{[y_t, X_t']'\}$. Under the alternative, the cointegrating relationship between $\{y_t\}$ and $\{X_t\}$ breaks down from some break fraction $\lfloor rT \rfloor$ onwards, for some $0 < m \leq r < 1$. Thus, the cointegrating relationship (40.4) turns into a spurious relationship at time point $\lfloor rT \rfloor$. For reasons discussed below, an initial period up to $\lfloor mT \rfloor$, in which the cointegrating relationship can safely be assumed to be present, is required. Clearly, in the absence of integrated regressors, with consequently $\dim(X_t) = 0$, the framework simplifies to monitoring trend stationarity of $\{y_t\}$.

To explain the idea of the monitoring procedure, assume for the moment that $\{u_t\}$ is observed and its long-run variance ω^2 known. Then the detector is given by

$$H^m(s) := \frac{1}{\omega^2}\left(\frac{1}{T}\sum_{i=\lfloor mT \rfloor+1}^{\lfloor sT \rfloor}\left(\frac{1}{\sqrt{T}}S_i\right)^2 - \frac{1}{T}\sum_{i=1}^{\lfloor mT \rfloor}\left(\frac{1}{\sqrt{T}}S_i\right)^2\right) \tag{40.7}$$

for $m \leq s \leq 1$ and with $S_i = \sum_{t=1}^{i} u_t$ denoting the partial sums of u_t. The detector is given by combining the well-known KPSS-statistic of Kwiatkowski et al. [3] for the null hypothesis of stationarity with the monitoring approach of Chu et al. [1]. Under the null hypothesis, it holds that

$$H^m(s) \Rightarrow_d \mathscr{H}^m(s) := \left(\int_m^s W(z)^2 dz - \int_0^m W(z)^2 dz\right). \tag{40.8}$$

Since under the alternative, the partial sum process as scaled in (40.7) diverges for $s > r$, the null hypothesis is rejected if an appropriately scaled version of the detector exceeds a critical value, i.e., when

$$T^m(s) := \left|\frac{H^m(s)}{w(s)}\right| > c(m, w, \alpha), \tag{40.9}$$

for some weighting function $w(s)$ and appropriate critical values $c(m, w, \alpha)$. The critical values are chosen such that with probability α, under the null hypothesis $T^m(s)$ is larger than $c(m, w, a)$ for some $s \in [m, 1]$. The first time $T^m(s)$ exceeds the critical value is called detection time. We use the same weighting function as Wagner and Wied [10], i.e., $w(s) = s^5$ in our specification with intercept and linear trend.

In practice, rather than the errors $\{u_t\}$ one only observes residuals, $\hat{u}_{t,m}$ say (indicating the dependence upon the calibration fraction m), and also the long-run variances are unknown and have to be estimated. It is well-known in the cointegration literature that due to the endogeneity of the regressors, as $\{u_t\}$ and $\{v_t\}$ are

allowed to be dynamically correlated, the OLS parameter estimators are consistent with their limiting distribution depending upon nuisance parameters relating to regressor endogeneity and error serial correlation. This, of course, implies that the limiting distribution of the properly scaled partial sum process of the OLS residuals also depends upon nuisance parameters. For this reason, residuals based on an estimator that corrects for endogeneity and that takes into account serial correlation have to be used. The literature offers several possibilities in this respect, with the most prominent being Fully Modified OLS (FM-OLS) of Phillips and Hansen [5], Dynamic OLS (D-OLS) of Saikkonen [6] and Integrated Modified OLS (IM-OLS) of Vogelsang and Wagner [7]. In our empirical analysis we use all three estimators.

Obtaining a nuisance parameter free limiting distribution of the properly scaled partial sum residual process rests upon appropriate estimation under the null hypothesis. This can be done in several ways, e.g., by using a moving window or by using a calibration period $1, \ldots, \lfloor mT \rfloor$ at the beginning of the sample. Wagner and Wied [10] opt, following Chu et al. [1], for the second route.

The null limiting distribution of $H^m(s)$, when calculated using residuals $\hat{u}_{t,m}$ as input, depends upon the deterministic components included, the number of integrated regressors, the calibration sample fraction m and the estimator chosen. Thus, critical values, for some chosen weighting function, can be obtained by simulation.

Looking at Eq. (40.4) it is clear that the monitoring procedure based on the partial sum residual process using parameter estimates based on the calibration period is not only consistent against the spurious regression alternative, but also against breaks in the parameters θ or β that occur at some time point $\lfloor rT \rfloor \geq \lfloor mT \rfloor$. In case of such a structural break the scaled partial sum residual process contains for observations later than $\lfloor rT \rfloor$ a divergent component, as $\hat{\theta}_m$ and $\hat{\beta}_m$, indicating in the notation here the dependence of the estimates on the calibration sample fraction, converge by construction to the pre-break values. Thus, detection of a structural change need not necessarily indicate a spurious relationship but can also indicate a structural change towards a cointegrating relationship with different slope and/or trend parameters.

40.3 Empirical Analysis

In Fig. 40.1 we display the monthly log RER indices over the period January 1991 to July 2014.[5] The red boxes included in the figure for each of the countries display the calibration period required for the monitoring procedure. The calibration period is set to end in December 1998 for all countries, i.e., it ends just before the Euro introduction at the beginning of 1999. For Austria the calibration period starts in January 1991, for Belgium, Finland, the Netherlands and Portugal in February 1994 and for France, Greece, Ireland, Italy and Spain in February 1996. This choice of the calibration period has been made to avoid the period of high exchange rate

[5]The price indices have been downloaded from the OECD webpage [4] and the exchange rates are taken from Eurostat [2].

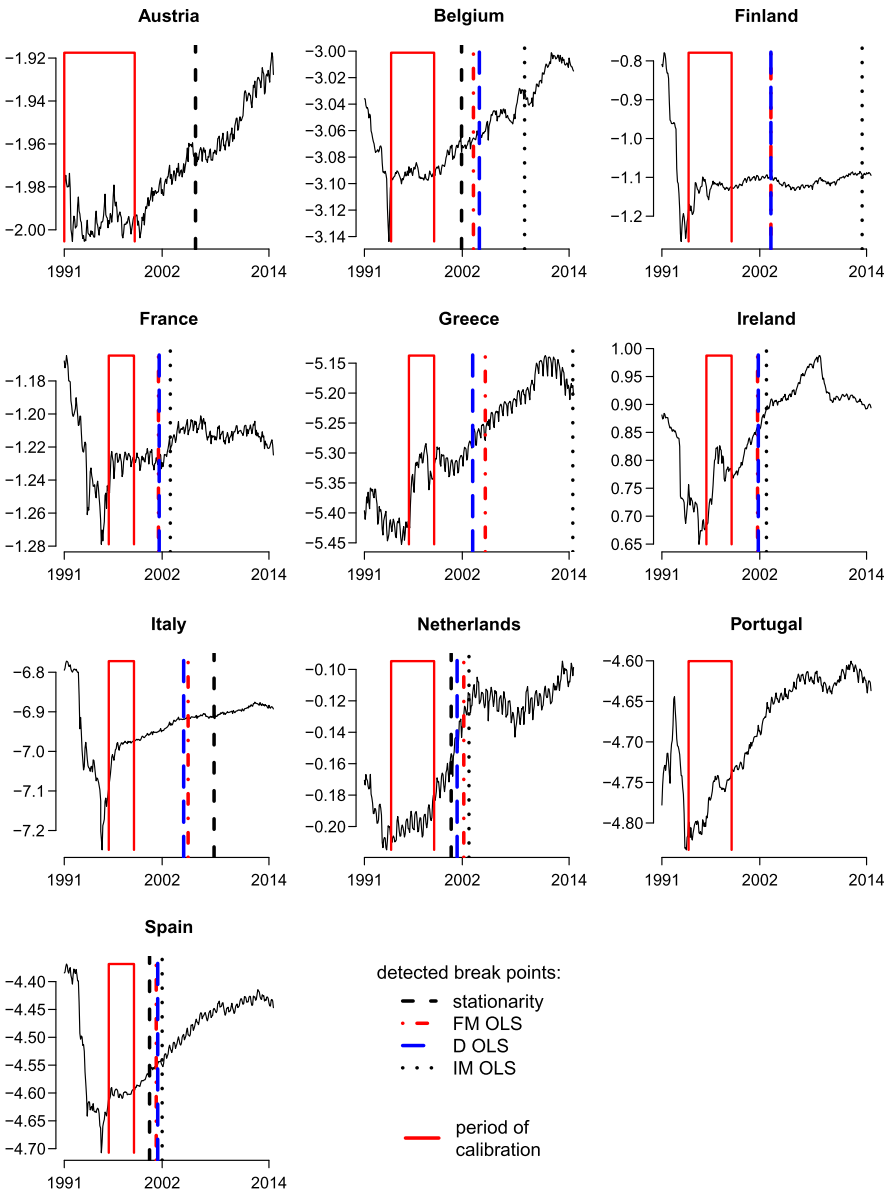

Fig. 40.1 Log RER indices, periods of calibration, and detected break points (intercept and linear trend)

volatility and instability in the aftermath of the 1992 UK currency crisis ("Black Wednesday"). Clearly, such a trimming is necessary as we need a period of stationarity, respectively cointegration, for calibration. The trimming also means that

Table 40.1 Detected break points

Country	*Calibration period*	*Trend stationarity*	*Cointegration* FM-OLS	*Cointegration* D-OLS	*Cointegration* IM-OLS
Austria	91(1)–98(12)	2005–10			
Belgium	94(2)–98(12)	2001–12	2003–04	2003–12	2009–01
Finland	94(2)–98(12)		2003–04	2003–04	2013–07
France	96(2)–98(12)		2001–08	2001–09	2002–12
Greece	96(2)–98(12)		2004–08	2003–03	2014–06
Ireland	96(2)–98(12)		2001–10	2001–11	2002–10
Italy	96(2)–98(12)	2007–11	2004–12	2004–06	
Netherlands	94(2)–98(12)	2000–10	2002–03	2001–06	2002–10
Portugal	94(2)–98(12)				
Spain	96(2)–98(12)	2000–08	2001–05	2001–07	2002–01

the calibration period is very short, which implies that parameter estimation can be expected to be imprecise.

Graphical inspection of the series shows that for most countries the RER appreciates with respect to Germany over the largest part of the period.[6] Also note that Finland's RER is the most stable one with respect to Germany after the period of Finland's severe crisis following the collapse of the Soviet Union.

In Table 40.1 we display the detected break points when trend stationarity of q_t as given in (40.2) or a cointegrating relationship of the form given in (40.3) is monitored. The main findings are: First, for all countries except Portugal a break point is detected. Second, all detected breaks occur well before the Euro area crisis, triggered in turn by the global financial crisis, has spread. Third, to a certain extent surprising, for four countries (Finland, France, Greece and Ireland) the more restrictive hypothesis of trend stationarity of the real exchange rate is not rejected, but the looser cointegration null hypothesis is. Fourth, by and large and as expected, the cointegration break dates are later than the stationarity break dates.

The detected break points are also indicated by vertical lines in Fig. 40.1. For some countries, e.g., Austria and France, the detected break points correspond to the first clearly "visible" changes in the behavior of the log RER indices. For other countries no such clear mapping between visual inspection and statistical analysis is present. A detailed investigation of the detected break points as well as an interpretation of the findings is beyond the scope of this paper that is merely meant to illustrate the cointegration monitoring procedure.

[6]Only at the end of the period one observes RER depreciation relative to Germany in the peripheral crisis countries like Greece, Ireland, Portugal and Spain in line with the deep recession and structural transformation process ongoing in these countries.

40.4 Summary and Conclusions

We have applied the stationarity and cointegration monitoring procedure of Wagner and Wied [10] to the RER indices, vis-*à*-vis Germany, of the first round Euro area member states. Clearly, our results are merely meant as an illustration and can only serve as one of many inputs into a thorough economic analysis of Euro area RER behavior. Nevertheless, the findings do indicate that methods for investigating the structural stability of stationary respectively cointegrating series may provide useful input for economic analysis. This in turn implies that several questions need to be addressed from an econometric theory perspective to provide potentially more useful tools: First, it may be relevant to flip null and alternative hypothesis, i.e., to monitor changes from I(1) or spurious to I(0) or cointegrating behavior to monitor entry into a period of "equilibrium". Second, multivariate monitoring procedures may be important for applied research in order to exploit the fact that often multiple series are affected at or at least around the same time. Exploiting also the cross-sectional dimension in such cases may lead to more powerful monitoring procedures. Third, especially important for monitoring data collected at higher frequencies, the effects of non-constant variances need to be investigated in detail. Robust, or correspondingly modified, procedures need to be developed for such situations.

Acknowledgements Financial support from Deutsche Forschungsgemeinschaft via the Collaborative Research Center 823: *Statistical Modelling of Nonlinear Dynamic Processes* (Projects A1, A3 and A4) is gratefully acknowledged. The second author additionally acknowledges financial support from the Jubiläumfonds of the Oesterreichische Nationalbank (Grant No. 15334). The authors furthermore thank two anonymous referees for valuable suggestions.

References

1. Chu C-SJ, Stinchcombe M, White H (1996) Monitoring structural change. Econometrica 64:1045–1065
2. Eurostat: Exchange rates. http://epp.eurostat.ec.europa.eu/portal/page/portal/exchange_rates/data/database. Cited 10 Sep 2014
3. Kwiatkowski D, Phillips PCB, Schmidt P, Shin Y (1992) Testing the null hypothesis of stationarity against the alternative of a unit root. J Econ 54:159–178
4. OECD (10 Sep 2014) Main economic indicators. http://stats.oecd.org/Index.aspx?DataSetCode=MEI_PRICES. Cited 10 Sep 2014
5. Phillips PCB, Hansen BE (1990) Statistical inference in instrumental variables regression with I(1) processes. Rev Econ Stud 57:99–125
6. Saikkonen P (1991) Asymptotically efficient estimation of cointegrating regressions. Econom Theory 7:1–21
7. Vogelsang TJ, Wagner M (2014) Integrated modified OLS estimation and fixed-*b* inference for cointegrating regressions. J Econ 178:741–760
8. Wagner M (2005) The Balassa–Samuelson effect in "East & West": differences and similarities. Rev Econ 56:230–248
9. Wagner M (2008) On PPP, unit roots and panels. Empir Econ 35:229–249
10. Wagner M, Wied D (2014) Monitoring stationarity and cointegration. SFB823 discussion paper 23/14. http://hdl.handle.net/2003/33430

Chapter 41
Approximating Markov Chains for Bootstrapping and Simulation

Roy Cerqueti, Paolo Falbo, Gianfranco Guastaroba, and Cristian Pelizzari

Abstract In this work we develop a bootstrap method based on the theory of Markov chains. The method moves from the two competing objectives that a researcher pursues when performing a bootstrap procedure: (i) to preserve the structural similarity – in statistical sense – between the original and the bootstrapped sample; (ii) to assure a diversification of the latter with respect to the former. The original sample is assumed to be driven by a Markov chain. The approach we follow is to implement an optimization problem to estimate the memory of a Markov chain (i.e. its order) and to identify its relevant states. The basic ingredients of the model are the transition probabilities, whose distance is measured through a suitably defined functional. We apply the method to the series of electricity prices in Spain. A comparison with the Variable Length Markov Chain bootstrap, which is a well established bootstrap method, shows the superiority of our proposal in reproducing the dependence among data.

41.1 Introduction

The heart of the bootstrap – introduced by Efron [10] – consists of resampling some given observations with the purpose of obtaining a good estimation of the statistical properties of the original population. Among the different bootstrap methods, a

R. Cerqueti
Department of Economics and Law, University of Macerata, Via Crescimbeni, 20–62100 Macerata MC, Italy
e-mail: roy.cerqueti@unimc.it

P. Falbo (✉) · G. Guastaroba · C. Pelizzari
Department of Economics and Management, University of Brescia, Contrada S. Chiara, 50–25122 Brescia BS, Italy
e-mail: paolo.falbo@unibs.it

G. Guastaroba
e-mail: gianfranco.guastaroba@unibs.it

C. Pelizzari
e-mail: cristian.pelizzari@unibs.it

A. Steland et al. (eds.), *Stochastic Models, Statistics and Their Applications*, Springer Proceedings in Mathematics & Statistics 122,
DOI 10.1007/978-3-319-13881-7_41

prominent role is played by those based on Markov chains (see e.g. Athreya and Fuh [2]; Bühlmann [4]; Horowitz [11]; Paroditis and Politis [13, 14]; Anatolyev and Vasnev [1]; Bertail and Clémençon [3]). The major advantage of this approach is that it is entirely data driven, so that it can smoothly capture the dependence structure of an observed time series, releasing a researcher from the risk of wrongly specifying the model, and from the difficulties of estimating its parameters.

In this paper we develop an original general approach to determine the relevant states and the memory (i.e. the order) of a Markov chain. The bootstrap procedure advanced here works similarly to that of Anatolyev and Vasnev [1], who propose a *Markov chain bootstrap* where states correspond to the intervals resulting from a partition of the state space (of an observed time series) into a fixed number of quantiles. However, differently from that work, our proposal places much greater care in identifying the states of the Markov chain. In particular, the approach we propose is based on the joint estimation of the relevant states and of the order of a Markov chain through an optimization problem. The solution identifies the partition which groups the states with the most similar transition probabilities. In this way the resulting groups emerge as the relevant states, that is the states which significantly influence the conditional distribution of the process. In this work we also extend theoretically the analysis in Cerqueti et al. [6–8] by introducing L^p norm based distance measures. We also show that the minimization of the objective function represented by the distance measure of the partitions, which is based on the transition probabilities of the states, corresponds to the minimization of the information loss function in the sense of Kolmogorov [12]. The optimization problem includes also a "multiplicity" constraint, which controls for a sufficient diversification of the resampled trajectories. Our proposal exploits the powerful conditioning tool provided by the transition probability matrix of Markov chains to model correctly and efficiently random processes with arbitrary dependence structure. The results shown in the application to the electricity prices of the Spanish market confirm the better performances of the method proposed here with respect to a well established bootstrap approach, such as the Variable Length Markov Chain (VLMC) bootstrap of Bühlmann and Wyner [5].

The paper is organized as follows. Section 41.2 introduces the settings of the model. Section 41.3 clarifies the theoretical foundation of the optimization problem we deal with. Section 41.4 formalizes the optimization problem. Section 41.5 provides a validation of the theoretical results through numerical experiments based on real data. Section 41.6 offers some conclusive remarks.

41.2 Model

We suppose that we observe N realizations homogeneously spaced in time of a data generating process and we introduce the set of such time-ordered observations as $E = \{y_1, \ldots, y_N\}$. There exist $J_N \geq 1$ distinct states $a_1, \ldots, a_{J_N} \in E$. The corresponding subsets of E, denoted as $E_1, \ldots, E_{J_N}$ and defined as

$$E_z = \{y_i \in E \mid y_i = a_z\}, \quad z = 1, \ldots, J_N, \ i = 1, \ldots, N,$$

constitute a partition of E. Moreover, fixing $z = 1, \ldots, J_N$, then the frequency of state a_z in the observed time series E is the cardinality of E_z. Let $A = \{a_1, \ldots, a_{J_N}\}$ be the range of the observed time series.

We now consider a time-homogeneous Markov chain of order $k \geq 1$, denoted as $X = \{X(t), t \geq 0\}$, with state space A. To ease the notation, in the following we will simply write Markov chain instead of time-homogeneous Markov chain. The k-lag memory of the Markov chain implies that the transition probability matrix should account for conditioning to trajectories of length k. Therefore, we refer hereafter to a *k-path transition probability matrix*.

Let us consider $a_z \in A$ and $\mathbf{a}_h = (a_{h,k}, \ldots, a_{h,1}) \in A^k$. The row vector $\mathbf{a}_h$ is the ordered set of k states $a_{h,w} \in A$, $w = 1, \ldots, k$, listed, in a natural way, from the furthest to the closest realization of the chain. The row vector $\mathbf{a}_h$ will be called k-path. This ordering of the realizations will be maintained throughout the paper. The Markov chain has transition probability from k-path $\mathbf{a}_h$ to state a_z given by

$$P(a_z|\mathbf{a}_h) = P\big(X(t) = a_z | X(t-1) = a_{h,1}, \ldots, X(t-k) = a_{h,k}\big). \quad (41.1)$$

According to Ching et al. [9], we estimate $P(a_z|\mathbf{a}_h)$ with the empirical frequencies $f(a_z|\mathbf{a}_h)$ related to N realizations of the phenomenon. For the sake of simplicity, we avoid introducing throughout the paper a specific notation for the estimates of the probabilities, therefore we estimate $P(a_z|\mathbf{a}_h)$ by

$$P(a_z|\mathbf{a}_h) = \begin{cases} \frac{f(a_z|\mathbf{a}_h)}{\sum_{j:a_j \in A} f(a_j|\mathbf{a}_h)}, & \text{if } \sum_{j:a_j \in A} f(a_j|\mathbf{a}_h) \neq 0, \\ 0, & \text{otherwise.} \end{cases}$$

Let us now introduce the set Λ of the partitions of A. A generic element $\lambda \in \Lambda$ can be written as $\lambda = \{A_1, \ldots, A_{|\lambda|}\}$, where $|\lambda|$ is the cardinality of λ, with $1 \leq |\lambda| \leq J_N$, and $\{A_q\}_{q=1,\ldots,|\lambda|}$ is a partition of nonempty subsets of A. The cardinality of Λ is $B(J_N)$, i.e. the Bell number of the J_N elements in set A.

Extending our notation to a multidimensional context, we consider the set Λ_k of k-dimensional partitions. The set Λ_k contains the partitions we will focus on in the present paper. A k-dimensional partition of Λ_k is denoted as $\boldsymbol{\lambda}$ and is defined as

$$\boldsymbol{\lambda} = \big\{A_{q_k,k} \times \cdots \times A_{q_w,w} \times \cdots \times A_{q_1,1} \,|\, q_w \in \big\{1, \ldots, |\lambda_w|\big\},\ w = 1, \ldots, k\big\},$$

where $A_{q_w,w}$ is a class of the partition λ_w and λ_w is a partition of A at time lag w. A k-dimensional partition of Λ_k can also be (more easily) represented by the k-tuple of the partitions λ_w, $w = 1, \ldots, k$, which the classes $A_{q_w,w}$ belong to. So the partition $\boldsymbol{\lambda}$ can also be identified with the notation $\boldsymbol{\lambda} = (\lambda_k, \ldots, \lambda_w, \ldots, \lambda_1)$. Such notation describes the fact that $\boldsymbol{\lambda}$ is a time-dependent partition of A, i.e. A is partitioned in different ways for each time lag w, $w = 1, \ldots, k$. The cardinality of Λ_k is $[B(J_N)]^k$, the cardinality of the partition $\boldsymbol{\lambda}$ is $|\boldsymbol{\lambda}| = \prod_{w=1}^{k} |\lambda_w|$.

We refer to the probability law P introduced in (41.1) and define

$$P(a_z|\mathbf{A}_q) = P\big(X(t) = a_z | X(t-1) \in A_{q_1,1}, \ldots, X(t-k) \in A_{q_k,k}\big), \quad (41.2)$$

where $\mathbf{A}_q = A_{q_k,k} \times \cdots \times A_{q_w,w} \times \ldots \times A_{q_1,1} \subseteq A^k$, and $a_z \in A$. The quantity in (41.2) is the transition probability to reach state a_z at time t after the process has

been in the classes $A_{q_k,k}, \ldots, A_{q_1,1}$ in the previous k times. The transition probabilities $P(a_z|\mathbf{A}_q)$ in (41.2) are estimated, as usual, through the empirical frequencies:

$$P(a_z|\mathbf{A}_q) = \begin{cases} \frac{\sum_{i:\mathbf{a}_i \in \mathbf{A}_q} f(a_z|\mathbf{a}_i)}{\sum_{i:\mathbf{a}_i \in \mathbf{A}_q} \sum_{j:a_j \in A} f(a_j|\mathbf{a}_i)}, & \text{if } \sum_{i:\mathbf{a}_i \in \mathbf{A}_q} \sum_{j:a_j \in A} f(a_j|\mathbf{a}_i) \neq 0, \\ 0, & \text{otherwise.} \end{cases}$$

The quantities $P(a_z|\mathbf{A}_q)$ estimate a new transition probability matrix. To keep the notation as simple as possible, we continue to refer to this matrix as to the k-path transition probability matrix.

We deal in our paper with a couple of questions related to finding the Markov chain which best describes the observed time series E:

- Which is the optimal k?
- Which is the optimal clustering of A for each time lag w, with $w = 1, \ldots, k$?

41.3 Theoretical Foundation of the Optimization Problem

In the context of bootstrapping, the conflicting scopes of a resampling procedure are two: on the one side, to maintain the statistical properties of the original sample (similarity); on the other side, to allow for a sufficient level of diversification between the original and the bootstrapped sample (multiplicity). In our model an optimal clustering procedure of the state space of a Markov chain – based on the fulfillment of similarity and multiplicity requirements – is implemented, to gain mathematical tractability when resampling.

The theoretical framework closer to our proposal is the field of information theory, with specific reference to information loss. We can, in general, define a functional space $\mathscr{G}$ whose elements g act on the Markov chain X by defining a new Markov chain $\tilde{X}$. The states of $\tilde{X}$ are the elements of a partition of A^k. There is a clear bijection between the g of $\mathscr{G}$ and the partitions λ_g of A^k, and they are associated to a specific amount of information. Let us write $\tilde{X} = X|\lambda_g$ to formalize that the new Markov chain is X conditioned to the information generated by the partition λ_g.

Since merging two k-paths cancels part of the information on the transition probabilities available letting them distinct, we can say that the partitions λ_g imply in general information loss. This argument is in line with Kolmogorov [12].

In order to measure such an information loss, a nonnegative functional $\eta_X \in [0, \bar{\eta}]$ can be introduced, such that $\eta_X(\tilde{X})$ represents a *distance measure* between X and $\tilde{X}$, which increases as the loss of information does. If $\eta(\tilde{X}) = 0$, no information is lost, while $\eta_X(\tilde{X}) = \bar{\eta}$ means that $\tilde{X}$ is generated by a partition providing the maximum level of information loss (no information left in passing from X to $\tilde{X}$).

The consistency requirements in the boundary situations of 0 and $\bar{\eta}$ lead to specific situations in our setting. We list them below, along with a brief explanation.

1. $\eta_X(X) = 0$. This is the case of full information and occurs when $\tilde{X} = X$. In this case the partition λ_g of the state space is the finest one: λ_g is the partition keeping separate all the states of the Markov chain (*singleton partition*).
2. If $\lambda_g = \{\emptyset, \Omega\}$, where Ω represents the sample space of the probability space where the Markov chain is defined, then $\eta_X(\tilde{X})$ attains its maximum. In this case the maximum level of information is lost. In fact, the corresponding partition λ_g collects all the elements of the state space in a unique set (*all-comprehensive partition*).

In the following section we will introduce a distance indicator, d_λ, and a multiplicity measure, m_λ, which will be used to measure similarity and multiplicity, respectively. They are two specific (information loss) distance measures η, which indeed satisfy conditions 1. and 2.

It can be expected that a partition of states of a Markov chain minimizing, in a controlled way, an information loss distance measure will condition the evolution of the bootstrapped samples more consistently than it would occur if that partition had been organized otherwise.

41.4 Optimization Problem: A Formalization

The concept of optimality must be intended as satisfying the requirements of the bootstrap procedures of statistical closeness between the original and the bootstrapped sample – minimization of a distance indicator – and a certain degree of diversification – constraint on the level of a multiplicity measure. A constrained minimization problem can be defined following this line. We enter into its details.

41.4.1 L^p-Type Distance Indicator

We define an L^p-type measure of the multidimensional class $\mathbf{A}_q$ as follows:

$$d_{\mathbf{A}_q} = \max_{i,j:\mathbf{a}_i,\mathbf{a}_j \in \mathbf{A}_q} d_{i,j}, \tag{41.3}$$

where

$$d_{i,j} = \sum_{z=1}^{J_N} \left| P(a_z|\mathbf{a}_i) - P(a_z|\mathbf{a}_j) \right|^p, \quad p > 0.$$

In this case, we preserve the similarity by imposing that the classes of a suitable partition have a low value of the indicator defined in (41.3). We can finally characterize the distance d_λ of partition $\boldsymbol{\lambda}$ with the average value of its classes distances:

$$d_{\boldsymbol{\lambda}} = \frac{1}{C} \cdot \sum_{q=1}^{|\boldsymbol{\lambda}|} d_{\mathbf{A}_q} \cdot |\mathbf{A}_q|,$$

where $|\mathbf{A}_q|$ is the cardinality of partition class $\mathbf{A}_q$ and $C = \sum_{q=1}^{|\boldsymbol{\lambda}|} |\mathbf{A}_q|$.

41.4.2 L^r-Type Multiplicity Measure

The multiplicity measures we propose are based on the size of the partition classes.

Let us define $l_{\boldsymbol{\lambda}}$ an *absolute multiplicity measure* of the partition $\boldsymbol{\lambda}$:

$$l_{\boldsymbol{\lambda}} = \sum_{q=1}^{|\boldsymbol{\lambda}|} |\mathbf{A}_q|^r, \quad r > 0.$$

We define the *relative multiplicity measure* m_{λ}, related to the partition $\boldsymbol{\lambda}$, by normalizing l_{λ} as follows:

$$m_{\boldsymbol{\lambda}} = \frac{\sqrt[r]{l_{\boldsymbol{\lambda}}} - \sqrt[r]{C}}{C - \sqrt[r]{C}}.$$

41.4.3 Optimization Problem

We now present the optimization problem based on the similarity and multiplicity criteria developed so far.

Definition 41.1 Consider $\gamma \in [0, 1]$, $k^* \in \{1, \ldots, N\}$, and $\boldsymbol{\lambda}^* = (\lambda^*_{k^*}, \ldots, \lambda^*_1) \in \Lambda_{k^*}$. The couple $(k^*, \boldsymbol{\lambda}^*)$ is said to be d-γ-optimal when it is the solution of the following minimization problem:

$$\min_{(k,\boldsymbol{\lambda}) \in \{1,\ldots,N\} \times \Lambda_k} d_{\boldsymbol{\lambda}} \quad \text{s.t.} \quad m_{\boldsymbol{\lambda}} \geq \gamma. \tag{41.4}$$

In Definition 41.1 we have that k^* is the optimal order of a Markov chain describing the evaluative phenomenon. Moreover, $\boldsymbol{\lambda}^*$ provides the optimal time-dependent clustering of the state space A, in order to have an approximation of the k^*-path transition probability matrix.

According to the definitions of $d_{\boldsymbol{\lambda}}$ and $m_{\boldsymbol{\lambda}}$, we can briefly discuss the optimization problem. Letting the multiplicity measure reach its minimum ($\gamma = 0$) is equivalent to allow for the singleton partition, which ensures the minimum distance ($d_{\boldsymbol{\lambda}} = 0$). Letting $\gamma = 1$ corresponds to forcing the maximum level of multiplicity. This boundary in our case is satisfied only by the all-comprehensive partition, when the distance indicator takes its maximum value.

Table 41.1 Percentiles and percentile ranks of the original daily Spanish electricity prices. Comparison between the VLMC bootstrap and the bootstrap method proposed here (case $p = 1$ and $r = 2$)

Statistics	Value[a]	VLMC bootstrap			Our bootstrap		
		5th pctl[b]	95th pctl[b]	Pctl rank[c]	5th pctl[b]	95th pctl[b]	Pctl rank[c]
Average	29.692	28.707	30.704	53	26.574	32.074	57
Standard dev.	9.570	8.157	10.581	72	7.113	10.979	68
Skewness	1.381	0.414	1.953	68	0.114	2.033	66
Kurtosis	5.081	0.293	9.352	59	−0.571	9.327	63
Minimum	5.469	5.726	9.311	0	4.546	11.754	58
Maximum	103.758	66.604	110.968	73	50.971	111.382	71
Aut. at lag 1	0.818	0.737	0.817	95	0.737	0.859	62
Aut. at lag 2	0.706	0.579	0.702	95	0.579	0.772	61
Aut. at lag 3	0.706	0.463	0.615	99	0.547	0.745	63
Aut. at lag 4	0.667	0.371	0.540	99	0.529	0.733	63
Aut. at lag 5	0.661	0.297	0.476	99	0.520	0.730	62
Aut. at lag 6	0.721	0.236	0.423	99	0.614	0.764	65
Aut. at lag 7	0.802	0.187	0.378	99	0.728	0.829	68
Aut. at lag 8	0.683	0.148	0.338	99	0.581	0.727	64

[a]Value is the actual value of the statistic observed in the original sample

[b]pctl stands for percentile

[c]pctl rank stands for percentile rank of the original sample value

41.5 Empirical Validation of the Model

This section aims at comparing the proposed method with another well established bootstrap procedure, namely the Variable Length Markov Chain (VLMC) bootstrap (Bühlmann and Wyner [5]). Only the case of $p = 1$ and $r = 2$ is discussed, to further support the strength of the method. Moreover, our method is bounded to order $k = 7$, while VLMC self-calibrates k. The original sample is the daily Mibel Spanish Electric System Arithmetic Average Price (euros per MWh) from January 2nd, 1998 to December 31st, 2003.

To assess the quality of the method, we analyze the statistical properties of the bootstrapped samples and compare them with the ones of the original sample. To this goal, we calculate the following statistics: average, standard deviation, skewness, kurtosis, minimum, maximum, and autocorrelations at lag k (where $k = 1, \ldots, 8$).

The comparison focuses on the percentile rank that the original sample takes with respect to the bootstrap distribution. A package written in R named "VLMC" (available at the web page http://cran.r-project.org/) was used to generate the bootstrapped samples for VLMC. For what concerns our method, the optimization problem (41.4) was solved heuristically by means of a Tabu Search algorithm in order to control for

its computational complexity (see Cerqueti et al. [6]). The number of bootstrapped samples is 5000.

The results of the comparison in Table 41.1 show that VLMC regularly generates narrower ranges between the 5th and the 95th percentiles than our method. However, they are only seldom consistent. In particular, autocorrelations at all lags are severely under-replicated in the VLMC bootstrapped samples. Such results confirm the expectation that the method proposed here, thanks to the minimum information loss pursued in our optimization problem, generates bootstrapped samples reproducing more carefully the original dependence among the data of an original sample.

41.6 Conclusive Remarks

This paper proposes an optimization problem to the goal of estimating the dimensions of the transition probability matrix of a Markov chain for simulation and bootstrap purposes. The optimization problem here formalized extends that presented in Cerqueti et al. [7], in that it introduces distance measures of L^p (L^r) type. The satisfactorily results obtained in the above-mentioned paper are theoretically further improved. The model is grounded on information theory, and it has been numerically validated through an experiment based on real data.

References

1. Anatolyev S, Vasnev A (2002) Markov chain approximation in bootstrapping autoregressions. Econ Bull 3(19):1–8
2. Athreya KB, Fuh CD (1992) Bootstrapping Markov chains: countable case. J Stat Plan Inference 33(3):311–331
3. Bertail P, Clémençon S (2007) Second-order properties of regeneration-based bootstrap for atomic Markov chains. Test 16:109–122
4. Bühlmann P (1997) Sieve bootstrap for time series. Bernoulli 3(2):123–148
5. Bühlmann P, Wyner AJ (1999) Variable length Markov chains. Ann Stat 27(2):480–513
6. Cerqueti R, Falbo P, Guastaroba G, Pelizzari C (2013) A tabu search heuristic procedure in Markov chain bootstrapping. Eur J Oper Res 227(2):367–384
7. Cerqueti R, Falbo P, Pelizzari C (2010) Relevant states and memory in Markov chain bootstrapping and simulation. Munich Personal RePEc Archive Paper 46254, University Library of Munich, Germany
8. Cerqueti R, Falbo P, Pelizzari C, Ricca F, Scozzari A (2012) A mixed integer linear programming approach to Markov chain bootstrapping. Quaderni del Dipartimento di Economia e Diritto dell'Università degli Studi di Macerata, n. 67, Università degli Studi di Macerata, Macerata, Italy
9. Ching W-K, Ng MK, Fung ES (2008) Higher-order multivariate Markov chains and their applications. Linear Algebra Appl 428(2-3):492–507
10. Efron B (1979) Bootstrap methods: another look at the jackknife. Ann Stat 7(1):1–26
11. Horowitz JL (2003) Bootstrap methods for Markov processes. Econometrica 71(4):1049–1082
12. Kolmogorov AN (1965) Three approaches to the quantitative definition of information. Probl Inf Transm 1(1):3–11

13. Paparoditis E, Politis DN (2001) Tapered block bootstrap. Biometrika 88(4):1105–1119
14. Paparoditis E, Politis DN (2001) A Markovian local resampling scheme for nonparametric estimators in time series analysis. Econom Theory 17(3):540–566

Chapter 42
Statistical Method to Estimate a Regime-Switching Lévy Model

Julien Chevallier and Stéphane Goutte

Abstract A regime-switching Lévy model combines jump-diffusion under the form of a Lévy process, and Markov regime-switching where all parameters depend on the value of a continuous time Markov chain. We start by giving general stochastic results. Estimation is performed following a two-step procedure. The EM-algorithm is extended to this new class of jump-diffusion regime-switching models. An empirical application is dedicated to the study of Asian equity markets.

42.1 Introduction

This paper proposes new statistical methods to estimate regime-switching Lévy models that are both efficient and practical. Our goal lies in estimating a Markov-switching model augmented by jumps, under the form of a Lévy process. This particular class of stochastic processes is entirely determined by a drift, a scaled Brownian motion and an independent pure-jump process. The estimation strategy relies on a two-step procedure: by estimating first the diffusion parameters in presence of switching, and second the Lévy jump component by means of separate Normal Inverse Gaussian distributions fitted to each regime. Computationally, the EM algorithm is extended to this new class of jump-diffusion regime-switching model. An empirical application is proposed for Asian equity markets.

J. Chevallier
Université Paris 8, Saint-Denis, France
e-mail: julien.chevallier04@univ-paris8.fr

J. Chevallier
IPAG Business School (IPAG Lab), Paris, France

S. Goutte (✉)
Université Paris 8 (LED), Saint-Denis, France
e-mail: stephane.goutte@univ-paris8.fr

S. Goutte
ESG Management School (ESG MS), Paris, France

A. Steland et al. (eds.), *Stochastic Models, Statistics and Their Applications*,
Springer Proceedings in Mathematics & Statistics 122,
DOI 10.1007/978-3-319-13881-7_42

The remainder of the paper is structured as follows. Section 42.2 introduces the rationale behind Lévy and Markov-switching modeling. Section 42.3 develops the stochastic model. Section 42.4 details the estimation method. Section 42.5 provides an empirical application. Section 42.6 concludes.

42.2 Background

In this preliminary section, we review the basic intuitions behind our modeling strategy. Lévy processes have many appealing properties in financial economics, and constitute the first building block of our model. Second, we recall the very intuitive interpretation of the aperiodic, irreducible and ergodic Markov chain.

Jumps are discontinuous variations in assets' prices. By nature, jumps consist of rare and dramatic events that dominate the trading days during which they occur. In financial economics, jumps are expected to appear due to dividend payments, microcrashes due to short-term liquidity challenges or news, such as macroeconomic announcements. Such events have been made partly accountable for the non-Gaussian feature of financial returns, as they can only be captured by fat-tailed distributions. Hence, by definition, jumps generate returns that lie outside their usual scale of value. Jumps matter both to investors, and to countries that produce and consume commodities. In the case of investors, jumps can be either significant investing opportunities or massive threats to profits and losses, depending on each investor's positioning. In each case, jumps modify expected returns in an unexpected way. The same logic applies to producers and consumers: sudden and large variation in asset prices endanger the forecasting of sales profit or the hedging strategies put in place to smooth costs. Hence, the higher the jump activity, the higher the uncertainty for market participants. This is why measuring jumps matters. Given that jumps are dramatic events from a financial history perspective, building statistical evidence around them seems of primary importance. Lévy processes can be thought of as a combination of a diffusion process and a jump process. Both Brownian motion (i.e. a pure diffusion process) and Poisson processes (i.e. pure jump processes) are Lévy processes. As such, Lévy processes represent a tractable extension of Brownian motion to infinitely divisible distributions. In addition, Lévy processes allow the modeling of discontinuous sample paths, whose properties match those of empirical phenomena such as financial time series.

The normal behavior of economies is occasionally disrupted by dramatic events that seem to produce quite different dynamics for the variables that economists study. Chief among these is the business cycle, in which economies depart from their normal growth behavior and a variety of indicators go into decline. The regime at any given date is presumed to be the outcome of a Markov chain whose realizations are unobserved to the econometrician. The task facing the econometrician is to characterize the regimes and the law that governs the transitions between them. These parameters estimates can then be used to infer which regime the process was in at any historical date. Although the state of the business cycle is not observed

directly by the econometrician, the statistical model implies an optimal way to form an inference about the unobserved variable and to evaluate the likelihood function of the observed data.

In this paper, we illustrate the statistical methods that allow to combine Markov-switching models with Lévy jump modeling.

42.3 The Stochastic Model

Let $(\omega, \mathscr{F}, P)$ be a filtered probability space and T be a fixed terminal time horizon. We propose in this paper to model the dynamic of a sequence of historical values of price using a regime-switching stochastic jump-diffusion. This model is defined using the class of Lévy processes.

Definition 42.1 A Lévy process L_t is a stochastic process such that

1. $L_0 = 0$.
2. For all $s > 0$ and $t > 0$, we have that the property of stationary increments is satisfied. i.e. $L_{t+s} - L_t$ as the same distribution as L_s.
3. The property of independent increments is satisfied. i.e. for all $0 \leq t_0 < t_1 < \cdots < t_n$, we have that $L_{t_i} - L_{t_{i-1}}$ are independent for all $i = 1, \ldots, n$.
4. L has a Cadlag paths. This means that the sample paths of a Lévy process are right continuous and admit a left limits.

Remark 42.1 In a Lévy process, the discontinuities occur at random times.

Definition 42.2 Let $(Z_t)_{t\in[0,T]}$ be a continuous time Markov chain on finite space $\mathscr{S} := \{1, 2, \ldots, K\}$. Denote $\mathscr{F}_t^Z := \{\sigma(Z_s); 0 \leq s \leq t\}$, the natural filtration generated by the continuous time Markov chain Z. The generator matrix of Z, denoted by Π^Z, is given by $\Pi_{ij}^Z \geq 0$, if $i \neq j$ for all $i, j \in \mathscr{S}$ and $\Pi_{ii}^Z = -\sum_{j\neq i} \Pi_{ij}^Z$ otherwise.

Remark 42.2 The quantity Π_{ij}^Z represents the switch from state i to state j.

Let us define the regime-switching Lévy Model:

Definition 42.3 For all $t \in [0, T]$, let Z_t be a continuous time Markov chain on finite space $\mathscr{S} := \{1, \ldots, K\}$ defined as in Definition 42.2. A regime-switching model is a stochastic process (X_t) which is solution of the stochastic differential equation given by

$$dX_t = \kappa(Z_t)\big(\theta(Z_t) - X_t\big)dt + \sigma(Z_t)dY_t \tag{42.1}$$

where $\kappa(Z_t)$, $\theta(Z_t)$ and $\sigma(Z_t)$ are functions of the Markov chain Z. Hence, they are constants which take values in $\kappa(\mathscr{S})$, $\theta(\mathscr{S})$ and $\sigma(\mathscr{S})$. Thus, $\kappa(\mathscr{S}) := \{\kappa(1), \ldots, \kappa(K)\} \in \mathbb{R}^{K^*}$, $\theta(\mathscr{S}) := \{\theta(1), \ldots, \theta(K)\}$ and $\sigma(\mathscr{S}) := \{\sigma(1), \ldots, \sigma(K)\} \in \mathbb{R}^{K^+}$. And finally, Y is a stochastic process which could be a Brownian motion or a Lévy process.

Remark 42.3 The following classic notations apply: κ denotes the mean-reverting rate; θ denotes the long-run mean; $\sigma_{\cdot}$ denotes the volatility of X.

Remark 42.4 In this model, there are two sources of randomness: the stochastic process Y appearing in the dynamics of X, and the Markov chain Z. There exists one randomness due to the market information which is the initial continuous filtration $\mathscr{F}$ generated by the stochastic process Y; and another randomness due to the Markov chain Z, $\mathscr{F}^Z$. Moreover, the Markov chain Z infers the unobservable state of the economy, i.e. expansion or recession. The processes Y^i estimated in each state, where $i \in \mathscr{S}$, capture: a different level of volatility in the case of Brownian motion (i.e. $Y^i \equiv W^i$), or a different jump intensity level of the distribution (and a possible skewness) in the case of Lévy process (i.e. $Y^i \equiv L^i$).

Barndorff–Nielsen [1] recalls the main properties of the Normal Inverse Gaussian (NIG) distribution, which is used as the Lévy distribution in this paper. The NIG density belongs to the family of normal variance-mean mixtures, i.e. one of the most commonly used parametric densities in financial economics. The NIG is a good alternative to the normal distribution since: (i) its distribution can model the heavy tails, kurtosis, and jumps, and (ii) the parameters of NIG distribution can be solved in a closed form.

42.4 Estimation

This section covers the methodology pertaining to the estimation task. In the first sub-section, we extend the EM algorithm to the class of Lévy regime-switching and explain how the likelihood can be evaluated. In the following sub-sections, the two-step estimation strategy as well as the initialization choice for the parameters are detailed.

The Expectation–Maximization algorithm used to estimate the regime-switching Lévy model in this paper is a generalization and extension of the EM-algorithm developed in Hamilton [3] and [4].

Our aim is to fit a regime-switching Lévy model such as (42.1) where the stochastic process Y is a Lévy process that follows a Normal Inverse Gaussian (NIG) distribution. Thus the optimal set of parameters to estimate is $\hat{\Theta} := (\hat{\kappa}_i, \hat{\theta}_i, \hat{\sigma}_i, \hat{\alpha}_i, \hat{\beta}_i, \hat{\delta}_i, \hat{\mu}_i, \hat{\Pi})$, for $i \in \mathscr{S}$.

We have the three parameters of the dynamics of X, the four parameters of the density of the Lévy process L, and the transition matrix of the Markov chain Z. Because the number of parameters grows rapidly in this class of jump-diffusion regime-switching models, direct maximization of the total log-likelihood is not practicable. To bypass this problem, we propose a method in two successive steps to estimate the global set of parameters.

Step 1: Estimation of the regime-switching model (42.1) in the Brownian case
Following the methodology of Janczura and Weron [6], we first take for the stochastic process Y a Brownian motion W. Moreover, suppose that the size of

historical data is $M+1$. Let Γ denote the corresponding increasing sequence of time from which the data values are taken:

$$\Gamma = \{t_j; 0 = t_0 \leq t_1 \leq \ldots t_{M-1} \leq t_M = T\}, \quad \text{with } \Delta_t = t_j - t_{j-1} = 1.$$

The discretized version of model (42.1) writes

$$X_{t+1} = \kappa(Z_t)\theta(Z_t) + \big(1 - \kappa(Z_t)\big)X_t + \sigma(Z_t)\varepsilon_{t+1}, \tag{42.2}$$

where $\varepsilon_t \sim \mathcal{N}(0,1)$ (since the process Y is a Brownian motion). We denote by $\mathscr{F}^X_{t_k}$ the vector of historical values of the process X until time $t_k \in \Gamma$. Thus, $\mathscr{F}^X_{t_k}$ is the vector of the $k+1$ last values of the discretized model and therefore, $\mathscr{F}^X_{t_k} = (X_{t_0}, X_{t_1}, \ldots, X_{t_k})$. The filtration generated by the Markov chain Z (i.e. $\mathscr{F}^Z$) is the one generated by the history values of Z in the time sequence Γ. For simplicity of notation, we will write in the sequel the model (42.2) as

$$X_{t+1} = \kappa_i\theta_i + (1-\kappa_i)X_t + \sigma_i\varepsilon_{t+1}.$$

This means that at time $t \in [0,T]$, the Markov chain Z is in state $i \in \mathscr{S}$ (i.e. $Z_t = i$) and Z jumps at time $t_j \in \Gamma$, $j \in \{0,1,\ldots,M-1\}$.
In the first step based on the EM-algorithm, the complete parameter space estimate $\hat{\Theta}$ is split into: $\hat{\Theta}_1 := (\hat{\kappa}_i, \hat{\theta}_i, \hat{\sigma}_i, \hat{\Pi})$, for $i \in \mathscr{S}$, which corresponds to the first subset of diffusion parameters. The transition probabilities are estimated according to the following formula

$$\Pi_{ij} = \frac{\sum_{k=2}^{M}[P(Z_{t_k} = j|\mathscr{F}^X_{t_M}; \hat{\Theta}_1)\frac{\Pi_{ij}P(Z_{t_{k-1}}=i|\mathscr{F}^X_{t_{k-1}};\hat{\Theta}_1)}{P(Z_{t_k}=j|\mathscr{F}^X_{t_{k-1}};\hat{\Theta}_1)}]}{\sum_{k=2}^{M}[P(Z_{t_{k-1}} = i|\mathscr{F}^X_{t_M}; \hat{\Theta}_1)]}. \tag{42.3}$$

The quantities $P(Z_{t_k} = j|\mathscr{F}^X_{t_M}; \hat{\Theta}_1)$, $P(Z_{t_{k-1}} = i|\mathscr{F}^X_{t_{k-1}}; \hat{\Theta}_1)$ refer to the smoothed inferences for the process being in state j at time t_k, based on starting values for the parameter vector Θ of the underlying process X (see Kim, C.-J. [7] or Janczura, J. and Weron, R. [5]).

Step 2: Estimation of the parameters of the Lévy process fitted to each regime
Using the regime classification obtained in the previous step, we estimate the second subset of parameters $\hat{\Theta}_2 := (\hat{\alpha}_i, \hat{\beta}_i, \hat{\delta}_i, \hat{\mu}_i)$, for $i \in \mathscr{S}$, which corresponds to the NIG distribution parameters of the Lévy jump process fitted for each regime. We assume the Lévy process L follows a Normal Inverse Gaussian (NIG) distribution. This family of distribution was introduced by Barndorff-Nielsen and Halgreen [2] and Barndorff-Nielsen [1]. Taking $\delta > 0$, $\alpha \geq 0$, then the density function of a NIG variable $NIG(\alpha, \beta, \delta, \mu)$ is given by

$$f_{NIG}(x;\alpha,\beta,\delta,\mu) = \frac{\alpha}{\pi}\exp\big(\delta\sqrt{\alpha^2-\beta^2} + \beta(x-\mu)\big) \times \frac{K_1(\alpha\delta\sqrt{1+(x-\mu)^2/\delta^2})}{\sqrt{1+(x-\mu)^2/\delta^2}}, \tag{42.4}$$

Table 42.1 Description of the Equity markets

Ticker	Description
TOPIX	JAPAN TOPIX Index
FBMKLCI	MALAYSIA FTSE Bursa Malaysia
CNXNIFTY	INDIA S&P CNX Nifty Index
DWJP	Dow Jones Japan Total Stock Market Index

Table 42.2 Estimated parameters of the regime-switching Lévy model for Asian equities

Parameters	Japan Topix		Malaysia FTSE		India S&P CNX		Dow Jones Japan	
	State 1	State 2	State 1	State 2	State 1	State 2	State 1	State 2
κ	0.0025	0.0174	0.0027	0.0027	0.0002	0.0064	0.0035	0.0280
θ	664.67	1079.30	1141,72	2061.37	4778.60	6652.69	417.7719	609.98
σ	85.06	480.50	173.36	35.33	4788.62	1894.17	25.06	246.93
P_{ii}^Z	0.99	0.96	0.88	0.95	0.99	0.99	0.98	0.89
α	1.22	0.05	1.20	0.02	0.01	0.02	0.81	0.12
β	−0.12	0.01	−0.30	0.00	0.00	−0.02	−0.03	0.06
δ	0.94	7.65	1.00	13.24	27.16	8.10	0.62	4.49
μ	0.09	−1.77	0.26	−2.54	−16.26	14.01	0.03	−2.47

where K_ν is the third Bessel kind function with index ν. It can be represented with the following integral $K_\nu(z) = \frac{1}{2}\int_0^\infty y^{\nu-1}\exp(-\frac{1}{2}z(y+y^{-1}))dy$. For a given real ν, the function K_ν satisfies the differential equation given by $x^2y'' + xy' - (x^2 + \nu^2)y = 0$. The estimation of the distribution parameters is achieved by constrained maximum likelihood: $\Phi^i := \{\alpha^i, \beta^i, \delta^i, \mu^i\}$, with $i \in \{1, 2\}$.

Proposition 42.1 *The log-likelihood function of the sequence of log-returns with distribution NIG* $(\alpha, \beta, \delta, \mu)$ *is given by*

$$L(\alpha, \beta, \delta, \mu) = n\log\left(\frac{\alpha}{\pi}\right) + n\delta\gamma + \sum_{t=0}^{n-1}\left[\beta\delta\tau_t - \log c_t + \log K_1(\alpha\delta c_t)\right],$$

where $\gamma = \sqrt{\alpha^2 - \beta^2}$. *For any* $t = 0, 1, \ldots n-1$, $\tau_t = \frac{r_t - \mu}{\delta}$ *and* $c_t = \sqrt{1 + \tau_t^2}$.

The initialization of the estimation is performed by the method of moments.

42.5 Application to Asian Equities

We apply these statistical methods to estimate regime-switching Lévy models in the context of Asian equities. The data is retrieved from Thomson Financial Datastream over the period going from July 20, 2010 to July 11, 2014 with a daily frequency, totaling 1281 observations. The names for each time series are given in Table 42.1.

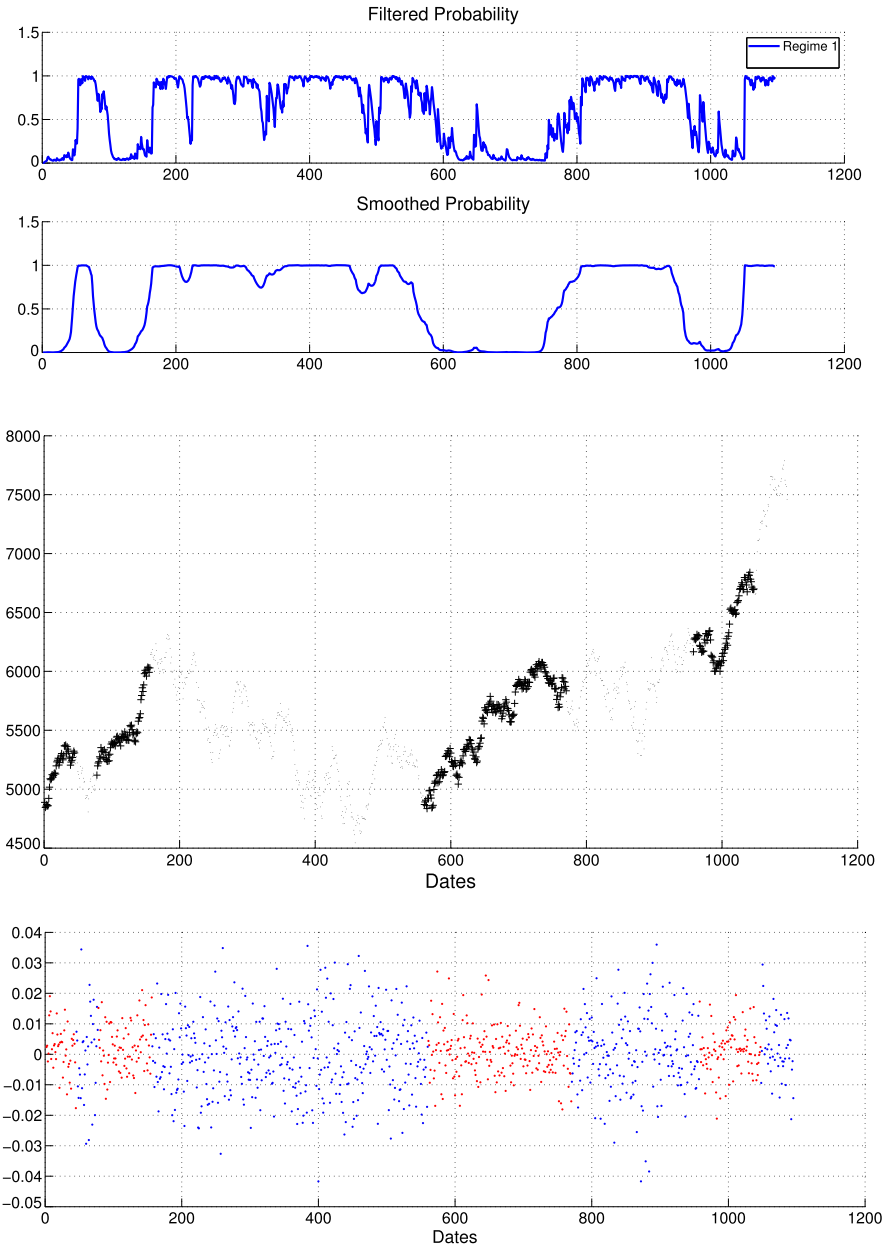

Fig. 42.1 Smoothed and filtered probabilities for the INDIA S&P CNX Nifty Index on *top*; Regime-switching classification in the *middle* and Log-returns classification at the *bottom*

We have recovered equity data in order to study the jump properties of stock markets under changing market conditions in the Pacific region.

Table 42.2 reports the results of: (i) the set of diffusion parameters, and (ii) the NIG density parameters of the Lévy jump process fitted to each regime. The remaining problem in this work is to specify the number of regimes in the Markov chain. For simplicity, we proceed with two regimes that relate to the 'boom' and 'bust' phases of the business cycle. We give now all estimated parameters for each time series in Table 42.2.

Regarding the estimated parameters in Table 42.2, we focus on the intensity jump parameters (i.e. α). For the NIG distribution, the smaller the value of α, the higher the intensity of jumps. For instance, for the Japan Topix, α in state 2 is equal to 0.05 which implies a high intensity of jumps. On the contrary, the value of α in state 1 is equal to 1.22 which indicates a Gaussian distribution in the NIG context (see Barndorff-Nielsen [1]). This result applies for all Asian equities. We can also discuss the asymmetry parameters β: changing signs between states 1 and 2 show the change in the distribution asymmetries.

We also report an illustrative plot (Fig. 42.1) where the regime switches are reported for the INDIA S&P CNX Nifty Index. To provide the reader with a clearer picture, we have chosen to plug the regimes identified back into the raw (non-stationary) data. Of course, all the estimates were performed on log-returns $r_t := \log(X_t) - \log(X_{t-1})$, e.g. stationary data. Below this first plot, the filtered and smoothed probabilities are displayed. They reflect the regime switches at stake.

42.6 Summary

Several conclusions are in order for the regime-switching Lévy model applied to Asian equities. First, we show the presence of two contrasted regimes in each time series. Second, we identify one jumpy regime and a rather quiet second regime. Therefore, it seems appropriate to model each regime separately, either with a pure Lévy-jump, or with a Brownian motion process. The two-step estimation strategy turns out as a straightforward approach. Taken together, the results gathered in the paper can encourage market practitioners or future researchers to use regime-switching Lévy models as a resourceful statistical procedure.

Acknowledgements For useful comments and suggestions on previous drafts, we wish to thank Marco Lombardi, Stelios Bekiros, Raphaelle Bellando, Gilbert Colletaz, Cem Ertur, Francesco Serranito, Daniel Mirza as well as participants at the 2014 Symposium of the Society for Nonlinear Dynamics & Econometrics (Baruch College, New York, USA), the 2014 Annual Conference of the International Association for Applied Econometrics (Queen Mary, University of London, UK), and the LEO Economic Seminar (Université d'Orléans).

References

1. Barndorff-Nielsen OE (1998) Processes of normal inverse Gaussian type. Finance Stoch 2:41–68

2. Barndorff-Nielsen O, Halgreen C (1977) Infinite divisibility of the hyperbolic and generalized inverse Gaussian distributions. Probab Theory Relat Fields 38(4):309–311
3. Hamilton JD (1989) A new approach to the economic analysis of non-stationary time series and the business cycle. Econometrica 57:357–384
4. Hamilton JD (1989) Rational-expectations econometric analysis of changes in regime. J Econ Dyn Control 12:385–423
5. Janczura J, Weron R (2010) An empirical comparison of alternative regime-switching models for electricity spot prices. Energy Econ 32:1059–1073
6. Janczura J, Weron R (2012) Efficient estimation of Markov regime-switching models: an application to electricity spot prices. AStA Adv Stat Anal 96:385–407
7. Kim CJ (1994) Dynamic linear models with Markov-switching. J Econom 60:1–22

Chapter 43
Wavelet Algorithm for Hierarchical Pattern Recognition

Urszula Libal and Zygmunt Hasiewicz

Abstract The idea, presented in this article, is based on a combination of hierarchical classifier with multiresolution representation of signals in the Daubechies wavelet bases. The paper concerns a multi-class recognition of random signals. It presents a multistage classifier with a hierarchical tree structure, based on a multiscale representation of signals in wavelet bases. Classes are hierarchically grouped in macro-classes and the established aggregation defines a decision tree. In each macro-class, the existence of deterministic pattern of signals is assumed. A global loss function with reject option is proposed for the multistage classifier and two strategies for the choice of loss function parameters are discussed. An analysis of risk is performed for a local (binary) attraction-limited minimum distance classifier for wavelet approximation of signals. This leads to proposals, relating to the upper estimate of the risk, called the guaranteed risk. Its value depends on the several parameters as the wavelet scale of signal representation, the support length of wavelet function, or the variance of the random noise in the macro-class. Finally, the guaranteed risk of the multistage classifier is derived.

43.1 Introduction

The paper is focused on automatic multistage classification of signals to one of the K classes. The multistage schema of signal recognition algorithm selects at each stage a smaller macro-class, being a child of the macro-class chosen in previous stage, by a binary classifier. There is introduced an additional option of stopping the hierarchical algorithm before terminal class is achieved and is called reject option in case of lack of decision at some stage. The tree structure of the algorithm allows the decomposition of the classification task to a number of local binary classifications. Therefore, binary classification problem is considered for signals given by a

U. Libal (✉) · Z. Hasiewicz
Department of Control Systems and Mechatronics, Wroclaw University of Technology,
Wybrzeze Wyspianskiego 27, 50-370 Wroclaw, Poland
e-mail: urszula.libal@pwr.edu.pl

Z. Hasiewicz
e-mail: zygmunt.hasiewicz@pwr.edu.pl

A. Steland et al. (eds.), *Stochastic Models, Statistics and Their Applications*,
Springer Proceedings in Mathematics & Statistics 122,
DOI 10.1007/978-3-319-13881-7_43

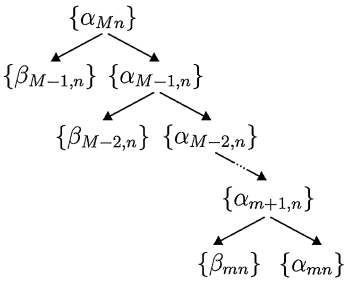

Fig. 43.1 A recursive method of determining wavelet approximation coefficients α_{jn} and detail coefficients β_{jn} for decreasing wavelet scale $j = M, M-1, \ldots, m$

model (43.1). In each macro-class, a deterministic prototype (pattern) is a source of signals which are obtained as noisy versions of patterns. The signals are sampled at time instants $t_1, t_2, \ldots, t_{p_M}$.

Assumption 43.1 *In macro-class* $k = 1, 2$, *the signals have a form*

$$s_k(t, \omega) = f_k(t) + \xi(t, \omega),$$
$$t \in \{t_1, t_2, \ldots, t_{p_M}\} \subset [0, 1], \ \omega \in \Omega, \tag{43.1}$$

where f_k *is a deterministic pattern,* $\xi \sim i.i.d.(0, \sigma_k^2)$ *is a stationary white noise with variance* σ_k^2, *and* $t_1, t_2, \ldots, t_{p_M}$ *are sampling times and* $p_M = 2^M$.

43.2 Signal Approximation in Wavelet Bases

In this section, the main idea of this article – i.e. a combination of hierarchical classifier with multiresolution representation of signals in the Daubechies wavelet bases [1] – is introduced. The hierarchical decomposition of signal in orthonormal bases of Daubechies wavelet functions can be performed by fast and easy to compute Mallat's algorithm [4]. The major inspiration for the fusion of a multistage classifier with the hierarchical procedure of wavelet decomposition of signals is the possibility of usage of wavelet representation of signals for various resolutions at every stage of this complex classifier.

The orthonormal basis property, partitioning the approximation space V_{j+1} into the approximation space V_j for a lower resolution, and detail space W_j, was applied by Stéphane Mallat to construct the recursive algorithm for wavelet coefficients computing (starting for the highest wavelet scale). The schema of this procedure is presented in Fig. 43.1.

In a basis of Daubechies wavelet family functions of order q, every signal s is represented by a vector of proper wavelet coefficients $\mathbf{w} = \alpha_{jn}$ (for details see [1]). The coefficient (feature) vector is

$$\mathbf{w} = \alpha_{jn} = \begin{bmatrix} \alpha_{jn_1} \\ \alpha_{jn_2} \\ \vdots \\ \alpha_{jn_p} \end{bmatrix} = \begin{bmatrix} \langle s, \phi_{jn_1} \rangle \\ \langle s, \phi_{jn_2} \rangle \\ \vdots \\ \langle s, \phi_{jn_p} \rangle \end{bmatrix}, \tag{43.2}$$

where the components in (43.2) are random variables of the form

$$\alpha_{jn_i} = \alpha_{jn_i}(\omega) = \left\langle s(.,\omega), \phi_{jn_i} \right\rangle = \int_{supp(\phi_{jn_i})} s(t,\omega)\phi_{jn_i}(t)\,dt. \tag{43.3}$$

The choice of wavelet scale j affects the width of the wavelet function support and hence the amount of detail in the signal representation. The length of Daubechies wavelet function support of order q is in particular

$$d(j) = \left|supp(\phi_{jn_i})\right| = \frac{2q-1}{2^j}. \tag{43.4}$$

The number of coefficients (features) for scale j is $p(j) = 2^j$ and decreases approximately twice (i.e. $p(j-1) \approx 2^{j-1}$) with the transition to a lower scale $j-1$, for every wavelet scale $j = M, M-1, \ldots, m$.

43.3 Hierarchical Pattern Recognition

A natural and obvious consequence of the use of a hierarchical representation of signal is multistage classification algorithm. The classification is performed sequentially in L steps by the use of local binary classifiers $\Psi_i, i = 1, 2, \ldots, L$. The vectors $\alpha_{j^{(i)}n}$ of wavelet coefficients are computed for a fixed scale $j^{(i)}$, as it was explained in previous section.

At each stage we consider a binary recognition task, with pre-defined two macro-classes. The macro-classes at ith stage are characterized by the following parameters and denotations:

- at ith stage there are 2 macro-classes of signals: $C_1(i)$, $C_2(i)$
- probabilities of macro-class appearance: $p_1(i)$, $p_2(i)$
- patterns of signals in macro-classes: $f_1(i)$, $f_2(i)$
- variances of noise in macro-classes: $\sigma_1^2(i)$, $\sigma_2^2(i)$

In the next point is defined a local attraction-limited minimum-distance classifier, used at each stage of the hierarchical classifier, but for a different pair of macro-classes and for a changed wavelet scale of signal approximation in wavelet bases.

The multistage recognition algorithm runs in L steps:

$$\begin{aligned}
&\text{stage 1: } \Psi_1(\alpha_{j^{(1)}n}) = C^{(1)},\\
&\text{stage 2: } \Psi_2(\alpha_{j^{(2)}n}) = C^{(2)},\\
&\qquad\vdots\\
&\text{stage } L\text{: } \Psi_L(\alpha_{j^{(L)}n}) = C^{(L)}.
\end{aligned}$$

Once again, it should be stressed that wavelet scales $j^{(i)}$ and pointed by the local classifiers Ψ_i macro-classes $C^{(i)}$ depends from the algorithm stage $i = 1, 2, \ldots, L$ (Fig. 43.2).

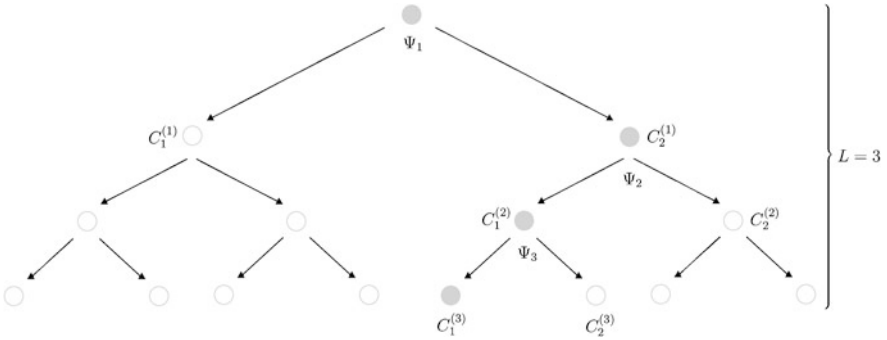

Fig. 43.2 Multistage hierarchical classification by a sequence of local binary classifiers

43.4 Attraction-Limited Minimum-Distance Classifier

We conduct a risk analysis for a particular form of the classifier, i.e. attraction-limited minimum-distance classifier [3], which is defined in Algorithm 43.1.

There are three decision areas determined by so called *clusters*, i.e. p-dimensional balls of *centers* in $\mathbf{c}_1$ and $\mathbf{c}_2$ and *radii* R_1 and R_2. In order to the radii R_1 and R_2 actually performed the function of limiting (i.e. guarantee of probabilistic separation) at the design of decision areas, it is assumed that R_1 and R_2 satisfy the following dependencies:

$$\mathbb{P}\big(\|\mathbf{c}_1 - \mathbf{w}\| \leq R_1 | \mathbf{w} \in 2\big) = \alpha, \tag{43.5}$$

$$\mathbb{P}\big(\|\mathbf{c}_2 - \mathbf{w}\| \leq R_2 | \mathbf{w} \in 1\big) = \alpha, \tag{43.6}$$

where parameter $\alpha \in [0, 1]$ reflects the probability that a cluster will include feature vectors from opposite macro-class, thus the value of this parameter should be set rather at a low level, e.g. 0.05.

The local classifier Ψ_i is defined for the following two cases:

Algorithm 43.1 *For disjoint clusters, i.e. when* $\|\mathbf{c}_1 - \mathbf{c}_2\| > R_1 + R_2$,

$$\Psi_i(\mathbf{w}) = \begin{cases} 1, & \text{if } \|\mathbf{c}_1 - \mathbf{w}\| \leq R_1, \\ 2, & \text{if } \|\mathbf{c}_2 - \mathbf{w}\| \leq R_2, \\ 0, & \text{if } (\|\mathbf{c}_1 - \mathbf{w}\| > R_1 \wedge \|\mathbf{c}_2 - \mathbf{w}\| > R_2). \end{cases} \tag{43.7}$$

For overlapping clusters, i.e. when $\|\mathbf{c}_1 - \mathbf{c}_2\| \leq R_1 + R_2$,

$$\Psi_i(\mathbf{w}) = \begin{cases} 1, & \text{if } \|\mathbf{c}_1 - \mathbf{w}\| \leq R_1 \wedge \|\mathbf{c}_2 - \mathbf{w}\| > R_2, \\ 2, & \text{if } \|\mathbf{c}_1 - \mathbf{w}\| > R_1 \wedge \|\mathbf{c}_2 - \mathbf{w}\| \leq R_2, \\ 0, & \text{if } (\|\mathbf{c}_1 - \mathbf{w}\| \leq R_1 \wedge \|\mathbf{c}_2 - \mathbf{w}\| \leq R_2) \\ & \quad \vee (\|\mathbf{c}_1 - \mathbf{w}\| > R_1 \wedge \|\mathbf{c}_2 - \mathbf{w}\| > R_2), \end{cases} \tag{43.8}$$

where "0" means lack of decision.

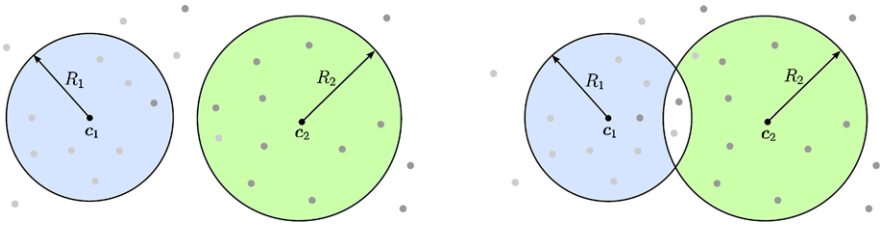

Fig. 43.3 Schema of decision areas for disjoint clusters (*left*) and overlapping clusters (*right*)

Vector **w** is given by the formula (43.2). The decision areas for disjoint and overlapping clusters are marked in Fig. 43.3 with colors: *blue* (classification to macro-class 1), *green* (classification to macro-class 2) and *white* (lack of decision or rejection).

43.5 Loss Function with Reject Option for Hierarchical Classifier

In pattern recognition tasks, the use of zero-one loss function [5] is the most often, because then the risk gains the interpretation as a probability of incorrect classification. The zero-one loss function is modified by introducing additional reject option [2] (i.e. lack of decision). This procedure requires the introduction of an additional parameter $r \in [0, 1]$, meaning a loss arising from a lack of decision. In addition, a loss forced by an incorrect decision is determined by a parameter $\rho \in [0, 1]$. The following definition of a local loss function $\mathscr{L}_i$, with values depending on the stage i of incorrect decision, is introduced in Definition 43.1.

Definition 43.1 Modified loss function $\mathscr{L}_i$ at ith stage has a form

$$\mathscr{L}_i\left(C^{(i)}, J^{(i)}\right) = \begin{cases} 0, & \text{if } C^{(i)} = J^{(i)}, \\ r\gamma(i), & \text{if } C^{(i)} = 0, \\ \rho\gamma(i), & \text{if } C^{(i)} \neq J^{(i)}, \end{cases} \tag{43.9}$$

where:

1. $\gamma(i)$ is a non-increasing function for growing stage index $i = 1, 2, \ldots, L$,
2. $\gamma(i) \in [0, 1]$,
3. $\sum_{i=1}^{L} \gamma(i) = 1$,
4. $r \in [0, 1]$,
5. $\rho \in [0, 1]$,
6. $\rho \geqslant r$.

The expression $r\gamma(i)$ is a loss resulting from the lack of classifier decision, and $\rho\gamma(i)$ – a loss resulting from incorrect decision, on the ith stage. It is assumed that the loss, established as a result of the multistage classification procedure with reject

option, is the sum of the losses incurred on subsequent stages. The design of loss function $\mathscr{L}^W$ for hierarchical multistage algorithm Ψ^W is therefore as follows.

$$\begin{aligned}\mathscr{L}^W\big(\big(C^{(1)}, C^{(2)}, \ldots, C^{(L)}\big), \big(J^{(1)}, J^{(2)}, \ldots, J^{(L)}\big)\big) \\ = \sum_{i=1}^{L} \mathscr{L}_i\big(C^{(i)}, J^{(i)}\big) \\ = \rho \sum_{i=1}^{L} \gamma(i) \mathbf{1}\big\{C^{(i)} \neq J^{(i)}\big\} + r \sum_{i=1}^{L} \gamma(i) \mathbf{1}\big\{C^{(i)} = 0\big\}. \end{aligned} \tag{43.10}$$

It should be noted that the random event consisting of incorrect classification at ith stage involves another wrong classifications at all subsequent steps, it is $i+1, i+2, \ldots, L$. On the other hand, the lack of decision at a certain ith stage, results that the classified signal is unallocated to any class or macro-class also at all subsequent steps $i+1, i+2, \ldots, L$.

According to the above, the loss from incorrect classification at ith stage, $C^{(i)} \neq J^{(i)}$, is

$$\rho . \sum_{k=i}^{L} \gamma(k), \tag{43.11}$$

and the loss as a result of the rejecting decision at ith stage of classification, $C^{(i)} = 0$, is

$$r \sum_{k=i}^{L} \gamma(k). \tag{43.12}$$

The correct classification to the terminal class $C^{(L)} = J^{(L)}$ is not assigned to any loss.

43.6 Selection Strategies of Loss Function Parameters

For the loss function $\mathscr{L}^W$ given by (43.10) the risk of multistage recognition algorithm $\Psi^W = (\Psi_1, \Psi_2, \ldots, \Psi_L)$ is

$$\mathscr{R}\big[\Psi^W\big] = \sum_{i=1}^{L} \mathscr{R}[\Psi_i], \tag{43.13}$$

that is equal to the sum of risk values for binary classifiers Ψ_i at various stages $i = 1, 2, \ldots, L$.

The value of the global risk depends on the strategy chosen when determining penalties for incorrect decisions or lack of decisions, by appropriate rescaling loss r and ρ on the stage by the factor $\gamma(i)$ (see Definition 43.1).

The prescale value at ith stage for *exponential strategy* is

$$\gamma(i) = c^{L-i}\frac{1-c}{1-c^L}, \tag{43.14}$$

and for *linear strategy*

$$\gamma(i) = (L-i+1)\frac{2}{L(L+1)}. \tag{43.15}$$

Strategy of the *exponential decrease of losses* puts the strongest emphasis on the correctness of decisions during the initial stages of recognition. Losses at the final stages are less significant. This approach is designed to protect against committing thick error in the initial phase, because choosing of incorrect macro-class at the first, results in wrong decisions on subsequent steps – without capability of repair. The strategy of the *linear decrease of losses* with the stage assigns the highest value of the loss to the first step. However, the decrease of the function value $\gamma(i)$ is slower, linear.

43.7 Guaranteed Risk of Hierarchical Classifier

The upper bound of classifier risk $\mathscr{R}$ is called *guaranteed risk* and denoted by $\mathscr{R}_{\max}$.

Theorem 43.1 *Guaranteed risk for local classifier* Ψ_i (*Algorithm* 43.1) *at stage* $i = 1, 2, \ldots, L$, *with known centers of clusters* $\mathbf{c}_1$, $\mathbf{c}_2$ *and with radii fulfilling the conditions* (43.5)–(43.6), *is*

$$\mathscr{R}_{\max}[\Psi_i] = \gamma(i)\Bigg[(\rho - r)\alpha + rd\big(j^{(i)}\big)p\big(j^{(i)}\big)\left(p_1(i)\left(\frac{\sigma_1(i)}{R_1(i)}\right)^2 + p_2(i)\left(\frac{\sigma_2(i)}{R_2(i)}\right)^2\right)\Bigg], \tag{43.16}$$

where $j^{(i)} \in \{m, m+1, \ldots, M\}$ *is a scale of signal approximation in wavelet bases, fixed for the stage* $i = 1, 2, \ldots, L$.

Proof The first steps of proof are Chebyshev inequalities applied to the expressions, in macro-class $k = 1, 2$,

$$\mathbb{P}\big(\|\mathbf{c}_k - \mathbf{w}\| > R_k \mid \mathbf{w} \in k\big) \leqslant \frac{\mathbb{E}(\|\mathbf{w} - \mathbb{E}\mathbf{w}\|^2 \mid \mathbf{w} \in k)}{R_k^2}. \tag{43.17}$$

The properties of Daubechies wavelet of order q give us the upper bound of variance in macro-class $k = 1, 2$,

$$Var(\alpha_{j^{(i)}n_l}) \leqslant \sigma_k^2 \big|supp\{\phi_{j^{(i)}n_l}\}\big| = \sigma_k^2 \frac{2q-1}{2^j}, \tag{43.18}$$

for wavelet coefficient

$$\alpha_{j^{(i)}n_l}(\omega) = \left\langle s_k(.,\omega), \phi_{j^{(i)}n_l}(.)\right\rangle. \tag{43.19}$$

□

Direct application of Theorem 43.1 and formula (43.16) leads to designation of the guaranteed risk for the multistage algorithm Ψ^W.

Corollary 43.1 *If the assumptions of Theorem 43.1 are fulfilled at each stage $i = 1, 2, \ldots, L$, of the hierarchical (multistage) classifier Ψ^W, then its guaranteed risk is*

$$\mathscr{R}_{\max}\left[\Psi^W\right] = (\rho - r)\alpha + r\sum_{i=1}^{L}\gamma(i)d\left(j^{(i)}\right)p\left(j^{(i)}\right) \times \left(p_1(i)\left(\frac{\sigma_1(i)}{R_1(i)}\right)^2 + p_2(i)\left(\frac{\sigma_2(i)}{R_2(i)}\right)^2\right). \tag{43.20}$$

The product of the length $d(j^{(i)})$ of Daubechies wavelet function support and the length $p(j^{(i)})$ of feature vector in scale $j^{(i)}$ can be estimated by value

$$d\left(j^{(i)}\right)p\left(j^{(i)}\right) \approx (2q - 1), \tag{43.21}$$

what is a consequence of the properties explained in Sect. 43.2 and where q is the order of Daubechies wavelets.

References

1. Daubechies I (1992) Ten lectures on wavelets. SIAM Edition, Philadelphia
2. Devroye L, Györfi L, Lugosi G (1996) A probabilistic theory of pattern recognition. Springer, New York
3. Hasiewicz Z, Libal U (2014) Upper bound of risk of attraction-limited minimum distance classifier. In: Proc 18th National Conference on Automation (in Polish) 8–10 September, Wroclaw
4. Mallat S (1989) A theory for multiresolution signal decomposition: the wavelet representation. IEEE Trans Pattern Anal Mach Intell 11(7):674–693
5. Webb AR, Copsey KD (2011) Statistical pattern recognition, 3rd edn. Wiley, New York

Chapter 44
Risk of Selection of Irrelevant Features from High-Dimensional Data with Small Sample Size

Henryk Maciejewski

Abstract In this work we demonstrate the effect of small sample size on the risk that feature selection algorithms will select irrelevant features when dealing with high-dimensional data. We develop a simple analytical model to quantify this risk; we verify this model by the means of simulation. These results (i) explain the inherent instability of feature selection from high-dimensional, small sample size data and (ii) can be used to estimate the minimum required sample size which leads to good stability of features. Such results are useful when dealing with data from high-throughput studies.

44.1 Problem formulation

High-throughput studies common in life sciences often yield data with small number of samples n given as vectors of d features, with $n \ll d$. An example might be gene expression studies, with the number of samples ($n \sim 10^2$–10^3) typically ranges of magnitude smaller than the number of gene expressions ($d \sim 10^4$). It is commonly observed that feature selection algorithms applied to such data yield unstable sets of features, i.e., small variation of the data leads to selection of feature sets with little overlapping with the previous sets [1, 2, 5, 6].

In this work we develop a simple model which can be used to quantify this effect in terms of the probability of selecting irrelevant (i.e. actually unassociated with the target) features rather than relevant features. This model can also be used to estimate the required sample size to guarantee acceptable stability of features. This work builds on and extends results shown in Chapter 3 of the Monograph [5].

We introduce the following notation. We denote the matrix with results of a massive throughput study as $X = (x_{ij})$, $i = 1, \ldots, d$, $j = 1, \ldots, n$, with the rows, denoted X_i, $i = 1, \ldots, d$, representing features measured for the n samples tested.

Electronic supplementary material Supplementary material is available in the online version of this chapter at doi:10.1007/978-3-319-13881-7_44.

H. Maciejewski (✉)
Institute of Computer Engineering, Control and Robotics, Wrocław University of Technology, ul. Janiszewskiego 11-17, 50-370 Wrocław, Poland
e-mail: Henryk.Maciejewski@pwr.edu.pl

A. Steland et al. (eds.), *Stochastic Models, Statistics and Their Applications*,
Springer Proceedings in Mathematics & Statistics 122,
DOI 10.1007/978-3-319-13881-7_44

Let $Y = (y_i)$, $i = 1, \ldots, n$ denote the target vector. Although Y can contain either qualitative or quantitative measurements, here we assume that Y is quantitative, i.e. $y_i \in R$, $i = 1, \ldots, n$.

We assume that the rows $X_1, \ldots, X_d$ and Y are samples of size n from the underlying random variables $\mathscr{X}_1, \ldots, \mathscr{X}_d$, and $\mathscr{Y}$. We assume that the variable $\mathscr{X}_i$ is not associated with the target ($\mathscr{X}_i$ and $\mathscr{Y}$ independent), and the variable $\mathscr{X}_j$ is associated with the target, with correlation $cor = cor(\mathscr{X}_j, \mathscr{Y}) > 0$. We expect that a feature selection procedure which estimates association of variables with the target would select feature j rather than i. We now estimate this probability as a function of the sample size n and correlation cor.

44.2 Probability of Selecting a Relevant Feature

Association of the feature i with the target can be estimated as the sample correlation coefficient $r_i = \frac{\sum_{k=1}^{n}(x_{ik}-\bar{X}_i)(y_k-\bar{Y})}{\sqrt{\sum_{k=1}^{n}(x_{ik}-\bar{X}_i)^2}\sqrt{\sum_{k=1}^{n}(y_k-\bar{Y})^2}}$ where $\bar{X}_i$, $\bar{Y}$ are means of X_i and Y. Similarly we calculate r_j as the sample correlation coefficient between X_j and Y.

The probability that the feature selection procedure selects the relevant feature j given features i and j equals

$$p = \Pr\big(|r_j| > |r_i|\big). \tag{44.1}$$

We provide approximate analytical formula for p as a function of n and cor and we quantify the quality of this approximation by the means of simulation. To simplify analytical approximation of p, we assume that $\mathscr{X}_i$, $\mathscr{X}_j$, and $\mathscr{Y}$ are normally distributed.

We start with the simulation study in which we observe p over a grid of sample sizes $n = 10, 20, 50, 100, 200, 500$ and correlations $cor = 0, 0.15, 0.2, 0.3, 0.4, 0.6, 0.8$. Technically, we generate 10 000 vectors of size n from each of $\mathscr{X}_i, \mathscr{X}_j, \mathscr{Y}$ following $N(0, 1)$, such that $\mathscr{X}_i, \mathscr{Y}$ are independent and $\mathscr{X}_j, \mathscr{Y}$ realize multivariate normal distribution with correlation cor. We calculate sample correlation coefficients r_i and r_j; variability of r_i and r_j over 10 000 realizations of the experiment is illustrated in Fig. 44.1.

We observe substantial overlapping of the observed sample correlation coefficients, with this effect clearly diminishing with increasing sample size n and increasing correlation cor.

The probability p can be estimated as the fraction of experiments out of 10 000 in which $|r_j| > |r_i|$. Results of this are shown in Fig. 44.2.

We observe in Fig. 44.2 that for small sample size (10–50) the probability $1 - p$ of selecting an irrelevant feature instead of the relevant feature remains not negligible even for high correlations ($\sim$0.6) between the relevant feature and the target.

Analytical approximate formula for p as a function of sample size and signal strength (i.e. correlation cor) can be obtained using the Fisher transformation [3, 4]. The sample correlation r calculated for normally distributed random variables can

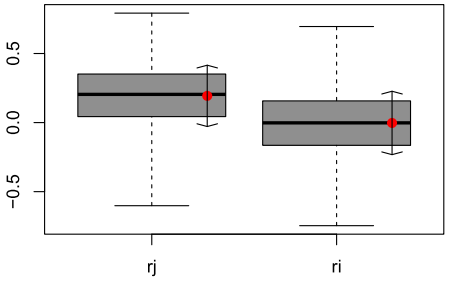

Fig. 44.1 Comparison of sample correlation coefficients for an irrelevant feature, r_i, and for a relevant feature, r_j. Results for sample size $n = 20$ and $cor = 0.2$. Whiskers of the boxplots extend over the whole range of observed data; the arrows overlaying the boxplots extend over mean ± standard deviation

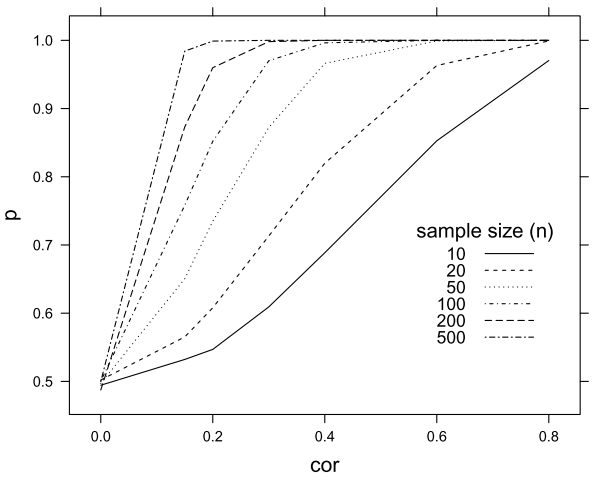

Fig. 44.2 Simulated probability $p = \Pr(|Z_j| > |Z_i|)$ of selecting the relevant feature X_j as a function of the sample size and correlation between X_j and Y

be transformed into $Z = \text{atanh}(r) = \frac{1}{2}\ln\frac{1+r}{1-r}$ which is approximately normally distributed $N(\mu, \sigma)$, with $\mu = \frac{1}{2}\ln\frac{1+\rho}{1-\rho}$ and $\sigma = \frac{1}{\sqrt{n-3}}$, where ρ is the true correlation coefficient between the underlying variables and n is the sample size.

Since the Fisher transformation is an increasing function, the probability p equals

$$p = \Pr\big(|Z_j| > |Z_i|\big). \tag{44.2}$$

Approximate formula for p can be obtained if we assume that Z_i and Z_j *are* normally distributed, $Z_i \sim N(\mu_i, \sigma_i)$, $Z_j \sim N(\mu_j, \sigma_j)$, with $\mu_i = 0$, $\mu_j = \frac{1}{2}\ln\frac{1+\rho}{1-\rho}$, and $\sigma_i = \sigma_j = \frac{1}{\sqrt{n-3}}$. Estimation of p as in Eq. (44.2) is then simple providing Z_i and Z_j are independent. [Discussion of this condition: if we take two independent samples each of size n from $(\mathscr{X}_i, \mathscr{Y})$ and from $(\mathscr{X}_j, \mathscr{Y})$ to estimate the sample correlation coefficients r_i and r_j, then these coefficients can be considered as realizations of two independent random variables. Now observing the property that for

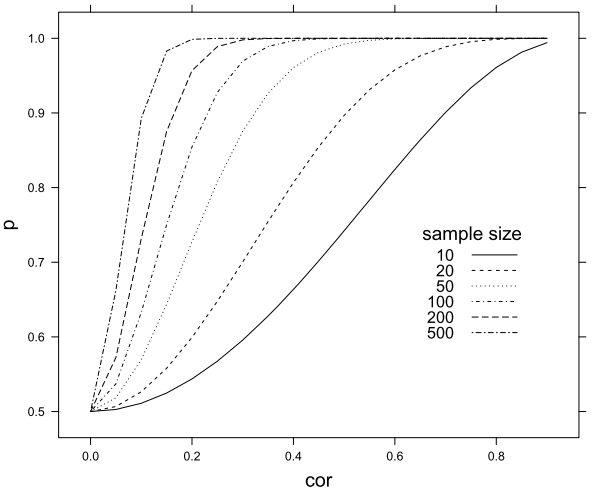

Fig. 44.3 Analytical approximation of the probability $p = \Pr(|Z_j| > |Z_i|)$ of selecting the relevant feature X_j rather than the irrelevant X_i, as a function of the sample size and correlation between X_j and Y

independent random variables U, V, the random variables $f(U)$, $g(V)$ are also independent for any (measurable) functions f and g, we obtain independence of Z_i, Z_j.]

Since distribution of two independent normally distributed random variables is bivariate normal, estimation of p becomes simple. We observe that $(Z_i, Z_j) \sim N(\boldsymbol{\mu}, \boldsymbol{\Sigma})$ with the mean $\boldsymbol{\mu} = [0 \ \mu_j] = \left[0 \ \frac{1}{2}\ln\frac{1+\rho}{1-\rho}\right]$ and the covariance matrix $\begin{bmatrix} \sigma_i^2 & 0 \\ 0 & {\sigma_j}^2 \end{bmatrix} = \begin{bmatrix} \frac{1}{n-3} & 0 \\ 0 & \frac{1}{n-3} \end{bmatrix}$.

Then p can be calculated as $p = \int\int_{|z_j|>|z_i|} f(z_i, z_j) dz_i dz_j$, where $f(z_i, z_j)$ is the density of (Z_i, Z_j). It can be shown (using transformation of variables) that p can be calculated as

$$p = 1 - 2 \int\int_{u_i>0, u_j>0} g(u_i, u_j) du_i du_j \tag{44.3}$$

where g is the density of the bivariate normal distribution with the mean $\boldsymbol{\mu} = \left[-\frac{1}{2\sqrt{2}}\ln\frac{1+\rho}{1-\rho} \ \frac{1}{2\sqrt{2}}\ln\frac{1+\rho}{1-\rho}\right]$ and the covariance matrix $\boldsymbol{\Sigma} = \begin{bmatrix} \frac{1}{n-3} & 0 \\ 0 & \frac{1}{n-3} \end{bmatrix}$.

In Fig. 44.3 we demonstrate p as a function of the sample size n and signal strength $cor = \rho$. We obtain this by numerically calculating the integral in Eq. (44.3).

Note that Eq. (44.3) is only an approximate formula for p, based on the assumption that Z_i and Z_j are normally distributed. We evaluated accuracy of this approximation by comparing p obtained from Eq. (44.3) (Fig. 44.3) with p observed in the simulation study (Fig. 44.2). Absolute difference between these two probabilities (denoted $p_{\text{Fig44.3}}$ and $p_{\text{Fig44.2}}$, respectively), calculated over the grid of n and cor values we used in the simulation study is shown in Fig. 44.4.

We conclude that the error of our approximation taken relative to the observed p does not exceed 4 %.

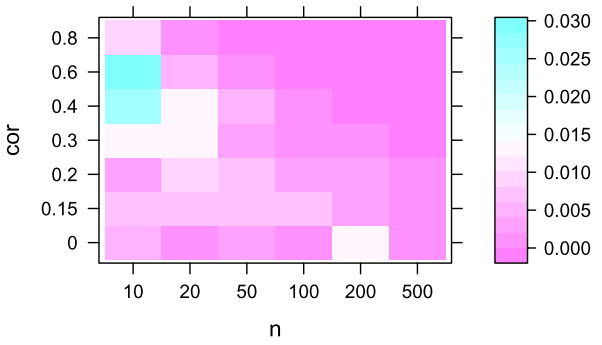

Fig. 44.4 Difference between simulated and analytical value of probability, i.e. $|p_{\text{Fig44.2}} - p_{\text{Fig44.3}}|$ as a function of the samples size n and correlation $cor(\mathscr{X}_j, \mathscr{Y})$

44.3 Feature Selection from High-Dimensional Data

The approximate formula (Eq. (44.3)) can be used to analyze the quality/stability of feature selection attempted for high-dimensional data with $d \gg n$. We now consider the case where n_V variables out of d are actually associated with the target, and $n_W = d - n_V$ are not associated with the target, with the condition $n_V \ll n_W$, as commonly encountered in practice.

We now analyze performance of a simple univariate feature selection procedure, similar to the one discussed in the previous section, which is used in order to find N_{TOP} variables most strongly associated with the target. To quantify performance of this feature selection procedure, we define the following measure

$$p_L = \Pr(\text{in the list of } N_{TOP} \text{ features at least } L \text{ are relevant}) \tag{44.4}$$

To estimate this probability we observe that the probability that a relevant feature i is selected by the algorithm rather than any of the n_W irrelevant features equals $\Pr(v_i > w_{(n_W)})$, where v_i denotes the Z-transformed sample correlation of the feature i with the target, and w_j, $j = 1, \ldots, n_w$ denote the Z-transformed sample correlation of irrelevant features with the target, and $w_{(n_W)}$ denotes the last order statistic of w_j, $j = 1, \ldots, n_w$. We further notice that p_L is equivalent to:

$$p_L = \Pr(v_{(n_V-(L-1))} > w_{(n_W-(N_{TOP}-L))}) \tag{44.5}$$

Applying the same approximation as in the previous section, i.e. taking v_i and w_j as normally distributed, their order statistics can be also obtained analytically (i.e. the pdf of the kth order statistic is $f_{k,n}(x) = n\binom{n-1}{k-1}(F(x))^{k-1}(1-F(x))^{n-k} f(x)$, where F and f are the population cdf and pdf). This allows to derive p_L from Eq. (44.5) (details of this are given in [5], pp. 34–39). Here we only provide conclusions from these approximate formulae derived in [5] in the form of p_L estimated for some selected values of the sample size n, signal strength in the relevant features cor and the number of relevant and irrelevant features n_V, n_W. These results are shown in Fig. 44.5. We observe that even for high signal strength and sample size around 100, it is virtually impossible to avoid irrelevant features among the selected features.

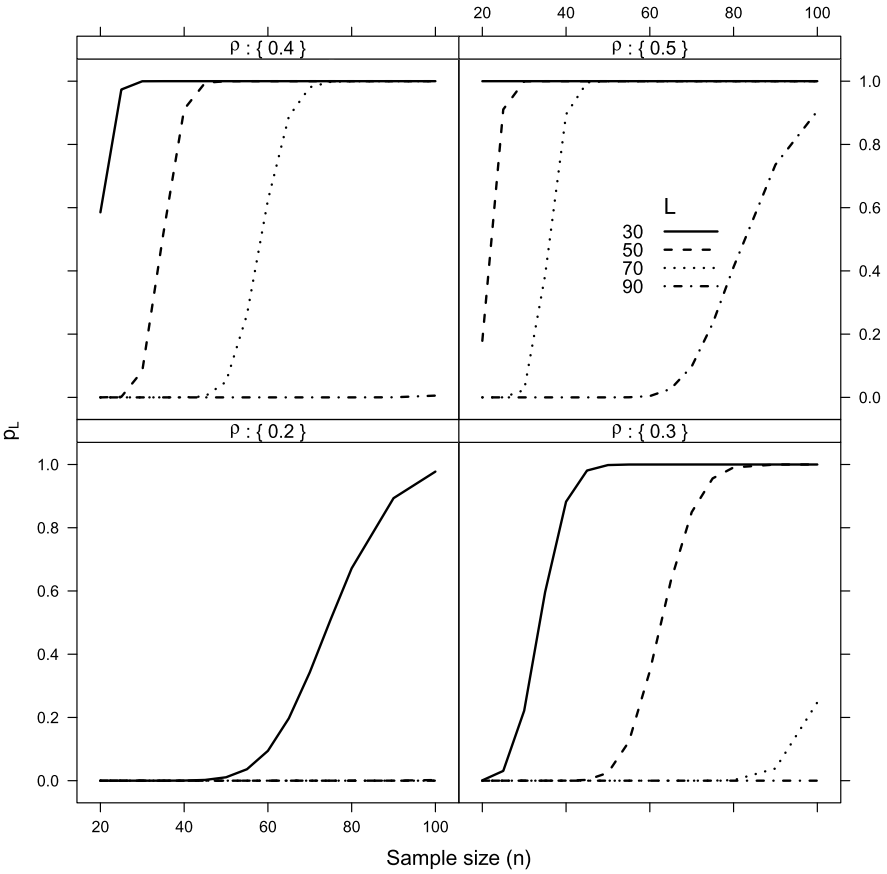

Fig. 44.5 Probability that at least L relevant features are selected among $N_{TOP} = 90$ features returned by a feature selection algorithm, as a function of the samples size n and correlation cor. Results for $n_V = 100$ relevant features and $n_w = 5000$ irrelevant features in data

44.4 Conclusions

Results presented in this work explain the inherent problem with feature selection from high-dimensional data. Instability of feature selection commonly observed when dealing with such data arises from the fact that small sample size leads to high variance of the observed measure of association of features with the target. This results in non-negligible probability of selection of irrelevant features and omitting the relevant ones, which translates into low quality of features selected from high-dimensional data, as illustrated in Fig. 44.5.

In the paper we derived approximate formulae, based on the simple probabilistic model, which allow us to quantify this effect in terms of the probability of selection of relevant features as a function of the sample size and signal strength. These

approximations can be useful for estimation of the required sample size which can bring desired quality of features under some expected signal strength.

References

1. Ein-Dor L, Kela I, Getz G, Givol D, Domany E (2005) Outcome signature genes in breast cancer: is there a unique set? Bioinformatics 21(2):171–178
2. Ein-Dor L, Zuk O, Domany E (2006) Thousands of samples are needed to generate a robust gene list for predicting outcome of cancer. Proc Natl Acad Sci 103(15):5923–5928
3. Fisher RA (1915) Frequency distribution of the values of correlation coefficient in samples from an indefinitely large population. Biometrica 10(4):507–521
4. Fisher RA (1921) On the "probable error" of a coefficient of correlation deduced from a small sample. Metron 1:3–32
5. Maciejewski H (2013) Predictive modelling in high-dimensional data: prior domain knowledge-based approaches. Oficyna Wydawnicza Politechniki Wrocławskiej, Wrocław
6. Wu MC, Lin X (2009) Prior biological knowledge-based approaches for the analysis of genome-wide expression profiles using gene sets and pathways. Stat Methods Med Res 18(6):577–593

Chapter 45
Fundamental and Speculative Shocks – Structural Analysis of Electricity Market

Katarzyna Maciejowska

Abstract In the paper, Structural Vector Autoregressive models (SVAR) are used to analyze effects of structural shocks on the electricity prices in UK. The shocks are identified via short run restrictions, which are imposed on the matrix of instantaneous effects. Two main types of shocks are considered: fundamental shocks, identified as demand and wind generation shocks and speculative shocks, which are associated solely with electricity prices. The results indicate that speculative shocks play an important role in the price setting process and account for more than 90 % of the unexpected electricity price variability. Moreover, wind generation shocks have larger input to the electricity price variance than demand shocks, particularly when peak hours are considered.

45.1 Introduction

Electricity market is very complex and difficult to model. The electricity demand depends strongly on the weather conditions and the business cycle. At the same time, it is price inelastic, which means that it responds weakly to price changes. Moreover, electricity cannot be economically stored but the power system stability requires that there is a constant balance between production and consumption [7]. As the result, electricity prices are very volatile and difficult to forecast (see [16] for a comprehensive review of forecasting methods).

The main objective of this paper is to investigate economic mechanisms, which make the forecasting process so difficult. In the research, a Structural VAR (SVAR) modeling approach is adopted. It allows to decompose forecast errors of electricity prices into structural innovations, which can be further related to particular eco-

This work was supported by funds from the National Science Centre (NCN, Poland) through grants No. 2011/01/B/HS4/01077

K. Maciejowska (✉)
Wrocław University of Technology, Wyspiańskiego 27, 50-370 Wrocław, Poland
e-mail: katarzyna.maciejowska@pwr.edu.pl

K. Maciejowska
CERGE-EI, Politickych veznu 7, 111 21 Praha 1, Czech Republic

A. Steland et al. (eds.), *Stochastic Models, Statistics and Their Applications*,
Springer Proceedings in Mathematics & Statistics 122,
DOI 10.1007/978-3-319-13881-7_45

nomic activities. This approach may help to answer questions on the sources of unexpected price changes.

A few papers have addressed the issue of structural modeling of electricity prices. Fezzi and Bunn [4, 5] and [12] applied structural VECM models to energy markets. The prime interest of [5] was the evaluation of a hypothesis of inelastic demand. Therefore, in the article, a two equation model of electricity prices and demand was used. The parameters were calibrated to the PJM market. Fezzi and Bunn [4] focused on the UK electricity market and the interactions between carbon and electricity prices. In [12], the US market was modeled and relations between electricity prices and fuel costs were analyzed. None of these articles have accounted for generation shocks, in particular, renewable generation shocks.

On the other hand, there is a growing literature on effects of renewable energy sources (RES) generation on electricity prices. Its impact on the average price behavior in various electricity market has been analyzed by [8, 9] and [6]. Refs. [6, 10] showed that an increasing wind generation lead to lower electricity prices. Moreover, it was proved that wind generation affects not only the price level but also the price volatility [10].

The aim of this paper is to identify and analyze the sources of unexpected variation of electricity price in UK. In 2013, RES accounted for around 8.7 % of total generation in UK. In the same year, according to [13], UK was one of the countries with the highest investment level in RES, in particular wind generation. Therefore it is plausible to include the wind generation in the analysis. The data describing the UK electricity market is used to estimate the SVAR model. It is applied to decompose the electricity price forecast errors into two groups of structural innovations: generation shocks (demand, wind generation and speculative shocks) and cost shocks (associated with gas, coal and CO_2 allowances prices). The results indicate that only the first group has a contemporaneous effect on electricity prices. It is shown that a positive wind generation shock reduces significantly the price level. Next, the input of generation innovations to the price volatility is investigated. It is proved that the majority of the price variance can be associated with speculative shocks. When fundamental shocks are considered, the wind generation shocks have a larger input to the price variance than the demand shocks.

Finally, the differences of the price setting mechanisms between the peak and off-peak hours are analyzed. It is well known, that the behavior of electricity prices changes over the day. During the morning and late evening hours, the prices are much lower and less volatile than during the peak hours. The paper attempts to verify, if these differences result from behavior of fundamental variables or rather reflect different attitudes of market agents.

The article is structured as follows. In Sect. 45.2 the data is described. Section 45.3 introduces an econometric model and discusses identification schemes used to estimate structural parameters. Section 45.4 presents the results of SVAR models applied separately to peak and off-peak hours. Finally, in Sect. 45.5 I conclude.

Table 45.1 Price data

Commodity	Description	Currency
Electricity	APX index, UK	GBP
UK natural gas	National balance point, UK	GBP
Thermal coal	ARA, Netherlands	USD
CO_2 emission rights	ECX CFI phase 3 futures 1-Pos	EUR

Note: In next sections, all prices are transformed into GBP

45.2 Data

In this research, I focus on the British electricity market. In this market, agents can trade electricity through power exchanges. The most popular exchange in the UK is APX. It publishes electricity price index, which is often considered as the reference prices. The daily price is computed as an average of 48 half-hourly prices (for details see www.apxende.com). On the basis of intra-day prices, two other price measures are constructed: peak (from 07:00 to 19:00) and off-peak (from 00:00 to 7:00 and from 19:00 to 00:00) price indexes. Additionally, National Grid provides information about the forecasted demand, the forecasted production from wind and realized production of electricity, with division into different fuel types. The data is published for half-hourly periods and allows computation of average values over peak and off-peak hours. In order to control for the generation costs, three cost variables: gas prices, coal prices and CO_2 allowance prices are included. The price data with short descriptions are presented in Table 45.1. All the data is transformed into natural logarithms to reduce variability.

The data spans the period from 01.01.2012 to 31.12.2012. Although, the longer sample is also available, I decide to estimate models with the data describing only one year (365 days) to ensure model stability. If the longer sample was used, I would have to cope with changes of the market structure, which result mainly from the increase of popularity of renewable energy sources (such as wind).

45.3 The Model

In this research, a structural vector autoregression model (SVAR) is used, in order to estimate and evaluate effects of structural shocks on electricity spot prices. This methodology was introduced by [14] and [1] and applied by many authors in macroeconomic analysis. It allows to give economic interpretation to shocks, which influence endogenous variables of interest. In a classical VAR model the endogenous variables are modeled as follows

$$y_t = Ax_t + \sum_{i=1}^{p} \Theta_i y_{t-i} + \varepsilon_t \tag{45.1}$$

where y_t is a $(K \times 1)$ vector of endogenous variables and x_t is $(M \times 1)$ vector of exogenous variables. The parameter A is a $(K \times M)$ matrix and Θ_i's are $(K \times K)$ matrices. Residuals, ε_t, are described by a $(K \times 1)$ vector. Although, the residuals are assumed not to be autocorrelated, they can be contemporaneously correlated. Therefore, they are often called forecast errors and don't have any direct economic interpretation.

A VAR model could be, in principle, viewed as a reduced form of a structural model. In the literature, a few types of structural models have been discussed (see [11] for detailed discussion). Here, I use so-called B-model, which assumes that forecast errors are a linear combination of independent, structural shocks. The model may be written as follows

$$y_t = Ax_t + \sum_{i=1}^{p} \Theta_i y_{t-i} + Bu_t \tag{45.2}$$

where u_t's are $(K \times 1)$ vectors of independent structural shocks with a diagonal variance-covariance matrix, $\Sigma_u = \Lambda$. The B matrix is called an instantaneous effect matrix and describes the contemporaneous relationship between structural shocks and endogenous variables. Due to linear relation between the forecast and structural errors, the following identity holds

$$\Sigma_\varepsilon = B\Lambda B' \tag{45.3}$$

It is often assumed that Λ is an identity matrix I_K. Here, I allow the variances of structural innovations to vary. In the same time, I restrict the diagonal elements of the B matrix to be equal to 1. I prefer this definition of the matrices B and Λ because it is more convenient for model comparison. It normalizes the responses of endogenous variables and enables a direct comparison of shock variances.

The reduced form VAR model can be easily estimated with a ML method. In the same time, the structural VAR cannot be directly applied because it is not identifiable. This means that the reduced form does not provide sufficient information to estimate all of parameters of the structural form. In particular, the structural model has $KM + pK^2 + K(K-1) + K$ parameters and the reduced form only $KM + pK^2 + K(K+1)/2$ parameters. Hence, in order to identify the model, at least $K(K-1)/2$ restrictions need to be imposed.

Different possible restrictions have been proposed in the literature. It is common to identify structural innovations, u_t, directly from the reduced form residuals, by imposing zero restriction on the B matrix. If the economic theory provides sufficient justification, a lower/upper triangular form of the B matrix can be assumed (e.g. [3]). It should be underlined that other zero restrictions on the B matrix are also possible.

45.3.1 Initial Analysis

The initial model uses two groups of endogenous variables: generation variables (wind generation W_t, total electricity demand D_t and electricity prices P_t) and cost

variables (gas prices G_t, coal prices C_t and CO_2 allowance prices $CO2_t$). Additionally, six exogenous variables are included in the model (x_t): a constant, a dummy for a day type, time trend, the length of the day (which is a proxy of yearly seasonality), forecasted demand and forecasted wind generation. The temperature is not included, as information about the forecasted temperature is already contained in the forecasted demand and forecasted wind production.

Lets define $y_t' = [W_t, D_t, P_t, G_t, C_t, CO2_t]$. First, I analyzed the estimates of the variance–covariance matrix of residuals based on (45.1). The block-diagonallity of the matrix Σ_e was tested with the Likelihood Ratio tests ($LR = 3.90$, $p - value = 0.082$), which indicated (at the significance level 10 %) that the forecast errors of variables describing electricity market (W_t, D_t and P_t) and describing generation costs (G_t, C_t and $CO2_t$) are uncorrelated. This outcome is in line with earlier results of [5] and [17], which indicate that changes in gas prices affect the electricity prices, on PJM and German markets, with some delay.

Because the main interest of this research is identification of shocks affecting contemporaneously electricity prices, the model could be simplified and expressed as follows

$$y_t = Ax_t + \sum_{i=1}^{p} \Theta_i y_{t-i} + \sum_{i=1}^{p} \Phi_i z_{t-i} + Bu_t \tag{45.4}$$

with $y_t' = [W_t, D_t, P_t]$ and $z_t' = [G_t, C_t, CO2_t]$.

45.3.2 Identification of Structural Parameters

In the model (45.4), there are three structural innovations, which are later called wind generation shock, demand shock and speculative shock. The first two innovations arise from a vast literature on electricity prices [5, 10, 15]. The speculative shock reflect the impact of bidding strategies of market participants on the final price [2]. Here, the following instantaneous relationships between innovations and endogenous variables (W_t, D_t and P_t) are assumed:

- The wind generation shock, u_{1t}, can affect all of the endogenous variables.
- The demand shock, u_{2t}, may influence all variables apart from wind generation.
- The speculative shock, u_{3t}, is the one, which influences only electricity prices. This identifying assumption reflects the fact that both the wind generation and demand (see [5]) are contemporaneously inelastic.

Hence, I restrict the B matrix to be lower triangular (45.5). There are three zero restrictions, which is sufficient to identify the structural form of the model (45.4). The diagonal elements of B are equal to one, which implies that responses of selected variables to particular innovations are unity. The variables are: W_t for the wind generation shock u_{1t}, D_t for the demand shock u_{2t} and P_t for the speculative shock u_{4t}

$$B = \begin{bmatrix} 1 & 0 & 0 \\ * & 1 & 0 \\ * & * & 1 \end{bmatrix} \tag{45.5}$$

45.4 Results

In order to compare the effects of structural shocks between the peak and off-peak hours, two separate models are estimated. The first one includes the peak prices and uses information about production and demand in these hours. The second one describes relations between variables during the off-peak hours. The lag structure in both models is selected with the AIC information criterion and consists of two lags: $p \in \{1, 7\}$.

45.4.1 Model Results

The estimates of the contemporaneous effect matrices, B, and estimates of standard deviations of structural shocks, diag($\sqrt{\Lambda}$), are presented in Table 45.2. Recall that due to the variable ordering, it is the last raw of the B matrix, which describes the relation between a particular shock and the electricity price.

The results lead to the following conclusions. First, as expected, a positive wind generation shock, u_{1t}, has a negative impact on electricity prices. The marginal cost of production from renewable resources is much lower than the marginal cost of production in conventional power plants. Hence, an unexpected rise of production from wind should decrease the final electricity price. The strength of the influence varies between period of a day. The responses of electricity prices to the supply shock are -0.088 and -0.051 for peak and off-peak hours, respectively. Both parameters are significant at $\alpha = 1$ %.

On the contrary, a positive demand shock, u_{2t}, leads to an increase of electricity prices. It is a natural consequence of a demand-supply price setting mechanism. The

Table 45.2 The estimates of the contemporaneous effects matrix, B, for Model 1 and Model 2

	Model 1 (Peak hours)			Model 2 (Off-peak hours)		
B	1	0	0	1	0	0
	-0.006^{**}	1	0	-0.006^{*}	1	0
	-0.088^{***}	0.753^{**}	1	-0.051^{***}	0.220	1
diag($\sqrt{\Lambda}$)	0.272	0.015	0.095	0.198	0.014	0.050
	(0.010)	(0.0006)	(0.0035)	(0.0074)	(0.0005)	(0.0019)

Note: The ML estimates of the unrestricted elements of the B matrices: *, ** and *** indicate parameters, which are significantly different from 0 at the significance levels 10 %, 5 % and 10 %, respectively; standard deviations of the parameters diag($\sqrt{\Lambda}$) are presented in parenthesis

Table 45.3 The input of structural shocks to the variance of electricity prices

		u_{1t}	u_{2t}	u_{3t}
Peak hours	Input	0.00057	0.00013	0.00902
	Share	5.89 %	1.36 %	92.75 %
Base hours	Input	0.00010	0.00001	0.00250
	Share	3.85 %	0.03 %	95.81 %

responses to the demand shock are 0.753 and 0.220 and are significantly different from zero for peak hours.

Next, the standard deviations, $\text{diag}(\sqrt{\Lambda})$, of structural disturbances are analyzed. It can be noticed that the wind generation shock varies more during the peak hours than off-peak hours. Its standard deviations are 0.272 and 0.198 in peak and base hours, respectively. The difference between variances in the two day periods is significant (when estimation errors of these parameters are taken into account). In the same time, the standard deviation of demand shocks is almost the same for both day periods, and equal to 0.015 and 0.014, respectively.

Moreover, similar to generation shocks, speculative shocks vary more during the peak hours than base hours. This outcome may reflect the complex bidding strategies of market players and nonlinear marginal costs curve of electricity producers.

Based on the estimated models, the input of structural shocks to the variance of electricity prices can be estimated. The results are presented in Table 45.3. It can be noticed that the speculative shocks account for more than 90 % of the variance of the electricity price, both in the peak and off-peak hours. This result indicates that unexpected deviations of bidding strategies are more important than shocks to fundamental variables. Second, wind generation shocks have a larger input to the price variance than demand shocks. This shows that the wind generation introduced an additional risk to the market, which should be taken into account by market participants.

45.5 Conclusions

In this research, structural (fundamental and speculative) shocks influencing electricity prices are identified via a Structural VAR (SVAR) model. The results indicate that not all of the fundamental shocks have contemporaneous effect on electricity prices. There is no evidence that electricity prices respond instantaneously to unexpected changes of gas, coal and CO_2 allowances prices. This result is in line with earlier finding of [5]. In the same time, the outcomes indicate that wind generation shocks and demand shocks play an important role in the price setting process.

The findings confirm that there are significant differences in price setting mechanisms between the peak and off-peak hours. This article underlines the importance of speculative shocks, which remains the most important source of electricity price forecast error volatility. When the wind supply shock is considered, the outcomes

indicate that it affects the price variability more than the demand shock. Although, its input to the variance of electricity prices is still small (varies between 4–6 %), it can be expected that it will rise in the following years.

References

1. Blanchard QJ, Quah D (1986) The dynamic effects of aggregate demand and supply disturbances. Am Econ Rev 34:523–533
2. David AK, Wen F (2000) Strategic bidding in competitive electricity markets: a literature survey. In: Power engineering society summer meeting 2000, vol 4. IEEE, New York, pp 2168–2173
3. Eichenbaum M, Evans C (1995) Some empirical evidence on the effects of shocks to the monetary polity on exchange rates. Q J Econ 110:975–1009
4. Fezzi C, Bunn D (2009) Structural interactions of European carbon trading and energy prices. J Energy Mark 4:53–69
5. Fezzi C, Bunn D (2010) Structural analysis of electricity demand and supply interactions. Oxford Bull Econ Stat 72:827–856
6. Forrest S, MacGill I (2013) Assessing the impact of wind generation on wholesale prices and generator dispatch in the Australian National Electricity Market. Energy Policy 59:120–132
7. Harris C (2006) Electricity markets: pricing, structures and economics. Wiley, Chichester
8. Jónssona T, Pinson P, Madsena H (2010) On the market impact of wind energy forecasts. Energy Econ 32:313–320
9. Kelesa D, Genoesea M, Möst D, Ortlieba S, Fichtner W (2013) A combined modeling approach for wind power feed-in and electricity spot prices. Energy Policy 59:213–225
10. Ketterer JC (2014) The impact of wind power generation on the electricity price in Germany. Energy Econ 44:270–280
11. Lütkepohl H (2005) New introduction to multiple time series analysis. Springer, Berlin
12. Mohammadi H (2009) Electricity prices and fuel costs: long-run relations and short-run dynamics. Energy Econ 31:503–509
13. REN21 (2014) Renewables 2014 – global status report. Available at http://www.ren21.net/REN21Activities/GlobalStatusReport.aspx
14. Sims C (1986) Are forecasting models usable for policy analysis. Q Rev - Fed Reserve Bank Minneap 1986:2–16
15. Weron R (2006) Modeling and forecasting electricity loads and prices: a statistical approach. Wiley, Chichester
16. Weron R (2014) Electricity price forecasting: a review of the state-of-the-art with a look into the future. Int J Forecast 30(4):1030–1081
17. Zachmann G, von Hrischhausen C (2008) First evidence of asymmetric cost pass-through of EU emission allowances: examining wholesale electricity prices in Germany. Econ Lett 99:465–469

Chapter 46
Decentralized Time-Constrained Scheduling for Sensor Network in Identification of Distributed Parameter Systems

Maciej Patan and Adam Romanek

Abstract An efficient approach to determine an activation policy for scanning sensor network monitoring a distributed process over some spatial domain is proposed. The scheduling problem is defined so as to maximize a criterion defined on the Fisher information matrix associated with the estimated parameters. Then, adopting pairwise communication schemes, the multi-exchange procedure is developed, which distributes the configuration process between the network nodes and take account to power consumption constraints. The approach is illustrated through an example on a sensor network scheduling problem for a convective diffusion process.

46.1 Introduction

Experimental design for spatio-temporal physical systems also called distributed parameter systems (DPSs) is often related to an optimal choice of measurement conditions in order to obtain the best information for estimating unknown parameters which can then be used, e.g., in optimal control. The impossibility to observe the system states over the entire spatial domain implies the question of where to locate discrete sensors and how to schedule the observations so as to accurately estimate the unknown system parameters. This question acquires especially vital importance in the context of recent advances in distributed sensor networks (SNs) which constitute a natural tools of monitoring distributed systems [3, 11, 18]. On one hand, SNs have recently come into prominence because they hold the potential to revolutionize observation systems. On the other hand, however, completely new challenges related to design problems are encountered.

Although laborious research on the development of strategies for efficient sensor placement has been conducted over the past years, the number of sensor placement

M. Patan (✉) · A. Romanek
Institute of Control and Computation Engineering, University of Zielona Góra, ul. Podgórna 50, 65-246 Zielona Góra, Poland
e-mail: M.Patan@issi.uz.zgora.pl

A. Romanek
e-mail: A.Romanek@weit.uz.zgora.pl

A. Steland et al. (eds.), *Stochastic Models, Statistics and Their Applications*,
Springer Proceedings in Mathematics & Statistics 122,
DOI 10.1007/978-3-319-13881-7_46

techniques developed to manage the problems of practical scale is very limited (cf. [6, 11, 18]), however some effective approaches have been proposed to cover various experimental settings, including stationary [7, 12, 14, 19], scanning [8–10, 13, 21] or moving observations [4, 5, 11, 15, 17, 20, 22].

The main aim of this work is to substantially extend the decentralized approach to scanning sensor configuration reported in [10] to the setting of sensor networks, where the observation system comprises multiple subnetworks and it is desired to activate only a subset of their nodes during a given time interval while the other sensors remain dormant. Additionally, the investigations include limitations on the power consumption of individual sensor nodes. Motivations come from technical limitations imposed on the time span of the measurements. These are inherent to sensor nodes, which are supplied with power from batteries, and therefore their total time of active work is limited.

46.2 Optimal Experimental Design Problem in Context

Let $y = y(x, t; \theta)$ denote the scalar state of a given DPS at a spatial point $x \in \Omega \subset \mathbb{R}^d$ and time instant $t \in T = [0, t_f]$, $t_f < \infty$. Here θ represents an unknown constant m-dimensional parameter vector which must be estimated using observations of the system. Further, let assume that the state y is observed directly by N pointwise sensors, from among only n are activated at time instants $0 < t_0 < t_1 < \cdots < t_K = t_f$ and will gather the continuous measurements for the duration of each subinterval $T_k = (t_{k-1}, t_k]$, $k = 1, \ldots, K$. Forming such an arbitrary partition on the time interval T, the considered 'scanning' observation strategy can be formally represented as

$$z_{\mathrm{m}}^{\ell}(t) = y\big(x_k^{\ell}, t; \theta\big) + \varepsilon\big(x_k^{\ell}, t\big), \quad t \in T_k,\ \ell = 1, \ldots, n,\ k = 1, \ldots K \tag{46.1}$$

where $z_{\mathrm{m}}^{\ell}(t)$ is the scalar output and $x_k^{\ell} \in X$ stands for the location of the ℓth sensor at time subinterval T_k, X signifies the part of the spatial domain Ω where the measurements can be made and $\varepsilon(x_k^{\ell}, t)$ denotes the measurement noise, which is customarily assumed to be zero-mean, Gaussian, spatial uncorrelated and white [18].

Given the model response $y(x_k^{\ell}, t; \theta)$ and the outcomes of the measurements $z_{\mathrm{m}}^{\ell}(\cdot)$, $\ell = 1, \ldots, n$ on time intervals T_k, estimate θ by $\widehat{\theta}$, a global minimizer of the output least-squares criterion [10, 18]. Since the covariance matrix $\mathrm{cov}(\widehat{\theta})$ of the least-squares estimator depends on the active sensor locations x_k^{ℓ}, therefore some measure Ψ quantifying the 'goodness' of different sensor configurations is required. Such criterion is customarily based on the concept of the *Fisher Information Matrix* (FIM) which is widely used in optimum experimental design theory for lumped systems [1, 18] as its inverse constitutes a good approximation of $\mathrm{cov}(\widehat{\theta})$.

The optimal sensor scheduling problem consists in seeking for each time subinterval T_k the best subset of n locations from among the N given potential ones. More precisely, the problem is to divide for each time subinterval the N available sensor nodes into n active ones and the remaining $N - n$ dormant ones so as to

maximize the criterion associated with the parameters to be estimated. However, since the available battery power for each node is limited, we impose the crucial constraints on total activation time for each individual sensor node in the form of the upper limit L denoting the maximal number of time subintervals the sensor is allowed to be active.

Introducing for each possible location x^i $(i = 1, \ldots, N)$ a set of variables v_k^is, each of them taking the value 1 or 0 depending on whether or not a sensor residing at x^i is activated during T_k. Therefore, in our setting, the FIM is given by [10]

$$M = \sum_{i=1}^{N} \sum_{k=1}^{K} v_k^i M_k\big(x^i\big), \tag{46.2}$$

where $M_k(x^i) = \frac{1}{t_f} \int_{T_k} g(x^i, t) g^{\mathsf{T}}(x^i, t) \mathrm{d}t$ and $g(x, t) = \big[\frac{\partial y(x,t;\vartheta)}{\partial \vartheta_1}, \ldots, \frac{\partial y(x,t;\vartheta)}{\partial \vartheta_m}\big]^{\mathsf{T}}_{\vartheta=\theta^0}$ stands for the so-called *sensitivity vector* (θ^0 is some preliminary estimate required for its calculation). As for a specific form of Ψ, various options exist [1], but the most popular criterion to be maximized, called the D-optimality criterion, is the log-determinant of the FIM, i.e. $\Psi(M) = \log\det(M)$. Hence, denoting as $v = [v_k^i]_{k=1,\ldots,K}^{i=1,\ldots,N}$, our design problem takes the following form:

Problem 46.1 Find v maximizing $\mathscr{P}(v) = \Psi(M)$, subject to $v_k^i \in \{0, 1\}$, $\sum_{i=1}^{N} v_k^i = n$, $k = 1, \ldots, K$ and $\sum_{k=1}^{K} v_k^i \le L$, $i = 1, \ldots, N$.

This constitutes a 0–1 integer programming problem which necessitates an original and efficient solution. Suppose that the matrix $M(v^\star)$ is nonsingular. It can be shown [11, Prop. 6.1, p. 162] that the matrix $v^\star$ constitutes a global solution to Problem 1 if, and only if, there exist numbers $\lambda_k^\star$, $k = 1, \ldots, K$ such that

$$\phi\big(i, k, v^\star\big) = \mathrm{tr}\big[M^{-1}\big(v^\star\big) M_k\big(x^i\big)\big] \begin{cases} \ge \lambda_k^\star & \text{if } v_k^{i\,\star} = 1, \\ \le \lambda_k^\star & \text{if } v_k^{i\,\star} = 0. \end{cases} \tag{46.3}$$

46.3 Decentralized Multi-exchange Algorithm

To make the outlined idea useful in applications, a numerical algorithm has to be employed. In [21] an effective computational scheme was developed and further improved in [11, 16] to effectively solve a similar problem based on the notion of so-called directly constrained design measures. Nevertheless, its fully centralized character makes it vulnerable with respect to the failures of individual network nodes. Therefore, the key property of the resulting procedure should be an efficient distribution of computations between the sensor nodes in a decentralized way. On the other hand, the fully distributed algorithm proposed in [10] may lead to significant rate of communications between individual sensors in the network, slowing down the convergence. Hence, the main aim of this work is to derive the algorithmic procedure which combines the advantages of those two approaches, providing

a compromise between reasonable rate of communications and distributed structure of computations.

The general idea is to construct a two-level structure of the network. First, we introduce the partitioning of network into G disjointed groups of sensors (subnetworks) with N_p sensors in the pth group, in such a way that $\sum_{p=1}^{G} N_p = N$. As the issue of optimal partitioning is far beyond the scope of this paper, here we assume that this is done arbitrarily. The resulting subnetworks are forming the lower level of our structure. Further, we assume that for each group we have the same superior entity, further called as *master node*, responsible for observation schedule optimization within the scope of individual group. These master nodes form the higher level of network which serves as the routing layer for exchanging the data between subnetworks, stores the local activation schedules and finally performs all the computations. The network nodes at lower level within each group communicate only with their master node to upload sensor readings during the actual experiment. In such a way, we obtain the mixed structure: centralized at level of subnetworks and decentralized on the level of master nodes which are responsible for distributing computations.

In the following we assume the asynchronous time model for the configuration process. Let $r = 0, 1, 2, \ldots$ be the discrete time index, which partition the continuous configuration time axis into time slots $Z_r = (z_{r-1}, z_r]$.

Owing to (46.3), $v_k^\star$ should be nonzero in the areas where $\phi_k(\cdot, \cdot, v^\star)$ takes on a larger value. Thus the central idea when constructing a computational algorithm for sensor density optimization is to move at configuration iteration r some observational activity from areas with smaller values of $\phi(\cdot, \cdot, v^{(r)})$ to those with larger values, as we expect that such a procedure will improve current solution $v^{(r)}$. The only component of $\phi(\cdot, \cdot, v^{(r)})$ which cannot be calculated independently of other nodes is the global information matrix (46.2) being a weighted average of the local information matrices $M_k(x^i)$. In such a way, our task is closely related to the problem of distributed averaging on a sensor network [2]. One of the simplest techniques dedicated for distributed averaging is a pairwise communication flooding, also known as a *gossip* scheme, which in its classic version assumes that at the rth time slot the pth sensor contacts some neighboring node q with probability P_{ij}, i.e., a pair $(p - q)$ is randomly and independently selected. At this time, both nodes set their values equal to the average of their current values.

In our setting the problem is slightly different as not all of the nodes contribute to the global estimate of FIM at the rth configuration slot. Therefore, apart from updating local estimates of the FIM the sensor nodes should be equipped with a mechanism to store and change the global activation schedule $v^{(r)}$. This can be achieved by the exchange of tokens representing the activation of the sensors at given subintervals T_k. Such tokens are transferred between nodes in the situation where a neighbor node at particular observation subinterval T_k is more informative in the sense of the function ϕ calculated on the current estimates of FIM (and, obviously, it is not activated yet). Furthermore, the total number of tokens at local node can be easy controlled with respect to the maximal number L of active time subintervals for individual sensor.

Algorithm 46.1 Distributed data exchange model. Indexes p and q denote, respectively, data from local repository and obtained from neighbor

procedure EXCHANGE_PROTCOL
  EXCHANGE(M^p, M^q)
  EXCHANGE($v(p)$, $v(q)$)
  $M^p \leftarrow$ RECENT(M^p, M^q)
  $M_{\text{avg}} \leftarrow$ AVG-NOT-NULL(M^p)
  for $k \leftarrow 1, K$ **do**
    for $\ell \leftarrow 1, N_p$ **do**
      $\phi_k^\ell \leftarrow \text{tr}[M_{\text{avg}}^{-1} M_k(x^\ell)]$
    end for
    EXCHANGE($(\phi_k^\ell)_{\ell=1}^{N_p}$, $(\phi_k^\ell)_{\ell=1}^{N_q}$)
    PASS-TOKEN($(\phi_k^\ell)_{\ell=1}^{N_p}$, $(\phi_k^\ell)_{\ell=1}^{N_q}$)
  end for
  $M_{new}(p) = \sum_{i=1}^{N_p} \sum_{k=1}^{K} v_k^i(p) M_k(x_i(p))$
  $M_p^p = (M_{new}(p), r)$
  EXCHANGE($M_{new}(p)$, $M_{new}(q)$)
  $M_q^p = (M_{new}(q), r)$
end procedure

Let M_j^m denote the local estimate of the FIM from the jth subnetwork stored at mth master node and the r_j^m be the configuration time when M_j^m has been updated for the last time. At $r = 0$ a sensor network starts with arbitrarily given token allocation and the following initial values of FIM estimates $M_j^m = \sum_{i=1}^{N_m} \sum_{k=1}^{K} v_k^i M_k(x^i)$ if $j = m$ and $M_j^m = \text{NULL}$ if $j \neq m$, where NULL means that FIM estimate is unknown. In that way, at mth master node the collection of pairs $M^m = (M_j^m, r_j^m)_{j=1}^G$ is stored. Then, at each subsequent time slot Z_r a random pair (p, q) of master nodes performs communication. The scheme of calculations form the point of view of pth node is embodied in Algorithm 46.1. The crucial operators of this procedure are:

- EXCHANGE operator stands for pairwise duplex exchange of data between two master nodes
- RECENT operator is responsible for building a list of the most recent values from pairs generated by iterating element-wise along both operands and updating the older value of FIM (i.e. $M_j^p \leftarrow M_j^q$ if $r_j^p < r_j^q$ and $M_j^q \leftarrow M_j^p$ otherwise)
- AVG-NOT-NULL operator computes the average of input collection of information matrices rejecting those the NULL ones (NULL values are simply treated to be missing)
- PASS-TOKEN operator determines for each time subinterval T_k, the worst active sensor within the subnetworks p and q (in terms of lowest current value of $\phi(\cdot, k, v^{(r)})$) and the best inactive sensor (in terms of greatest current value of $\phi(\cdot, k, v^{(r)})$), which is currently active in less than L time subintervals (so that it could become active). If no such sensors exist then the operator does nothing. If

$\phi(\text{worst}, k, v^{(r)}) < \phi(\text{best}, k, v^{(r)})$ then $v_k^{\text{worst}} \leftarrow 0$ (deactivation of worst active) and $v_k^{\text{best}} \leftarrow 1$ (activation of best inactive). In particular, for this purpose, some existing efficient exchange algorithms can be applied [10, 18, 21].

46.4 Simulation Example

Consider the problem of sensor configuration for parameter estimation in the process of air pollutant transport-chemistry over a given urban area Ω, being a square with a side of length 1 km. In this domain, two active sources of pollution are present, which yield the pollutant spatial concentration $y = y(x,t)$. The evolution of y over the observation interval $T = (0, 1000]$ (in seconds) is described by the following initial–boundary problem:

$$\begin{aligned} &\frac{\partial y(x,t)}{\partial t} + \nabla \cdot \big(v(x,t)y(x,t)\big) = \nabla \cdot \big(\kappa \nabla y(x,t)\big) + f_1(x) + f_2(x), \quad x \in \Omega \\ &\frac{\partial y(x,t)}{\partial n} = 0, \quad \text{on } \partial\Omega \times T, \qquad y(x,0) = y_0, \quad \text{in } \Omega, \end{aligned} \tag{46.4}$$

where terms $f_\ell(x) = \mu_\ell \exp(-100\|x - \chi^\ell\|^2)$, $\ell = 1, 2$ represent the pollutant sources with emission intensities μ_ℓ located at the points $\chi^\ell = (\chi_1^\ell, \chi_2^\ell)$, $\ell = 1, 2$, and $\partial y/\partial n$ stands for the partial derivative of y with respect to the outward normal to the boundary $\partial\Omega$. The average spatio-temporal changes of the wind velocity field over Ω were approximated according to the model (scaled in [km/h]) $v(x,t) = 7.2 \cdot (x_1 + x_2 - t \cdot 10^{-3}; (2x_1 - 1)t \cdot 10^{-3} + x_2 - 1)$. Furthermore, κ denotes an unknown turbulent diffusion coefficient.

The goal of this simulation is to determine the locations of the pollutant sources, their emission intensities and the unknown diffusion coefficient. In order to estimate the parameter vector $\theta = (\mu_1, \chi_1^1, \chi_2^1, \mu_2, \chi_1^2, \chi_2^2, \kappa)$ a sensor network with scanning nodes has been applied. The observation horizon was split into 5 evenly partitioned subintervals $T_k = (200(k-1), 200k]$, $k = 1, \ldots, 5$.

The initial values of the parameters to be identified were assumed to be $\theta_0 = (12\ \text{kg/s}, 0.4\ \text{km}, 0.7\ \text{km}, 15\ \text{kg/s}, 0.8\ \text{km}, 0.3\ \text{km}, 50\ \text{m}^2/\text{s})$. The possible sensor locations were chosen from the mesh of $N = 460$ points uniformly distributed over the area Ω (depicted in Fig. 46.1). The problem was to design a D-optimal schedule to activate at each subinterval T_k a subset of $n = 100$ out of $N = 460$ sensors that would take the measurements, simultaneously providing that a single node would be active for no more than L time subintervals. It was assumed that all master nodes form a fully connected communication graph with uniform probability distribution of a single communication between a given pair of them. The number of groups G was set to 21. Such two-level structure allowed to reduce the number of sensor pairwise communications by the factor of 10^3 in comparison to fully distributed communication scheme [10]. For the purpose of this experiment we assumed that the resulting groups should be of sim-

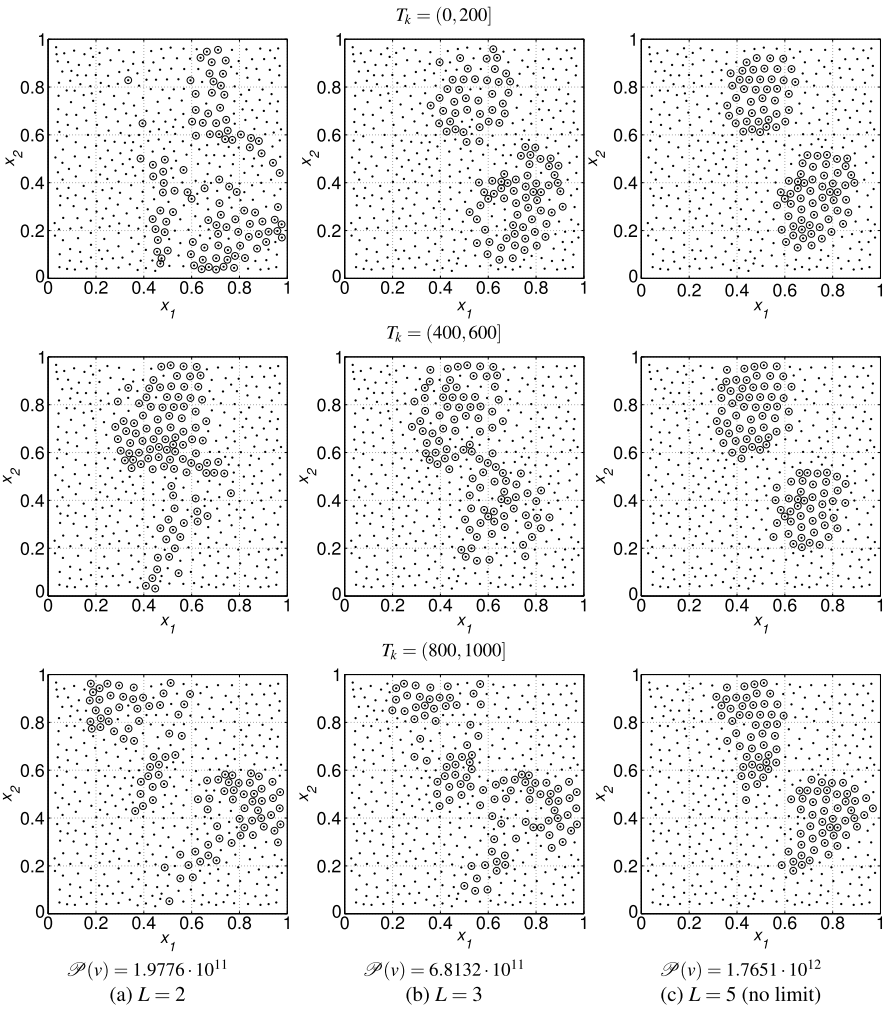

Fig. 46.1 Final allocation of active sensors at selected time subintervals subject to various time activation constraints **(a)**–**(b)** and without time constraints **(c)**

ilar cardinality. The initial sensor configuration was chosen randomly for each time subinterval T_k. The activation schedules obtained for various upper limits L are shown in Fig. 46.1. The network activation patterns follow the complex changes in the concentration of the pollutant proliferating from two sources. It becomes clear that the restrictive constraints on activation time lead to slight decrease in solution efficiency, but provides better distribution of measurement effort between the network nodes as the activated clusters are more spatially scattered.

46.5 Conclusion

The sensor scheduling problem in view of accurate parameter estimation for distributed parameter systems subject to limitations both on the total number of activated sensor nodes and activation time has been addressed. As a result, an exchange algorithm is developed which operates efficiently in a decentralized manner.

Further research will be directed toward the open issue of the sensor partitioning scheme which is of great importance from the point of view of convergence rate. Finally, the current solution allows two master nodes to exchange only one token for each time interval during a single communication. Therefore, some more efficient token exchange schemes will be investigated as well.

References

1. Atkinson AC, Donev AN, Tobias RD (2007) Optimum experimental designs, with SAS. Oxford University Press, Oxford
2. Boyd S, Ghosh A, Prabhakar B, Shah D (2006) Randomized gossip algorithms. IEEE Trans Inf Theory 52(6):2508–2530
3. Cassandras CG, Li W (2005) Sensor networks and cooperative control. Eur J Control 11(4–5):436–463
4. Demetriou MA, Hussein I (2009) Estimation of spatially distributed processes using mobile spatially distributed sensor network. SIAM J Control Optim 48(1):266–291
5. Jeremić A, Nehorai A (2000) Landmine detection and localization using chemical sensor array processing. IEEE Trans Signal Process 48(5):1295–1305
6. Kubrusly CS, Malebranche H (1985) Sensors and controllers location in distributed systems—a survey. Automatica 21(2):117–128
7. Nehorai A, Porat B, Paldi E (1995) Detection and localization of vapor-emitting sources. IEEE Trans Signal Process 43(1):243–253
8. Patan M (2006) Optimal activation policies for continuous scanning observations in parameter estimation of distributed systems. Int J Syst Sci 37(11):763–775
9. Patan M (2008) A parallel sensor scheduling technique for fault detection in distributed parameter systems. In: Luque E, Margalef T, Benitez D (eds) Euro-Par 2008: parallel processing. Lecture notes in computer science, vol 5168, pp 833–843
10. Patan M (2012) Distributed scheduling of sensor networks for identification of spatio-temporal processes. Int J Appl Math Comput Sci 22(2):299–311
11. Patan M (2012) Optimal sensor networks scheduling in identification of distributed parameter systems. Lecture notes in control and information sciences, vol 425. Springer, Berlin, doi:10.1007/978-3-642-28230-0
12. Patan M, Uciński D (2008) Configuring a sensor network for fault detection in distributed parameter systems. Int J Appl Math Comput Sci 18(4):513–524
13. Patan M, Uciński D (2010) Time-constrained sensor scheduling for parameter estimation of distributed systems. In: Proc 49th IEEE conference on decision and control, Atlanta, USA, 16–19 Dec. 2010, pp 7–12. Published on CD-ROM, doi:10.1109/CDC.2010.5717912
14. Rafajłowicz E (1983) Optimal experiment design for identification of linear distributed-parameter systems: frequency domain approach. IEEE Trans Autom Control 28(7):806–808
15. Rafajłowicz E (1986) Optimum choice of moving sensor trajectories for distributed parameter system identification. Int J Control 43(5):1441–1451

16. Romanek A, Patan M (2014) Decentralized multi-exchange scheduling of sensor networks for parameter estimation of distributed systems. In: Proc 19th int conference on methods and models in automation and robotics 2014, Miedzyzdroje, Poland, 2–5 September 2014. Published on CD-ROM, doi:10.1109/MMAR.2014.6957426
17. Tricaud C, Patan M, Uciński D, Chen Y (2008) D-optimal trajectory design of heterogeneous mobile sensors for parameter estimation of distributed systems. In: Proc 2008 American control conference, Seattle, WA, 11–13 June. Published on CD-ROM, doi:10.1109/ACC.2008.4586568
18. Uciński D (2005) Optimal measurement methods for distributed-parameter system identification. CRC Press, Boca Raton
19. Uciński D (2012) Sensor network scheduling for identification of spatially distributed processes. Int J Appl Math Comput Sci 22(1):25–40
20. Uciński D, Chen Y (2005) Time-optimal path planning of moving sensors for parameter estimation of distributed systems. In: Proc 44th IEEE conference on decision and control, and the European control conference 2005, Seville, Spain. Published on CD-ROM
21. Uciński D, Patan M (2002) Optimal location of discrete scanning sensors for parameter estimation of distributed systems. In: Proc 15th IFAC World Congress, Barcelona, Spain, 22–26 July 2002, pp 22–26. Published on CD-ROM
22. Uciński D, Patan M (2010) Sensor network design for the estimation of spatially distributed processes. Int J Appl Math Comput Sci 20(3):459–481

Chapter 47
Least Squares Estimators of Peptide Species Concentrations Based on Gaussian Mixture Decompositions of Protein Mass Spectra

Andrzej Polanski, Michal Marczyk, Monika Pietrowska, Piotr Widlak, and Joanna Polanska

Abstract In this paper we propose to use Gaussian mixture decompositions of protein mass spectral signals to construct least squares estimators of peptide species concentrations in proteomic samples and further to use these estimators as spectral features in cancer versus normal spectral classifiers. For a real dataset we compare variances of least squares estimators to variances of analogous estimators based on spectral peaks. We also evaluate performance of spectral classifiers with features defined by either least squares estimators or by spectral peaks by their power to differentiate between patterns specific for case and control samples of head and neck cancer patients. Cancer/normal classifiers based on spectral features defined by Gaussian components achieved lower average error rates than classifiers based on spectral peaks.

47.1 Introduction

Majority of procedures for processing of proteomic mass spectral profiles involve direct detection and alignment of individual peaks in the spectra, with the underlying

A. Polanski (✉)
Institute of Informatics, Silesian University of Technology, Gliwice, Poland
e-mail: andrzej.polanski@polsl.pl

M. Marczyk · J. Polanska
Data Mining Group, Silesian University of Technology, Gliwice, Poland

J. Polanska
e-mail: joanna.polanska@polsl.pl

M. Marczyk
e-mail: michal.marczyk@polsl.pl

M. Pietrowska · P. Widlak
Maria Sklodowska-Curie Memorial Cancer Center and Institute of Oncology, Gliwice, Poland

P. Widlak
e-mail: widlak@io.gliwice.pl

M. Pietrowska
e-mail: m-pietrowska@io.gliwice.pl

A. Steland et al. (eds.), *Stochastic Models, Statistics and Their Applications*,
Springer Proceedings in Mathematics & Statistics 122,
DOI 10.1007/978-3-319-13881-7_47

hypotheses that each spectral peak corresponds to a specific protein/peptide ion registered, and positions and heights of peaks carry information on compositions of the analyzed samples. Consequently, the largest portion of the published mass spectral classifiers for distinguishing between case and control samples in proteomic data include procedures for direct extraction of spectral peaks and using their parameters for classification, e.g., [1–4, 8, 10, 17].

Obviously, reducing the MS signal to a list of spectral peaks leads, at least in principle, to the loss of information. Some of structural elements of the MS signal can be lost and peaks heights data can be corrupted by noise of excessive level. These concerns can be addressed by representing the MS signals with the use of more developed mathematical model. An obvious choice is a mixture model with Gaussian distribution functions as a natural option for the component functions. Application of mixtures of Gaussian probability distribution functions to dissolve mass spectra of protein mix has been already studied. Several aspects of using Gaussian mixture modeling for protein MS spectra were highlighted in [6, 11, 14, 15, 20]. In particular, in the cases where there are overlaps between components (peaks), mixture models enable detecting components "hidden" behind others. Components of mixture models of MS spectra are characterized by both positions and shapes (widths), while in peak detection methods the information on shapes is missing.

However, none of the mentioned papers analyzed mixture models in the context of developing proteomic mass spectral features and their practical validation in classification experiments. In this paper we point out that, on the basis of Gaussian mixture decomposition of the MS signal [11, 13] it is possible to define least-squares estimators of peptide species concentrations in the protein mix and to propose a method for classification of proteomic MALDI-ToF mass spectra, based on defining the spectral features by these least-square estimators.

The proposed methodology has been applied to the MALDI-ToF mass spectra dataset, comprising spectra of plasma samples of head and neck cancer patients and healthy donors [16]. In computational experiments we demonstrated improvements achieved by the use of the proposed method. We verified the proposed spectral features by comparing variances of estimators of features defined by least-squares to those defined by peak heights and by comparing spectral classifiers based on either least-squares estimates or peak heights.

47.2 Estimators of Peptide Concentrations

A MALDI-ToF mass spectrum contains information about exact mass-to-charge (m/z) values of registered peptide ions and their abundance (i.e., numbers of counts from ion detector). We denote measurement points along the m/z axis by x_n. The numbers of ion counts corresponding to times of flights x_n are denoted by y_n, $n = 1, 2, \ldots N$. N is the number of data points in the spectrum. Real experimental data always consist of more than one spectrum. To each point x_n along the m/z axis correspond counts y_{mn}, $m = 1, 2, \ldots, M$, where m denotes the index of the

spectrum and M is the number of the spectra. The assumption that the sets of values at the m/z axis, x_n, $n = 1, 2, \ldots N$, are identical for all spectra in the dataset is frequently not true; mass spectrometers often generate different sets and different numbers of measurement points x_n along the m/z axis for different spectra. In order to unify values of x_n among all spectra, methods of linear interpolation and trimming are typically applied. Unifying the m/z scale among different spectra by interpolation and trimming is often combined with the operation of binning, which reduces the size of the data and also rejects some of the noise.

The protein mix in the analyzed sample contains a set of peptide species, whose presence in the sample is manifested by maxima (peaks) of the MS signals. We think on one peptide species in the analyzed protein mix sample and we denote its concentration by θ. Below we describe two methods of estimating the value of θ.

47.2.1 Peak Estimator

When we use a spectral peak to estimate θ then the formula for estimator, denoted by $\hat{\theta}_P$ can be written, with some simplification, as follows

$$\hat{\theta}_P = K \max_n y_n \tag{47.1}$$

where K is a constant. The above estimator is called a spectral peak estimator of θ. The simplification follows from the fact, that peak detection algorithms [21] often include additional smoothing operators for reducing the influence of noise on the estimation, which can change the exact position of the maximum. The value of the constant K scales units of peptide concentration to numbers of ion counts registered in the spectra. For the purpose of analyses performed in this paper, we assume that $K = 1$.

47.2.2 Least Squares Estimator

By contemplating the plots of fragments of the spectra in Fig. 47.1 (left panel) we come to the conclusion that the spectral signal y_n provides repeated measurements of the concentration θ. Due to finite resolution of protein mass spectrometers and due to the presence of isotopic forms of atoms in molecules the concentration θ is reflected in all values of the spectral signal y_n at m/z coordinates in the vicinity of $\max(y_n)$. We assume that the values of the spectral signal are related to θ by the following linear model

$$y_n = b_n\theta + e_n \tag{47.2}$$

In the above b_n and e_n describe, respectively, the gain coefficient between spectral signal and the concentration θ, and a random error. After writing Eq. (47.2) in the vector form

$$y = b\theta + e \tag{47.3}$$

where y and b are column vectors composed of elements y_n and b_n, respectively, (with the appropriate range of indices n) one can compute the least-squares estimate of θ as follows (e.g., [5])

$$\hat{\theta} = a^T y, \tag{47.4}$$

where

$$a = \frac{b}{b^T b}. \tag{47.5}$$

In order to apply the least squares estimator (47.4) to a dataset we additionally need to know (estimate) values of the gain coefficients b_n. With an abundance of data provided by proteomic spectra, we can reliably estimate b by the following procedure. We average over all spectra in the analyzed dataset, which strongly reduces the influence of the random error. We assume that fragment of the average spectrum modeled by a Gaussian component corresponds to the error-free version of the relation (47.2). The Gaussian component function corresponding to θ can be written as follows

$$f_\theta(x_n) = \alpha_\theta \frac{1}{\sqrt{\pi}\sigma_\theta} \exp\left[-\frac{(x_n - \mu_\theta)^2}{2\sigma_\theta^2}\right]. \tag{47.6}$$

In the above formula α_θ denotes the Gaussian component scaling factor and μ_θ and σ_θ are, respectively, its expectation and dispersion. Using the notation in (47.6) we obtain the formula for b_n

$$b_n = f_\theta(x_n), \tag{47.7}$$

which allows for efficient use of the least squares estimator (47.4).

We want to compare peak and least squares estimators, which requires that they are scaled equally. Assuming noise free environment and comparing (47.1) with $K = 1$ to (47.4) we derive appropriately scaled least squares estimator of θ, denoted by $\hat{\theta}_{LS}$, defined as follows

$$\hat{\theta}_{LS} = \frac{a^T y}{\sum a_n}. \tag{47.8}$$

47.3 Gaussian Mixture Decomposition of the MS Dataset

The analyzed dataset [16] includes 52 MALDI-ToF mass spectra of plasma proteome. Blood samples were collected in a group of 22 head and neck squamous-cell cancer male patients and in a group of 30 sex- and age-matched healthy donors. The theoretical resolution of the spectrometer used for our experiments was 0.01 %. Spectral fragments ranging from 2,000 to 10,000 Da have been selected for analyses. For each of the 52 samples, mass spectra were registered 4 times and the mean

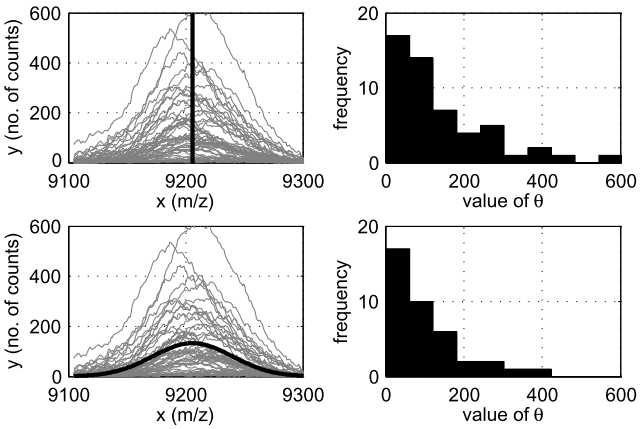

Fig. 47.1 *Left panel*, *upper plot*: Fragments of all 52 protein spectra from the head and neck dataset, from the range defined by the fourth component $\mu_4 - 3\sigma_4 < x < \mu_4 - 3\sigma_4$. Additionally, the m/z position of the peak $mz = 9205.5$ Da detected in the range of the fragments is shown by a vertical line. *Left panel, lower plot*: Again fragments of all 52 protein spectra, the same as in the *upper plot*, are shown. Additionally, the (*scaled*) probability density function corresponding to μ_4, σ_4 is drawn. *Right panel*: Histograms of values of the peptide concentrations (with m/z coordinate close to 9205.9 Da) concentrations, estimated with the use of peak estimator (*upper plot*), and estimated with the use of least squares estimator (*lower plot*)

over 4 experimental repetitions was taken for further analyses. Spectral signals were binned with the resolution 1 Da and, after removing baselines and normalizing [18] average spectrum y_n^A was computed.

Gaussian mixture decomposition of the average spectrum was estimated with the use of an appropriate version of the EM algorithm iterations [6, 11, 13, 19]. EM iterations were started by using the "inverse CDF" method and augmented by some modifications that prevented divergence [19].

47.4 Comparison of Estimators by Variances of Estimated Concentrations

Lest squares estimator (47.8) should, in principle, provide better (lower variance) estimates of the concentration θ than "isolated point" peak estimator (47.1). However, due to simplifying assumption in our derivations, the hypothesis on the advantage of least squares over peak estimators can get support by additional verification on the real dataset.

In order to compute peak estimators we used the algorithm and the computer program CWT described in [7] publicly available in the Internet, for detection of peaks of the proteomic spectra. This algorithm is considered as one of the best among algorithms for spectral peak extraction [21]. We used the program CWT with the settings reported as optimal in [21] which led to the detection of $K = 60$ peaks

and to obtaining values of heights of these peaks for the spectra. Since the obtained number of peaks was rather low (in view of visual inspection for the average spectrum) we additionally modified the parameter ampTh from the default 0.01 to 0.005, which led to obtaining the second, larger set of $K = 84$ peaks. (Parameter ampTh is the lowest threshold value, expressed relatively to the value of the highest detected peak, for the peak to be considered above the noise).

In order to compute least squares estimators two Gaussian decomposition models were found on the basis of EM iterations, where numbers of components were assumed $K = 80$ and $K = 100$. In the next step we have identified five Gaussian components, $\mu_1 = 2013{,}3$ Da, $\sigma_1 = 3.39$ Da, $\mu_2 = 6698.1$ Da, $\sigma_2 = 33.55$ Da, $\mu_3 = 8995.4$ Da, $\sigma_3 = 26.79$ Da, $\mu_4 = 9205.9$ Da, $\sigma_4 = 33.87$ Da, $\mu_5 = 9479.3$ Da, $\sigma_5 = 46.93$ Da. These Gaussian components appear in both decompositions $K = 80$ and $K = 100$ and they are quite well separated from other components. For all these five components we can also easily assign spectral peaks computed by using CWT, present both in $K = 60$ peaks and $K = 84$ peaks decompositions. We have chosen "clear" components separated from others due to simple assignment between Gaussian components and peaks, and because the fact that for overlapping components the assumption of equal scaling of peptide in (47.1) and (47.8) estimates can be violated.

We have computed sample variances of estimates (47.1) and (47.8) for all five locations. Variances of least squares estimators were always lower than variances of peak estimators. Distributions of estimates of concentrations are strongly skewed (see plots in the right panel of Fig. 47.1). Therefore we have used Levene's test [12] for comparing samples variances and we have obtained the following p-values, corresponding to successive locations: 0.1156, 0.0463, 0.2092, 0.0360, 0.0074. P-values are "low" and in three out of five locations the hypothesis on equal variances can be rejected at the significance level less than 0.05.

In the left panel of Fig. 47.1 we show fragments of all 52 protein spectra in the range defined by the fourth component $\mu_4 - 3\sigma_4 < x < \mu_4 - 3\sigma_4$. In the upper plot in the left panel we illustrate the idea of computing peak estimators by drawing a vertical bold line at the position of the detected spectral peak. In the lower plot of the left panel we illustrate the idea of the least squares estimator by drawing (bold line) the (scaled) probability density function corresponding to μ_4, σ_4. In the right panel we present histograms of values of the peptide concentrations (with m/z coordinate close to 9205.9 Da) concentrations, estimated with the use of peak estimator (47.1) – upper plot, and estimated with the use of least squares estimator (47.8) – lower plot.

47.5 Comparison of Spectral Features by Accuracy of Classification

In addition to comparison of variances of selected estimators we have also compared precisions of classifiers based on spectral features defined by estimators of peptide concentrations, peak estimator (47.1) and least squares estimator (47.8).

Table 47.1 Prediction powers of SVM classifiers based on four systems of spectral features. Abbreviations: LS $K = 80$ – least squares features, 80 Gaussian components, LS $K = 100$ – least squares features 100 Gaussian components, Peaks $K = 60$ – peak features, 60 peaks, Peaks $K = 84$ – peak features, 84 peaks

Classifier	LS $KS = 80$	LS $K = 100$	Peaks $K = 60$	Peaks $K = 84$
Lowest error rate	0.17	0.19	0.24	0.23

Then we have carried out standard training – validation experiments for classifiers based on biomarkers chosen from sets of spectral features. Construction of the classifier involved using the training set to recruit a number (2–50) of top differentiating spectral features based on the values of the t statistics. We were using Matlab implementations of the SVM [9] training – classification algorithms. The procedure of 10 – fold validation was repeated 500 times to estimate the average error rate and its standard deviation. We have tried SVM classification algorithms with different kernels and we report predictive powers of the SVM classifier, optimized with respect to the choice of the kernel type (linear, quadratic, Gaussian). For both types of spectral features, best classification results were obtained by using the SVM classifier with the Gaussian kernel (option named rbf in the Matlab procedure). For all classifiers lowest error rates were achieved for numbers of differentiating spectral features from the same range 10–15.

The prediction powers of the SVM classifiers represented as best (lowest) percentage of errors in the 10-fold cross validation experiments are shown in Table 47.1 below. As one can see for spectral classifier based on features defined by least squares estimators the error rates are lower than those obtained in classification based on spectral peaks.

47.6 Conclusion

Computational experiments for a real proteomic MS signals dataset prove that the idea of using Gaussian mixture decompositions of spectral signals to construct least squares estimators of peptide species concentrations in the protein mix and further to construct spectral classifiers can lead to useful results. In the real dataset variances of least squares estimators were statistically significantly lower than variances of peak estimators and classifiers based on features defined by least squares estimators achieved lower average error rates than classifiers based on spectral peaks.

Acknowledgements This work was financially supported by the Polish National Science Centre UMO-2011/01/B/ST6/06868 grant (A.P.), GeCONiI project number POIG.02.03.01-24-099/13 (M.M.) and internal grant from Silesian University of Technology BK/265/RAU-1/2014 t.10 (J.P.). All the calculations were carried out using GeCONiI infrastructure funded by project number POIG.02.03.01-24-099/13.

References

1. Barla A, Jurman G, Riccadonna S, Merler S, Chierici M, Furlanello C (2008) Machine learning methods for predictive proteomics. Brief Bioinform. doi:10.1093/bib/bbn008
2. Baggerly KA, Morris JS, Wang J, Gold D, Xiao LC, Coombes KR (2003) A comprehensive approach to the analysis of matrix-assisted laser desorption/ionization-time of flight proteomics spectra from serum samples. Proteomics 3:1667–1672
3. Baggerly KA, Morris JS, Coombes KR (2004) Reproducibility of SELDI-TOF protein patterns in serum: comparing datasets from different experiments. Bioinformatics 20:777–785
4. Bao-Ling A, Qu Y, Davis JW, Ward MD, Clements MA, Cazares LH, Semmes OJ, Schellhammer PF, Yasui Y, Feng Z, Wright GL Jr (2002) Serum protein fingerprinting coupled with a pattern-matching algorithm distinguishes prostate cancer from benign prostate hyperplasia and healthy men. Cancer Res 62:3609–3614
5. Deutsch R (1965) Estimation theory. Prentice Hall, New York
6. Dijkstra M, Roelofsen H, Vonk RJ, Jansen RC (2006) Peak quantification in surface-enhanced laser desorption/ionization by using mixture models. Proteomics 6(19):5106–5116
7. Du P, Kibbe WA, Lin SM (2006) Improved peak detection in mass spectrum by incorporating continuous wavelet transform-based pattern matching. Bioinformatics 22(17):2059–2065
8. Hale JE, Gelfanova V, Ludwig JR, Knierman MD (2003) Application of proteomics for discovery of protein biomarkers. Brief Funct Genomics Proteomics 2:185–193
9. Hastie T, Tibshirani R, Friedman J (2009) The elements of statistical learning: data mining, inference, and prediction. Springer, Berlin
10. Karpievitch YV, Hill EG, Smolka AJ, Morris JS, Coombes KR, Baggerly KA, Almeida JS (2007) PrepMS: TOF MS data graphical preprocessing tool. Bioinformatics 23(2):264–265
11. Kempka M, Sjodahl J, Bjork A, Roeraade J (2004) Improved method for peak picking in matrix-assisted laser desorption/ionization time-of-flight mass spectrometry. Rapid Commun Mass Spectrom 18:1208–1212
12. Levene H (1960) In: Olkin I, Hotelling H et al (eds) Contributions to probability and statistics: essays in honor of Harold hotelling. Stanford University Press, Stanford, pp 278–292
13. McLachan GJ, Peel W (2000) Finite mixture distributions. Wiley, New York
14. Noy K, Fasulo D (2007) Improved model-based, platform-independent feature extraction for mass spectrometry. Bioinformatics 23(19):2528–2535
15. Pelikan R, Hauskrecht M (2010) Efficient peak-labeling algorithms for whole-sample mass spectrometry proteomics. IEEE/ACM Trans Comput Biol Bioinform 7(1):126–137
16. Pietrowska M, Polanska J, Walaszczyk A, Wygoda A, Rutkowski T, Skladowski K, Marczak L, Stobiecki M, Marczyk M, Polanski A, Widlak P (2011) Association between plasma proteome profiles analysed by mass spectrometry, a lymphocyte-based DNA-break repair assay and radiotherapy-induced acute mucosal reaction in head and neck cancer patients. Int J Radiat Biol 87(7):711–719
17. Ressom HW, Varghese RS, Drake SK, Hortin GL, Abdel-Hamid M, Loffredo CA, Goldman R (2007) Peak selection from MALDI-TOF mass spectra using ant colony optimization. Bioinformatics 23:619–626
18. Sauve AC, Speed TP (2004) Normalization, baseline correction and alignment of high-throughput mass spectrometry data. In: Proceedings gensips
19. Sokol R, Polanski A (2013) Comparison of methods for initializing EM algorithm for estimation of parameters of Gaussian multi component heteroscedastic mixture models. Studia Inform 34(1):1–25
20. Wang Y, Zhou X, Wang H, Li K, Yao L, Wong ST (2008) Reversible jump MCMC approach for peak identification for stroke SELDI mass spectrometry using mixture model. Bioinformatics 24(13):407–413
21. Yang C, He Z, Yu W (2009) Comparison of public peak detection algorithms for MALDI mass spectrometry data analysis. BMC Bioinformatics 10:4

Chapter 48
Detection of Essential Changes in Spatio-Temporal Processes with Applications to Camera Based Quality Control

Ewaryst Rafajłowicz

Abstract Our aim in this paper is to propose a simple detector of changes in time that is well suited for parallel use at a large number of spatial sites, since our main motivation is change detection in a sequence of images that are dedicated for quality control of continuously running industrial processes.

48.1 Introduction

Our aim is to propose a new look at change detection tasks that arise when we observe a large number of parallel processes that may change in time. To motivate our approach, consider a sequence of images provided by a camera that follows the quality of a certain production process. Each image contains millions of pixels. Fixing our attention at a particular pixel we can observe fluctuations of its grey levels in time as one time series. Applying a change detector (e.g., EWMA, CUSUM etc.) to all time series arising from observing each pixel, for each instant of time we obtain a set of YES/NO decisions concerning the presence or absence of a change. It is clear that the change at one pixel only is rather unimportant from the view point of the production quality control. We should rather concentrate on more massive changes that arise in a spatially concentrated area at the same (or approximately the same) time.

From the statistical point of view quite similar change detection tasks arise when a bank observes the amount of money collected on accounts of its clients. Even a sharp change of deposits of one or several clients is usually not important. However, when we detect essential deposit changes of a larger group of clients approximately at the same time (and possibly in the same city or region), then it should be an indicator that something important may happened in the banking market.

One more example of a need for detecting massive changes of parallel processes comes from following intensity of the traffic in the Internet. The growth of the traffic intensity approximately at the same time to a group of web pages is well known

E. Rafajłowicz (✉)
Institute of Computer Engineering, Control and Robotics, Wrocław University of Technology, Wrocław, Poland
e-mail: ewaryst.rafajlowicz@pwr.wroc.pl

A. Steland et al. (eds.), *Stochastic Models, Statistics and Their Applications*,
Springer Proceedings in Mathematics & Statistics 122,
DOI 10.1007/978-3-319-13881-7_48

indicator of hackers attack. In this case a geographical closeness may not appear, but attacked web pages may have similarities of other kind, e.g., the same owner.

In the same vain one can consider:

– a health care system, when the growing number of patients in a certain area should be detected as a possible indicator of an epidemia,
– a stock market – prices of shears of enterprises can fluctuate, but a rapid reduction of them at a certain area can be a symptom of certain economic changes.

All the above examples have the following common features:

1. observed processes run in parallel, but not necessarily independently, in time at different sites (spatial locations),
2. change detection along time axis at one or even a few site(s) (pixels) can be neglected, unless they have very high or very low values in comparison to typical (in-control) state,
3. moderate in size changes of observed variables, arising in time and at moderate area in space are typical cases to be detected,
4. smaller changes of observed variables, but arising at larger areas in the spatial domain should (or at least could) be considered as an alarm,
5. changes along time axis may arise not necessarily at the same time instant, but can be spread in a certain time interval.

Additionally, one should distinguish between up and down changes, because at a certain area the number of up changes may dominate largely the number of down changes and the former can be neglected.

Clearly, the terms used above like: “high” and “low” changes as well as “close” time instants and “larger area” are problem dependent and require to be defined precisely at scales relevant to an application at hand.

The above list of possible changes of interest can be named spatio-temporal change detection problems. One can try to solve some of them using the classic control charts and aggregating observations over the spatial domain. However, such approaches may lead to overlooking changes along time axis when the aggregation covers larger spatial regions. Furthermore, not all the above sketched problems can be solved using a spatial aggregation.

For these reasons it seems justified to consider new kinds of spatio-temporal change detectors. Apparently, it is not possible to propose change detectors for all the above mentioned problems in one paper.

We propose a simple change detector of changes in time that is well suited for parallel use at a large number of spatial sites. The idea is based on exponentially weighted moving average smoothing (EWMAS), but the detector itself is different than the one that is used in the classic EWMA chart. In particular, it allows to distinguish between jumps of a moderate size and those that are large. It keeps the main advantage of the classic EWMA chart, namely, there is no need to store historical data, i.e., for the current decision it suffices to have the present smoothed state and the current observation, which is crucial importance when we have to monitor millions of sites or pixels. The EWMAS is based on the idea of vertical weighting that was used for detecting changes in space (edges) in [14].

Detection of spatio-temporal changes may also include

1. changes along curves at the spatial domain that are observed at the same (or close) time instant(s) can also be of interest (e.g., as in edge detection tasks in image sequence processing),
2. changes of the observed variable that "travels" in time along curves at the spatial domain.

These tasks are much more difficult than those listed above and they are outside the scope of this paper.

Quality control of continuously running industrial production processes is the subject of research for many years (see [10] and the bibliography cited therein and [16, 18] for recently proposed nonparametric control charts). These charts as well as classic control charts like the Shewhart one, CUSUM, EWMA are well suited for detecting changes in time. In the stream of research called spatial statistics (see [3] and the bibliography cited therein) the topic of detecting changes in space domain is present. Somewhat unexpectedly, detecting changes simultaneously in time and space has not so rich bibliography as one might expect. The main contributions in this direction come from applications of image sequences processing and their applications in geoscience (see [1, 5, 6, 11, 17]). Quickest detection of significant changes in a sensor net that is based on a non-cooperative stopping game which is a model of the multivariate disorder detection has been proposed in [19]. The approach proposed in [12] also covers spatio-temporal changes as a special case of detecting jumps of time series with values in a Banach space.

In recent years one can observe a rapid development of relatively cheap, high resolution and high speed industrial cameras that are well suited for quality monitoring of such processes (see [7]). Simultaneously, a high speed, running in parallel computers and graphical processing units (GPU) made it possible to process sequences of high resolution images on-line. As a result, the stream of research on control charting with image data, which is closely related to this paper, is rapidly growing (see [9] for a stimulating review and [8, 13] for more recent contributions).

The paper is organized as follows. In the next section we describe our version of EWMAS temporal change detector and present its elementary properties. Then, we shall describe how a bank of such change detectors can be used to detect spatio-temporal changes. Finally, we present an example of application to quality control of a copper slab using images from a camera.

48.2 EWMA Smoothed Jump Detector

For simplicity, we shall describe our jump detector in 2D spatial case, but the extension to larger dimensions is immediate. Let $x = (x^{(1)}, x^{(2)}) \in \Omega$ denotes a spatial position (e.g., of a pixel or site) in a rectangular domain[1] (image) Ω. By $t = 1, 2, \ldots$

[1] It is convenient to work with a rectangular domain, but all the considerations convey easily to other domains, integer lattices or finite sets.

we denote time instants when observations are made (e.g., images from a camera are sampled). Observed real-valued random field (e.g., grey-level image) $Y(x,t)$ results from observing an unknown function $m(x,t)$ with zero mean, finite variance additive errors $\varepsilon(x,t)$, i.e.,

$$Y(x,t) = m(x,t) + \varepsilon(x,t), \quad x \in \Omega,\ t = 1,2,\ldots. \tag{48.1}$$

The probability distribution of $\varepsilon(x,t)$ is unknown, but – for simplicity of the exposition – we assume that there exists its p.d.f., denoted by f_ε, which does not depend on x and t and it is symmetric. We also assume that $Y(x,t)$ and $Y(x',t')$ are uncorrelated for $t \neq t'$, $t,t' = 1,2,\ldots$, $x,x' \in \Omega$, even if $x = x'$. However, for each t a spatial correlation is allowed. This assumption will be used only when theoretical properties of our jump detector are investigated.

Consider a symmetric and unimodal kernel $K : R \to R^+$ such that $K(0) = 1$ and $K(z) \to 0$ as $|z| \to \infty$. In particular, the gaussian $K_G(z) = \exp(-z^2/2)$ kernel and the uniform one: $K_U(z) = 1$ for $|z| \leq 1$ and $K_U(z) = 0$ for $|z| > 1$ are of special interest.

Then, for $m(x,t)$ we have the following nonlinear equation (see [15] for the proof that can be adopted to the case considered here):

$$m(x,t) = \kappa^{-1} E\big[Y(x,t)K\big(\big(Y(x,t) - m(x,t)\big)/H\big)\big],$$
$$x \in \Omega,\ t = 1,2,\ldots \tag{48.2}$$

where $\kappa \stackrel{def}{=} \int_{-\infty}^{\infty} K(z/H) f_\varepsilon(z)dz$. Equation (48.2) can be the source of many empirical versions for estimating $m(x,t)$. We select one of the simplest that can be run in parallel w.r.t. time for each site (pixel) $x \in \Omega$. Namely,

$$\hat{m}(x,t+1) = (1-\alpha)\hat{m}(x,t) + \frac{\alpha}{\hat{\kappa}} Y(x,t) K\big(\big(Y(x,t) - \hat{m}(x,t)\big)/H\big), \tag{48.3}$$

where $t = 1,2,\ldots$, $x \in \Omega$, while $0 < \alpha < 1$ is a smoothing parameter. Also K and $H > 0$ are selected by the statistician. $\hat{\kappa}$ can be estimated from residuals, because $\kappa = E[K(\varepsilon(x,t)/H)]$. If the variance of $\varepsilon(x,t)$ is small in comparison to H^2, then κ is close to 1 and later on we take $\hat{\kappa} = 1$.

A really fast version of (48.3) one obtains for the uniform kernel:

$$\hat{m}(x,t+1) = (1-\alpha)\hat{m}(x,t) + \begin{cases} 0, & \text{if } |Y(x,t) - \hat{m}(x,t)| > H \\ \alpha Y(x,t) & \text{if } |Y(x,t) - \hat{m}(x,t)| \leq H \end{cases} \tag{48.4}$$

From (48.4) it is clear that $\hat{m}(x,t+1)$ is essentially updated only if there is no jump larger than $H > 0$.

Spatio-Temporal Change Detector – Basic Version

Step 1 – Detection of changes in time. For current time instant t and for every $x \in \Omega$ calculate matrix $B(x,t)$ of the same size as Ω in the following way:

$$B(x,t) = \begin{cases} 1, & \text{if } |Y(x,t) - \hat{m}(x,t)| > H \\ 0, & \text{if } |Y(x,t) - \hat{m}(x,t)| \leq H \end{cases} \tag{48.5}$$

Step 2 – First decision. If $\sum_{x\in\Omega} B(x,t) \le \theta_0$, set $t = t+1$, calculate (48.4) and go to Step 1, otherwise, go to Step 3. Here $\theta_0 \ge 0$ is a threshold preselected in such a way that if we met only a few number of sites with time changes, we can decide that there were no essential changes in the space–time domain.

Step 3 – Removing small clusters in the space domain. For fixed t one can interpret $B(x,t)$ as a binary image and apply image processing tools like morphological erosion or blob analysis (see [2]) in order to remove single sites or small clusters of them by setting the corresponding $B(x,t) = 0$.

Step 4 – Final decision. Select $\theta_1 > \theta_0$ as a threshold for declaring essential spatio-temporal change. If $\sum_{x\in\Omega} B(x,t) \ge \theta_1$, then declare essential change, set $t = t+1$ and go to Step 1. Otherwise, calculate (48.4) and also set $t = t+1$ and go to Step 1.

Remark Only (48.4) and Step 1 can be run in parallel, but these are the most time consuming operations, because they are repeated for all $x \in \Omega$ and all t.

If we skip Step 2 and Step 3 and fix a particular $x \in \Omega$, then we can compare the above algorithm for change detection in time with other control charts. As one can notice, (48.4) runs as the EWMA chart with two exceptions. Namely, $\hat{m}(x,t)$ is updated only when new observation is close to it. Thus, $\hat{m}(x,t)$ estimates the process mean, but only in-control states. In contrary, in EWMA chart $\hat{m}(x,t)$ also jumps are incorporated into $\hat{m}(x,t)$, if they were not detected. The second difference is in that in the classic EWMA chart $\hat{m}(x,t)$ is compared to the threshold in order to detect jumps. Here, the decision is based on the difference $Y(x,t) - \hat{m}(x,t)$, which resembles the Shewhart control chart, however with important difference that the smoothed in-control behavior $\hat{m}(x,t)$ is the base for comparisons. One may hope that the proposed combination of the EWMA smoothing idea and the Shewhart chart gives a detector that will be useful for spatio-temporal change detection.

By simple modifications one can easily tune the above basic algorithm to a variety of particular applications.

1. When only jumps above the mean are of interest, i.e., the conditions in (48.4) and in (48.5) are replaced by $Y(x,t) - \hat{m}(x,t) > H$ (resp. $\le H$), then in Step 4 the final decision can take also jump heights into account as follows: $\sum_{x\in\Omega}(Y(x,t) - \hat{m}(x,t))B(x,t) \ge \theta_1$.
2. In Step 4 the final decision takes into account changes detected at the same time instant. When sampling rate in time is high, one can consider also changes that occurred at several earlier time instants $J \ge 1$, i.e., $\sum_{j=0}^{J}\sum_{x\in\Omega} B(x,t-j) \ge \theta_1$ at all spatial points. This require to store $(J+1)$th previous $B(x,t-j)$ matrices.
3. One can replace the conditions in (48.5) by the following:

$$\left| Y(x,t) - z^{-1} \sum_{x\in Z(x)} \hat{m}(x,t) \right| > H \quad (\le H, \text{ resp.}),$$

where $Z(x)$ is a neighborhood of x, while z is its cardinality. This version is less sensitive to false alarms, but not so easy to run on parallel processors as (48.5).

48.3 Some Properties of the Spatio-Temporal Change Detector

In this section we announce simple properties of the basic version of our spatio-temporal change detector. By the lack of space, we omit most of the proofs that will be published elsewhere. For simplicity, we assume that in the basic algorithm Step 3 and Step 4 is omitted.

For simplicity we assume that random errors are commonly bounded, i.e., there exists $\mathscr{E}$ such that with probability 1, $|\varepsilon(x,t)| \le \mathscr{E}$. H is selected such that $H \ge 2\mathscr{E}$, which means that there are no guarantees of detecting jumps smaller than $2\mathscr{E}$.

In Control Behavior Let us assume for a while that there are no spatio-temporal jumps, i.e., $Y(x,t) = M(x) + \varepsilon(x,t)$, $x \in \Omega$, $t = 1, 2, \ldots$, where $M(x)$ is a stationary proper background process. If our algorithm starts from $\hat{m}(x,0) = Y(x,0)$, then the following properties can be proved.

InC1 $E[\hat{m}(x,t)] = M(x)$, $x \in \Omega$, $t = 1, 2, \ldots$.

InC2 The false alarm probability is zero for all $x \in \Omega$ and $t > 1$. Notice that this is the consequence of the assumptions: $|\varepsilon(x,t)| \le \mathscr{E}$ and $H \ge 2\mathscr{E}$.

InC3 For $x \in \Omega$ and $t = 1, 2, \ldots$, define $\hat{\varepsilon}(x,t) = M(x) - \hat{m}(x,t)$. Then, for $\hat{\varepsilon}$ the following recurrent relationships hold:

$$\hat{\varepsilon}(x,t) = (1-\alpha)\hat{\varepsilon}(x,t-1) + \alpha\varepsilon(x,t), \quad t = 1, 2, \ldots \tag{48.6}$$

with the initial condition $\hat{\varepsilon}(x,0) = \varepsilon(x,0)$. Furthermore, (48.6) implies $|\hat{\varepsilon}(x,t)| \le \mathscr{E}$.

InC4 For $x \in \Omega$ and $t = 1, 2, \ldots$ we have $|Y(x,t) - \hat{m}(x,t)| \le 2\mathscr{E}$.

Change Detection We firstly consider change detection in time for arbitrary but fixed spatial site $x \in \Omega$. To this end we assume that at a certain time instant $t_0 > 1$ for the first time

$$Y(x,t_0) = M(x) + r(x,t_0) + \varepsilon(x,t_0), \quad x \in \Omega \tag{48.7}$$

where $r(x,t_0)$ is a jump to be detected, which is assumed to be persistent ((48.7) holds also for $t > t_0$) and bounded away from 0, i.e., there exists $R > 0$ such that $r(x,t_0) > R$, $x \in \Omega$.

We shall assume that R is known and $R > 3\mathscr{E}$, because it defines the smallest jump that we are able to detect immediately, as we shall see below. Select $H > 0$ such that

$$\mathscr{E} \le H < R - 2\mathscr{E}. \tag{48.8}$$

Let us note that $\hat{m}(x,t_0) = M(x) + \hat{\varepsilon}(x,t_0)$, according to (48.6), which can be invoked here, because there was no jump before t_0. Hence, using this equality and (48.7) we obtain

$$\left|Y(x,t_0) - \hat{m}(x,t_0)\right| = \left|r(x,t_0) + \varepsilon(x,t_0) - \hat{\varepsilon}(x,t_0)\right| \ge R - 2\mathscr{E}. \tag{48.9}$$

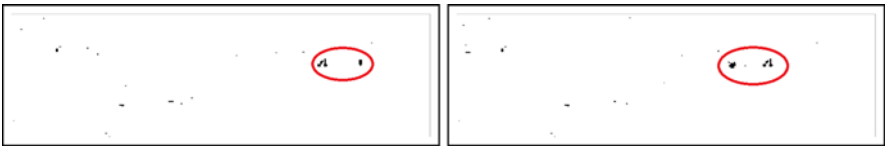

Fig. 48.1 Defects detected on the copper slab – two subsequent frames (the left image was taken first)

The last inequality follows from the following facts: $r(x,t_0) > R$, $|\varepsilon(x,t_0)| \leq \mathscr{E}$, which also implies $|\hat{\varepsilon}(x,t_0)| \leq \mathscr{E}$ with probability one. In the worst case $r(x,t_0) + \varepsilon(x,t_0) - \hat{\varepsilon}(x,t_0) = R - \mathscr{E} - \mathscr{E}$, which finishes the proof of (48.9). According to (48.8) this implies $|Y(x,t_0) - \hat{m}(x,t_0)| > H$.

Corollary 48.1 *Under the above assumptions the jump is detected immediately after its occurrence at each site $x \in \Omega$ where it appears.*

The above corollary was obtained under idealized assumptions. In practice, $\mathscr{E}$ is not known and should be estimated from previous runs. If the errors have a distribution with infinite support, then one can select $\mathscr{E}$ so as with probability $0 < \beta < 1$ errors are contained in the interval $[-\mathscr{E}, \mathscr{E}]$. Then, repeating the above reasoning, we can say that with probability at least β jumps will be detected at time t_0 at all sites where they happened. Hence, if jumps appeared at $K > \theta_1$ sites, then the probability that less than θ_1 of them will be detected at t_0 can easily be calculated from the binomial distribution, since the events of detecting or not detecting a jump at each site at t_0 are independent. If a jump in a certain site is not detected at t_0 it will be detected later with a high probability, but evaluating it is not so easy, because heights of the undetected jumps enter into $\hat{m}(x, t_0 + j)$, $j = 1, 2, \ldots$.

Example The above approach to spatio-temporal change detection can be used for quality control of continuously running processes like production of plain fabrics, paper, steel sheets, wires, slabs, uniformly painted surfaces etc. The idea is based on a simple constatation that it is very difficult to detect a motion of a uniformly painted or produced surface. In contrary, any defects, having different grey levels than the proper surface, are easier to detect as moving objects, because they are frequently visible at several subsequent images. Additional feature of our approach is its ability to follow slow changes of a background, caused, e.g., by changes of its temperature (see also [4]).

Exactly such circumstances appear when we want to detect defects (darker places) on a proper (bright) surface of a hot copper slab continuously moving before a camera. Slow changes of the proper surface temperature make the task more difficult. Applying the proposed approach with the uniform kernel K, $\alpha = 0.5$ and $H = 6$ grey levels (scale $[0, 255]$) provides the results shown in Fig. 48.1, where matrices $B(x,t)$ and $B(x,t+1)$ are displayed as images. As one can notice, the results are quite satisfactory – the same configuration of two cluster of defects was

detected in two subsequent images (enclosed by ellipse) and in the next two, which are not displayed.

Acknowledgements The paper was supported by the National Council for Research of Polish Government under grant 2012/07/B/ST7/01216, internal code 350914 of Wrocław University of Technology.

The author would like to express his thanks to anonymous referees for comments clarifying the presentation.

References

1. Bhamare SM, Agone V (2011) Change detection of surface temperature and its consequence using multi-temporal remote sensing data and GIS application to Tapi Basin of India. In: Proceedings of the global conference on global warming, Lisbon, Portugal, 11–14 July, 2011
2. Davies ER (2005) Machine vision: theory, algorithms, practicalities. Morgan Kaufmann, San Mateo
3. Gaetan C, Guyon X (2010) Spatial statistics and modeling. Springer, Berlin
4. Garcial Rube DF, et al (2002) Shape inspection system for variable-luminance steel plates with real-time adaptation capabilities to luminance variations. Real-Time Imaging 8:303–315
5. Hima EP (2013) Video objects detection using spatial and temporal segmentation. Int J Sci Res, India Online 2(7):255
6. Ji M, Jensen JR (1999) Effectiveness of subpixel analysis in detecting and quantifying urban imperviousness from landsat thematic mapper imagery. Geocarto Int 14(4):33–41
7. Malamasa EN, et al (2003) A survey on industrial vision systems, applications and tools. Image Vis Comput 21:171–188
8. Megahed FM, Wells J, Camelio JA, Woodall WH (2012) A spatiotemporal method for the monitoring of image data. Qual Reliab Eng Int 28(8):967–980
9. Megahed FM, Woodall WH, Camelio JA (2011) A review and perspective on control charting with image data. J Qual Technol 43(2):83–98
10. Montgomery DC (1996) Introduction to statistical quality control. Wiley, New York
11. Panigrahi N, Mohan BK, Athithan G (2011) Differential geometric approach to change detection using remotely sensed images. J Adv Inf Technol 2(3):134–138
12. Pawlak M, Rafajłowicz E, Steland A (2004) On detecting jumps in time series: nonparametric setting. J Nonparametr Stat 16(3/4):329–347
13. Prause A, Steland A (2015) Detecting changes in spatial-temporal image data based on quadratic forms In: Stochastic models, statistics and their applications, Chapter 16
14. Rafajłowicz E (2007) SUSAN edge detector reinterpreted, simplified and modified. In: International workshop on multidimensional (nD) systems, Aveiro, Portugal, pp 69–74
15. Rafajłowicz E, Pawlak M, Steland A (2008) Nonlinear image processing and filtering: a unified approach based on vertically weighted regression. Int J Appl Math Comput Sci 18(1):49–61
16. Rafajłowicz E, Pawlak M, Steland A (2010) Nonparametric sequential change-point detection by a vertically trimmed box method. IEEE Trans Inf Theory 56(7):3621–3634
17. Ristivojevic M, Konrad J (2006) Space–time image sequence analysis: object tunnels and occlusion volumes. IEEE Trans Image Proc 15(2):364–376
18. Steland A, Rafajlowicz E (2014) Decoupling change-point detection based on characteristic functions: methodology, asymptotics, subsampling and application. J Stat Plan Inference 145:49–73
19. Szajowski K (2011) Multi-variate quickest detection of significant change process. In: Baras JS, Katz J, Altman E (eds) Decision and game theory for security. Lecture notes in computer science, vol 7037. Second international conference, GameSec 2011 College Park, MD, Maryland, USA, November 14–15, 2011, pp 56–66

Chapter 49
The Impact of Renewables on Electricity Prices and Congestion in a Regime Switching Model: Evidence from the Italian Grid

Alessandro Sapio

Abstract In this paper, the cross-zonal impact of renewable energy (RE) on electricity prices is assessed by means of a time-varying regime switching model, focusing on the highly congested line connecting Sicily with the Italian peninsula.

In the base regime, there is no congestion and the price in Sicily (which equals the system marginal price) depends on national electricity demand and RE supply. In the congested regime, the Sicilian price depends on the local electricity demand and RE supply, as well as on market power by local generators. The transition between regimes is modeled through a dynamic probit, including, as explanatory variables, the RE supply on both sides of the potentially congested line.

The regime switching model is estimated using hourly data from the Italian day-ahead electricity market for the year 2012. As shown by results, congestion is determined by the total amount of renewables in mainland Italy, but when the RE supply is disaggregated into different sources, one finds that congestion is mainly due to photovoltaics (from the peninsula) and hydropower (wherever located), whereas wind power has a negative effect on congestion regardless of localization.

49.1 Introduction

The regime switching model is now a staple in econometric research on liberalized electricity markets. Indeed, it allows to account for the spikes that characterize the time series of electricity prices, as in Huisman and Mahieu [5], Weron et al. [11], Karakatsani and Bunn [8], and Janczura and Weron [6] among others. Typically, regimes are assumed unknown, and transitions are modeled by means of a Markov process. However, one key reason why spikes occur is congestion in the transmission grid, causing the emergence of local market power. This has led Haldrup and Nielsen [3, 4] to build a regime switching model with *known* regimes delimited by observable congestion episodes. This model is much easier to estimate, and lends itself to a more straightforward economic interpretation. There was, however, one

A. Sapio (✉)
Department of Business and Economic Studies, Parthenope University of Naples, Via Generale Parisi 13, 80132 Naples, Italy
e-mail: alessandro.sapio@uniparthenope.it

A. Steland et al. (eds.), *Stochastic Models, Statistics and Their Applications*,
Springer Proceedings in Mathematics & Statistics 122,
DOI 10.1007/978-3-319-13881-7_49

important limitation in Haldrup and Nielsen: constant transition probabilities. Theoretical reasons [7] as well as goodness of fit [6] call for time-varying transitions. Exploring what lies behind regime switches can also be a source of interesting policy insights.

This paper uses a time-varying regime switching model of electricity prices to study a key issue in energy policy, namely, how grid congestion and the supply of renewable energy sources interact to determine electricity prices. The downward pressure on electricity prices that renewables exert in the short run, due to their relatively low marginal cost, can be offset if they cause congestion and the ensuing emergence of local market power. The impact of renewables can moreover depend on the location of the generating plants.

The model comprises a base regime, with no congestion, and a congested regime. Transitions depend on power demand and on the supply of renewable energy (RE) at both ends of the potentially congested line. The model is estimated using hourly data from the Italian day-ahead electricity market, observed in the year 2012, focusing on the highly congested line linking two regions that are rich in renewables, such as Sicily and the southern part of the Italian peninsula.

The next two sections illustrate the dataset, the methods and the results, before a last section of concluding remarks.

49.2 Data and Methods

In order to assess the impact of RE supply on zonal electricity prices, it is useful to conceive the Sicilian wholesale electricity price as going through two regimes. In a base regime, there is no congestion and the price in Sicily equals the system marginal price at the national level. Hence, it depends on the demand and supply forces that determine the electricity market equilibrium at the national level. In the congested regime, the Sicilian price differs from the other zonal prices, as it only reflects the demand from local users and the supply from generators located on the island.

Formally, let $p_t^z, d_t^z, r_t^z, m_t^z$ be, respectively, the power price, power demand, RE supply, and a market power index in zone z in period (hour) t, all in natural logarithms, where $z \in \{Sicily, RoI, Italy\}$ (RoI stands for Rest of Italy, i.e. the aggregate of all zones different from Sicily).[1] Let $\pi_t = Prob(c_t = 1) \in [0, 1]$ denote the probability that the line connecting Sicily with the neighboring South zone is congested (c_t stands for congestion at time t). In the base regime, $p_t^{Sicily} = p_t^{Italy}$, hence we assume the following model:

$$p_t^{Sicily} = \eta_b p_{t-k}^{Sicily} + \alpha_b d_t^{Italy} + \beta_b r_t^{Italy} + \varepsilon_{b,t} \tag{49.1}$$

where η_b, α_b and β_b are constant coefficients, k is a time lag, $\varepsilon_{b,t}$ is an i.i.d. error term with μ_b mean and standard deviation σ_b, and b refers to the base regime.

[1] In order to avoid missing values, 1 was added to the variables before taking logs.

In the congested regime, $p_t^{Sicily} \neq p_t^{Italy}$, motivating the following model for the Sicilian price:

$$p_t^{Sicily} = \eta_c p_{t-k}^{Sicily} + \alpha_c d_t^{Sicily} + \beta_c r_t^{Sicily} + \gamma_c m_t^{Sicily} + \varepsilon_{c,t} \tag{49.2}$$

where the coefficients are defined as in the base regime, with the addition of γ_c (c stands for congested).[2]

By assumption, the probability that the Sicily-South line is congested at time t, π_t, is driven by a dynamic probit:

$$\pi_t = \Phi\left(\alpha_1 d_t^{Sicily} + \alpha_2 d_t^{RoI} + \beta_1 r_t^{Sicily} + \beta_2 r_t^{RoI} + \psi c_{t-k}\right) \tag{49.3}$$

where $\Phi(.)$ denotes the Gaussian probability distribution function, and c_t is a dummy equal to 1 if congestion occurred in period t, ψ tunes the dependency of the congestion probability on congestion observed in previous period $t-k$.[3] Along with demand and renewables from Sicily, the set of regressors includes demand and renewables from the rest of Italy. The error term of the selection equation is allowed to correlate with both $\varepsilon_{b,t}$ and $\varepsilon_{c,t}$. The correlation coefficients, to be estimated, are respectively θ_b and θ_c.

In line with the evidence on the short-term impact of renewables on electricity prices (as reviewed e.g. by Guerci and Sapio [2]), we expect $\beta_b < 0$ and $\beta_c < 0$, while basic microeconomic intuition suggests $\alpha_b > 0$ and $\alpha_c > 0$. The downward pressure of renewables on electricity prices can however be (at least partly) offset for Sicilian consumers if $\beta_2 > 0$, because in that case, RE produced in the rest of Italy causes congestion and leads to higher Sicilian prices.

The estimated impact of renewables, as from the outlined model, may hide differences across sources, such as hydropower, wind, and photovoltaics, that are characterized by rather different dynamics. Hence, in an alternative specification of the model, r_t^z is replaced by the vector $[h_t^z, w_t^z, pv_t^z]$ (respectively: hydropower, wind, photovoltaics, in natural logs). Specifications using the aggregate and disaggregated RE penetration rates are also considered.[4]

Data and Variables Data on the wholesale day-ahead electricity market for the year 2012 have been collected from the Italian Power Exchange (IPEX) website (www.mercatoelettrico.it).[5] These hourly-frequency data include, for each zone: prices in Euros/MWh, sold and purchased quantities in MWh, and Residual Supply

[2]Thermal power supply is not included among regressors, as its setting is supposedly strategic. Yet, we control for it indirectly by means of the RSI market power indicator m_t^{Sicily} in the congested regime. This was not included in the base regime, as our data source does not provide market power indices at the national level.

[3]This is known as a dynamic probit, not to be confused with the autocorrelated probit, where the lagged probability appears as a regressor. See Kim et al. [9].

[4]The RE penetration rate for a zone is defined as the ratio between the RE supply and the demand in that zone.

[5]The wholesale market is run 24/7 with a hourly frequency. Year 2012 was an interesting one for these purposes, as the Sicily-South line was congested for about 84 % of the hours. When the

Indexes (RSI).[6] Zonal sold quantities for individual RE technologies (wind, photovoltaics, hydropower), measured from individual bid data (source: Terna, the Italian transmission system operator), and their sums across sources and zones are the main explanatory variables. Congestion is measured as a dummy variable taking value equal to 1 when prices in Sicily and in the South zone differ, 0 otherwise. For each variable, 8784 data points are available.[7]

Summary statistics for the sample are given in Table 49.1.[8] As clear from the table, congestion is almost always from the Italian peninsula to Sicily, resulting in higher prices in Sicily (on average, about 102 Eur/MWh under congestion vs. 61 Eur/MWh). Hence, renewables produced in the peninsula may be key drivers of congestion.

It is worth noting that correlations across sources are weak and negative: −0.067 between wind and solar in Sicily, and −0.086 in the rest of Italy. Such mild correlations are confirmed when we consider the penetration rates. Hence, different RE sources may be responsible for congestion to different degrees. Also, if we plot the congestion frequencies against the RE supply quantiles for each RE source, we find a negative relationship between wind supply in the rest of Italy and congestion to Sicily, in contrast with the apparently positive impact of photovoltaics (see Table 49.2).[9]

49.3 Results

Maximum Likelihood estimates of the model outlined in Eqs. (49.1) to (49.3) (following Maddala [10]) are presented in Table 49.3. Four specifications are presented: in the first, power demand and RE supply (aggregated across sources) enter as determinants of prices and switching probabilities. In the second, RE supply is disaggregated into hydro, wind, and photovoltaics. The third and fourth specifications are similar to the first and second, respectively, except that in the congestion equation, RE penetration rates appear instead of supply volumes. Daily dummies, accounting

transmission lines are used below capacity, the same price is received by all generating companies across Italy. Whenever congestion arises, the market is split in up to 6 zones (North, Center-North, Center-South, South, Sicily, and Sardinia), 5 limited production poles, and 6 virtual foreign zones; hence, zonal prices dispersion arises. Sicily is only connected with the South zone.

[6]The RSI is defined as the sum of the overall quantities offered for sale, minus the number of operators multiplied by the difference between the sum of the overall quantities offered for sale and the sum of the overall quantities sold. This is equal to minus the sum (over companies) of the RSI index presented by Gianfreda and Grossi [1], hence it is increasing in market power.

[7]Year 2012 had 366 days.

[8]Unit root tests (Augmented Dickey-Fuller, Phillips-Perron) performed on the time series of electricity prices, demand, and supply variables cannot reject the null of mean stationarity. Hence, no first differencing is needed before performing the econometric analysis.

[9]In Table 49.2, values for the 2nd to 5th deciles for photovoltaics are not reported, as its supply was null for about half of the hours in 2012.

Table 49.1 Summary statistics

	Units	Obs.	Rel. freq.		Min	Max
Congestion		8784	0.841	0.366	0	1
Congestion from Sicily		8784	0.085	0.279	0	1
Congestion to Sicily		8784	0.756	0.430	0	1
			Mean	Std. Dev.		
Power price, Sicily	Eur/MWh	8784	95.28	48.689	0	3000
Power price, Sicily (cong.)	Eur/MWh	7389	101.73	49.56	0	3000
Power price, Sicily (no cong.)	Eur/MWh	1395	61.11	23.04	0	212
Price (PUN), Italy	Eur/MWh	8784	75.48	22.177	12.14	324.2
Power demand, Sicily	MWh	8784	2267.22	423.27	1344.61	3445.04
Power demand, rest of Italy	MWh	8784	31734.15	6611.90	18052.95	48042.39
Power demand, Italy	MWh	8784	34001.37	6964.08	19582.34	51185.33
Hydropower production, Sicily	MWh	8784	50.48	80.25	0	497
Hydropower production, rest of Italy	MWh	8784	3911.77	1954.89	637	15429
Hydropower production, Italy	MWh	8784	3962.25	1986.74	651	15535
Wind power production, Sicily	MWh	8784	334.28	308.61	0	2318
Wind power production, rest of Italy	MWh	8784	1165.33	876.35	6	6239
Wind power production, Italy	MWh	8784	1499.61	1092.62	11	6783
Solar power production, Sicily	MWh	8784	4.764	7.459	0	27
Solar power production, rest of Italy	MWh	8784	102.39	145.579	0	500
Solar power production, Italy	MWh	8784	107.15	152.07	0	525
RSI, Sicily		8784	139.95	224.46	0	2141.2

Table 49.2 Congestion frequencies across quantiles of RE supply in the South zone (overall congestion and congestion towards Sicily)

Wind, South Deciles	Cong. to Sicily Freq.	Cong., overall Freq.	Photovolt., South Deciles	Cong. to Sicily Freq.	Cong., overall Freq.
1	0.8476	0.9176	1	0.6694	0.8012
2	0.8295	0.8924	2		
3	0.7782	0.8783	3		
4	0.7777	0.8780	4		
5	0.7993	0.8940	5		
6	0.7585	0.8451	6	0.8195	0.8963
7	0.7446	0.8400	7	0.8647	0.8947
8	0.7200	0.7874	8	0.8562	0.8907
9	0.7167	0.7816	9	0.8113	0.8508
10	0.5861	0.6956	10	0.8713	0.8784

for deterministic weekly patterns, are included in all specifications. We consider a 24-hour lag for prices in both regimes and for congestion, a natural choice in view of the daily patterns of electricity consumption.

Here is a description of the findings. Generally speaking, renewables exercise a downward pressure on electricity prices in both regimes. This can be grasped by noting the negative sign of the overall amount of renewables in the price equations for the base and congested regimes. Such evidence confirms the price reduction effect found in the previous empirical literature (Guerci and Sapio [2] and references therein). However, when renewable energy technologies are considered separately, results show that this effect is due to wind and photovoltaic power, whereas hydropower supply drives the price upwards, although only in the congested regime. Inspecting market data, it turns out that prices in Sicily averaged about 154 Euros/MWh when hydro pumped storage was the marginal technology (totaling 513 hours), suggesting its use to offset the price drops and variability caused by other renewables.

These estimates account for the *direct* effect of renewables on electricity prices. As to the indirect effects working through the transmission grid, total renewables produced in Sicily decrease congestion, whereas those generated in the rest of Italy increase it (specification 1). This holds also when the penetration rates are considered instead of the sheer generated volumes (specification 3). Again, different RE technologies do not behave alike. In specifications 2 and 4, hydropower increases congestion and wind decreases it regardless of their localization. Photovoltaic energy determines congestion if produced in the rest of Italy, and relieves it when flowing from Sicily, but this is true only in specification 2, although the coefficient of photovoltaics produced in the rest of Italy retains its positive sign also in specification 4. If hydropower is used strategically, its systematically positive association with congestion causes no wonder. What is really surprising is that wind from the rest of Italy seemed to relieve congestion, perhaps reflecting the curtailment of wind plants by the grid operator in the South zone for reliability reasons (0.5 % of power demand in 2012; source: Terna).

Concerning the other explanatory variables, one finds that, in the congested regime, the electricity price in Sicily is less autocorrelated and less sensitive to RE supply. Market power, measured by means of the RSI, leads to higher prices in all specifications.

49.4 Conclusion

One of the main drawbacks of supporting RE sources involves its difficult integration with transmission and distribution grids conceived under the centralized power generation paradigm. The expected downward pressure on electricity prices may be offset by the emergence of congestion rents and by the sheer under-utilization of (subsidized) RE plants. The preliminary results presented here show that whether renewables aggravate congestion depends on the localization of the RE plants, and that some sources (hydro, photovoltaics) are more likely to determine congestion.

Table 49.3 Regime switching models of day-ahead electricity prices in Sicily

	(1)	(2)	(3)	(4)
Non-congested regime				
p_{t-24}^{Italy}	0.486*** (19.54)	0.403*** (17.10)	0.485*** (19.65)	0.404*** (17.17)
d_t^{Italy}	0.657*** (14.94)	0.984*** (19.02)	0.653*** (15.03)	0.936*** (18.19)
r_t^{Italy}	−0.0643*** (−3.84)		−0.0487** (−3.01)	
h_t^{Italy}		0.0120 (1.25)		0.0173 (1.90)
pv_t^{Italy}		−0.0373*** (−13.43)		−0.0334*** (−12.19)
w_t^{Italy}		−0.0326*** (−4.41)		−0.0247*** (−3.33)
Constant	−4.289*** (−12.67)	−7.603*** (−17.05)	−4.366*** (−13.11)	−7.229*** (−16.24)
Daily dummies	yes	yes	yes	yes
Congested regime				
p_{t-24}^{Sicily}	0.361*** (9.17)	0.299*** (7.04)	0.367*** (9.91)	0.316*** (8.07)
d_t^{Sicily}	0.734*** (15.44)	0.840*** (14.50)	0.744*** (15.99)	0.805*** (15.26)
r_t^{Sicily}	−0.0291*** (−5.21)		−0.0280*** (−5.21)	
h^{Sicily}	0.0114*** (5.82)	0.00394* (1.98)	0.0107*** (5.54)	0.00393 (1.95)
pv^{Sicily}		0.0198*** (4.73)		0.0230*** (5.72)
w^{Sicily}		−0.0248*** (−5.56)		−0.0193*** (−4.68)
m^{Sicily}		−0.0355*** (−8.30)		−0.0323*** (−8.05)
Constant	−2.573*** (−10.34)	−3.090*** (−10.21)	−2.681*** (−10.67)	−2.934*** (−10.25)
Daily dummies	yes	yes	yes	yes

Table 49.3 (*continued*)

	(1)	(2)	(3)	(4)
Switching eq.				
d_t^{Sicily}	1.926*** (7.13)	0.900*** (3.39)	1.608*** (6.52)	0.930*** (3.74)
d_t^{RoI}	−0.0979 (−0.65)	−0.114 (−0.76)	0.0368 (0.21)	0.305* (1.99)
r_t^{Sicily}	−0.277*** (−10.56)			
r_t^{RoI}	0.120 (1.80)			
h_t^{Sicily}		0.0634*** (4.96)		
h_t^{RoI}		0.270*** (6.88)		
pv_t^{Sicily}		−0.192*** (−6.30)		
pv_t^{RoI}		0.101*** (7.02)		
w_t^{Sicily}		−0.157*** (−6.31)		
w_t^{RoI}		−0.110*** (−4.94)		
Penetr. RE, Sicily			−1.915*** (−11.23)	
Penetr. RE, RoI			0.754** (2.61)	
Penetr. hydro, Sicily				2.955*** (3.84)
Penetr. hydro, RoI				1.871*** (4.47)
Penetr. pv, Sicily				−33.79*** (−3.58)
Penetr. pv, RoI				9.980 (1.36)
Penetr. wind, Sicily				−1.625*** (−8.56)
Penetr. wind, RoI				−2.620*** (−4.74)

Table 49.3 (*continued*)

	(1)	(2)	(3)	(4)
Constant	−12.17*** (−9.82)	−5.508*** (−3.67)	−11.45*** (−10.59)	−9.038*** (−7.16)
Daily dummies	yes	yes	yes	yes
$\ln \sigma_b$	−1.476*** (−41.52)	−1.573*** (−36.88)	−1.502*** (−41.71)	−1.571*** (−34.00)
$\ln \sigma_c$	−0.905*** (−19.14)	−0.911*** (−19.68)	−0.914*** (−19.32)	−0.922*** (−19.69)
ρ_b	−0.421*** (−6.27)	−0.424*** (−5.03)	−0.398*** (−5.85)	−0.436*** (−4.76)
ρ_c	−0.639*** (−4.57)	−0.704*** (−4.39)	−0.617*** (−4.65)	−0.660*** (−4.62)
Observations	8760	8760	8760	8760

t statistics in parentheses

* $p < 0.05$. ** $p < 0.01$. *** $p < 0.001$

All variables in natural logarithms, except dummies and ratios

Legend – d: log-demand; r: log total RE supply; h: log hydropower supply;

pv: log photovoltaic power supply; w: log wind supply

While this is not enough to cancel source-specific subsidies, some conditionality in awarding the subsidies, based on economic impacts, will be probably needed, as well as a careful allocation of the administrative responsibilities in the authorization process. This is a key issue in power markets, such as the Italian one, that break down into zonal markets as congestion arises.

Further empirical exercises will be needed to develop these implications. On the one hand, it may be useful to apply principal component analysis in order to take care of the positive correlation between RE supply at both sides of the transmission line. On the other hand, the impact of renewables on directional congestion may be assessed by means of a 3-stage regime switching model.

References

1. Gianfreda A, Grossi L (2012) Forecasting Italian electricity zonal prices with exogenous variables. Energy Econ 34(6):2228–2239
2. Guerci E, Sapio A (2012) High wind penetration in an agent-based model of the electricity market. Rev OFCE 5:415–447
3. Haldrup N, Nielsen M (2006) A regime switching long memory model for electricity prices. J Econom 135(1):349–376
4. Haldrup N, Nielsen M (2006) Directional congestion and regime switching in a long memory model for electricity prices. Stud Nonlinear Dyn Econ 10(3). doi:10.2202/1558-3708.1367
5. Huisman R, Mahieu R (2003) Regime jumps in electricity prices. Energy Econ 25(5):425–434
6. Janczura J, Weron R (2010) An empirical comparison of alternate regime-switching models for electricity spot prices. Energy Econ 32(5):1059–1073
7. Kanamura T, Ohashi K (2008) On transition probabilities of regime switching in electricity prices. Energy Econ 30(3):1158–1172
8. Karakatsani N, Bunn D (2008) Intra-day and regime-switching dynamics in electricity price formation. Energy Econ 30(4):1776–1797
9. Kim CJ, Piger J, Startz R (2008) Estimation of Markov regime-switching regression models with endogenous switching. J Econom 143(2):263–273
10. Maddala GS (1983) Limited-dependent and qualitative variables in econometrics. Cambridge University Press, Cambridge
11. Weron R, Bierbrauer M, Trück S (2004) Modeling electricity prices: jump diffusion and regime switching. Physica A 336(1):39–48

Chapter 50
On Hammerstein System Nonlinearity Identification Algorithms Based on Order Statistics and Compactly Supported Functions

Przemysław Śliwiński, Paweł Wachel, and Zygmunt Hasiewicz

Abstract Nonparametric algorithms recovering the nonlinearity in Hammerstein systems are examined. The algorithms are based on ordered measurements and on compactly supported functions. The contribution of the note consists in that the probability density function of the input signal does not need to be strictly bounded from zero but can vanish in a finite number of points. In this setting, the convergence is established for nonlinearities being piecewise-Lipschitz functions. It is also verified that for p times locally differentiable nonlinearities, the algorithms attain the convergence rate $O(n^{-2p/(2p+1)})$, the best possible nonparametric one. Noteworthy, the rate is not worsened by irregularities of the input probability density function.

50.1 Introduction

In system identification we deal with two kind of knowledge: a priori information, possessed before experiment in a form of the laws governing the behavior of the investigated system or object, and the empirical one, i.e., the measurement data obtained in the experiment. If the former is rich enough, the parametric algorithms are usually employed. Otherwise, one should apply the nonparametric technique (in case when the prior knowledge is not fully validated, one could also consider the semiparametric approach).

Considered in this note Hammerstein system identification problem has been a subject of a thorough investigation for many years; see e.g. [6, 12], or e.g. [15] for various parametric, nonparametric or semi-parametric algorithms. The system has been applied in various fields, e.g. in biocybernetics [10], chemistry [9], control [16], power delivery [11], economy [1], and in signal processing [3].

P. Śliwiński (✉) · P. Wachel · Z. Hasiewicz
Institute of Computer Engineering, Control and Robotics, Wrocław University of Technology, Wybrzeże Wyspiańskiego 27, Wrocław, Poland
e-mail: przemyslaw.sliwinski@pwr.edu.pl

P. Wachel
e-mail: pawel.wachel@pwr.edu.pl

Z. Hasiewicz
e-mail: zygmunt.hasiewicz@pwr.edu.pl

A. Steland et al. (eds.), *Stochastic Models, Statistics and Their Applications*,
Springer Proceedings in Mathematics & Statistics 122,
DOI 10.1007/978-3-319-13881-7_50

We focus on the system nonlinearity recovery. The nonparametric identification algorithms are of the Gasser–Müller type and use compactly supported kernel or wavelet functions. We examine their convergence conditions for piecewise-Lipschitz nonlinearities and convergence rates for the smoother ones. It is verified that the rates are the best possible and, contrary to the Nadaraya–Watson-type algorithms, are not worsened by irregularity of the input signal probability density function. Application of the Gasser–Müller estimate to the Hammerstein system nonlinearity recovery problem was proposed and thoroughly examined in [5].

50.2 Identification Problem

The Hammerstein system is a cascade of a nonlinear static element followed by a linear dynamics; see Fig. 50.1. By m and $\{k_i\}$, $i = 0, \ldots, \infty$, we denote the nonlinear characteristic and the impulse response of the dynamic part, respectively. Our goal is to recover the nonlinearity from random input–output measurements $(U_1, Y_1), (U_2, Y_2), \ldots, (U_n, Y_n)$ of the whole system (as the internal signal W_n is, by assumption, not available for measurements). The following assumptions hold:

A. The input signal $\{U_n; n = \cdots - 1, 0, 1, 2, \ldots\}$ is a stationary white random process with an unknown probability density function f. We assume that $-1 \leq U_n \leq 1$ and that

$$f(u) > 0, \tag{50.1}$$

for all $u \in [-1, 1]$, except, maybe, of a finite number of points.

B. The nonlinearity m satisfies locally a Lipschitz inequality

$$\left|m(u) - m(u \pm \varepsilon)\right| \leq c\varepsilon, \tag{50.2}$$

for some unknown $c, \varepsilon > 0$.

C. The dynamic subsystem is asymptotically stable, i.e., $\sum_{i=0}^{\infty} |k_i| < \infty$.

D. Noise $\{Z_n; n = \cdots - 1, 0, 1, 2, \ldots\}$ is a stationary white random process independent of the input signal and has zero mean and finite variance.

The class of locally Lipschitz characteristics (which consists of e.g. discontinuous, piecewise polynomial functions) cannot be parameterized and hence Assumption **B** makes our problem *nonparametric*. According to Assumption **C**, the dynamic part can be any stable ARMA system. The novelty of the paper is that – contrary to e.g. [6, Chap. 8] and [14, Chaps. V and VI] – Assumption **A** admits densities which are not bounded from zero, e.g. triangle and parabolic ones.

The input–output equation describing the Hammerstein system can be rearranged in the following way

$$Y_n = \sum_{i=0}^{\infty} k_i m(U_{n-i}) + Z_n = \underbrace{\mu(U_n)}_{\text{a static system}} + \underbrace{\xi_n + Z_n}_{\text{a correlated noise}},$$

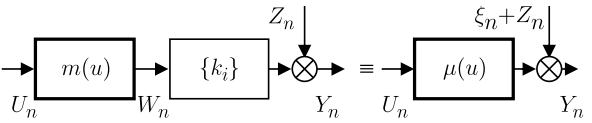

Fig. 50.1 Hammerstein system and its static equivalence

where

$$\mu(u) = \alpha m(u) + \beta, \quad \text{with } \alpha = k_0 \text{ and } \beta = Em(U_0) \sum_{i=1}^{\infty} k_i,$$

and where

$$\xi_n = \sum_{i=1}^{\infty} k_i \big[m(U_{n-i}) - Em(U_0) \big].$$

Thanks to that, the Hammerstein system can be reduced to its static nonlinear counterpart, represented by $\mu(u)$, with the new artificial signal $\xi_n + Z_n$ playing a role of an additive correlated and zero-mean output noise. The idea of the nonparametric approach is based on the fact that

$$E\big\{ Y_n | U_n = u \big\} = \mu(u) \tag{50.3}$$

which means that the nonlinearity $\mu(u)$ is a regression function. Hence, estimating the regression in (50.3), we recover the system nonlinearity m, albeit up to unknown constants α and β.

Remark 50.1 The fact that the nonlinearity can be recovered up to that constants is a consequence of the cascade structure of the system and the inaccessibility of the interconnecting signal W_n.

Remark 50.2 While Assumption **A** extends a class of admissible input probability density functions, it nevertheless still excludes non compactly-supported ones; e.g. the Gauss or Cauchy densities.

50.3 Algorithms

We examine two nonparametric algorithms recovering μ, i.e., the kernel and the multiscale wavelet one. Rather than on the original sequence of measurement pairs $(U_1, Y_1), (U_2, Y_2), \ldots, (U_n, Y_n)$, they both operate on its ordered version, $(U_{(1)}, Y_{[1]}), (U_{(2)}, Y_{[2]}), \ldots, (U_{(n)}, Y_{[n]})$, arranged *w.r.t.* the increasing input values.

The *kernel identification algorithm* has a form of the Gasser–Müller estimate:

$$\hat{\mu}(u) = \frac{1}{h(n)} \sum_{j=1}^{n} Y_{[j]} \int_{U_{(j-1)}}^{U_{(j)}} K\left(\frac{u - v}{h(n)} \right) dv, \tag{50.4}$$

with K being a bounded, compactly supported kernel function (see Table 50.1 in Appendix B for exemplary kernels), and where $\{h(n)\}$ is some positive number sequence.

The *multiscale wavelet algorithm* is of the form (cf. [14]):

$$\bar{\mu}(u) = \sum_{l=l_{\min}(u)}^{l_{\max}(u)} \bar{c}_{q(n),l}\varphi_{q(n),l}(u), \tag{50.5}$$

with

$$\bar{c}_{q(n),l} = \sum_{j=1}^{n} Y_{[j]} \int_{U_{(j-1)}}^{U_{(j)}} \varphi_{q(n),l}(v)dv, \tag{50.6}$$

where $\varphi_{kl}(u) = 2^{k/2}\varphi(2^k u - l)$ are scaled and translated copies of the compactly supported wavelet scaling functions $\varphi(u)$, $\{q(n)\}$ is a positive integer sequence and $l_{\min}(u)$, $l_{\max}(u)$ are appropriate summation limits; see Table 50.2 in Appendix B. Both presented algorithms are based on compactly supported functions and this fact plays an important role in proving algorithms' properties. The following theorems establish convergence of the algorithms.

Theorem 50.1 *If*

$$h(n) \to 0 \quad \textit{and} \quad nh(n) \to \infty, \tag{50.7}$$

then

$$E\big[\mu(u) - \hat{\mu}(u)\big]^2 \to 0,$$

as $n \to \infty$, *at every point* $u \in (-1, 1)$, *at which* (50.1) *holds*.

Theorem 50.2 *If*

$$2^{q(n)} \to \infty \quad \textit{and} \quad n^{-1}2^{q(n)} \to 0, \tag{50.8}$$

then

$$E\big[\mu(u) - \bar{\mu}(u)\big]^2 \to 0,$$

as $n \to \infty$, *at every point* $u \in (-1, 1)$, *at which* (50.1) *holds*.

As number sequences one can choose, e.g., $h(n) = n^{-\alpha}$ and $2^{q(n)} = n^{\alpha}$ with $\alpha \in (0, 1)$. Our next two theorems deal with convergence rate of the algorithms.

Theorem 50.3 *Let* m *have* p *derivatives and let* p*th derivative be bounded in the* ε*-neighborhood of* u. *Let* K *in* (50.4) *be compactly supported and have* p *vanishing moments* (*see Appendix B*). *If*

$$h(n) \sim n^{-1/(2p+1)},$$

then, for any $0 < \varepsilon < 1$,

$$E\big[\mu(u) - \hat{\mu}(u)\big]^2 = O\big(n^{-2p/(2p+1)}\big). \tag{50.9}$$

Theorem 50.4 *Let m have p derivatives and let pth derivative be bounded in the ε-neighborhood of u. Let $\{\varphi_{kl}\}$ in (50.5)–(50.6) be the pth compactly supported wavelet scaling functions. If*

$$2^{q(n)} \sim n^{1/(2p+1)},$$

then, for any $0 < \varepsilon < 1$,

$$E\big[\mu(u) - \bar{\mu}(u)\big]^2 = O\big(n^{-2p/(2p+1)}\big). \tag{50.10}$$

The theorems show that convergence rate is related to p (which describes the smoothness of m and the number of vanishing moments of the function used in the estimates): the smoother m (the larger p), the better convergence rate. For instance, for $p = 1$ the rate is $O(n^{-2/3})$ and grows to $O(n^{-6/7})$ for $p = 3$. For large p, the rate is close to $O(n^{-1})$, the order typical for parametric inference.

Moreover, the rate is indeed independent of the regularity of the input probability density f. This property is an important advantage of the algorithms derived from ordered observations over other types known in the literature (cf. e.g. [6]), which convergence rate is worsened by irregularity of f. Recall that the obtained rate is the best possible for algorithms based on nonparametric a priori information; cf. [13].

50.4 Final Remarks

The following conclusions about the algorithms can be drawn:

- The novelty of the paper is that both convergence and convergence rate of the algorithms are independent of the shape of f for densities not necessarily bounded from zero. It means that irregularities of f don't worsen the speed at which the estimates converge. Owing to that, the rate holds for, e.g., the triangle and parabolic densities.
- The class of admissible nonlinearities includes all functions satisfying (locally) the Lipschitz inequality (50.2).
- In spite of the poor a priori information, convergence rate is not so far from $O(n^{-1})$, i.e., the rate typical for the parametric inference.

It should also be eventually remarked that the proposed algorithms are computationally simple (as integration of functions in (50.4) and (50.6) can readily be replaced by subtraction of their indefinite integrals; cf. [14]). This property, together with those already established in the paper, make the algorithms a valuable alternative in all situations in which the a priori knowledge does not allow to apply a parametric model.

Acknowledgements The idea of the paper has been derived from the private correspondence with W. Greblicki, in which he demonstrates that, under the assumption in (50.1), **the global convergence** of the algorithm (50.4) can be shown even for non compactly supported kernels (provided that the input density f grows in the vicinities of its roots sufficiently fast). The convergence rate, however, becomes dependent on the rate of this growth.

Appendix A: Theorems' Proofs

We start with proofs of Theorems 50.1 and 50.9 concerning the kernel algorithm (50.4).

Proof Recall that

$$\hat{\mu}(u) = \sum_{j=1}^{n} \big[Z_{[j]} + \xi_{[j]} + \mu(U_{(j)})\big] \frac{1}{h(n)} \int_{U_{(j-1)}}^{U_{(j)}} K\left(\frac{u-v}{h(n)}\right) dv$$

and define

$$\mu_{h(n)}(u) = \frac{1}{h(n)} \int_{-1}^{1} \mu(v) K\big((u-v)/h(n)\big) dv.$$

Clearly

$$\begin{aligned} \mu_{h(n)}(u) = &\sum_{j=1}^{n} \frac{1}{h(n)} \int_{U_{(j-1)}}^{U_{(j)}} \mu(v) K\left(\frac{u-v}{h(n)}\right) dv \\ &+ \frac{1}{h(n)} \int_{U_{(n)}}^{U_{(n+1)}} \mu(v) K\left(\frac{u-v}{h(n)}\right) dv. \end{aligned}$$

Denote now by $S_{h(n)} = \operatorname{supp} K(u/h(n))$ the support of the kernel function K. Noting that the $S_{h(n)}$ can be arbitrary small with growing $h(n)$, we simply infer that for any $u \in S_{h(n)}$, such that the restriction (50.1) holds, it exists a constant $\delta > 0$ for which $f(u) \geq \delta$. Thus, the theorem is verified by applying the following inequality proven in [4, Lemma 5.1, Theorem 5.1]:

$$E\big[\hat{\mu}(u) - \mu_{h(n)}(u)\big]^2 \leq c\big\{W_1 + W_2 + W_3 + W_4 + \big[\mu(u) - \mu_{h(n)}(u)\big]^2\big\}$$

where

$$W_1 = \operatorname{var} Z_1 \sum_{j=1}^{n} E\left[\frac{1}{h(n)} \int_{U_{(j-1)}}^{U_{(j)}} K\left(\frac{u-v}{h(n)}\right) dv\right]^2 \leq c \frac{1}{nh(n)}$$

$$W_2 = E\left[\sum_{j=1}^{n} \xi_{[j]} \frac{1}{h(n)} \int_{U_{(j-1)}}^{U_{(j)}} K\left(\frac{u-v}{h(n)}\right) dv\right]^2 \leq c \frac{1}{nh(n)}$$

$$W_3 = E\left[\sum_{j=1}^{n} \frac{1}{h(n)} \int_{U_{(j-1)}}^{U_{(j)}} \big[\mu(U_{(j)}) - \mu(v)\big] K\left(\frac{u-v}{h(n)}\right) dv\right]^2 \leq c \frac{1}{n^2 h(n)}$$

$$W_4 = E\left[\frac{1}{h(n)} \int_{U_{(n)}}^{U_{(n+1)}} K\left(\frac{u-v}{h(n)}\right) dv\right]^2 \leq c \frac{1}{n^2 h(n)}$$

for some generic $c > 0$, and by using the following lemma; cf. [4, Lemma C2]:

Lemma 50.1 *For a bounded and compactly supported K and μ satisfying (50.2) it holds that*

$$\left[\mu(u) - \mu_{h(n)}(u)\right]^2 \to 0 \quad as\ h(n) \to 0.$$

To prove Theorem 50.3 we need another lemma [4, Lemma 6.1]:

Lemma 50.2 *For a bounded and compactly supported K with p vanishing moments and μ having p bounded derivatives it holds that*

$$\left[\mu(u) - \mu_{h(n)}(u)\right]^2 = O\left(h^{2p}(n)\right).$$

Selecting $h(n) \sim n^{-1/(2p+1)}$ results in the convergence rate (50.9).

To prove Theorems 50.2 and 50.4 dealing with the wavelet version, it suffices to recall that the algorithm (50.5)–(50.6) can be rewritten in a kernel-like form

$$\bar{\mu}(u) = \sum_{j=1}^{n} Y_{[j]} \int_{U_{(j-1)}}^{U_{(j)}} \phi_{q(n),l}(u, v)dv,$$

with the summation kernel

$$\phi_{kl}(u, v) = \sum_{l=l_{\min}(u)}^{l_{\max}(u)} \varphi_{kl}(u)\varphi_{kl}(v),$$

of the corresponding scaling function $\varphi_{kl}(u)$; see e.g. [7].

Appendix B: Kernel and Wavelet Functions

The following kernel functions, with compact supports in $[-1, 1]$, can be used in algorithms (see Table 50.1, e.g. [8]),where I is the indicator function. As the compactly supported wavelet scaling functions one can apply both the classic Daubechies functions, or symmlets, or the Cohen–Daubechies–Vial wavelets (orthogonal on an interval) (Table 50.2); see e.g. [2].

Table 50.1 Exemplary kernels with compact support and vanishing moments

Kernel function	Vanishing moments
$I_{[\lvert u\rvert \le 1]}(u) \cdot \frac{1}{2}$	0
$I_{[\lvert u\rvert \le 1]}(u) \cdot \frac{3}{4}(1 - u^2)$	1
$I_{[\lvert u\rvert \le 1]}(u) \cdot \frac{1}{8}(9 - 15u^2)$	2
$I_{[\lvert u\rvert \le 1]}(u) \cdot \frac{3}{8}(3 - 5u^2)$	3

Table 50.2 Basic properties of exemplary wavelet scaling functions (p – wavelet number)

	pth Daubechies function/symmlet
$l_{\min}(u)$	$\lfloor 2^k x \rfloor - 2p + 2$
$l_{\max}(u)$	$\lceil 2^k x \rceil - 1$
Supports of φ and ϕ	$[0, 2p - 1]$

References

1. Capobianco E (2002) Hammerstein system representation of financial volatility processes. Eur Phys J B 27(2):201–211
2. Cohen A (2003) Numerical analysis of wavelets methods. Studies in mathematics and its applications. Elsevier, Amsterdam
3. Gilabert P, Montoro G, Bertran E (2011) FPGA implementation of a real-time NARMA-based digital adaptive predistorter. IEEE Trans Circuits Syst II, Express Briefs 58(7):402–406
4. Greblicki W (1996) Nonlinearity estimation in Hammerstein systems based on ordered observations. IEEE Trans Signal Process 44(5):1224–1233
5. Greblicki W, Pawlak M (1994) Dynamic system identification with order statistics. IEEE Trans Inf Theory 40(5):1474–1489
6. Greblicki W, Pawlak M (2008) Nonparametric system identification. Cambridge University Press, New York
7. Hasiewicz Z (2001) Non-parametric estimation of non-linearity in a cascade time series system by multiscale approximation. Signal Process 81(4):791–807
8. Härdle W (1990) Applied nonparametric regression. Cambridge University Press, Cambridge
9. Jeng JC, Huang HP (2008) Nonparametric identification for control of MIMO Hammerstein systems. Ind Eng Chem Res 47(17):6640–6647
10. Kukreja S, Kearney R, Galiana H (2005) A least-squares parameter estimation algorithm for switched Hammerstein systems with applications to the VOR. IEEE Trans Biomed Eng 52(3):431–444
11. Meilera M, Schmida O, Schudya M, Hoferb E (2008) Dynamic fuel cell stack model for real-time simulation based on system identification. J Power Sources 176(2):523–528
12. Söderström T, Stoica P (1989) System identification. Prentice Hall, New York
13. Stone CJ (1980) Optimal rates of convergence for nonparametric regression. Ann Stat 8(6):1348–1360
14. Śliwiński P (2013) Nonlinear system identification by Haar wavelets. Lecture notes in statistics, vol 210. Springer, Heidelberg
15. Śliwiński P, Rozenblit J, Marcellin MW, Klempous R (2009) Wavelet amendment of polynomial models in Hammerstein system identification. IEEE Trans Autom Control 54(4):820–825
16. Wang J, Wang D, Moore P, Pu J (2001) Modelling study, analysis and robust servo control of pneumatic cylinder actuator systems. IEE Proc, Control Theory Appl 148(1):35–42

Chapter 51
An Algorithm for Construction of Constrained D-Optimum Designs

Dariusz Uciński

Abstract A computational algorithm is proposed for determinant maximization over the set of all convex combinations of a finite number of nonnegative definite matrices subject to additional box constraints on the weights of those combinations. The underlying idea is to apply a simplicial decomposition algorithm in which the restricted master problem reduces to an uncomplicated multiplicative weight optimization algorithm.

51.1 Introduction

Optimum experimental design seeks to allocate measurement resources in regression problems so to maximize the relevant design criterion. Feasible allocations are identified with probability measures on the design region called continuous designs [1, 7]. To determine optimal measures, a numerical procedure is most often required. A straightforward strategy is to cover the design region with a suitable network, $\mathscr{N}$, of points which should be rich enough to contain close approximations to the points likely to have positive mass in the optimal design, and to focus solely on optimizing the masses associated with elements in $\mathscr{N}$. For the D-optimal design criterion, a simple multiplicative computational procedure was devised and analyzed in [3, 7, 9, 10].

Some studies have been undertaken in order to extend the appealing framework of the multiplicative algorithm to more complex settings which are encountered in applications [4, 5, 13]. They are limited, however, to equality constraints on the design weights [10]. In practice, various inequality constraints must be sometimes considered which are due to cost limitations, required design measure space restrictions for achieving certain robustness properties, or restrictions on the experimental space. Although much work has been done in this respect [2], the number of publications on the algorithmic aspects of constrained design is still very limited.

D. Uciński (✉)
Institute of Control and Computation Engineering, University of Zielona Góra, ul. Podgórna 50, 65-246 Zielona Góra, Poland
e-mail: D.Ucinski@issi.uz.zgora.pl

A. Steland et al. (eds.), *Stochastic Models, Statistics and Their Applications*,
Springer Proceedings in Mathematics & Statistics 122,
DOI 10.1007/978-3-319-13881-7_51

The aim of this paper is to propose an extension of the multiplicative algorithm to maximization of the D-optimality criterion subject to additional box constraints on the design weights. The underlying idea is to apply simplicial decomposition [6] which iterates by alternately solving a linear programming subproblem within the set of all feasible points and a nonlinear master problem within the convex hull of a subset previously generated points. The former problem is solved here using an algorithm being almost as simple as a closed form solution and the latter problem reduces to employing the original multiplicative algorithm mentioned above.

Throughout the paper, $\mathbb{R}_+$ and $\mathbb{R}_{++}$ stand for the sets of nonnegative and positive real numbers, respectively. The set of real $m \times n$ matrices is denoted by $\mathbb{R}^{m\times n}$. We use $\mathbb{S}^m$ to denote the set of symmetric $m \times m$ matrices, $\mathbb{S}^m_+$ to denote the set of symmetric nonnegative definite $m \times m$ matrices, and $\mathbb{S}^m_{++}$ to denote the set of symmetric positive definite $m \times m$ matrices. The curled inequality symbols $\succeq$ and $\succ$ between vectors represents componentwise inequalities, while between symmetric matrices, they represents the Löwner ordering. The symbols $\mathbf{1}$ and $\mathbf{0}$ denote vectors whose all components are one and zero, respectively. Given a set of points A, $\mathrm{co}(A)$ stands for its convex hull. The probability (or canonical) simplex in $\mathbb{R}^n$ is defined as $S_n = \{\mathbf{p} \in \mathbb{R}^n_+ \mid \mathbf{1}^\mathsf{T}\mathbf{p} = 1\}$. Given two vectors $\boldsymbol{x}$ and $\boldsymbol{y}$ of dimension n, $\boldsymbol{x} \cdot \boldsymbol{y}$ is an n-vector whose ith component is $x_i y_i$ (the componentwise multiplication operator).

51.2 Optimum Experimental Design for Multiresponse Models

Consider d-dimensional observations $\mathbf{y}_{ij}$ of a vector $\mathbf{y}$ of response variables, performed at fixed values $\mathbf{x}_i$ of the l-dimensional vector $\mathbf{x}$ of explanatory variables,

$$\mathbf{y}_{ij} = \mathbf{F}(\mathbf{x}_i)^\mathsf{T}\boldsymbol{\theta} + \boldsymbol{\varepsilon}_{ij}, \quad j = 1, \ldots, r_i,\ i = 1, \ldots, n, \tag{51.1}$$

where $\mathbf{F}(\mathbf{x}_i) \in \mathbb{R}^{m\times d}$, $i = 1, \ldots, n$ are known, $\mathbf{x}_i \neq \mathbf{x}_k$ if $i \neq k$, and $\boldsymbol{\theta} \in \mathbb{R}^m$ is a vector of unknown parameters. The observations are replicated $r_i \geq 0$ times for the setting $\mathbf{x}_i$, so that the total number of experimental runs is $N = \sum_{i=1}^n r_i$. The d-dimensional vectors of additive random errors $\boldsymbol{\varepsilon}_{ij}$ are sampled from a distribution satisfying $E(\boldsymbol{\varepsilon}_{ij}) = \mathbf{0}$, $E(\boldsymbol{\varepsilon}_{ij}\boldsymbol{\varepsilon}_{k\ell}^\mathsf{T}) = \delta_{ij}\delta_{k\ell}\mathbf{V}(\mathbf{x}_i)$, where the dispersion matrices $\mathbf{V}(\mathbf{x}_i) \in \mathbb{S}^d_{++}$, $i = 1, \ldots, n$ are known and δ_{ij} signifies the Kronecker delta.

Set $\mathbf{M}_i = \mathbf{F}(\mathbf{x}_i)\mathbf{V}(\mathbf{x}_i)^{-1}\mathbf{F}(\mathbf{x}_i)^\mathsf{T} \in \mathbb{S}^m_+$, $i = 1, \ldots, n$. If the matrix $\widetilde{\mathbf{M}} = \sum_{i=1}^n r_i\mathbf{M}_i$, called the *Fisher information matrix* (FIM), has full rank, then its inverse is the covariance matrix of the weighted LS estimator of $\boldsymbol{\theta}$. The values of $\mathbf{x}_i$, $i = 1, \ldots, n$ are fixed and may not be altered, but we have full control over the corresponding numbers of replications r_i, $i = 1, \ldots, n$. To construct a D-optimum design means to pick the r_i's which maximize the D-optimality criterion $\Phi[\widetilde{\mathbf{M}}] = \log\det(\widetilde{\mathbf{M}})$ [1, 7].

In order to circumvent the combinatorial nature of this optimization problem, it is customary to extend the definition of the solution. In the relaxed formulation, instead of the r_i's, we operate on the weights $p_i = r_i/N$, $i = 1, \ldots, n$, unequivocally representing the allocation of experimental runs to the support points. Note that $\mathbf{p} = (p_1, \ldots, p_n)$ satisfies $\mathbf{1}^\mathsf{T}\mathbf{p} = 1$, $\mathbf{p} \succeq \mathbf{0}$. It is also more convenient to operate on the so-called *normalized* FIM

$$\mathbf{M}(\mathbf{p}) = \sum_{i=1}^{n} p_i \mathbf{M}_i \tag{51.2}$$

in lieu of $\widetilde{\mathbf{M}}$. Clearly, a $\mathbf{p}$ which maximizes $\Phi[\mathbf{M}(\mathbf{p})]$ yields multiplicities $r_1, \ldots, r_n$ which maximize $\Phi[\widetilde{\mathbf{M}}]$. For large N the feasible p_i's can be considered as any non-negative reals which sum up to unity, and not necessarily integer multiples of $1/N$. As a result, the mathematical formulation becomes more tractable and is extensively used in optimum experimental theory [1, 7].

One of the criticisms of this relaxed approach is that the resulting designs concentrate at a relatively small number of support points, rather than spreading the measurement effort around appropriately [2]. This gave rise to investigations aiming at imposing the appropriate limitations on the form of the optimal designs. Following this line of research, we are interested in solving the following problem:

Problem 51.1 Given a vector $\mathbf{b} \in \mathbb{R}^n_{++}$ satisfying $\mathbf{1}^\mathsf{T}\mathbf{b} \geq 1$, find a vector of weights $\mathbf{p} \in \mathbb{R}^n$ to maximize

$$\Phi\big[\mathbf{M}(\mathbf{p})\big] = \log\det\big(\mathbf{M}(\mathbf{p})\big) \tag{51.3}$$

over the convex set $P = \{\mathbf{p} \mid \mathbf{0} \preceq \mathbf{p} \preceq \mathbf{b},\ \mathbf{1}^\mathsf{T}\mathbf{p} = 1\}$.

Note that the performance index Φ is concave over the canonical simplex $S_n = \big\{\mathbf{p} \in \mathbb{R}^n_+ \mid \mathbf{1}^\mathsf{T}\mathbf{p} = 1\big\}$ and differentiable at points in S_n yielding nonsingular FIMs,

$$\boldsymbol{\phi}(\mathbf{p}) := \nabla\Phi(\mathbf{p}) = \Big[\operatorname{trace}\big\{\mathbf{M}(\mathbf{p})^{-1}\mathbf{M}_1\big\}, \ldots, \operatorname{trace}\big\{\mathbf{M}(\mathbf{p})^{-1}\mathbf{M}_n\big\}\Big]^\mathsf{T}. \tag{51.4}$$

51.3 Simplicial Decomposition for Problem 51.1

51.3.1 Algorithm Model

Simplicial decomposition (SD) proved extremely useful for large-scale pseudoconvex programming problems [6]. It proceeds by alternately solving linear and nonlinear programming subproblems, called the *column generation problem* (CGP) and the *restricted master problem* (RMP), respectively. In the RMP, the original problem is relaxed by replacing the original constraint set P with its inner approximation being the convex hull of a finite set of feasible solutions. In the CGP, this inner approximation is improved by incorporating a point in the original constraint set that lies furthest along the gradient direction computed at the solution of the RMP. A marked characteristic of the SD method is that the sequence of solutions to the RMP tends to a solution to the original problem in such a way that the objective function strictly monotonically approaches its optimal value.

Tailoring the SD scheme to our needs, we obtain Algorithm 51.1. In the sequel, its consecutive steps will be discussed in turn.

Algorithm 51.1 Algorithm model for solving Problem 51.1 via simplicial decomposition

Step 0: (Initialization)
Guess an initial solution $\mathbf{p}^{(0)} \in P$ such that $\mathbf{M}(\mathbf{p}^{(0)})$ is nonsingular. Set $I = \{1, \ldots, n\}$, $Q^{(0)} = \{\mathbf{p}^{(0)}\}$ and $k = 0$.

Step 1: (Termination check)
Set $I_{\mathrm{ub}}^{(k)} = \{i \in I \mid p_i^{(k)} = b_i\}$, $I_{\mathrm{im}}^{(k)} = \{i \in I \mid 0 < p_i^{(k)} < b_i\}$, $I_{\mathrm{lb}}^{(k)} = \{i \in I \mid p_i^{(k)} = 0\}$. If

$$\phi_i\big(\mathbf{p}^{(k)}\big) \begin{cases} \geq \lambda & \text{if } i \in I_{\mathrm{ub}}^{(k)}, \\ = \lambda & \text{if } i \in I_{\mathrm{im}}^{(k)}, \\ \leq \lambda & \text{if } i \in I_{\mathrm{lb}}^{(k)} \end{cases} \tag{51.5}$$

for some $\lambda \in \mathbb{R}_+$, then STOP and $\mathbf{p}^{(k)}$ is optimal.

Step 2: (Solution of the column generation subproblem)
Compute

$$\mathbf{q}^{(k+1)} = \arg\max_{\mathbf{p} \in P} \boldsymbol{\phi}\big(\mathbf{p}^{(k)}\big)^{\mathsf{T}} \mathbf{p} \tag{51.6}$$

and set

$$Q^{(k+1)} = Q^{(k)} \cup \{\mathbf{q}^{(k+1)}\}. \tag{51.7}$$

Step 3: (Solution of the restricted master subproblem)
Find

$$\mathbf{p}^{(k+1)} = \arg \max_{\mathbf{p} \in \mathrm{co}(Q^{(k+1)})} \Phi\big[\mathbf{M}(\mathbf{p})\big] \tag{51.8}$$

and purge $Q^{(k+1)}$ of all extreme points with zero weights in the resulting expression of $\mathbf{p}^{(k+1)}$ as a convex combination of elements in $Q^{(k+1)}$. Increment k by one and go back to Step 1.

51.3.2 Termination of Algorithm 51.1

The computation is stopped if the current point $\mathbf{p}^{(k)}$ satisfies the condition of nonincrease, to first order, in performance measure value in the whole constraint set, $\max_{\mathbf{p} \in P} \boldsymbol{\phi}(\mathbf{p}^{(k)})^{\mathsf{T}}(\mathbf{p} - \mathbf{p}^{(k)}) \leq 0$. The condition (51.5) is less costly in terms of the number of floating-point operations. It results from the following equivalence theorem which follows from direct application of Lemma 1 in [12] after setting $f(\mathbf{p}) = \Phi(\mathbf{M}(\mathbf{p}))$, see also [8].

Proposition 51.1 *Suppose that* $\mathbf{M}(\mathbf{p}^\star)$ *is nonsingular for some* $\mathbf{p}^\star \in P$. *The vector* $\mathbf{p}^\star$ *is a global maximum of* Φ *over* P *if, and only if, there is a number* $\lambda^\star$ *such that*

$$\phi_i\left(p^\star\right)\begin{cases}\geq \lambda^\star & \text{if } p_i^\star = b_i,\\ = \lambda^\star & \text{if } 0 < p_i^\star < b_i,\\ \leq \lambda^\star & \text{if } p_i^\star = 0\end{cases} \tag{51.9}$$

for $i = 1, \ldots, n$.

Implementation of (51.5) requires some alterations to guarantee termination in a finite number of iterations, but their description is beyond the scope of this paper.

51.3.3 Solution of the Column Generation Subproblem

In Step 2 of Algorithm 51.1 we deal with the linear programming problem

$$\text{maximize } \mathbf{c}^\mathsf{T}\mathbf{p} \quad \text{subject to } \mathbf{p} \in P, \tag{51.10}$$

where $\mathbf{c} = \boldsymbol{\phi}(\mathbf{p}^{(k)})$. We can develop an algorithm to solve this problem, which is almost as simple as a closed-form solution. The key idea is to make use of the following assertion being a direct consequence of Lemma 1 in [12].

Proposition 51.2 *A vector* $\mathbf{q} \in P$ *constitutes a global solution to the problem* (51.10) *if, and only if, there exists a scalar* ρ *such that*

$$c_i\begin{cases}\geq \rho & \text{if } q_i = b_i,\\ = \rho & \text{if } 0 < q_i < b_i,\\ \leq \rho & \text{if } q_i = 0\end{cases} \tag{51.11}$$

for $i = 1, \ldots, n$.

Thus, in order to solve (51.10), it is sufficient to pick the consecutive largest components c_i of $\mathbf{c}$ and set the corresponding weights q_i as their maximal allowable values b_i. The process is repeated until the sum of the assigned weights exceeds one. Then the value of the last weight which was set in this manner should be corrected so as to satisfy the constraint $\mathbf{1}^\mathsf{T}\mathbf{p} = 1$ and the remaining (i.e., unassigned) weights are set as zeros. This scheme is implemented as Algorithm 51.2.

51.3.4 Solution of the Restricted Master Subproblem

Suppose that in the $(k+1)$-th iteration of Algorithm 51.1, we have $Q^{(k+1)} = \{\mathbf{q}_1, \ldots, \mathbf{q}_r\}$, possibly with $r < k+1$ owing to the built-in deletion mechanism of points in $Q^{(j)}$, $1 \leq j \leq k$, which did not contribute to the convex combinations yielding the corresponding iterates $\mathbf{p}^{(j)}$. Step 3 of Algorithm 51.1 involves maximization of (51.3) over $\mathrm{co}(Q^{(k+1)}) = \{\sum_{j=1}^r w_j\mathbf{q}_j | \mathbf{w} \succeq \mathbf{0},\ \mathbf{1}^\mathsf{T}\mathbf{w} = 1\}$.

From the representation of $\mathbf{p} \in \mathrm{co}(Q^{(k+1)})$ as $\mathbf{p} = \sum_{j=1}^r w_j\mathbf{q}_j$, or, componentwise, $p_i = \sum_{j=1}^r w_j q_{j,i}$, $i = 1, \ldots, n$, $q_{j,i}$ being the ith component of $\mathbf{q}_j$, we get

Algorithm 51.2 Algorithm model for solving the column generation subproblem

Step 0: (Initialization)
Set $j = 0$ and $v^{(0)} = 0$.

Step 1: (Sorting)
Sort the elements of $\mathbf{c}$ in nonincreasing order, i.e., find a permutation π on the index set $I = \{1, \ldots, n\}$ such that

$$c_{\pi(i)} \geq c_{\pi(i+1)}, \quad i = 1, \ldots, n-1. \tag{51.12}$$

Step 2: (Identification of nonzero weights)

Step 2.1: If $v^{(j)} + b_{\pi(j+1)} < 1$ ($\mathbf{b}$ has been defined in Problem 51.1) then set

$$v^{(j+1)} = v^{(j)} + b_{\pi(j+1)}. \tag{51.13}$$

Otherwise, go to Step 3.

Step 2.2: Increment j by one and go to Step 2.1.

Step 3: (Form the ultimate solution)
Set

$$q_{\pi(i)} = \begin{cases} b_{\pi(i)} & \text{for } i = 1, \ldots, j, \\ 1 - v^{(j)} & \text{for } i = j+1, \\ 0 & \text{for } i = j+2, \ldots, n. \end{cases} \tag{51.14}$$

$$\mathbf{M}(\mathbf{p}) = \sum_{i=1}^{n} p_i \mathbf{M}_i = \sum_{j=1}^{r} w_j \left(\sum_{i=1}^{n} q_{j,i} \mathbf{M}_i \right) = \sum_{j=1}^{r} w_j \mathbf{M}(\mathbf{q}_j). \tag{51.15}$$

From this, we see that the RMP can equivalently be formulated as

Problem 51.2 Find the sequence of weights $\mathbf{w} \in \mathbb{R}^r$ to maximize

$$\Psi(\mathbf{w}) = \log\det\big(\mathbf{H}(\mathbf{w})\big) \tag{51.16}$$

subject to the constraints

$$\mathbf{1}^{\mathsf{T}}\mathbf{w} = 1, \quad \mathbf{w} \succeq \mathbf{0}, \tag{51.17}$$

where

$$\mathbf{H}(\mathbf{w}) = \sum_{j=1}^{r} w_j \mathbf{H}_j, \quad \mathbf{H}_j = \mathbf{M}(\mathbf{q}_j), \ j = 1, \ldots, r. \tag{51.18}$$

Its solution can be determined numerically using the multiplicative algorithm analyzed in [3, 7, 9, 10] or [11, p. 62]. Its RMP version proceeds as summarized in Algorithm 51.3.

Algorithm 51.3 Algorithm model for the restricted master problem

Step 0: (Initialization)
Select a weight vector $\mathbf{w}^{(0)} \in S_r \cap \mathbb{R}^r_{++}$, e.g., set $\mathbf{w}^{(0)} = (1/r)\mathbf{1}$. Set $\ell = 0$.

Step 1: (Termination check)
If

$$\frac{1}{m}\boldsymbol{\psi}\left(\mathbf{w}^{(\ell)}\right) \preceq \mathbf{1} \tag{51.19}$$

then STOP.

Step 2: (Multiplicative update)
Evaluate

$$\mathbf{w}^{(\ell+1)} = \frac{1}{m}\boldsymbol{\psi}\left(\mathbf{w}^{(\ell)}\right) \cdot \mathbf{w}^{(\ell)}. \tag{51.20}$$

Increment ℓ by one and go to Step 1.

51.4 Numerical Example

The reactant concentrations $[A]$, $[B]$ and $[C]$ in a batch reactor are governed by

$$\begin{cases} \dfrac{\mathrm{d}[A]}{\mathrm{d}t} = -k_1[A]^{\gamma_1}, & [A]_{t=0} = 1, \\ \dfrac{\mathrm{d}[B]}{\mathrm{d}t} = k_1[A]^{\gamma_1} - k_2[B]^{\gamma_2}, & [B]_{t=0} = 0, \\ \dfrac{\mathrm{d}[C]}{\mathrm{d}t} = k_2[B]^{\gamma_2}, & [C]_{t=0} = 0, \end{cases} \tag{51.21}$$

where k_1 and k_2 are the rates and γ_1 and γ_2 are the orders of the reactions. The vector of coefficients $\boldsymbol{\theta} = (k_1, k_2, \gamma_1, \gamma_2)$ is to be estimated from measurements of all concentrations at feasible time points $t_i = 0.2i$, $i = 1, \ldots, n = 100$. We wish to design the observation process so that the experiment is maximally informative.

We fit this situation into the framework of Sect. 51.3 by setting $\mathbf{x}_i = t_i$ for $i = 1, \ldots, n$. We assume that the measurements of individual responses are independent of one another, i.e., $\mathbf{V}(t_i) = \mathbf{I}_3$, the 3×3 identity matrix, $i = 1, \ldots, n$. We set $\mathbf{F}(t_i)^{\mathsf{T}} = \partial\boldsymbol{\eta}/\partial\boldsymbol{\theta}(t_i, \boldsymbol{\theta}^0)$, $i = 1, \ldots, n$, where $\boldsymbol{\eta}(t, \boldsymbol{\theta}) = ([A](t; \boldsymbol{\theta}), [B](t; \theta), [C](t; \boldsymbol{\theta}))$, $[A](\cdot; \boldsymbol{\theta})$, $[B](\cdot; \boldsymbol{\theta})$ and $[C](\cdot; \boldsymbol{\theta})$ denote the solution to (51.21) for a given value of the parameter vector θ, $\partial\boldsymbol{\eta}/\partial\boldsymbol{\theta}$ is the Jacobian matrix and $\boldsymbol{\theta}^0 = (0.7, 0.2, 1.1, 1.5)$ is a prior estimate to $\boldsymbol{\theta}$. This constitutes a usual procedure in optimum design for nonlinear regression, cf. [1, 11].

A computer program was written in MATLAB to implement Algorithms 51.1–51.3. The computations were started from the 'uniform' design $\mathbf{p}^{(0)} = (1/n)\mathbf{1} = 0.01\,\mathbf{1}$. The results are displayed in Fig. 51.1.

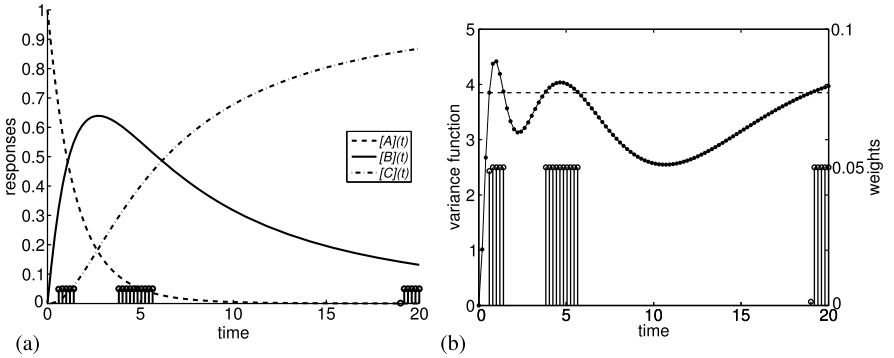

Fig. 51.1 Simulation results for the 'uniform' upper bound $\mathbf{b} = 0.05 \cdot \mathbf{1}$: **(a)** Time evolution of the reactant concentrations and optimum designs pictorially represented by vertical stems starting at points whose abscissas coincide with the design support points and terminating with circles whose ordinates reflect the corresponding weights. **(b)** Variance function $\phi_i(\mathbf{p}^\star)$ for the computed D-optimum designs. Vertical stems constitute a pictorial representation of the design weights and the *dashed horizontal* line is drawn at a level of λ underlying the optimality conditions (51.9)

References

1. Atkinson AC, Donev AN, Tobias RD (2007) Optimum experimental designs, with SAS. Oxford University Press, New York
2. Cook D, Fedorov V (1995) Constrained optimization of experimental design. Statistics 26:129–178
3. Fellman J (1974) On the allocation of linear observations (Thesis). Comment Phys Math 44(2):27–78
4. Harman R, Trnovská M (2009) Approximate D-optimal designs of experiments on the convex hull of a finite set of information matrices. Math Slovaca 59:693–704
5. Patan M (2012) Distributed scheduling of sensor networks for identification of spatio-temporal processes. Int J Appl Math Comput Sci 22(2):299–311
6. Patriksson M (2001) Simplicial decomposition algorithms. In: Floudas CA, Pardalos PM (eds) Encyclopedia of optimization, vol 5. Kluwer, Dordrecht, pp 205–212
7. Pázman A (1986) Foundations of optimum experimental design. Reidel, Dordrecht
8. Sahm M, Schwabe R (2001) A note on optimal bounded designs. In: Atkinson A, Bogacka B, Zhigljavsky A (eds) Optimum design 2000. Kluwer, Dordrecht, pp 131–140
9. Torsney B (1981) Algorithms for a constrained optimisation problem with applications in statistics and optimum design. Unpublished Ph.D. Thesis, University of Glasgow. Available at http://theses.gla.ac.uk/1088/1/1981torsneyphd.pdf
10. Torsney B, Mandal S (2004) Multiplicative algorithms for constructing optimizing distributions: further developments. In: Di Bucchianico A, Läuter H, Wynn HP (eds) *mODa 7*. Proc 7th int workshop on model-oriented data analysis. Physica-Verlag, Heidelberg, pp 163–171
11. Uciński D (2005) Optimal measurement methods for distributed-parameter system identification. CRC Press, Boca Raton
12. Uciński D (2012) Sensor network scheduling for identification of spatially distributed processes. Int J Appl Math Comput Sci 22(1):25–40
13. Uciński D, Patan M (2007) D-optimal design of a monitoring network for parameter estimation of distributed systems. J Glob Optim 39(2):291–322

Chapter 52
The Analysis of Stochastic Signal from LHD Mining Machine

Agnieszka Wyłomańska and Radosław Zimroz

Abstract In this paper a novel procedure for LHD (Load-Haul-Dump) machine temperature signal analysis is proposed. In this procedure the signal segmentation and its decomposition into trend and residuals is made. Moreover in the next step the novel technique for further decomposition of residuals is proposed and stochastic analysis procedure is applied. The stochastic analysis is based on the ARMA (autoregressive moving average) models with Gaussian and strictly stable distribution. Different nature of extracted sub-signals offers specific opportunity to use them for condition monitoring as well as process monitoring purposes. Appropriate processing techniques give a chance to observe specific character in the acquired data. In this paper we present basic theory related to the applied methodology as well as practical example obtained by application of proposed techniques.

52.1 Introduction

Recent trends in mining industry are focused on monitoring of processes and machines monitoring. The reasons of that are, among others, improvement of production efficiency, optimisation of processes, cost reduction, increasing of safety, etc. A very special case is monitoring of underground machines. Due to unusually harsh conditions, efficient operation of machines and safe working conditions for mining staff are the highest priority. In this paper a novel procedure for machine temperature signals analysis is proposed. Investigated data come from underground LHD machine, namely loader, that is used for copper ore transport. Basically, the procedure is based on signal segmentation, [19], decomposition into trend and residuals,

A. Wyłomańska (✉)
Hugo Steinhaus Center, Institute of Mathematics and Computer Science, Wrocław University of Technology, Wrocław, Poland
e-mail: agnieszka.wylomanska@pwr.edu.pl

R. Zimroz (✉)
Diagnostics and Vibro-Acoustics Science Laboratory, Wrocław University of Technology and KGHM CUPRUM Ltd CBR, Wrocław, Poland
e-mail: radoslaw.zimroz@pwr.edu.pl

A. Steland et al. (eds.), *Stochastic Models, Statistics and Their Applications*,
Springer Proceedings in Mathematics & Statistics 122,
DOI 10.1007/978-3-319-13881-7_52

further decomposition and, finally, the stochastic analysis of decomposed parts of the signal [10, 11, 15, 20]. Different nature of extracted sub-signals offers specific opportunity to use them for condition monitoring as well as process monitoring purposes. Appropriate processing techniques give a chance to observe specific character in the acquired data. It should be also highlighted, that due to harsh conditions, many collected signals should be validated first. Again, there is a strong link to phenomena reported in the literature related to vibration analysis [8]. In the paper all mentioned issues are addressed. Both basic theory related to the method as well as practical example obtained by application of proposed techniques to real data will be discussed.

52.2 Methodology

In this section we describe in details the whole procedure of temperature signal analysis. Basic assumption for signal analysis here is that due to complexity of the signal there is a need to "decompose" it into much simpler sub-signals. It is related to extraction of part of the signal called "segment" that corresponds to continuous operation of machine (machine on – machine off) in one of the regimes. The primary decomposition is made on the basis of the increments of the examined signal $X_1, X_2, \ldots, X_N$. Those points for which the absolute value of increments exceed the given threshold ε, might mean beginning of a new segment. The alternative methods of segmentation one can find for instance in [4]. As it will be mentioned in next section, it was found that each segment is constituted from two very different processes. The first one, commonly used in diagnostic is a trend-like signal. It stands for low frequency variation of the machine temperature that depends on time of operation, condition of the machine, temperature in the given mining corridor underground, etc. Second process is very different. It is related to relatively high frequency fluctuation of temperature and it corresponds to time varying machine operation. To identify and understand both processes, it is proposed to decompose the signal into deterministic trend and residual signal related to the mentioned fluctuations. So, in the next step for each specified sub-signal we fit a polynomial which represents the deterministic trend. In order to fit the polynomial corresponding to each sub-signal we use the least squares method. Denoting the sub-signal as $Y_1, Y_2, \ldots, Y_m$, the coefficients $a_1, a_2, \ldots, a_p$ of the polynomial of order p are calculated by solving the following equation:

$$(a_0, a_1, \ldots, a_p) = argmin \sum_{i=1}^{m} r_i^2, \tag{52.1}$$

where r_i is a residuum corresponding to the observation i, $r_i = Y_i - \sum_{j=0}^{p} a_j i^j$, $i = 1, 2, \ldots, m$ and $f(i) = \sum_{j=0}^{p} a_j i^j$ is a fitted polynomial of order p.

After fitting the polynomials to appropriate sub-signals in the next step of our procedure we examine the residual sub-signals. In each segment we observe that

there are parts with similar statistical behaviour. The decomposition of residuum corresponding to each segment we perform on the basis of the time-frequency representation of examined sub-signal. We decompose the residuum sub-signals into a set of narrowband sub-signals using a time-frequency representation. Here we propose to use the discrete short-time Fourier transform (STFT) that for residuum $r_1, r_2, \ldots, r_m$, frequency $f \in F$ and time $t \in T$ is defined as follows: $\mathrm{STFT}(t, f) = \sum_{k=0}^{m-1} r_{k+1} w(t-k) e^{2i\pi f k/m}$, where $w(t-k)$ is a shifted window. Note that signal segmentation might be performed in different manners [3, 5, 7, 12, 13, 16]. Our hypothesis is that switching between regimes might cause different spectral contents of the signal (due to different nature of operation for that regime) and, moreover, might cause a kind of singularity in the signal. This procedure can be described mathematically in the following way: for each residuum sub-signal we first calculate the STFT and next, for each time point t we sum the absolute values of the STFT according to frequencies, that means we calculate the following value: $d(t) = \sum_{f \in F} |\mathrm{STFT}(t, f)|$. Finally, on the basis of $d(t)$ function we can find such point t for which the function reaches local minima. The local minima we can find by setting a threshold and then by finding such time point for which the $d(t)$ function exceeds it. The STFT-based segmentation is just an approximation due to poor time-frequency resolution. It gives preliminary knowledge if and when change might appear. Within the validation part, one might also refer to other variables, that are probably more clear to interpret – as engine torque or engine rotational speed. In our analysis we improve the STFT-based segmentation by using engine torque variable. The final step of our methodology is to fit appropriate model to each segment – short part of the signal with homogeneous nature. Here we use methods of time series analysis, namely to description of the residual sub-signals we use the general class of autoregressive moving average (ARMA) models [1]. The ARMA time series $\{X_t\}$ with orders p and q is defined as follows:

$$X_t - \sum_{i=1}^{p} a_p X_{t-1} = Z_i + \sum_{i=1}^{q} b_i Z_{t-i}, \tag{52.2}$$

where $\{a_i\}_{i=1}^{p}$ and $\{b_i\}_{i=1}^{q}$ are coefficients and $\{Z_i\}$ is the residual series of the model. First, for each residual sub-signal we chose the proper ARMA order on the basis of Bayesian information criterion (BIC) [1]. Then, for the chosen ARMA order we estimate the parameters of the time series by using maximum likelihood method [1]. Then we analyse the residuals of fitted ARMA models. More precisely, we examine if the ARMA residuals exhibit behaviour adequate to independent identically distributed random variables, i.e. their autocorrelation and partial autocorrelation functions (ACF and PACF) are close to zero for all lags different than zero and the data are homogeneous. In this analysis we also concentrate on the distribution of the ARMA residuals. By using Jacque–Bera (JB) test [6] we check Gaussianity. If the ARMA residuals are not Gaussian, then we check if they can be modelled by using more general class of distributions, namely stable one [14, 17]. Let us mention, the stable distribution is defined via its characteristic function. Namely, the random variable X has stable distribution with parameters $0 < \alpha \leq 2$, $-1 \leq \beta \leq 1$, $\sigma > 0$ and $\mu \in R$ if its characteristic function is given by [17]:

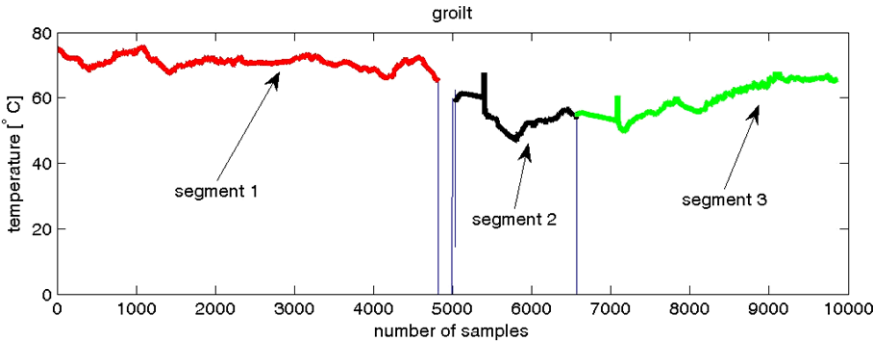

Fig. 52.1 The segmented analysed signal groilt

$$E\exp\{i\theta X\} = \begin{cases} \exp\{-\sigma^\alpha|\theta|^\alpha(1-i\beta(\operatorname{sign}\theta)\tan(\pi\alpha/2))+i\mu\theta\} & \text{for } \alpha \neq 1 \\ \exp\{-\sigma|\theta|(1-i\beta\pi/2(\operatorname{sign}\theta)\log|\theta|)+i\mu\theta\} & \text{for } \alpha = 1. \end{cases}$$

To test the stable distribution we use the Anderson–Darling (AD) test [2, 15, 18]. After recognition the proper distribution of ARMA residuals we can estimate the chosen distributions' parameters. To estimate the Gaussian distribution parameters (μ and σ) we use the maximum likelihood method, while for stable distribution ($\alpha, \sigma, \beta, \mu$) we propose to use the regression method [9]. In order the prove the fitted ARMA model is appropriate to examined sub-signals, we simulate the trajectory of fitted model with estimated parameters and fitted ARMA residuals' distributions. The first goodness-of-fit criterion is the similar behaviour of simulated series and examined signal. This similarity can be manifested in the behaviour of time series itself but also in the measures of dependence, such as ACF and PACF. Here we compare those measures calculated for examined residual sub-signals and ACFs and PACFs for fitted models.

52.3 Application

As it was mentioned earlier raw temperature data are very difficult to interpret and model. The data represent nearly $3h$ of machine operation. During that time one might notice short breaks in operation. We have selected groilt data (GeaR OIL Temperature) because it reveals interesting properties: it is clearly seen that there are some parts of the signal that seem to be artifacts, see Fig. 52.1. It is physically impossible that machine with temperature c.a. 70 °C will be cooled in few second to 0 °C. It is probably related to switching off the machine. As reported in [8, 21] data validation in industrial conditions is a key step in signal processing. According to the presented in previous section methodology, the primary segmentation is made on the basis of increments of the signals. Results of the first step of segmentation are presented in Fig. 52.1 where considered signal (groilt) is segmented and plotted in different colours. Deep analysis of the shape of each segment provide an interesting conclusion that there is a mixture of trend-like component and high frequency

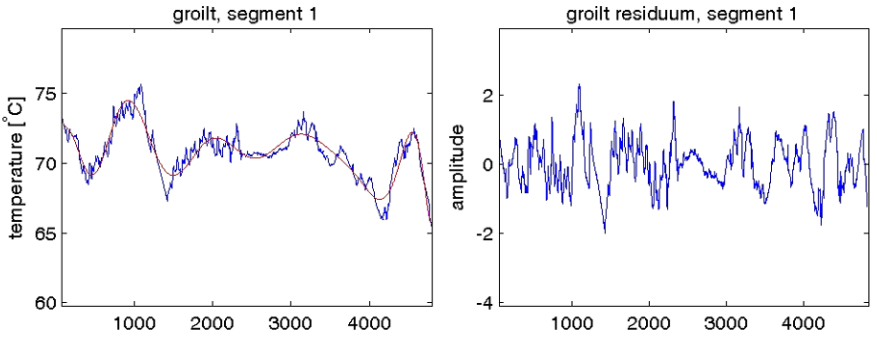

Fig. 52.2 Decomposition results for segment 1: *left* – trend signals in red plotted on raw data, *right* – residuals

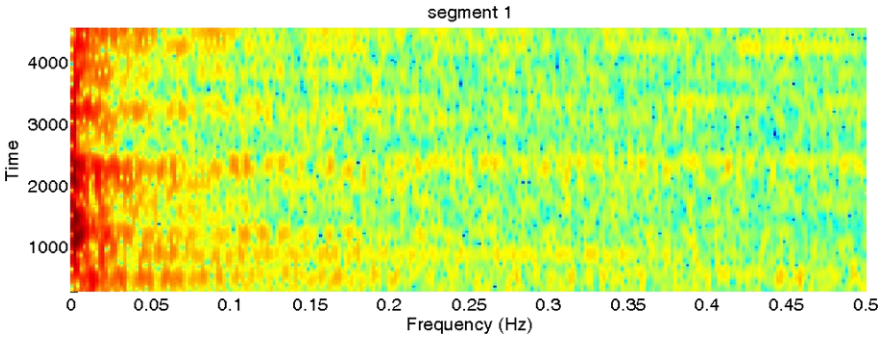

Fig. 52.3 Time-frequency representations of residuum from groilt signal from segment 1

fluctuation. A procedure for trend and residuals estimation has been applied to segment 1 (S1) and 3 (S3) of examined groilt data and results of its application for segment 1 are shown in Fig. 52.2. We decided to avoid analysis for segment 2 due to its relatively short duration.

As it was mentioned, trend analysis might be used for condition monitoring purposes (alarm providing due to overheating of the system or short time prognosis when such level will be achieved). Residual part of the signal reveals (at least at some parts of the signal) cyclic nature. These cycles were barely visible in raw data due to dynamics of the signal (tens of C). The key questions are: Is it possible to extract information about machine operation regimes from residual signal? If yes - how to do it? and if it really corresponds to cyclic behaviour of machine? To answer for that questions further signal segmentation based on time-frequency signal representation has been done. In Fig. 52.3 we present the STFT for segment 1 of residuum corresponding to groilt signal. As we observe there are time points for which the energy distribution is smaller. On the basis of this we can conclude on the further decomposition of residual series.

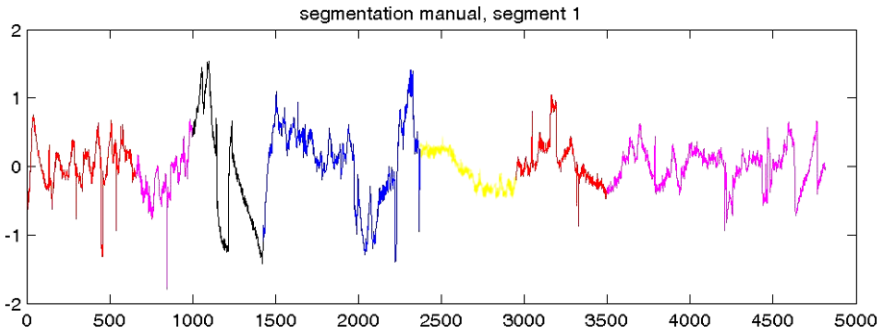

Fig. 52.4 Final result of segmentation of residuals from segments 1 (STFT segmentation with manual selection of segments)

According to presented methodology in order to make additional segmentation we analyse the $d(t)$ function that corresponds to groilt residuum series for segment 1 and 3. On the basis of the $d(t)$ we can find the time points which split the examined residual series into sub-signals with similar behaviour. Local minimum of $d(t)$ indicate change of regime. The final result of the segmentation for segment 1 (after validation with engine torque signal) is presented in Fig. 52.4.

According to the described statistical modelling procedure, the best ARMA orders were chosen on the basis of BIC criterion. Result of this step is presented in Table 52.1. In the next step we estimated the ARMA parameters of selected parts from segment 1 (P1–P7) and segment 3 (P1–P5) and on the basis of fitted models we calculate the ARMA residuals. In Table 52.2 we present the result of testing distributions for ARMA residuals corresponding to segment 1 and segment 3 together with the estimated parameters of appropriate distributions. In Fig. 52.5 we show the validation of our stochastic modelling procedure and show the simulated trajectory of P4 corresponding to segment 1 and ACFs and PACFs of P4 and those measures for fitted ARMA models. As we observe the simulated trajectory have similar behaviour as analysed data set. Moreover the analysed measures of dependence are similar.

52.4 Conclusions

In this paper a novel procedure for temperature signals analysis is proposed. In this procedure the signal segmentation and its decomposition into trend and residuals is made. Moreover in the next step the novel technique for further decomposition of residuals is proposed and modelling procedure is applied. Because of the different nature of extracted sub-signals on the basis of them we can monitor both the machine condition and processes that are associated with its operation. In the real data analysis it has been shown that a slowly varying trend is much important than high frequency oscillation with small amplitudes and the local variation of temperature is related to machine operation regime (loading, unloading, moving with

Table 52.1 The orders of ARMA models for appropriate residual sub-signals corresponding to segment 1 and 3 and BIC statistic

Segment 1	AR order	MA order	BIC statistic	Segment 3	AR order	MA order	BIC statistic
P1	2	1	$-0.121673 \cdot 10^4$	P1			
P2	4	5	$-0.135290 \cdot 10^4$	P2	1	1	$-0.139259 \cdot 10^4$
P3				P3			
P4	5	5	$-0.184909 \cdot 10^4$	P4	2	5	$-0.863022 \cdot 10^4$
P5	4	0	$-0.247935 \cdot 10^4$	P5	3	3	$-0.200873 \cdot 10^4$
P6	3	3	$-0.595945 \cdot 10^3$				
P7	5	5	$-0.358021 \cdot 10^4$				

Table 52.2 The p-values of JB and AD tests for Gaussian and stable distribution for ARMA residuals corresponding to segment 1 and segment 3 and estimated parameters of appropriate distributions

Segment 1/Segment 3	p-value of JB	p-value of AD	Stable/Gaussian
P1(S1/S3)	0.001/	0.02/	None/
P2(S1/S3)	0.44/0.001	0.78/0	Gaussian/None $\mu = 0, \sigma = 0.084/$
P3(S1/S3)			
P4(S1/S3)	0.001/0.001	0.08/0.54	Stable/Stable $\alpha = 1.36,\ \sigma = 0.03/\alpha = 1.1,\ \sigma = 0.043$ $\beta = 0.32,\ \mu = 0.01/\beta = 0.22,\ \mu = 0.01$
P5(S1/S3)	0.001/0.001	0/0.16	None/Stable $/\alpha = 1.2,\ \sigma = 0.02$ $/\beta = 0.17,\ \mu = 0.001$
P6(S1)	0.001	0.9	Stable $\alpha = 1.32,\ \sigma = 0.02$ $\beta = 0.21,\ \mu = 0.03$
P7(S1)	0.001	0.08	Stable $\alpha = 1.54,\ \sigma = 0.02$ $\beta = -0.15,\ \mu = -0.00015$

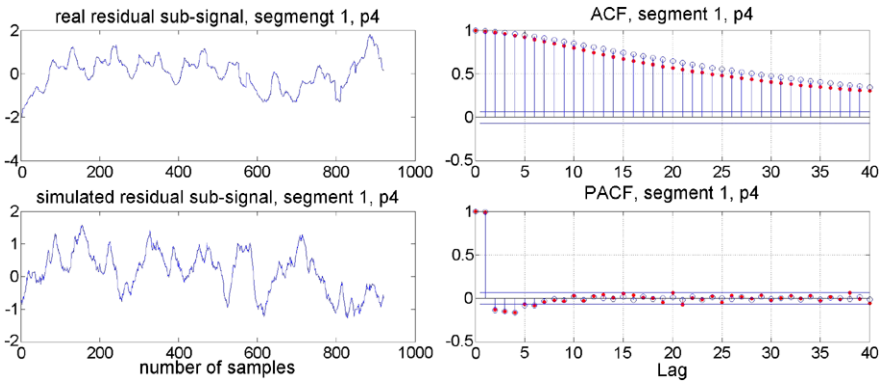

Fig. 52.5 *Left figure*: Real residual sub-signal corresponding to P4 from segment 1 (*top panel*) and simulated residual sub-signal on the basis of fitted ARMA model and *right figure*: ACFs (*top panel*) and PACFs (*bottom panel*) for real residual sub-signal corresponding to P4 from segment 1 (*red line*) and those measures for fitted ARMA models (*blue line*)

approx. stable speed, acceleration, deceleration etc.). From theoretical point of view operation of loader should reveal cyclic nature. Unfortunately, in practise these data might be very different for some segments which may be related to different state of the machine. Therefore no cyclic behaviour will appear in any available data. This causes that more advanced techniques and methods should be used to examine real data. Additional channel (Engine Torque, ET) used for validation allowed us to confirm/validated discovered information. It should be highlight, that using ET data only, these conclusion would be difficult to achieve.

References

1. Brockwell PJ, Davis RA (1996) Introduction to time series and forecasting. Springer, New-York
2. Burnecki K, Wylomanska A, Beletskii A, Gonchar V, Chechkin A (2012) Recognition of stable distribution with Levy index alpha close to 2. Phys Rev E 85:056711
3. Crossman JA, Guo H, Murphey YL, Cardillo J (2003) Automotive signal fault diagnostics – part I: Signal fault analysis, signal segmentation, feature extraction and quasi-optimal feature selection. IEEE Trans Veh Technol 52(4):1063
4. Gajda J, Sikora G, Wylomanska A (2013) Regime variance testing – a quantile approach. Acta Phys Pol B 44(5):1015
5. Hory C, Martin N, Chehikian A (2002) Spectrogram segmentation by means of statistical features for non-stationary signal interpretation. IEEE Trans Signal Process 50(12):2915
6. Jarque CM, Bera AK (1987) A test for normality of observations and regression residuals. Int Stat Rev 55:163
7. Karlsen HA, Tjostheim D (1990) Autoregressive segmentation of signal traces with applications to geological dipmeter measurements. IEEE Trans Geosci Remote Sens 28(2):171
8. Kepski P, Barszcz T (2012) Validation of vibration signals for diagnostics of mining machinery. Diagnostyka 64(4):25
9. Koutrouvelis IA (1980) Regression-type estimation of the parameters of stable laws. J Am Stat Assoc 75:18

10. Maciejewska M, Szczurek A, Janczura J, Wylomanska A (2013) Stochastic modeling of indoor air temperature. J Stat Phys 152:979
11. Makowski RA, Zimroz R (2011) Adaptive bearings vibration modelling for diagnosis. In: Bouchachia A (ed) ICAIS 2011. LNAI, vol 6943. Springer, Berlin, p 248
12. Mahmood S, Sharif BS (2006) Noise reduction, smoothing and time interval segmentation of noisy signals using an energy optimisation method. IEE Proc, Vis Image Signal Process 153(2):101–108
13. Millioz F, Martin N (2006) Invited conference, time-frequency segmentation for engine speed monitoring. In: Special session on "Pattern recognition in acoustics and vibration", thirteen international congress on sound and vibration, ICSV13, Vienna, Austria, 2–6 July
14. Nowicka-Zagrajek J, Wylomanska A (2008) Measures of dependence for stable AR(1) models with time-varying coefficients. Stoch Models 24(1):58
15. Obuchowski J, Wylomanska A, Zimroz R (2013) Stochastic modeling of time series with application to local damage detection in rotating machinery. In: Damage assessment of structures. Key engineering materials, vol 569, p 441
16. Popescu TD, Aiordachioaie D (2013) Signal segmentation in time-frequency plane using Rényi entropy. In: Application in seismic signal processing 2013 conference on control and fault-tolerant systems (SysTol), Nice, France, 9–11 October
17. Samorodnitsky G, Taqqu MS (1994) Stable non-Gaussian random processes. Chapman &Hall, New York
18. Weron R (2004) In: Gentle JE, Hardle WH, Mori Y (eds) Handbook of computational statistics: concepts and methods. Springer, Berlin
19. Wylomanska A, Zimroz R (2014) Signal segmentation for operational regimes detection of heavy duty mining mobile machines – a statistical approach. Diagnostyka 15:33
20. Xiuzhong X, Xiong Hu H, Jiang S (2010) Statistic analysis and predication of crane condition parameters based on svm. In: Proceedings of the 2010 IEEE international conference on automation and logistics, Hong Kong and Macau, 16–20 August
21. Zimroz R, Wodecki J, Krol R, Andrzejewski M, Sliwinski P, Stefaniak P (2014) Self-propelled mining machine monitoringsystem – data validation, processing and analysis. In: Mine planning and equipment selection, doi 10.1007/978-3-319-02678-7-124.1285

Chapter 53
Evaluating the Performance of VaR Models in Energy Markets

Saša Žiković, Rafał Weron, and Ivana Tomas Žiković

Abstract We analyze the relative performance of 13 VaR models using daily returns of WTI, Brent, natural gas and heating oil one-month futures contracts. After obtaining VaR estimates we evaluate the statistical significance of the differences in performance of the analyzed VaR models. We employ the simulation-based methodology proposed by Žiković and Filer in Czech J Econ Finan 63(4):327–359, 2013, which allows us to rank competing VaR models. Somewhat surprisingly, the obtained results indicate that for a large number of different VaR models there is no statistical difference in their performance, as measured by the Lopez size adjusted score. However, filtered historical simulation (FHS) and the BRW model stand out as robust and consistent approaches that – in most cases – significantly outperform the remaining VaR models.

53.1 Introduction

Fossil fuels are commodities that are the primary source of energy for electricity production, transportation and industrial production. Their importance and multiplicative effect on almost all branches of the economy dictates the necessity for deeper insight into the ways of measuring and protecting against risks stemming from changes in their prices. Energy markets differ from traditional financial markets for several reasons, but two of the most important ones are the nature of production and consumption and geopolitical fragility. Their return distributions exhibit a higher variance and are more leptokurtic and skewed compared to those of classical financial assets. These characteristics make risk modeling a challenging task. Moreover, energy risk management is not only relevant for financial investors but even more so for energy producers and consumers who need to hedge from both the ris-

S. Žiković (✉) · I. Tomas Žiković
Faculty of Economics, University of Rijeka, Rijeka, Croatia
e-mail: szikovic@efri.hr

R. Weron
Department of Operations Research, Wrocław University of Technology, Wrocław, Poland
e-mail: rafal.weron@pwr.edu.pl

A. Steland et al. (eds.), *Stochastic Models, Statistics and Their Applications*,
Springer Proceedings in Mathematics & Statistics 122,
DOI 10.1007/978-3-319-13881-7_53

ing and falling energy prices. In order to be able to hedge against such risks the first step is to correctly evaluate the market risk of a particular energy commodity. Value at Risk (VaR) is an essential tool for this purpose. Within energy markets, VaR can be used to quantify the price risk of energy commodities associated with the desired probability level. The use of the VaR risk models in order to forecast market risk is widely used in the financial industry, where profits and losses are calculated daily, a process known as marking-to-market. VaR methodology is not yet widely used in non-financial companies, one of the reasons being the lack of regulatory requirement to daily mark-to-market their holdings. Although energy companies do not report their daily changes in value, VaR methodology is appropriate for these non-financial companies since their revenues and expenditures often fluctuate daily due to significant volatility in prices of their inputs and outputs.

The volatility of energy commodities has been widely studied in the energy economics literature. In particular, Mohammadi and Su [16] consider weekly oil spot prices in 11 markets and compare the forecasting accuracy of four GARCH-class models under two loss functions using the DM test. Wei et al. [17] conclude that no single model is superior for WTI and Brent across different loss functions. Agnolucci [1] studies the market volatility of WTI futures and finds extensions of GARCH models with asymmetric effects and different error distributions to outperform implied volatility models in terms of predictive accuracy. Studying electricity spot prices, Weron [18] finds that deseasonalized (with respect to the weekly patterns and long-term trends) returns exhibit heavy or semi-heavy tails, that can be captured well by generalized hyperbolic or Levy-stable laws.

In the risk management context, Hung et al. [10] show that in general the assumption of a Gaussian distribution leads to an underestimation of risk and highlight the importance of selecting the appropriate distribution in a GARCH context. They further find that the Value-at-Risk (VaR) of crude oil and oil products is better captured by fat-tailed distributions. Marimoutou et al. [14] find that extreme value based models perform well in the oil markets and that they offer a major improvement over the traditional (non-parametric and parametric) methods. Žiković and Vlahinić-Dizdarević [22] analyze WTI, natural gas and coal prices at the 95, 99 and 99.5 % confidence levels and conclude that the best performance across all of the tested confidence levels is achieved for the EVT-GARCH model. Bunn et al. [3] show that a structural linear quantile regression model outperforms skewed GARCH-*t* and CAViaR models regarding the accuracy of out-of-sample forecasts of VaR. Finally, a number of authors find long range memory in energy returns and report as their top VaR performers models based on this characteristic, i.e. APARCH, FIGARCH and FIAPARCH [2, 7, 13]. Overall the findings reported in the literature on the subject of VaR estimation for energy commodities are mixed. A situation that is similar to the one found in the electricity price forecasting literature [19].

Apart from known VaR problems that refer to sub-additivity and tail events, there is also an often overlooked systemic problem with risk model comparison and ranking. Backtesting VaR or expected shortfall (ES) figures yields only a comparison for a single realization of the underlying data generating process. The VaR literature is vast but it rarely addresses the issue of statistical significance in performance

of different models. Sometimes it may be only a matter of chance that for some commodity over a particular time horizon a certain model performs better than the competing ones.

The goal of this paper is to evaluate the performance of a wide array of VaR models for WTI, Brent, natural gas (NG) and heating oil (HO) one-month futures contracts during the ongoing global economic crisis, which includes periods of both backwardation and contango. After obtaining the VaR estimates we proceed to evaluate the statistical significance of the differences in performance of the analyzed VaR models. We employ the methodology for comparing VaR model performance presented in [21], allowing us to consistently rank competing VaR models. The obtained information is equally important for the risk management purposes, policy making as well as for the pricing of structured commodity derivatives.

The rest of the paper is organized as follows. In Sect. 53.2 we present the VaR ranking procedure that we use in our analysis. In Sect. 53.3 we outline the data and the methodology. VaR backtesting and rankings are presented in Sect. 53.4. Finally, in Sect. 53.5 we wrap up the results and conclude.

53.2 Comparing and Ranking VaR Models

In the risk literature there are a number of methods that test the hypothesis whether a certain model is better than some other model, such as the superior predictive ability (SPA) of Hansen [8], the equal predictive ability (EPA) of Diebold and Mariano [6] and the reality check (RC) of White [20]. The question of interest in all of these tests is whether any alternative forecast is better than the benchmark forecast, or equivalently, whether the best alternative forecasting model is better than the benchmark. This question can be addressed by testing the null hypothesis that the benchmark is not inferior to any alternative forecast. Using such tests is useful for a forecaster who wants to explore whether a better forecasting model than the model currently being used is available. After a search over several alternative models, the relevant question is whether the observed excess performance by an alternative model is significant or not.

To implement forecast evaluation, it is necessary to specify a loss function, and a number of different loss functions have been proposed in the literature. Lopez [12] suggested a size-adjusted loss function that is simple, symmetrical and intuitive:

$$C_t = \begin{cases} 1 + (L_t - VaR_t)^2 & \text{if } L_t > VaR_t, \\ 0 & \text{if } L_t \leq VaR_t. \end{cases}$$

Unlike the usually employed VaR tests where large VaR exceedances are treated in the same way as the smaller ones, this loss function allows for the sizes of tail losses to influence the final rating of a VaR model. A VaR model that generates higher tail losses would generate higher values under this size adjusted loss function than a VaR model that generates lower tail losses, ceteris paribus. No asymptotic distribution theory or critical values have been derived for this statistic but it is very suitable for

ranking the performance of competing models. The ranking procedure proposed in [21] consists of five steps:

1. Fitting an ARMA-GARCH model to the time series in order to obtain independent and identically distributed (IID) errors. Then estimating the empirical CDF of each time series (applying it to the non-tail regions of the distribution) with a Gaussian kernel. This allows to smooth the CDF, eliminating the stepwise pattern of the sample CDF.
2. Finding the upper and lower thresholds such that a percentage of the residuals are reserved for each tail and fitting the amount by which those extreme residuals in each tail fall beyond the associated threshold to a parametric GPD.
3. Generating N simulated paths for the residuals from the obtained semi-parametric distribution (each path is T observations long) and adding the ARMA-GARCH model to the residuals to obtain $N \times T$ simulated time series returns.
4. Calculating VaR for each of the $N \times T$ simulated returns for each VaR model and Lopez scores for each of the N VaR-simulated return pairs, for each VaR model.
5. Comparing if the mean values of the Lopez scores for different VaR models are significantly different from each other. For this purpose the Kruskal–Wallis test is employed.

The Kruskal–Wallis test is a nonparametric version of the classical one-way analysis of variance (ANOVA), and tests the null hypothesis that all samples are drawn from the same population, or equivalently, from different populations with the same distribution [9]. Kruskal–Wallis test is used since it makes only mild assumptions about the data, and is appropriate when the distribution of the data is non-normal.

53.3 Data and Methodology

We analyze the performance of 13 VaR models: a simple moving average (VCV), the RiskMetrics approach, historical simulation (HS 250 and HS 500; the number indicates the number of past observations used to compute VaR), mirrored historical simulation (MHS 250 and MHS 500), BRW simulation with decay factors $\lambda = 0.97$ and 0.99, a GARCH model, filtered historical simulation (FHS), the unconditional EVT approach using the generalized Pareto distribution (GPD) and the conditional EVT approach (EVT GARCH). In the analysis we employ the log-daily returns of WTI, Brent, natural gas (NG – Henry Hub and New York Harbour) and heating oil (HO – NYMEX) one-month futures contracts. Returns were collected from the Bloomberg website for the period January 1, 1995 through July 1st, 2014, which includes a period of the latest surge and fall in prices of energy commodities. The roll-over of contracts is performed at time $T - 2$ days. The transitions are smooth and there is no change in the price between the two contracts since any difference would provide an arbitrage opportunity and, hence, would be quickly exploited.

The VaR figures are calculated for a one-day ahead long position and the 99 % confidence level.

The analyzed VaR models are tested by using: the Kupiec [11] test, the Christoffersen [4] test of independence (IND) and the Lopez [12] size adjusted test. As pointed out in [21], the Christoffersen unconditional coverage (UC) test is problematic since it gives a distorted image of the performance of VaR models. Because it is chi-square distributed with one degree of freedom, deviations from the test's expected value that occur on the conservative side (i.e. with number of exceedances lower than their expected value) are penalized more severely. This characteristic is not compatible with risk-averse or risk-neutral assumptions. Thus, from the regulatory standpoint, the Kupiec [11] binomial test is preferable to the Christoffersen [4] UC test, because it is more desirable to have positive than negative deviations. The same logic extends to the Christoffersen conditional coverage (CC) test since it is the sum of the UC and IND tests. In our two-stage backtesting procedure, the best performing VaR model must first satisfy both the Kupiec [11] and Christoffersen [4] independence (IND) tests and then provide the minimal deviation from the expected value of losses by minimizing the Lopez [12] error statistics.

53.4 Backtesting Results

To secure the same out-of-the-sample backtesting period for all of the examined energy commodities, the out-of-the-sample data sets are formed by removing the 1000 most recent observations from each commodity price series. The remaining observations are used to calculate GPD tail parameters, VaR starting values and calibrate volatility. The length of the tail-loss data set used for backtesting depends on the number of errors generated by each VaR model. Data from all the commodities shows leptokurtosis, asymmetry and significant heteroskedasticity, with pronounced autoregression that shows periodicity.

Based on the Akaike and Bayesian information criterion the best GARCH representation of volatility with GED and Student t distribution was used to capture the dynamics of data-generating processes of each commodity. The asymmetry parameter in the GARCH model was significantly different from zero only for WTI. The asymmetry parameter, which controls the asymmetric impact of positive and negative shocks on conditional variance, indicates significantly higher conditional volatility after positive shocks, i.e. price increases. Estimation of the tail index is crucial in applying EVT models which are directly linked to threshold value u that defines the level above which returns are considered extreme. The threshold value for each index was determined by comparing the Hill estimator with the mean excess plot and the quantile–quantile (QQ) plot [5]. The same procedure of estimating the threshold value was also performed on IID innovations required for the implementation of the EVT-GARCH model [15]. The mean excess and QQ plots, Hill estimator and maximum likelihood estimates (MLE) all show that tail indexes for all commodities are equal to or greater than zero, implying fat tails and that the

Table 53.1 Lopez [12] size adjusted scores for 13 VaR models and four commodities (WTI, Brent, natural gas – NG, and heating oil – HO) at the 99 % confidence level are reported in columns 2–5. The observation period covers 1000 days from July 2010 to July 1st, 2014. Scores for models not satisfying the Kupiec [11] test and/or the Christoffersen [4] independence test at the 10 % significance level are underlined. The lowest Lopez scores, i.e. the smallest deviations from the expected values, are emphasized in bold. Rankings of VaR models based on the Lopez [12] size adjusted scores are reported in columns 6–10. They were obtained for 2000 simulated trajectories and a forecasting horizon of 1000 days. Lower values indicate better VaR models. If multiple models have the same score there is no statistically significant difference between them.

VaR model	WTI	Brent	NG	HO	WTI	Brent	NG	HO	Total
	Lopez scores				*Rankings*				
HS 250	3.13	**1.10**	7.27	2.16	3	2	4	2	3
HS 500	−1.88	−4.92	2.21	−2.87	2	2	2	2	2
MHS 250	−1.93	−5.93	**−1.90**	−3.87	2	3	1	2	2
MHS 500	−3.92	−6.94	−4.92	−4.89	3	3	4	3	4
BRW $\lambda = 0.97$	8.15	7.15	9.26	10.18	4	3	4	4	5
BRW $\lambda = 0.99$	**−0.92**	−1.92	3.20	**0.13**	1	1	3	1	1
Normal VCV	4.17	6.16	5.26	1.17	5	5	4	4	7
Risk metrics	10.22	13.20	2.12	11.18	5	5	2	4	6
GARCH	7.17	9.18	**0.09**	6.17	5	5	1	4	5
HW	8.15	10.16	9.17	16.20	5	5	4	5	8
FHS	**−0.92**	**−0.90**	−6.98	−2.88	1	1	3	1	1
EVT GARCH	−5.95	−3.93	−3.96	**−0.87**	3	2	2	1	2
GPD	−10.00	−10.00	−10.00	−10.00	5	5	4	4	7

GPD belongs to the Gumbel domain of attraction. This suggests that the normal distribution is not appropriate for describing tail events.

Columns 2–5 in Table 53.1 present our out-of-sample VaR model ranking according to minimal Lopez size adjusted scores for WTI, Brent, natural gas (NG) and heating oil (HO) at the 99 % confidence level. We conduct a two stage ranking since we allow a model to be ranked only after it satisfies both the Kupiec [11] and the Christoffersen [4] independence test. Satisfactory performance with regards to coverage and independence criteria is recorded for nonparametric models (HS, MHS), as well as FHS and extreme value based approaches. Very weak performance is recoded for GARCH, VCV, RiskMetrics and Hull–White models. Regarding the closeness of fit performance – which we measure by the Lopez [12] score – FHS, EVT GARCH and HS/MHS models provide the best fit.

In the next step, we apply the methodology discussed in Sect. 53.2 to test whether there is any statistically significant difference in the performance of the tested VaR models. The data is simulated based on the distribution of returns in the period July 2010–July 2014. For each commodity 2000 simulated trajectories of 1000 days are considered. The Lopez size adjusted score yields the best performing model as the one that is the closest to zero. After obtaining 2000 Lopez size adjusted scores for each VaR model and for each commodity, we apply the Kruskal–Wallis test to

compare the differences among the tested VaR models. The results are reported in columns 6–10 in Table 53.1.

When the simulated mean value of a given VaR model lies outside the 95 % confidence bands of all the other tested VaR models, it is ranked according to its relative performance. If a model is not significantly different from the other models it shares the same ranking as the VaR models not significantly different from it. Looking at the ranking results presented in columns 6–10 in Table 53.1, we see that for a large number of different models there is no statistically significant difference in their performance measured by our loss function.

When considering the overall performance for the tested commodities, the best performing VaR models that are statistically different from other tested models are the filtered historical simulation (FHS) and the BRW ($\lambda = 0.99$) model. These models are followed by the conditional EVT GARCH model and two simple nonparametric models (HS and MHS). The worst performance, measured by the distance from expected losses, be it positive or negative is recorded for Hull–White, VCV and unconditional GPD models. Although we tested 13 VaR models, we see that for all the tested commodities the number of statistically different models never surpasses five, and in the case of natural gas all the VaR models are concentrated in just four groups. To some extent our results confirm the findings in [10] and [14], but at the same time they pose a serious question of whether there are any significant differences among the tested VaR models in the mentioned papers. It is impossible to fully compare the results since we have no knowledge about the statistical significance of their VaR rankings.

53.5 Conclusions

Our empirical study shows that for a large number of different VaR models there is no statistical difference measured by the Lopez [12] size adjusted score as the loss function. Overall, statistically significant top performers are the filtered historical simulation (FHS) and the BRW ($\lambda = 0.99$) model. An additional benefit to risk management practitioners lies in the fact that these two models are very simple to compute and implement in everyday operations. As our loss function is the size adjusted Lopez score, these VaR models provide the closest fit to the actual level of risk encountered in the analyzed energy commodities. Simpler parametric models, such as the VCV, Hull–White and RiskMetrics, were the worst performers in our VaR comparison. Poor performance with regard to our loss function is also recorded for a very conservative unconditional GPD model. Unlike the aforementioned parametric models this is due to the fact that it constantly overestimated the level of risk that was recorded in the four commodities during the 2010–2014 period, i.e. it was overly conservative.

It is also interesting to note that although historical simulation based models are clearly theoretically inferior to EVT models in VaR estimation, their empirical track record is impressive. This finding may suggest that during the analyzed period there

were a large number of extreme events that allowed the simpler nonparametric models to correctly asses the true level of VaR. Advanced models based on conditional EVT and FHS as well as the very simple nonparametric models, such as mirrored historical simulation, yield very robust and consistent results. Models that span between these two extremes are not successful in energy markets and yield inconsistent risk estimates.

Acknowledgements This work was supported by the Croatian Science Foundation under Grant number IP-2013-11-2203.

References

1. Agnolucci P (2009) Volatility in crude oil futures: a comparison of the predictive ability of GARCH and implied volatility models. Energy Econ 31:316–321
2. Aloui C (2008) Value-at-risk analysis for energy commodities: long-range dependencies and fat tails in return innovations. J Energy Mark 1(1):31–63
3. Bunn D, Andresen A, Chen D, Westgaard S (2013) Analysis and forecasting of electricity price risks with quantile factor models. London Business School working paper. Available from http://www.ceem-dauphine.org/assets/dropbox/Derek_BUNN.pdf
4. Christoffersen PF (1998) Evaluating interval forecasts. Int Econ Rev 39(4):841–862
5. Danielsson J, de Vries C (1997) Tail index and quantile estimation with very high frequency data. J Empir Finance 4:241–257
6. Diebold FX, Mariano R (1995) Comparing predictive accuracy. J Bus Econ Stat 13:253–263
7. Giot P, Laurent S (2003) Market risk in commodity markets: a VaR approach. Energy Econ 25:435–457
8. Hansen PR (2005) A test for superior predictive ability. J Bus Econ Stat 23(4):365–380
9. Hollander M, Wolfe DA (1999) Nonparametric statistical methods. Wiley, Hoboken
10. Hung JC, Lee MC, Liu HC (2008) Estimation of value-at-risk for energy commodities via fat-tailed GARCH models. Energy Econ 30(3):1173–1191
11. Kupiec P (1995) Techniques for verifying the accuracy of risk management models. J Deriv 3:73–84
12. Lopez AJ (1999) Methods for evaluating value-at-risk estimates. Econ Policy Rev (Federal Reserve Bank of New York) 2:3–17
13. Mabrouk S (2011) Value-at-risk and expected shortfall estimations based on GARCH-type models: evidence from energy commodities. J Energy Dev 35:279–314
14. Marimoutou V, Raggad B, Trabelsi A (2009) Extreme value theory and value at risk: application to oil market. Energy Econ 31:519–530
15. McNeil AJ, Frey R (2000) Estimation of tail-related risk measures for heteroscedastic financial time series: an extreme value approach. J Empir Finance 7:271–300
16. Mohammadi H, Su L (2010) International evidence on crude oil price dynamics: applications of ARIMA-GARCH models. Energy Econ 32(5):1001–1008
17. Wei Y, Wang Y, Huang D (2010) Forecasting crude oil market volatility: further evidence using GARCH-class models. Energy Econ 32(6):1477–1484
18. Weron R (2009) Heavy-tails and regime-switching in electricity prices. Math Methods Oper Res 69(3):457–473
19. Weron R (2014) Electricity price forecasting: a review of the state-of-the-art with a look into the future. Int J Forecast 30(4):1030–1081
20. White H (2000) A reality check for data snooping. Econometrica 68:1097–1126

21. Žiković S, Filer RK (2013) Ranking of VaR and ES models: performance in developed and emerging markets. Czech J Econ Finan 63(4):327–359
22. Žiković S, Vlahinić-Dizdarević N (2011) Similarities between expected shortfall and value at risk: application to energy markets. Int J Manag Cases 13(3):386–399

ERRATUM

Erratum to: Detection of Essential Changes in Spatio-Temporal Processes with Applications to Camera Based Quality Control

Ewaryst Rafajłowicz

Erratum to: Chapter 48 in: ***Stochastic Models, Statistics and Their Applications,***
Steland, Ansgar, Rafajłowicz, Ewaryst,
Szajowski, Krzysztof (Eds.),
DOI 10.1007/978-3-319-13881-7_48

Page 440 — **Acknowledgements** The paper was supported by the National Council for Research of Polish Government under grant 2012/07/B/ST7/01216, internal code 350914 of Wrocław University of Technology.
The author would like to express his thanks to anonymous referees for comments clarifying the presentation.

Must read:
Acknowledgements The paper was supported by **The National Science Centre Poland** under grant 2012/07/B/ST7/01216, internal code 350914 of Wrocław University of Technology.
The author would like to express his thanks to anonymous referees for comments clarifying the presentation.

The online version of the original chapter can be found under 10.1007/978-3-319-13881-7_48

E. Rafajłowicz (✉)
Institute of Computer Engineering, Control and Robotics, Wrocław University of Technology, Wrocław, Poland
e-mail: ewaryst.rafajlowicz@pwr.wroc.pl

A. Steland et al. (eds.), *Stochastic Models, Statistics and Their Applications*,
Springer Proceedings in Mathematics & Statistics 122,
DOI 10.1007/978-3-319-13881-7_54

Author Index

A. Steland et al. (eds.), *Stochastic Models, Statistics and Their Applications*,
Springer Proceedings in Mathematics & Statistics 122,
DOI 10.1007/978-3-319-13881-7